

Norwegian University of Life Sciences
Faculty of Chemistry, Biotechnology
and Food Science

Philosophiae Doctor (PhD)
Thesis 2021:80

Polycyclic aromatic compounds (PACs) in ambient air of Svalbard. Concentrations, seasonal trends, sources, and transformation processes

Polyaromatiske sykliske komponenter (PAC)
i omgivelsesluft på Svalbard. Konsentrasjoner,
sesong trender, kilder og transformasjons
prosesser

Tatiana Drotikova

Polycyclic aromatic compounds (PACs) in ambient air of Svalbard. Concentrations, seasonal trends, sources, and transformation processes

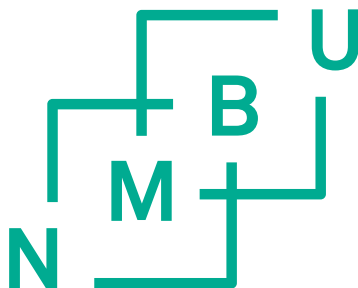
Polyaromatiske sykliske komponenter (PAC) i omgivelsesluft på Svalbard.
Konsentrasjoner, sesong trender, kilder og transformasjons prosesser

Philosophiae Doctor (PhD) Thesis

Tatiana Drotikova

Norwegian University of Life Sciences
Faculty of Chemistry, Biotechnology and Food Science

Ås / Longyearbyen (2021)

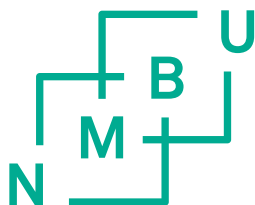


Thesis number 2021:80
ISSN 1894-6402
ISBN 978-82-575-1857-8

Preface

The thesis is submitted in fulfilment of the requirements for the degree of Philosophiae Doctor (PhD) at the Faculty of Chemistry, Biotechnology and Food Science, Norwegian University of Life Science (NMBU), Ås, Norway. The study was carried out at and funded by the University Centre in Svalbard (UNIS). The sample analyses were performed at NMBU, UNIS, French National Institute for Industrial Environment and Risks (Ineris), and Norwegian Institute for Air Research (NILU). The study relevant courses were taken at UNIS, NMBU, University of Oslo (UiO), and University of Copenhagen (UCPH). 25% of the project time was dedicated to the annual teaching of the graduate AT-324/824 chemistry course at UNIS.

Additional financial support was provided by the Research Council of Norway (Svalop 940015 and Barelab RIS ID 10628 projects). During my doctoral training, I have also been enrolled in the Atmopart project supported by the Svalbard Environmental Protection Fund on “Characterization of direct fossil fuel burning particulate emissions in Svalbard”. I was also a partner of the “Strengthening cooperation on air pollution research in Svalbard” project funded by the Research Council of Norway.



Supervisors and Evaluation Committee

Main supervisor:

Prof. Roland Kallenborn, Norwegian University of Life Sciences (NMBU) and University Centre in Svalbard (UNIS)

Co-supervisors:

Dr. Anne Karine Halse, Norwegian Institute for Air Research (NILU)

Dr. Helena Reinardy, Scottish Association for Marine Science (SAMS) and UNIS

Prof. Stephan Weinbruch, Technical University of Darmstadt (TU Darmstadt)

Prof. Arne Aalberg, Norwegian University of Science and Technology (NTNU) and UNIS

Evaluation Committee:

Dr. Hayley Hung, Environment and Climate Change Canada, Canada

Prof. Øyvind Mikkelsen, Environmental and Analytical Chemistry, NTNU, Norway

Prof. Yngve H. Stenstrøm, Organic chemistry, NMBU, Norway

*This work is dedicated to
my son Lev (10) and daughter Julia (5),
who live in the Arctic since sea ice was still in the fjords*

Acknowledgements

I remember the day when my main supervisor, Roland Kallenborn, said that I am going to have a “flight start” of the PhD project and sent me out for field work. So, on my first official day of the PhD, I found myself climbing to the top of the Longyearbyen power plant (95 m) together with my other enthusiastic and brave co-supervisor, Stephan Weinbruch, to collect my first, very important (*sarcastic*) samples. Climbing inside a moving (unexpectedly) chimney tower in complete darkness without a headlamp was insane. Due to strong windy conditions, the tower was swinging though I have been thinking that the actual reason was my nervousness accompanied by dizzy feelings. I nearly expected to soon be unconscious when I stopped at what felt like the middle of the ascent to estimate if the distance up to the top was shorter than turning back down to the ground. Since nobody was at the bottom to meet and “rescue” me and Stephan has already made it to the top, I decided to follow him. Now I think it was a sign of how complicated and wild this PhD study would be but still possible - I have made it to the top then and I made it now!

For the opportunity to do this PhD and for a wise choice of the research topic I am passionate about now, I would like to thank Roland Kallenborn, the initiator of this work. Thank you, Roland, for being supportive from the first day of my PhD until the present, for continuous generation of research ideas, being respectful and patient to my work progress delays, and letting me work independently though always being controlled.

Except for my first PhD day experience (the climb ☺), I am also thankful to Stephan Weinbruch for always caring for me, both when I stayed in Germany and during his short visits to Longyearbyen. Stephan, you are a stickler for punctuality and a responsible supervisor indeed. It was a pleasure to work with you and to learn from you.

I think it is cool to have a cool supervisor and I have certainly had one, Anne Karine Halse! Kine, you have been a trustable friend, a strict supervisor, and a committed field assistant, all in one. Your support and encouragement (during days and nights) throughout my PhD was invaluable. I am very thankful for it. Me and Lev and Svalbard miss you very much <3.

I was lucky to get Helena Reinardy as my co-supervisor later in these PhD years when deadlines were already close, and a level of stress was elevated. Receiving your comments on my writings was always a trembling moment with thoughts like “Did I fail it again?” I am truly impressed by how logical, accurate, skilful, strait, unemotional, and

astute your suggestions have always been. I gained a lot of knowledge from you, and I am very grateful for it indeed.

I am deeply thankful to my UNIS co-supervisor, Arne Aalberg, for always providing me with the best possible work conditions, taking care of my mental and social health and the PhD progress, helping to balance between edges and find solutions, and even caring and installing my bulky sampling equipment! I will remember our snowmobile trips, dinners, and your delicious homemade cakes. Hope we will repeat it all multiple times again!

I owe a special debt of gratitude to my unofficial co-supervisor, Dr. Alexandre Albinet, from the French National Institute for Industrial Environment and Risks (Ineris), France. This work would never have been completed with this level of competence and great achievements if it weren't his insightful knowledge on PACs and endless enthusiasm. He was the one who pushed my edges, always digging deeper and asking for more at the same time providing enormous help and supervision. Our collaboration helped me to believe in myself as a researcher and build my scientific confidence and maturity.

I thank Svalbard Satellite Station, Longyearbyen lokalstyre, and Store Norske for collaboration and assistance on samples and data collection. Financial support of Research Council of Norway and Svalbard Miljøvernfond have been very appreciated. This field-based study would never be successful without great assistance of the UNIS engineers. I thank my dear friend, Jessica Bosch Birkeland (former UNIS employee), with whom we have started this PhD journey together, for always being a reliable, skilful, and responsible field leader. I did not need to use my brain much when on a field with you as every little detail and potential failure were thought over by you, thanks! I also thank Sebastian Sikora for finalizing my summer 2018 sampling campaign when I had to leave the island urgently and for multiple help with on-site equipment installation. Furthermore, I thank the Logistics Department of UNIS for extensively teaching me to shoot, drive a snowmobile, swim in cold water, glacier and avalanche practical precautions, and for all the assistance.

I wish to thank all my friends and colleagues in town and on the mainland, who were always cheerful, supportive and willing to share non-work-related activities. I owe a special thanks to Kari Elise Moxnes and Thor Johansen, who hosted and treated me as a daughter in their family during my visits to Ås for lab works in NMBU. I am deeply

grateful for your love, hospitality, protection, and care. You and Kajaveien 22 are always in my heart. Finally, I thank my sweet kids, my son Lev and daughter Julia, for their love and joy and for being an anchor to the “normal” life. I thank my mom, Elena, for always supporting my education and help during my PhD. My deepest gratitude and appreciation go to my dear husband, Aleksey, for his continuous support and help during this long PhD journey.

Tatiana Drotikova
Longyearbyen, August 2021

Summary

Polycyclic aromatic compounds (PACs) are ubiquitous organic, gaseous, and particulate chemicals primarily emitted from incomplete combustion of fossil fuels, waste, and open biomass burning, including wildfires. Several PACs are classified as known, probable or possible carcinogens and toxicants. Atmospheric transport is the most efficient way for PACs' global distribution. Due to a tendency to increase in environmental compartments and biota and low degradation rates in polar conditions, PACs have been identified as chemicals of emerging Arctic concern.

PACs comprise several thousand different molecules, which are traditionally represented by 16 unsubstituted polycyclic aromatic hydrocarbons (PAHs). An extended suite of PAHs, including the 16 priority PAHs, were studied in this thesis. The list of target 91 PACs consisted of 23 PAHs, 31 oxy-PAHs, and 37 nitro-PAHs. Oxy- and nitro-PAHs are equally or more toxic and may act as direct mutagens and carcinogens in biota. In addition to primary emissions, oxy- and nitro-PAHs can also be photochemically produced in the atmosphere by oxidation of PAHs. While background Arctic air concentrations of PAHs are known, little is documented about local contributions of anthropogenic emissions, and the levels of oxy- and nitro-PAHs in the Arctic air are largely unknown.

The primary aim of the study was to quantify PACs in the ambient air of Longyearbyen (78.22° N, 15.65° E), the largest populated settlement in Svalbard, the northernmost land in the European Arctic. To better assess the influence of local emissions, gaseous and particulate air samples were collected within the boundary layer height (below 50 m asl) at rural and urban sites and on an adjacent mountain top. The sampling campaign lasted for almost a year (from November 2017 until October 2018) and covered all seasons accompanied by an extreme shift from conditions of polar night to full polar day. Seasonal transport regimes of air masses from lower latitudes and local meteorology have been investigated to assess remote sources and the near-ground local emissions' dispersion. For detailed source emissions' characterization, plume samples of the local coal-burning power plant were collected for analysis. Additional attention of the study was given to investigation of physicochemical processing of atmospheric PACs to understand their fate under polar conditions.

Measured seasonal PAC concentrations in ambient air of Longyearbyen were highly variable and span sixteen-folds of magnitude. Winter air quality was mainly controlled

by transported air masses from the European sector, including Scandinavia, Northern Europe, Western Russia, and the West Siberian plain. The study revealed the predominant influence of local anthropogenic emissions during spring and summer. Specific polar climate conditions caused near-ground pollution accumulation and resulted in the highest annual PAC concentrations in spring. The concentrations were comparable and partly exceeded the European annual mean levels. Local vehicle traffic, specifically snowmobiles, was presumed as the major source. Contrary to observations at background Arctic air monitoring stations, PAC summer levels exceeded winter levels. Up to four times higher PAC concentrations were determined when high marine traffic was present at the local port. Ambient emissions from coal-burning in Longyearbyen were evident on the days with northwesterly winds. This thesis provides new data on snowmobile and coal-burning characteristic PAC emissions and ambient seasonal profiles of PACs in general.

This thesis is the first study showing the evidence of rapid halogen-initiated oxidation of atmospheric PACs under natural conditions. Long exposure time and absence of photodegradation in the polar night enabled detection of several ozonation products of PACs, which have previously been detected in laboratory studies. Significant phase repartitioning was determined for a number of PACs in response to changing ambient conditions, implying their high potencies for evaporation from contaminated surfaces in the predicted warmer Arctic future.

As knowledge was limited to monitoring only 16 PAHs in background Arctic air, this thesis opens up many novel aspects about occurrence, seasonal variations, sources, atmospheric behaviour, degradation, and persistence of a large suite of selected PACs. It plays a crucial role in understanding the environmental fate of PACs as key chemicals of emerging concern in the Arctic. The work highlights an essential contribution of local anthropogenic sources and sensitivity of the Arctic environment to accumulation and lack of pollutants degradation.

Norsk sammendrag

Polysykliske aromatiske komponenter (PAC) er organiske, flyktige og partikulært bundne kjemikalier som primært slippes ut fra ufullstending forbrenning av fossilt brensel, avfall og åpen biomassebrenning inkludert skogbranner. Mange PAC-er er klassifiserte som, sannsynlige og/eller potensielt kreftfremkallende forbindelser og toksiske. Atmosfærisk transport er den mest effektive måten for global transport og fordeling av PAC-er. Grunnet disse komponentenes evne til opphoping i miljøet, i tillegg til lang tilstedeværelse i biota på grunn av dens lave nedbrytningshastighet, har PAC blitt identifisert som prioriterte forurensninger i Arktis.

PAC-er omfatter flere tusen ulike molekyler men blir normalt representert av 16 ikke-substituerte polysykliske aromatiske hydrokarboner (PAH). I dette arbeidet så har et utvidet antall PAC-er, inkludert 16 prioriterte PAHene (US-EPA16), blitt studert. Listen over 91 PAC, studert, inkluderer 23 PAHs, 31 oksy-PAH og 37 nitro-PAH. Oksy- og nitro-PAH er like eller mer toksiske enn ikke-substituerte PAH-er, de kan være mutagene og kreftfremkallende. I tillegg til utslipp fra primære kilder, så dannes oksy- og nitro-PAH gjennom fotokjemisk oksidasjon av ikke-substituert PAH-er. Mens bakgrunnkonsentrasjoner av ikke-substituerte PAH i luft fra Arktis er kjent fra tidligere undersøkelser, så er det lite som er kjent rundt nivåer og bidrag fra potensielle menneskeskapte kilder av oksy- og nitro-PAH i Arktis.

Hovedmålet for dette studiet var derfor å bestemme PAC-er i luftprøver fra Longyearbyen (78.22° N, 15.65° E). Longyearbyen er den største bosetningen på Spitsbergen som er den største øya i Svalbard (Norsk Arktis). For å bedre kunne vurdere påvirkningen av lokale utslipp, ble det tatt luftprøver av gassformige og partikkelbundne PAC-er innenfor atmosfæriske grenselaget (50 moh), i Longyearbyen og omegn. Prøvetakingen foregikk på urbane, rurale lokasjoner og en nærliggende fjelltopp, og forgikk i nesten i 1 år (fra november 2017 til oktober 2018). Dermed ble også PAC konsentrasjoner og fordelingsmønster i overgangsperioden mellom polarnatt til midnattssol undersøkt. Sesongavhengige transportregimer av luftmasser fra lavere breddegrader og lokal meteorologi, har blitt inkludert i studien for å kartlegge og vurdere bidraget fra fjerntliggende kilder samt PAC fordelingen fra lokale kilder. For mer detaljert karakterisering av utslipp fra kilden, ble det også tatt avgass-prøver fra pipeuttak ved det lokale kullkraftverket. Ytterligere fokus for studien var å studere

fotokjemiske nedbrytningsprosesser av PAC-er for å bedre forstå sesongavhengig transformasjon av atmosfærisk PAC under polare forhold.

Dette studiet bidrar med nytt faglig innsyn rundt utslipp, fordeling og kilder til karakteristiske PAC-er. Det er en tydelig trend i PAC nivåer gjennom hele målekampanjen, hvor nivåene later til å være sesongavhengige og varierer over seksten størrelsesordener. Luftkvaliteten om vinteren var i stor grad kontrollert av langtransporterte luftmasser fra europeiske kilder, i.e. Skandinavia, Nord-Europa, Vest-Russland og de vest-sibiriske slettene. Studien bekrefter hvor innflytelse lokale utslippkilder har på vår og sommerhalvåret. De spesielle klimaforholdene (sesonalitet, temperturforandringer, inversoner, etc) bidro til akkumulering av forurensing i den lave atmosfæren, og dette medfører at årskonsentrasjonen av PAC-er er høyest om våren og sommeren. Målte nivåer av PAC-er ble funnet på samme nivå eller overskred det årlige europeiske gjennomsnittet av PAC-er. Lokale trafikkforhold, men spesielt snøscootere ble identifisert som en av hovedkildene. I motsetning til bakgrunnobservasjoner på Zeppelin stasjonen (Ny-Ålesund og andre arktiske overvåkingsstasjoner), var nivåene av PAC høyest om sommeren sammenlignet med vinteren. Det ble målt opptil fire ganger så høye PAC luftkonsentrasjoner under cruiseskip sesongen sammenlignet med andre tidsperioder. Utslipp fra kullkraftverket i Longyearbyen var tydelig i PAC målingene i tidsperioder med nordvestlig vindretning.

Videre så har det blitt avdekket det har foregått en rask halogen initiert oksidering av atmosfæriske PAC-er under naturlige forhold. Lang eksponeringstid og fravær av fotodegradering i polarnatten muliggjør påvisning av flere nedbrytningsprodukter av ozonering. Slike forbindelser ble tidligere kun detektert i kontrollerte laboratoriestudier. Kunnskapen om PAC i Arktis har hittil vært begrenset til overvåking av et relativt lite antall av PAH i luft. Dermed bidrar denne studien med nye faglig opplysninger rund forekomst, sesongvariasjoner, kilder, atmosfæriske egenskaper, nedbrytningsveier, miljøskjebne og stabilitet for de undersøkte PACer. Denne nye informasjonen kan spille en viktig rolle for en bedre forståelse av miljøskjebnen i et Arktis under endring.

Table of content

Preface.....	iii
Supervisors and Evaluation Committee	v
Acknowledgements	ix
Summary.....	xiii
Norsk sammendrag.....	xv
List of papers.....	1
Reprint copyrights	3
Acronyms and abbreviations	5
1 Introduction	7
1.1 Identity and physico-chemical properties of PACs.....	7
1.2 PAC sources and environmental fate	9
1.3 Atmospheric removal processes of PACs	12
1.4 Exposure and toxicity	14
1.5 Regulations on PACs.....	18
1.6 Emissions and atmospheric transport of PACs to the Arctic.....	19
1.7 PACs as chemicals of emerging Arctic concern (CEACs)	22
2 Thesis objectives	25
3 Methods	27
3.1 Study area.....	27
3.2 Sampling locations and sample collection.....	28
3.3 Sample preparation and analysis.....	32
3.4 Quality assurance and quality control.....	34
3.5 Statistical analysis	34
3.6 Local meteorology and LRAT analysis.....	35
4 Results and discussion	37
4.1 LRAT seasonal influence	37

4.2 PAC seasonal concentrations and sources	41
4.2.1 Winter	41
4.2.2 Spring	43
4.2.3 Summer	44
4.2.4 Autumn	46
4.2.5 Summary notes.....	46
4.3 Coal power plant emissions characterization	47
4.4 Gas/particle partitioning of atmospheric PACs	49
4.5 Secondary formation of PACs in the polar atmosphere.....	52
4.5.1 Polar night chemistry	53
4.5.2 Polar spring chemistry.....	54
4.5.3 Polar day summer chemistry.....	56
5 Conclusions	59
6 Future perspectives.....	63
7 References.....	66
8 Appendix.....	89
Papers	103
Paper I.....	103
Paper II.....	167
Paper III	215

List of papers

PAPER I Drotikova, T., Ali, A. M., Halse, A. K., Reinardy, H. C., and Kallenborn, R.: Polycyclic aromatic hydrocarbons (PAHs) and oxy- and nitro-PAHs in ambient air of the Arctic town Longyearbyen, Svalbard, *Atmos. Chem. Phys.*, 20, 9997-10014, 10.5194/acp-20-9997-2020, 2020. Published.

PAPER II Drotikova, T., Dekhtyareva, A., Kallenborn, R., and Albinet, A.: Polycyclic aromatic hydrocarbons (PAHs) and their nitrated and oxygenated derivatives in the Arctic boundary layer: Seasonal trends and local anthropogenic influence, *Atmos. Chem. Phys. Discuss.*, 2021, 1-27, 10.5194/acp-2021-193, 2021. Manuscript accepted for final publication.

PAPER III Drotikova, T., Kallenborn, R., and Albinet A.: Insights the physicochemical processes of atmospheric polycyclic aromatic hydrocarbons (PAHs) and their derivatives under polar conditions in Svalbard. Manuscript in preparation.

Publications not included for the thesis evaluation:

Marquès, M., Sierra, J., Drotikova, T., Mari, M., Nadal, M., and Domingo, J. L.: Concentrations of polycyclic aromatic hydrocarbons and trace elements in Arctic soils: A case-study in Svalbard, *Environ. Res.*, 159, 202-211, 10.1016/j.envres.2017.08.003, 2017.

Dekhtyareva A., Drotikova T., Nikulina A., Hermansen O., Chernov D.G., Mateos D., Herreras M., Petroselli C., Ferrero L., Gregorič A., 2021. Summer air pollution in Svalbard: emission sources, meteorology and air quality. Manuscript in preparation.

Weinbruch, S., Benker, N., Kandler, K., Schutze, K., Kling, K., Berlinger, B., Thomassen, Y., Drotikova, T., and Kallenborn, R.: Source identification of individual soot agglomerates in Arctic air by transmission electron microscopy, *Atmos. Environ.*, 172, 47-54, 10.1016/j.atmosenv.2017.10.033, 2018.

Weinbruch, S., **Drotikova, T.**, Benker, N., and Kallenborn, R.: Particulate and gaseous emissions of power generation at Svalbard (AtmoPart), Governor of Svalbard, Svalbard Environmental Protection Fund, 20 pp., 2015.

Weinbruch, S., Zou, L., Ebert, M., Benker, N., **Drotikova, T.**, Kallenborn, R., and Ellingsen, D.: Emission of primary nanoparticles from coal and diesel-fired power plants on Svalbard: An electron microscopy study, 2021. Manuscript in preparation.

Reprint copyrights

- Figure 2 Reprinted with permission from Shen, H., Huang, Y., Wang, R., Zhu, D., Li, W., Shen, G., Wang, B., Zhang, Y., Chen, Y., Lu, Y., Chen, H., Li, T., Sun, K., Li, B., Liu, W., Liu, J., and Tao, S.: Global Atmospheric Emissions of Polycyclic Aromatic Hydrocarbons from 1960 to 2008 and Future Predictions, *Environ. Sci. Technol.*, 47, 6415-6424, <https://doi.org/10.1021/es400857z>, 2013. Copyright © 2013 American Chemical Society
- Figure 4 Reprinted with permission from Riva, M., Healy, R. M., Flaud, P.-M., Perraudin, E., Wenger, J. C., and Villenave, E.: Gas- and Particle-Phase Products from the Chlorine-Initiated Oxidation of Polycyclic Aromatic Hydrocarbons, *J. Phys. Chem. A*, 119, 11170-11181, <https://doi.org/10.1021/acs.jpca.5b04610>, 2015. Copyright © 2015 American Chemical Society
- Figure 5 Reprinted with permission from Albinet, A., Leoz-Garziandia, E., Budzinski, H., Villenave, E., and Jaffrezo, J. L.: Nitrated and oxygenated derivatives of polycyclic aromatic hydrocarbons in the ambient air of two French alpine valleys. Part 1: Concentrations, sources and gas/particle partitioning, *Atmos. Environ.*, 42, 43-54, <http://doi.org/10.1016/j.atmosenv.2007.10.009>, 2008. Copyright © 2007 Elsevier Ltd
- Figure 6 Reprinted with permission from Fu, P. P., Xia, Q., Sun, X., and Yu, H.: Phototoxicity and environmental transformation of polycyclic aromatic hydrocarbons (PAHs)—light-induced reactive oxygen species, lipid peroxidation, and DNA damage, *Journal of Environmental Science and Health, Part C*, 30, 1-41, <https://doi.org/10.1080/10590501.2012.653887>, 2012. Copyright © 2012 Taylor & Francis
- Figure 7 AMAP (2015b), open access

Acronyms and abbreviations

AhR	Aryl hydrocarbon receptor
AMAP	Arctic Monitoring and Assessment Programme
ASL	Above sea level
BLH	Boundary layer height
CEAC	Chemical of emerging Arctic concern
CYP	Cytochrome P450 enzymes
DNA	Deoxyribonucleic acid
EC	Elemental carbon
EPA PAHs	Priority PAHs listed by the US Environmental Protection Agency
GC-EI-MS/MS	Gas chromatography with electron ionization tandem mass spectrometry detection
GC-NICI-MS	Gas chromatography with negative ion chemical ionization mass spectrometry
HMW	Heavy molecular weight
K_{aw}	Air-water partitioning coefficient
K_{oa}	<i>n</i> -Octanol-air partitioning coefficient
K_{ow}	<i>n</i> -Octanol-water partitioning coefficient
LMW	Low molecular weight
LRAT	Long-range atmospheric transport
NIST	National Institute of Standards and Technology
OC	Organic carbon
PACs	Polycyclic aromatic compounds (PAHs, oxy-PAHs, nitro-PAHs, and other substituted and heterocyclic PAHs together)
PAH	Polycyclic aromatic hydrocarbon
PCA	Principal component analysis
PSE	Pressurized solvent extraction
PUF	Polyurethane foam
QFF	Quartz fiber filter
QuEChERS	Quick Easy Cheap Effective Rugged and Safe extraction
ROS	Reactive oxygen species
SPE	Solid phase extraction

TEF	Toxic equivalency factor
TIS	Temperature inversion strength
UHPLC/Fluo	Ultra high-performance liquid chromatography with fluorescence detection
UNIS	University Centre in Svalbard
%PM	Percentage in particulate matter

The list of compound names and abbreviations is provided in Appendix Table S1.

1 Introduction

The Arctic region is a receptor of air pollution from diverse source regions at mid-latitudes and a sentinel of global contaminants propagation. Processes controlling air pollution in the Arctic are largely complex and present a web of interactions between polar climate, vertical structure of Arctic troposphere, local boundary layer meteorology, and unique regional chemistry. Changes in mid-latitude emissions and climate-driven changes in atmospheric transport patterns accompanied by increasing local emissions are expected to shift the balance among contaminants source contributions in future (Arnold et al., 2016). Polycyclic aromatic compounds (PACs) are among several groups of chemicals of emerging concern in the Arctic environment as they are emitted from various combustion sources and may have adverse effects on humans and the Arctic ecosystem (AMAP, 2021a). Sea ice retreat facilitates industrialization of the region, and the local PAC emissions within the Arctic are expected to increase. Studies have shown that PACs measured in Arctic marine waters and sediments mainly originate from natural underwater hydrocarbon seeps, while airborne PACs better reflect ongoing emissions (Yu et al., 2019; Dahle et al., 2006). This thesis gains knowledge on occurrence, levels, environmental behaviour, and principal sources and processes of atmospheric PACs, most of which have not been investigated in the high Arctic before. Svalbard in the Norwegian Arctic was chosen as the study area. Warm Atlantic waters along its west coast assure sea ice-free conditions and promote human activities in Svalbard, as well as this area frequently receives air masses from Eurasia (Stohl, 2006). Extreme variation of solar insolation and ambient temperatures between polar night and polar day drive many feedbacks in the Arctic air contamination by PACs. In this thesis, PACs refers to a suite of polycyclic hydrocarbons (PAHs) and their oxygenated and nitrated derivatives (oxy- and nitro-PAHs).

1.1 Identity and physico-chemical properties of PACs

PAHs are a class of organic compounds with two or more fused aromatic rings in linear, angular, or clustered arrangements. Due to their ubiquitous presence and toxicity, PAHs have been studied for more than four decades since the US Environmental Protection Agency (EPA) released a list of 16 representative PAHs in 1976 based on their toxicity, ability to be analyzed, and environmental occurrence at the time (Lawrence, 2015). This set of 16 analytes became commonly used for monitoring in all the environmental

compartments, and due to consistency over time, most statements about temporal and spatial trends apply to them. However, PACs comprise several thousand molecules with nitro-, oxy-, hydroxy-, chloro-, bromo-, amino-, and N-, S- O-heterocyclic functionalization (Fig. 1; Achten and Andersson, 2015; Andersson and Achten, 2015).

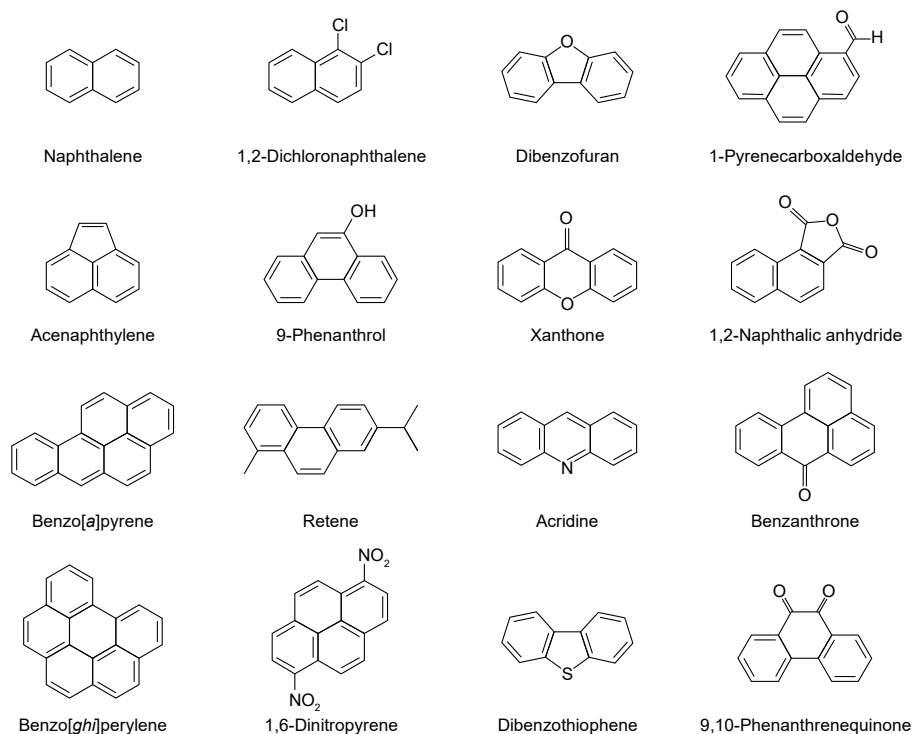


Figure 1. Structural formulas of selected polycyclic aromatic compounds (PACs). Compounds studied in the thesis, their abbreviation names, and properties are outlined in Table S1.

The physico-chemical properties of PACs generally correlate with the molecular weight. Vapour pressure and water solubility decrease with the number of aromatic rings in the PAC structure, while octanol-water partition coefficients (K_{ow}) increase (Table S1). Accordingly, heavy molecular weight (HMW; > 4 rings) PACs mainly exist in particulate phase, are low soluble in water, and sufficiently lipophilic to bioaccumulate in organisms (Petersen and Kristensen, 1998; Bruner et al., 1994; Nfon et al., 2008). HMW PACs are also more persistent as they are shielded from degradation processes when incorporated into a particle pore structure (Lammel, 2015a; Niu et al., 2007). The lighter molecular weight (LMW; < 4 rings) PACs with vapour pressure in the range of 10^{-6} - 10^{-2} Pa are considered as semi-volatile and partition between gaseous and particulate

phases under ambient conditions (Bidleman, 1988; Lammel et al., 2009; Finlayson-Pitts and Pitts Jr., 1999). The presence of polar functional groups in the PAC structure increase the hydrophilicity in the order $\text{NO}_2 < \text{COOH} < \text{OH} < \text{CN} < \text{NH}_2 < \text{dione}$ (Achten and Andersson, 2015). Consequently, oxy-PAHs, and notably quinones, have higher water solubility and lower K_{ow} than PAHs and nitro-PAHs with a similar ring number, explaining greater mobility of oxy-PAHs in soil and sediment (Idowu et al., 2019). Nitro-PAHs have lower vapour pressure, water solubility and K_{ow} than their related PAHs. Lower water solubility of nitro-PAH can be explained by the higher MW than a corresponding PAH (Bandowe and Meusel, 2017). The higher K_{oa} of nitro-PAHs indicates that the introduction of nitro-groups leads to higher migration into a more hydrophobic octanol phase, as well as greater partitioning into particulate matter. Thereby, physico-chemical properties of PACs determine their transport, behaviour, persistence, and effects on biological systems.

1.2 PAC sources and environmental fate

PACs are unintentionally produced during incomplete combustion and pyrolysis of fossil fuels (coal, crude oil, and natural gas), biomass, and inorganic waste (Bandowe and Meusel, 2017; Ravindra et al., 2008). They are therefore emitted into the environment from transports, industrial, residential and agricultural sectors. The most important industrial sources of PACs are aluminium, iron and steel production, cement manufacture, asphalt industries, and coal-fired power plants (Abbas et al., 2018). Global atmospheric PAC emission is estimated as 504 000 tonnes/year with 54 % contribution from Asian countries (Fig. 2; Shen et al., 2013). It is dominated by biomass burning (74 %), with transportation and industrial sources making up only 20 % of the global total. More than 70 % of PAC emissions are anthropogenic. Natural emission sources include wildfires and volcanic eruption.

In contrast to PAHs, oxy- and nitro-PAHs can also be secondary formed via homogeneous (in gas phase) or heterogeneous (gas-particle reactions) oxidation processes of PAHs by tropospheric oxidants such as OH or NO_3 radicals, NO_2 , and O_3 (Atkinson and Arey, 1994; Vione et al., 2004; Keyte et al., 2013) or by direct photolysis.

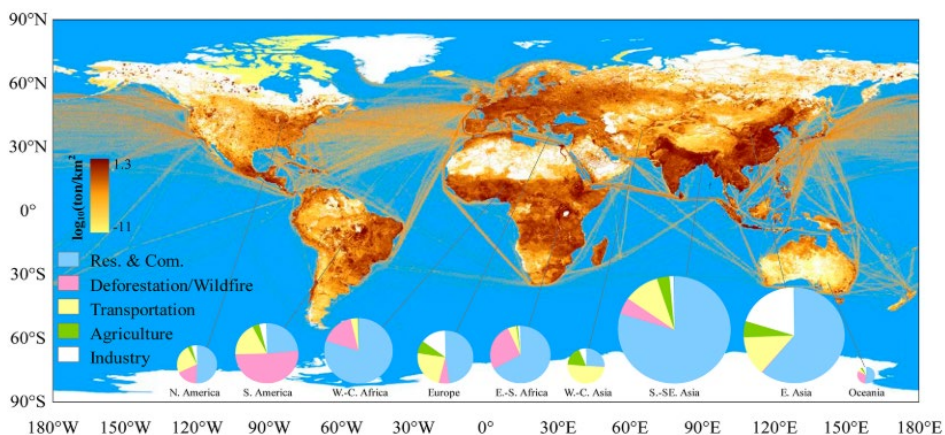


Figure 2. Global spatial distributions of 16 PAH emissions in 2007 according to Shen et al. (2013). Relative contribution of major sources is shown as pie charts. Note “Res. & Com.” is residential and commercial emissions.

Oxy- and nitro-PAH by-products are less volatile than unsubstituted PAHs and tend to be more particle-associated (Sect. 1.3 & Fig. 5). The reactions with OH (daytime) and NO₃ (night-time) radicals are the main transformation pathways of gas-phase PAHs (Fig. 3). The established mechanism of PAH reactions with the radicals involves the addition of the OH or NO₃ radical to the aromatic ring to form an energy-rich PAH-X (X = OH, NO₃) adduct. Further reaction of this adduct with NO₂ will yield nitro-PAHs, while adduct reaction with O₂ will form a peroxy-radical intermediate which can further react or decompose via a number of different pathways to yield ring-retaining products such as quinones or a wide range of ring-opened products such as acids, aldehydes and anhydrides (Keyte et al., 2013). In most environments, the reaction with OH, generated by the photolysis of ozone and water during daytime hours, plays the dominant role, ensuring PAHs’ transformation into oxy- and nitro-PAHs faster than one day in most cases (Atkinson and Arey, 1994; Keyte et al., 2013). For some gaseous PAHs (e.g., Ace, Acy, Phe), night-time oxidation by NO₃ is much quicker than during a day (Vione et al., 2004), as well as the yields of nitro-PAH products from the NO₃-initiated reaction are notably higher than that of the corresponding reaction initiated by OH radicals (Keyte et al., 2013). NO₃ radicals are formed in polluted air via a reaction between nitrogen dioxide and ozone and present in the atmosphere at a significant level only at night due to rapid photolysis of NO₃ (Brown and Stutz, 2012). As in gas phase, particle-bound PACs react with atmospheric OH (gas/particle heterogeneous processes) via the adduct

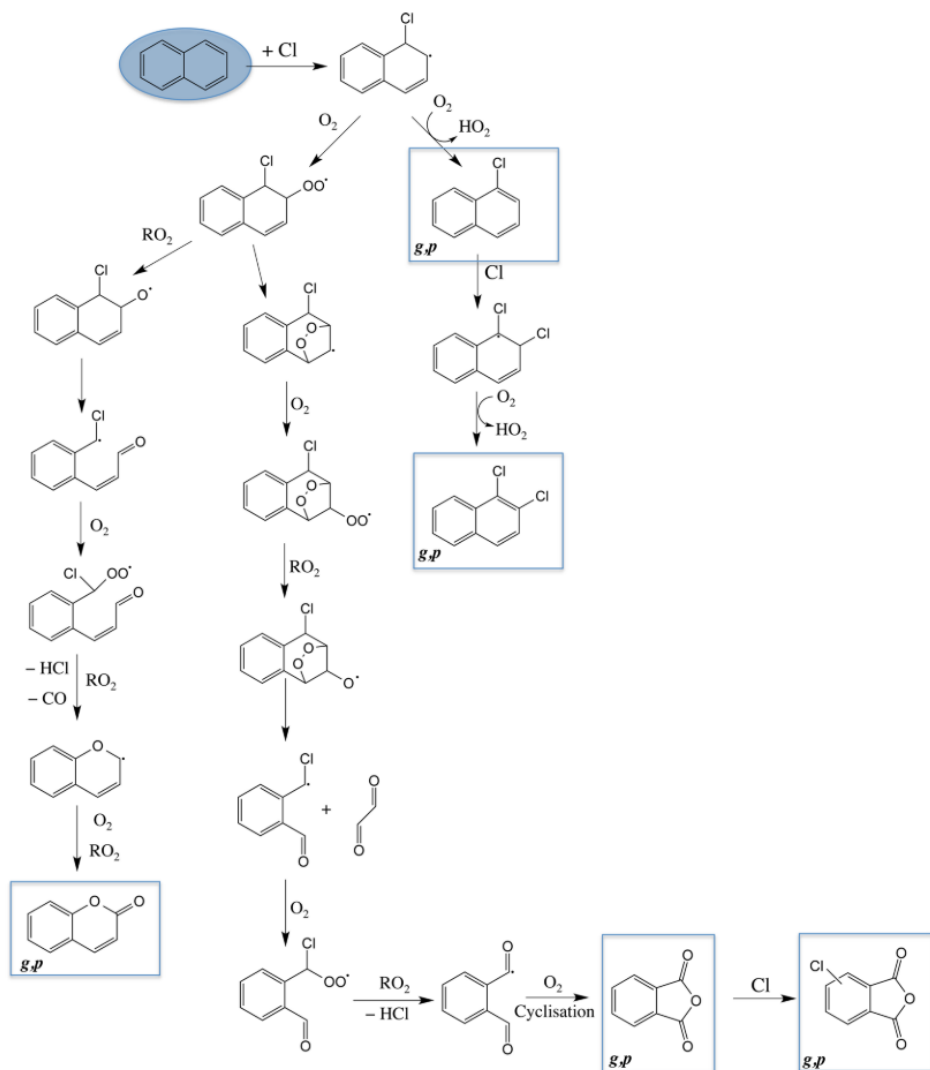


Figure 4. Mechanism for Cl atom-initiated oxidation of naphthalene proposed by Riva et al. (2015). Incomplete list of products is presented. The phase of the observed products (gas = g; particle = p) is indicated in boxes.

1.3 Atmospheric removal processes of PACs

Once emitted in the atmosphere at source regions, PACs undergo dry deposition, removal by precipitation, photodegradation, and oxidation by tropospheric gases during their transport. The rate of each of these sink/transformation processes largely depends on whether the PAC is in gaseous phase or bound to particle.

Many PACs are semi-volatile compounds (3-4 rings), repartitioning between phases in response to changing meteorological conditions. Gas-particle partitioning of these compounds primarily depends on their physicochemical properties (such as vapour pressure, K_{oa} and K_{aw} coefficients) and generally correlates with a PAC molecular weight (Fig. 5). Cold conditions favour repartitioning of PACs into particulate phase (Shahpoury et al., 2016; Albinet et al., 2008; Tomaz et al., 2016). Due to lower vapour pressure and higher K_{oa} coefficient, nitro-PAHs have a greater tendency to sorb to particles (Bandowe and Meusel, 2017).

Particulate phase PACs have slower photo-chemical degradation rate than the gaseous phase compounds. This is likely due to incorporation of a compound in a particle matrix, which shields the portion of the PAC in the particle pores from light and an oxidant attack (Lammel, 2015b). Consequently, size, chemical composition, surface area, porosity, and other particle properties play crucial role in outcome of the heterogeneous reactions of PACs (Lohmann and Lammel, 2004). For majority of PACs, the gas phase atmospheric reactions have faster kinetics than the heterogeneous reactions (Keyte et al., 2013). The PAC's degradation is lowest on dark coloured particles like black carbon and soot, largely emitted together with PACs after biomass, forest, and fossil fuel burning. For example, anthracene has a half-life of 0.5 h on alumina (white) and 310 h on black carbon (Abdel-Shafy and Mansour, 2016). Longer atmospheric lifetimes allow greater geographic dispersal of bound to particles PACs (Lammel, 2015b).

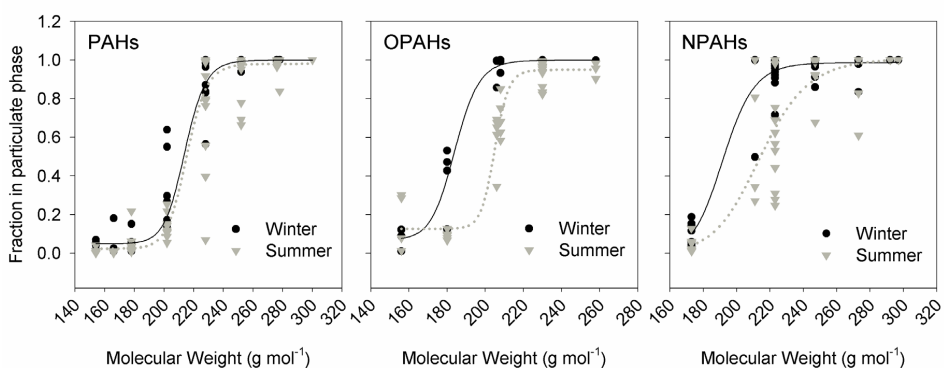


Figure 5. Phase state partitioning of PAHs, oxy-PAHs, and nitro-PAHs according to their molecular weight in winter and summer (Albinet et al., 2008).

PACs can be removed from the atmosphere by dry deposition and more efficiently by wet scavenging (Shahpoury et al., 2018). In general, PACs present in the gas phase dissolve within clouds and into raindrops, whereas particle-bound PACs are washed out from the atmosphere by precipitation (Ravindra et al., 2008; Škrdlíková et al., 2011). Higher water solubility of oxy-PAHs and some LMW PAHs plays an additional role in the substance wet scavenging (Walgraeve et al., 2010; Škrdlíková et al., 2011). Particles scavenging by precipitation was concluded to be greater than gas scavenging (Shahpoury et al., 2018), though Wania et al. (1999) stated that the gaseous PACs can efficiently be removed by snow, while it does not affect fine particles (Zhang et al., 2013). Adsorption of gaseous molecules to the surface of snowflakes could contribute to the phase transfer process (Simcik, 2004). Fallout of PACs adsorbed to particles (dry deposition) depends on the aerosol abundance and its type (mass, size, aerodynamic properties, shape, and chemical composition; Weinbruch et al., 2018), as well as dynamic conditions of the atmosphere (e.g., wind speed, atmospheric stratification, cloud characteristics; Lei and Wania, 2004; Willis et al., 2018).

In addition, PACs can be photolyzed under solar ultraviolet UVA irradiation (320-400 nm). Light absorption by gaseous PACs induces photodimerization and photooxidation (Vione et al., 2004; Bandowe and Meusel, 2017). Location of a substituted group is important as it influences a rearrangement of the excited state (electrons) in a molecule. For example, 1-NNap lifetime with respect to photolysis is 0.5 h, while it is 11 h for its isomer, 2-NNap (Feilberg et al., 1999). Particulate phase oxy-PAHs are more stable against photo-irradiation than nitro-PAHs. Atmospheric lifetimes of the compounds due to photodecomposition were calculated to be 0.5–22 h for nitro-PAHs and 4.5–35 h for oxy-PAHs (Kameda, 2018; Fan et al., 1996). PACs with a perpendicular to the aromatic ring group have greater photodegradation kinetics than those having parallel ones (Warner et al., 2004; Kameda, 2018).

1.4 Exposure and toxicity

Humans and wildlife are exposed to PACs via inhalation, diet, absorption through skin, or by maternal transfer. The relative importance of the exposure routes varies among organisms, their living environmental compartment, and life stage (Wallace et al., 2020; Kim et al., 2013; Ramesh and Archibong, 2011). Once absorbed, the distribution of PACs among tissues appears to be compound- and organ-specific, and not driven solely by

passive partitioning according to their lipophilicity (Wallace et al., 2020). PACs with $\log K_{oa} > 5$ can bioaccumulate in adipose tissues and breast milk (Wallace et al., 2020). Because many species can metabolize PACs, it is generally assumed that trophic transfer is not important and PACs are not expected to biomagnify (Laender et al., 2011).

Metabolism controls the nature and extent of exposure to PACs by changing excretion rates. PACs are mainly metabolised in liver, though it may also take place in many other tissues (e.g., kidney and lung; Wallace et al., 2020). Biotransformation starts when some PACs bind to the aryl hydrocarbon receptor (AHR), resulting in the induction of PAC-metabolizing enzymes, primarily cytochrome P450 1A (CYP1A) enzymes (Hwang et al., 2020; Pampanin and Sydnes, 2013). Further on, a polar reactive group is added to the PAC's structure, often entailing hydroxylation and epoxidation. Hydroxylated metabolites are then excreted both as free hydroxylated metabolites and as hydroxylated metabolites conjugated to glucuronic acid and sulfate (Abbas et al., 2018; Wallace et al., 2020).

Metabolism of PACs can be associated with harm. During biotransformation, unstable and highly reactive metabolites are produced, such as diol epoxides, radical cations, and quinone (Fig. 6), which may react with DNA to produce DNA adducts (Shimada, 2006; Bolton et al., 2000). Formation of DNA adducts can cause a mismatch in DNA replication and altered promoter binding, leading to an inheritable DNA mutation or abnormal gene expression, and ultimately tumorigenesis (Moorthy et al., 2015). Furthermore, generated quinones are highly redox active molecules. Redox cycling of quinones can amplify the generation of reactive oxygen species (ROS), such as superoxide, hydrogen peroxide, and ultimately the hydroxyl radical (Zhang et al., 2012). ROS can cause severe oxidative stress within cells through formation of oxidized lipids, proteins, and DNA (Bolton et al., 2000); oxidative DNA damage can further mediate carcinogenesis (Moorthy et al., 2002). Thereby, metabolic activation of PACs can cause oxidative stress, genotoxic, mutagenic, and carcinogenic effects.

Metabolic activation of PAHs to electrophiles is required to exert their harmful effects (Bolton et al., 2000), while oxy- and nitro-PAHs may also act as direct mutagens and carcinogens (Idowu et al., 2019). Oxy-PAHs play a major role in stimulation of oxidative stress (Dasgupta et al., 2014; Bolton et al., 2000), and nitro-PAHs have a high affinity to produce covalently bonded DNA adducts through ring oxidation or nitro reduction pathways (Watt et al., 2007). These compounds have very low acute toxicity (Onduka et

al., 2012; Bolton et al., 2000; Knecht et al., 2013) and are also more bioavailable than unsubstituted PAHs due to their higher hydrophilicity and mobility (Idowu et al., 2019; Lammel et al., 2020). In combination with direct toxicity, it implies that oxy- and nitro-PAHs can cause mutations and cancer regardless of a general trophic dilution of PACs and an organism detoxification capacity (Idowu et al., 2019). In general, despite their lower concentrations in the environment, oxy- and nitro-PAHs show comparable or greater (up to orders of magnitude) mutagenic and carcinogenic effects than unsubstituted PAHs (Durant et al., 1996; Wang et al., 2011; Bandowe and Meusel, 2017; Idowu et al., 2019; Lammel et al., 2020; WHO, 2003). Due to their carcinogenic properties, almost 30 PACs are classified as known, probable or possible carcinogens to humans and wildlife (International Agency for Research on Cancer, 2020), including several oxy- and nitro-PAHs (Table 1).

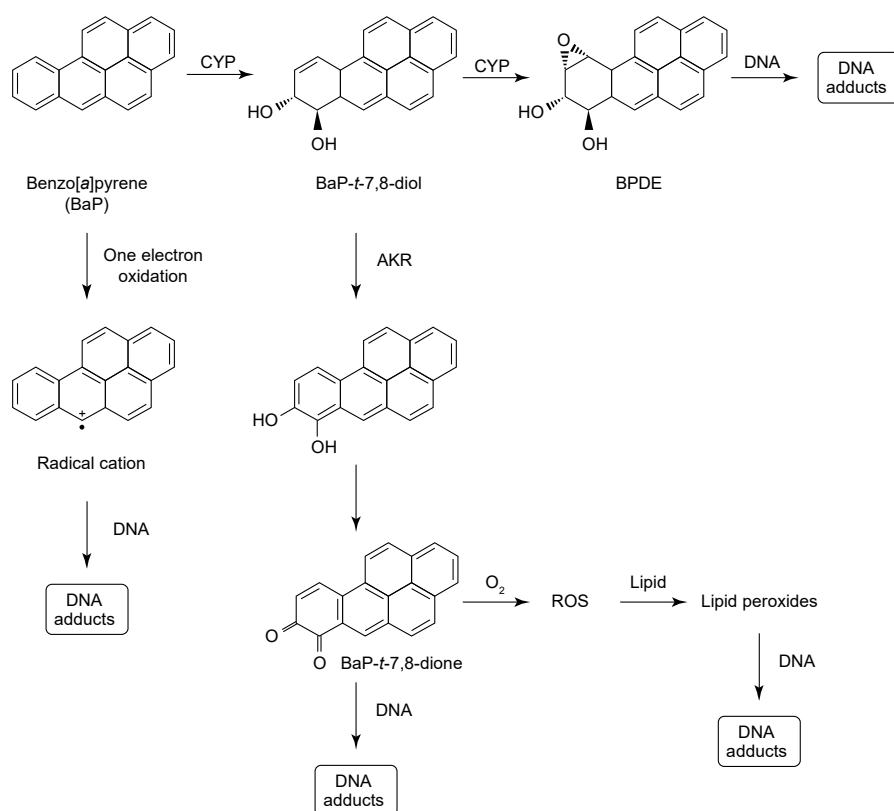


Figure 6. Metabolic activation pathways of benzo[a]pyrene (BaP) leading to cancer initiation (Fu et al., 2012). Cytochrome P450 (CYP) enzymes, aldo-keto reductase (AKR) enzymes, BaP-7,8-diol-9,10-epoxide (BPDE), reactive oxygen species (ROS).

Table 1. Classification of selected PACs into carcinogenic groups by International Agency for Research on Cancer (2020). Groups: 1- carcinogenic to humans, 2A- probably carcinogenic to humans, 2B- possibly carcinogenic to humans, 3- not classifiable as to its carcinogenicity to humans.

Compound	Group	EPA priority	Compound	Group	EPA priority
Benzo[<i>a</i>]pyrene	1	x	1,3-Dinitropyrene	2B	
2-Naphthylamine	1		1,6-Dinitropyrene	2B	
Dibenzo[<i>a,l</i>]pyrene	2A		1,8-Dinitropyrene	2B	
Cyclopenta[<i>cd</i>]pyrene	2A		2-Nitrofluorene	2B	
Dibenzo[<i>a,h</i>]anthracene	2A	x	Benzophenone	2B	
Dibenzo[<i>a,j</i>]acridine	2A		9,10-Anthraquinone	2B	
1-Nitropyrene	2A		1-Hydroxyanthraquinone	2B	
6-Nitrochrysene	2A		1,8-Dihydroxyanthraquinone	2B	
Indeno[1,2,3- <i>cd</i>]pyrene	2B	x	Fluoranthene	3	x
Benzo[<i>j</i>]fluoranthene	2B	x	2-Methylfluoranthene	3	
Benzo[<i>b</i>]fluoranthene	2B	x	Anthracene	3	x
Benzo[<i>k</i>]fluoranthene	2B	x	Pyrene	3	x
Chrysene	2B	x	Benzo[<i>ghi</i>]perylene	3	x
Benzo[<i>a</i>]anthracene	2B	x	Anthanthrene	3	x
3,7-Dinitrofluoranthene	2B		Benzo[<i>e</i>]pyrene	3	x
3-Nitrobenzanthrone	2B		Acenaphthene	3	x
3,9-Dinitrofluoranthene	2B		Phenanthrene	3	x
4-Nitropyrene	2B		Fluorene	3	x

Several studies have also documented embryotoxic effects caused by PAC exposure (Vignet et al., 2014; Logan, 2007; Albers, 2006; Le Bihanic et al., 2015). In mammals, PACs are able to cross the placental barrier and reach the fetal organs (Perera et al., 2019), which can impair a fetus normal growth and development and may cause toxic and carcinogenic effects. Low birth weight, premature delivery, and delayed child development are possible adverse birth outcomes, and can lead to perinatal diseases and mortality as well as health issues later in life including tumours, asthma, brain, and central nervous system development issues (Perera et al., 2005; Perera et al., 2019). Some PACs are also endocrine disrupting compounds and affect reproduction (Bolden et al., 2017; Wallace et al., 2020; Honda and Suzuki, 2020). Overexpression of AhR by PACs causes antagonistic suppression of sex steroid hormones, which can result in impaired fertilization and loss of normal ovarian function in fish, birds, and mammals, including humans (Booc et al., 2014; Bidgoli et al., 2011; Bolden et al., 2017; Onduka et al., 2015; Douben, 2003).

Under the same exposure dose, the toxicity of many oxy- and nitro-PAHs are greater than PAHs. For example, the toxic equivalency factor (TEF = compound toxicity compared against toxicity of BaP assigned as 1) of 1,6-DNPyr is four orders of magnitude greater than TEF of its parent PAH namely Pyr (Table 2). It should be noted that TEF is a metric based on carcinogenic potential and does not account for other effects such as ROS generation, while many studies confirm oxidative stress mediated toxicity of oxy-PAHs compared to other known PAHs (Idowu et al., 2019 and the references therein).

Table 2. Toxic equivalency factors (TEFs = compound toxicity compared against toxicity of benzo[*a*]pyrene assigned as 1) of studied compounds (Nisbet and LaGoy, 1992; Samburova et al., 2017; Durant et al., 1996; Doornaert and Pichard, 2005; Harrison and Hester, 1998; OEHHA, 2009). No TEFs are available for the other studied compounds not listed here.

Compound	TEF	Compound	TEF
EPA priority PAHs		Non-prioritized PACs	
Naphthalene	0.001	1-Methylnaphthalene	0.001
Acenaphthylene	0.001	2-Methylnaphthalene	0.001
Acenaphthene	0.001	2-Methylfluoranthene	0.001
Fluorene	0.001	Retene	0.001
Phenanthrene	0.001	Benzo[<i>e</i>]pyrene	1
Anthracene	0.01	Benzo[<i>j</i>]fluoranthene	0.1
Fluoranthene	0.001	Coronene	0.001
Pyrene	0.001	9,10-Anthraquinone	0.018
Benzo[<i>a</i>]anthracene	0.1	5-Nitroacenaphthene	0.01
Chrysene	0.01	2-Nitrofluorene	0.01
Benzo[<i>b</i>]fluoranthene	0.1	9-Nitroanthracene	0.0032
Benzo[<i>k</i>]fluoranthene	0.1	2-Nitrofluoranthene	0.05
Benzo[<i>a</i>]pyrene	1	1-Nitropyrene	0.1
Indeno[1,2,3- <i>cd</i>]pyrene	0.1	4-Nitropyrene	0.1
Benzo[<i>ghi</i>]perylene	0.01	6-Nitrochrysene	10
Dibenzo[<i>a,h</i>]anthracene	5	1,3-Dinitropyrene	0.031
		1,6-Dinitropyrene	10
		1,8-Dinitropyrene	1

1.5 Regulations on PACs

International environmental quality guidelines are limited to a small fraction of the thousands (>100 000) of different PAC congeners. Atmospheric 16 EPA PAHs are regulated in the USA, Canada, and UK, though in European Union only 7 PAHs are targeted (US EPA, 2011; Ontario Ministry of the Environment and Climate Change, 2020;

UK Air DEFRA, 2007; EU Directive 2004/107/EC, 2005). Because PACs occur in complex mixtures of compounds with multiple modes of action, BaP is used as a reference PAH compound. BaP annual average target value varies between countries and typically range between 0.1 and 1 ng/m³ in PM₁₀, (particulate matter of aerodynamic diameter below 10 µm; Ravindra et al., 2008). Due to potential adverse effects on the environment, wildlife or human health, PACs are included in the list of target chemicals of the Convention for the Protection of the Marine Environment of the North-East Atlantic (OSPAR, 2009; Boitsov et al., 2020) and to the List of Toxic Substances of the Canadian Environmental Protection Act (CEPA; Environment Canada and Health Canada, 1994).

Despite high toxicity, similar to the 16 EPA PAHs sources and properties, oxy- and nitro-PAHs are not regulated, though sporadically included in national screening programs in Europe (Brorström-Lundén et al., 2010; Vikelsøe, 2002) and considered to be regularly monitored in the US and Europe (Bandowe and Meusel, 2017; CEN, 2016). Recent estimates on the Canadian ambient air toxicity showed up to a factor of six increase when PACs beyond the EPA PAHs were considered (Tevlin et al., 2021), confirming the toxicological irrelevance of recent years guidelines (Samburova et al., 2017; Andersson and Achten, 2015).

1.6 Emissions and atmospheric transport of PACs to the Arctic

PACs emissions within the Arctic is small compared to other world regions, and long-range atmospheric transport (LRAT) is considered as the primary delivery path of pollution released in the lower latitudes (AMAP, 2017a; Friedman et al., 2014; Halsall et al., 1997; Wang et al., 2010). As such, PACs are included in the Convention on Long-Range Transboundary Air Pollution (United Nations Economic Commission for Europe UNECE, 1998). About 150 000 tons of PACs are annually released in the atmosphere by circumpolar and neighbouring countries corresponding to 30 % of global emissions (AMAP, 2017a). Biomass burning and vehicle emissions are the key sources in Russia, Canada, and the USA, the largest PAC emitters among the Arctic countries. In the USA, the majority of PAC emissions that are attributable to biomass burning arise from residential wood combustion, while wildfires are of greater importance in Canada and Russia (Kukavskaya et al., 2013; Berthiaume et al., 2021; Shen et al., 2013; Luo et al., 2020). PAC industrial emissions in Russia have a higher contribution (20 %) than in the

North American countries, mainly from coke and aluminium production (Shen et al., 2013; AMAP, 2021a). It is worth mentioning that PACs are constituted of crude oil and coal as they were formed over millions of years at relatively low temperatures about 100 °C (Abdel-Shafy and Mansour, 2016; Huang et al., 2014), including areas in the Arctic (Dahle et al., 2006; AMAP, 2010; Foster et al., 2015).

The PACs that escape the listed sink processes (Sect. 1.3) can be long-range transported from polluted regions to the Arctic. However, the lower troposphere (< 2 km) of the high Arctic is in general well isolated from the free troposphere and towards lower latitudes. The cold Arctic air masses build the so-called polar dome with the Arctic front as its boundary, formed by the surfaces of constant potential temperature (Klonecki, 2003; AMAP, 2015). Air masses inside and outside the polar dome have different chemical compositions (Bozem et al., 2019; Klonecki, 2003; Willis et al., 2018), confirming the barrier function of the dome. Only the air masses cooled to similar low potential temperatures as within the polar dome area can penetrate it (Klonecki, 2003).

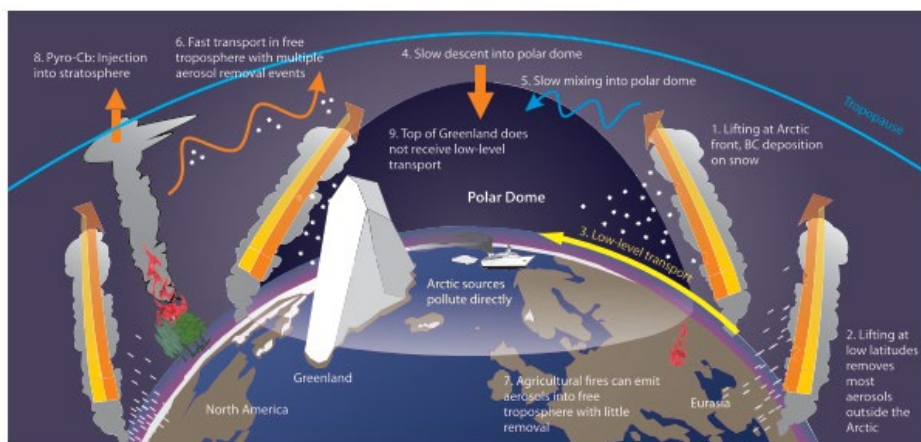


Figure 7. Atmospheric transport pathways to the Arctic based on the study by Stohl (2006) from AMAP (2015).

For polluted air to reach the lower Arctic troposphere on time scales shorter than a few weeks, the pollution source regions must be sufficiently cold and thus located north of the Arctic front (Stohl, 2006). This situation only occurs in winter and early spring over cold, snow-covered areas in northern Eurasia where the Arctic front can be located as far south as 40°N in January (AMAP, 2015). During this period, the cold polluted air masses can be quick (without uplifting as it is sufficiently cold; pathway 3, Fig. 7) and

effectively transported to the Arctic lower troposphere (where all the air quality monitoring is performed). The winter low-level air transport is on the time scale of 10 to 15 days (Stohl, 2006; pathway 3). Pollution emitted into the relatively warm air masses south of the Arctic front gets lifted and is typically associated with cloud formation and precipitation by which soluble pollutants and aerosols can be scavenged from the atmosphere (pathways 1 and 2, Fig. 7). These air masses are delivered into the Arctic middle or upper troposphere, and their descent to the local boundary layer (lowest 500 m) takes several weeks due to slow cooling (Stohl, 2006). Hereby, LRAT of pollution to the Arctic has strong seasonality with an increased tendency during winter and low efficiency in summer. Furthermore, the pollutant source region for the Arctic near-surface receptor location differs from that for the middle or upper polar troposphere (Hirdman et al., 2010).

The efficiency of northward LRAT of PACs is controlled by weather along the transport pathway and also by the sea ice extent. The sea ice influences the heat and moisture exchange between the ice/ocean and the transporting air masses that could impact wet deposition, enhance vertical mixing (i.e., reduced dry deposition; Vihma et al., 2014), and cause PACs' phase repartitioning. In contrast to the low-level winter transport (pathway 3, Fig. 7), the agricultural and forest fire plumes are often injected to higher altitudes directly above the source into the free troposphere and even the stratosphere, thus reducing the efficiency of dry and wet deposition (AMAP, 2015; Stohl, 2006).

Local Arctic meteorology significantly controls vertical exchange between the boundary layer and the free troposphere. The dominance of ice in the Arctic facilitates surface heat losses during the polar night when the sun remains below the horizon for several months. Sea ice also isolates the atmosphere from oceanic heat and moisture and reflects solar radiation. Winter and spring sea ice maximum favours Arctic atmospheric stability and causes surface-based thermal inversions, which promote the accumulation of near-surface emissions and thus prioritize the importance of local sources. Furthermore, high static stability of the polar air masses is associated with low turbulence of air (AMAP, 2015). In such conditions, the particle dry deposition is slower (Willis et al., 2018), increasing the risk of PACs inhalation exposure. In summer, warm rain, frequent drizzle, and ubiquitous low-level clouds in the Arctic cause efficient removal of particles (Browse et al., 2012), as well as gaseous phase water-soluble pollutants, including the PACs (Lei and Wania, 2004). The wet scavenging efficiently

removes accumulation-mode aerosol. Thus, finer particles prevail in the Arctic summer air (AMAP, 2015), which are more difficult to wash out, though their concentrations are significantly lower than in winter and spring (Croft et al., 2016).

1.7 PACs as chemicals of emerging Arctic concern (CEACs)

The Arctic regions have undergone rapid climatic changes in the past decades. The rates of polar atmosphere warming are 3 times higher than what is observed globally, with a change in near-surface air temperature by 3.1-10.6°C (AMAP, 2021b; IPCC, 2021). A greater temperature change near the poles than the rest of the globe is commonly referred to as 'Arctic amplification' (Hanssen-Bauer et al., 2019). It is mainly driven by the feedback mechanisms to a sea ice cover reduction and intensified northward heat transport (Kokhanovsky and Tomasi, 2020; Wickström, 2020) due to changes in large-scale atmospheric and oceanic circulations (Spielhagen et al., 2011; Mitchell et al., 2012). Diminishing Arctic sea ice cover increases heat and moisture transfer to the atmosphere from the ocean and amplifies absorption of solar radiation due to a surface albedo change (Serreze et al., 2009; Graversen and Wang, 2009).

Climate-related impacts offset global emissions reductions and maintain PAC air concentrations in the high Arctic (Muir and Galarneau, 2021). Warmer global climate increases forest fire activity and enhances multi-hopping LRAT of pollutants to the North. The low Arctic temperatures make contaminants less mobile and prevent their entering the ecosystem. With rising temperatures this barrier is broken, and PAC concentrations are expected to increase via re-emission from contaminated surfaces in the Arctic and releases from melted soil permafrost, ice, and glaciers (Granberg et al., 2017; Yu et al., 2019). A sea ice decline opens up shipping routes in the Arctic Ocean and subarctic waters. The maritime activities in the region have increased by 75 % since 2013 (PAME, 2020) and are mainly associated with fishing. Shipping in the Arctic is likely to increase with the development of natural resource extraction and tourism. It will require appropriate infrastructure and maritime services development promoting growth and urbanization of local Arctic settlements (AMAP, 2017b). It will increase fossil fuel combustion emissions, as well as risk for occasional releases of PACs from oil spills during hydrocarbon exploration, extraction, or transport (Svavarsson et al., 2021).

Exposure to PACs is associated with potential harm for Arctic wildlife. High lipid content, immobility, slower enzymatic biotransformation, depuration, and growth rates

in cold water conditions, as well as generally longer life span stimulate biomagnification of PACs in marine Arctic invertebrates (AMAP, 2010; Camus et al., 2003; Agersted et al., 2018). Over the past three decades in the Norwegian Arctic, there has been a 10-30 fold increase in PAC concentrations in lower trophic level organisms (Laender et al., 2011). Fish, mammals (marine and terrestrial), and birds are considered to have more efficient detoxification systems (Wallace et al., 2020). However, PACs accumulate in Arctic top predators, such as harp seals and beluga whales (Béland et al., 1993; Martineau et al., 2002; Hellou et al., 1991), and their metabolism leads to the formation of harmful metabolites (oxy- and nitro-PAHs and other; Hwang et al., 2020). Cancer, deformities, cardiotoxicity, DNA damage, and other health effects were associated with the environmental exposure of the Arctic long-lived mammals to PACs (Wilson et al., 2005; Poirier et al., 2019).

Arctic wildlife is recently exposed to multiple stressors, including changing climate conditions, legacy persistent organic pollutants (POPs), numerous CEACs, increased shipping, and human presence in general. Weather fluctuation and sea ice diminishing cause energetic stress to ice-associated species (polar bears and seals) due to loss of habitat and access to food and breeding areas (Sonne et al., 2021). Multi-decadal exposure to legacy POPs remarkably impaired their metabolism, endocrine and immune systems (Tartu et al., 2017; Sonne et al., 2021; Desforges et al., 2018), and thus increased the populations' vulnerability. Exposure to harmful PACs is an additional stressor, which may result in exceeding the threshold levels of toxicological concern associated with effects on immunity, reproductive capacity, and infectious diseases in Arctic marine mammals (Routti et al., 2019; Letcher et al., 2010; Sonne et al., 2021). Furthermore, due to a lipid-rich diet, Arctic top predators are among the most polluted species in the world (Letcher et al., 2010). Their bodies contain a large variety of organic lipophilic contaminants (e.g., PCBs), which in combination with PACs will increase the mixture complexity and likely result in synergetic effects at lower concentrations than those applied in laboratory studies (Sonne et al., 2021; Wallace et al., 2020).

Regional meteorology promotes persistence and accumulation of PACs. Low ambient temperatures favour the partitioning of semi-volatile PACs to the particulate phase. The particle-bound compounds are protected from reaction with atmospheric oxidants and light, which results in longer atmospheric lifetimes (Lohmann and Lammel, 2004). Particulate PACs deposit to snow, ocean, and ultimately soil and sediment, where they

can persist over decades (AMAP, 2010; Bandowe and Meusel, 2017) and cause chronic exposure to wildlife. Due to extended winter darkness in the Arctic, photodegradation of PAHs is inhibited for several months. Moreover, the dilution of near-ground emissions is limited to a very shallow, inversion-capped layer of cold air, characterized by low vertical turbulence. It leads to emissions accumulation in the Arctic boundary layer. The dominant loss process of atmospheric PACs, the reactions with OH radicals (Keyte et al., 2013), is largely suppressed in the polar atmosphere as the production of OH radicals under dark and dry Arctic conditions is low. Oxidation capacity of Arctic troposphere remarkably increases by spring, when sunlit snow contributes to the active halogen photochemistry (Grannas et al., 2007; Simpson et al., 2007). It presumably enhances the level of airborne oxy- and nitro-PAHs, the compounds with high acute toxicity (Idowu et al., 2019). Warmer and wetter future Arctic conditions may significantly influence the chemistry of the lower polar troposphere. Moisture increase promotes higher concentrations of OH radicals in the atmosphere. In addition, a retreat of sea ice enhances the amount of sea salt aerosols to be deposited into the snow, increasing the concentration of halides, the halogen atom precursors (Raso, 2018). Hereby, due to a predicted increase of the regional emissions, lower degradation rates, accumulation in environmental compartments and biota, additional toxicological stress to vulnerable Arctic wildlife, changing atmospheric transport patterns, potential enhancement of atmospheric oxidation capacity, and ambiguous feedbacks to changing Arctic climate in general, PACs have been identified as chemicals of emerging Arctic concern (CEACs; Laender et al., 2011; AMAP, 2017a, 2021a; Sonne et al., 2021), which require detailed investigation.

2 Thesis objectives

The Arctic region is a primary harbinger of global climate change and a receiver of pollution from lower latitudes. Despite global emissions reduction, PAC concentrations have a tendency to increase in the Arctic environment presumably due to the climate-driven changes: frequent forest fires at mid-latitudes, amplified LRAT, and increased local Arctic emissions, including anthropogenic and re-volatilization of previously-deposited PACs (Muir and Galarneau, 2021). PACs are therefore of emerging concern in the Arctic (Sect. 1.7). The occurrence of selected PAHs (11-21 compounds) has been monitored at Canadian, Finish, and Norwegian Arctic air monitoring stations for over 30 years (AMAP, 2017a). While background Arctic air concentrations of PAHs are known, local anthropogenic emission contributions are poorly documented (Balmer et al., 2019) and the levels of oxy- and nitro-PAHs in the Arctic air are largely unknown (AMAP, 2017a, 2021a). Only two studies have previously reported the concentrations of two nitro-PAHs and five oxy-PAHs measured in the air samples from the late 1900s collected in Svalbard (Cecinato et al., 2000) and Nunavut (Singh et al., 2017), respectively, which do not represent the recent Arctic air quality.

This study was carried out in Svalbard, the northernmost land in the European Arctic. Surrounded by warm atmospheric and oceanic currents, the region is an epicentre of ongoing climate change (Isaksen et al., 2016) and the central receiver of air pollution from high-latitude Eurasian sources (Stohl, 2006; AMAP, 2017a). The overall motivation of this PhD work was to study the concentration levels, seasonal trends, sources, and processes of PAHs, oxy-PAHs, and nitro-PAHs (91 compounds in total) in the Arctic atmosphere. For such purposes, this work was conducted in the most populated high Arctic town of Longyearbyen (78.22° N, 15.65° E) on the west coast of Svalbard allowing the study potential influence of local anthropogenic emissions. Contrary to background air monitoring at the mountain sampling sites with minimal impact from near-ground pollution plumes, ambient air samples (gaseous and particulate) were collected from within the boundary layer height to better assess the influence of local emissions. Taking the advantage of high-litudinal ambient conditions with the unique light and weather extreme seasonality and the region-specific chemistry, atmospheric PACs physicochemical processes were investigated to understand their formation and fate in the Arctic. Specific objectives for the three papers that form the backbone of the thesis are as follows:

Paper I “Polycyclic aromatic hydrocarbons (PAHs) and oxy- and nitro-PAHs in ambient air of the Arctic town Longyearbyen, Svalbard”. The Longyearbyen coal-fired power plant was hypothesized to be the major local source of PACs. The main goal was to evaluate PAC emissions from the local power plant and to examine the plume changes with distance from the source by combining the obtained stack emissions pattern, characteristic literature data of various sources, and statistical analysis. The paper is based on the stack emission and ambient air samples simultaneously collected at the two sites downwind the power plant.

Paper II “Polycyclic aromatic hydrocarbons (PAHs) and their nitrated and oxygenated derivatives in the Arctic boundary layer: Seasonal trends and local anthropogenic influence”. The main goal was to assess the potential influence of local versus remote source emissions delivered by LRAT. This was accomplished through the following objectives: (1) to study transport regimes of the near-surface, potentially polluted air masses from mid-latitudes to the Arctic and to examine the polar boundary layer meteorology to reveal the main remote sources and its seasonality, (2) to investigate local seasonal snowmobile and ship traffic emission levels and patterns using port registry data, national holiday schedule, and local meteorological conditions. The study is based on the urban ambient air samples from Longyearbyen and contrasted to the background PAC levels of Ny-Ålesund.

Paper III “Insights the physicochemical processes of atmospheric polycyclic aromatic hydrocarbons (PAHs) and their derivatives under polar conditions in Svalbard”. The main goal was to study secondary formation of oxy-PAHs and highlight the specific chemical processes observed under Arctic conditions (daytime, night-time, and halogen chemistry). Addition objectives included studying prevailing seasonal sources based on urban, rural, and altitudinal air samples and a deeper understanding of the potential influence of local anthropogenic emissions by the level’s comparison between the sites. The paper also provides the main data suite on the PACs’ phase repartitioning in response to the ambient conditions.

3 Methods

3.1 Study area

The study was performed in the vicinity of Longyearbyen town (78.22° N, 15.65° E) on the west coast of Svalbard archipelago, in the Arctic European sector (Fig. 8). Longyearbyen is the largest populated among the northernmost settlements, with about 2460 permanent residents (Statistics Norway, 2021) and a seasonal increase of up to 16000 monthly townsmen due to tourism, mainly in spring and summer (Statistics Norway, 2016). Local human activities include tourism, transport, coal mining, and research. The local coal-fired power plant (30771 ton/year of coal and 419 ton/year of diesel consumption (Miljødirektoratet, 2018)) and car traffic (1558 vehicles (Statistics Norway, 2018)) are the primary permanent local sources of anthropogenic emissions, while snowmobiles (2135 vehicles (Statistics Norway, 2018)) and marine (718 local boats (Statistics Norway, 2018) and 345 cruise ships (Kystdatahuset, 2018)) traffic are seasonal. There is no local waste incineration and wood burning registered in the town.

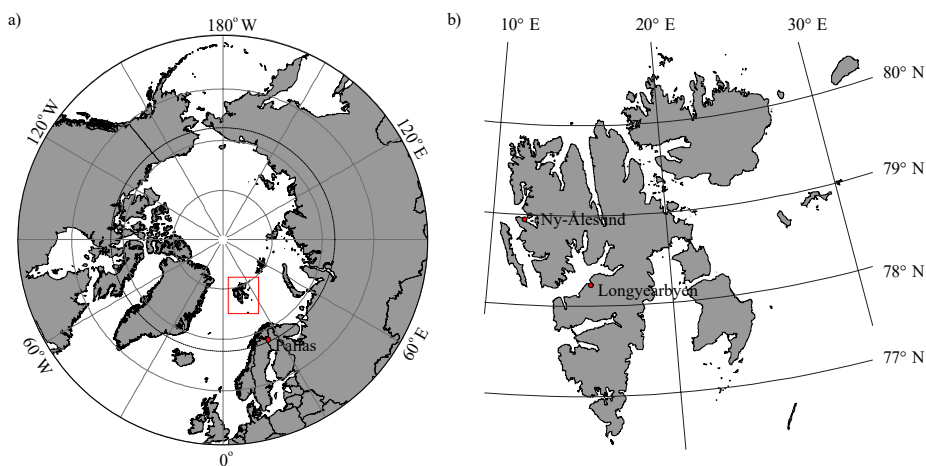


Figure 8. Location of Svalbard in the Arctic (a) and map of Svalbard (b).

Svalbard is located at the gateway of both atmospheric and oceanic heat transport into the Arctic (Serreze et al., 2007), and it is the warmest region in the Arctic above 76° N latitude (Serreze and Barry, 2014; Wickström et al., 2020a). Warm Atlantic water is transported northward along Svalbard's west coast via West Spitsbergen Current

(branch of the Gulf Stream; Nilsen et al., 2016). The North Atlantic cyclone track approaches Svalbard from the southwest bringing mid-latitude air masses to the Arctic. Consequently, the west coast of Svalbard remains ice-free throughout the winter, while the north and east parts bear a seasonal ice cover (Isaksen et al., 2016). Ice-free conditions create a warmer climate in the vicinity of Longyearbyen, with more precipitation events occurring in the fall (Hanssen-Bauer et al., 2019). The mean annual precipitation measured in the Longyearbyen area is about 200 mm only, which is lower than the driest areas on the Norwegian mainland. The annual mean temperature in Longyearbyen during the period 2000-2020 was approximately -3 °C (Hanssen-Bauer et al., 2019). The ambient temperature ranges between -30 °C (-15 °C as monthly average) in winter/spring and +22 °C (+7 °C as monthly average) in summer (data for 2020 available at: <https://www.yr.no>, 2021). For the Longyearbyen latitude, the polar night period of continuous darkness lasts for 2.5 months from the middle of November until the end of January, followed by the about 3 weeks-long twilight period (Fig. S2 in **Paper II**). Sun returns to the town by the mid of February and the light conditions increase gradually until April (daylight), when the period of 5 months of midnight sun begins (polar day).

3.2 Sampling locations and sample collection

Ambient air sampling was performed from November 2017 to September 2018 (**Papers I-III**), at three locations (Fig. 8): the roof of the University Centre in Svalbard (UNIS, 25 m asl, urban location, 250 m from the fjord), the former northern lights observatory in Adventdalen valley (Adventdalen, 10 m asl, rural location, 4.6 km upwind UNIS), and Svalbard satellite station on Platåberget mountain by the antenna N°1 (Svalsat, 450 m asl, background location, 6 km downwind UNIS). Sampling was not simultaneous unless specified (**Paper I**). Due to high avalanche danger, sampling at Svalsat was not possible to perform in spring. Considering south-easterly prevailing wind direction and katabatic winds from Longyearbreen and Larsbreen glaciers, nearly all year-round UNIS is located downwind from the town (600 m distance), and the two main gateways (Adventdalen and Longyeardalen valleys), largely used for snowmobile driving during winter and spring. Due to reverse sea-land surfaces temperature gradient in summer, the wind direction can temporarily change to northwesterly, making UNIS position downwind the coal-burning power plant (1 km distance to UNIS) and the harbour (5 km distance

to UNIS). UNIS is also surrounded by paved roads that are used by cars all year round. For the coal-fired power plant emission analysis (**Paper I**), stack emission air samples were collected at the source and two locations at transect distance: UNIS and Adventdalen (Fig. 8). Sampling at UNIS and Adventdalen was performed simultaneously in early autumn 2018 on days with a predicted northwesterly wind direction (downwind the plant; **Paper I**).

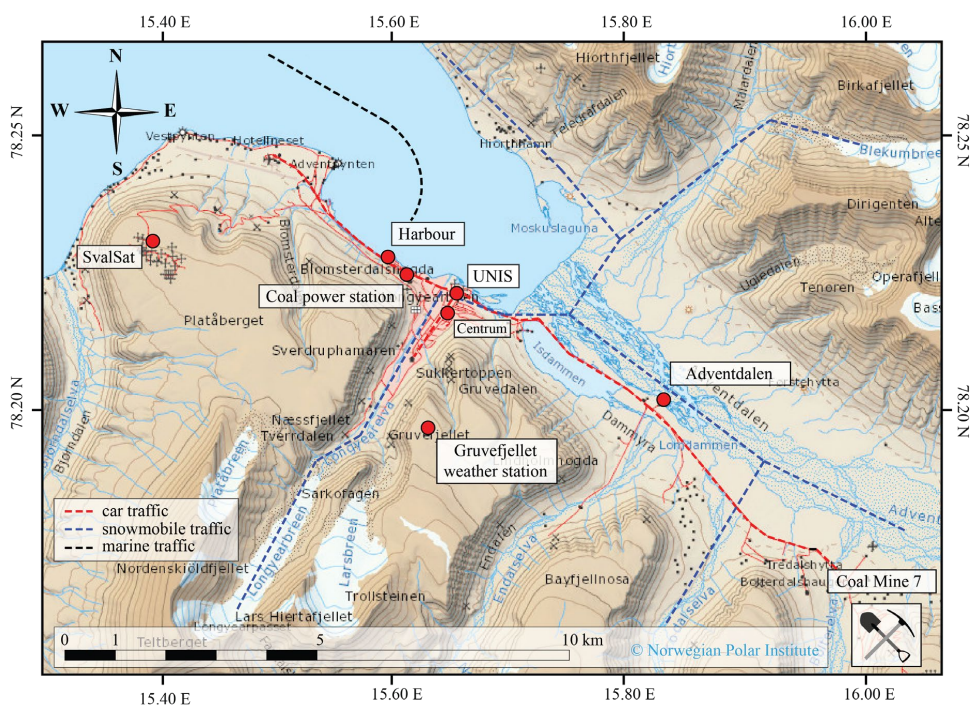


Figure 9. Sampling sites in the vicinity of Longyearbyen, Svalbard. Ambient air samples were collected at UNIS (urban), Adventdalen (rural), and Svalsat (background) sites.

About 370 m³ of ambient air was collected over 24 h per sample using a high-volume air sampler (TISCH-1000-BLXZ, TISCH Environmental Inc., USA; Fig. 10) following the US EPA standard procedure TO-13A (US EPA, 1999). Particulate PACs were collected on quartz fiber filters (QFF; pre-burnt at 450 °C for 6 h; $\varnothing = 103$ mm; no binder; Munktell/Ahlstrom, Finland). Gaseous PACs were collected on polyurethane foams (PUF; Soxhlet pre-cleaned in toluene for 24 h followed by 24 h acetone wash; $\varnothing = 65$ mm; L = 100 mm; Klaus Ziemer GmbH, Germany). Upon on-site installation and every 360 sampling hours, the equipment was calibrated to maintain sampling accuracy following the producer operation manual (Tisch Environmental Inc., 2021).

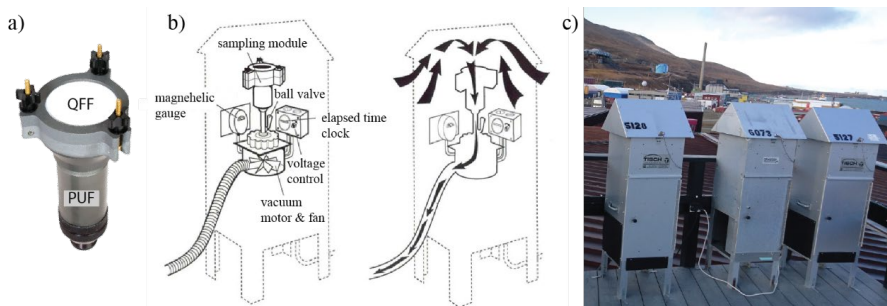


Figure 10. Large volume ambient air sampling equipment: (a) sampling module with quartz fiber filter QFF and polyurethane foam PUF to collect particulate and gaseous phases, respectively, (b) air flow direction, (c) the equipment installed on the roof of UNIS in Longyearbyen.

The power plant stack emission samples (1.3-3.0 m³) were collected after all flue gas cleaning steps (Fig. 11). Details on the plant purification system are provided in Sect. 2.1 of **Paper I**. The sampling probe was situated to face the direction of the flue gas. A custom-made low-volume, battery-powered air sampler (Digitel, Switzerland) was used to pump the flue gas (35 L/min) through the sampling material placed in a stainless-steel cartridge (Fig. 12). Like the ambient samples, the particulate phase was collected on QFF ($\varnothing = 47$ mm; no binder; Pallflex, USA) and the gaseous phase on PUF ($\varnothing = 50$ mm; L = 75 mm; Klaus Ziemer GmbH, Germany). The flue gas parameters (temperature, moisture, flow speed, and density) were measured during the sampling by an FKT3DP1A multi-meter equipped with an S-type pitot probe (FlowKinetics LLC, USA). All samples were kept intact inside the sampling unit after collection. In order to reduce the risk of post-collection contamination, the unit was sealed in two plastic bags for transportation to the lab, where samples were removed from the unit, sealed with layers of aluminium foil, and stored airtight in two plastic bags. Samples were kept frozen at -20 °C until analysis.

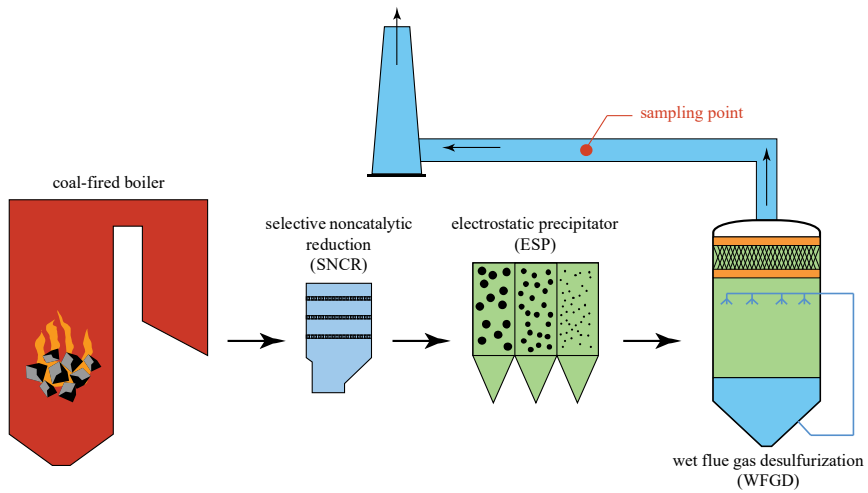


Figure 11. Exhaust sampling point at the Longyearbyen coal-fired power plant.

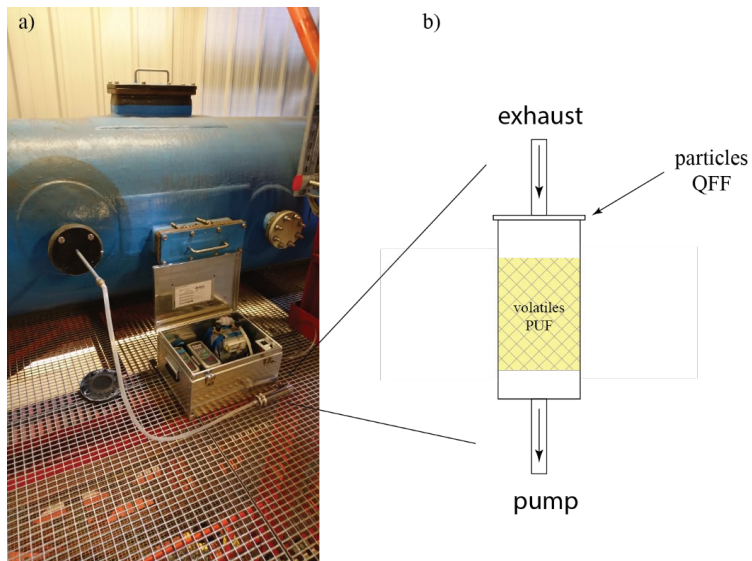


Figure 12. Portable low volume air sampling equipment used for the coal-fired power plant exhaust sampling (a) and a sample unit to trap particles and volatiles (b).

3.3 Sample preparation and analysis

Full details on analytical procedures, including methods validation, chemicals, and instrumentation used, are outlined in Sect. S1-S2 of **Paper I** and Sect. 2.4 of **Paper II** and the references therein. Only a simplified description of sample preparation is provided here (Fig. 13). In brief, a known amount of several (11-25) deuterated PAC surrogate standards were added to the samples prior to extraction in order to monitor potential loss of analytes during extraction and clean up. QFF samples (particulate phase) were extracted applying a QuEChERS-like (Quick Easy Cheap Effective Rugged and Safe) method using dichloromethane (**Paper I**) and acetonitrile as solvents (**Papers II & III**; Albinet et al., 2013). PUF samples (gaseous phase) were extracted using Soxhlet (**Paper I**) or pressurized solvent extractions (PSE; **Papers II & III**) using dichloromethane and acetone, respectively. The extracts were concentrated and fractionated according to their polarity following solid phase extraction (SPE): first with neutral alumina Al_2O_3 to remove macromolecules and polar interfering compounds, then with unmodified silica gel SiOH to separate the alkane fraction from the aromatic one (Albinet et al., 2006). Elutes were dried under a gentle nitrogen stream and reconstituted with about 100 μ L solvent. The purified samples were spiked with a known amount of two isotope-labelled standards to evaluate the surrogate recoveries.

PAHs were analyzed via two different methods. For **Paper I**, the 16 PAHs were quantified by gas chromatography with electron ionization tandem mass spectrometry detection GC-EI-MS/MS (Agilent 7890B GC coupled to 7000C Triple Quad MS, Agilent Technologies, USA) using a low-polar TG-5SILMS capillary column (5 % Phenyl Methylpolysiloxane; 30 m with 5 m safeguard \times 0.25 mm \times 0.25 μ m film thickness; Thermo Scientific Trace GC Ultra, USA; 1 μ L injected). For **Papers II & III**, PAH analysis was performed following the European Committee for Standardization (CEN) standard procedures EN 15549:2008 and TS 16645:2014 (CEN, 2008, 2014). 22 PAHs were analyzed by ultra-high-performance liquid chromatography with fluorescence detection UHPLC/Fluo (Dionex Ultimate 3000, Thermo Scientific, USA) using a C18 UHPLC column (Zorbax Eclipse PAH, 2.1 mm \times 150 mm \times 1.8 μ m, Agilent, USA; 3 μ L injected).

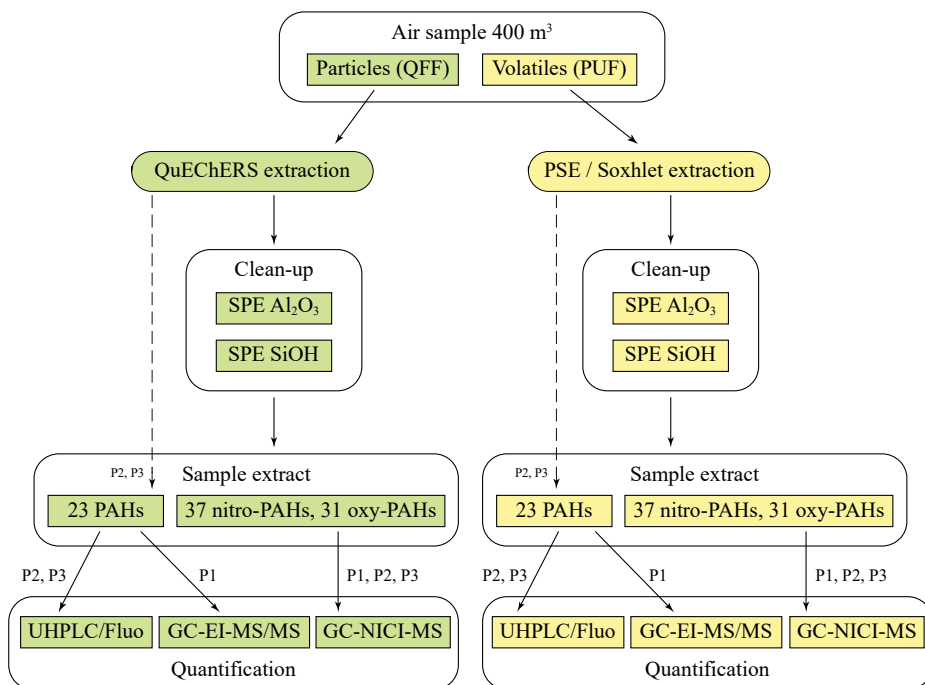


Figure 13. Air sample preparation procedures. Note “P” is for paper 1-3.

Very low ambient concentration of nitro- and oxy-PAHs (few pg/m³) required higher sensitivity quantification method with reduced contribution from the sample matrix. Gas chromatography with negative ion chemical ionization mass spectrometry (GC-NICI-MS) operated in single ion monitoring (SIM) mode was applied for analysis of 31 oxy-PAHs and 37 nitro-PAHs (**Papers I-III**). The use of methane as a reagent gas minimized molecular fragmentation while allowing ionization of nitro- and oxy-PAHs by resonance capture of the thermal electrons. Agilent 7890B/7000C and 7890A/5975C GC/MS systems (Agilent Technologies, USA) were used in **Paper I** and **Papers II & III**, respectively. 1 µl of the purified extracts has been injected. In **Paper I**, like for the PAH’s analysis, the target compounds were separated on a TG-5SILMS capillary column. In **Papers II & III**, the separation was carried out by use of a fused silica Rxi-PAH column (30 m × 250 µm × 0.10 µm, Restek, USA).

3.4 Quality assurance and quality control

In order to evaluate the background contamination related to sample collection and analysis, QFF and PUF field and laboratory blanks were performed and analyzed along with the exposed samples. Compounds showing field blank values higher than 30 % of the seasonal average concentrations were excluded from the final results. In **Paper I** (Sect. S2 and Table S9-S11), the method detection limits (MDLs) defined as the smallest quantity of analyte that is significantly different from the blank were determined based on laboratory blanks and applied. In **Papers II & III**, MDL was determined based on signal to noise ratio of a reagent blank analysis, and from the calibration solution of the lowest concentration, according to standard procedures EN 15549:2008 and TS 16645:2014 (CEN, 2008, 2014). No blank correction was performed for the concentration calculations. Samples showing PAC concentrations below the instrumental limit of quantification (LOQ) were replaced by LOQ/2 for further calculations.

Acceptable PAC surrogate recoveries were obtained and ranged between 50-120 % (**Papers I-III**). The method accuracy was also checked using NIST standard reference material (SRM 1649b, urban dust; n=3) for **Papers II & III**. Results obtained (Table S8 in **Paper II**) were in good agreement with NIST certified, reference or indicative concentration values and with those previously reported in the literature for oxy- and nitro-PAHs (Albinet et al., 2013; Albinet et al., 2014; Albinet et al., 2006) as certified or reference concentration values in SRM do not exist for several compounds. Because a certified reference material was not available in the laboratory at the time of the samples' analysis for **Paper I**, a sample spiking test (n=4) was performed using all analytes. The results showed about 80-100 % recovery for most PAHs; the recovery rates of the derivatives were slightly lower (Table S7 in **Paper I**). Relative standard deviations (RSTD) were within 20 %, indicating good precision of the analysis.

3.5 Statistical analysis

Statistical analyses of compound concentrations were performed with Minitab 20 Statistical Software (Minitab LLC, Pennsylvania, USA). Normality and homogeneity of variances were tested with Shapiro–Wilk and Levene's tests, respectively. A Mann–Whitney U test was performed to test significant differences between sampling locations. Spearman's correlation was used to investigate relationships between

different variables. The statistical significance was set at $p < 0.05$ unless stated. Principal component analysis (PCA) was performed for PACs' source apportionment (**Paper I**).

3.6 Local meteorology and LRAT analysis

Meteorological parameters, including ambient temperature, atmospheric pressure, wind speed and direction, relative humidity, and UV radiation, were recorded at Gruvefjellet (78°12' N 15°37' E; 464 m asl) and Adventdalen (78°12' N 15°49' E; 15 m asl) automatic weather stations in 2.6 and 4.6 km distance to UNIS, respectively (Fig. 9). A wind rose analysis has been performed via MATLAB and Statistics Toolbox Release 2020b, The MathWorks, Inc., Natick, Massachusetts, USA. The temperature inversion strength (TIS, K) and turbulence probability (atmospheric stratification) within the atmospheric layer between the Adventdalen (15 m asl) and Gruvefjellet (464 m asl) weather stations were studied as described in Sect. 2.3 in **Paper II**. The global reanalysis dataset ERA5 with hourly output frequency, the horizontal and vertical resolutions of 31 km and 137 levels, respectively (Copernicus C3S, 2017), has been utilized to investigate the synoptic-scale meteorological conditions and boundary layer height (BLH) over Svalbard for the measurement period (**Paper II**).

The Hybrid Single-Particle Lagrangian Integrated Trajectory model (HYSPLIT; **Paper I**; Stein et al., 2015) and the Lagrangian air parcels dispersion model FLEXPART V8.2 based on meteorological data from European Centre for Medium-Range Weather Forecasts' (ECMWF) ERA-Interim reanalysis (**Paper II**; Stohl et al., 2005) were used to study LRAT of air masses to the measurement sites. Ten-day backward trajectories were obtained for air arriving at the lowest 500 m height above the ground in the region covering both Ny-Ålesund and Longyearbyen. In **Paper II** (Sect. 2.3), to investigate LRAT of air pollutants from ground-based emissions at mid-latitudes to Svalbard, only the trajectories that reach latitudes below 70° N and end up below the local BLH were considered. The trajectories' points corresponding to the first day of the simulation were not considered since most of them were over the Svalbard region. The potential removal of atmospheric pollutants with precipitation during their LRAT was investigated based on ECMWF ERA-Interim reanalysis data on the specific humidity at each time step along the back-trajectories (Table S5 in **Paper II**).

4 Results and discussion

4.1 LRAT seasonal influence

Atmospheric transport is the most efficient way for PAHs, released in the lower latitudes, to reach the Arctic (Friedman et al., 2014). Multidecadal observations at the Arctic monitoring stations confirm intercontinental atmospheric transport of PAHs to the high North (Yu et al., 2019; Halsall et al., 1997; Becker et al., 2006; Sofowote et al., 2011; Friedman and Selin, 2012; Prevedouros et al., 2004). The PAH concentrations observed at background Arctic sites peak in winter, decreasing throughout spring, with minimal annual levels during summers (Prevedouros et al., 2004; Singh et al., 2017; Yu et al., 2019; Fu et al., 2009). This concentrations trend in the polar atmosphere is mainly driven by LRAT seasonal mechanism and its efficiency (Klonecki, 2003; Stohl, 2006) as discussed in Sect. 1.6. PACs are also “seasonal contaminants” due to increased fossil fuels burning for residential heating and car driving in winter (Yu et al., 2019; Tomaz et al., 2016; Albinet et al., 2008; Ringuet et al., 2012a) and higher photochemical degradation during summer at source regions and in the Arctic (Barrie, 1996). Similar annual PAH concentrations' trend with the maximal levels in winter was observed at the background Svalbard site, Zeppelin atmospheric monitoring station in Ny-Ålesund (78°58' N, 11°53' E, 474 m asl) during the 2017/2018 season (Fig. 14). The same period sampling campaign in Longyearbyen revealed a different seasonal profile of PAHs, as well as oxy- and nitro-PAHs (Fig. 16), likely due to local anthropogenic emissions associated with the annual light cycle and tourism activities (**Paper II**).

The atmospheric boundary layer is defined as the lowest part of the troposphere directly influenced by the earth's surface and responds to surface forcing (the exchange of heat, momentum, and moisture) on a short timescale. It is also the layer of the atmosphere through which primary emissions from the surface would be mixed vertically (Simpson et al., 2007; Hu, 2015). The annual transport regimes of potentially polluted (started at the near-surface) air masses from a source area to the Arctic boundary layer in the region of interest in Svalbard were studied, as well as precipitation events along the pollution delivery (**Paper II**). The 10-day backward trajectory probability analysis of more than 11 thousand individual trajectories revealed the air masses transport during winter mainly from the European sector, including the areas of Scandinavia, Northern Europe, Western Russia, and the West Siberian plain (Fig. 15). In spring, the source regions shifted from east to west and

significantly up north: from continental locations in Russia and Europe to marine ones over the North Atlantic, mainly from the area north of the 75 °N latitude. Summer air transport up north was from the Atlantic sector with many precipitation events (rain), and thus significant scavenging of pollutants. As discussed in Sect. 1.6, summer air transport is directed to the higher troposphere (Klonecki, 2003; Bozem et al., 2019), and the near-ground polar air is 13-17 days old (Stohl, 2006). Accordingly, significant winter LRAT of potentially polluted air masses to the local boundary layer in Svalbard has been concluded, while it was weak in summer.

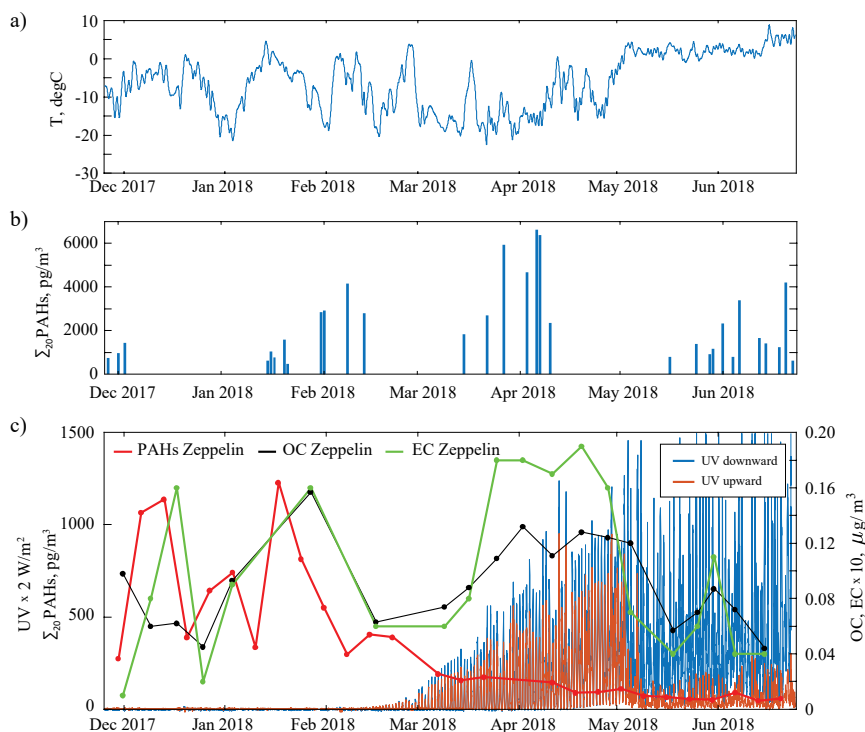


Figure 14. Annual trends of (a) ambient air temperature, (b) Σ_{20} PAH total (G+P; pg/m^3) concentrations measured in Svalbard air at UNIS (Longyearbyen; urban) and (c) Zeppelin (Ny-Ålesund; background) stations, as well as concentrations of organic and elemental carbon (OC and EC, respectively; $\mu\text{g}/\text{m}^3$). The figure is a modified reprint of Figure S3 in Paper II.

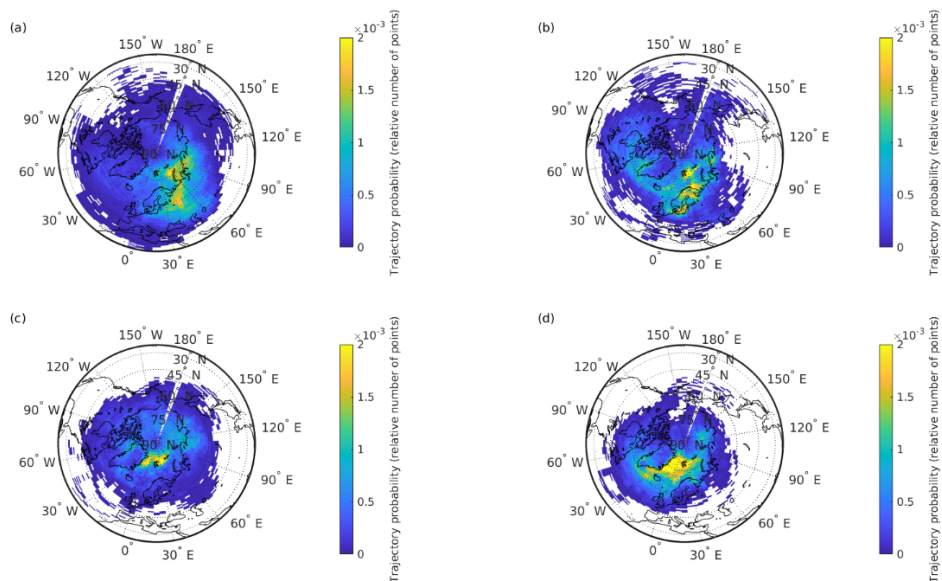


Figure 15. 10-day backward trajectory probability maps for air masses originated from a source area boundary layer and arrived at 0-500 m above the region of interest in Svalbard. Data are for (a) November-January, (b) February, (c) March-April, and (d) May-June periods. The figure is a reprint of Figure 3 in Paper II.

The Arctic boundary layer meteorology plays an important role in modulating the ambient concentrations of pollutants through different ways. Continuous radiative cooling of snow-covered surfaces during several months of polar night and stable synoptic conditions in spring resulted in low temperatures at the ground (-13.8 ± 3.4 °C as average) in March-April and stably stratified conditions ($Ri_{bulk} > 5.25$ %) with deep and persistent thermal inversions (TIS 4.5 K; Fig. 16) during the sampling period. At that time, the BLH was as low as 100 ± 79 m. As consequence, the spring near-ground PAC measured concentrations were greatly influenced by local emissions, which were trapped beneath an inversion layer, and their dilution was limited to a very shallow volume of cold air under suppressed vertical mixing conditions.

Thereby, the northward LRAT mechanism seasonality and specific meteorology of the polar boundary layer drive the source contribution strength (LRAT vs the local Arctic) and the vertical distribution of pollutants. Based on the investigations in **Paper II**, LRAT influence was pronounced during winter, while local emissions contribution was predominant in spring and summer for the PAC concentrations measured at sea level stations (UNIS and Adventdalen) in Longyearbyen vicinity. It resulted in the different

PACs' annual trend than at the Zeppelin station on the mountain top (about 500 m asl) above the boundary layer (Fig. 16). This outcome is consistent with the earlier observations of the altitudinal gradient Arctic air pollution in spring and summer (Brock et al., 2011; Kupiszewski et al., 2013; AMAP, 2015), though interannual variations are possible due to changing cyclone activities in the Arctic (Wickström et al., 2020b) and sea ice expend (Onarheim et al., 2014).

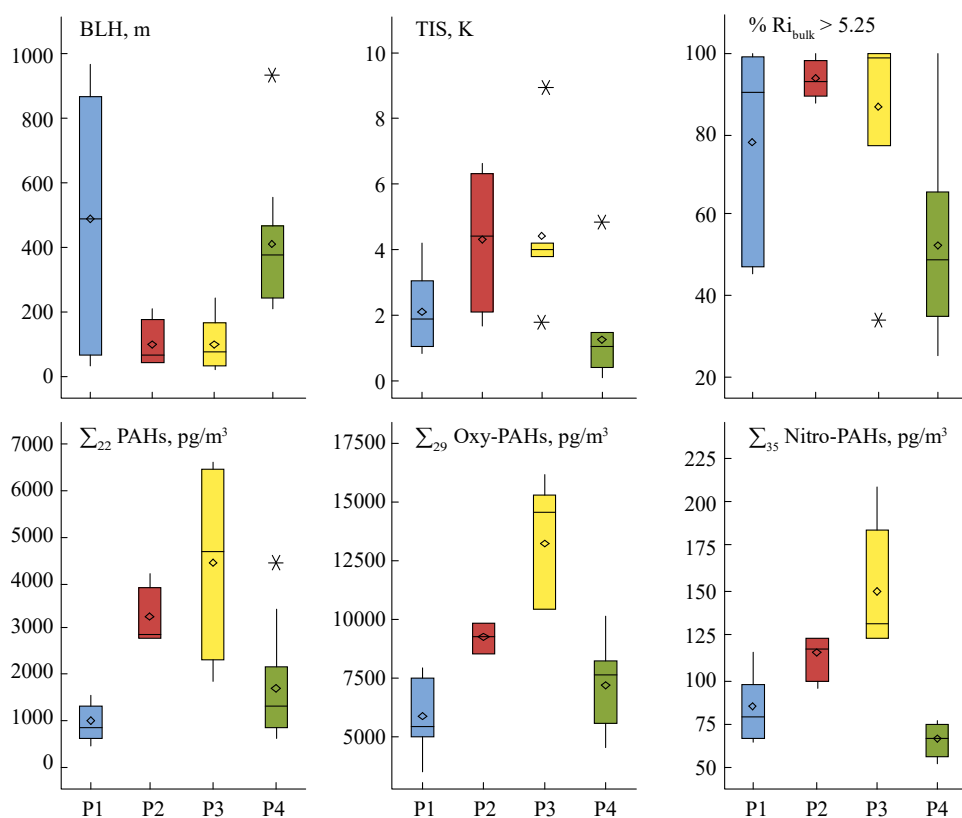


Figure 16. Atmospheric characteristics and sum PAC concentrations in urban air of Longyearbyen. Top panels: boundary layer height BLH, thermal inversion strength TIS, bulk Richardson number Ri_{bulk} as a characteristic of thermal stability of air layer. Bottom panels: sum concentrations (G+P; pg/m³) of PAHs, oxy-PAHs, and nitro-PAHs. Data are for the November-January (P1; n=8), February (P2; n=4), March-April (P3; n=7), and May June (P4; n=12) periods in 2017/2018. The figure is a modified version of Figure 2 in Paper II.

4.2 PAC seasonal concentrations and sources

This thesis was focused on quantification of 23 PAHs, 31 oxy-PAHs, and 37 nitro-PAHs in Svalbard air in winter, spring, summer (**Papers II & III**), and early autumn (**Paper I**). A complete list of compounds studied, their abbreviated names, and physicochemical properties are provided in Table S1. Individual concentrations (gaseous and particulate) of the 91 PACs measured at urban (UNIS), rural (Adventdalen), and altitudinal (Svalsat) sites are reported in **Papers I-III** as described in Table 3.

Table 3. Guidance on the reports of full results (quantified PAC concentrations) in the papers.

	Urban		Rural		Background		Source	
	UNIS		Adventdalen		Svalsat		Coal-burning	
	Paper	Table	Paper	Table	Paper	Table	Paper	Table
winter-summer	II	S1-S3	III	S1-S3	III	S1-S3		
autumn	I	1	I	1			I	1

4.2.1 Winter

The polar night winter period is characterized by the most considerable weather fluctuations caused by high cyclone activity and efficient pollution delivery via LRAT (Sect. 3.1.1 in **Paper II**). The \sum_{22} PAH winter concentrations were found similar (within 16 % difference) at the three sampling sites in Longyearbyen (Fig. 17). The \sum_{20} PAHs concentrations were in good agreement with the background levels in Ny-Ålesund in 115 km northwest of Longyearbyen (Table S6 in **Paper III**), confirming predominant influence of LRAT of air masses to Svalbard, which were mainly from northwestern Eurasia (Sect. 4.1). Similar was observed for the atmospheric PAH derivatives with slightly (10-20 %) higher sum concentrations at Svalsat (Fig. 17). Higher levels at the mountain rule out the primary sources' influence and support the LRAT predominance. Comparing to the Eurasian winter levels, the \sum_{11} PAHs concentrations measured in Svalbard were a factor of 2 lower than in the background continental air in Northern Finland (Pallas, Matorova station, 68°00' N, 24°14' E, 340 m asl; Table S7 in **Paper II**) and the \sum_{21} PAHs concentrations were a factor of 40 lower than in the central European air (Tomaz et al., 2016). The \sum_{29} oxy-PAHs and \sum_{35} nitro-PAH winter levels in Longyearbyen were 3 and 5 times lower, respectively, compared to the urban European air (Tomaz et al., 2016; same compounds considered). This comparison may provide a rough estimation of the PAC's LRAT efficiency from the Eurasian sector though it largely depends on weather and atmospheric losses along the transport pathway (Sect. 1.3), as

well as meteorological conditions and photochemical transformation within the Arctic (Sect. 4.5).

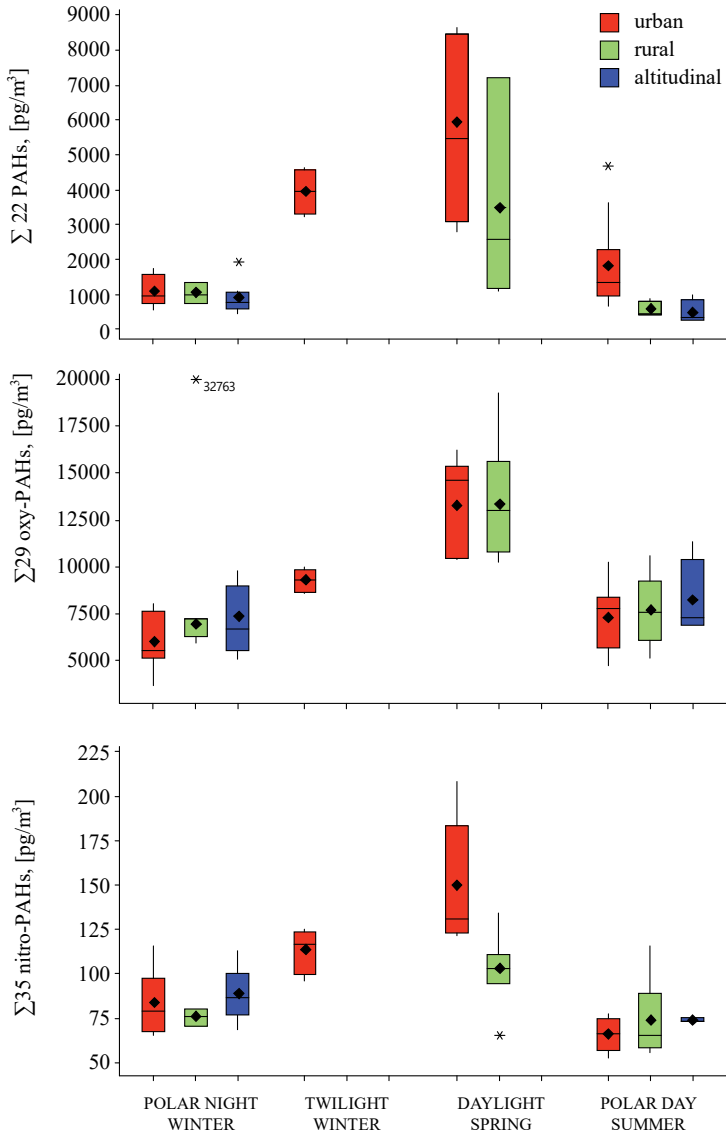


Figure 17. Sum seasonal concentrations (G+P; pg/m^3) of PACs measured at three sites in Longyearbyen air in the period from November 2017 until July 2018 (Papers II & III). Smaller suite of different PACs was analyzed in the autumn air samples (Paper I), presented as Figure S1 in Appendix.

In agreement with the earlier report by Yu et al. (2019), Phe and Flu were the predominant compounds in Longyearbyen air in winter (0.3 ng/m^3 as the individual compound seasonal mean concentrations; Table S1 in **Paper III**) and accounted for about 60 % of the PAHs winter profile (Fig. 5 in **Paper II**). BZPh, PhAn, and 9-FluO represent 80 % of the oxy-PAHs ($0.8\text{-}1.8 \text{ ng/m}^3$ as the individual compound seasonal mean concentrations) and 1-NNap and dinitropyrenes account for about 40 % of the total nitro-PAHs (11 pg/m^3 as the individual compound seasonal mean concentrations).

4.2.2 Spring

Local meteorological conditions favoured accumulation of ground-level emissions in spring (Sect. 4.1), which resulted in the annual highest PAC levels. As the UNIS is located downwind Adventdalen (Fig. 8), 40-80 % higher \sum_{22} PAHs, \sum_{35} nitro-PAHs, elemental and organic carbon (EC and OC, respectively) concentrations were measured at UNIS compared to the levels in the valley (**Paper III**). The \sum_{29} oxy-PAH concentrations at urban and rural sites in spring were similar (Fig. 17). Focusing on the UNIS site (urban), the spring \sum_{22} PAH concentrations ($5902 \pm 2421 \text{ pg m}^{-3}$) were a factor of 6 higher those in winter and the \sum_{29} oxy-PAHs ($13229 \pm 2681 \text{ pg m}^{-3}$) and \sum_{35} nitro-PAH ($150 \pm 34 \text{ pg m}^{-3}$) levels increased by a factor of 2 (Fig. 16). As discussed in **Paper II**, these urban Arctic levels are about one order of magnitude lower than the average European urban and suburban PAC concentrations (Tomaz et al., 2016; Albinet et al., 2008; Degrendele et al., 2021), though the difference is less pronounced with the annual levels in background air (Nežiková et al., 2020): the spring concentrations of \sum_{15} PAHs and \sum_4 HMW oxy-PAHs were about a factor of 2 lower, while \sum_4 LMW oxy-PAHs and \sum_{15} nitro-PAHs were in a similar range to up to one order of magnitude higher. Considering individual PAC concentrations, several of them significantly exceeded (more than twice) the annual mean urban levels in central Europe (Tomaz et al., 2016; Albinet et al., 2008). As for the Arctic scale, the \sum_{20} PAHs average seasonal concentration in Longyearbyen urban air was a factor of 30 higher than those in Ny-Ålesund, considering the same compounds measured during the same spring period in 2018 (Table S7 in **Paper II**). This observation reveals notable contribution of the anthropogenic emissions in Longyearbyen as the UNIS and Zeppelin stations have similar air masses transport from lower latitudes, but the stations have different elevations.

The coal-burning emissions from the power plant were upwind during all the sampling days in spring (Table S6 in **Paper II**). Thus, this source likely had low impact on the concentrations and patterns observed. Car traffic intensity is quite steady through winter to spring, and the same emission intensities are presumed as similarly cold ambient temperatures during these periods. However, significantly higher spring values of the ratio $(\text{BghiP}+\text{Cor})/\sum_{12}\text{PAHp}$ (sum of filter concentrations of PAHs mainly present in the particulate phase (PAHp)) and EC and OC concentrations indicated accumulation of gasoline emissions (Marchand et al., 2004; Albinet et al., 2007) with air pollution peak on weekends and during the Easter holidays likely indicating contribution of the snowmobile emissions (2135 vehicles; Statistics Norway, 2018). No scientific studies on PAC emissions from snowmobiles have been reported. Nonetheless, snowmobile driving is a well-documented major source of CO, NO_x, particles, volatile organic compounds (VOCs), aromatic hydrocarbons (Sive et al., 2003; Bishop et al., 2001; Shively et al., 2008; Zhou et al., 2010; GYC, 2011), and PAHs were detected in snow along snowmobile tracks (McDaniel and Zielinska, 2014; Rhea et al., 2005; Oanh et al., 2019). Svalbard air pollution by snowmobile emissions has previously been documented (Reimann et al., 2009; Vestreng et al., 2009; Dekhtyareva, 2019). The detailed comparison of the PAC weekend profiles with the rest of the cold period day profiles revealed the compounds presumably associated with the snowmobile emissions (Sect. 3.2 in **Paper II**).

4.2.3 Summer

Summer composition of the Arctic lower troposphere is primarily controlled by local weather conditions and local anthropogenic and natural emission sources due to less efficient LRAT mechanism and enhanced removal of PACs (Sect. 4.1). Increased incoming solar radiation (24 h of sunlight) and warmer ambient temperatures (+3.6 °C as average) are the most notable changes of high-latitude summer. After a snow melt, surface albedo decreases and warmed surface heats the air. Warm air rises, causing turbulence, and thus increasing vertical mixing of local plumes. Furthermore, wind direction is unstable in Longyearbyen area during summer. Due to channeling inside the fjord, the main summer directions are northwesterly and southeasterly, which are along with the three sampling sites, local coal-burning power plant, and the harbour (Fig. 8). Thereby, efficient pollutants dispersion can be expected in summer in the absence of

precipitation events. Indeed, uniform distribution of nitro-PAHs, oxy-PAHs, EC, and OC between the three sampling sites in Longyearbyen was observed (Fig. 17), and the difference of the \sum_{22} PAHs concentrations in Adventdalen and Svalsat did not exceed 20 % being higher at the lower altitude site (Table S1-S3 in **Paper III**). However, the concentrations of \sum_{22} PAHs, OC and EC were a factor of 3 higher in urban air.

The UNIS sampling site is located in close proximity to central Longyearbyen, as well as to the power plant and the harbour. A factor of 4 higher concentrations of particulate phase PAHs were measured on the days, when UNIS was downwind the plant and the harbour (Sect. 3.1.2 **Paper II**). This observation proposed the prevailing influence of ship emissions as only about 6 % of the power plant total PAC emissions were associated to the particulate phase (**Paper I**). The total (arrival + departure) gross tonnage of vessels (Kystdatahuset, 2018) was used as indicator of ship traffic. Local air pollution was found to correlate with the source strength (summed total tonnage of ships registered in the harbour during the sampling hours) and the OC/EC ratio values indicated the ship emissions contribution (**Paper II**). Detailed analysis of the summer PAC profiles based on different prevailing wind directions and determined (**Paper I**) pattern of the local power plant-specific emissions let us reveal the PACs likely characteristic of the local harbour emissions, also consistent with literature (Sect. 3.2 in **Paper II**). A proportion increase of some oxy-PAHs could not be attributed to any local emissions. Their secondary generation in the atmosphere was further evaluated in **Paper III**.

Comparing the summer 2018 altitudinal Svalbard air samples from Longyearbyen and Ny-Ålesund, the \sum_{20} PAHs concentrations at Svalsat were on average a factor of 4 higher the background levels measured at Zeppelin during the same summer period (Table S6 in **Paper III**). The difference was up to one order of magnitude, when several cruise boats were present in the harbour of Longyearbyen. Due to increased vertical mixing, buoyant exhaust from large ships equipped with high smokestacks can likely reach the Svalsat sampling site on the adjacent mountain (475 m asl). Gaseous phase compounds, Flu (41 pg/m³) and Phe (99 pg/m³), were the most abundant in Svalsat air, which might indicate the coal power plant emissions contribution, as Flu and Phe are the main PAHs determined in the plant exhaust samples (**Paper I**).

4.2.4 Autumn

The annual lowest PAC concentrations were detected in autumn (Fig. S1). Low contribution of remote sources was concluded as the traced air masses predominantly originated from the areas north of Svalbard and Greenland (Fig. S4 in **Paper I**), and Σ_{14} PAH concentrations in Longyearbyen were one order of magnitude higher than the background levels at Zeppelin (Table S2). Multivariate statistical analysis (PCA) revealed local coal combustion and vehicle and marine traffic emissions as the predominant sources of PACs in autumn (Sect. 4 in **Paper I**). Due to closer proximity to the active coal mine, Adventdalen station was also affected by diesel emissions likely from trucks, which regularly transport produced coal via road nearby the sampling site. Twice higher PAC concentrations were measured at the urban site than rural (Table 1 in **Paper I**), though they were about a factor of 2 lower than those measured during summer (Table S2). This is likely due to lower ship traffic in the local fjord at the end of a sailing season (Fig. S5 in **Paper I**) and different weather conditions. The Arctic early autumn is characterised by ambient temperatures about freezing and frequent precipitation events, both snow and rain. Precipitation and humid conditions enhance removal of PACs from air (Škrdlíková et al., 2011). Effective wet scavenging of several particle-bound HMW, as well as semi-volatile PACs was indicated by significant negative correlations (Spearman correlation, $p < 0.05$) between the PAC concentrations and amount of precipitation and mass of water vapour in the air (specific humidity; Sect. 3.2.2 in **Paper I**). The UNIS and Adventdalen chemical profiles of PAHs and oxy-PAHs were similar, while the profiles of nitro-PAHs differ (Fig. S2 in **Paper I**). Proportions of 1- and 2-NNap were higher in UNIS samples (about 60 % of Σ_{22} nitro-PAHs), while 9-NAnt and 2+3-NFlt showed higher contributions into the nitro-PAH profile of samples from Adventdalen (about 55 % of Σ_{22} nitro-PAHs).

4.2.5 Summary notes

Measured seasonal PAC concentrations in ambient air of Longyearbyen are highly variable and span up to sixteen-folds of magnitude (Σ_{22} PAHs; Table S1 in **Paper III**). Higher concentrations of primary origin species, PAHs and EC, as well as OC, were determined in urban air, followed by the rural and altitudinal, indicating contribution of anthropogenic emissions in Longyearbyen. Primary origin of oxy- and nitro-PAHs was less obvious, as equal or higher sum concentrations were quantified in rural and

altitudinal air (Fig. 17). In contrast to PAHs, which only degrade with time, oxy- and nitro-PAHs can also be generated in atmosphere at source area and/or during LRAT to the Arctic. Thus, these compounds have different occurrence rates in the atmosphere.

- LRAT of north-western Eurasian air masses was predominant in winter. The PAC concentrations were fairly uniform in all three sites in Longyearbyen and Ny-Ålesund in winter (Sect. 4.2.1).
- Compared to the Svalbard background air quality (UNIS vs Zeppelin; Table S7 in **Paper II**), maximum local air pollution in Longyearbyen was revealed in spring (x31) and summer (x19). It was predominantly caused by local seasonal snowmobile and ship traffic, respectively, with continuous contribution from car and coal-burning emissions (**Paper II**).
- Highest PAC concentrations were measured in spring (Fig. 17), the coldest period in the high Arctic with frequent thermal inversions. The region-specific meteorological conditions promoted accumulation of local fossil fuel (snowmobiles and cars) emissions and likely isolation of the local boundary layer from air masses delivered via LRAT to the higher layers of polar atmosphere (Sect. 4.1).
- Summer air quality in Longyearbyen correlates with wind direction. Northwesterly winds, characteristic to summer mainly, deliver emissions from the local coal power plant and notably from the port (Sect. 4.2.3). Up to twice higher PAC concentrations were measured under northwesterly winds.
- Annual lowest PAC concentrations were observed in early autumn (September), even when wind blew from the harbour and the plant. The atmospheric pollutants scavenging was caused by frequent precipitation events (Sect. 4.2.4).

4.3 Coal power plant emissions characterization

Coal combustion is one of the main sources of PAHs, NPAHs and OPAHs worldwide, which also exists in the high Arctic. PACs are constituents of raw coal and can also be produced during high temperature coal combustion through pyrolysis of methane, acetylene, butadiene, and different other compounds (Huang et al., 2014; Tarafdar and Sinha, 2019). The Longyearbyen power plant coal consumption is about 30 000 ton/year. It provides the community with sufficient electricity (45 000MW) and central heating supply (70 000MW) throughout the year (Bøckman, 2019). The plant was

hypothesized to be a key contributor (**Paper I**) as 68 % of Svalbard air pollution by PAHs was accounted to coal combustion emissions (Yu et al., 2019). The annual prevailing local wind direction is from the southeast and the power plant emissions are upwind the town most of the time. In summer, when the soil surface in Adventdalen becomes warmer than the water surface in Adventfj¸rd, the wind direction can temporarily change to northwesterly on the days with no strong large-scale winds. To assess the PAC emissions (concentrations and pattern) and their environmental fate, the power plant exhaust and ambient air samples were simultaneously collected downwind the power plant in the beginning of autumn to avoid the summer pick of marine traffic at the harbour, located close to the power plant (Fig. 8). Due to efficient removal of particles by the power plant exhaust cleaning system, 89 % of the PAC emissions from the power plant were in gaseous phase, prevailed by the LMW compounds Nap and Phe (80 %), Flu, Flt, Pyr (Fig. 2 in **Paper I**) in agreement with previous reports (Hsu et al., 2016). Emissions of the 16 PAHs from the coal-burning power plants operated worldwide, equipped with analogous exhaust cleaning systems and/or burning the same type of coal were considered for comparison (Table S12 in **Paper I** and Fig. 18). Significantly lower amount of \sum_{16} PAHs of 0.106 $\mu\text{g}/\text{m}^3$ (corresponds to 1.5 $\mu\text{g}/\text{kg}$ coal) was determined for the Longyearbyen power plant mainly due to smaller amount of dust in the power plant plume and low boilers capacity (64 MW total). Operation conditions, combustion temperature, and geological maturity of coal can have significant effects on emitted PAH chemical profiles and concentrations too (Huang et al., 2014; Wang et al., 2015; Peng et al., 2016). The emission factors of oxy- and nitro-PAHs were not reported earlier. Thus, no comparison is possible with literature data. Compared to the amount of emitted 16 PAHs, a factor of 3 and an order of magnitude lower \sum_8 oxy-PAHs (32.6 \pm 20.9 ng/m^3) and \sum_{22} nitro-PAHs (4.5 \pm 2.1 ng/m^3) were determined, respectively. The chemical profiles were dominated by 9,10-AntQ, 9-Flu and 1-NNap, 3-NPhe, 7-NBaAnt (Fig. 2 in **Paper I**). Generation of oxy-PAHs during coal combustion was concluded, while production of nitro-PAHs was not revealed perhaps due to low content of NO_x in the flue gas to react with PAHs (Lundgjerdingen, 2017) and/or decomposition of nitro-PAHs at 1000 °C.

A dilution effect with a factor of 2 was observed for the transect ambient air samples: 1.26 \pm 0.16 and 0.63 \pm 0.14 ng/m^3 were the sum of all 47 PAH derivatives for UNIS and

Adventdalen, respectively, under 1 °C and 3.5 m/s wind from NW ambient conditions accompanied by few precipitation events of rain and snow.

The determined indicatory PACs (**Paper I**) and the PAH diagnostic ratio Flu/(Flu+Pyr) = 0.64±0.11 were further applied in order to trace the Longyearbyen power plant emissions. Multivariate statistical analysis confirmed local coal combustion, as well as vehicle and marine traffic emissions, as the predominant sources of PACs in Longyearbyen in the early autumn (**Paper I**) and during summer (**Papers II & III**). Furthermore, observed PAH concentrations at the Zeppelin station were higher than model simulations, indicating influence of local Arctic sources. Coal combustion was identified as the main source of air pollution in Ny-Ålesund, and Phe, Flu, Flt, and Pyr were the main contributors (Yu et al., 2019), most likely attributable to the Longyearbyen power plant located 115 km southeast of Ny-Ålesund. Hereby, though generally low emissions of PACs from the coal burning in Longyearbyen were determined, large volume of flue gas daily emissions remain the power plant to be an important local Arctic anthropogenic source of air pollution with average daily emissions of \sum_{16} PAHs, \sum_8 oxy-PAHs, and \sum_{22} nitro-PAHs of 98.7, 31.3, and 4.3 mg, respectively (note non-isokinetic sampling regime).

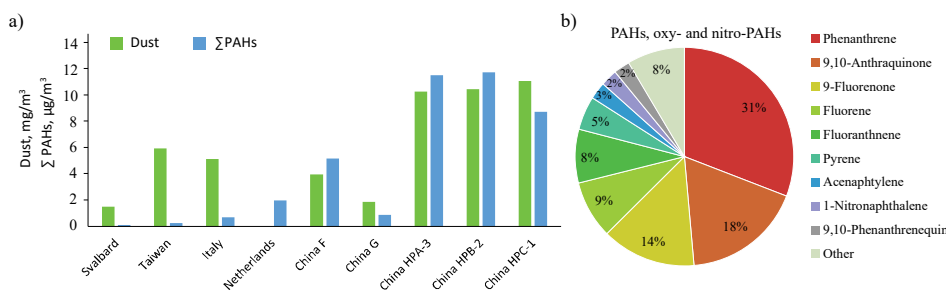


Figure 18. The 16 PAHs (G+P) and dust emissions from the coal power plant in Longyearbyen (Svalbard) compared to the world operating plants equipped with similar exhaust purification systems and/or burning the same type of coal (based on the data from Table S12 in Paper I), and the PACs' chemical profile of the Longyearbyen plant emissions (modified Figure 2 in Paper I).

4.4 Gas/particle partitioning of atmospheric PACs

PACs are semi-volatile compounds repartitioning between phases in response to ambient conditions change (Robinson et al., 2007; Donahue et al., 2012). A compound phase state determines its atmospheric lifetime (reactivity, photolysis, and deposition), LRAT potential, persistence in environmental compartments, and thus total

environmental fate, as well as the toxic potential of exposure (bioaccessibility; Yaffe et al., 2001; Su et al., 2006; Nováková et al., 2020). A compound migration from gaseous to particulate phase is influenced by both adsorption on particle and absorption into organic matter processes (Pankow, 1994; Lohmann and Lammel, 2004), which are strongly temperature-dependent (Thuens et al., 2014). Furthermore, humidity notably affects the partitioning of the more polar contaminants, such as oxy- and nitro-PAHs (Hu et al., 2019; Shahpoury et al., 2018; Mu et al., 2018). Hence seasonal, altitude, and latitude variations in the gas/particle partitioning of PACs are expected.

Gas/particle partitioning of PACs was investigated under a large span of atmospheric conditions, which contrasts to mid-latitude conditions studies. The sampling campaigns for **Papers I & III** were conducted from late Arctic summer until early autumn. During this period, the air temperature varied from -20 °C in February to +9 °C in June (dT=29 °C), and the mass of water vapour in the air (specific humidity) increased by a factor of 3 in summer. More humid conditions in summer are due to increased solar insolation and large areas of the open ocean available after the sea ice melt.

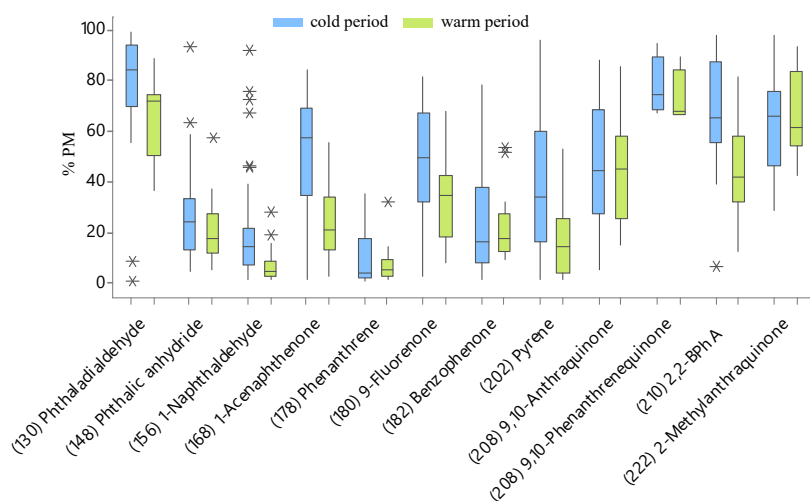


Figure 19. Percentage of selected PACs determined in particulate phase (%PM) in cold (November-April; n=35) and warm (May-July; n=22) seasons illustrating gas/particle partitioning in response to ambient conditions change. Full results are provided in Paper III. Compound molecular mass (g/mol) is given in parentheses.

LMW PAHs were primarily found in the gas phase, while HMW PAHs were present in the particulate phase (Tables S6 & S7 in **Paper III**), which is in accordance with their physico-chemical properties. Statistically reliable evaluation of %PM for many nitro-PAHs was not possible due to the high number of concentration values below the method quantification limit. Compared to the earlier reported data for mid-latitude European winters (Tomaz et al., 2016; Nežiková et al., 2020; Degrendele et al., 2021; Albinet et al., 2008), higher values of %PM were found for several semi-volatile PACs: up to 30 % repartitioning between phases was determined for Flt, PhtA, 1-NapA, 2-FCinA, 1-AceO, 9-FluO, and 2,2-BPhA (Fig. 19). It implies a significant phase state sensitivity of these compounds to the ambient conditions. In turn, it alerts for their careful use in the modelling studies on LRAT and chemical transformation in the atmosphere. Statistically significant (Spearman correlation, $p < 0.05$) negative correlations of %PM values with ambient temperature and absolute humidity were confirmed for most of these compounds, reflecting their repartitioning to a particulate phase at colder conditions and migration to a vapour phase at warmer and wetter Arctic conditions in summer. Fresh pollution plumes and their rates' variabilities might have been responsible for a different outcome and an absence of statistically reliable correlations with the ambient conditions (e.g., for Flt and 2-FCinA).

Up to 4 times higher emissions of the particle-bound PACs from local ship traffic was determined (**Paper II**), which explains higher %PM of Xan, 2,3-NapAn, DBPone, and BbFlu in the warmer period than during the winter days. In general, higher %PM of PACs was determined at the urban location (UNIS), likely due to closer proximity to the stationary (coal power plant and ships) and mobile (car and snowmobile traffic) local fossil fuel burning sources compared to Adventdalen.

Due to the warming Arctic climate, re-volatilization of LMW PACs from polluted surfaces like ocean, snow, ice, and soil is expected (Yu et al., 2019; Muir and Galarneau, 2021). More than 60 % of the total environmental mass of PAHs with a molecular mass below 216 g/mol (2-MeFlt) and oxy-PAH with a molecular mass below 210 g/mol (BPhA) were determined in the gas phase (%PM < 40 %) during the Arctic summer (**Papers I & III**), confirming their high re-volatilization potential.

4.5 Secondary formation of PACs in the polar atmosphere

Due to sufficient concentrations and high oxidation potential ($E^0 = 2.59$ V; Vione et al., 2004), the OH radical is usually regarded as the main atmospheric oxidant of PAHs during their transport and the only oxidant considered in most of the modelling studies (Lammel et al., 2009; Friedman and Selin, 2012; Galarneau et al., 2014). Dry Arctic conditions and the absence of solar radiation for a long time do not let the regional atmospheric chemistry follow this rule, but different oxidation pathways are driven, which are discussed herein. Chemical transformation of primary PAC emissions can be significant in the polar atmosphere under special seasonal ambient conditions with sufficient amount of local reactants. These transformation processes should be included in modelling studies for valid simulation of the distribution of PAC emissions and examination of source contributions.

To get insights of atmospheric photooxidation processes of PACs, seasonal evolution of the product/parent PAC ratios based on total individual concentrations has been investigated for all three sampling sites (**Paper III**). The seasonal results are discussed separately and combined with literature knowledge, OC/EC ratio values, and meteorological parameters to highlight specific origin or predominant seasonal oxidants. Summary of photochemical transformation pathways identified in this thesis is provided in Table 4.

Table 4. Potential PACs' transformation pathways in polar troposphere based on this thesis results.

PAC	Oxidant	Conditions	Oxy-PAH
Naphthalene	O ₃	full polar night, cold, winter	1,4-Naphthoquinone
2-Methylnaphthalene			Phthalic anhydride
1-Methylnaphthalene			1-Naphthaldehyde
Benzo[<i>a</i>]anthracene			Benzo[<i>a</i>]anthracene-7,12-dione
Pyrene			9-Phenanthrenecarboxaldehyde
Fluorene	•Hal > •OH	day/night, cold, spring	Benzo[<i>b</i>]fluorenone, 6 <i>H</i> -Dibenzo[<i>b,d</i>]pyran-6-one
9-Fluorenone			6 <i>H</i> -Dibenzo[<i>b,d</i>]pyran-6-one
Phenanthrene			6 <i>H</i> -Dibenzo[<i>b,d</i>]pyran-6-one
2-Formyl- <i>trans</i> -cinnamaldehyde			Phthaldialdehyde
Anthracene			9,10-Anthraquinone, Anthrone, Xanthone, 9-Fluorenone, 1,2-Naphthalic anhydride
9,10-Anthraquinone			Anthrone
Naphthalene	•OH	full polar day, warmest, summer	1,2-Naphthoquinone, 1-Naphthaldehyde, 2-Formyl- <i>trans</i> -cinnamaldehyde, Phthalic anhydride
Phthaldialdehyde			Phthalic anhydride

4.5.1 Polar night chemistry

An extended over several months polar night period in the high Arctic provides a unique environment for field-based research on night-time atmospheric transformation of PACs. This period is dominated by LRAT air masses from lower latitude regions. Polar air masses may reside in the dark for longer than 10 days due to the efficiency of the Polar Dome in inhibiting transport to lower latitudes (Klonecki et al., 2003; Stohl, 2006). Hence even very slow dark-time reactions may be important due to the long exposure period to the night oxidants and absence of photodegradation of the product. Investigation of the product/parent ratios for nitro-PAHs did not show clear evidence of the night-time formation of nitro-PAHs under polar conditions. Though, the observed

ratios of 1,4-NapQ/Nap, PhtAn/2-MeNap, 1-NapA/1-MeNap, BaAnt-7,12/BaAnt, and 9-PheA/Pyr were notably higher in winter at Svalsat and also at the other two locations (Fig. 3 in **Paper III**), suggesting formation of oxy-PAHs. As many PAH derivatives can also be primary emitted, the background site (Svalsat) data with no direct emission sources provides strong evidence on the secondary process to appear. The OC/EC ratio is a suitable tracer for evaluation of the origin of carbonaceous matter in the atmosphere (Srivastava et al., 2018b; Wu and Yu, 2016; Pio et al., 2011). While EC has only primary origin from carbon fuel-based combustion processes, OC can also be secondary formed. Thus, high winter OC/EC ratio values at Svalsat (24.3 as median; Table S4 in **Paper III**) reveal the great potential of atmospheric formation processes during a polar night.

The nitrate radical NO_3 and ozone O_3 are the main acting oxidants in the nocturnal atmosphere in many environments (Brown and Stutz, 2012). The Arctic is a low NO_x environment, and nitrogen oxides are primarily present in stable reservoir forms like N_2O_5 , peroxyacetyl nitrate (PAN), HNO_3 , and others (Solberg et al., 1997; AMAP, 2015; Björkman et al., 2013). Thermal and photolytic decompositions of the reservoir species are reduced under low temperature dark conditions (Brown and Stutz, 2012; Thompson et al., 2015; Simpson et al., 2007); thus, NO_3 radical production is likely weak during the permanent night-time period (Solberg et al., 1997; Brown et al., 2011). Hence, we may conclude that the nocturnal oxidation of PAHs was mainly via ozonolysis. The reaction of PAHs with ozone is enhanced on particles in comparison with reactions in the gas phase (Keyte et al., 2013). Experimental studies have reported the high loss of BaAnt and Pyr under exposure to O_3 (Ringuet et al., 2012b; Jariyasopit et al., 2014) and 1,4-NapQ, PhtAn, 1-NapA, 9-PheA, and BaAnt-7,12 were found among products of ozonation of PAHs (Reisen and Arey, 2002; Riva et al., 2016; Kramer et al., 2019; Perraudin et al., 2007; Rindone et al., 2010; Cochran et al., 2016). Furthermore, BaAnt-7,12 was confirmed to be exclusively formed by ozonation of BaAnt, unlike by the reaction with OH radicals (Ringuet et al., 2012b).

4.5.2 Polar spring chemistry

The return of sunlight to the Arctic significantly increases the oxidation capacity of the polar boundary layer (Simpson et al., 2007; Hornbrook et al., 2016; Peterson et al., 2015; Simpson et al., 2017; Thompson et al., 2015), which affects the lifetime of PACs and changes their fates in the environment. Due to ubiquitous presence of saline surfaces,

such as coastal snowpack, sea ice surfaces, and sea salt aerosol (Abbatt et al., 2012), the Arctic region is a rich source of atmospheric reactive halogen species (Monks, 2005; AMAP, 2016; Zhao et al., 2016; Sihler et al., 2012; Begoin et al., 2010). Molecular halogens Cl₂, BrCl, Br₂, I₂ are known halogen atom precursors emitted from photochemical reactions occurring on snowpack and aerosol surfaces (McNamara et al., 2019; Raso et al., 2017; Custard et al., 2017). Light initiated active halogen photochemistry causes depletion of tropospheric ozone with frequent near zero surface concentrations, which may last over several days (Thompson et al., 2015; Fan and Jacob, 1992). In combination with dry conditions, it results in low hydroxyl radical OH production in spring and thus domination of the halogen photochemistry (Simpson et al., 2007), especially within the BLH (Strong et al., 2020).

While bromine and iodine atoms are primarily responsible for ozone depletion (Simpson et al., 2015; Strong et al., 2020; Thompson et al., 2015), a large chemical flux of carbonyl compounds as oxidation products of extensive chlorine-atom processing of numerous saturated and unsaturated organics (including aromatic) is widely reported (Grannas et al., 2002; Simpson et al., 2007; Hornbrook et al., 2016; Thompson et al., 2015). Simultaneous degradation of PAHs and increase of oxidation by-products (acids) in the high Canadian Arctic in spring have earlier been observed (Fu et al., 2009; Singh et al., 2017). Furthermore, the calculated rate constant of an adduct formation with Cl is a factor of 3 higher than with OH for Ace and Acy and the easier formation of NAnt and NPy_r via Cl-initiated mechanism was concluded (Dang and He, 2016).

In **Paper III**, significantly greater ratios of 9,10-AntQ/Ant, ANO/Ant, Xan/Ant, 9-FluO/Ant, and PhtA/2-FCinA were determined for the spring P3 period compared to the dark/twilight P1-P2 and summer P4 periods at urban and remote sites (Fig. 4 in **Paper III**; no samples were taken at the background site), suggesting the secondary formation of 9,10-AntQ, ANO, Xan, 9-FluO and PhtA from the reaction of the parent PAH Ant triggered by halogen radical attack under daylight polar conditions (Fig. 4). Ant has a sterically unhindered molecule, and it is one of the most reactive PAHs (Keyte et al., 2013). In addition, the Cl atom-initiated atmospheric oxidation of Ant is highly exothermic, with no potential barrier process (Dang and He, 2016), and significant degradation of Ant was revealed during a simulated tidal flat conditions experiment on photochemical halogenation of PAHs by Sankoda et al. (2013). Formation of 9,10-AntQ and ANO as products of chlorination of Ant has earlier been proposed by Jin et al.

(2020b). Similar can be presumed for PhtA and 2-FCinA as significantly higher values of the PhtA/2-FCinA ratio were determined in P3 period (Fig. 4 in **Paper III**). PhtA is reported in the literature as a second-generation product resulting from further oxidation of 2-FCinA (Chan et al., 2009; Tomaz et al., 2017; Arey and Atkinson, 2003), which is the main by-product from the OH-initiated oxidation of Nap (Qu et al., 2006; Keyte et al., 2013). Our observations are leading to the conclusion that these compounds can also be formed by halogen-initiated reaction pathways.

Blowing saline snow and sea salt aerosol particles are responsible for halogen chemistry inland, far from marine influence (Strong et al., 2020). However, the impact is presumed to be higher at coastal sites with greater seawater spray influence, sea salt aerosol concentrations, and halogens' release by marine organisms at low tide (Simpson et al., 2015). High spring ratios of BbFluo/Flu, DBPone/Flu, DBPone/9Fluo, DBPone/Phen, 1,2-NapQ/Ant, and ANO/9,10-AntQ were obtained at UNIS located 250 m from the fjord (no sea ice; 12 h tide period; Fig. 4 in **Paper III**), while it was less evident at Adventdalen site located at 3.5 km distance from the sea (Fig. 8). These data strongly imply a higher exposure to halogens and reveal secondary production of BbFluo, DBPone, 1,2NapQ, and ANO during spring and likely via halogen-initiated reactions. All these compounds have been previously reported as by-products of the oxidation of PAHs and/or oxy-PAHs by OH and O₃ (Perraudin et al., 2007; Lee and Lane, 2009; Lee et al., 2012). DBPone was also proposed as a marker of PAH's secondary formation in the atmosphere (Tomaz et al., 2017).

4.5.3 Polar day summer chemistry

Due to limited northward LRAT in summer, Arctic air masses mainly represent regional emissions undergoing locally induced transformation. Increased ambient temperatures, humidity, and solar radiation in this period change the main drivers of polar atmospheric chemistry. Photolysis and reactions with OH radicals primarily control the atmospheric degradation of PACs in summer. Photolysis of ozone in the presence of water vapour produces OH radical, which peaks in concentration in summer (Solberg et al., 1996), while ozone levels become minimal and NO₃ radical (react directly with PAH; Keyte et al., 2013) is rapidly photolyzed (within few seconds) under midnight sun conditions (Solberg et al., 1997; Monks and Hey, 2020).

Significant increase of the product/parent PAC summer ratios provides evidence of atmospheric oxidation of Nap by OH radicals and consequent formation of 1,2-NapQ, 1-NapA, 2-FCinA, PhtAn, and PhtA (Fig. 5 in **Paper III**), though these compounds may also be emitted after combustion processes (Oda et al., 2001; Jakober et al., 2007; Tomaz et al., 2017). However, the high ratios at the rural and the background altitudinal sites support the assumption about the secondary formation of these compounds (Lee and Lane, 2009; Reisen and Arey, 2002; Chan et al., 2009; Perraudin et al., 2007; Arey and Atkinson, 2003), likely as an additional source to their primary emissions.

Full details on the PACs' physicochemical processes in the polar atmosphere and the conclusions making are described in Sect. 3.3 of **Paper III**.

5 Conclusions

PACs are toxic, ubiquitous chemicals of concern in the Arctic environment. In this thesis, the occurrence, seasonal and spatial concentration trends, environmental behaviour, and potential sources of 91 gaseous and particulate PACs in Svalbard air have been investigated. The selected PACs included 23 PAHs and, for the first time, an extensive suite of their oxygenated and nitrated derivatives (31 oxy-PAHs and 37 nitro-PAHs), making it the most detailed study of these contaminants in the Arctic to date.

The results obtained in this thesis showed that seasonal PAC concentrations in ambient air of Longyearbyen, the largest settlement in Svalbard, are highly variable and span up to sixteen-folds of magnitude. Measured PAC concentrations in Svalbard were about one order of magnitude lower than the average European urban and suburban levels. Investigation of air masses transport and local meteorology indicated efficient delivery of contaminated air from lower latitudes in winter and high sensitivity of measured ambient PAC concentrations to the regional climatology and local Arctic emissions during other seasons.

Local meteorology plays a predominant role in modulating extent of the polar air contamination. Sustained cold, stably stratified conditions in the lower Arctic troposphere in spring favoured pollution accumulation in the near-ground air layer and atmospheric chemical processing (oxidation) of primary contaminants. Dispersion of local emissions was inhibited due to frequent thermal inversions in March and April. These polar spring-specific ambient conditions coincided with a significant increase in local human activities followed the several months of winter darkness. The annual highest PAC concentrations in Longyearbyen air were observed in this period, with a factor of 30 higher \sum_{20} PAH concentrations than in background air at Zeppelin monitoring station in Svalbard, being comparable to the European annual mean levels. Alarming concentrations of individual oxy- and nitro-PAHs were observed. Local vehicle traffic, specifically snowmobiles, seemed the predominant source of PAC emissions. Significant evidence of photochemical PAC formation under polar spring conditions was observed.

The measured PAC winter concentrations were in agreement with data reported from circumpolar monitoring stations. Contrary to the observations at background Arctic sites, PAC summer levels exceeded the winter ones. The average summer \sum_{20} PAH concentrations were a factor of 23 higher compared to Svalbard background levels

(Zeppelin), demonstrating significant contribution of local anthropogenic emissions and masking the PAH's degradation under midnight sun polar conditions. Evidence from ambient concentrations examined at the local scale in Longyearbyen showed that summer PAC levels correlate with wind direction. Up to twice higher PAC concentrations were measured under north-westerly winds delivering emissions from the local coal power plant and notably from the port. In autumn, frequent precipitation events (rain and snow) caused annual lowest PAC levels in Longyearbyen. As during spring, secondary formation of PAH derivatives was also evident in winter, summer, and autumn.

Pronounced PAC concentration gradients were found on relatively small spatial scale in urban, rural, and altitudinal sites in the vicinity of Longyearbyen, except for the winter period when PACs were evenly distributed due to strong inflow of LRAT air masses. Spatial variability in PAC concentrations was consistent with proximity to local emission sources (e.g., snowmobile, car, and marine traffic and the coal power plant) being greatest at the urban site. PAC levels were lowest at the altitudinal mountain top site (Svalsat), although on summer days with high marine traffic, the concentrations were comparable to those at the rural site in Adventdalen.

For the first time, plume samples of the coal-burning power plant in Longyearbyen, one of two active plants in the high Arctic, were analyzed. Generally, low emissions of PACs were determined ($\sum_{16} \text{PAHs} = 1.5 \mu\text{g/kg coal}$), confirming an efficient exhaust purification by a modern cleaning system. However, a large volume of daily flue gas emissions remains the power plant an important local anthropogenic source of atmospheric contaminants in the Arctic. The source markers for the plant coal burning were determined, and production of oxy-PAHs (not nitro-PAHs) during high-temperature coal combustion was concluded. Results align with existing literature and can assist interpretation of deviations between the monitored and modelled PAH concentrations in Svalbard background air (Zeppelin). Successful application of the determined diagnostic ratio of $\text{Flu}/(\text{Flu}+\text{Pyr}) > 0.64$ confirmed the high reliability of its use for qualitative identification of coal-burning emissions from the Longyearbyen plant.

To the best knowledge, this study is the first to report phase-separated PAC concentrations in the Arctic air. The compound phase state firmly controls the lifetime and LRAT potential of PACs, key parameters for modelling studies. For most LMW PACs

the dominant presence in the gaseous phase was confirmed under extremely cold conditions. Significant phase partitioning was revealed for the number of PACs in response to changes in ambient conditions (temperature and humidity). Higher proportion of these compounds in gaseous phase were found in summer than in the winter-spring cold period. These findings imply potencies of some semi-volatile PACs for evaporation from contaminated surfaces in the warmer Arctic future.

The present study also contributes new knowledge on the photochemical transformation of PACs under polar conditions. Distinct atmospheric oxidant capacity and various potential transformation pathways of PACs have been studied in each key season (winter (polar night), spring (daylight), and summer (full polar day)). Unique oxidation products from PAH ozonation observed during the winter period highlight ozone being a sole PAH oxidant during the night-time period. In spring, the evidence of rapid halogen-initiated oxidation of atmospheric PAHs has been highlighted in agreement with the fact that polar air masses are enriched in halogen reactive species (X^{\bullet} , X_2 , XO , XY , and HOX with X and Y being Cl , Br or I) in this period. In summer, PAC atmospheric processes are driven by photolysis and OH radical chemistry, as ozone and nitrogen oxides are photolyzed (full polar day conditions) and can also be hydrolyzed. As an effect of polar sunrise, PAHs are traditionally considered degraded, and their further environmental fate is disregarded. Photochemical production of more harmful PAC derivatives (oxy-PAHs, halogenated PAH, and other PACs) from PAHs demonstrated in this thesis highlights that the environmental fate by PACs should not be ignored after the polar sunrise but should instead be the focus of research.

To conclude, this thesis closes vast knowledge gaps on the occurrence of PAH derivatives in the Arctic atmosphere, the compounds with significantly greater toxicity than the traditional 16 PAHs, which were defined almost five decades ago with substantially lower knowledge and available analytical analyses. Novel aspects presented here play a crucial role in understanding levels, sources, fate, and transport of atmospheric PACs. This knowledge is essential for authorities working on national and regional regulatory monitoring and remediation strategies and might further provide confidence for choosing new candidates to be routinely measured in densely populated areas and the Arctic.

6 Future perspectives

Significant contribution of local anthropogenic sources on the PAC concentration levels in Svalbard was highlighted in this PhD thesis. Emissions caused by high human activity together with specific seasonal meteorological conditions and strong oxidation capacity of the polar atmosphere may cause severe local air pollution in spring. Results obtained from observations made in Longyearbyen suggests that snowmobile traffic induces dramatic seasonal PAC concentration peaks. However, emissions from diesel and gasoline driven cars and coal burning together with LRAT contribute to the local PAC background concentration levels. In order to better understand and evaluate the different PAC, PM and gaseous pollutant source contributions, further source apportionment studies should be performed in Svalbard and notably in the urban location of Longyearbyen. Such work might be based on extended chemical characterization of the particulate (and/or gaseous phases) and applying statistical source-receptor modes (e.g., positive mass factorization, PMF; Karagulian et al., 2015; Hopke et al., 2020). For instance, in addition to PACs, the analysis of PM chemical species such as elemental and organic carbon (EC/OC), major ions, metals but also key molecular markers of primary (e.g., levoglucosan marker of biomass burning (Simoneit et al., 1999; Bhattarai et al., 2019)) and secondary organic aerosol sources would allow getting detailed PM, as well as PAC, source discrimination and evaluation (Lanzafame et al., 2021; Srivastava et al., 2018c; Srivastava et al., 2018a; Srivastava et al., 2021). In such strategy, the monitoring of PM mass, O₃, NO_x, CO, SO₂ is also required. This highlights that air quality monitoring in Longyearbyen is still lacking. Furthermore, in order to increase the confidence in source identification, specific local source chemical profiles (snowmobile, boat, coal plant, diesel and gasoline car emissions) could also be obtained based on direct emission and/or down-wind sampling strategies (Belis et al., 2014). In addition, substantial air contamination by PACs from the local marine traffic in summer was highlighted in this thesis. As ship traffic is expected to increase in the near future, further studies should primarily address this source notably over the entire sailing season combined with port registry data.

As demonstrated in this PhD thesis, the Arctic region is enriched with halogen species, activated at polar sunrise in spring, when local PAC emissions are high and can be converted into potential more harmful contaminants (e.g., oxy- and nitro-PAHs). Reactions of PACs with halogens are faster than with the OH radical, and higher

concentrations of halogen species are predicted in the warmer Arctic future (Raso, 2018). Therefore, it would be of high interest for the scientific community to better understand the chemical processes involved in the PAC halogen chemistry and expand knowledge on the formed reaction products based on laboratory experiments using smog chambers or oxidation flow reactors. For stronger evidence of the halogen-driven oxidation of PACs, intensive spring sampling campaigns are advised together with measurements of ozone and long-lived gaseous elemental mercury. Ozone depletion events correlate with mercury oxidation, mainly driven by Br radical chemistry (Kokhanovsky and Tomasi, 2020), while Cl and I radicals are assumed to induce PACs oxidation. The knowledge on the PAC halogen chemistry is poorly documented, and thus it is likely that analyzed in this thesis suite of PACs does not include some major transformation products like other oxygenated PACs, polycyclic aromatic acids and halogenated PAHs (Singh et al., 2017; Jin et al., 2020b). Halogenated PAHs have potential similar or higher toxicity than polychlorinated dibenzo-p-dioxins and dibenzofurans and may significantly contribute to environmental and human risks (Jin et al., 2020a). In such context, non-target screening (NTS) analytical strategy of air samples would be of great support to highlight new analytes of interest (Röhler et al., 2020). As a first attempt, the quantification of chlorinated-PAHs and/or NTS analyses could be performed on the remaining QFF from this PhD work collected in spring period.

Considering the high sensitivity of the Arctic environment to local pollutant accumulation in the lowest troposphere (BLH) and high oxidation capacity of the polar atmosphere in spring, the use of old vehicles (cars and snowmobiles) equipped with poor exhaust cleaning systems should be re-evaluated and likely banned by the local Svalbard authorities. Furthermore, recent studies have shown significant snow and likely soil and vegetation contamination along snowmobile tracks (McDaniel and Zielinska, 2014). Soil in the Arctic is largely permafrost, which acts as a barrier preventing contaminants from entering groundwater (Granberg et al., 2017). It makes Arctic soil being a storage of contaminants, increasing the potential for toxicological effects on terrestrial biota (e.g., reindeers) exposed to contamination. It would be interesting to quantify levels of PACs in soil from the main snowmobile routes, for example, in Adventdalen valley.

In addition, the global research community is attempting to define a list of toxicologically relevant PACs appropriate for measurement in various environmental

media. In this thesis, several oxy-PAHs have been quantified in the Svalbard air at pronounced levels with comparable and sometimes higher concentrations than in Europe. These compounds are among ROS precursors and have high acute toxicity. From a method perspective, oxy-PAHs may be analyzed with the same instrumentation as the PAHs (GC/MS-EI-SIM). Therefore, it is suggested to include the most representative oxy-PAH candidates into ongoing atmospheric monitoring programmes, as well as quantify their occurrence in other Arctic environmental compartments.

In the big picture, atmospheric circulation is a key element in the environmental linkages between the Arctic and the mid-latitudes (Walsh, 2014). Atmospheric circulation responses to the ongoing climate change are not well understood yet. Sea ice diminishing in the Arctic drives changes in the Arctic Oscillation and cyclone activity, which are expected to be accompanied by alterations of pathways and efficiency of LRAT pollution delivery northward. The warmer and wetter climate is predicted in the Arctic (Wickström et al., 2020b), which might have a potential effect on the PAC's partitioning into the gaseous phase, increase wet scavenging of these compounds during their intercontinental delivery, and likely increase the oxidation capacity of the polar atmosphere supplying it by hydroxyl radicals. Wildfire emissions are projected to increase under climate warming and semi-volatile PACs have the potential for reemission from previously contaminated soil and water in the Arctic (Muir and Galarneau, 2021; Berthiaume et al., 2021). Greater economic activity in the north will cause the emissions increase from shipping, industrial development, and further urbanization of local Arctic settlements. To summarize, uncertain climate change responses and growth of anthropogenic and natural PAC emissions in the region demand continued monitoring of an extended suite of PACs in the Arctic.

7 References

Abbas, I., Badran, G., Verdin, A., Ledoux, F., Roumié, M., Courcot, D., and Garçon, G.: Polycyclic aromatic hydrocarbon derivatives in airborne particulate matter: sources, analysis and toxicity, *Environ. Chem. Lett.*, 16, 439–475, <https://doi.org/10.1007/s10311-017-0697-0>, 2018.

Abbatt, J. P. D., Thomas, J. L., Abrahamsson, K., Boxe, C., Granfors, A., Jones, A. E., King, M. D., Saiz-Lopez, A., Shepson, P. B., Sodeau, J., Toohey, D. W., Toubin, C., von Glasow, R., Wren, S. N., and Yang, X.: Halogen activation via interactions with environmental ice and snow in the polar lower troposphere and other regions, *Atmos. Chem. Phys.*, 12, 6237–6271, <https://doi.org/10.5194/acp-12-6237-2012>, 2012.

Abdel-Shafy, H. I., and Mansour, M. S. M.: A review on polycyclic aromatic hydrocarbons: Source, environmental impact, effect on human health and remediation, *Egypt. J. Pet.*, 25, 107–123, <https://doi.org/10.1016/J.EIPE.2015.03.011>, 2016.

Achten, C., and Andersson, J. T.: Overview of Polycyclic Aromatic Compounds (PAC), *Polycyclic Aromat. Compd.*, 35, 177–186, <https://doi.org/10.1080/10406638.2014.994071>, 2015.

Agersted, M. D., Møller, E. F., and Gustavson, K.: Bioaccumulation of oil compounds in the high-Arctic copepod *Calanus hyperboreus*, *Aquat. Toxicol.*, 195, 8–14, <https://doi.org/10.1016/j.aquatox.2017.12.001>, 2018.

Albers, P. H.: Birds and polycyclic aromatic hydrocarbons, *Avian and Poultry Biology Reviews*, 17, 125–140, 2006.

Albinet, A., Leoz-Garziandia, E., Budzinski, H., and Villenave, E.: Simultaneous analysis of oxygenated and nitrated polycyclic aromatic hydrocarbons on standard reference material 1649a (urban dust) and on natural ambient air samples by gas chromatography–mass spectrometry with negative ion chemical ionisation, *J. Chromatogr. A*, 1121, 106–113, <https://doi.org/10.1016/j.chroma.2006.04.043>, 2006.

Albinet, A., Leoz-Garziandia, E., Budzinski, H., and Viilenave, E.: Polycyclic aromatic hydrocarbons (PAHs), nitrated PAHs and oxygenated PAHs in ambient air of the Marseilles area (South of France): Concentrations and sources, *Sci. Total Environ.*, 384, 280–292, <https://doi.org/10.1016/j.scitotenv.2007.04.028>, 2007.

Albinet, A., Leoz-Garziandia, E., Budzinski, H., Villenave, E., and Jaffrezo, J. L.: Nitrated and oxygenated derivatives of polycyclic aromatic hydrocarbons in the ambient air of two French alpine valleys. Part 1: Concentrations, sources and gas/particle partitioning, *Atmos. Environ.*, 42, 43–54, <http://doi.org/10.1016/j.atmosenv.2007.10.009>, 2008.

Albinet, A., Tomaz, S., and Lestremau, F.: A really quick easy cheap effective rugged and safe (QuEChERS) extraction procedure for the analysis of particle-bound PAHs in ambient air and emission samples, *Sci. Total Environ.*, 450–451, 31–38, <https://doi.org/10.1016/j.scitotenv.2013.01.068>, 2013.

Albinet, A., Nalin, F., Tomaz, S., Beaumont, J., and Lestremau, F.: A simple QuEChERS-like extraction approach for molecular chemical characterization of organic aerosols: application to nitrated and oxygenated PAH derivatives (NPAH and OPAH) quantified by GC–NICIMS, *Anal. Bioanal. Chem.*, 406, 3131–3148, <https://doi.org/10.1007/s00216-014-7760-5>, 2014.

AMAP: Assessment 2007: Oil and Gas Activities in the Arctic - Effect and Potential Effects. Volume 2, Arctic Monitoring and Assessment Programme (AMAP), Oslo, Norway, vii + 277 pp., 2010.

AMAP: AMAP Assessment 2015: Black carbon and ozone as Arctic climate forcers, Arctic Monitoring and Assessment Programme (AMAP), Oslo, Norway, vii + 116 pp., 2015.

AMAP: AMAP Assessment 2015: Temporal trends in persistent organic pollutants in the Arctic, Arctic Monitoring and Assessment Programme (AMAP), Oslo, Norway, vi +71 pp., 2016.

AMAP: AMAP Assessment 2016: Chemicals of Emerging Arctic Concern, Arctic Monitoring and Assessment Programme (AMAP), Oslo, Norway, xvi + 353 pp., 2017a.

AMAP: Adaptation actions for a changing Arctic: perspectives from the Barents area, Arctic Monitoring and Assessment Programme (AMAP), Oslo, Norway, xiv + 267 pp., 2017b.

AMAP: POPs and Chemicals of Emerging Arctic Concern: Influence of Climate Change. Summary for Policy-makers, Arctic Monitoring and Assessment Programme (AMAP), Tromsø, Norway, 16 pp., 2021a.

AMAP: Arctic Climate Change Update 2021: Key Trends and Impacts. Summary for Policy-makers, Arctic Monitoring and Assessment Programme (AMAP), Oslo, Norway, 16 pp., 2021b.

Andersson, J. T., and Achten, C.: Time to say goodbye to the 16 EPA PAHs? Toward an up-to-date use of PACs for environmental purposes, *Polycyclic Aromat. Compd.*, 35, 330-354, <https://doi.org/10.1080/10406638.2014.991042>, 2015.

Arey, J., and Atkinson, R.: Photochemical reactions of PAHs in the atmosphere, in: *PAHs: An Ecotoxicological Perspective*, edited by: Douben, P. E. T., John Wiley & Sons Ltd, England, 47-64, <https://doi.org/10.1002/0470867132.ch4>, 2003.

Arnold, S. R., Law, K. S., Brock, C. A., Thomas, J. L., Starkweather, S. M., von Salzen, K., Stohl, A., Sharma, S., Lund, M. T., and Flanner, M. G.: Arctic air pollution: Challenges and opportunities for the next decade, *Elementa: Science of the Anthropocene*, 4, P000104, <http://doi.org/10.12952/journal.elementa.000104>, 2016.

Atkinson, R., and Arey, J.: Atmospheric chemistry of gas-phase polycyclic aromatic hydrocarbons: formation of atmospheric mutagens, *Environ. Health Perspect.*, 102, 117-126, <https://doi.org/10.1289/ehp.94102s4117>, 1994.

Balmer, J. E., Hung, H., Yu, Y., Letcher, R. J., and Muir, D. C. G.: Sources and environmental fate of pyrogenic polycyclic aromatic hydrocarbons (PAHs) in the Arctic, *Emerging Contaminants*, 5, 128-142, <https://doi.org/10.1016/j.emcon.2019.04.002>, 2019.

Bandowe, B. A. M., and Meusel, H.: Nitrated polycyclic aromatic hydrocarbons (nitro-PAHs) in the environment - A review, *Sci. Total Environ.*, 581-582, 237-257, <https://doi.org/10.1016/j.scitotenv.2016.12.115>, 2017.

Barrie, L. A.: Occurrence And Trends of Pollution in the Arctic Troposphere, in: *Chemical Exchange Between the Atmosphere and Polar Snow*. NATO ASI Series (Series I: Global Environmental Change), edited by: Wolff, E. W., and Bales, R. C., 43, Springer, Berlin, Heidelberg, 93-129, https://doi.org/10.1007/978-3-642-61171-1_5, 1996.

Becker, S., Halsall, C. J., Tych, W., Hung, H., Attewell, S., Blanchard, P., Li, H., Fellin, P., Stern, G., Billeck, B., and Friesen, S.: Resolving the Long-Term Trends of Polycyclic Aromatic Hydrocarbons in the Canadian Arctic Atmosphere, *Environ. Sci. Technol.*, 40, 3217-3222, <https://doi.org/10.1021/es052346l>, 2006.

Begoin, M., Richter, A., Weber, M., Kaleschke, L., Tian-Kunze, X., Stohl, A., Theys, N., and Burrows, J. P.: Satellite observations of long range transport of a large BrO plume in the Arctic, *Atmos. Chem. Phys.*, 10, 6515-6526, <https://doi.org/10.5194/acp-10-6515-2010>, 2010.

Béland, P., DeGuise, S., Girard, C., Lagacé, A., Martineau, D., Michaud, R., Muir, D. C. G., Norstrom, R. J., Pelletier, É., Ray, S., and Shugart, L. R.: Toxic Compounds and Health and Reproductive Effects in St. Lawrence Beluga Whales, *J. Great Lakes Res.*, 19, 766-775, [https://doi.org/10.1016/S0380-1330\(93\)71264-2](https://doi.org/10.1016/S0380-1330(93)71264-2), 1993.

Belis, C. A., Larsen, B. R., Amato, F., El Haddad, I., Favez, O., Harrison, R. M., Hopke, P. K., Nava, S., Paatero, P., Prevot, A., Quass, U., Vecchi, R., and Viana, M.: European guide on air pollution source apportionment with receptor models, EUR 26080, JRC European Commission, Publication Office of the European Union, Luxembourg, 88 pp., <https://doi.org/10.2788/9307>, 2014.

Berthiaume, A., Galarneau, E., and Marson, G.: Polycyclic aromatic compounds (PACs) in the Canadian environment: Sources and emissions, *Environ. Pollut.*, 269, 116008, <https://doi.org/10.1016/j.envpol.2020.116008>, 2021.

Bhattarai, H., Saikawa, E., Wan, X., Zhu, H., Ram, K., Gao, S., Kang, S., Zhang, Q., Zhang, Y., Wu, G., Wang, X., Kawamura, K., Fu, P., and Cong, Z.: Levoglucosan as a tracer of biomass burning: Recent progress and perspectives, *Atmos. Res.*, 220, 20-33, <https://doi.org/10.1016/j.atmosres.2019.01.004>, 2019.

Bidgoli, S. A., Karimi, M., Asami, Z., Baher, H., and Djamali Zavarhei, M.: Association between testicular Aryl hydrocarbon Receptor levels and idiopathic male infertility: A case-control study in Iran, *Sci. Total Environ.*, 409, 3267-3273, <https://doi.org/10.1016/j.scitotenv.2011.03.024>, 2011.

Bidleman, T. F.: Atmospheric processes, *Environ. Sci. Technol.*, 22, 361-367, <https://doi.org/10.1021/es00169a002>, 1988.

Bishop, G. A., Morris, J. A., and Stedman, D. H.: Snowmobile contributions to mobile source emissions in Yellowstone National Park, *Environ. Sci. Technol.*, 35, 2874-2881, <https://doi.org/10.1021/es010513l>, 2001.

Björkman, M., Kühnel, R., Partridge, D., Roberts, T., Aas, W., Mazzola, M., Viola, A., Hodson, A., Ström, J., and Isaksson, E.: Nitrate dry deposition in Svalbard, *Tellus Ser. B*, 65, 19071, <https://doi.org/10.3402/tellusb.v65i0.19071>, 2013.

Boitsov, S., Klungsøyr, J., and Jensen, H. K. B.: Background concentrations of polycyclic aromatic hydrocarbons (PAHs) in deep core sediments from the Norwegian Sea and the Barents Sea: A proposed update of the OSPAR Commission background values for these sea areas, *Chemosphere*, 251, 126344, <https://doi.org/10.1016/j.chemosphere.2020.126344>, 2020.

Bolden, A. L., Rochester, J. R., Schultz, K., and Kwiatkowski, C. F.: Polycyclic aromatic hydrocarbons and female reproductive health: A scoping review, *Reprod. Toxicol.*, 73, 61-74, <https://doi.org/10.1016/j.reprotox.2017.07.012>, 2017.

Bolton, J. L., Trush, M. A., Penning, T. M., Dryhurst, G., and Monks, T. J.: Role of Quinones in Toxicology, *Chem. Res. Toxicol.*, 13, 135-160, <https://doi.org/10.1021/tx9902082>, 2000.

Booc, F., Thornton, C., Lister, A., MacLatchy, D., and Willett, K. L.: Benzo[a]pyrene Effects on Reproductive Endpoints in *Fundulus heteroclitus*, *Toxicol. Sci.*, 140, 73-82, <https://doi.org/10.1093/toxsci/kfu064>, 2014.

Bozem, H., Hoor, P., Kunkel, D., Köllner, F., Schneider, J., Herber, A., Schulz, H., Leaitch, W. R., Aliabadi, A. A., Willis, M. D., Burkart, J., and Abbatt, J. P. D.: Characterization of transport regimes and the polar dome during Arctic spring and summer using in situ aircraft measurements, *Atmos. Chem. Phys.*, 19, 15049-15071, <https://doi.org/10.5194/acp-19-15049-2019>, 2019.

Brock, C. A., Cozic, J., Bahreini, R., Froyd, K. D., Middlebrook, A. M., McComiskey, A., Brioude, J., Cooper, O., Stohl, A., and Aikin, K.: Characteristics, sources, and transport of aerosols measured in spring 2008 during the aerosol, radiation, and cloud processes affecting Arctic Climate (ARCPAC) Project, *Atmos. Chem. Phys.*, 11, 2423-2453, <https://doi.org/10.5194/acp-11-2423-2011>, 2011.

Brorström-Lundén, E., Remberger, M., Kaj, L., Hansson, K., Palm Cousins, A., and Andersson, H.: Results from the Swedish national screening programme 2008, IVL Swedish Environmental Research Institute, Göteborg, Sweden, 69 pp., <https://www.ivl.se/webdav/files/Rapporter/B1944.pdf>, 2010.

Brown, S. S., Dubé, W. P., Peischl, J., Ryerson, T. B., Atlas, E., Warneke, C., de Gouw, J. A., de Lintel Hekkert, S., Brock, C. A., Flocke, F., Trainer, M., Parrish, D. D., Feshenfeld, F. C., and Ravishankara, A. R.: Budgets for nocturnal VOC oxidation by nitrate radicals aloft during the 2006 Texas Air Quality Study, *J. Geophys. Res. Atmos.*, 116, D24305, <https://doi.org/10.1029/2011JD016544>, 2011.

Brown, S. S., and Stutz, J.: Nighttime radical observations and chemistry, *Chem. Soc. Rev.*, 41, 6405-6447, <https://doi.org/10.1039/C2CS35181A>, 2012.

Browse, J., Carslaw, K. S., Arnold, S. R., Pringle, K., and Boucher, O.: The scavenging processes controlling the seasonal cycle in Arctic sulphate and black carbon aerosol, *Atmos. Chem. Phys.*, 12, 6775-6798, <https://doi.org/10.5194/acp-12-6775-2012>, 2012.

Bruner, K. A., Fisher, S. W., and Landrum, P. F.: The Role of the Zebra Mussel, *Dreissena polymorpha*, in Contaminant Cycling: I. The Effect of Body Size and Lipid Content on the Bioconcentration of PCBs and PAHs, *J. Great Lakes Res.*, 20, 725-734, [http://dx.doi.org/10.1016/S0380-1330\(94\)71190-4](http://dx.doi.org/10.1016/S0380-1330(94)71190-4), 1994.

Bøckman, R.: Fremtidens energiutfordringer på Svalbard (in Norwegian), Longyearbyen Lokaltstyre, Norway, Open file at www.uit.no (last access: 28 January 2020), 10 pp., 2019.

Camus, L., Birkely, S. R., Jones, M. B., Børseth, J. F., Grøsvik, B. E., Gulliksen, B., Lønne, O. J., Regoli, F., and Depledge, M. H.: Biomarker responses and PAH uptake in *Mya truncata* following exposure to oil-contaminated sediment in an Arctic fjord (Svalbard), *Sci. Total Environ.*, 308, 221-234, [https://doi.org/10.1016/S0048-9697\(02\)00616-2](https://doi.org/10.1016/S0048-9697(02)00616-2), 2003.

Carrara, M., Wolf, J.-C., and Niessner, R.: Nitro-PAH formation studied by interacting artificially PAH-coated soot aerosol with NO₂ in the temperature range of 295–523 K, *Atmos. Environ.*, 44, 3878-3885, <https://doi.org/10.1016/j.atmosenv.2010.07.032>, 2010.

Cecinato, A., Mabilia, R., and Marino, F.: Relevant organic components in ambient particulate matter collected at Svalbard Islands (Norway), *Atmos. Environ.*, 34, 5061-5066, [https://doi.org/10.1016/S1352-2310\(00\)00188-6](https://doi.org/10.1016/S1352-2310(00)00188-6), 2000.

CEN: European Committee for Standardization (CEN, French: Comité Européen de Normalisation), EN 15549:2008 Air quality - Standard method for the measurement of the concentration of benzo[a]pyrene in ambient air, CEN, Brussels, Belgium, 50 pp., 2008.

CEN: European Committee for Standardization (CEN, French: Comité Européen de Normalisation), PB CEN/TS16645:2014 Ambient Air - Method for the measurement of benz[a]anthracene,

benzo[b]fluoranthene, benzo[j]fluoranthene, benzo[k]fluoranthene, dibenz[a,h]anthracene, indeno[1,2,3-cd]pyrene and benzo[ghi]perylene, CEN, Brussels, Belgium, 51 pp., 2014.

CEN: European Committee for Standardization (CEN, French: Comité Européen de Normalisation): PD CEN/TR 16998:2016 Ambient air - Report on nitro- and oxy-PAHs - Origin, toxicity, concentrations and measurement methods, CEN, Brussels, Belgium, 59 pp., 2016.

Chan, A. W. H., Kautzman, K. E., Chhabra, P. S., Surratt, J. D., Chan, M. N., Crouse, J. D., Kürten, A., Wennberg, P. O., Flagan, R. C., and Seinfeld, J. H.: Secondary organic aerosol formation from photooxidation of naphthalene and alkylnaphthalenes: implications for oxidation of intermediate volatility organic compounds (IVOCs), *Atmos. Chem. Phys.*, 9, 3049-3060, <https://doi.org/10.5194/acp-9-3049-2009>, 2009.

Cochran, R. E., Jeong, H., Haddadi, S., Fisseha Derseh, R., Gowan, A., Beránek, J., and Kubátová, A.: Identification of products formed during the heterogeneous nitration and ozonation of polycyclic aromatic hydrocarbons, *Atmos. Environ.*, 128, 92-103, <https://doi.org/10.1016/j.atmosenv.2015.12.036>, 2016.

Copernicus C3S: Copernicus Climate Change Service (C3S), ERA5: Fifth generation of ECMWF atmospheric reanalyses of the global climate, Copernicus Climate Change Service Climate Data Store (CDS), 2017.

Croft, B., Martin, R. V., Leaitch, W. R., Tunved, P., Breider, T. J., D'Andrea, S. D., and Pierce, J. R.: Processes controlling the annual cycle of Arctic aerosol number and size distributions, *Atmos. Chem. Phys.*, 16, 3665-3682, <https://doi.org/10.5194/acp-16-3665-2016>, 2016.

Custard, K. D., Raso, A. R. W., Shepson, P. B., Staebler, R. M., and Pratt, K. A.: Production and Release of Molecular Bromine and Chlorine from the Arctic Coastal Snowpack, *ACS Earth and Space Chemistry*, 1, 142-151, <https://doi.org/10.1021/acsearthspacechem.7b00014>, 2017.

Dahle, S., Savinov, V., Petrova, V., Klungsoyr, J., Savinova, T., Batova, G., and Kursheva, A.: Polycyclic aromatic hydrocarbons (PAHs) in Norwegian and Russian Arctic marine sediments: concentrations, geographical distribution and sources, *Norw. J. Geol.*, 86, 41-50, 2006.

Dang, J., and He, M.: Mechanisms and kinetic parameters for the gas-phase reactions of anthracene and pyrene with Cl atoms in the presence of NO_x, *RSC Adv.*, 6, 17345-17353, <https://doi.org/10.1039/C5RA25959B>, 2016.

Dasgupta, S., Cao, A., Mauer, B., Yan, B., Uno, S., and McElroy, A.: Genotoxicity of oxy-PAHs to Japanese medaka (*Oryzias latipes*) embryos assessed using the comet assay, *Environ. Sci. Pollut. Res.*, 21, 13867-13876, <https://doi.org/10.1007/s11356-014-2586-4>, 2014.

Degrendele, C., Kanduč, T., Kocman, D., Lammel, G., Cambelová, A., Dos Santos, S. G., Horvat, M., Kukučka, P., Holubová Šmejkalová, A., Mikeš, O., Nuñez-Corcuera, B., Příbylová, P., Prokeš, R., Saňka, O., Maggos, T., Sarigiannis, D., and Klánová, J.: NPAHs and OPAHs in the atmosphere of two central European cities: Seasonality, urban-to-background gradients, cancer risks and gas-to-particle partitioning, *Sci. Total Environ.*, 793, 148528, <https://doi.org/10.1016/j.scitotenv.2021.148528>, 2021.

Dekhtyareva, A.: On local and long-range transported air pollution in Svalbard, Doctoral thesis, The Arctic University of Norway (UiT), Tromsø, Norway, 191 pp., <https://hdl.handle.net/10037/16297>, 2019.

Desforges, J.-P., Hall, A., McConnell, B., Rosing-Asvid, A., Barber, J. L., Brownlow, A., De Guise, S., Eulaers, I., Jepson, P. D., Letcher, R. J., Levin, M., Ross, P. S., Samarra, F., Víkingsson, G., Sonne, C., and Dietz, R.: Predicting global killer whale population collapse from PCB pollution, *Science*, 361, 1373, <https://doi.org/10.1126/science.aat1953>, 2018.

Donahue, N. M., Kroll, J., Pandis, S. N., and Robinson, A. L.: A two-dimensional volatility basis set-Part 2: Diagnostics of organic-aerosol evolution, *Atmos. Chem. Phys.*, 12, 615-634, <https://doi.org/10.5194/acp-12-615-2012>, 2012.

Doornaert, B., and Pichard, A.: Analysis and proposal of methods for evaluating the dose-response relations between polycyclic aromatic hydrocarbon blends and carcinogenic effects, *Environnement, Risques & Santé*, 4 (3), 205-220, 2005.

Douben, P. E. T.: PAHs: An Ecotoxicological Perspective, *Ecological and environmental toxicology series*, John Wiley & Sons Ltd, Chichester, West Sussex, England, 406 pp., 2003.

Durant, J. L., Busby Jr, W. F., Lafleur, A. L., Penman, B. W., and Crespi, C. L.: Human cell mutagenicity of oxygenated, nitrated and unsubstituted polycyclic aromatic hydrocarbons associated with urban aerosols, *Mutat. Res. Genet. Toxicol.*, 371, 123-157, [https://doi.org/10.1016/S0165-1218\(96\)90103-2](https://doi.org/10.1016/S0165-1218(96)90103-2), 1996.

Environment Canada and Health Canada: Canadian Environmental Protection Act. Priority Substance List Report: Polycyclic Aromatic Hydrocarbons, Ottawa, Canada, 68 pp., 1994.

EU Directive 2004/107/EC: Directive 2004/107/EC of the European Parliament and the Council of 15 December 2004 relating to arsenic, cadmium, mercury, nickel and polycyclic aromatic hydrocarbons in ambient air, *Official Journal of the European Union*, 23, 3-16, <http://data.europa.eu/eli/dir/2004/107/oj>, 2005.

Fan, S.-M., and Jacob, D. J.: Surface ozone depletion in Arctic spring sustained by bromine reactions on aerosols, *Nature*, 359, 522-524, <https://doi.org/10.1038/359522a0>, 1992.

Fan, Z., Kamens, R. M., Hu, J., Zhang, J., and McDow, S.: Photostability of Nitro-Polycyclic Aromatic Hydrocarbons on Combustion Soot Particles in Sunlight, *Environ. Sci. Technol.*, 30, 1358-1364, <https://doi.org/10.1021/es9505964>, 1996.

Feilberg, A., Kamens, R. M., Strommen, M. R., and Nielsen, T.: Photochemistry and Partitioning of Semivolatile Nitro-PAH in the Atmosphere, *Polycyclic Aromat. Compd.*, 14, 151-160, <https://doi.org/10.1080/10406639908019121>, 1999.

Finlayson-Pitts, B. J., and Pitts Jr., J. N.: *Chemistry of the upper and lower atmosphere: theory, experiments, and applications*, 1 ed., Academic Press, San Diego, California, USA, 969 pp., <https://doi.org/10.1016/B978-0-12-257060-5.X5000-X>, 1999.

Foster, K. L., Stern, G. A., Carrie, J., Bailey, J. N. L., Outridge, P. M., Sanei, H., and Macdonald, R. W.: Spatial, temporal, and source variations of hydrocarbons in marine sediments from Baffin Bay, Eastern Canadian Arctic, *Sci. Total Environ.*, 506-507, 430-443, <http://dx.doi.org/10.1016/j.scitotenv.2014.11.002>, 2015.

Friedman, C. L., and Selin, N. E.: Long-range atmospheric transport of polycyclic aromatic hydrocarbons: a global 3-D model analysis including evaluation of Arctic sources, *Environ. Sci. Technol.*, 46, 9501-9510, <https://doi.org/10.1021/es301904d>, 2012.

Friedman, C. L., Zhang, Y., and Selin, N. E.: Climate Change and Emissions Impacts on Atmospheric PAH Transport to the Arctic, *Environ. Sci. Technol.*, 48, 429-437, <https://doi.org/10.1021/es403098w>, 2014.

Fu, P., Kawamura, K., and Barrie, L. A.: Photochemical and Other Sources of Organic Compounds in the Canadian High Arctic Aerosol Pollution during Winter–Spring, *Environ. Sci. Technol.*, 43, 286-292, <https://doi.org/10.1021/es803046g>, 2009.

Fu, P. P., Xia, Q., Sun, X., and Yu, H.: Phototoxicity and environmental transformation of polycyclic aromatic hydrocarbons (PAHs)—light-induced reactive oxygen species, lipid peroxidation, and DNA damage, *J. Environ. Sci. Health, Part C*, 30, 1-41, <https://doi.org/10.1080/10590501.2012.653887>, 2012.

Galarneau, E., Makar, P. A., Zheng, Q., Narayan, J., Zhang, J., Moran, M. D., Bari, M. A., Pathela, S., Chen, A., and Chlumsky, R.: PAH concentrations simulated with the AURAMS-PAH chemical transport model over Canada and the USA, *Atmos. Chem. Phys.*, 14, 4065-4077, <https://doi.org/10.5194/acp-14-4065-2014>, 2014.

Granberg, M. E., Ask, A., and Gabrielsen, G. W.: Local contamination in Svalbard: Overview and suggestions for remediation actions, *Norsk Polarinstitutt, Tromsø, Norway*, 044, 50 pp., 2017.

Grannas, A. M., Shepson, P. B., Guimbaud, C., Sumner, A. L., Albert, M., Simpson, W., Dominé, F., Boudries, H., Bottenheim, J., Beine, H. J., Honrath, R., and Zhou, X.: A study of photochemical and physical processes affecting carbonyl compounds in the Arctic atmospheric boundary layer, *Atmos. Environ.*, 36, 2733-2742, [https://doi.org/10.1016/S1352-2310\(02\)00134-6](https://doi.org/10.1016/S1352-2310(02)00134-6), 2002.

Grannas, A. M., Jones, A. E., Dibb, J., Ammann, M., Anastasio, C., Beine, H. J., Bergin, M., Bottenheim, J., Boxe, C. S., Carver, G., Chen, G., Crawford, J. H., Dominé, F., Frey, M. M., Guzmán, M. I., Heard, D. E., Helmig, D., Hoffmann, M. R., Honrath, R. E., Huey, L. G., Hutterli, M., Jacobi, H. W., Klán, P., Lefer, B., McConnell, J., Plane, J., Sander, R., Savarino, J., Shepson, P. B., Simpson, W. R., Sodeau, J. R., von Glasow, R., Weller, R., Wolff, E. W., and Zhu, T.: An overview of snow photochemistry: evidence, mechanisms and impacts, *Atmos. Chem. Phys.*, 7, 4329-4373, <https://doi.org/10.5194/acp-7-4329-2007>, 2007.

Graversen, R. G., and Wang, M.: Polar amplification in a coupled climate model with locked albedo, *Clim. Dyn.*, 33, 629-643, <https://doi.org/10.1007/s00382-009-0535-6>, 2009.

GYC: Existing Research and Data Regarding the Status of Air Quality in the Greater Yellowstone Ecosystem: A Bibliography, edited by: Hettinger, K., Greater Yellowstone Coalition (GYC), Jackson, WY, USA, 72 pp., 2011.

Halsall, C. J., Barrie, L. A., Fellin, P., Muir, D. C. G., Billeck, B. N., Lockhart, L., Rovinsky, F. Y., Kononov, E. Y., and Pastukhov, B.: Spatial and Temporal Variation of Polycyclic Aromatic Hydrocarbons in the Arctic Atmosphere, *Environ. Sci. Technol.*, 31, 3593-3599, <https://doi.org/10.1021/es970342d>, 1997.

Hanssen-Bauer, I., Førland, E. J., Hisdal, H., Mayer, S., Sandø, A. B., and Sorteberg, A.: Climate in Svalbard 2100 - a knowledge base for climate adaptation, Norwegian Centre for Climate Services (NCCS), Oslo, Norway, 1/2019, 105 pp., <https://www.miljodirektoratet.no/globalassets/publikasjoner/m1242/m1242.pdf>, 2019.

Harrison, R., and Hester, R.: Air pollution and health, *Issues in Environmental Science and Technology*, The Royal Society of Chemistry's, 142 pp., <https://doi.org/10.1039/9781847550095>, 1998.

Hellou, J., Upshall, C., Ni, I. H., Payne, J. F., and Huang, Y. S.: Polycyclic aromatic hydrocarbons in harp seals (*Phoca groenlandica*) from the Northwest Atlantic, *Arch. Environ. Contam. Toxicol.*, 21, 135-140, <https://doi.org/10.1007/BF01055568>, 1991.

Hirdman, D., Sodemann, H., Eckhardt, S., Burkhardt, J. F., Jefferson, A., Mefford, T., Quinn, P. K., Sharma, S., Ström, J., and Stohl, A.: Source identification of short-lived air pollutants in the Arctic using statistical analysis of measurement data and particle dispersion model output, *Atmos. Chem. Phys.*, 10, 669-693, <https://doi.org/10.5194/acp-10-669-2010>, 2010.

Honda, M., and Suzuki, N.: Toxicities of polycyclic aromatic hydrocarbons for aquatic animals, *Int. J. Environ. Res. Public Health*, 17, 1363, <https://doi.org/10.3390/ijerph17041363>, 2020.

Hopke, P. K., Dai, Q., Li, L., and Feng, Y.: Global review of recent source apportionments for airborne particulate matter, *Sci. Total Environ.*, 740, 140091, <https://doi.org/10.1016/j.scitotenv.2020.140091>, 2020.

Hornbrook, R. S., Hills, A. J., Riemer, D. D., Abdelhamid, A., Flocke, F. M., Hall, S. R., Huey, L. G., Knapp, D. J., Liao, J., Mauldin III, R. L., Montzka, D. D., Orlando, J. J., Shepson, P. B., Sive, B., Staebler, R. M., Tanner, D. J., Thompson, C. R., Turnipseed, A., Ullmann, K., Weinheimer, A. J., and Apel, E. C.: Arctic springtime observations of volatile organic compounds during the OASIS-2009 campaign, *J. Geophys. Res. Atmos.*, 121, 9789-9813, <https://doi.org/10.1002/2015JD024360>, 2016.

Hsu, W. T., Liu, M. C., Hung, P. C., Chang, S. H., and Chang, M. B.: PAH emissions from coal combustion and waste incineration, *J. Hazard. Mater.*, 318, 32-40, <http://doi.org/10.1016/j.jhazmat.2016.06.038>, 2016.

<https://www.yr.no>. Longyearbyen airport weather station data for 2020: <https://www.yr.no/nb/historikk/graf/1-2759929/Norge/Svalbard/Svalbard/Longyearbyen> (last access: 25 June 2021), 2021.

Hu, H., Tian, M., Zhang, L., Yang, F., Peng, C., Chen, Y., Shi, G., Yao, X., Jiang, C., and Wang, J.: Sources and gas-particle partitioning of atmospheric parent, oxygenated, and nitrated polycyclic aromatic hydrocarbons in a humid city in southwest China, *Atmos. Environ.*, 206, 1-10, <https://doi.org/10.1016/j.atmosenv.2019.02.041>, 2019.

Hu, X. M.: Boundary layer (atmospheric) and air pollution | Air Pollution Meteorology, in: *Encyclopedia of Atmospheric Sciences*, 2 ed., edited by: North, G. R., Pyle, J., and Zhang, F., Academic Press, Oxford, UK, 227-236, <https://doi.org/10.1016/B978-0-12-382225-3.00499-0>, 2015.

Huang, W., Huang, B., Bi, X., Lin, Q., Liu, M., Ren, Z., Zhang, G., Wang, X., Sheng, G., and Fu, J.: Emission of PAHs, NPAHs and OPAHs from residential honeycomb coal briquette combustion, *Energy & Fuels*, 28, 636-642, <https://doi.org/10.1021/ef401901d>, 2014.

Hwang, J.-H., Kannan, K., Evans, T. J., Iwata, H., and Kim, E.-Y.: Assessment of Risks of Dioxins for Aryl Hydrocarbon Receptor-Mediated Effects in Polar Bear (*Ursus maritimus*) by in Vitro and in Silico Approaches, *Environ. Sci. Technol.*, 54, 1770-1781, <https://doi.org/10.1021/acs.est.9b05941>, 2020.

Idowu, O., Semple, K. T., Ramadass, K., O'Connor, W., Hansbro, P., and Thavamani, P.: Beyond the obvious: Environmental health implications of polar polycyclic aromatic hydrocarbons, *Environ. Int.*, 123, 543-557, <https://doi.org/10.1016/j.envint.2018.12.051>, 2019.

Inazu, K., Kobayashi, T., and Hisamatsu, Y.: Formation of 2-nitrofluoranthene in gas-solid heterogeneous photoreaction of fluoranthene supported on oxide particles in the presence of nitrogen dioxide, *Chemosphere*, 35, 607-622, [https://doi.org/10.1016/S0045-6535\(97\)00124-0](https://doi.org/10.1016/S0045-6535(97)00124-0), 1997.

International Agency for Research on Cancer: List of classifications, in: IARC Monographs on the Identification of Carcinogenic Hazards to Humans (Updated 2020-06-26), World Health Organization, Geneva, Switzerland, <https://monographs.iarc.fr/list-of-classifications> (last access: 04 June 2021), 2020.

IPCC: Summary for Policymakers, in: *Climate Change 2021: The Physical Science Basis. Contribution of Working Group I to the Sixth Assessment Report of the Intergovernmental Panel on Climate Change (IPCC)*, edited by: Masson-Delmotte, V., P. Zhai, A. Pirani, S. L. Connors, C. Péan, S. Berger, N. Caud, Y. Chen, L. Goldfarb, M. I. Gomis, M. Huang, K. Leitzell, E. Lonnoy, J.B.R. Matthews, T. K. Maycock, T. Waterfield, O. Yelekçi, R. Yu and B. Zhou, Cambridge University Press, UK, 41 pp., https://www.ipcc.ch/report/ar6/wg1/downloads/report/IPCC_AR6_WGI_SPM.pdf, 2021.

Isaksen, K., Nordli, Ø., Førland, E. J., Łupikasza, E., Eastwood, S., and Niedźwiedz, T.: Recent warming on Spitsbergen—Influence of atmospheric circulation and sea ice cover, *J. Geophys. Res. Atmos.*, 121, 11913-11931, <https://doi.org/10.1002/2016JD025606>, 2016.

Jakober, C. A., Riddle, S. G., Robert, M. A., Destaillets, H., Charles, M. J., Green, P. G., and Kleeman, M. J.: Quinone Emissions from Gasoline and Diesel Motor Vehicles, *Environ. Sci. Technol.*, 41, 4548-4554, <https://doi.org/10.1021/es062967u>, 2007.

Jariyasopit, N., Zimmermann, K., Schrlau, J., Arey, J., Atkinson, R., Yu, T.-W., Dashwood, R. H., Tao, S., and Simonich, S. L. M.: Heterogeneous Reactions of Particulate Matter-Bound PAHs and NPAHs with NO₃/N₂O₅, OH Radicals, and O₃ under Simulated Long-Range Atmospheric Transport Conditions: Reactivity and Mutagenicity, *Environ. Sci. Technol.*, 48, 10155-10164, <https://doi.org/10.1021/es5015407>, 2014.

Jin, R., Bu, D., Liu, G., Zheng, M., Lammel, G., Fu, J., Yang, L., Li, C., Habib, A., Yang, Y., and Liu, X.: New classes of organic pollutants in the remote continental environment – Chlorinated and brominated polycyclic aromatic hydrocarbons on the Tibetan Plateau, *Environ. Int.*, 137, 105574, <https://doi.org/10.1016/j.envint.2020.105574>, 2020a.

Jin, R., Zheng, M., Lammel, G., Bandowe, B. A. M., and Liu, G.: Chlorinated and brominated polycyclic aromatic hydrocarbons: Sources, formation mechanisms, and occurrence in the environment, *Prog. Energy Combust. Sci.*, 76, 100803, <https://doi.org/10.1016/j.pecs.2019.100803>, 2020b.

Kameda, T.: Atmospheric Reactions of PAH Derivatives: Formation and Degradation, in: *Polycyclic Aromatic Hydrocarbons: Environmental Behavior and Toxicity in East Asia*, edited by: Hayakawa, K., Springer Singapore, Singapore, 75-91, https://doi.org/10.1007/978-981-10-6775-4_7, 2018.

Karagulian, F., Belis, C. A., Dora, C. F. C., Prüss-Ustün, A. M., Bonjour, S., Adair-Rohani, H., and Amann, M.: Contributions to cities' ambient particulate matter (PM): A systematic review of local source contributions at global level, *Atmos. Environ.*, 120, 475-483, <https://doi.org/10.1016/j.atmosenv.2015.08.087>, 2015.

Keyte, I. J., Harrison, R. M., and Lammel, G.: Chemical reactivity and long-range transport potential of polycyclic aromatic hydrocarbons – a review, *Chem. Soc. Rev.*, 42, 9333-9391, <https://doi.org/10.1039/C3CS60147A>, 2013.

Kim, K.-H., Jahan, S. A., Kabir, E., and Brown, R. J. C.: A review of airborne polycyclic aromatic hydrocarbons (PAHs) and their human health effects, *Environ. Int.*, 60, 71-80, <https://doi.org/10.1016/j.envint.2013.07.019>, 2013.

Klonecki, A.: Seasonal changes in the transport of pollutants into the Arctic troposphere-model study, *J. Geophys. Res.*, 108, 8367, <http://doi.org/10.1029/2002jd002199>, 2003.

Knecht, A. L., Goodale, B. C., Truong, L., Simonich, M. T., Swanson, A. J., Matzke, M. M., Anderson, K. A., Waters, K. M., and Tanguay, R. L.: Comparative developmental toxicity of environmentally relevant oxygenated PAHs, *Toxicol. Appl. Pharmacol.*, 271, 266-275, <https://doi.org/10.1016/j.taap.2013.05.006>, 2013.

Kokhanovsky, A., and Tomasi, C.: *Physics and Chemistry of the Arctic Atmosphere*, 1 ed., Springer Polar Sciences, Springer Nature Switzerland AG, Cham, Switzerland, 717 pp., <https://doi.org/10.1007/978-3-030-33566-3>, 2020.

Kramer, A. L., Suski, K. J., Bell, D. M., Zelenyuk, A., and Massey Simonich, S. L.: Formation of Polycyclic Aromatic Hydrocarbon Oxidation Products in α -Pinene Secondary Organic Aerosol Particles Formed through Ozonolysis, *Environ. Sci. Technol.*, 53, 6669-6677, <https://doi.org/10.1021/acs.est.9b01732>, 2019.

Kukavskaya, E. A., Soja, A. J., Petkov, A. P., Ponomarev, E. I., Ivanova, G. A., and Conard, S. G.: Fire emissions estimates in Siberia: evaluation of uncertainties in area burned, land cover, and fuel consumption, *Can. J. For. Res.*, 43, 493-506, <https://doi.org/10.1139/cjfr-2012-0367>, 2013.

Kupiszewski, P., Leck, C., Tjernström, M., Sjogren, S., Sedlar, J., Graus, M., Müller, M., Brooks, B., Swietlicki, E., and Norris, S.: Vertical profiling of aerosol particles and trace gases over the central Arctic Ocean during summer, *Atmos. Chem. Phys.*, 13, 12405-12431, <https://doi.org/10.5194/acp-13-12405-2013>, 2013.

Kystdatahuset: Longyearbyen port traffic as of 2018: <https://kystdatahuset.no/> (last access: 05 June 2020), 2018.

Laender, F. D., Hammer, J., Hendriks, A. J., Soetaert, K., and Janssen, C. R.: Combining Monitoring Data and Modeling Identifies PAHs as Emerging Contaminants in the Arctic, *Environ. Sci. Technol.*, 45, 9024-9029, <https://doi.org/10.1021/es202423f>, 2011.

Lammel, G., Sehili, A. M., Bond, T. C., Feichter, J., and Grassl, H.: Gas/particle partitioning and global distribution of polycyclic aromatic hydrocarbons – A modelling approach, *Chemosphere*, 76, 98-106, <http://doi.org/10.1016/j.chemosphere.2009.02.017>, 2009.

Lammel, G.: Polycyclic Aromatic Compounds in the Atmosphere – A Review Identifying Research Needs, *Polycyclic Aromat. Compd.*, 35, 1-14, <https://doi.org/10.1080/10406638.2014.931870>, 2015a.

Lammel, G.: Long-range atmospheric transport of polycyclic aromatic hydrocarbons is worldwide problem - results from measurements at remote sites and modelling, *Acta Chimica Slovenica*, 62, 729-735, <https://doi.org/10.17344/acsi.2015.1387>, 2015b.

Lammel, G., Kitanovski, Z., Kukučka, P., Novák, J., Arangio, A. M., Codling, G. P., Filippi, A., Hovorka, J., Kuta, J., Leoni, C., Příbylová, P., Prokeš, R., Sáníka, O., Shahpoury, P., Tong, H., and Wietzorek, M.: Oxygenated and Nitrated Polycyclic Aromatic Hydrocarbons in Ambient Air - Levels, Phase Partitioning,

Mass Size Distributions, and Inhalation Bioaccessibility, *Environ. Sci. Technol.*, 54, 2615-2625, <https://doi.org/10.1021/acs.est.9b06820>, 2020.

Lanzafame, G. M., Srivastava, D., Favez, O., Bandowe, B. A. M., Shahpoury, P., Lammel, G., Bonnaire, N., Alleman, L. Y., Couvidat, F., Bessagnet, B., and Albinet, A.: One-year measurements of secondary organic aerosol (SOA) markers in the Paris region (France): Concentrations, gas/particle partitioning and SOA source apportionment, *Sci. Total Environ.*, 757, 143921, <https://doi.org/10.1016/j.scitotenv.2020.143921>, 2021.

Lawrence, H. K.: The source of US EPA's sixteen PAH priority pollutants, *Polycyclic Aromat. Compd.*, 35, 147-160, <https://doi.org/10.1080/10406638.2014.892886>, 2015.

Le Bihanic, F., Somnard, V., Perrine, d. L., Pichon, A., Grasset, J., Berrada, S., Budzinski, H., Cousin, X., Morin, B., and Cachot, J.: Environmental concentrations of benz[a]anthracene induce developmental defects and DNA damage and impair photomotor response in Japanese medaka larvae, *Ecotox. Environ. Safe.*, 113, 321-328, <http://dx.doi.org/10.1016/j.ecoenv.2014.12.011>, 2015.

Lee, J. Y., and Lane, D. A.: Unique products from the reaction of naphthalene with the hydroxyl radical, *Atmos. Environ.*, 43, 4886-4893, <https://doi.org/10.1016/j.atmosenv.2009.07.018>, 2009.

Lee, J. Y., Lane, D. A., Heo, J. B., Yi, S.-M., and Kim, Y. P.: Quantification and seasonal pattern of atmospheric reaction products of gas phase PAHs in PM_{2.5}, *Atmos. Environ.*, 55, 17-25, <https://doi.org/10.1016/j.atmosenv.2012.03.007>, 2012.

Lei, Y. D., and Wania, F.: Is rain or snow a more efficient scavenger of organic chemicals?, *Atmos. Environ.*, 38, 3557-3571, <https://doi.org/10.1016/j.atmosenv.2004.03.039>, 2004.

Letcher, R. J., Bustnes, J. O., Dietz, R., Jenssen, B. M., Jørgensen, E. H., Sonne, C., Verreault, J., Vijayan, M. M., and Gabrielsen, G. W.: Exposure and effects assessment of persistent organohalogen contaminants in arctic wildlife and fish, *Sci. Total Environ.*, 408, 2995-3043, <http://dx.doi.org/10.1016/j.scitotenv.2009.10.038>, 2010.

Liao, J., Huey, L. G., Liu, Z., Tanner, D. J., Cantrell, C. A., Orlando, J. J., Flocke, F. M., Shepson, P. B., Weinheimer, A. J., Hall, S. R., Ullmann, K., Beine, H. J., Wang, Y., Ingall, E. D., Stephens, C. R., Hornbrook, R. S., Apel, E. C., Riemer, D., Fried, A., Mauldin, R. L., Smith, J. N., Staebler, R. M., Neuman, J. A., and Nowak, J. B.: High levels of molecular chlorine in the Arctic atmosphere, *Nat. Geosci.*, 7, 91-94, <https://doi.org/10.1038/ngeo2046>, 2014.

Logan, D. T.: Perspective on ecotoxicology of PAHs to fish, *Human and Ecological Risk Assessment*, 13, 302-316, <https://doi.org/10.1080/10807030701226749>, 2007.

Lohmann, R., and Lammel, G.: Adsorptive and absorptive contributions to the gas-particle partitioning of polycyclic aromatic hydrocarbons: state of knowledge and recommended parametrization for modeling, *Environ. Sci. Technol.*, 38, 3793-3803, <http://doi.org/10.1021/es035337q>, 2004.

Lundgerdingen, K. S.: Teknisk rapport Longyearbyen Energiverket (in Norwegian), Applica Test & Certification AS, Longyearbyen, Norway, Available by request from Longyearbyen Lokaltstyre, 23 pp., 2017.

Luo, J., Han, Y., Zhao, Y., Huang, Y., Liu, X., Tao, S., Liu, J., Huang, T., Wang, L., Chen, K., and Ma, J.: Effect of northern boreal forest fires on PAH fluctuations across the arctic, *Environ. Pollut.*, 261, 114186, <https://doi.org/10.1016/j.envpol.2020.114186>, 2020.

Marchand, N., Besombes, J. L., Chevron, N., Masclet, P., Aymoz, G., and Jaffrezo, J. L.: Polycyclic aromatic hydrocarbons (PAHs) in the atmospheres of two French alpine valleys: sources and temporal patterns, *Atmos. Chem. Phys.*, 4, 1167-1181, <https://doi.org/10.5194/acp-4-1167-2004>, 2004.

Martineau, D., Lemberger, K., Dallaire, A., Labelle, P., Lipscomb Thomas, P., Michel, P., and Mikaelian, I.: Cancer in wildlife, a case study: beluga from the St. Lawrence estuary, Québec, Canada, *Environ. Health Perspect.*, 110, 285-292, <https://doi.org/10.1289/ehp.02110285>, 2002.

McDaniel, M., and Zielinska, B.: Polycyclic Aromatic Hydrocarbons in the Snowpack and Surface Water in Blackwood Canyon, Lake Tahoe, CA, as Related to Snowmobile Activity, *Polycyclic Aromat. Compd.*, 35, 102-119, <https://doi.org/10.1080/10406638.2014.935449>, 2014.

McNamara, S. M., W. Raso, A. R., Wang, S., Thanekar, S., Boone, E. J., Kolesar, K. R., Peterson, P. K., Simpson, W. R., Fuentes, J. D., Shepson, P. B., and Pratt, K. A.: Springtime Nitrogen Oxide-Influenced Chlorine Chemistry in the Coastal Arctic, *Environ. Sci. Technol.*, 53, 8057-8067, <https://doi.org/10.1021/acs.est.9b01797>, 2019.

Miet, K., Le Menach, K., Flaud, P., Budzinski, H., and Villenave, E.: Heterogeneous reactions of ozone with pyrene, 1-hydroxypyrene and 1-nitropyrene adsorbed on particles, *Atmos. Environ.*, 43, 3699-3707, <https://doi.org/10.1016/j.atmosenv.2009.04.032>, 2009.

Miljødirektoratet: Longyearbyen power plant coal and diesel consumption as of 2018: <https://www.norskeutslipp.no/no/Diverse/Virksomhet/?CompanyID=5115> (last access: 12 November 2020), 2018.

Mitchell, D. M., Osprey, S. M., Gray, L. J., Butchart, N., Hardiman, S. C., Charlton-Perez, A. J., and Watson, P.: The effect of climate change on the variability of the Northern Hemisphere stratospheric polar vortex, *J. Atmos. Sci.*, 69, 2608-2618, <https://doi.org/10.1175/JAS-D-12-021.1>, 2012.

Monks, P., and Hey, J. V.: Tropospheric chemistry and air pollution, in: *Atmospheric science for environmental scientists*, 2 ed., edited by: Hewitt, C. N., and Jackson, A. V., Wiley-Blackwell, UK, 159-202, 2020.

Monks, P. S.: Gas-phase radical chemistry in the troposphere, *Chem. Soc. Rev.*, 34, 376-395, <https://doi.org/10.1039/b307982c>, 2005.

Moorthy, B., Chu, C., and Carlin, D. J.: Polycyclic aromatic hydrocarbons: from metabolism to lung cancer, *Toxicol Sci.*, 145, 5-15, <https://doi.org/10.1093/toxsci/kfv040>, 2015.

Mu, Q., Shiraiwa, M., Octaviani, M., Ma, N., Ding, A., Su, H., Lammel, G., Pöschl, U., and Cheng, Y.: Temperature effect on phase state and reactivity controls atmospheric multiphase chemistry and transport of PAHs, *Sci. Adv.*, 4, eaap7314, <https://doi.org/10.1126/sciadv.aap7314>, 2018.

Muir, D. C. G., and Galarneau, E.: Polycyclic aromatic compounds (PACs) in the Canadian environment: Links to global change, *Environ. Pollut.*, 273, 116425, <https://doi.org/10.1016/j.envpol.2021.116425>, 2021.

Nežiková, B., Degrendele, C., Bandowe, B. A. M., Holubová Šmejkalová, A., Kukučka, P., Martíník, J., Mayer, L., Prokeš, R., Příbylová, P., Klánová, J., and Lammel, G.: Three years of atmospheric concentrations of nitrated and oxygenated polycyclic aromatic hydrocarbons and oxygen heterocycles at a central European background site, *Chemosphere*, 269, 128738, <https://doi.org/10.1016/j.chemosphere.2020.128738>, 2020.

Nfon, E., Cousins, I. T., and Broman, D.: Biomagnification of organic pollutants in benthic and pelagic marine food chains from the Baltic Sea, *Sci. Total Environ.*, 397, 190-204, <http://dx.doi.org/10.1016/j.scitotenv.2008.02.029>, 2008.

Nilsen, F., Skogseth, R., Vaardal-Lunde, J., and Inall, M.: A simple shelf circulation model: Intrusion of Atlantic water on the West Spitsbergen shelf, *J. Phys. Oceanogr.*, 46, 1209-1230, <https://doi.org/10.1175/JPO-D-15-0058.1>, 2016.

Nisbet, I. C. T., and LaGoy, P. K.: Toxic equivalency factors (TEFs) for polycyclic aromatic hydrocarbons (PAHs), *Regul. Toxicol. Pharm.*, 16, 290-300, [https://doi.org/10.1016/0273-2300\(92\)90009-X](https://doi.org/10.1016/0273-2300(92)90009-X), 1992.

Niu, J., Sun, P., and Schramm, K.-W.: Photolysis of polycyclic aromatic hydrocarbons associated with fly ash particles under simulated sunlight irradiation, *J. Photochem. Photobiol. A*, 186, 93-98, <https://doi.org/10.1016/j.jphotochem.2006.07.016>, 2007.

Nováková, Z., Novák, J., Kitanovski, Z., Kukučka, P., Smutná, M., Wietzorek, M., Lammel, G., and Hilscherová, K.: Toxic potentials of particulate and gaseous air pollutant mixtures and the role of PAHs and their derivatives, *Environ. Int.*, 139, 105634, <https://doi.org/10.1016/j.envint.2020.105634>, 2020.

Oanh, P. K., Kazushi, N., Yoshie, N., Tatsuya, T., Yusuke, F., Miho, A., Toshimitsu, S., Kenji, K., Hideaki, M., Hien, T. O. T., and Norimichi, T.: Concentrations of polycyclic aromatic hydrocarbons in Antarctic snow polluted by research activities using snow mobiles and diesel electric generators, *Bull. Glaciol. Res.*, 37, 23-30, <https://doi.org/10.5331/bgr.19A02>, 2019.

Oda, J., Nomura, S., Yasuhara, A., and Shibamoto, T.: Mobile sources of atmospheric polycyclic aromatic hydrocarbons in a roadway tunnel, *Atmos. Environ.*, 35, 4819-4827, [https://doi.org/10.1016/S1352-2310\(01\)00262-X](https://doi.org/10.1016/S1352-2310(01)00262-X), 2001.

OEHHA: Technical support document for cancer potency factors: Methodologies for derivation, listing of available values, and adjustments to allow for early life stage exposures, Office of Environmental Health Hazard Assessment (OEHHA), California EPA, USA, 88 pp., <https://oehha.ca.gov/media/downloads/crntr/tsdcancerpotency.pdf>, 2009.

Onarheim, I. H., Smedsrud, L. H., Ingvaldsen, R. B., and Nilsen, F.: Loss of sea ice during winter north of Svalbard, *Tellus Ser. A*, 66, 23933, <https://doi.org/10.3402/tellusa.v66.23933>, 2014.

Onduka, T., Ojima, D., Kakuno, A., Ito, K., Koyama, J., and Fujii, K.: Nitrated polycyclic aromatic hydrocarbons in the marine environment: acute toxicities for organisms at three trophic levels, *Jpn. J. Environ. Toxicol.*, 15, 1-10, <https://doi.org/10.11403/jset.15.1>, 2012.

Onduka, T., Ojima, D., Ito, K., Mochida, K., Koyama, J., and Fujii, K.: Reproductive toxicity of 1-nitronaphthalene and 1-nitropyrene exposure in the mummichog, *Fundulus heteroclitus*, *Ecotoxicology*, 24, 648-656, <https://doi.org/10.1007/s10646-014-1412-6>, 2015.

Ontario Ministry of the Environment and Climate Change: Ambient Air Quality Criteria, Toronto, Canada, 45 pp., <https://www.ontario.ca/page/ontarios-ambient-air-quality-criteria-sorted-contaminant-name>, 2020.

OSPAR: Background Document on Polycyclic Aromatic Hydrocarbons (PAHs), Oil Spill Prevention, Administration and Response (OSPAR), 34 pp., <https://www.ospar.org/work-areas/hasec/hazardous-substances/priority-action>, 2009.

PAME: The increase in Arctic shipping 2013-2019. Arctic shipping status report #1, Protection of the Arctic marine environment (PAME), 11 pp., <https://storymaps.arcgis.com/stories/592bfe70251741b48b0a9786b75ff5d0>, 2020.

Pampanin, D. M., and Sydnes, M. O.: Polycyclic Aromatic Hydrocarbons a Constituent of Petroleum: Presence and Influence in the Aquatic Environment, in: Hydrocarbon, edited by: Kutcherov, V., and Kolesnikov, A., InTech, Rijeka, Croatia, 83-118, <http://dx.doi.org/10.5772/48176>, 2013.

Pankow, J. F.: An absorption model of gas/particle partitioning of organic compounds in the atmosphere, *Atmos. Environ.*, 28, 185-188, [https://doi.org/10.1016/1352-2310\(94\)90093-0](https://doi.org/10.1016/1352-2310(94)90093-0), 1994.

Peng, N., Li, Y., Liu, Z., Liu, T., and Gai, C.: Emission, distribution and toxicity of polycyclic aromatic hydrocarbons (PAHs) during municipal solid waste (MSW) and coal co-combustion, *Sci. Total Environ.*, 565, 1201-1207, <https://doi.org/10.1016/j.scitotenv.2016.05.188>, 2016.

Perera, F., Tang, D., Whyatt, R., Lederman, S. A., and Jedrychowski, W.: DNA damage from polycyclic aromatic hydrocarbons measured by benzo[a]pyrene - DNA adducts in mothers and newborns from Northern Manhattan, the World Trade Center Area, Poland, and China, *Cancer Epidemiology and Prevention Biomarkers*, 14, 709-714, <https://doi.org/10.1158/1055-9965.EPI-04-0457>, 2005.

Perera, F., Ashrafi, A., Kinney, P., and Mills, D.: Towards a fuller assessment of benefits to children's health of reducing air pollution and mitigating climate change due to fossil fuel combustion, *Environ. Res.*, 172, 55-72, <https://doi.org/10.1016/j.envres.2018.12.016>, 2019.

Perraudin, E., Budzinski, H., and Villenave, E.: Identification and quantification of ozonation products of anthracene and phenanthrene adsorbed on silica particles, *Atmos. Environ.*, 41, 6005-6017, <https://doi.org/10.1016/j.atmosenv.2007.03.010>, 2007.

Petersen, G. I., and Kristensen, P.: Bioaccumulation of lipophilic substances in fish early life stages, *Environ. Toxicol. Chem.*, 17, 1385-1395, <https://doi.org/10.1002/etc.5620170724>, 1998.

Peterson, P. K., Simpson, W. R., Pratt, K. A., Shepson, P. B., Frieß, U., Zielcke, J., Platt, U., Walsh, S. J., and Nghiem, S. V.: Dependence of the vertical distribution of bromine monoxide in the lower troposphere on meteorological factors such as wind speed and stability, *Atmos. Chem. Phys.*, 15, 2119-2137, <https://doi.org/10.5194/acp-15-2119-2015>, 2015.

Pio, C., Cerqueira, M., Harrison, R. M., Nunes, T., Mirante, F., Alves, C., Oliveira, C., Sanchez De La Campa, A., Artíñano, B., and Matos, M.: OC/EC ratio observations in Europe: Re-thinking the approach for apportionment between primary and secondary organic carbon, *Atmos. Environ.*, 45, 6121-6132, <https://doi.org/10.1016/j.atmosenv.2011.08.045>, 2011.

Poirier, M. C., Lair, S., Michaud, R., Hernández-Ramon, E. E., Divi, K. V., Dwyer, J. E., Ester, C. D., Si, N. N., Ali, M., Loseto, L. L., Raverty, S. A., St. Leger, J. A., Van Bonn, W. G., Colegrove, K., Burek-Huntington, K. A., Suydam, R., Stimmelmayer, R., Wise, J. P., Wise, S. S., Beauchamp, G., and Martineau, D.: Intestinal polycyclic aromatic hydrocarbon - DNA adducts in a population of beluga whales with high levels of gastrointestinal cancers, *Environ. Mol. Mutagen.*, 60, 29-41, <https://doi.org/10.1002/em.22251>, 2019.

Prevedouros, K., Brorström-Lundén, E., J. Halsall, C., Jones, K. C., Lee, R. G. M., and Sweetman, A. J.: Seasonal and long-term trends in atmospheric PAH concentrations: evidence and implications, *Environ. Pollut.*, 128, 17-27, <https://doi.org/10.1016/j.envpol.2003.08.032>, 2004.

Qu, X., Zhang, Q., and Wang, W.: Mechanism for OH-initiated photooxidation of naphthalene in the presence of O₂ and NO_x: A DFT study, *Chem. Phys. Lett.*, 429, 77-85, <https://doi.org/10.1016/j.cplett.2006.08.036>, 2006.

Ramesh, A., and Archibong, A. E.: Chapter 43 - Reproductive toxicity of polycyclic aromatic hydrocarbons: occupational relevance, in: *Reproductive and Developmental Toxicology*, edited by: Gupta, R. C., Academic Press, San Diego, California, USA, 577-591, <https://doi.org/10.1016/B978-0-12-382032-7.10043-8>, 2011.

Raso, A. R.: Iodine, Bromine, and Chlorine in the Arctic atmosphere – Emission Rates, Sources, and Impacts, Doctoral thesis, Purdue University, West Lafayette, Indiana, USA, 249 pp., <https://doi.org/10.25394/PGS.7479356.v1>, 2018.

Raso, A. R. W., Custard, K. D., May, N. W., Tanner, D., Newburn, M. K., Walker, L., Moore, R. J., Huey, L. G., Alexander, L., Shepson, P. B., and Pratt, K. A.: Active molecular iodine photochemistry in the Arctic, *Proceedings of the National Academy of Sciences*, 114, 10053-10058, <https://doi.org/10.1073/pnas.1702803114>, 2017.

Ravindra, K., Sokhi, R., and Van Grieken, R.: Atmospheric polycyclic aromatic hydrocarbons: Source attribution, emission factors and regulation, *Atmos. Environ.*, 42, 2895-2921, <https://doi.org/10.1016/j.atmosenv.2007.12.010>, 2008.

Reimann, S., Kallenborn, R., and Schmidbauer, N.: Severe Aromatic Hydrocarbon Pollution in the Arctic Town of Longyearbyen (Svalbard) Caused by Snowmobile Emissions, *Environ. Sci. Technol.*, 43, 4791-4795, <https://doi.org/10.1021/es900449x>, 2009.

Reisen, F., and Arey, J.: Reactions of Hydroxyl Radicals and Ozone with Acenaphthene and Acenaphthylene, *Environ. Sci. Technol.*, 36, 4302-4311, <https://doi.org/10.1021/es025761b>, 2002.

Rhea, D. T., Gale, R. W., Orazio, C. E., Peterman, P. H., Harper, D. D., and Farag, A. M.: Polycyclic aromatic hydrocarbons in water, sediment, and snow, from lakes in Grand Teton National Park, Wyoming, USGS-CERC, Columbia, South Carolina, USA, 91344, 30 pp., https://www.cerc.usgs.gov/pubs/center/pdfDocs/PAH_2-05.pdf, 2005.

Rindone, B., Saliu, F., and Suarez-Bertoa, R.: The Synthesis of Phthalic Anhydride via Ozonation of Naphthalene, *Ozone Sci. Eng.*, 32, 161-165, <https://doi.org/10.1080/01919511003788001>, 2010.

Ringuet, J., Albinet, A., Leoz-Garziandia, E., Budzinski, H., and Villenave, E.: Diurnal/nocturnal concentrations and sources of particulate-bound PAHs, OPAHs and NPAHs at traffic and suburban sites in the region of Paris (France), *Sci. Total Environ.*, 437, 297-305, <https://doi.org/10.1016/j.scitotenv.2012.07.072>, 2012a.

Ringuet, J., Albinet, A., Leoz-Garziandia, E., Budzinski, H., and Villenave, E.: Reactivity of polycyclic aromatic compounds (PAHs, NPAHs and OPAHs) adsorbed on natural aerosol particles exposed to atmospheric oxidants, *Atmos. Environ.*, 61, 15-22, <https://doi.org/10.1016/j.atmosenv.2012.07.025>, 2012b.

Riva, M., Healy, R. M., Flaud, P.-M., Perraudin, E., Wenger, J. C., and Villenave, E.: Kinetics of the gas-phase reactions of chlorine atoms with naphthalene, acenaphthene, and acenaphthylene, *J. Phys. Chem. A*, 118, 3535-3540, <https://doi.org/10.1021/jp500943a>, 2014.

Riva, M., Healy, R. M., Flaud, P.-M., Perraudin, E., Wenger, J. C., and Villenave, E.: Gas- and Particle-Phase Products from the Chlorine-Initiated Oxidation of Polycyclic Aromatic Hydrocarbons, *J. Phys. Chem. A*, 119, 11170-11181, <https://doi.org/10.1021/acs.jpca.5b04610>, 2015.

Riva, M., Healy, R. M., Tomaz, S., Flaud, P.-M., Perraudin, E., Wenger, J. C., and Villenave, E.: Gas and particulate phase products from the ozonolysis of acenaphthylene, *Atmos. Environ.*, 142, 104-113, <https://doi.org/10.1016/j.atmosenv.2016.07.012>, 2016.

Robinson, A. L., Donahue, N. M., Shrivastava, M. K., Weitkamp, E. A., Sage, A. M., Grieshop, A. P., Lane, T. E., Pierce, J. R., and Pandis, S. N.: Rethinking organic aerosols: Semivolatile emissions and photochemical aging, *Science*, 315, 1259-1262, <https://doi.org/10.1126/science.1133061>, 2007.

Routti, H., Atwood, T. C., Bechshoft, T., Boltunov, A., Ciesielski, T. M., Desforges, J.-P., Dietz, R., Gabrielsen, G. W., Jenssen, B. M., Letcher, R. J., McKinney, M. A., Morris, A. D., Rigét, F. F., Sonne, C., Styriahve, B., and Tartu, S.: State of knowledge on current exposure, fate and potential health effects of contaminants in polar bears from the circumpolar Arctic, *Sci. Total Environ.*, 664, 1063-1083, <https://doi.org/10.1016/j.scitotenv.2019.02.030>, 2019.

Röhler, L., Schlabach, M., Haglund, P., Breivik, K., Kallenborn, R., and Bohlin-Nizzetto, P.: Non-target and suspect characterisation of organic contaminants in Arctic air – Part 2: Application of a new tool for identification and prioritisation of chemicals of emerging Arctic concern in air, *Atmos. Chem. Phys.*, 20, 9031-9049, <https://doi.org/10.5194/acp-20-9031-2020>, 2020.

Samburova, V., Zielinska, B., and Khlystov, A.: Do 16 Polycyclic Aromatic Hydrocarbons Represent PAH Air Toxicity?, *Toxics*, 5, 17, <https://doi.org/10.3390/toxics5030017>, 2017.

Sankoda, K., Nomiya, K., Kuribayashi, T., and Shinohara, R.: Halogenation of Polycyclic Aromatic Hydrocarbons by Photochemical Reaction under Simulated Tidal Flat Conditions, *Polycyclic Aromat. Compd.*, 33, 236-253, <https://doi.org/10.1080/10406638.2013.770406>, 2013.

Serreze, M. C., Barrett, A. P., Slater, A. G., Steele, M., Zhang, J., and Trenberth, K. E.: The large-scale energy budget of the Arctic, *J. Geophys. Res.*, 112, D11122, <https://doi.org/10.1029/2006jd008230>, 2007.

Serreze, M. C., Barrett, A. P., Stroeve, J. C., Kindig, D. N., and Holland, M. M.: The emergence of surface-based Arctic amplification, *The Cryosphere*, 3, 11-19, <https://doi.org/10.5194/tc-3-11-2009>, 2009.

Serreze, M. C., and Barry, R. G.: *The Arctic climate system*, Cambridge Atmospheric and Space Science Series, edited by: Dessler, A. J., Houghton, J. T., and Rycroft, M. J., Cambridge University Press, UK, 404 pp., <https://doi.org/10.1017/CB09781139583817>, 2014.

Shahpoury, P., Lammel, G., Albinet, A., Sofuoğlu, A., Dumanoğlu, Y., Sofuoğlu, S. C., Wagner, Z., and Zdimar, V.: Evaluation of a Conceptual Model for Gas-Particle Partitioning of Polycyclic Aromatic Hydrocarbons Using Polyparameter Linear Free Energy Relationships, *Environ. Sci. Technol.*, 50, 12312-12319, <https://doi.org/10.1021/acs.est.6b02158>, 2016.

Shahpoury, P., Kitanovski, Z., Lammel, G. J. A. C., and Physics: Snow scavenging and phase partitioning of nitrated and oxygenated aromatic hydrocarbons in polluted and remote environments in central Europe and the European Arctic, *Atmos. Chem. Phys.*, 18, 13495-13510, <https://doi.org/10.5194/acp-18-13495-2018>, 2018.

Shen, H., Huang, Y., Wang, R., Zhu, D., Li, W., Shen, G., Wang, B., Zhang, Y., Chen, Y., Lu, Y., Chen, H., Li, T., Sun, K., Li, B., Liu, W., Liu, J., and Tao, S.: Global Atmospheric Emissions of Polycyclic Aromatic

Hydrocarbons from 1960 to 2008 and Future Predictions, *Environ. Sci. Technol.*, 47, 6415-6424, <https://doi.org/10.1021/es400857z>, 2013.

Shimada, T.: Xenobiotic-Metabolizing Enzymes Involved in Activation and Detoxification of Carcinogenic Polycyclic Aromatic Hydrocarbons, *Drug Metab. Pharmacokinet.*, 21, 257-276, <https://doi.org/10.2133/dmpk.21.257>, 2006.

Shively, D. D., Pape, B. M. C., Mower, R. N., Zhou, Y., Russo, R., and Sive, B. C.: Blowing Smoke in Yellowstone: Air Quality Impacts of Oversnow Motorized Recreation in the Park, *Environmental Management*, 41, 183-199, <https://doi.org/10.1007/s00267-007-9036-8>, 2008.

Sihler, H., Platt, U., Beirle, S., Marbach, T., Kühl, S., Dörner, S., Verschaeve, J., Frieß, U., Pöhler, D., Vogel, L., Sander, R., and Wagner, T.: Tropospheric BrO column densities in the Arctic derived from satellite: retrieval and comparison to ground-based measurements, *Atmos. Meas. Tech.*, 5, 2779-2807, <https://doi.org/10.5194/amt-5-2779-2012>, 2012.

Simcik, M. F.: The importance of surface adsorption on the washout of semivolatile organic compounds by rain, *Atmos. Environ.*, 38, 491-501, <https://doi.org/10.1016/j.atmosenv.2003.09.013>, 2004.

Simoneit, B. R. T., Schauer, J. J., Nolte, C. G., Oros, D. R., Elias, V. O., Fraser, M. P., Rogge, W. F., and Cass, G. R.: Levoglucosan, a tracer for cellulose in biomass burning and atmospheric particles, *Atmos. Environ.*, 33, 173-182, [https://doi.org/10.1016/S1352-2310\(98\)00145-9](https://doi.org/10.1016/S1352-2310(98)00145-9), 1999.

Simpson, W. R., von Glasow, R., Riedel, K., Anderson, P., Ariya, P., Bottenheim, J., Burrows, J., Carpenter, L. J., Frieß, U., Goodsite, M. E., Heard, D., Hutterli, M., Jacobi, H. W., Kaleschke, L., Neff, B., Plane, J., Platt, U., Richter, A., Roscoe, H., Sander, R., Shepson, P., Sodeau, J., Steffen, A., Wagner, T., and Wolff, E.: Halogens and their role in polar boundary-layer ozone depletion, *Atmos. Chem. Phys.*, 7, 4375-4418, <https://doi.org/10.5194/acp-7-4375-2007>, 2007.

Simpson, W. R., Brown, S. S., Saiz-Lopez, A., Thornton, J. A., and von Glasow, R.: Tropospheric Halogen Chemistry: Sources, Cycling, and Impacts, *Chem. Rev.*, 115, 4035-4062, <https://doi.org/10.1021/cr5006638>, 2015.

Simpson, W. R., Peterson, P. K., Frieß, U., Sihler, H., Lampel, J., Platt, U., Moore, C., Pratt, K., Shepson, P., Halfacre, J., and Nghiem, S. V.: Horizontal and vertical structure of reactive bromine events probed by bromine monoxide MAX-DOAS, *Atmos. Chem. Phys.*, 17, 9291-9309, <https://doi.org/10.5194/acp-17-9291-2017>, 2017.

Singh, D. K., Kawamura, K., Yanase, A., and Barrie, L. A.: Distributions of polycyclic aromatic hydrocarbons, aromatic ketones, carboxylic acids, and trace metals in Arctic aerosols: Long-range atmospheric transport, photochemical degradation/production at polar sunrise, *Environ. Sci. Technol.*, 51, 8992-9004, <https://doi.org/10.1021/acs.est.7b01644>, 2017.

Sive, B. C., Shively, D., and Pape, B.: Spatial variation of volatile organic compounds associated with snowmobile emissions in Yellowstone National Park, U.S. National Park Service, 85 pp., https://www.nps.gov/yell/learn/management/upload/sive_report.pdf, 2003.

Škrdlíková, L., Landlová, L., Klánová, J., and Lammel, G.: Wet deposition and scavenging efficiency of gaseous and particulate phase polycyclic aromatic compounds at a central European suburban site, *Atmos. Environ.*, 45, 4305-4312, <https://doi.org/10.1016/j.atmosenv.2011.04.072>, 2011.

Sofowote, U. M., Hung, H., Rastogi, A. K., Westgate, J. N., Deluca, P. F., Su, Y., and McCarry, B. E.: Assessing the long-range transport of PAH to a sub-Arctic site using positive matrix factorization and potential source contribution function, *Atmos. Environ.*, 45, 967-976, <https://doi.org/10.1016/j.atmosenv.2010.11.005>, 2011.

Solberg, S., Schmidbauer, N., Semb, A., Stordal, F., and Hov, Ø.: Boundary-layer ozone depletion as seen in the Norwegian Arctic in spring, *J. Atmos. Chem.*, 23, 301-332, 1996.

Solberg, S., Krognnes, T., Stordal, F., Hov, O., Beine, H. J., Jaffe, D. A., Clemitshaw, K. C., and Penkett, S. A.: Reactive Nitrogen Compounds at Spitsbergen in the Norwegian Arctic, *J. Atmos. Chem.*, 28, 209-225, <https://doi.org/10.1023/A:1005883323285>, 1997.

Sonne, C., Dietz, R., Jenssen, B. M., Lam, S. S., and Letcher, R. J.: Emerging contaminants and biological effects in Arctic wildlife, *Trends Ecol. Evol.*, 36, 421-429, <https://doi.org/10.1016/j.tree.2021.01.007>, 2021.

Spielhagen, R. F., Werner, K., Sørensen, S. A., Zamelczyk, K., Kandiano, E., Budeus, G., Husum, K., Marchitto, T. M., and Hald, M.: Enhanced modern heat transfer to the Arctic by warm Atlantic water, *Science*, 331, 450-453, <https://doi.org/10.1126/science.1197397>, 2011.

Srivastava, D., Favez, O., Bonnaire, N., Lucarelli, F., Haefelin, M., Perraudin, E., Gros, V., Villenave, E., and Albinet, A.: Speciation of organic fractions does matter for aerosol source apportionment. Part 2: Intensive short-term campaign in the Paris area (France), *Sci. Total Environ.*, 634, 267-278, <https://doi.org/10.1016/j.scitotenv.2018.03.296>, 2018a.

Srivastava, D., Favez, O., Perraudin, E., Villenave, E., and Albinet, A.: Comparison of Measurement-Based Methodologies to Apportion Secondary Organic Carbon (SOC) in PM_{2.5}: A Review of Recent Studies, *Atmosphere*, 9, 452, <https://doi.org/10.3390/atmos9110452>, 2018b.

Srivastava, D., Tomaz, S., Favez, O., Lanzafame, G. M., Golly, B., Besombes, J.-L., Alleman, L. Y., Jaffrezo, J.-L., Jacob, V., Perraudin, E., Villenave, E., and Albinet, A.: Speciation of organic fraction does matter for source apportionment. Part 1: A one-year campaign in Grenoble (France), *Sci. Total Environ.*, 624, 1598-1611, <https://doi.org/10.1016/j.scitotenv.2017.12.135>, 2018c.

Srivastava, D., Daellenbach, K. R., Zhang, Y., Bonnaire, N., Chazeau, B., Perraudin, E., Gros, V., Lucarelli, F., Villenave, E., Prévôt, A. S. H., El Haddad, I., Favez, O., and Albinet, A.: Comparison of five methodologies to apportion organic aerosol sources during a PM pollution event, *Sci. Total Environ.*, 757, 143168, <https://doi.org/10.1016/j.scitotenv.2020.143168>, 2021.

Statistics Norway: This is Svalbard 2016. What the figures say, Oslo, Norway, 28 pp., <https://www.ssb.no/en/befolkning/artikler-og-publikasjoner/this-is-svalbard-2016>, 2016.

Statistics Norway: Registered vehicles, by region, statistical variable per year, data for 2018: <https://www.ssb.no/statbank/table/11823/> (last access: 05 June 2020), 2018.

Statistics Norway: Longyearbyen and Ny-Ålesund population as of 4th May 2021: <https://www.ssb.no/befolkning/folketall/statistikk/befolkningen-pa-svalbard> (last access: 25 June 2021), 2021.

Stein, A., Draxler, R. R., Rolph, G. D., Stunder, B. J., Cohen, M., and Ngan, F.: NOAA's HYSPLIT atmospheric transport and dispersion modeling system, *Bull. Am. Meteorol. Soc.*, 96, 2059-2077, <https://doi.org/10.1175/BAMS-D-14-00110.1>, 2015.

Stohl, A., Forster, C., Frank, A., Seibert, P., and Wotawa, G.: Technical note: The Lagrangian particle dispersion model FLEXPART version 6.2, *Atmos. Chem. Phys.*, 5, 2461-2474, <https://doi.org/10.5194/acp-5-2461-2005>, 2005.

Stohl, A.: Characteristics of atmospheric transport into the Arctic troposphere, *J. Geophys. Res. Atmos.*, 111, D11306, <https://doi.org/10.1029/2005jd006888>, 2006.

Strong, K., Simpson, W. R., Bognar, K., Lindenmaier, R., and Roche, S.: Trace Gases in the Arctic Atmosphere, in: *Physics and Chemistry of the Arctic Atmosphere*, edited by: Kokhanovsky, A., and Tomasi, C., Springer International Publishing, Cham, Switzerland, 153-207, https://doi.org/10.1007/978-3-030-33566-3_3, 2020.

Su, Y., Lei, Y. D., Wania, F., Shoeib, M., and Harner, T.: Regressing Gas/Particle Partitioning Data for Polycyclic Aromatic Hydrocarbons, *Environ. Sci. Technol.*, 40, 3558-3564, <https://doi.org/10.1021/es052496w>, 2006.

Svavarsson, J., Guls, H. D., Sham, R. C., Leung, K. M. Y., and Halldórsson, H. P.: Pollutants from shipping - new environmental challenges in the subarctic and the Arctic Ocean, *Mar. Pollut. Bull.*, 164, 112004, <https://doi.org/10.1016/j.marpolbul.2021.112004>, 2021.

Tarafdar, A., and Sinha, A.: Polycyclic Aromatic Hydrocarbons (PAHs) Pollution Generated from Coal-Fired Thermal Power Plants: Formation Mechanism, Characterization, and Profiling: Characterization and Control, in: *Pollutants from Energy Sources*, edited by: Agarwal, R. A., Agarwal, A. K., Gupta, T., and Sharma, N., Energy, Environment, and Sustainability, Springer Nature Singapore Pte. Ltd., Singapore, 73-90, https://doi.org/10.1007/978-981-13-3281-4_5, 2019.

Tartu, S., Lille-Langøy, R., Størseth, T. R., Bourgeon, S., Brunsvik, A., Aars, J., Goksøyr, A., Jenssen, B. M., Polder, A., Thiemann, G. W., Torget, V., and Routti, H.: Multiple-stressor effects in an apex predator: combined influence of pollutants and sea ice decline on lipid metabolism in polar bears, *Sci. Rep.*, 7, 16487, <https://doi.org/10.1038/s41598-017-16820-5>, 2017.

Thompson, C. R., Shepson, P. B., Liao, J., Huey, L. G., Apel, E. C., Cantrell, C. A., Flocke, F., Orlando, J., Fried, A., Hall, S. R., Hornbrook, R. S., Knapp, D. J., Mauldin Iii, R. L., Montzka, D. D., Sive, B. C., Ullmann, K., Weibring, P., and Weinheimer, A.: Interactions of bromine, chlorine, and iodine photochemistry during ozone depletions in Barrow, Alaska, *Atmos. Chem. Phys.*, 15, 9651-9679, <https://doi.org/10.5194/acp-15-9651-2015>, 2015.

Thuens, S., Blodau, C., Wania, F., and Radke, M.: Comparison of Atmospheric Travel Distances of Several PAHs Calculated by Two Fate and Transport Models (The Tool and ELPOS) with Experimental Values Derived from a Peat Bog Transect, *Atmosphere*, 5, 324-341, <https://doi.org/10.3390/atmos5020324>, 2014.

Tisch Environmental Inc.: Operation manual, TE-1000BL PUF Poly-Urethane Foam, High Volume Air Sampler, Cleves, Ohio, USA, 36 pp., 2021.

Tomaz, S., Shahpoury, P., Jaffrezo, J.-L., Lammel, G., Perraudin, E., Villenave, E., and Albinet, A.: One-year study of polycyclic aromatic compounds at an urban site in Grenoble (France): Seasonal variations, gas/particle partitioning and cancer risk estimation, *Sci. Total Environ.*, 565, 1071-1083, <http://doi.org/10.1016/j.scitotenv.2016.05.137>, 2016.

Tomaz, S., Jaffrezo, J.-L., Favez, O., Perraudin, E., Villenave, E., and Albinet, A.: Sources and atmospheric chemistry of oxy- and nitro-PAHs in the ambient air of Grenoble (France), *Atmos. Environ.*, 161, 144-154, <https://doi.org/10.1016/j.atmosenv.2017.04.042>, 2017.

UK Air DEFRA: The air quality strategy for England, Scotland, Wales and Northern Ireland, Department for Environment, Food and Rural Affairs (DEFRA), UK Air, 1, 56 pp., https://assets.publishing.service.gov.uk/government/uploads/system/uploads/attachment_data/file/69336/pb12654-air-quality-strategy-vol1-070712.pdf, 2007.

United Nations Economic Commission for Europe UNECE: The 1998 Aarhus protocol on persistent organic pollutants (POPs), UNECE, Aarhus, Danmark, 49 pp., https://www.unece.org/env/lrtap/pops_h1.html, 1998.

US EPA: Compendium of Methods for the Determination of Toxic Organic Compounds in Ambient Air. Second Edition. Compendium Method TO-13A. Determination of Polycyclic Aromatic Hydrocarbons (PAHs) in Ambient Air Using Gas Chromatography/Mass Spectrometry (GC/MS), US EPA, Cincinnati, Ohio, USA, 84 pp., <https://www.epa.gov/sites/production/files/2019-11/documents/to-13arr.pdf>, 1999.

US EPA: Polycyclic Aromatic Hydrocarbons on the Gulf Coastline: [https://archive.epa.gov/emergency/bpspill/web/html/pahs.html#:~:text=Polycyclic%20Aromatic%20Hydrocarbons%20\(PAHs\)%20are,commonly%20called%20'weathered%20oil'](https://archive.epa.gov/emergency/bpspill/web/html/pahs.html#:~:text=Polycyclic%20Aromatic%20Hydrocarbons%20(PAHs)%20are,commonly%20called%20'weathered%20oil') (last access: 04 July 2021), 2011.

Vestreng, V., Kallenborn, R., and Økstad, E.: Norwegian Arctic climate: climate influencing emissions, scenarios and mitigation options at Svalbard, Miljødirektoratet, Oslo, Norway, 56 pp., <https://www.miljodirektoratet.no/globalassets/publikasjoner/klif2/publikasjoner/2552/ta2552.pdf>, 2009.

Vignet, C., Le Menach, K., Mazurais, D., Lucas, J., Perrichon, P., and Le Bihanic, F.: Chronic dietary exposure to pyrolytic and petrogenic mixtures of Pahs causes physiological disruption in zebrafish - Part 1: Survival and growth, *Environ. Sci. Pollut. Res.*, 21, 13804–13817, <https://doi.org/10.1007/s11356-014-2629-x>, 2014.

Vihma, T., Pirazzini, R., Fer, I., Renfrew, I. A., Sedlar, J., Tjernström, M., Lüpkes, C., Nygård, T., Notz, D., Weiss, J., Marsan, D., Cheng, B., Birnbaum, G., Gerland, S., Chechin, D., and Gascard, J. C.: Advances in understanding and parameterization of small-scale physical processes in the marine Arctic climate system: a review, *Atmos. Chem. Phys.*, 14, 9403-9450, <https://doi.org/10.5194/acp-14-9403-2014>, 2014.

Vikelsøe, J., Thomsen, M., Carlsen, L., Johansen, E., : Persistent Organic Pollutants in Soil, Sludge and Sediment. A Multianalytical Field Study of Selected Organic Chlorinated and Brominated Compounds, National Environmental Research Institute (NERI), Ministry of the Environment, Copenhagen, Denmark, 402, 98 pp., https://www.dmu.dk/1_viden/2_Publikationer/3_fagrappporter/rapporter/FR402.pdf, 2002.

Vione, D., Barra, S., de Gennaro, G., de Rienzo, M., Gilardoni, S., Perrone, M. G., and Pozzoli, L.: Polycyclic Aromatic Hydrocarbons in the Atmosphere: Monitoring, Sources, Sinks and Fate. II: Sinks and Fate, *Ann. Chim. (Rome)*, 94, 257-268, <https://doi.org/10.1002/adic.200490031>, 2004.

Walgraeve, C., Demeestere, K., Dewulf, J., Zimmermann, R., and Van Langenhove, H.: Oxygenated polycyclic aromatic hydrocarbons in atmospheric particulate matter: Molecular characterization and occurrence, *Atmos. Environ.*, 44, 1831-1846, <https://doi.org/10.1016/j.atmosenv.2009.12.004>, 2010.

Wallace, S. J., de Solla, S. R., Head, J. A., Hodson, P. V., Parrott, J. L., Thomas, P. J., Berthiaume, A., and Langlois, V. S.: Polycyclic aromatic compounds (PACs) in the Canadian environment: Exposure and effects on wildlife, *Environ. Pollut.*, 265, 114863, <https://doi.org/10.1016/j.envpol.2020.114863>, 2020.

Walsh, J. E.: Intensified warming of the Arctic: Causes and impacts on middle latitudes, *Global Planet. Change*, 117, 52-63, <https://doi.org/10.1016/j.gloplacha.2014.03.003>, 2014.

Wang, R., Tao, S., Wang, B., Yang, Y., Lang, C., Zhang, Y., Hu, J., Ma, J., and Hung, H.: Sources and Pathways of Polycyclic Aromatic Hydrocarbons Transported to Alert, the Canadian High Arctic, *Environ. Sci. Technol.*, 44, 1017-1022, <https://doi.org/10.1021/es902203w>, 2010.

Wang, R., Liu, G., and Zhang, J.: Variations of emission characterization of PAHs emitted from different utility boilers of coal-fired power plants and risk assessment related to atmospheric PAHs, *Sci. Total Environ.*, 538, 180-190, <http://doi.org/10.1016/j.scitotenv.2015.08.043>, 2015.

Wang, W., Jariyasopit, N., Schrlau, J., Jia, Y., Tao, S., Yu, T.-W., Dashwood, R. H., Zhang, W., Wang, X., and Simonich, S. L. M.: Concentration and Photochemistry of PAHs, NPAHs, and OPAHs and Toxicity of PM_{2.5} during the Beijing Olympic Games, *Environ. Sci. Technol.*, 45, 6887-6895, <https://doi.org/10.1021/es201443z>, 2011.

Wania, F., Mackay, D., and Hoff, J. T.: The importance of snow scavenging of polychlorinated biphenyl and polycyclic aromatic hydrocarbon vapors, *Environ. Sci. Technol.*, 33, 195-197, <https://doi.org/10.1021/es980806n>, 1999.

Warner, S. D., Farant, J.-P., and Butler, I. S.: Photochemical degradation of selected nitropolycyclic aromatic hydrocarbons in solution and adsorbed to solid particles, *Chemosphere*, 54, 1207-1215, <https://doi.org/10.1016/j.chemosphere.2003.09.020>, 2004.

Watt, D. L., Utzat, C. D., Hilario, P., and Basu, A. K.: Mutagenicity of the 1-Nitropyrene-DNA Adduct N-(Deoxyguanosin-8-yl)-1-aminopyrene in Mammalian Cells, *Chem. Res. Toxicol.*, 20, 1658-1664, <https://doi.org/10.1021/tx700131e>, 2007.

Weinbruch, S., Benker, N., Kandler, K., Schütze, K., Kling, K., Berlinger, B., Thomassen, Y., Drotikova, T., and Kallenborn, R.: Source identification of individual soot agglomerates in Arctic air by transmission electron microscopy, *Atmos. Environ.*, 172, 47-54, <https://doi.org/10.1016/j.atmosenv.2017.10.033>, 2018.

WHO: Environmental health criteria 229. Selected nitro- and nitro-oxy-polycyclic aromatic hydrocarbons, World Health Organization (WHO), Geneva, Switzerland, 511 pp., http://whqlibdoc.who.int/ehc/WHO_EHC_229.pdf, 2003.

Wickström, S.: Warmer and wetter winters over the high-latitude North Atlantic: an atmospheric circulation perspective, Doctoral thesis, The University of Bergen (UiB), Bergen, Norway, 174 pp., <http://hdl.handle.net/1956/22191>, 2020.

Wickström, S., Jonassen, M. O., Cassano, J. J., and Vihma, T.: Present Temperature, Precipitation, and Rain-on-Snow Climate in Svalbard, *J. Geophys. Res. Atmos.*, 125, e2019JD032155, <https://doi.org/10.1029/2019JD032155>, 2020a.

Wickström, S., Jonassen, M. O., Vihma, T., and Uotila, P.: Trends in cyclones in the high-latitude North Atlantic during 1979–2016, *Q. J. R. Meteorolog. Soc.*, 146, 762-779, <https://doi.org/10.1002/qj.3707>, 2020b.

Willis, M. D., Leaitch, W. R., and Abbatt, J. P. D.: Processes controlling the composition and abundance of Arctic aerosol, *Rev. Geophys.*, 56, 621-671, <https://doi.org/10.1029/2018rg000602>, 2018.

Wilson, J. Y., Cooke, S. R., Moore, M. J., Martineau, D., Mikaelian, I., Metner, D. A., Lockhart, W. L., and Stegeman, J. J.: Systemic Effects of Arctic Pollutants in Beluga Whales Indicated by CYP1A1 Expression, *Environ. Health Perspect.*, 113, 1594-1599, <https://doi.org/10.1289/ehp.7664>, 2005.

Wu, C., and Yu, J. Z.: Determination of primary combustion source organic carbon-to-elemental carbon (OC/EC) ratio using ambient OC and EC measurements: secondary OC-EC correlation minimization method, *Atmos. Chem. Phys.*, 16, 5453-5465, <https://doi.org/10.5194/acp-16-5453-2016>, 2016.

Yaffe, D., Cohen, Y., Arey, J., and Grosovsky, A. J.: Multimedia Analysis of PAHs and Nitro-PAH Daughter Products in the Los Angeles Basin, *Risk Anal.*, 21, 275-294, <https://doi.org/10.1111/0272-4332.212111>, 2001.

Yu, Y., Katsoyiannis, A., Bohlin-Nizzetto, P., Brorström-Lundén, E., Ma, J., Zhao, Y., Wu, Z., Tych, W., Mindham, D., Sverko, E., Barresi, E., Dryfhout-Clark, H., Fellin, P., and Hung, H.: Polycyclic aromatic hydrocarbons not declining in Arctic air despite global emission reduction, *Environ. Sci. Technol.*, 53, 2375-2382, <https://doi.org/10.1021/acs.est.8b05353>, 2019.

Zhang, L., Jin, Y., Huang, M., and Penning, T.: The Role of Human Aldo-Keto Reductases in the Metabolic Activation and Detoxication of Polycyclic Aromatic Hydrocarbons: Interconversion of PAH Catechols and PAH o-Quinones, *Front. Pharmacol.*, 3, 193, <https://doi.org/10.3389/fphar.2012.00193>, 2012.

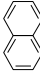
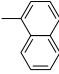
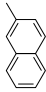
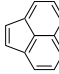
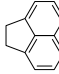
Zhang, L., Wang, X., Moran, M., and Feng, J.: Review and uncertainty assessment of size-resolved scavenging coefficient formulations for below-cloud snow scavenging of atmospheric aerosols, *Atmos. Chem. Phys.*, 13, 10005-10025, <https://doi.org/10.5194/acp-13-10005-2013>, 2013.

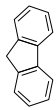
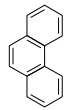
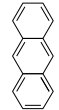
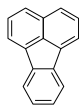

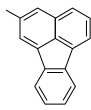
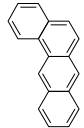
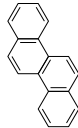
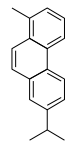
Zhao, X., Strong, K., Adams, C., Schofield, R., Yang, X., Richter, A., Friess, U., Blechschmidt, A.-M., and Koo, J.-H.: A case study of a transported bromine explosion event in the Canadian high arctic, *J. Geophys. Res. Atmos.*, 121, 457-477, <https://doi.org/10.1002/2015JD023711>, 2016.

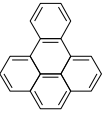
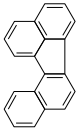
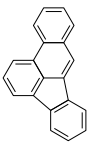
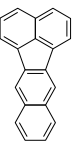
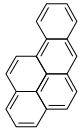
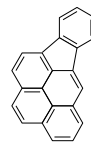

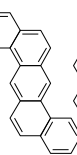

Zhou, Y., Shively, D., Mao, H., Russo, R. S., Pape, B., Mower, R. N., Talbot, R., and Sive, B. C.: Air Toxic Emissions from Snowmobiles in Yellowstone National Park, *Environ. Sci. Technol.*, 44, 222-228, <https://doi.org/10.1021/es9018578>, 2010.

8 Appendix

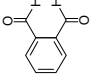
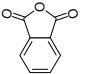
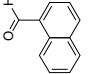
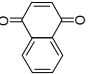
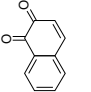
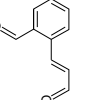
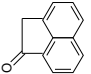
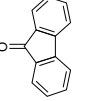
Table S1. Estimated physico-chemical properties of studied compounds (25 °C, 101.3 kPa). Data acquired from EPI Suite, U.S. EPA: Estimation Programs Interface Suite™ for Microsoft® Windows, v 4.11. 2019, United States Environmental Protection Agency: Washington, DC, USA. Data includes molecular weight (MW), octanol-air (K_{OA}), octanol-water (K_{OW}), and air-water (K_{AW}) partition coefficients, as well as water solubility (WS), vapour pressure (P), and rate coefficient of reaction with OH radical (K_{OH}).

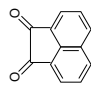
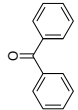
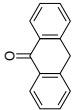
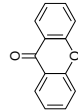
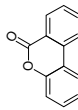
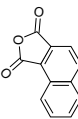
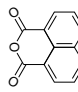
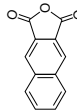
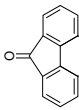
Compound	Abbreviation	CAS	MW, [g mol ⁻¹]	Log K_{OA}	Log K_{OW}	Log K_{AW}	WS, [mg L ⁻¹]	P, [Pa]	K_{OH} , [cm ³ molec ⁻¹ sec ⁻¹]	Structure
Naphthalene	Nap	91-20-3	128.17	5.0	3.3	-1.7	1.42E+02	5.39E+00	2.16E-11	
1-Methylnaphthalene	1-MeNap	90-12-0	142.2	5.5	3.9	-1.7	4.06E+01	4.91E+00	5.65E-11	
2-Methylnaphthalene	2-MeNap	91-57-6	142.2	5.5	3.9	-1.7	4.14E+01	4.60E+00	5.65E-11	
Acenaphthylene	Acy	208-96-8	152.19	6.3	3.9	-2.3	2.49E+00	1.67E-01	7.55E-11	
Acenaphthene	Ace	83-32-9	154.21	6.0	3.9	-2.1	2.53E+00	1.72E-01	6.69E-11	

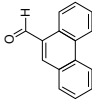
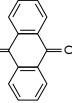
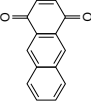
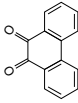
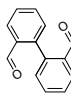
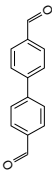
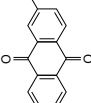
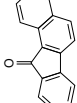
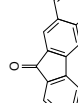
Fluorene	Flu		166.22	6.6	4.2	-2.4	1.34E+00	4.40E-02	8.85E-12	
Phenanthrene	Phe	85-01-8	178.23	7.2	4.5	-2.8	6.77E-01	5.76E-03	1.30E-11	
Anthracene	Ant	120-12-7	178.23	7.1	4.5	-2.6	6.91E-01	2.89E-04	4.00E-11	
Fluoranthene	Flt	206-44-0	202.25	8.6	5.2	-3.4	2.03E-01	6.07E-04	8.69E-11	
Pyrene	Pyr	129-00-0	202.25	8.2	4.9	-3.3	2.25E-01	4.59E-05	5.00E-11	
2-Methylfluoranthene	2-MeFlt	33543-31-6	216.28	8.9	5.5	-3.4	5.84E-02	2.33E-04	5.05E-11	
Benzo[a]anthracene	BaAnt	56-55-3	228.29	9.1	5.8	-3.3	2.91E-02	3.63E-05	5.00E-11	
Chrysene	Chry	218-01-9	228.29	9.5	5.8	-3.7	2.64E-02	2.08E-07	5.00E-11	
Retene	Ret	483-65-8	234.3	8.7	6.4	-2.3	8.48E-03	3.52E-04	4.17E-11	

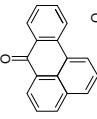
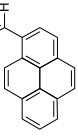
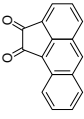
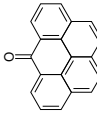
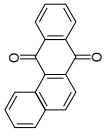
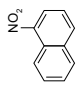
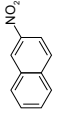
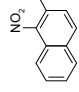
Benzo[e]pyrene	BePyr	192-97-2	252.3	11.4	6.4	-4.9	5.64E-03	2.59E-06	5.00E-11	
Benzo[j]fluoranthene	BjFlt	205-82-3	252.3	10.6	6.1	-4.5	1.08E-02	3.20E-06	8.69E-11	
Benzo[b]fluoranthene	BbFlt	205-99-2	252.31	10.4	5.8	-4.6	1.08E-02	3.20E-06	8.69E-11	
Benzo[k]fluoranthene	BkFlt	207-08-9	252.31	10.7	6.1	-4.6	1.08E-02	3.20E-06	6.21E-11	
Benzo[a]pyrene	BaP	50-32-8	252.31	10.9	6.1	-4.7	1.04E-02	1.31E-07	5.00E-11	
Indeno[1,2,3-cd]pyrene	IPyr	193-39-5	276.33	11.5	6.7	-4.8	2.49E-03	1.17E-07	8.69E-11	
Benzo[ghi]perylene	BghiP	191-24-2	276.33	11.5	6.6	-4.9	2.49E-03	1.17E-07	5.00E-11	
Dibenzo[a,h]anthracene	DBAnt	53-70-3	278.35	11.8	6.5	-5.2	3.30E-03	1.85E-09	5.00E-11	
Coronene	Cor	191-07-1	300.4	13.7	7.6	-6.1	2.83E-04	1.14E-11	5.00E-11	

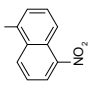
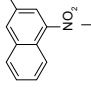
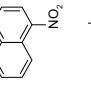
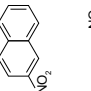
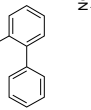
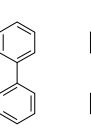
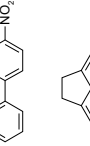
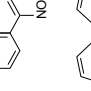
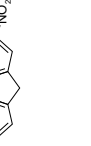
Oxy-PAHs

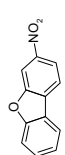
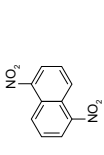
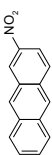
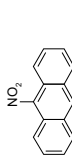
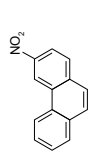
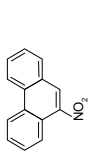
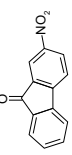
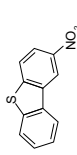
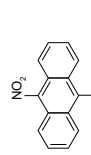
Phthalaldehyde	PhA	643-79-8	134.13	7.3	1.4	-5.9	5.35E+03	1.99E+00	3.41E-11	
Phthalic anhydride	PhAn	85-44-9	148.12	7.8	1.6	-6.2	3.33E+03	2.96E-02	7.49E-13	
1-Naphthaldehyde	1-NapA	66-77-3	156.18	7.2	2.9	-4.3	2.44E+02	3.33E-01	2.78E-11	
1,4-Naphthoquinone	1,4-NapQ	130-15-4	158.15	8.8	1.7	-7.1	2.42E+03	2.25E-02	3.01E-12	
1,2-Naphthoquinone	1,2-NapQ	524-42-5	158.15	8.9	2.1	-6.8	1.10E+03	1.44E-02	1.30E-11	
2-Formyl- <i>trans</i> -cinnamaldehyde	2-FCinA	61650-52-0	160.17	8.3	1.5	-6.8	3.34E+03	3.01E-01	5.39E-11	
1-Acenaphthenone	1-AceO	2235-15-6	168.19	7.6	2.8	-4.8	2.00E+01	1.30E-02	2.37E-11	
9-Fluorenone	9-FluO	486-25-9	180.2	8.1	3.6	-4.6	3.74E+00	7.63E-03	6.18E-12	

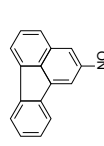
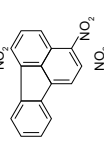
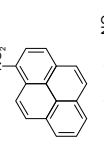
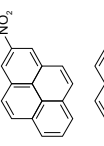
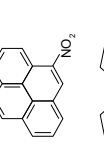
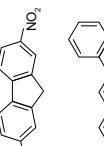
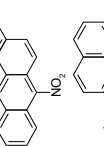
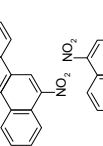
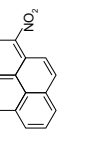
Acenaphthenequinone	AceQ	82-86-0	182.17	8.8	2.0	-6.9	9.01E+01	4.53E-05	8.30E-12	
Benzophenone	BZPh	119-61-9	182.22	7.3	3.2	-4.1	1.03E+02	1.21E-01	3.55E-12	
Anthrone	ANO	90-44-8	194.23	8.2	3.7	-4.5	2.72E+00	2.44E-03	9.77E-12	
Xanthone	Xan	90-47-1	196.2	8.5	3.4	-5.1	4.52E+00	4.76E-04	8.97E-12	
6 <i>H</i> -Dibenzo[<i>b,d</i>]pyran-6-one	DBPone	2005-10-9	196.2	5.7	2.0	-3.7	7.13E+01	9.01E-04	5.58E-12	
1,2-Naphthalic anhydride	1,2-NapAn	5343-99-7	198.17	7.8	3.2	-4.6	7.57E+01	5.97E-03	8.30E-12	
1,8-Naphthalic anhydride	1,8-NapAn	81-84-5	198.17	7.8	3.2	-4.6	5.88E+00	5.49E-05	8.30E-12	
2,3-Naphthalene-dicarboxylic anhydride	2,3-NapAn	716-39-2	198.18	7.8	3.2	-4.6	7.57E+01	5.97E-03	8.30E-12	
4 <i>H</i> -Cyclopenta(<i>def</i>)-phenanthrene-4-one	CPPhcO	5737-13-3	204.22	9.6	4.1	-5.5	9.44E-01	3.56E-04	5.00E-12	

9-Phenanthrene-carboxaldehyde	9-PheA	4707-71-5	206.24	9.3	4.1	-5.3	1.07E+00	7.65E-04	2.35E-11	
9,10-Anthraquinone	9,10-AntQ	84-65-1	208.21	9.4	3.4	-6.0	3.92E+00	5.11E-06	1.50E-12	
1,4-Anthraquinone	1,4-AntQ	635-12-1	208.21	10.9	2.8	-8.1	1.50E+02	3.21E-04	1.06E-11	
9,10-Phenanthrene-quinone	9,10-PheQ	84-11-7	208.21	9.5	2.5	-7.0	2.17E+01	1.14E-04	6.18E-12	
2,2'-Biphenyldicarboxaldehyde	2,2-BPhA	1210-05-5	210.23	10.2	3.2	-7.0	7.29E+01	8.35E-04	3.60E-11	
4,4'-Biphenyldicarboxaldehyde	4,4-BPhA	66-98-8	210.23	10.2	3.2	-7.0	7.29E+01	8.35E-04	3.60E-11	
2-Methylanthraquinone	2-MeAntQ	84-54-8	222.24	10.7	3.9	-6.8	1.23E+00	1.16E-04	2.84E-12	
Benzo[<i>a</i>]fluorenone	BaFluO	479-79-8	230.26	10.3	4.7	-5.6	2.16E-01	5.16E-05	1.80E-11	
Benzo[<i>b</i>]fluorenone	BbFluO	NA	230.26	10.4	3.9	-6.5	1.54E+01	1.67E-04	1.06E-10	

Benzenanthrone	BZT	82-05-3	230.26	10.4	4.8	-5.6	1.84E-01	2.95E-05	1.80E-11	
1-Pyreneboxaldehyde	1-PyrA	3029-19-4	230.26	10.3	4.2	-6.1	5.75E-01	2.87E-05	4.22E-11	
Acenanthrenequinone	AAntQ	6373-11-1	232.23	12.0	4.2	-7.9	6.63E-01	1.27E-05	1.54E-11	
6 <i>H</i> -Benzo[<i>cd</i>]pyren-6-one	BPyrO	3074-00-8	254.28	11.8	5.3	-6.5	5.03E-02	2.01E-06	1.92E-11	
Benzo[<i>a</i>]anthracene-7,12-dione	BaA-7,12Q	2498-66-0	258.3	12.3	4.4	-7.9	2.89E-01	5.17E-06	9.05E-12	
Nitro-PAHs										
1-Nitronaphthalene	1-NNap	86-57-7	173.17	7.3	3.2	-4.1	4.57E+01	9.72E-02	2.70E-12	
2-Nitronaphthalene	2-NNap	581-89-5	173.17	7.3	3.2	-4.1	4.14E+01	3.77E-02	2.70E-12	
2-Methyl-1-nitronaphthalene	2-Me-1-NNap	881-03-8	187.19	7.6	3.5	-4.0	1.98E+01	2.17E-02	4.17E-12	

1-Methyl-5-nitro-naphthalene	1-Me-5-NNap	91137-27-8	187.19	7.6	3.5	-4.0	1.98E+01	1.45E-02	4.17E-12	
2-Methyl-4-nitro-naphthalene	2-Me-4-NNap	13615-38-8	187.19	7.6	3.5	-4.0	1.98E+01	1.45E-02	4.17E-12	
1-Methyl-4-nitro-naphthalene	1-Me-4-NNap	880-93-3	187.19	7.6	3.5	-4.0	1.98E+01	2.73E-02	4.17E-12	
1-Methyl-6-nitro-naphthalene	1-Me-6-NNap	105752-67-8	187.19	7.6	3.5	-4.0	1.98E+01	1.45E-02	4.17E-12	
2-Nitrobiphenyl	2-NBPh	86-00-0	199.2	7.7	3.6	-4.2	1.59E+01	6.95E-02	2.92E-12	
3-Nitrobiphenyl	3-NBPh	2113-58-8	199.2	8.0	3.9	-4.2	8.91E+00	1.35E-02	2.79E-12	
4-Nitrobiphenyl	4-NBPh	92-93-3	199.2	8.0	3.8	-4.2	9.84E+00	4.01E-03	2.92E-12	
5-Nitroacenaphthene	5-NAce	602-87-9	199.2	8.2	3.9	-4.3	7.20E-01	5.45E-03	8.30E-12	
2-Nitrofluorene	2-NFlu	607-57-8	211.22	7.9	3.4	-4.6	1.60E+00	5.91E-04	4.16E-12	

3-Nitrobenzofuran	3-NDBF	5410-97-9	213.19	9.0	3.9	-5.2	1.14E+00	6.55E-04	7.50E-13	
1,5-Dinitronaphthalene	1,5-DNNap	605-71-0	218.17	9.1	2.6	-6.5	8.98E+01	5.33E-05	2.36E-13	
2-Nitroanthracene	2-NAnt	3586-69-4	223.23	9.2	4.2	-5.1	2.92E-01	1.80E-04	5.00E-12	
9-Nitroanthracene	9-NAnt	602-60-8	223.23	9.9	4.8	-5.1	8.66E-02	1.60E-04	5.00E-12	
3-Nitrophenanthrene	3-NPhe	17024-19-0	223.23	9.2	4.2	-5.1	2.92E-01	1.80E-04	1.62E-12	
9-Nitrophenanthrene	9-NPhe	954-46-1	223.23	9.2	4.2	-5.1	2.92E-01	1.80E-04	1.62E-12	
2-Nitro-9-fluorenone	2-N-9-Fluo	3096-52-4	225.2	10.0	3.1	-7.0	1.36E+00	1.19E-04	2.66E-12	
2-Nitrobenzo-thiophene	2-NDBT	6639-36-7	229.26	9.3	4.0	-5.3	3.85E-01	1.06E-04	1.01E-12	
9-Methyl-10-nitroanthracene	9-Me-10-NAnt	84457-22-7	237.25	9.7	4.7	-5.0	8.35E-02	8.51E-05	7.61E-12	

2-Nitrofluoranthene	2-NFlu	13177-29-2	247.25	8.5	4.3	-4.2	6.79E-02	7.36E-06	4.39E-12	
3-Nitrofluoranthene	3-NFlu	892-21-7	247.25	10.6	4.8	-5.9	6.79E-02	7.36E-06	4.39E-12	
1-Nitropyrene	1-NPyr	5522-43-0	247.25	10.9	5.1	-5.9	3.70E-02	1.11E-05	6.25E-12	
2-Nitropyrene	2-NPyr	789-07-1	247.25	10.6	4.8	-5.9	6.79E-02	7.36E-06	6.25E-12	
4-Nitropyrene	4-NPyr	57835-92-4	247.25	10.6	4.8	-5.9	6.79E-02	7.36E-06	6.25E-12	
2,7-Dinitrofluorene	2,7-DNFlu	5405-53-8	256.209	10.3	3.4	-7.0	9.52E-01	1.88E-07	1.36E-12	
7-Nitrobenzo[a]anthracene	7-NBaA	20268-51-3	273.3	11.4	5.3	-6.1	1.53E-02	1.01E-06	6.25E-12	
6-Nitrochrysene	6-NChry	7496-02-8	273.3	11.4	5.3	-6.1	1.53E-02	1.01E-06	6.25E-12	
1,3-Dinitropyrene	1,3-DNPyr	75321-20-9	292.24	12.8	4.6	-8.3	0.05404	1.21E-07	5.46E-13	

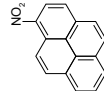
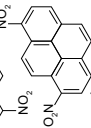
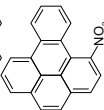
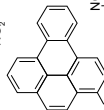
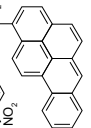
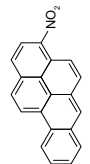
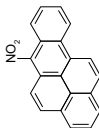
1,6-Dinitropyrene	1,6-DNPyr	42397-64-8	292.24	12.8	4.6	-8.3	5.40E-02	1.21E-07	5.46E-13	
1,8-Dinitropyrene	1,8-DNPyr	42397-65-9	292.24	12.8	4.6	-8.3	5.40E-02	1.21E-07	5.46E-13	
1-Nitrobenzo[e]pyrene	1-NBePyr	91259-16-4	297.3	12.8	5.9	-6.9	3.49E-03	4.13E-08	6.25E-12	
3-Nitrobenzo[e]pyrene	3-NBePyr	81340-58-1	297.3	12.8	5.9	-6.9	3.49E-03	4.13E-08	6.25E-12	
1-Nitrobenzo[a]pyrene	1-NBaPyr	70021-99-7	297.3	12.8	5.9	-6.9	3.49E-03	4.13E-08	6.25E-12	
3-Nitrobenzo[a]pyrene	3-NBaPyr	70021-98-6	297.3	12.8	5.9	-6.9	3.49E-03	4.13E-08	6.25E-12	
6-Nitrobenzo[a]pyrene	6-NBaPyr	63041-90-7	297.3	12.8	5.9	-6.9	3.49E-03	4.13E-08	6.25E-12	

Table S2. Sum concentrations (G+P; pg/m³) of 14 EPA PAHs* in the air of Longyearbyen compared to the levels at the background station in Svalbard (Zeppelin) measured during the same periods in 2017/2018. The determined periods are November-January (P1), February (P2), March-April (P3), May-June (P4), September (P5).

Location	Coordinates	Period	N samples	Mean	SD	Min	Median	Max	Data from Paper
UNIS (urban), Longyearbyen, Svalbard	78.22° N, 15.65° E, 25 m asl	P1	8	839	366	416	772	1432	II
		P2	4	2733	772	2107	2483	3857	II
		P3	7	3290	1721	1163	4040	5023	II
		P4	12	1392	998	347	1091	3754	II
		P5	6	749	73	687	723	867	I
Adventdalen (rural), Longyearbyen, Svalbard	78°12' N 15°49' E, 15 m asl	P1	3	663	258	492	537	960	III
		P2	-						
		P3	7	1239	1057	267	844	2994	III
		P4	6	304	160	68	296	524	III
		P5	6	366	64	279	356	448	I
Svalsat (altitudinal), Longyearbyen, Svalbard	78.23° N, 15.39° E, 457 m asl	P1	8	540	206	299	504	996	III
		P2	-						
		P3	-						
		P4	4	337	237	151	257	682	III
		P5	-						
Zeppelin (background), Ny-Ålesund, Svalbard	78°58' N, 11°53' E, 474 m asl	P1	9	429	215	162	427	767	II
		P2	3	247	71	173	253	315	II
		P3	5	124	76	59	108	254	II
		P4	8	40	9	30	36	61	II
		P5	5	33	5	27	34	40	I

*Summed 14 PAHs are Ace, Flu, Phe, Ant, Flt, Pyr, BaAnt, Chry, BbFlt, BkFlt, BaP, IPyr, DBAnt, BPer
Note that sets of 15-22 PAHs were measured in Papers I-III

Figure S1. Sum seasonal atmospheric concentrations (G+P; pg/m^3) of PACs at the three sites in Longyearbyen. The same selected compounds from Paper I-III were included into consideration.

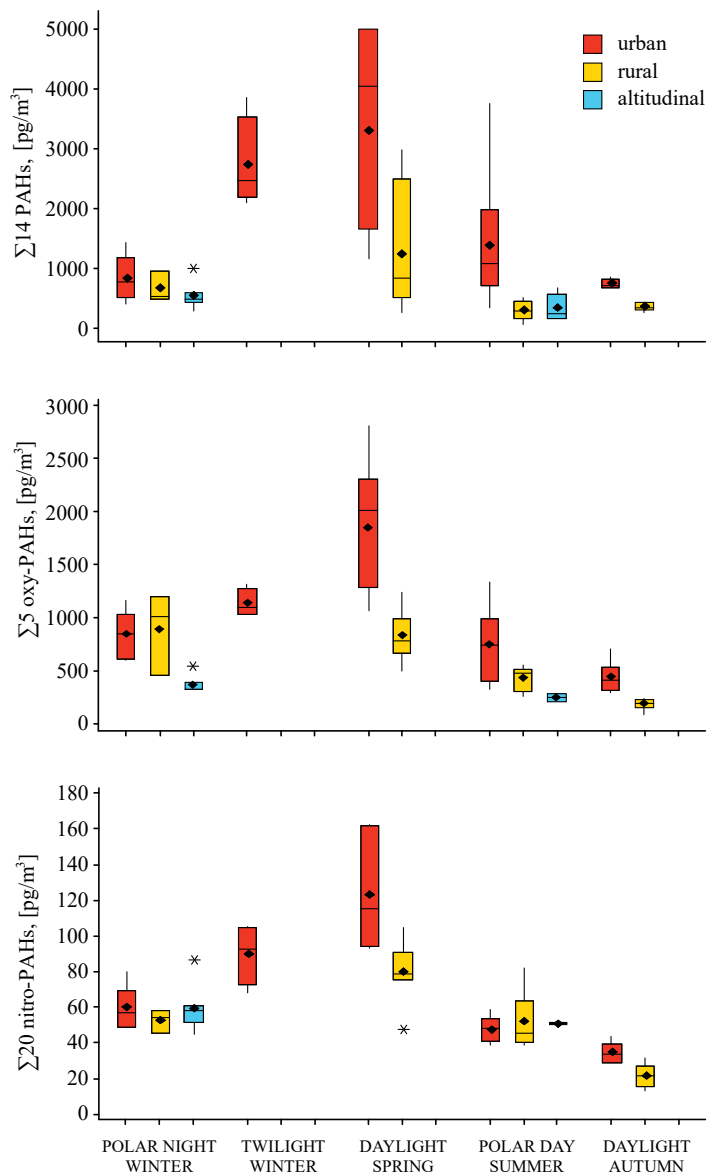
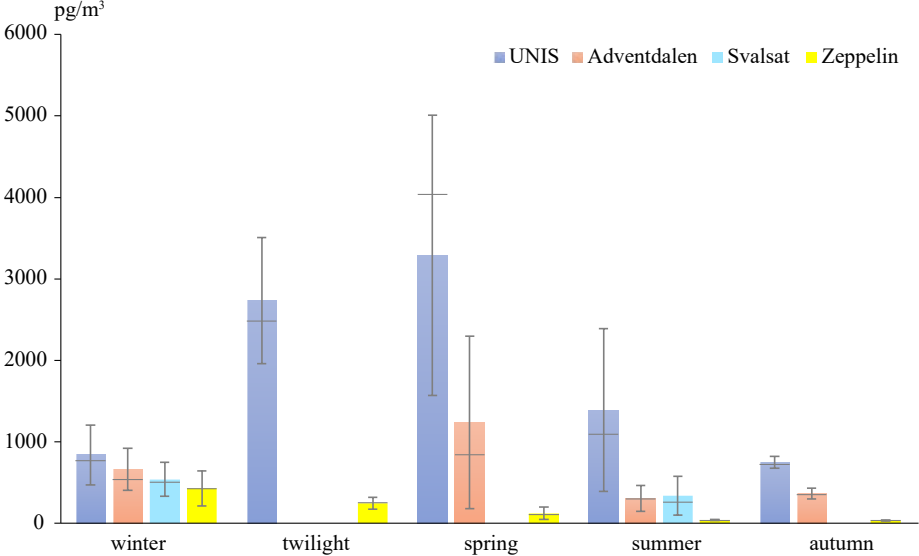


Figure S2. Sum concentrations of 14 EPA PAHs* (G+P; pg/m^3) in urban (UNIS), rural (Adventdalen), altitudinal (Svalsat), and background (Zeppelin) air of Svalbard. Data are for the November-January (winter), February (twilight), March-April (spring), May-July (summer), and September (autumn) 2017/2018 periods. The bar charts represent mean values with standard deviation error bars. The lines represent median values.



*Summed 14 PAHs are Ace, Flu, Phe, Ant, Flt, Pyr, BaAnt, Chry, BbFlt, BkFlt, BaP, IPyr, DBAnt, BPer

Paper I

Polycyclic aromatic hydrocarbons (PAHs) and oxy- and nitro-PAHs in ambient air of the Arctic town Longyearbyen, Svalbard.

Drotikova, T., Ali, A. M., Halse, A. K., Reinardy, H. C., and Kallenborn, R.

Published.



Polycyclic aromatic hydrocarbons (PAHs) and oxy- and nitro-PAHs in ambient air of the Arctic town Longyearbyen, Svalbard

Tatiana Drotikova^{1,2}, Aasim M. Ali³, Anne Karine Halse⁴, Helena C. Reinardy^{1,5}, and Roland Kallenborn^{1,2}

¹Department of Arctic Technology, University Centre in Svalbard (UNIS), Longyearbyen, 9171, Norway

²Faculty of Chemistry, Biotechnology and Food Sciences, Norwegian University of Life Sciences (NMBU), Ås, 1432, Norway

³Department of Contaminants and Biohazards, Institute of Marine Research (IMR), Bergen, 5817, Norway

⁴Department of Environmental Chemistry, Norwegian Institute for Air Research (NILU), Kjeller, 2007, Norway

⁵Scottish Association for Marine Science (SAMS), Oban, Argyll, PA37 1QA, United Kingdom

Correspondence: Tatiana Drotikova (tatiana.drotikova@unis.no)

Received: 16 February 2020 – Discussion started: 28 February 2020

Revised: 6 June 2020 – Accepted: 17 June 2020 – Published: 27 August 2020

Abstract. Polycyclic aromatic hydrocarbons (PAHs) are not declining in Arctic air despite reductions in their global emissions. In Svalbard, the Longyearbyen coal-fired power plant is considered to be one of the major local sources of PAHs. Power plant stack emissions and ambient air samples, collected simultaneously at 1 km (UNIS) and 6 km (Adventdalen) transect distance, were analysed (gaseous and particulate phases separately) for 22 nitro-PAHs, 8 oxy-PAHs, and 16 parent PAHs by gas chromatography in combination with single quadrupole electron capture negative ionization mass spectrometry (GC-ECNI-MS) and gas chromatography in combination with triple quadrupole electron ionization mass spectrometry (GC-EI-MS/MS). Results confirm low levels of PAH emissions ($\sum 16$ PAHs = $1.5 \mu\text{g kg}^{-1}$ coal) from the power plant. Phenanthrene, 9,10-anthraquinone, 9-fluorenone, fluorene, fluoranthene, and pyrene accounted for 85 % of the plant emission (not including naphthalene). A dilution effect was observed for the transect ambient air samples: 1.26 ± 0.16 and $0.63 \pm 0.14 \text{ ng m}^{-3}$ were the sum of all 47 PAH derivatives for UNIS and Adventdalen, respectively. The PAH profile was homogeneous for these recipient stations with phenanthrene and 9-fluorenone being most abundant. Multivariate statistical analysis confirmed coal combustion and vehicle and marine traffic as the predominant sources of PAHs. Secondary atmospheric formation of 9-nitroanthracene and 2 + 3-nitrofluoranthene was evaluated and concluded. PAHs partitioning between gaseous and particulate phases showed a strong dependence on ambient tem-

peratures and humidity. The present study contributes important data which can be utilized to eliminate uncertainties in model predictions that aim to assess the extent and impacts of Arctic atmospheric contaminants.

1 Introduction

Traditionally, Arctic regions are considered to be pristine and remote from the majority of potential large-scale emission sources in industrialized mid-latitude countries (Armitage et al., 2011; Macdonal et al., 2000; Barrie et al., 1992). Atmospheric transport is the most efficient way for polycyclic aromatic hydrocarbons (PAHs), released in the lower latitudes, to reach the Arctic (Friedman et al., 2014). Long-range atmospheric transport (LRAT) to Arctic regions has strong seasonality with an increased tendency during winter and spring (Willis et al., 2018). This is driven by a different mean circulation direction across the Arctic in winter compared to summer, the extension and significantly increased permeability of the Arctic front in winter, and the absence of wet removal of particles during transport (Willis et al., 2018). These factors explain observed maximum near-surface pollutant concentrations during winter and minimum levels during summer (Klonecki, 2003). Fossil fuel sources dominate total aerosol organic carbon in Arctic winter air, with a predominance of alkanes, PAHs, and phthalates (Fu et al., 2009). During the past decades, the background monitoring of at-

atmospheric pollutants in Ny-Ålesund, Svalbard, and Alert, Canada, have been an important data repository for information on the occurrence and LRAT of anthropogenic contaminants including persistent organic pollutants and PAHs in the Arctic regions. The data demonstrate ubiquitous distribution of PAHs on a global scale, including the Arctic. Confirmed occurrence of a pollutant in a polar environment is an important criterion considered by the Stockholm, Basel, and Rotterdam conventions (Fiedler et al., 2019). The United Nations Economic Commission for Europe (UNECE) has incorporated PAHs in the Convention on Long-range Transboundary Air Pollution (UNECE, 1998). Atmospheric PAHs are regulated in the USA, Canada, UK, and Europe (US EPA, 2011; Ontario Ministry of the Environment and Climate Change, 2016; UK Air DEFRA, 2007; EU Directive 2004/107/EC, 2005). PAHs are also included in the list of target chemicals of the Convention for the Protection of the Marine Environment of the North-East Atlantic (OSPAR). PAH concentrations are not declining in the Arctic despite global emission reductions (Yu et al., 2019), and PAHs are listed as “chemicals of emerging concern in the Arctic” (Balmer and Muir, 2017).

PAHs are byproducts of different incomplete combustion processes, mainly fossil fuels and biomass burning (Ravindra et al., 2008a). Their toxic and carcinogenic effects on both human health and ecosystems are well documented (Kim et al., 2013; Reynaud and Deschaux, 2006; Macdonald et al., 2010). Under unique Arctic weather conditions, with extreme temperatures, wind, and light seasonality, atmospheric PAHs may behave differently compared to in temperate climatic conditions. Low temperatures favour the partitioning of semi-volatile PAHs from gas phase to particulate phase, which makes them more persistent in the Arctic environment (Lammel, 2015). Due to extended winter darkness in the Arctic, photodegradation of PAHs is limited for several months. The transition from dark polar winter to the light spring and summer brings a large increase in the amount of available solar radiation and oxidants in the Arctic troposphere (Willis et al., 2018). PAHs react with a number of atmospheric oxidants, most notably the hydroxyl radical, ozone, the nitrate radical, and nitrogen dioxide (Keyte et al., 2013). This leads to their transformation into more toxic oxygenated and nitrated PAH derivatives (oxy-PAHs and nitro-PAHs). Oxy- and nitro-PAHs are also constituents of raw coal and can be emitted with PAHs following the same combustion processes (W. Huang et al., 2014). Oxy- and nitro-PAHs have high toxicity (Onduka et al., 2012); they can act as direct mutagens, carcinogens, and oxidative stressors in biota (Durant et al., 1996). The biological effects of nitro- and oxy-PAHs can be greater than those of the parent PAHs (WHO, 2003). In remote locations they are found at concentrations near detection limits and thus are mostly not included in monitoring programmes, and the level of nitro- and oxy-PAHs in the Arctic atmosphere is unknown (Balmer and Muir, 2017).

The Arctic is warming at a higher rate than the global average and visible changes happen rapidly here. Thus, it is a key area for modelling studies on climate effects on contaminants with a main focus on LRAT from lower latitudes. As a consequence, local Arctic sources are usually disregarded, and a lack of information on local emission sources is a source of uncertainty in model predictions that often deviate significantly from observations (Schmale et al., 2018). Local emission sources may be of high importance in winter, when strong temperature atmospheric inversions can be frequent in Arctic region (Bradley et al., 1992). These episodes inhibit the mass and heat fluxes from the surface to the atmosphere, and consequently the dilution of surface emissions (Janhall et al., 2006; Li et al., 2019). This trapping of emissions results in poor air quality and can be potentially harmful to local people. Climate change introduces additional sources of PAHs to the Arctic region. In the past decade, human activities such as resource exploration, research, tourism, fisheries, and maritime traffic have increased substantially due to warming and corresponding reduction of sea ice, opening up new shipping routes (Jörundsdóttir et al., 2014). Warming may also enhance the volatilization of low molecular-weight (LMW) PAHs from ground surfaces (Friedman et al., 2014) and melting sea ice (Yu et al., 2019). The reactivity of PAHs in the gas phase is significantly greater than when associated with particles (Keyte et al., 2013); therefore increasing air temperatures can be expected to lead to increased levels of toxic nitro- and oxy-PAHs.

The need for a comprehensive assessment of local contaminant sources in Svalbard was acknowledged and initiated in the international Arctic Monitoring and Assessment Programme (AMAP); with the major focus on persistent organic pollutants (Pedersen et al., 2011), there is a scarcity of data on local sources of PAHs in Svalbard. A back-trajectory analysis of 20 years of data for three representative PAHs (Phe, Pyr, and BaPyr; see Table 1 for full names) suggested that Svalbard is impacted by air masses coming from eastern Russia, northern Europe, and northwest Russia during winter (Yu et al., 2019). Overall, combined European and Russian emissions accounted for more than 80 % of episodic high-concentration events in Svalbard in 2007 (Balmer and Muir, 2017; Friedman and Selin, 2012). However, observed concentrations of Phe and Pyr from the Zeppelin station, Svalbard, were higher than model simulations, indicating important contributions of local sources of PAHs to the Arctic atmosphere, too (Yu et al., 2019). This study focused on the main settlement in Svalbard, Longyearbyen, with a population of approximately 2400 inhabitants and a high level of (partially seasonal) human activities (transport, coal mining, industry, tourism, and research). The local coal-fired power plant (PP) was hypothesized to be the major local source of PAHs, and the overall objectives of this study were to (1) evaluate PAH emissions from the local power plant, (2) examine concentrations and profile changes with distance from the PP, (3) quantify concentrations of PAHs and nitro-

Table 1. Concentrations of PAHs (G+P) and percentage in the particulate phase (%PM) in Longyearbyen power plant, UNIS, and Adventdalen. Data are average, minimum, and maximum; $n = 6$ for each location.*

Compound name	Abbreviated name	Power plant			UNIS			Adventdalen		
		Mean ng m ⁻³	Min–max ng m ⁻³	Mean %PM	Mean pg m ⁻³	Min–max pg m ⁻³	Mean %PM	Mean pg m ⁻³	Min–max pg m ⁻³	Mean %PM
Naphthalene	Nap	51.82	32.74–59.82	7.4	< MDL	< MDL	–	< MDL	< MDL	–
Acenaphthylene	Acy	2.30	1.22–3.80	0.6	16.89	7.14–29.15	0.0	2.40	1.10–5.13	0.0
Acenaphthene	Ace	0.87	0.30–2.18	8.4	48.48	24.29–72.99	0.0	3.84	1.25–6.62	0.0
Fluorene	Flu	7.61	3.68–12.16	4.6	170.50	136.5–236.0	1.1	59.96	38.49–95.82	1.8
Phenanthrene	Phe	27.32	12.01–44.87	5.6	409.20	368.5–470.0	6.5	236.30	191.7–270.8	3.7
Anthracene	Ant	1.06	0.23–2.13	0.0	18.04	12.29–25.52	0.0	14.25	10.46–19.33	3.5
Fluoranthene	Flt	6.99	1.43–12.49	3.9	28.45	24.14–36.06	40.5	19.14	10.76–38.54	23.2
Pyrene	Pyr	4.40	1.08–7.35	8.3	39.47	30.72–47.84	26.8	27.17	20.91–35.89	15.8
Benzo(a)anthracene	BaAnt	0.13	0.04–0.20	0.0	2.17	0.01–5.83	68.2	n.d.	n.d.	–
Chrysene	Chry	0.28	0.06–0.42	0.0	7.32	2.60–13.47	81.7	3.12	0.11–7.11	64.1
Benzo(b+k)fluoranthene	BbkFlt	n.d.	n.d.	–	2.23	0.01–5.87	100.0	0.75	0.01–2.79	100.0
Benzo(a)pyrene	BaPyr	n.d.	n.d.	–	0.89	0.01–2.46	100.0	0.34	0.01–1.16	100.0
Indeno(1,2,3-cd)pyrene	IPyr	n.d.	n.d.	–	1.63	0.07–3.79	100.0	0.71	0.07–2.67	100.0
Dibenzo(a,h)anthracene	DBAnt	n.d.	n.d.	–	n.d.	n.d.	–	n.d.	n.d.	–
Benzo(g,h,i)perylene	BPer	n.d.	n.d.	–	3.92	1.44–8.12	100.0	1.21	0.08–3.83	100.0
∑16 PAHs		102.8	61.9–139.1	–	749.2	687.4–866.9	–	369.1	279.0–454.5	–
9-Fluorenone	9-Flu	12.35	5.57–19.54	19.2	270.30	128.2–543.8	41.7	139.40	110.2–177.2	25.5
9,10-Antraquinone	9,10-AntQ	15.76	4.60–47.00	21.3	163.50	105.2–269.1	37.5	71.70	11.4–118.4	43.9
4H-Cyclopenta(def)-phenanthrene-4-one	cPphe-4	1.30	0.51–2.55	15.8	27.23	20.16–35.80	65.5	18.77	11.97–39.10	38.1
9,10-Phenanthrenequinone	9,10-PheQ	2.13	0.96–4.40	0.0	< MDL	< MDL	–	< MDL	< MDL	–
Benzo(a)fluorene-11-one	BaFlu-11	0.16	0.08–0.23	27.6	6.07	1.79–11.08	100.0	2.23	0.71–4.36	100.0
Benzanthrone	BZT	0.87	0.14–1.31	0.0	1.76	0.02–4.32	96.7	0.10	0.02–0.58	100.0
Benzo(a)anthracene-7,12-dione	BaAnt-7,12	n.d.	n.d.	–	2.20	0.01–4.86	100.0	0.93	0.01–2.21	100.0
6H-Benzo(cd)pyrene-6-one	BPyr-6	n.d.	n.d.	–	n.d.	n.d.	–	n.d.	n.d.	–
∑8 oxy-PAHs		32.6	15.8–73.1	–	471.0	325.9–741.4	–	233.1	124.7–337.1	–
1-Nitronaphthalene	1-NNap	2.19	0.99–4.69	61.7	16.97	13.36–21.53	0.1	5.02	1.91–9.84	1.5
2-Nitronaphthalene	2-NNap	0.26	0.11–0.40	31.7	5.08	2.44–7.33	3.1	1.88	1.29–2.83	5.4
2-Nitrophenyl	2-NBip	0.16	0.07–0.29	39.9	0.99	0.82–1.20	10.1	0.98	0.81–1.29	5.9
4-Nitrobiphenyl	4-NBip	n.d.	n.d.	–	2.23	1.51–2.68	0.0	2.45	0.29–4.10	0.0
1,5-Dinitronaphthalene	1,5-DNNap	n.d.	n.d.	–	0.80	0.05–2.17	80.0	0.93	0.05–3.72	53.9
5-Nitroacenaphthene	5-NAce	n.d.	n.d.	–	0.15	0.05–0.38	0.0	0.30	0.05–1.62	0.0
2-Nitrofluorene	2-NFlu	0.04	0.02–0.14	0.0	0.21	0.07–0.78	15.1	0.59	0.07–1.05	4.2
9-Nitroanthracene	9-NAnt	0.08	0.02–0.23	0.0	0.62	0.19–0.91	n.d.	2.26	0.12–4.70	57.8
9-Nitrophenanthrene	9-NPhe	n.d.	n.d.	–	0.20	0.09–0.37	n.d.	0.44	0.09–1.17	25.0
3-Nitrophenanthrene	3-NPhe	0.76	0.0003–1.93	96.1	n.d.	n.d.	–	n.d.	n.d.	–
2-Nitroanthracene	2-NAnt	0.31	0.07–0.62	0.0	n.d.	n.d.	–	n.d.	n.d.	–
2 + 3-Nitrofluoranthene	2 + 3-NFlt	0.52	0.06–1.14	0.0	9.50	7.32–11.37	94.5	12.30	4.68–26.66	79.8
4-Nitropyrene	4-NPyr	0.11	0.03–0.17	0.0	n.d.	n.d.	–	n.d.	n.d.	–
1-Nitropyrene	1-NPyr	n.d.	n.d.	–	n.d.	n.d.	–	n.d.	n.d.	–
2,7-Dinitrofluorene	2,7-DNFlu	0.06	0.001–0.14	0.0	n.d.	n.d.	–	n.d.	n.d.	–
7-Nitrobenzo(a)anthracene	7-NBaAnt	0.58	0.11–0.93	0.0	n.d.	n.d.	–	n.d.	n.d.	–
6-Nitrochrysene	6-NChry	n.d.	n.d.	–	n.d.	n.d.	–	n.d.	n.d.	–
1,3-Dinitropyrene	1,3-DNPyr	n.d.	n.d.	–	n.d.	n.d.	–	n.d.	n.d.	–
1,6-Dinitropyrene	1,6-DNPyr	n.d.	n.d.	–	n.d.	n.d.	–	n.d.	n.d.	–
1,8-Dinitropyrene	1,8-DNPyr	n.d.	n.d.	–	n.d.	n.d.	–	n.d.	n.d.	–
6-Nitrobenzo(a)pyrene	6-NBaPyr	n.d.	n.d.	–	n.d.	n.d.	–	n.d.	n.d.	–
∑22 nitro-PAHs		4.5	2.0–7.8	–	36.8	30.3–46.1	–	27.2	13.5–44.4	–

* Full results are given in the Supplement (Tables S9–S11); < MDL: below method detection limit; n.d. – not detected.

and oxy-PAHs, in both gaseous and particulate phases, and (4) determine other potential local sources of PAHs and nitro- and oxy-PAHs.

2 Material and methods

2.1 Sampling site

Svalbard is an archipelago located between latitudes 77 and 81° N in the western Barents Sea. Longyearbyen, being the largest populated settlement, was chosen as the study area. The local PP was installed in Longyearbyen in the 1980s and provides the community with sufficient electricity (45 000 MW) and central heating supply (70 000 MW) throughout the year (Bøckman, 2019). The PP is fuelled by coal produced in a nearby mine at Breinosa (mine no. 7). This coal has a distinct quality (brown, high-volatility bituminous coal with vitrinite reflectance $R_o = 0.78\%$; Marshall et al., 2015) and is well suited for energy production. Coal consumption is about 25 000–30 000 t yr⁻¹. The PP has two boilers (32 MW each). The coal burning temperature is about 1000 °C (Bøckman, 2019). Since December 2015, the flue gas purification system consists of a selective non-catalytic reduction (SNCR) system, an electrostatic precipitator (ESP), and a wet flue gas desulfurization (WFGD) scrubber. After SNCR the NO_x content in the flue gas is reduced by 50 % by spraying urea solution as a reduction agent into the boiler. Further, in the ESP step, dust is electrically charged and deflected toward the collection electrodes. In the WFGD scrubber, the flue gas is cooled and desulfurized by sea water. Low emissions are reported: dust 1.5 ± 0.2, SO₂ 0.3 ± 0.1, NO_x 244 ± 19, and CO 63 ± 5 mg Nm⁻³ (Lundgerdingen, 2017), reflecting the high efficiency of the flue gas cleaning system.

For PP emission analysis, stack emission air samples were collected at source (PP) and two locations at transect distance: the roof of the University Centre in Svalbard (UNIS, urban location, 1 km from PP) and the former northern lights observatory in Adventdalen (Adventdalen, rural location, 6 km from PP, 7 km to the active coal mine no. 7; Fig. 1). Sampling at UNIS and Adventdalen was performed simultaneously.

2.2 Sample collection

2.2.1 Power plant

A total of six low-volume (1.3–3.0 m³) samples of the PP stack emission were collected (Table S1 in the Supplement) under normal operating conditions on 27 September (PP1–PP3) and 2 October (PP4–PP6) 2018. Sampling was performed downstream from the WFGD scrubber, after all flue gas cleaning steps. The sampling probe (inner $\varnothing = 11$ mm) was situated to face the direction of the flue gas. A custom-made low-volume, battery-powered air sampler

(Digitel, Switzerland) was used to pump the flue gas through the sampling material placed in a stainless steel cartridge (16249, Sartorius Stedim Biotech GmbH, Germany). The particulate phase was collected on quartz fibre filter (QFF; pre-burnt at 450 °C for 6 h; $\varnothing = 47$ mm; no binder; Pallflex, USA) and the gaseous phase on polyurethane foam (PUF; Soxhlet pre-cleaned in toluene for 24 h followed by 24 h acetone wash; $\varnothing = 50$ mm; $L = 75$ mm; Klaus Ziemer GmbH, Germany). Although the pump was operated at the maximum speed (35 L min⁻¹, which corresponds to 6.1 m s⁻¹ probe intake flow speed), an isokinetic sampling regime was not achieved. The flue gas parameters (temperature 8.9 ± 0.5 °C, moisture 28 ± 2 %, flow speed 18.1 ± 0.8 m s⁻¹, and density 1.24 ± 0.2 kg m⁻³) were measured during the sampling by an FKT3DP1A multi-meter equipped with an S-type pitot probe (FlowKinetics LLC, USA).

2.2.2 UNIS and Adventdalen

The prevailing wind direction in Longyearbyen and Adventdalen is from the southeast. In summer, when the soil surface in Adventdalen becomes warmer than the water surface in Adventfjorden, the wind direction can temporarily change to northwesterly (Dekhtyareva et al., 2016; Esau et al., 2012). To focus on PP emission and avoid the peak of marine traffic in the summer, simultaneous sampling at UNIS and Adventdalen was carried out from 28 August to 28 September 2018 (Table S1) on days with a predicted northwesterly wind direction (Fig. S1 in the Supplement), using high-volume air samplers (TISCH-1000-BLXZ, TISCH Environmental Inc., USA) equipped with a dual-chamber sampling module (particle filter, stainless screen and vapour filter, glass cartridge). About 370 m³ of ambient air was collected over 24 h per sample (Table S1). For each station, six high-volume air samples were collected for particulate (QFF; pre-burnt at 450 °C for 6 h; $\varnothing = 103$ mm; no binder; Munktell/Ahlstrom, Finland) and gaseous (PUF; Soxhlet pre-cleaned in toluene for 24 h followed by 24 h acetone wash; $\varnothing = 65$ mm; $L = 100$ mm; Klaus Ziemer GmbH, Germany) phases. Weather parameters including ambient temperature, relative humidity, UV radiation, wind direction, and precipitation were recorded (Table S2). All samples (PP, UNIS, and Adventdalen) were kept intact inside the sampling unit after collection. In order to reduce the risk of post-collection contamination, the unit was sealed in two plastic bags for transportation to the lab, where samples were removed from the unit, sealed with layers of aluminium foil, and stored airtight in two plastic bags. Samples were kept frozen at -20 °C until analysis. A total of 18 samples (18 QFFs and 18 PUFs) and 8 field blanks (4 for PP and 4 for UNIS and Adventdalen) were collected.

2.3 Analytical procedure

In total, 16 PAHs and 8 oxy- and 22 nitro-PAHs (Table S3) were quantified using gas chromatography in combination

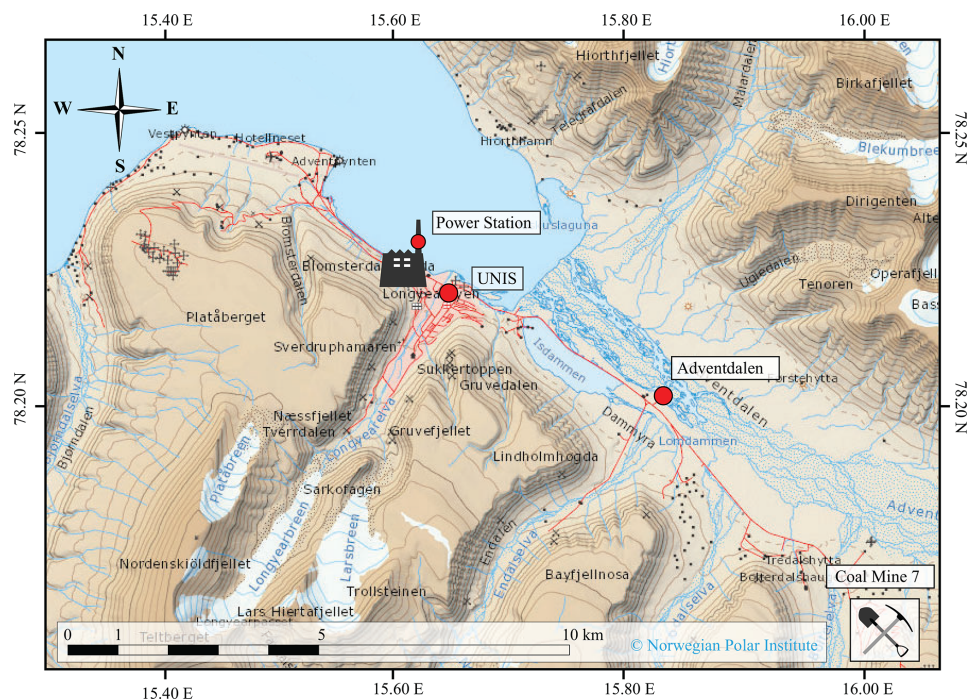


Figure 1. Air sampling transect locations in the vicinity of Longyearbyen.

with electron ionization triple quadrupole mass spectrometry (GC-EI-MS/MS) and gas chromatography in combination with electron capture negative ionization single quadrupole mass spectrometry (GC-ECNI-MS), respectively. Full details on analytical methods, including equipment and procedures, are outlined in the Supplement (Sect. S1, Tables S4 and S5). In brief, all QFF (particulate phase) and PUF (gaseous phase) samples were extracted separately by two different methods, followed by the same clean-up procedure. Several ^2H -labelled PAH (dPAH) surrogates (16 dPAHs, 3 dOxy-PAHs, and 6 dNitro-PAHs) were added to samples prior to extraction. QFF samples were extracted with dichloromethane using a quick, easy, cheap, effective, rugged, and safe QuEChERS-like procedure developed previously for the analysis of particulate bound PAHs (Albinet et al., 2013, 2014). PUF samples were Soxhlet extracted with dichloromethane for 24 h. The extracts were concentrated and cleaned up first with neutral alumina Al_2O_3 and then with neutral silica SiO_2 . Elutes were dried under gentle nitrogen stream and redissolved in approximately 100 μL *n*-hexane. The purified samples were spiked with three labelled standards to evaluate the surrogate recoveries.

2.4 Quality assurance

Detailed information on method validation and quality control is provided in the Supplement (Sect. S2). Field ($n = 4$ for PP, $n = 4$ for UNIS and Adventdalen combined) and laboratory ($n = 3$ for PP, $n = 3$ for UNIS and Adventdalen combined) blanks were analysed in order to evaluate possible contamination during sample transport and analysis. The method detection limit (MDL) was determined based on blank values for each sampling material type (Table S6). High contamination of PUF blank samples by Nap and 9,10-PhEQ for UNIS and Adventdalen was found; these compounds were excluded from the final results. No blank correction was performed for the concentration calculations. Samples with PAH concentrations below the instrumental limit of quantification (LOQ) were replaced by LOQ/2 for statistical analysis. The method efficiency was tested using QFF ($n = 4$) and PUF ($n = 4$) spiked samples (Table S7). Acceptable recoveries ranged between 63 %–109 % for dPAHs, 56 %–68 % for dOxy-PAHs, and 44 %–89 % for dNitro-PAHs (Table S8).

2.5 Statistical analysis

Statistical analyses of compound concentrations were performed with Minitab 18 Statistical Software (Minitab LLC, Pennsylvania, USA). Normality and homogeneity of variances were tested with Shapiro–Wilk and Levene’s tests, respectively. A Mann–Whitney *U* test was performed to test significant differences between sampling locations. Spearman’s correlation was used to investigate relationships between different variables. The statistical significance was set at $p < 0.05$, unless stated.

Principle component analysis (PCA) was performed for PAH source apportionment. A 6×29 matrix (sample number $\times 29$ detected compounds, including 14 PAHs and 15 nitro- and oxy-PAHs) dataset was used to assess the source contribution to PAHs for each location (UNIS and Adventalen). Total PAH concentrations (gaseous and particulate, G+P) were used to minimize the influence of partitioning, ageing, and photochemical degradation (Kim et al., 2009). PCA was based on a correlation matrix to standardize scales and weight all variables equally (Holmes et al., 2017). PCA was first applied on the concentrations matrix only, and then additional parameters (weather and diagnostic ratios) were carefully included in order to explain the observed sample groupings.

3 Results and discussion

3.1 Longyearbyen power plant PAH emission profile

Individual concentrations and phase distribution (percentage of particulate matter, %PM) of target PAHs are summarized in Table 1. The sum of total (G+P) concentration of the 16 priority PAHs ($\sum 16$ PAHs; U.S. Environmental Protection Agency) in the purified flue gases emitted from the PP is $0.106 \mu\text{g m}^{-3}$, which corresponds to $1.5 \mu\text{g kg}^{-1}$ coal. Currently, there is no PAH emissions standard for coal-fired power plants in Norway. However, compared to the Canadian emission limits of PAHs for municipal solid waste incinerators of $5 \mu\text{g m}^{-3}$ (Li et al., 2016), the Longyearbyen PP emissions are a factor of 3 lower. About 94% of 16 PAHs were emitted in a gas phase, in agreement with earlier studies (Li et al., 2016; Wang et al., 2015; Yang et al., 1998). The emission profile of the Longyearbyen PP is dominated by LMW PAHs (two and three rings), which represents 89% of $\sum 16$ PAHs emission; high molecular-weight (HMW) PAHs (5–7 rings) were not detected, likely due to their low vapour pressure and thus association with particles. A combination of ESP and WFGD has a removal efficiency of PM of up to 99.9% (Wang et al., 2019). Fine cooling of the PP flue gas ($8.9 \pm 0.5^\circ\text{C}$) by cold sea water facilitates high PM collection efficiency as well (Noda and Makino, 2010; Wang et al., 2019). As a result, PP dust emissions are below the ultra-low standard of 5 mg m^{-3} (Zhao et

Table 2. Ratios of individual oxy- and nitro-PAHs to their corresponding parent PAHs (G+P) in Longyearbyen power plant; averages of individual ratio values ($n = 6$) with standard deviation are presented.

Ratio	Mean \pm SD
Nitro-PAH / PAH	
2-NFlu / Flu	0.004 ± 0.005
3-NPhe / Phe	0.028 ± 0.028
2-NAnt / Ant	0.15 ± 0.11
9-NAnt / Ant	0.04 ± 0.03
2 + 3-NFlt / Flt	0.03 ± 0.02
7-NBAnt / BaAnt	5.37 ± 3.87
Oxy-PAH / PAH	
9,10-PheQ / Phe	0.08 ± 0.01
cPhen-4 / Pyr	0.31 ± 0.11
BaFlu-11 / Chry	0.65 ± 0.34
9-Flu / Phe	0.47 ± 0.13
9-Flu / Flu	1.67 ± 0.29
9,10-AntQ / Ant	12.17 ± 7.31

al., 2017) at $1.5 \pm 0.2 \text{ mg m}^{-3}$ (Lundgjerdingen, 2017). The PAH emissions profile was dominated by Nap and Phe, accounting for 53% and 27% of $\sum 16$ PAHs, followed by Flu, Flt, and Pyr. Nap and Phe are often reported as major emitted compounds from power plants equipped with analogous exhaust cleaning systems and/or burning the same type of coal (Hsu et al., 2016; Li et al., 2016; Wang et al., 2015). A similar PAH emissions profile was reported by Hsu et al. (2016) for the power plant in central Taiwan (Table S12). A higher flue gas dust concentration and different coal sources resulted in 40% emissions of four-ringed PAHs compared to 11% for Longyearbyen PP. Operation conditions and boiler type can have significant effects on emitted PAH profiles and concentrations (Wang et al., 2015) as can combustion temperature (Peng et al., 2016) and geological maturity (W. Huang et al., 2014).

Nitro- and oxy-PAHs are constituents of raw coal and can also be produced from parent PAH compounds during high-temperature coal combustion (W. Huang et al., 2014). The yields of individual nitro-PAHs from the PP were 1–2 orders of magnitude lower than those of their corresponding parent PAHs, and individual concentrations were at or below 1.7 ng m^{-3} ; 1-NNap was the most abundant nitro-PAH. W. Huang et al. (2014) investigated the same type of coal (bituminous, $R_0 = 0.77\%$), burnt at lower temperatures in a honeycomb briquette stove; nitro-PAHs were absent in the raw coal and calculated nitro-PAH / PAH ratios were > 1 , confirming the formation of nitro-PAH compounds during coal combustion. In contrast, in the present work, the same daughter-to-parent PAH ratios were < 1 (Table 2), indicating an absence of nitro-PAH formation during coal combustion or possible thermal degradation of nitro-PAH at 1000°C .

The yields of oxy-PAHs were orders of magnitude higher than nitro-PAHs because oxy-PAHs can be produced by reaction of PAH with O[•] or [•]OH radicals generated continuously by radical chain reactions during combustion (W. Huang et al., 2014). 9-Flu and 9,10-AntQ were the most abundant among the oxy-PAHs (12.4 and 15.6 ng m⁻³, respectively), and concentration of 9,10-PheQ was a factor of 6 lower. The calculated ratios of oxy-PAH to corresponding parent PAH were lowest for 9,10-PheQ/Phe and highest for 9,10-AntQ/Ant (Table 2). This can be due to a higher content of Phe in coal, as well as different reaction rates of Phe, Ant, and Flu with O[•] or [•]OH radicals. Difference between the reaction rates of Flu and Ant can possibly be explained by different reaction pathways; Flu undergoes H atom abstraction at the 9-position to form 9-Flu, while Ant requires [•]OH attack on the aromatic ring (Brubaker and Hites, 1998). Ant and Phe have essentially the same three-ring structure, only differing by the relative position of their aromatic rings. However, Ant appears to be significantly more reactive, due to the sterically unhindered molecular structure of Ant (Keyte et al., 2013). The formation of specific PAHs is also a temperature-dependent process (Peng et al., 2016).

Ant, BaAnt, and Chry are often used as indicators of coal combustions (Zheng et al., 2019; Wu et al., 2014; Wang et al., 2009); however, their concentrations in the flue gas of the Longyearbyen PP were negligible. This demonstrates the strong importance of determining indicative PAH profiles for individual combustion sources for correct source identification. PAH emissions from different coal plants are hard to compare because they are affected by many factors including coal type, boiler load, combustion mode (Wang et al., 2015), and flue gas cleaning systems. Nap was the most abundant PAH emitted from the Longyearbyen PP. Due to its ubiquitous presence, Nap was not regarded as a suitable marker. Further, Phe, Flu, Flt, Pyr, 9-Flu, and 9,10-AntQ were the main PAHs and oxy-PAHs detected in the Longyearbyen PP flue gas (Fig. 2); therefore the presence and diagnostic ratios (Table 3) of these compounds were used as markers of the PP source in the present work. In Yu et al. (2019), coal combustion was identified as the main source (68 % contribution) of PAHs, at the Zeppelin monitoring station at Ny-Ålesund, Svalbard, and Phe, Flu, Flt, and Pyr were the main contributors, most likely attributable to the Longyearbyen PP located 115 km southeast of Ny-Ålesund. Overall, the total flue gas emissions were 960 000 Nm³ d⁻¹ (Lundgjerdingen, 2017), and average daily emissions of Σ 16 PAHs, Σ 8 oxy-PAHs, and Σ 22 nitro-PAHs are 98.7, 31.3, and 4.3 mg, respectively.

3.2 UNIS and Adventdalen

3.2.1 Ambient concentrations and PAH profiles

The concentrations of PAHs and oxy-PAHs measured at UNIS were a factor of 2 higher than at Adventdalen,

while nitro-PAH levels differed less (Table 1). Σ 15 PAHs were 749.2 ± 72.6 (UNIS) and 369.1 ± 66.7 pg m⁻³ (Adventdalen); Σ 7 Oxy-PAHs were 471.0 ± 150.8 (UNIS) and 233.1 ± 68.3 pg m⁻³ (Adventdalen); Σ 22 nitro-PAHs were an order of magnitude lower than both parent PAHs and oxy-PAHs, with average values of 36.8 ± 6.2 (UNIS) and 27.2 ± 11.1 pg m⁻³ (Adventdalen). The UNIS and Adventdalen chemical profiles of PAHs and oxy-PAHs were similar, while the profiles of nitro-PAHs differ (Fig. S2). Proportions of 1- and 2-NNap were higher in UNIS samples (about 60 % of Σ 22 nitro-PAHs), while 9-Nant and 2 + 3-NFlt showed higher contributions into the nitro-PAH profile of samples from Adventdalen (about 55 % of Σ 22 nitro-PAHs).

Among the parent PAHs, Phe (ranging from 191.7 to 470.0 pg m⁻³) and Flu (ranging from 38.5 to 236.0 pg m⁻³) were the most abundant in the present study. The Phe and Flu concentrations measured in Longyearbyen (UNIS and Adventdalen) were 2 orders of magnitude higher than those detected at the Zeppelin station and the same order of magnitude as in Birkenes (southern mainland Norway) for the same period (Table S13). The PAH profiles were dominated by Phe and Flu at all sites (Fig. S3). A higher proportion of Phe was observed in Longyearbyen samples. The measured PAH concentrations in the present study were in agreement with the 2-decade average data reported for the Arctic monitoring stations in Svalbard (Zeppelin) and Finland (Pallas) and were about an order of magnitude higher compared to the Canadian Arctic (Alert) concentrations (Yu et al., 2019). The PAH levels observed in Longyearbyen were significantly (up to 2 orders of magnitude) lower compared to rural sites in Europe and China (Table S14).

Among measured oxy-PAHs, concentrations of 9-Flu and 9,10-AntQ were the highest in the present study. The 9-Flu level (270.3 ± 146.9 pg m⁻³ at UNIS and 139.4 ± 24.9 pg m⁻³ in Adventdalen) was a factor of 3 higher than reported for Pallas and Råö (southern Sweden) background stations (Brorström-Lundén et al., 2010), while 9,10-AntQ (163.5 ± 57.4 pg m⁻³ at UNIS and 71.7 ± 39.2 pg m⁻³ in Adventdalen) in Longyearbyen was equal to the winter levels in central European background air (Lammel et al., 2020). The sum of oxy-PAHs detected at UNIS was similar to rural sites in eastern England (Alam et al., 2014) and the central Czech Republic (Lammel et al., 2020) but was significantly lower than in rural southern China (B. Huang et al., 2014) and the French Alps (Albinet et al., 2008).

1-NNap and 2 + 3-NFlt were the most abundant nitro-PAHs detected at UNIS and Adventdalen. The level of 2 + 3-NFlt (9.5 ± 1.6 at UNIS and 12.3 ± 7.7 pg m⁻³ in Adventdalen) was an order of magnitude higher than that at Råö and Pallas stations (Brorström-Lundén et al., 2010), and 1-NNap average concentrations were 17.0 ± 3.0 at UNIS and 5.0 ± 3.2 pg m⁻³ in Adventdalen. Overall, nitro-PAH concentrations were similar to those reported for the Pallas and Råö Scandinavian stations (Brorström-Lundén et al., 2010) and

Table 3. Source identification based on diagnostic ratios derived from total (G+P) concentrations; averages of individual ratio values ($n = 6$) with standard deviation are presented.

	Mean value	Potential source	Reference
IPyr / (IPyr+BPer)			
Power plant	n.d.	–	
UNIS	0.32 ± 0.01	< 0.35 gasoline	Ravindra et al. (2008b)
Adventdalen	0.45 ± 0.05	0.35–0.70 diesel	Kavouras et al. (2001); Ravindra et al. (2008b)
Flu / (Flu+Pyr)			
Power plant	0.64 ± 0.11	–	
UNIS	0.81 ± 0.04	> 0.5 coal combustion > 0.5 diesel	Yunker et al. (2002); Katsoyiannis and Breivik (2014); Ravindra et al. (2008b)
Adventdalen	0.68 ± 0.05	0.64 local power plant > 0.5 coal combustion	This study Yunker et al. (2002); Katsoyiannis and Breivik (2014)
Flt / (Flt+Pyr)			
Power plant	n.d.	–	
UNIS	0.42 ± 0.02	0.31–0.42 marine fuel	Zhang et al. (2019)
Adventdalen	0.40 ± 0.08	< 0.5 petrol emission	Yunker et al. (2002)
BbkFlt / BPer			
Power plant	n.d.	–	
UNIS	0.48 ± 0.03	< 0.4 gasoline	Kuo et al. (2013)
Adventdalen	0.87 ± 0.25	0.78 diesel	Kuo et al. (2013)

the rural site in the Czech Republic which is representative of central European background levels (Lammel et al., 2020).

3.2.2 Gas–particle partitioning

Gas–particle partitioning is an important process that controls transport, degradation, and distribution patterns of contaminants in and between environmental compartments (Finlayson-Pitts and Pitts, 1999; Lammel et al., 2009; Franklin et al., 2000). The sampling campaign in the present study was conducted from late Arctic summer until early autumn and during this period the air temperature varied from +6.8 in August to –4.4 °C in September and several precipitation events (snow and rain) occurred. In general, LMW PAHs were found in the gas phase, while HMW PAHs were present in the particulate phase (Table 1), which is in accordance with their physico-chemical parameters, such as the octanol–air partition coefficient, vapour pressure, and molecular weight (Table S3; Tomaz et al., 2016; Shahpoury et al., 2016). Repartitioning between phases (Fig. 3) mainly impacted semi-volatile compounds with three and four aromatic rings (Flt, Pyr, BaAnt, Chry; 2-NFlu, 9-Flu, cPPhe-4, 9,10-AntQ, 9-NAnt, and 2+3-NFlt) as a response to changing meteorological conditions (Hu et al., 2019). Strong negative correlations of the percentage of PAH determined in particulate

phase (%PM) with ambient temperature were confirmed for most of these compounds (Table S15). %PM also depends on aerosol surface area, organic matter, and black carbon content (Lohmann and Lammel, 2004).

Compared to Adventdalen, the urban UNIS location ensures a higher level of PAHs emitted from different nearby anthropogenic sources, including the PP. Furthermore, low ambient temperature reinforces the partitioning of freshly emitted gaseous PAHs to the particulate phase. As a result, %PM at UNIS was higher than in Adventdalen. Deposition (wet and dry) and chemical reactions with atmospheric oxidants are important removal processes of PAH from air (Keyte et al., 2013). On the local scale, within an hour of travel time from PP to Adventdalen, it is not expected that photolytically initiated transformation of the freshly emitted PAHs has a strong influence on gas phase concentrations and consequently on %PM. Dry deposition rates vary depending on the type of adsorbing particle (mass, size, aerodynamic properties, shape, and chemical composition) and the atmospheric conditions (Weinbruch et al., 2018) and may be a dominant PAH removal process in source areas (Sharma and McBean, 2002).

The influence of wet deposition was indicated by a significant negative correlation between the amount of precipitation and concentrations of several particle-bound HMW

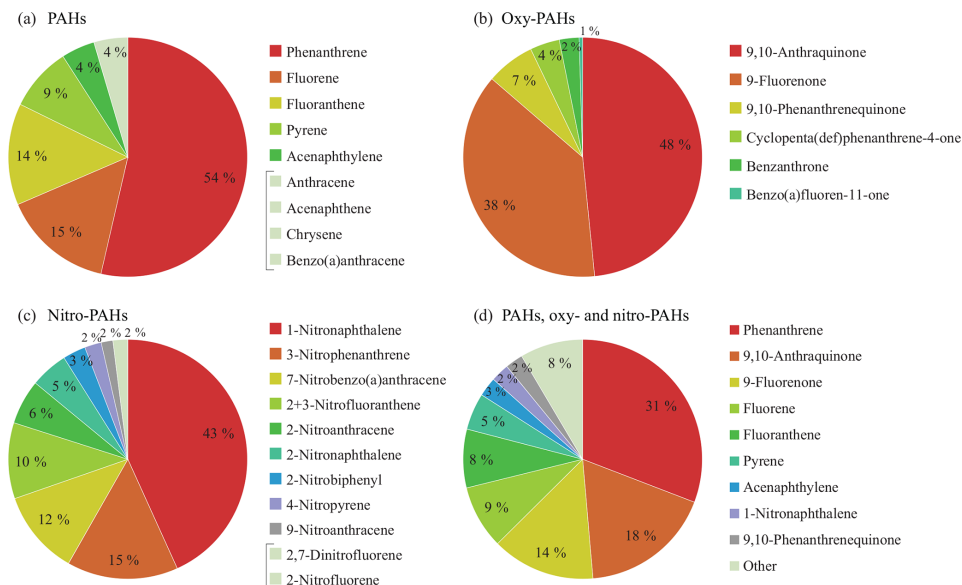


Figure 2. Proportion of (a) PAHs, (b) oxy-PAHs, (c) nitro-PAHs, and (d) all the PAH derivatives (G+P; excluding Nap) in the Longyearbyen power plant emission ($n = 6$).

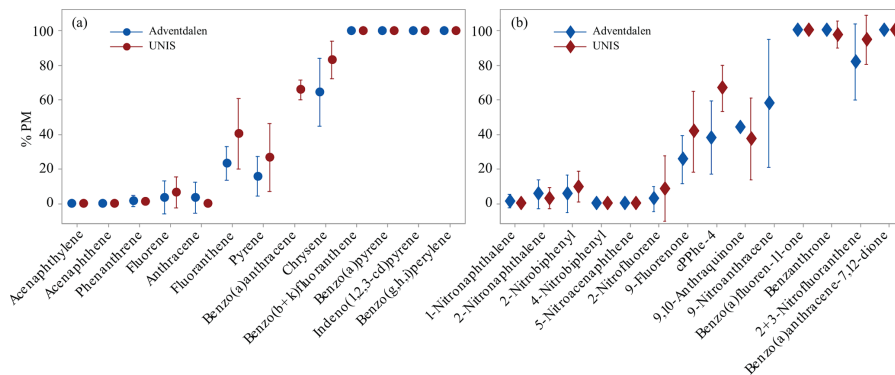


Figure 3. Percentage of (a) PAHs and (b) nitro- and oxy-PAHs determined in particulate phase (% PM) at UNIS ($n = 6$) and Adventdalen ($n = 6$); individual standard deviations are used to calculate the intervals.

PAHs (Chry, BbkFlt, IPyr, BPer, BaFlu-11, and BaAnt-7,12) as well as semi-volatile Phe, Flt, and Pyr, which are more predominant in the gaseous phase (Spearman correlation, $p < 0.05$; Table S16). Effective wet scavenging of Phe, Flt, and Pyr has been suggested earlier (Škrdlíková et al., 2011). Furthermore, a strong negative correlation with the mass of water vapour in the air (specific humidity) was determined for most of the compounds (Spearman correlation, $p < 0.05$;

Table S17). Particle-associated HMW compounds are readily scavenged by precipitation, while water solubility and polarity (for nitro- and oxy-PAHs) play an additional role in wet scavenging processes (Shahpoury et al., 2018). The gas phase removal from the atmosphere is due to substance dissolution in water droplets, which enhances the scavenging effect at higher humidity. A higher sensitivity of gas scavenging com-

pared with particle scavenging towards liquid water content was also indicated by Škrdlíková et al. (2011).

In general, the obtained %PM was in agreement with those reported earlier (Table S18). A higher %PM of 9,10-AntQ and several nitro-PAHs (1- and 2-NNap, 2-NFlu, 9-NAnt, 9-NPhen) was detected in French Alpine sites in winter (Albinet et al., 2008), while a higher %PM of Flt, 9-Flu, and cPPhe-4 found in the present study contrasts with those reported for temperate urban and rural sites in China and Europe (B. Huang et al., 2014; Tomaz et al., 2016). Source difference, weather influence such as precipitation and temperature, and different atmospheric conditions (e.g. number of suspended particles, mass size particle distribution, and specific humidity) are likely responsible for these variations.

4 Source identification

Due to changes in the Arctic front, more frequent precipitation, and low levels of wood and coal burning for residential heating in the Northern Hemisphere in the summer, the LRAT of PAHs to the Arctic is low in summer. Sampling was performed on days with predicted northwesterly wind, and according to the 5 d back-trajectory analysis, the air arriving to Longyearbyen in the sampling period mainly came from the north and from Greenland (Fig. S4). As discussed in Sect. 3.2.1, up to 2 orders of magnitude lower PAH concentrations were detected at the Zeppelin monitoring station compared to the levels in Longyearbyen at the same time. Thus, local emissions were the main sources of PAHs in Longyearbyen in this study.

Besides the PP emission, vehicles are another obvious local source of PAHs. In 2018, 1558 vehicles, including cars, lorries, and buses, were registered in Longyearbyen (Table S19; Statistics Norway, 2018). Longyearbyen maintains about 50 km of paved and unpaved roads dedicated to traffic (Bore, 2012). Sampling was conducted at the end of summer in order to avoid peak emissions from marine traffic and to focus on PP emissions; however, it is likely that some of the 718 registered private boats were active in Adventfjorden and several larger ocean-going vessels were in the port around the sampling period (weeks 34–38, Fig. S5). Thus, shipping emissions could not be eliminated as a potential source of PAHs. Note that there is no local waste incineration and wood burning.

PCA was applied to samples from Adventdalen ($n = 6$) and UNIS ($n = 6$) to determine potential PAH sources in each location. Total PAH (G+P) concentrations were used to minimize the influence of partitioning, ageing, and photochemical degradation. Selected PAH diagnostic ratios (Table 3) and weather parameters were utilized as additional supportive tools for sources interpretation, and their values were used as variables. Diagnostic ratios may be affected by large-scale mixing of PAHs in the atmosphere, differing emission rates of PAH from the same source, the in-

fluence of changing environmental conditions, and the atmospheric processing of individual PAH compounds with different atmospheric lifetimes and reactivities (Alam et al., 2013; Tobiszewski and Namieśnik, 2012; Katsoyannis and Breivik, 2014). Ratios based on highly reactive compounds such as Ant and BaAnt were not included, while more stable HMW PAHs diagnostic ratios were interpreted with greater confidence (Galarneau, 2008; Alam et al., 2014). Yunker et al. (2002) previously proposed the ratio of IPyr / (IPyr+BPer) to differentiate vehicle from coal combustion emissions. BbkFlt / BPer was selected as an additional marker ratio for traffic due to the greater capacity to discriminate between diesel and gasoline emissions, as well as due to its wider value range (Kuo et al., 2013). The Flt / (Flt+Pyr) ratio is often used for source identification and, in particular, to understand if PAHs are mainly emitted from petroleum sources or from combustion processes (Yu et al., 2019). The Flu / (Flu+Pyr) ratio was selected as a specific indicator for coal combustion due to its strong correlation with the local PP determined markers, and the ratio value was also in agreement with the literature (Yunker et al., 2002; Katsoyannis and Breivik, 2014). Two principal components (PCs) for Adventdalen (74 %) and two PCs for UNIS (74 %) were focused on.

4.1 Adventdalen

The first and the second PCs described 51 % and 23 % of the total variance, respectively (Table S20). Three groups of compounds suggest three different potential sources. The first group include Flt, Pyr, cPPhe-4, BaFlu-11, and BaAnt-7,12. Strong correlations between their concentrations and the IPyr / (IPyr+BPer) ratio suggest a traffic origin for these compounds (Yunker et al., 2002) and specifically diesel emissions (Tables 3; S21; Ravindra et al., 2006, 2008a). Because of the rural position, car traffic is much lower at this location. At the same time, due to the proximity to an active mine (Fig. 1), heavy-duty vehicles (coal trucks, tourist buses, geotechnical drilling machinery) are thus the main candidate source for PAH vehicle emissions. Produced coal is regularly delivered from the mine to PP and storage area in the harbour on a road situated 150 m away from the Adventdalen sampling station. Coal is transported by Volvo FH540 trucks (built in 2018–2020) driven on diesel CFPP-12 (NS-EN 590; Per Nilssen, Store Norske, personal communication, 2020; Table S23). The trucks have Euro 6 standard compliant Volvo D13K engines (HC 0.13, CO 1.5, NO_x 0.4, PM 0.01 g (kWh)⁻¹; DieselNet, 2020) fitted with exhaust gas recirculation, diesel particulate filter, diesel oxidation catalyst, selective catalytic reduction, and ammonia oxidation catalyst (Volvo Trucks, 2020). These allow high operation temperatures and high efficiencies in reducing particle and NO_x emissions. Numerous studies showed substantial reduction in gaseous and particulate emissions of PAH and nitro- and oxy-PAHs as the result of such mitigation in particle and NO_x

emissions (Hu et al., 2013; Gerald Liu et al., 2010; Khalek et al., 2015; Huang et al., 2015). An up to 10 orders of magnitude reduction in emission from similar to Volvo D13K heavy-duty engine was reported for several nitro-PAHs (6-NChry, 1-NPyr, 2-NPyr, 4-NPyr, 7-NBaAnt; Liu et al., 2015; Gerald Liu et al., 2010), which were not detected in the present study, most likely due to low vehicle numbers in Adventdalen. However, Flt, Phe, and Pyr have been widely reported to be emitted after diesel emissions (Albinet et al., 2007; Ravindra et al., 2008a; Wingfors, 2001) as have BaFlu-11, BaAnt-7,12, and cPPhen (Nyström et al., 2016; Ahmed et al., 2018; Rogge et al., 1993). 9-Flu, 9,10-AntQ, and 1-NNap were the main oxy- and nitro-PAHs emitted from modern technology heavy-duty diesel engines (Liu et al., 2015; Gerald Liu et al., 2010; Guan et al., 2017), supporting the traffic origin of the group 1 compounds too.

9-Flu, 9,10-AntQ, and 1-NNap, together with Phe and Flu (group 2), seem to have a double origin. On a PCA loading plot these compounds have a similar proximity to the traffic emission ratio (PC1), as well as to the coal combustion ratio (PC2). As reported earlier, Phe, Flu, 9,10-AntQ, 9-Flu, and 1-NNap together accounted for 74 % of the total PAH emission from the local PP (Fig. 2) and a Mann–Whitney U statistical test ($n = 6$, $p \leq 0.05$) showed no significant difference between values of the Flu / (Flu+Pyr) coal combustion diagnostic ratio based on the measured Flu and Pyr concentrations in Adventdalen and in the local PP stack emission.

The PC1 emphasized a positive correlation of 2 + 3-NFlt and 9-NAnt (group 3) with temperature, humidity, and UV radiation, as well as a negative correlation with primary PAHs (Fig. 4, Table S17), suggesting a secondary source of origin. The daughter-to-parent PAH ratios, 9-NAnt/Ant and 2 + 3-NFlt / Flt (Table S24), showed statistically significant correlations with temperature, humidity, and UV radiation (Spearman correlation, $p < 0.10$; Table S25). Moreover, 2 + 3-NFlt and 9-NAnt had a strong positive correlation with each other and negatively correlated with their parent compounds (Spearman correlation, Table S26), by reason of assumed chemical transformation. It should be noted that 9-NAnt and 2 + 3-NFlt were detected in the PP flue gas at low levels (0.08 and 0.5 ng m⁻³, respectively), and further statistical analysis (Spearman correlation, Table S26, Fig. 4) showed no correlation with established PP tracers (Phe, 9,10-AntQ, and 9-Flu), suggesting a different source of origin. These results indicate atmospheric formation as an additional source of 9-NAnt and 2 + 3-NFlt, in agreement with other studies (Lin et al., 2015; Hayakawa et al., 2000; Shahpoury et al., 2018). Sampling close to a major source of NO_x emission such as the local power plant can result in concentrations of NO₃ and NO₂ at high enough levels for atmospheric transformation of PAHs to occur (Keyte et al., 2013). Relative contribution of primary and secondary sources of nitro-PAHs could be evaluated by applying a 2-NFlt / 1-NPyr ratio (Ringuet et al., 2012; Ciccioli et al., 1996), but 1-NPyr was not detected in our study.

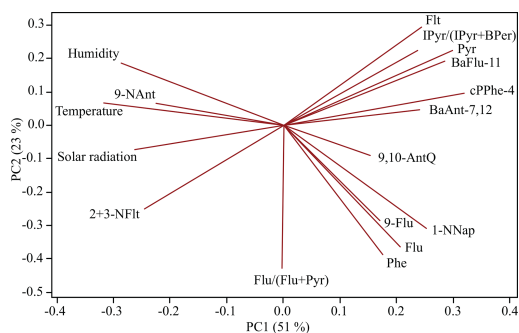


Figure 4. Principal component analysis loading plot of PC1 and PC2 for Adventdalen samples (G+P; $n = 6$).

The two PCs explain 74 % of the total variance. Traffic emission (mainly diesel exhaust) and the coal burning PP are concluded as the main local sources of PAHs and nitro- and oxy-PAHs in Adventdalen, and atmospheric transformation of PAHs is an additional source of nitro-PAHs.

4.2 UNIS

The proximity of the UNIS sampling location to central Longyearbyen, as well as to the PP and the port, makes the UNIS location more complex for source identification. This site is mainly influenced by passenger car traffic, although heavy-duty vehicles also pass UNIS. Overall, 1114 private cars were registered in Longyearbyen in 2018 (Statistics Norway, 2018), including old- and modern-technology cars (Euro 3–7 emission standard), approximately equally balanced between gasoline and diesel fuel. Gasoline 95 (with up to 5 % bioethanol) and diesel CFPP-12 (with up to 7 % biodiesel) are the exclusive fuels used in summer time and comply with the Norwegian standard NS-EN 228 and NS-EN 590, respectively, with ultra-low (< 10 ppm or 0.001 %) sulfur content (Jøran Storø, LNS Spitsbergen, personal communication, 2020). Details of the fuel parameters can be found in Tables S22 and S23.

Muñoz et al. (2018) undertook a study under similar vehicle and fuel conditions to Longyearbyen and reported a predominance of LMW PAHs for both fuels. Flt, Pyr, and Phe and BPer, BaPyr, Chry, and BbFlt were found to be the most abundant compounds in gaseous and particulate phases, respectively, in agreement with earlier studies (Nyström et al., 2016). A similar PAH pattern was found for UNIS samples. On the PCA plot (Fig. 5) Flt, Pyr, BPer, BaPyr, Chry, and BbFlt are grouped together (group 1) and have equally high loadings on the PC1 (Table S27). The compound concentrations are significantly correlated with the traffic ratio BbFlt / BPer ($p < 0.05$, Table S28) suggesting the same origin of the compounds. The BbFlt / BPer ratio varied from

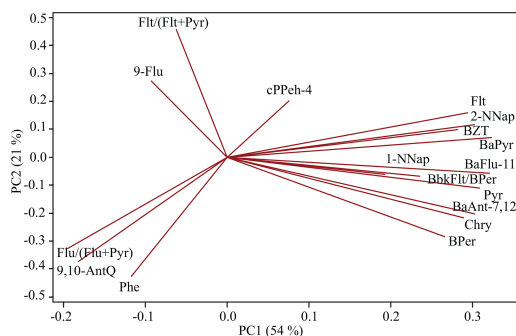


Figure 5. Principal component analysis loading plot of PC1 and PC2 for UNIS samples (G+P; $n = 6$).

0.43 to 0.72 indicating either diesel or gasoline emissions (Kuo et al., 2013). The diesel emission predominance was found for 2 out of the 6 sampling days, although particulate phase 1-NPyr, a marker of diesel emissions, was not detected. 1-NPyr forms in the combustion chamber of diesel engines by the addition of nitrogen oxide or nitrogen dioxide to free Pyr radicals (IARC, 2014). Its generation is facilitated by the high engine temperatures (IARC, 2014; Karavalakis et al., 2010; Guan et al., 2017; Huang et al., 2015), which likely cannot be reached in Longyearbyen due to short driving distances and a low speed limit. The use of high-quality ultra-low sulfur fuel with substantially reduced emissions of NO_x leads to reduced nitration of PAHs during fuel combustion (Heeb et al., 2008; T. Zhao et al., 2020) and together with low total vehicle number results in low nitro-PAH emissions. The atmospheric deposition which occurred may be of influence too.

Gaseous phase 1-NNap and 2-NNap have large loadings on the PC1. They are often reported in traffic emissions (Alam et al., 2015; Albinet et al., 2007; Keyte et al., 2016), as well as oxy-PAHs such as BaFlu-11, BaAnt-7,12, and BZT (Nyström et al., 2016; Albinet et al., 2007; Ahmed et al., 2018; Karavalakis et al., 2010). All these nitro- and oxy-PAHs have a strong positive correlation with the traffic ratio (Table S28). Thus, we conclude the traffic (diesel and gasoline) is the source for Flt, Pyr, Chry, BPer, BaPyr, 1-NNap, 2-NNap, BaFlu-11, BaAnt-7,12, and BZT at the UNIS location.

A second group of compounds (Phe, Flu, and 9,10-AntQ) was strongly correlated with the coal combustion ratio $\text{Flu} / (\text{Flu} + \text{Pyr})$ (Fig. 5, Table S28), supported by their predominance (along with 9-Flu) in the PP emissions (Fig. 2). 9-Flu may have other possible sources, including diesel and gasoline vehicle exhaust, coal powder, and road dust particles (Keyte et al., 2013), and may be locally produced, transported a longer range, or secondarily formed in the atmosphere (Kojima et al., 2010). Interestingly, despite heavy rain

during sampling, 9-Flu was found in its maximum concentration (about 2-fold higher the average detected level) on the second sampling day, which may suggest a strong local emission on that day in addition to the daily PP emissions. 9-Flu showed a strong positive correlation with the $\text{Flt} / (\text{Flt} + \text{Pyr})$ ratio, indicating petrol or marine fuel sources (Zhang et al., 2019). The ratio did not correlate with the traffic-emitted compounds and the traffic ratio (group 1); thus marine fuel emission was regarded as a potential source. Despite the intention to collect air samples at the end of summer to avoid the peak marine traffic, four large boats (fishing, two cruise vessels, and oil tanker; Fig. S5) and some private boats were registered in Longyearbyen harbour during sampling day 2 (Kystdatahuset, 2018). Our assumption is supported by reports of 9-Flu, cPPeh-4, and 9,10-AntQ as major oxy-PAHs in ship emissions (Czech et al., 2017; J. Zhao et al., 2020, 2019). According to Svalbard environmental law, vessels entering Svalbard coastal waters are required to use distillate marine fuel (DMA ISO 8217:2017) instead of heavy marine oil to satisfy regulations requiring a fuel sulfur content below 1.0 % (Governor of Svalbard, 2014). Ultra-low sulfur diesel CFPP-12 (NS-EN 590, with sulfur content below 0.001 %, Table S23) is also used for private boats. Such predominance of distillate marine diesel explains the strong correlation of 9-Flu with the marine fuel ratio and no correlation with 9,10-AntQ, which is mainly emitted from heavy-fuel oil (Huang et al., 2018). The use of high-quality fuels decreases the emissions of particles (Anderson et al., 2015). A reduction of up to 94 % particulate PAH emission was reported when burning low-sulfur fuel compared to heavy-fuel oil (Huang et al., 2018; Gregoris et al., 2016; Kotchenruther, 2017; Czech et al., 2017). This explains the absence of particle-bound PAHs correlating with the marine ratio $\text{Flt} / (\text{Flt} + \text{Pyr})$.

The two PCs explain 74 % of the total variance of the UNIS samples. PP coal burning, traffic, and marine shipping emissions are determined as potential sources of PAHs and nitro- and oxy-PAHs.

5 Conclusions

The results provide insights into local sources of atmospheric PAHs and nitro- and oxy-PAHs in Svalbard. Source markers for the coal burning PP in Longyearbyen were determined, and generally low emissions of PAHs confirmed an efficient exhaust cleaning system. However, PAHs are emitted daily from coal burning and, due to a large volume of flue gas emissions, the PP remains an important local anthropogenic source of atmospheric contaminants. Overall, nitro- and oxy-PAH concentrations were the same order of magnitude as detected at other background Scandinavian and European air sampling stations, and PAHs were 1 order of magnitude higher than in Ny-Ålesund, Svalbard. The gas-particle partitioning of PAHs and nitro- and oxy-PAHs was dependent on air temperature and humidity and mainly impacted

semi-volatile compounds with three and four aromatic rings. Vehicle and marine traffic were other contributors to PAH emissions. The results also revealed secondary atmospheric formation as an additional source of 2 + 3-NFlt and 9-NAnt. The present study contributes to understanding the fate and distribution of PAHs in the Arctic, and it provides important information on the phase-separated concentrations of PAHs and nitro- and oxy-PAHs in Arctic air, as well as markers of the Longyearbyen PP emissions. This data can eliminate uncertainties in model predictions that aim to assess the extent and impacts of Arctic atmospheric contaminants. Furthermore, the knowledge on local emissions level can be important in case of temperature inversion in the lower atmosphere when vertical dilution is limited and contaminants are trapped near the ground, which may be adverse to public health.

Data availability. The dataset used in this paper is included in the Supplement, and further information is available from the corresponding author at tatiana.drotikova@unis.no.

Supplement. The supplement related to this article is available online at: <https://doi.org/10.5194/acp-20-9997-2020-supplement>.

Author contributions. RK, AKH, and HCR designed the campaign. TD conducted the field and lab works. TD, with support from AMA and RK, optimized, validated, and performed GC analysis and further quantification. TD processed and interpreted PCA outcome. TD prepared the paper with contributions from all co-authors. TD, AMA, and AKH prepared the Supplement.

Competing interests. The authors declare that they have no conflict of interest.

Acknowledgements. We gratefully acknowledge Longyearbyen Lokalstyre (Longyearbyen Community Council), specifically Kim Rune Røkenes (a former leader of Energyverket), for the support in performing the PP exhaust sampling. We also thank Rasmus Bøckman (Lokalstyre, Energyverket) for providing information on the PP system operating parameters; Morten Hogsnes and Kristin Lundgjerdingen (Applica Test & Certification AS) for sharing their knowledge on PP flue gas sampling; Siiri Wickström (UNIS) for helping with weather prediction; Marcos Porcires (UNIS) for on-site installation of weather station; Øyvind Mikkelsen (Norwegian University of Science and Technology) for teaching on the PCA topic; and Malte Jochmann (UNIS/Store Norske) for fruitful discussions on Svalbard coal quality. This research was financially supported by UNIS, NMBU, and the Svalbard Environmental Protection Fund (AtmoPart project).

Financial support. This research has been supported by the Svalbard Environmental Protection Fund (grant no. 940010).

Review statement. This paper was edited by Ralf Ebinghaus and reviewed by two anonymous referees.

References

- Ahmed, T. M., Bergvall, C., and Westerholm, R.: Emissions of particulate associated oxygenated and native polycyclic aromatic hydrocarbons from vehicles powered by ethanol/gasoline fuel blends, *Fuel*, 214, 381–385, <https://doi.org/10.1016/j.fuel.2017.11.059>, 2018.
- Alam, M. S., Delgado-Saborit, J. M., Stark, C., and Harrison, R. M.: Using atmospheric measurements of PAH and quinone compounds at roadside and urban background sites to assess sources and reactivity, *Atmos. Environ.*, 77, 24–35, <https://doi.org/10.1016/j.atmosenv.2013.04.068>, 2013.
- Alam, M. S., Delgado-Saborit, J. M., Stark, C., and Harrison, R. M.: Investigating PAH relative reactivity using congener profiles, quinone measurements and back trajectories, *Atmos. Chem. Phys.*, 14, 2467–2477, <https://doi.org/10.5194/acp-14-2467-2014>, 2014.
- Alam, M. S., Keyte, I. J., Yin, J., Stark, C., Jones, A. M., and Harrison, R. M.: Diurnal variability of polycyclic aromatic compound (PAC) concentrations: Relationship with meteorological conditions and inferred sources, *Atmos. Environ.*, 122, 427–438, <https://doi.org/10.1016/j.atmosenv.2015.09.050>, 2015.
- Albinet, A., Leoz-Garziandia, E., Budzinski, H., and Viilenave, E.: Polycyclic aromatic hydrocarbons (PAHs), nitrated PAHs and oxygenated PAHs in ambient air of the Marseilles area (South of France): Concentrations and sources, *Sci. Total Environ.*, 384, 280–292, <https://doi.org/10.1016/j.scitotenv.2007.04.028>, 2007.
- Albinet, A., Leoz-Garziandia, E., Budzinski, H., Villenave, E., and Jaffrezo, J. L.: Nitrated and oxygenated derivatives of polycyclic aromatic hydrocarbons in the ambient air of two French alpine valleys. Part I: Concentrations, sources and gas/particle partitioning, *Atmos. Environ.*, 42, 43–54, <https://doi.org/10.1016/j.atmosenv.2007.10.009>, 2008.
- Albinet, A., Tomaz, S., and Lestremau, F.: A really quick easy cheap effective rugged and safe (QuEChERS) extraction procedure for the analysis of particle-bound PAHs in ambient air and emission samples, *Sci. Total Environ.*, 450–451, 31–38, <https://doi.org/10.1016/j.scitotenv.2013.01.068>, 2013.
- Albinet, A., Nalin, F., Tomaz, S., Beaumont, J., and Lestremau, F.: A simple QuEChERS-like extraction approach for molecular chemical characterization of organic aerosols: application to nitrated and oxygenated PAH derivatives (NPAH and OPAH) quantified by GC–NICIMS, *Anal. Bioanal. Chem.*, 406, 3131–3148, <https://doi.org/10.1007/s00216-014-7760-5>, 2014.
- Anderson, M., Salo, K., Hallquist, Å. M., and Fridell, E.: Characterization of particles from a marine engine operating at low loads, *Atmos. Environ.*, 101, 65–71, <https://doi.org/10.1016/j.atmosenv.2014.11.009>, 2015.
- Armitage, J. M., Quinn, C. L., and Wania, F.: Global climate change and contaminants—an overview of opportunities and priorities for modelling the potential implications for long-term human expo-

- sure to organic compounds in the Arctic, *J. Environ. Monitor.*, 13, 1532–1546, <https://doi.org/10.1039/c1em10131e>, 2011.
- Balmer, J. and Muir, D.: Polycyclic aromatic hydrocarbons (PAHs), in: *AMAP Assessment 2016: Chemicals of emerging Arctic concern*, edited by: Hung, H., Letcher, R., and Yu, Y., Arctic Monitoring and Assessment Programme (AMAP), Oslo, Norway, 219–238, 2017.
- Barrie, L. A., Gregor, D., Hargrave, B., Lake, R., Muir, D., Shearer, R., Tracey, B., and Bidleman, T.: Arctic contaminants: Sources, occurrence and pathways, *Sci. Total Environ.*, 122, 1–74, [https://doi.org/10.1016/0048-9697\(92\)90245-n](https://doi.org/10.1016/0048-9697(92)90245-n), 1992.
- Bøckman, R.: Fremtidens energiutfordringer på Svalbard (in Norwegian), Longyearbyen Lokalstyre, Norway, 10 pp., available at: <https://www.uit.no> (last access: 28 January 2020), 2019.
- Bore, R. R., Andreassen, I., Kristiansen, J. E., and Modig, I.: Dette er Svalbard 2012. Hva tallene forteller, Statistics Norway, Oslo, Norway, 24 pp., 2012 (in Norwegian).
- Bradley, R. S., Keimig, F. T., and Diaz, H. F.: Climatology of surface-based inversions in the North American Arctic, *J. Geophys. Res.*, 97, 15699, <https://doi.org/10.1029/92JD01451>, 1992.
- Brorström-Lundén, E., Remberger, M., Kaj, L., Hansson, K., Palm Cousins, A., and Andersson, H.: Results from the Swedish national screening programme 2008, IVL Swedish Environmental Research Institute, Göteborg, Sweden, 69 pp., 2010.
- Brubaker, W. W. and Hites, R. A.: OH reaction kinetics of polycyclic aromatic hydrocarbons and polychlorinated dibenzo-p-dioxins and dibenzofurans, *J. Phys. Chem. A*, 102, 915–921, <https://doi.org/10.1021/jp9721199>, 1998.
- Ciccio, P., Cecinato, A., Brancaleoni, E., Frattoni, M., Zacchei, P., Miguel, A. H., and De Castro Vasconcellos, P.: Formation and transport of 2-nitrofluoranthene and 2-nitropyrene of photochemical origin in the troposphere, *J. Geophys. Res.*, 101, 19567–19581, <https://doi.org/10.1029/95jd02118>, 1996.
- Czech, H., Stengel, B., Adam, T., Sklorz, M., Streibel, T., and Zimmermann, R.: A chemometric investigation of aromatic emission profiles from a marine engine in comparison with residential wood combustion and road traffic: Implications for source apportionment inside and outside sulphur emission control areas, *Atmos. Environ.*, 167, 212–222, <https://doi.org/10.1016/j.atmosenv.2017.08.022>, 2017.
- Dekhtyareva, A., Edvardsen, K., Holmén, K., Hermansen, O., and Hansson, H. C.: Influence of local and regional air pollution on atmospheric measurements in Ny-Ålesund, *Int. J. Sust. Dev. Plan.*, 11, 578–587, <https://doi.org/10.2495/sdp-v11-n4-578-587>, 2016.
- DieselNet: EU emission standards for heavy-duty truck and bus engines: available at: <https://www.dieselnet.com/standards/>, last access: 5 June 2020.
- Durant, J. L., Busby Jr., W. F., Lafleur, A. L., Penman, B. W., and Crespi, C. L.: Human cell mutagenicity of oxygenated, nitrated and unsubstituted polycyclic aromatic hydrocarbons associated with urban aerosols, *Mutat. Res.-Genet. Tox.*, 371, 123–157, [https://doi.org/10.1016/S0165-1218\(96\)90103-2](https://doi.org/10.1016/S0165-1218(96)90103-2), 1996.
- Esau, I., Argentini, S., Przybylak, R., Repina, I., and Sjöblom, A.: Svalbard Meteorology, *Adv. Meteorol.*, 2012, 818473, <https://doi.org/10.1155/2012/818473>, 2012.
- EU Directive 2004/107/EC: Directive 2004/107/EC of the European Parliament and the Council of 15 December 2004 relating to arsenic, cadmium, mercury, nickel and polycyclic aromatic hydrocarbons in ambient air, in: *Official Journal of the European Union*, 2005.
- Fiedler, H., Kallenborn, R., Boer, J. D., and Sydnæs, L. K.: The Stockholm Convention: A tool for the global regulation of persistent organic pollutants, *Chem. Int.*, 41, 4–11, <https://doi.org/10.1515/ci-2019-0202>, 2019.
- Finlayson-Pitts, B. J. and Pitts Jr., J. N.: *Chemistry of the upper and lower atmosphere: theory, experiments, and applications*, Elsevier, 1999.
- Franklin, J. A., Atkinson, R., Howard, P. H., Orlando, J. J., Seigneur, C., Wallington, T. J., and Zetzsch, C.: Quantitative determination of persistence in air, in: *Evaluation of persistence and long-range transport of chemicals in the environment*, edited by: Klečka, G. M., Mackay, D., Boethling, R. S., Calamari, D., Cowan-Ellsberry, C., Eisenreich, S., Franklin, J., Grady Jr., C. P. L., Graham, D. G., Hansen, B., Howard, P. H., Jones, K. C., Kannan, K., Larson, R. J., Macdonald, R. W., McKone, T., Muir, D., Parkerton, T., Thibodeaux, L., van de Meent, D., Wallington, T., and Zetzsch, C., SETAC Press, Pensacola, Florida, USA, 7–62, 2000.
- Friedman, C. L. and Selin, N. E.: Long-range atmospheric transport of polycyclic aromatic hydrocarbons: a global 3-D model analysis including evaluation of Arctic sources, *Environ. Sci. Technol.*, 46, 9501–9510, <https://doi.org/10.1021/es301904d>, 2012.
- Friedman, C. L., Zhang, Y., and Selin, N. E.: Climate change and emissions impacts on atmospheric PAH transport to the Arctic, *Environ. Sci. Technol.*, 48, 429–437, <https://doi.org/10.1021/es403098w>, 2014.
- Fu, P., Kawamura, K., Chen, J., and Barrie, L. A.: Isoprene, monoterpene, and sesquiterpene oxidation products in the high Arctic aerosols during late winter to early summer, *Environ. Sci. Technol.*, 43, 4022–4028, <https://doi.org/10.1021/es803669a>, 2009.
- Galarneau, E.: Source specificity and atmospheric processing of airborne PAHs: Implications for source apportionment, *Atmos. Environ.*, 42, 8139–8149, <https://doi.org/10.1016/j.atmosenv.2008.07.025>, 2008.
- Gerald Liu, Z., Berg, D. R., Vasys, V. N., Dettmann, M. E., Zielinska, B., and Schauer, J. J.: Analysis of C₁, C₂, and C₁₀ through C₃₃ particle-phase and semi-volatile organic compound emissions from heavy-duty diesel engines, *Atmos. Environ.*, 44, 1108–1115, <https://doi.org/10.1016/j.atmosenv.2009.11.036>, 2010.
- Governor of Svalbard: Heavy fuel oil ban in the protected areas of Svalbard, available at: <https://www.syssemmannen.no/en/heavy-fuel-oil-ban-in-the-protected-areas/> (last access: 5 June 2020), 2014.
- Gregoris, E., Barbaro, E., Morabito, E., Toscano, G., Donato, A., Cesari, D., Contini, D., and Gambaro, A.: Impact of maritime traffic on polycyclic aromatic hydrocarbons, metals and particulate matter in Venice air, *Environ. Sci. Pollut. Res.*, 23, 6951–6959, <https://doi.org/10.1007/s11356-015-5811-x>, 2016.
- Guan, C., Cheung, C. S., Li, X., and Huang, Z.: Effects of oxygenated fuels on the particle-phase compounds emitted from a diesel engine, *Atmos. Pollut. Res.*, 8, 209–220, <https://doi.org/10.1016/j.apr.2016.08.005>, 2017.
- Hayakawa, K., Murahashi, T., Akutsu, K., Kanda, T., Tang, N., Kakimoto, H., Toriba, A., and Kizu, R.: Comparison of polycyclic aromatic hydrocarbons and nitro-

- cyclic aromatic hydrocarbons in airborne and automobile exhaust particulates, *Polycycl. Aromat. Comp.*, 20, 179–190, <https://doi.org/10.1080/10406630008034784>, 2000.
- Heeb, N. V., Schmid, P., Kohler, M., Gujer, E., Zennegg, M., Wenger, D., Wichser, A., Ulrich, A., Gfeller, U., Honegger, P., Zeyer, K., Emmenegger, L., Petermann, J.-L., Czerwinski, J., Mosimann, T., Kasper, M., and Mayer, A.: Secondary effects of catalytic diesel particulate filters: conversion of PAHs versus formation of nitro-PAHs, *Environ. Sci. Technol.*, 42, 3773–3779, <https://doi.org/10.1021/es7026949>, 2008.
- Holmes, D., Moody, P., Dine, D., and Trueman, L.: *Research methods for the biosciences*, Third ed., Oxford University Press, Oxford, United Kingdom, 2017.
- Hsu, W. T., Liu, M. C., Hung, P. C., Chang, S. H., and Chang, M. B.: PAH emissions from coal combustion and waste incineration, *J. Hazard. Mater.*, 318, 32–40, <https://doi.org/10.1016/j.jhazmat.2016.06.038>, 2016.
- Hu, H., Tian, M., Zhang, L., Yang, F., Peng, C., Chen, Y., Shi, G., Yao, X., Jiang, C., and Wang, J.: Sources and gas-particle partitioning of atmospheric parent, oxygenated, and nitrated polycyclic aromatic hydrocarbons in a humid city in southwest China, *Atmos. Environ.*, 206, 1–10, <https://doi.org/10.1016/j.atmosenv.2019.02.041>, 2019.
- Hu, S., Herner, J. D., Robertson, W., Kobayashi, R., Chang, M. C. O., Huang, S.-M., Zielinska, B., Kado, N., Collins, J. F., Rieger, P., Huai, T., and Ayala, A.: Emissions of polycyclic aromatic hydrocarbons (PAHs) and nitro-PAHs from heavy-duty diesel vehicles with DPF and SCR, *J. Air Waste Manage.*, 63, 984–996, <https://doi.org/10.1080/10962247.2013.795202>, 2013.
- Huang, B., Liu, M., Bi, X., Chaemfa, C., Ren, Z., Wang, X., Sheng, G., and Fu, J.: Phase distribution, sources and risk assessment of PAHs, NPAHs and OPAHs in a rural site of Pearl River Delta region, China, *Atmos. Pollut. Res.*, 5, 210–218, <https://doi.org/10.5094/APR.2014.026>, 2014.
- Huang, C., Hu, Q., Wang, H., Qiao, L., Jing, S. a., Wang, H., Zhou, M., Zhu, S., Ma, Y., Lou, S., Li, L., Tao, S., Li, Y., and Lou, D.: Emission factors of particulate and gaseous compounds from a large cargo vessel operated under real-world conditions, *Environ. Pollut.*, 242, 667–674, <https://doi.org/10.1016/j.envpol.2018.07.036>, 2018.
- Huang, L., Bohac, S. V., Chernyak, S. M., and Batterman, S. A.: Effects of fuels, engine load and exhaust after-treatment on diesel engine SVOC emissions and development of SVOC profiles for receptor modeling, *Atmos. Environ.*, 102, 228–238, <https://doi.org/10.1016/j.atmosenv.2014.11.046>, 2015.
- Huang, W., Huang, B., Bi, X., Lin, Q., Liu, M., Ren, Z., Zhang, G., Wang, X., Sheng, G., and Fu, J.: Emission of PAHs, NPAHs and OPAHs from residential honeycomb coal briquette combustion, *Energ. Fuel.*, 28, 636–642, <https://doi.org/10.1021/ef401901d>, 2014.
- IARC: Diesel and gasoline engine exhausts and some nitroarenes. 1-Nitropyrene, IARC Monographs on the Evaluation of Carcinogenic Risks to Humans, International Agency for Research on Cancer, Lyon, France, 2014.
- Janhäll, S., Olofsson, K., Andersson, P., Pettersson, J., and Halqvist, M.: Evolution of the urban aerosol during winter temperature inversion episodes, *Atmos. Environ.*, 40, 5355–5366, <https://doi.org/10.1016/j.atmosenv.2006.04.051>, 2006.
- Jörundsdóttir, H. Ó., Jensen, S., Hylland, K., Holth, T. F., Gunnlaugsdóttir, H., Svavarsson, J., Ólafsdóttir, Á., El-Taliawy, H., Rigét, F., Strand, J., Nyberg, E., Bignert, A., Høydal, K. S., and Halldórsson, H. P.: Pristine Arctic: background mapping of PAHs, PAH metabolites and inorganic trace elements in the North-Atlantic Arctic and sub-Arctic coastal environment, *Sci. Total Environ.*, 493, 719–728, <https://doi.org/10.1016/j.scitotenv.2014.06.030>, 2014.
- Karavalakis, G., Stourmas, S., Ampatzoglou, D., Bakeas, E., and Spanos, A.: Regulated and unregulated emissions of a Euro 4 SUV operated with diesel and soy-based biodiesel blends, *SAE Int. J. Fuels Lubr.*, 2, 115–131, 2010.
- Katsoyiannis, A. and Breivik, K.: Model-based evaluation of the use of polycyclic aromatic hydrocarbons molecular diagnostic ratios as a source identification tool, *Environ. Pollut.*, 184, 488–494, <https://doi.org/10.1016/j.envpol.2013.09.028>, 2014.
- Kavouras, I. G., Koutrakis, P., Tspakis, M., Lagoudaki, E., Stephanou, E. G., Von Baer, D., and Oyola, P.: Source apportionment of urban particulate aliphatic and polynuclear aromatic hydrocarbons (PAHs) using multivariate methods, *Environ. Sci. Technol.*, 35, 2288–2294, <https://doi.org/10.1021/es001540z>, 2001.
- Keyte, I. J., Harrison, R. M., and Lammel, G.: Chemical reactivity and long-range transport potential of polycyclic aromatic hydrocarbons – a review, *Chem. Soc. Rev.*, 42, 9333–9391, <https://doi.org/10.1039/C3CS60147A>, 2013.
- Keyte, I. J., Albinet, A., and Harrison, R. M.: On-road traffic emissions of polycyclic aromatic hydrocarbons and their oxy- and nitro- derivative compounds measured in road tunnel environments, *Sci. Total Environ.*, 566–567, 1131–1142, <https://doi.org/10.1016/j.scitotenv.2016.05.152>, 2016.
- Khalek, I. A., Blanks, M. G., Merritt, P. M., and Zielinska, B.: Regulated and unregulated emissions from modern 2010 emissions-compliant heavy-duty on-highway diesel engines, *J. Air Waste Manage.*, 65, 987–1001, <https://doi.org/10.1080/10962247.2015.1051606>, 2015.
- Kim, D., Kumfer, B. M., Anastasio, C., Kennedy, I. M., and Young, T. M.: Environmental aging of polycyclic aromatic hydrocarbons on soot and its effect on source identification, *Chemosphere*, 76, 1075–1081, <https://doi.org/10.1016/j.chemosphere.2009.04.031>, 2009.
- Kim, K.-H., Jahan, S. A., Kabir, E., and Brown, R. J. C.: A review of airborne polycyclic aromatic hydrocarbons (PAHs) and their human health effects, *Environ. Int.*, 60, 71–80, <https://doi.org/10.1016/j.envint.2013.07.019>, 2013.
- Klonecki, A.: Seasonal changes in the transport of pollutants into the Arctic troposphere-model study, *J. Geophys. Res.*, 108, 8367, <https://doi.org/10.1029/2002jd002199>, 2003.
- Kojima, Y., Inazu, K., Hisamatsu, Y., Okochi, H., Baba, T., and Nagoya, T.: Influence of secondary formation on atmospheric occurrences of oxygenated polycyclic aromatic hydrocarbons in airborne particles, *Atmos. Environ.*, 44, 2873–2880, <https://doi.org/10.1016/j.atmosenv.2010.04.048>, 2010.
- Kotchenruther, R. A.: The effects of marine vessel fuel sulfur regulations on ambient PM_{2.5} at coastal and near coastal monitoring sites in the U.S., *Atmos. Environ.*, 151, 52–61, <https://doi.org/10.1016/j.atmosenv.2016.12.012>, 2017.
- Kuo, C.-Y., Chien, P.-S., Kuo, W.-C., Wei, C.-T., and Rau, J.-Y.: Comparison of polycyclic aromatic hydrocarbon emis-

- sions on gasoline- and diesel-dominated routes, *Environ. Monit. Assess.*, 185, 5749–5761, <https://doi.org/10.1007/s10661-012-2981-6>, 2013.
- Kystdatahuset: Longyearbyen port traffic for 2018: available at: <https://kystdatahuset.no/> (last access: 5 June 2020), 2018.
- Lammel, G.: Long-range atmospheric transport of polycyclic aromatic hydrocarbons is worldwide problem – results from measurements at remote sites and modelling, *Acta Chim. Slov.*, 729–735, <https://doi.org/10.17344/acsi.2015.1387>, 2015.
- Lammel, G., Sehili, A. M., Bond, T. C., Feichter, J., and Grassl, H.: Gas/particle partitioning and global distribution of polycyclic aromatic hydrocarbons – A modelling approach, *Chemosphere*, 76, 98–106, <https://doi.org/10.1016/j.chemosphere.2009.02.017>, 2009.
- Lammel, G., Kitanovski, Z., Kukucka, P., Novak, J., Arangio, A. M., Codling, G. P., Filippi, A., Hovorka, J., Kuta, J., Leoni, C., Pribylova, P., Prokes, R., Sanka, O., Shahpoury, P., Tong, H. J., and Wietzorek, M.: Oxygenated and nitrated polycyclic aromatic hydrocarbons in ambient air-levels, phase partitioning, mass size distributions, and inhalation bioaccessibility, *Environ. Sci. Technol.*, 54, 2615–2625, <https://doi.org/10.1021/acs.est.9b06820>, 2020.
- Li, J., Li, X., Li, M., Lu, S., Yan, J., Xie, W., Liu, C., and Qi, Z.: Influence of air pollution control devices on the polycyclic aromatic hydrocarbon distribution in flue gas from an ultralow-emission coal-fired power plant, *Energy Fuels*, 30, 9572–9579, <https://doi.org/10.1021/acs.energyfuels.6b01381>, 2016.
- Li, J., Chen, H., Li, Z., Wang, P., Fan, X., He, W., and Zhang, J.: Analysis of low-level temperature inversions and their effects on aerosols in the lower atmosphere, *Adv. Atmos. Sci.*, 36, 1235–1250, <https://doi.org/10.1007/s00376-019-9018-9>, 2019.
- Lin, Y., Qiu, X., Ma, Y., Ma, J., Zheng, M., and Shao, M.: Concentrations and spatial distribution of polycyclic aromatic hydrocarbons (PAHs) and nitrated PAHs (NPAHs) in the atmosphere of North China, and the transformation from PAHs to NPAHs, *Environ. Pollut.*, 196, 164–170, <https://doi.org/10.1016/j.envpol.2014.10.005>, 2015.
- Liu, Z. G., Wall, J. C., Ottinger, N. A., and McGuffin, D.: Mitigation of PAH and Nitro-PAH emissions from non-road diesel engines, *Environ. Sci. Technol.*, 49, 3662–3671, <https://doi.org/10.1021/es505434r>, 2015.
- Lohmann, R. and Lammel, G.: Adsorptive and absorptive contributions to the gas-particle partitioning of polycyclic aromatic hydrocarbons: state of knowledge and recommended parametrization for modeling, *Environ. Sci. Technol.*, 38, 3793–3803, <https://doi.org/10.1021/es035337q>, 2004.
- Lundgjerdingen, K. S.: Teknisk rapport Longyearbyen Energiverket (in Norwegian), Applica Test & Certification AS, Longyearbyen, Norway, Available by request from Longyearbyen Lokalstyre, 23, 2017.
- Macdonald, R. W., Barrie, L. A., Bidleman, T. F., Diamond, M. L., Gregor, D. J., Semkin, R. G., Strachan, W. M., Li, Y. F., Wania, F., Alae, M., Alexeeva, L. B., Backus, S. M., Bailey, R., Bewers, J. M., Gobeil, C., Halsall, C. J., Harner, T., Hoff, J. T., Jantunen, L. M., Lockhart, W. L., Mackay, D., Muir, D. C., Pudykiewicz, J., Reimer, K. J., Smith, J. N., and Stern, G. A.: Contaminants in the Canadian Arctic: 5 years of progress in understanding sources, occurrence and pathways, *Sci. Total Environ.*, 254, 93–234, [https://doi.org/10.1016/s0048-9697\(00\)00434-4](https://doi.org/10.1016/s0048-9697(00)00434-4), 2000.
- Macdonald, C., Lockhart, L., and Gilman, A.: Effects of oil and gas activity on the environment and human health, in: *Assessment 2007: Oil and gas activities in the Arctic – effect and potential effects*, Arctic Monitoring and Assessment Programme (AMAP), Oslo, Norway, 5, 1–164, 2010.
- Marshall, C., Uguno, J., Large, D. J., Meredith, W., Jochmann, M., Friis, B., Vane, C., Spiro, B. F., Snape, C. E., and Orheim, A.: Geochemistry and petrology of palaeocene coals from Spitzbergen – Part 2: Maturity variations and implications for local and regional burial models, *Int. J. Coal Geol.*, 143, 1–10, <https://doi.org/10.1016/j.coal.2015.03.013>, 2015.
- Muñoz, M., Haag, R., Honegger, P., Zeyer, K., Mohn, J., Comte, P., Czerwinski, J., and Heeb, N. V.: Co-formation and co-release of genotoxic PAHs, alkyl-PAHs and soot nanoparticles from gasoline direct injection vehicles, *Atmos. Environ.*, 178, 242–254, <https://doi.org/10.1016/j.atmosenv.2018.01.050>, 2018.
- Noda, N. and Makino, H.: Influence of operating temperature on performance of electrostatic precipitator for pulverized coal combustion boiler, *Adv. Powder Technol.*, 21, 495–499, <https://doi.org/10.1016/j.apt.2010.04.012>, 2010.
- Nyström, R., Sadiktsis, I., Ahmed, T. M., Westerholm, R., Kögler, J. H., Blomberg, A., Sandström, T., and Boman, C.: Physical and chemical properties of RME biodiesel exhaust particles without engine modifications, *Fuel*, 186, 261–269, <https://doi.org/10.1016/j.fuel.2016.08.062>, 2016.
- Onduka, T., Ojima, D., Kakuno, A., Ito, K., Koyama, J., and Fujii, K.: Nitrated polycyclic aromatic hydrocarbons in the marine environment: acute toxicities for organisms at three trophic levels, *Jpn. J. Environ. Toxicol.*, 15, 1–10, <https://doi.org/10.11403/jset.15.1>, 2012.
- Ontario Ministry of the Environment and Climate Change: Ontario Ambient Air Quality Criteria, available at: <https://www.ontario.ca/page/ontarios-ambient-air-quality-criteria-sorted-contaminant-name> (last access: 5 June 2020), 2016.
- Pedersen, H., Kallenborn, R., Ottesen, R., Gabrielsen, G., Schrum, C., Evensen, A., Ruus, A., Benjaminsen, H., Sagerup, K., and Christensen, G.: PCBs on Svalbard, Norwegian Environment Agency and Governor of Svalbard, Longyearbyen, Norway, 99 pp., 2011.
- Peng, N., Li, Y., Liu, Z., Liu, T., and Gai, C.: Emission, distribution and toxicity of polycyclic aromatic hydrocarbons (PAHs) during municipal solid waste (MSW) and coal co-combustion, *Sci. Total Environ.*, 565, 1201–1207, <https://doi.org/10.1016/j.scitotenv.2016.05.188>, 2016.
- Ravindra, K., Bencs, L., Wauters, E., de Hoog, J., Deutsch, F., Roekens, E., Bleux, N., Berghmans, P., and Van Grieken, R.: Seasonal and site-specific variation in vapour and aerosol phase PAHs over Flanders (Belgium) and their relation with anthropogenic activities, *Atmos. Environ.*, 40, 771–785, <https://doi.org/10.1016/j.atmosenv.2005.10.011>, 2006.
- Ravindra, K., Sokhi, R., and Vangrieken, R.: Atmospheric polycyclic aromatic hydrocarbons: Source attribution, emission factors and regulation, *Atmos. Environ.*, 42, 2895–2921, <https://doi.org/10.1016/j.atmosenv.2007.12.010>, 2008a.
- Ravindra, K., Wauters, E., and Van Grieken, R.: Variation in particulate PAHs levels and their relation with the transboundary movement of the air masses, *Sci. Total Environ.*, 396, 100–110, <https://doi.org/10.1016/j.scitotenv.2008.02.018>, 2008b.

- Reynaud, S. and Deschaux, P.: The effects of polycyclic aromatic hydrocarbons on the immune system of fish: A review, *Aquat. Toxicol.*, 77, 229–238, <https://doi.org/10.1016/j.aquatox.2005.10.018>, 2006.
- Ringuet, J., Albinet, A., Leoz-Garziandia, E., Budzinski, H., and Villenave, E.: Diurnal/nocturnal concentrations and sources of particulate-bound PAHs, OPAHs and NPAHs at traffic and suburban sites in the region of Paris (France), *Sci. Total Environ.*, 437, 297–305, <https://doi.org/10.1016/j.scitotenv.2012.07.072>, 2012.
- Rogge, W. F., Hildemann, L. M., Mazurek, M. A., Cass, G. R., and Simoneit, B. R.: Sources of fine organic aerosol. 2. Noncatalyst and catalyst-equipped automobiles and heavy-duty diesel trucks, *Environ. Sci. Technol.*, 27, 636–651, <https://doi.org/10.1021/es00041a007>, 1993.
- Schmale, J., Arnold, S. R., Law, K. S., Thorp, T., Anenberg, S., Simpson, W. R., Mao, J., and Pratt, K. A.: Local Arctic air pollution: A neglected but serious problem, *Earth's Future*, 6, 1385–1412, <https://doi.org/10.1029/2018ef000952>, 2018.
- Shahpoury, P., Lammel, G., Albinet, A., Sofuoğlu, A., Dumanoglu, Y., Sofuoğlu, S. C., Wagner, Z., and Zdimal, V.: Evaluation of a conceptual model for gas-particle partitioning of polycyclic aromatic hydrocarbons using poly-parameter linear free energy relationships, *Environ. Sci. Technol.*, 50, 12312–12319, <https://doi.org/10.1021/acs.est.6b02158>, 2016.
- Shahpoury, P., Kitanovski, Z., and Lammel, G.: Snow scavenging and phase partitioning of nitrated and oxygenated aromatic hydrocarbons in polluted and remote environments in central Europe and the European Arctic, *Atmos. Chem. Phys.*, 18, 13495–13510, <https://doi.org/10.5194/acp-18-13495-2018>, 2018.
- Sharma, M. and McBean, E. A.: Atmospheric PAH deposition: deposition velocities and washout ratios, *J. Environ. Eng.*, 128, 186–195, [https://doi.org/10.1061/\(ASCE\)0733-9372\(2002\)128:2\(186\)](https://doi.org/10.1061/(ASCE)0733-9372(2002)128:2(186)), 2002.
- Škrdlíková, L., Landlová, L., Klánová, J., and Lammel, G.: Wet deposition and scavenging efficiency of gaseous and particulate phase polycyclic aromatic compounds at a central European suburban site, *Atmos. Environ.*, 45, 4305–4312, <https://doi.org/10.1016/j.atmosenv.2011.04.072>, 2011.
- Statistics Norway: Registered vehicles, by region, statistical variable per year, data for 2018, available at: <https://www.ssb.no/statbank/table/11823/> (last access: 5 June 2020), 2018.
- Tobiszewski, M. and Namieśnik, J.: PAH diagnostic ratios for the identification of pollution emission sources, *Environ. Pollut.*, 162, 110–119, <https://doi.org/10.1016/j.envpol.2011.10.025>, 2012.
- Tomaz, S., Shahpoury, P., Jaffrezo, J.-L., Lammel, G., Perraudin, E., Villenave, E., and Albinet, A.: One-year study of polycyclic aromatic compounds at an urban site in Grenoble (France): Seasonal variations, gas/particle partitioning and cancer risk estimation, *Sci. Total Environ.*, 565, 1071–1083, <https://doi.org/10.1016/j.scitotenv.2016.05.137>, 2016.
- UK Air DEFRA: The air quality strategy for England, Scotland, Wales and Northern Ireland, Department for Environment, Food and Rural Affairs, UK Air, 1, 56 pp., available at: https://assets.publishing.service.gov.uk/government/uploads/system/uploads/attachment_data/file/69336/pb12654-air-quality-strategy-vol1-070712.pdf (last access: 5 June 2020), 2007.
- UNECE: The 1998 Aarhus protocol on persistent organic pollutants (POPs), 49 pp., available at: https://www.unece.org/env/lrtap/pops_h1.html (last access: 5 June 2020), 1998.
- US EPA: Polycyclic Aromatic Hydrocarbons on the Gulf Coastline: available at: [https://archive.epa.gov/emergency/bpspill/web/html/pahs.html#:~:text=PolycyclicAromaticHydrocarbons\(PAHs\)are,commonlycalled%27weatheredoil%27](https://archive.epa.gov/emergency/bpspill/web/html/pahs.html#:~:text=PolycyclicAromaticHydrocarbons(PAHs)are,commonlycalled%27weatheredoil%27) (last access: 5 June 2020), 2011.
- Volvo trucks: Volvo D13 Engine family: available at: https://www.volvotrucks.us/-/media/vtna/files/shared/powertrain/revised4147_101-volvo_d13_engine-brochure_low-res.pdf, last access: 5 June 2020.
- Wang, G., Ma, Z., Deng, J., Li, Z., Duan, L., Zhang, Q., Hao, J., and Jiang, J.: Characteristics of particulate matter from four coal-fired power plants with low–low temperature electrostatic precipitator in China, *Sci. Total Environ.*, 662, 455–461, <https://doi.org/10.1016/j.scitotenv.2019.01.080>, 2019.
- Wang, K., Shen, Y., Zhang, S., Ye, Y., Shen, Q., Hu, J., and Wang, X.: Application of spatial analysis and multivariate analysis techniques in distribution and source study of polycyclic aromatic hydrocarbons in the topsoil of Beijing, China, *Environ. Geol.*, 56, 1041–1050, <https://doi.org/10.1007/s00254-008-1204-5>, 2009.
- Wang, R., Liu, G., and Zhang, J.: Variations of emission characterization of PAHs emitted from different utility boilers of coal-fired power plants and risk assessment related to atmospheric PAHs, *Sci. Total Environ.*, 538, 180–190, <https://doi.org/10.1016/j.scitotenv.2015.08.043>, 2015.
- Weinbruch, S., Benker, N., Kandler, K., Schutze, K., Kling, K., Berlinger, B., Thomassen, Y., Drotikova, T., and Kallenborn, R.: Source identification of individual soot agglomerates in Arctic air by transmission electron microscopy, *Atmos. Environ.*, 172, 47–54, <https://doi.org/10.1016/j.atmosenv.2017.10.033>, 2018.
- WHO: Environmental health criteria 229. Selected nitro- and nitro-oxy-polycyclic aromatic hydrocarbons, World Health Organization, 2003.
- Willis, M. D., Leitch, W. R., and Abbatt, J. P. D.: Processes controlling the composition and abundance of Arctic aerosol, *Rev. Geophys.*, 56, 621–671, <https://doi.org/10.1029/2018rg000602>, 2018.
- Wingfors, H.: Characterisation and determination of profiles of polycyclic aromatic hydrocarbons in a traffic tunnel in Gothenburg, Sweden, 35, 6361–6369, [https://doi.org/10.1016/s1352-2310\(01\)00389-2](https://doi.org/10.1016/s1352-2310(01)00389-2), 2001.
- Wu, D., Wang, Z., Chen, J., Kong, S., Fu, X., Deng, H., Shao, G., and Wu, G.: Polycyclic aromatic hydrocarbons (PAHs) in atmospheric PM_{2.5} and PM₁₀ at a coal-based industrial city: Implication for PAH control at industrial agglomeration regions, China, *Atmos. Res.*, 149, 217–229, <https://doi.org/10.1016/j.atmosres.2014.06.012>, 2014.
- Yang, H.-H., Lee, W.-J., Chen, S.-J., and Lai, S.-O.: PAH emission from various industrial stacks, *J. Hazard. Mater.*, 60, 159–174, [https://doi.org/10.1016/s0304-3894\(98\)00089-2](https://doi.org/10.1016/s0304-3894(98)00089-2), 1998.
- Yu, Y., Katsoyiannis, A., Bohlin-Nizzetto, P., Brorström-Lundén, E., Ma, J., Zhao, Y., Wu, Z., Tych, W., Mindham, D., Sverko, E., Barresi, E., Dryfhout-Clark, H., Fellin, P., and Hung, H.: Polycyclic aromatic hydrocarbons not declining in Arctic air despite global emission reduction, *Environ. Sci. Technol.*, 53, 2375–2382, <https://doi.org/10.1021/acs.est.8b05353>, 2019.

- Yunker, M. B., Macdonald, R. W., Vingarzan, R., Mitchell, R. H., Goyette, D., and Sylvestre, S.: PAHs in the Fraser river basin: a critical appraisal of PAH ratios as indicators of PAH source and composition, *Org. Geochem.*, 33, 489–515, [https://doi.org/10.1016/s0146-6380\(02\)00002-5](https://doi.org/10.1016/s0146-6380(02)00002-5), 2002.
- Zhang, F., Chen, Y., Cui, M., Feng, Y., Yang, X., Chen, J., Zhang, Y., Gao, H., Tian, C., Matthias, V., and Liu, H.: Emission factors and environmental implication of organic pollutants in PM emitted from various vessels in China, *Atmos. Environ.*, 200, 302–311, <https://doi.org/10.1016/j.atmosenv.2018.12.006>, 2019.
- Zhao, J., Zhang, Y., Wang, T., Sun, L., Yang, Z., Lin, Y., Chen, Y., and Mao, H.: Characterization of PM_{2.5}-bound polycyclic aromatic hydrocarbons and their derivatives (nitro-and oxy-PAHs) emissions from two ship engines under different operating conditions, *Chemosphere*, 225, 43–52, <https://doi.org/10.1016/j.chemosphere.2019.03.022>, 2019.
- Zhao, J., Zhang, Y., Chang, J., Peng, S., Hong, N., Hu, J., Lv, J., Wang, T., and Mao, H.: Emission characteristics and temporal variation of PAHs and their derivatives from an ocean-going cargo vessel, *Chemosphere*, 249, 126194, <https://doi.org/10.1016/j.chemosphere.2020.126194>, 2020.
- Zhao, S., Duan, Y., Yao, T., Liu, M., Lu, J., Tan, H., Wang, X., and Wu, L.: Study on the mercury emission and transformation in an ultra-low emission coal-fired power plant, *Fuel*, 199, 653–661, <https://doi.org/10.1016/j.fuel.2017.03.038>, 2017.
- Zhao, T., Yang, L., Huang, Q., Zhang, W., Duan, S., Gao, H., and Wang, W.: PM_{2.5}-bound polycyclic aromatic hydrocarbons (PAHs) and nitrated-PAHs (NPAHs) emitted by gasoline vehicles: Characterization and health risk assessment, *Sci. Total Environ.*, 727, 138631, <https://doi.org/10.1016/j.scitotenv.2020.138631>, 2020.
- Zheng, L., Ou, J., Liu, M., Chen, Y., Tang, Q., and Hu, Y.: Seasonal and spatial variations of PM₁₀-bounded PAHs in a coal mining city, China: Distributions, sources, and health risks, *Ecotox. Environ. Safe.*, 169, 470–478, <https://doi.org/10.1016/j.ecoenv.2018.11.063>, 2019.

Supplement of Atmos. Chem. Phys., 20, 9997–10014, 2020
<https://doi.org/10.5194/acp-20-9997-2020-supplement>
© Author(s) 2020. This work is distributed under
the Creative Commons Attribution 4.0 License.



Supplement of

Polycyclic aromatic hydrocarbons (PAHs) and oxy- and nitro-PAHs in ambient air of the Arctic town Longyearbyen, Svalbard

Tatiana Drotikova et al.

Correspondence to: Tatiana Drotikova (tatiana.drotikova@unis.no)

The copyright of individual parts of the supplement might differ from the CC BY 4.0 License.

Table of Contents

	Text S1. Analytical procedures	2
	Text S2. Method validation and quality control	3
	Table S1. Sampling dates and sample volumes	7
5	Table S2. Meteorological data for UNIS (samples U1-U7) and Adventdalen (samples A1-A7) sampling stations	7
	Table S3. Physico-chemical properties of target compounds	8
	Table S4. GC–EI-MS/MS parameters used for PAHs determination and instrumental limits of quantification (LOQ).....	14
10	Table S5. GC-ECNI-MS parameters used for nitro- and oxy-PAHs determination and instrumental limits of quantification (LOQ).....	15
	Table S6. Blank values and method detection limits (MDL) for different sampling materials.....	16
	Table S7. Average recovery rates (Rec, %) and relative standard deviations (RSTD, %) for <i>spiked</i> samples	17
	Table S8. Average recovery rates (Rec, %) of internal standards (ISTDs) for <i>ambient air</i> samples	19
15	Table S9. Concentrations of PAHs (G+P) and percentage in the particulate phase (%PM) in <i>Longyearbyen power plant</i> (n=6), as well as MDLs for gaseous (PUF) and particulate (QFF) phases, and instrumental LOD and LOQ; all values are in pg m^{-3}	20
	Table S10. Concentrations of PAHs (G+P) and percentage in the particulate phase (%PM) at <i>UNIS</i> (n=6), as well as MDLs for gaseous (PUF) and particulate (QFF) phases, and instrumental LOD and LOQ; all values are in pg m^{-3}	21
20	Table S11. Concentrations of PAHs (G+P) and percentage in the particulate phase (%PM) at <i>Adventdalen</i> (n=6), as well as MDLs for gaseous (PUF) and particulate (QFF) phases, and instrumental LOD and LOQ; all values are in pg m^{-3}	22
	Table S12. Comparison of Longyearbyen power plant 16 PAH emissions with other coal-burning plants operated worldwide	23
25	Table S13. UNIS and Adventdalen air concentrations (G+P) of 16 PAHs compared to national and regional background concentrations detected in <i>autumn 2018</i>	24
	Table S14: Comparison of average concentrations (G+P; pg m^{-3}) of PAHs, oxy-PAHs and nitro-PAHs measured in Longyearbyen with those previously reported in the literature for rural sites <i>worldwide</i>	25
30	Table S15. Spearman correlation of selected PAH %PMs with ambient temperature and specific humidity for Adventdalen data (n=6).....	26
	Table S16. Spearman correlation of selected PAH concentrations (G+P) with precipitation for UNIS data (n=6)	26
	Table S17. Spearman correlation of PAH concentrations (G+P) with weather parameters for Adventdalen data (n=6).....	27
35	Table S18. %PM obtained in this study compared to literature data	28
	Table S19. Combustion engine vehicles in Longyearbyen as of 2018	29
	Table S20. Eigenanalysis of the correlation matrix and Eigenvectors for Adventdalen data.....	30
	Table S21. Spearman correlation of PAH concentrations (G+P; n=6) with diagnostic ratios for Adventdalen data	30
40	Table S22. Extractions from certificate of quality: unleaded <i>gasoline</i> , RON95, Norway, summer.....	31
	Table S23. Extractions from certificate of quality: B-base automotive <i>diesel</i> , CFPP-12, Norway.....	31
	Table S24. Ratios of nitro- and oxy-PAH to corresponding parent PAH at three locations	32

	Table S25. Spearman correlation of nitro- and oxy-PAH to corresponding parent PAH ratios with weather parameters in Adventdalen (n=6).....	32
45	Table S26. Spearman correlation of concentrations (G+P) of PAHs, nitro- and oxy-PAHs with each other for Adventdalen data (n=6).....	33
	Table S27. Eigenanalysis of the correlation matrix and Eigenvectors for UNIS data.....	34
	Table S28. Spearman correlation of PAH concentrations (G+P; n=6) with diagnostic ratios for UNIS data.....	34
50	Figure S1. Wind rose diagrams for UNIS (samples U1-U7) and Adventdalen (samples A1-A7) sampling stations.....	35
	Figure S2. UNIS and Adventdalen chemical profiles of (a) PAHs, (b) oxy-PAHs, and (c) nitro-PAHs.....	37
	Figure S3. The 15 PAH profiles for different stations in Svalbard (UNIS, Adventdalen, Zeppelin) and the mainland Norway (Birkenes) measured in <i>autumn 2018</i>	38
	Figure S4. 5-day back trajectories of Longyearbyen.....	38
55	Figure S5. Port Longyearbyen statistics 2018.....	41
	References.....	42

Text S1. Analytical procedures

Chemicals

Dichloromethane (DCM), *n*-hexane, and acetone (GC–MS grade), were purchased from VWR International AS, Oslo, Norway. Standards of PAHs, nitro- and oxy-PAHs in *c*-hexane (>98.0 % purity) were purchased from Chiron AS, Trondheim, Norway.

Sample preparation

QFFs (particulate phase) and PUFs (gaseous phase) samples were extracted separately by two different methods, followed by the same clean-up procedure. Fifty ng of 25 ²H-labelled PAH (dPAH) internal standards (ISTDs), including 16 EPA priority dPAHs (Table S4), 3 dOxy-PAHs, and 6 dNitro-PAHs (Table S5), were added before extraction. Previously reported methods (Albinet et al., 2006; Albinet et al., 2013; Albinet et al., 2014) were combined, modified and validated for the current trace quantitative analysis. QFF was placed in a centrifuge glass tube. After addition of 12-15 mL DCM, the tube was vortexed for 1.5 min (VWR 12620-848, Oslo, Norway). The sample was then centrifuged (Hettich, Universal 320, Germany) for 5 min at 4,000 rpm at 10°C and the supernatant was transferred to a clean glass vial. The extraction procedure was repeated three times. Combined supernatants (about 40 ml) were concentrated to about 500 µL under gentle nitrogen stream (5.5 quality; AGA, Norway) using Reacti-vap 18780 (Pierce Biotechnology Inc., Sweden). PUF samples were Soxhlet extracted with DCM for 24 hours. The extract (about 300 mL) was reduced to about 500 µL (Zymark, Turbovap 500, Sweden).

The QFF and PUF extracts were first cleaned on neutral alumina Al₂O₃ SPE cartridge (500 mg, Macherey Nagel, Germany). PAHs, nitro- and oxy-PAHs were eluted with 9 mL DCM. After concentration under a gentle nitrogen stream, the residue was dissolved in 200 µL *n*-hexane. Samples were further cleaned-up with neutral silica SiO₂ SPE cartridge (500 mg, Macherey Nagel, Germany). The alkane fraction was eluted with 1 mL *n*-hexane and discarded. PAHs, nitro- and oxy-PAHs were thereafter eluted with 9 mL 35:65 (v/v) DCM-*n*-hexane. The elute was dried under a gentle nitrogen stream and redissolved in 100 µL *n*-hexane. Subsequently, the purified samples were spiked with 10 ng of three recovery standards (RSTDs; 1,2,3,4-tetrachloronaphthalene, Flt-d10, and 1-NPyr-d9) and analyzed by GC-MS.

GC-MS analysis

16 priority PAHs, 8 oxy-PAHs, and 21 nitro-PAHs were analyzed via two different methods using a 7890B Agilent GC chromatograph coupled to 7000C Agilent Triple Quad MS (Agilent Technologies, Santa Clara, California). All compounds were separated on the low-polar TG-5SILMS capillary column (5% Phenyl Methylpolysiloxane; 30 m with 5 m safe guard \times 0.25 mm \times 0.25 μ m film thickness; cat. 26096-1425, Thermo Scientific Trace GC Ultra. A sample injection volume was 1 μ L; pulsed splitless injection mode using a 4 mm ID splitless, single taper, no wool ultra inert liner (5190-2292, Agilent, USA). Agilent MassHunter software (Version B.07.00 /Build 7.0.457.0, 2008) was used for instrument control, method validation and quantification.

PAH analysis by GC-EI-MS/MS method

The injector temperature was 300 $^{\circ}$ C in pulsed splitless mode at 35 psi for 1.5 min (1.6 min splitless time). Ultra pure He (quality 6.0; AGA, Norway) was used as carrier gas, at a constant flow rate of 1.0 mL min⁻¹. The GC oven temperature program was as follows: initial temperature was hold at 70 $^{\circ}$ C for 3 min, increased to 170 $^{\circ}$ C at 40 $^{\circ}$ C min⁻¹, with further increase to 240 $^{\circ}$ C at 10 $^{\circ}$ C min⁻¹, followed by a ramp to 310 $^{\circ}$ C at 5 $^{\circ}$ C min⁻¹ and hold for 2 min. Transfer line temperature was 325 $^{\circ}$ C. The ion source temperature was 280 $^{\circ}$ C and quadrupoles temperatures were 150 $^{\circ}$ C.

The MS was run in electron ionization (EI) mode. The solvent delay time was 5.0 min. Nitrogen (quality 6.0; AGA, Norway) was used as collision gas at a flow rate of 1.5 mL min⁻¹. Helium quench gas was set at 2.25 mL min⁻¹. Electron ionization was operated at 70 eV. Analyses were performed in multiple reaction monitoring (MRM) mode. Table S4 gives the retention times (RTs) and the monitored transitions for each compound and collision energy adopted from (Kanan et al., 2012). For the deuterated internal standards, the chosen transitions were parent molecular ion-parent molecular ion, at collision energy 0 eV.

Nitro- and oxy-PAH analysis by GC-ECNI-MS method

The injector temperature was 230 $^{\circ}$ C in pulsed splitless mode at 40 psi for 1.5 min (1.6 min splitless time). The carrier gas (He) flow rate was 1.2 mL min⁻¹. The GC temperature program started at 70 $^{\circ}$ C for 2 min, then ramped to 250 $^{\circ}$ C at 45 $^{\circ}$ C min⁻¹ and held for 5 min, followed by a ramp to 310 $^{\circ}$ C at 5 $^{\circ}$ C min⁻¹. Transfer line temperature was 325 $^{\circ}$ C.

The MS was run in electron capture negative ion (ECNI) mode. The MS parameters were as follows: ion source temperature was 280 $^{\circ}$ C and quadrupole temperature was 150 $^{\circ}$ C. Methane (quality 6.0; AGA, Norway) was used as a reagent gas with a flow of 2.5 mL min⁻¹, electron energy was 150 eV and the emission current was 50 μ A. Analyses were performed in selected ion monitoring mode (SIM). Monitored ions and RT are shown in Table S5.

Text S2. Method validation and quality control

115 Calibration

Quantification of each individual PAH was based on eight-point calibration curve from 1 to 600 pg μ L⁻¹ (gravimetrically diluted) in *n*-hexane. Calibration curves were linear with $R^2 > 0.987$ for all compounds. Quantification of nitro- and oxy-PAHs was based on nine-point calibration curves from 0.5 to 400 pg μ L⁻¹ (gravimetrically diluted) in *n*-hexane. Calibration curves were linear with $R^2 > 0.99$ for all compounds. The linear range of 9,10-PheQ was from 5 pg μ L⁻¹ to 400 pg μ L⁻¹ with R^2 of 0.97. Individual calibration curves for all

ISTDs were based on eight concentration levels (5-250 pg μL^{-1}) with constant concentration of RSTDs (100 pg μL^{-1}), prepared in *n*-hexane.

Recovery rates

Apparent recovery (Recovery, %) for all analytes was calculated using Eq. (1):

$$125 \quad \text{Recovery, \%} = \frac{M_{\text{exp}}}{M_{\text{ref}}} \times 100, \quad (1)$$

where M_{exp} is amount of target compound experimentally obtained from calibration graph and M_{ref} is a known added amount (Burns et al., 2002). Recovery of ISTD was calculated relative to RSTD added prior to GC analysis. Recoveries of target analytes were calculated relative to ISTD for spiked samples. The spiked samples were prepared by adding a known amount of native (16 PAHs, 19 nitro-PAHs, 8 oxy-PAHs) and internal (16 dPAHs, 6 dNitro-PAHs, 2 dOxy-PAHs) standards to the blank sample material before extraction. The spiked samples were treated as real samples. Four replicate samples for each sampling material were performed (QFF, $n=4$ and PUF, $n=4$).

Detection limits

Instrumental limits of detection (LOD) and quantification (LOQ) were calculated according to the calibration curve method (Konieczka and Namieśnik, 2009; Shrivastava and Gupta, 2011; Şengül, 2016) based on residual standard deviation ($\text{STDEV}_{\text{res}}$) of the calibration curve in lowest concentration range (from 1 to 5 pg μL^{-1} for PAHs and from 0.1 to 5 pg μL^{-1} for nitro- and oxy-PAHs; $n=15$ measurements). $\text{STDEV}_{\text{res}}$, LOD, and LOQ were calculated by Eq. (2), (3) and (4), respectively.

$$140 \quad \text{STDEV}_{\text{res}} = \sqrt{\frac{\sum(Y - Y_{\text{eq}})^2}{n-2}}, \quad (2)$$

where Y is the observed value of a compound peak area and Y_{eq} is the value calculated using the determined linear regression equation.

$$\text{LOD} = 3.3 \times \text{STDEV}_{\text{res}}/\text{slope} \quad (3)$$

$$\text{LOQ} = 10 \times \text{STDEV}_{\text{res}}/\text{slope} \quad (4)$$

Samples showed analyte concentrations below limit of quantification (LOQ) were replaced by LOQ/2 for statistical analysis.

In order to evaluate the background contamination related to sample collection and analysis, PUF and QFF field blanks (exposed filters without any air filtration; $n=4$ for PP and $n=4$ for UNIS/Adventdalen) and laboratory blanks ($n=3$ for PP and $n=3$ for UNIS/Adventdalen) were treated and analyzed by the same methods as real samples. Laboratory blanks were prepared for each extraction batch. MDL was calculated based on blanks according to Eq. (5):

$$150 \quad \text{MDL} = \bar{X} + 3 \times \text{STD}_b, \quad (5)$$

where \bar{X} is the blank mean concentration, and STD_b is the standard deviation of the replicate blank sample concentrations.

Results of method validation and quality control

155 Ambient atmospheric concentrations of nitro- and oxy-PAHs are in the range of few pg m^{-3} to a few ng m^{-3} , which are about 1–3 orders of magnitude lower than those of PAHs. Thus, a sensitive GC-ECNI-MS method was applied for the trace quantification of nitro- and oxy-PAHs. PAHs were identified based on compound specific RTs and two characteristic MRM transitions, while nitro- and oxy-PAHs were identified based on their RTs and monitored ions in SIM mode. The calculated instrumental LOD and LOQ values are summarized in
160 Table S4 and Table S5. LOQ for PAHs (GC-EI-MS/MS) ranged from 0.98 to 3.69 pg. The HMW PAHs exhibited higher LODs. This may be due to interference from the stationary phase for later-eluting compounds. LOQ for nitro-PAHs (GC- ECNI-MS) ranged from 0.09 to 2.04 pg, while LOQ for oxy-PAHs (GC- ECNI-MS) were slightly higher, and ranged from 0.49 to 5.35 pg, and LOQ for 9,10-PheQ is 26.87 pg. This is because
165 nitro-PAHs have higher affinity for negative ion formation, while the carbonyl group within oxy-PAHs is able to stabilize the excess negative charge associated with the capture of thermal electrons within the NICI process (Han et al., 2019). The linearity of instrumental response was evaluated over the range from 1 to 600 $\text{pg } \mu\text{L}^{-1}$ for PAHs and 1 to 400 $\text{pg } \mu\text{L}^{-1}$ for nitro- and oxy-PAHs. High values of regression coefficient r^2 were determined: $r^2 > 0.987$ for all PAHs and $r^2 > 0.990$ for all nitro- and oxy-PAHs, except 0.97 for 9,10-PheQ.

The recoveries percent of PAHs, nitro- and oxy-PAHs and their internal standards were calculated using *spiked*
170 QFFs and PUFs samples. The recovery percent and accuracy (%RSTD) results are summarized in Table S7. Relative standards deviations (RSTDs) were in the range 5-15%, indicating a good repeatability. The recovery rates of native compounds from *spiked QFFs* samples were in the range 38-119 % for PAHs, 43-74 % for NPAHs, and 38-57 % for OPAHs, while recoveries of labeled internal standards were 65-111% for dPAHs, 40-77% for dNitro-PAHs, and 40-41% for dOxy-PAHs. The recovery rates of native compounds from *spiked PUFs*
175 samples were in the range 44-121 % for PAHs, 56-104 % for nitro-PAHs, and 43-110 % for Oxy-PAHs, while recoveries of labeled internal standards were 54-101% for dPAHs, 69-104% for dNitro-PAHs, 50-74% for dOxy-PAHs. Native nitro- and oxy-PAHs, such as BPy-6, 6-NBaPyr, 1,3-, 1,6-, and 1,8-DNPyr, showed low recovery (< 30 %) and therefore were excluded from quantification in air samples.

Samples spiking test (Table S7) showed that applying individual isotope labeled ISTD for each of 16 PAHs,
180 resulted in higher apparent recovery rates (~80%-100% for most of the compounds) compared to nitro- and oxy-PAHs, where only 8 deuterated ISTDs were used for 31 nitro- and oxy-PAHs. Recovery rates for all ISTDs showed satisfying recoveries (40 – 111%). dPAHs showed nearly equal, high extraction rates for the both methods applied for QFF and PUF spiked samples. The relatively low but still satisfying recovery for dNap, 54% for PUF and 65% for QFF, could be attributed to higher volatility of the compound, which leads to higher
185 losses during sample preparation. dNitro- and dOxy-PAHs extracted from QFF exhibited lower recovery compared to those Soxhlet extracted from PUFs. This either indicates co-extraction of PUF matrix or higher extraction efficiency of nitro- and oxy-PAHs by hot solvent circulation through PUF over long period of time (24 h).

The ISTD recoveries obtained for QFF and PUF air samples (Table S8) were in acceptable range, 63-105 % for
190 dPAHs, 56-69% dOPAHs, 44-89% dNAPHs.

Field (n=8) and laboratory (n=6) blanks were analysed in order to monitor and control possible contamination during sample transport and laboratory work. Method detection limit (Table S6) was determined based on blank levels. High contamination of blank samples by 9,10-PheQ (UNIS and Adventdalen), and 2-NFlu (PP) was

found. Thus, concentrations for these compounds were excluded from the final results. No blank correction was
195 performed for the concentration calculations.

Table S1. Sampling dates and sample volumes

Sample	Date	Power plant	Sample	Start date*	UNIS	Sample	Start date*	Adventdalen
		Volume, m ³			Volume, m ³			Volume, m ³
PP1	27.09.2018	2.7	U1	28.08.2018	349.2	A1	28.08.2018	359.5
PP2	27.09.2018	3.0	U2	30.08.2018	376.1	A2	30.08.2018	349.7
PP3	27.09.2018	1.7	U4	13.09.2018	365.6	A3	06.09.2018	451.5
PP4	02.10.2018	1.5	U5	25.09.2018	384.5	A4	13.09.2018	354.2
PP5	02.10.2018	1.3	U6	26.09.2018	355.7	A5	25.09.2018	403.8
PP6	02.10.2018	1.5	U7	27.09.2018	365.2	A7	27.09.2018	272.1

*sampling duration 23-31 hours

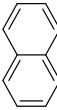
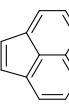
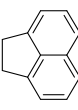
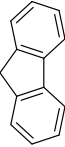
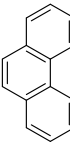
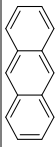
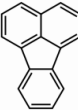

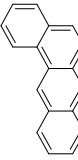
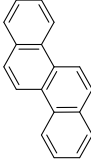
200 **Table S2. Meteorological data for UNIS (samples U1-U7) and Adventdalen (samples A1-A7) sampling stations**

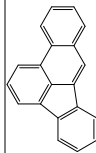
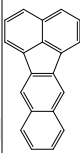
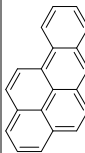
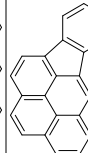
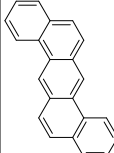
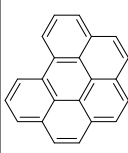
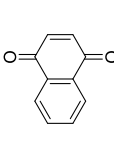
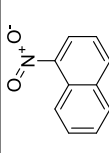
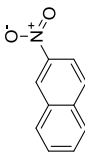
Sample name	Solar radiation, W m ⁻²	Air temp, °C	Pressure, hPa	RH, %	Specific humidity* _i , kg kg ⁻¹	Wind from** , degree	Precipitation, mm	Type of precipitation
U1	88.7±137.6	5.2±1.0	1011.5	74.7	0.0041	130.0	0.1	rain
U2	42.2±45.3	4.7±0.9	1000.1	78.0	0.0042	230.0	4.2	rain
U4	31.0±34.7	1.2±0.9	1003.3	79.5	0.0033	150.0	0.0	-
U5	18.3±24.4	-1.1±1.3	984.3	83.7	0.0030	220.0	2.8	snow
U6	27.9±39.0	-3.3±0.5	990.4	67.5	0.0020	260.0	0.3	snow
U7	16.9±28.7	-3.1±0.4	994.2	68.9	0.0020	260.0	0.2	snow
A1	88.7±137.6	4.9±0.9	1011.5	77.0	0.0041	120.0	0.1	rain
A2	42.2±45.3	5.0±1.0	1000.1	75.4	0.0042	260.0	4.2	rain
A3	76.4±110.7	3.1±1.0	1016.9	78.9	0.0040	270.0	0.0	-
A4	31.0±34.7	0.7±0.8	1003.3	85.4	0.0033	120.0	0.0	-
A5	18.3±24.4	-1.8±1.0	984.3	82.2	0.0030	210.0	2.8	snow
A7	16.9±28.7	-2.7±0.3	994.2	63.5	0.0020	250.0	0.2	snow

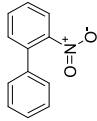
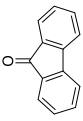
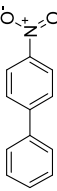
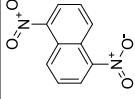
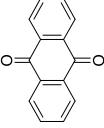
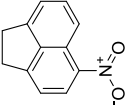
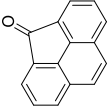
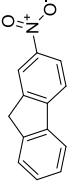
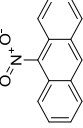
*calculated according to Launiainen and Vihma (1990)

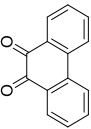
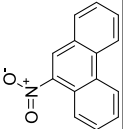
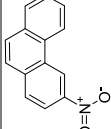
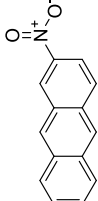
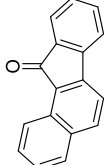
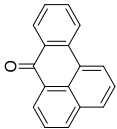
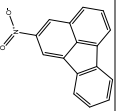
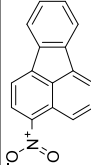
**wind roses are presented as Figure S1

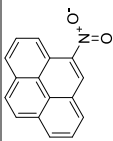
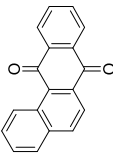
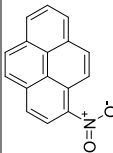
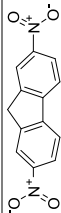
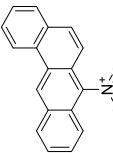
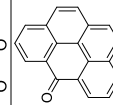
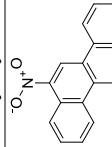
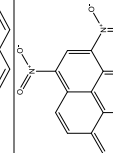
Table S3. Physico-chemical properties of target compounds

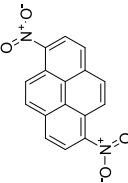
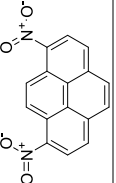
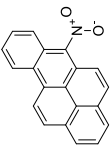
Compound	Abbreviation	CAS number	Structure ¹⁾	Log K _{oa} ²⁾	Water solubility, (estimated) ²⁾ mg L ⁻¹	Water solubility (experimental) ²⁾ mg L ⁻¹	Boiling point ³⁾ °C	Log K _{ow} ²⁾
Naphthalene	Nap	91-20-3		5.04	142.1	31.0	221.5±7.0	3.30
Acenaphthylene	Acy	208-96-8		6.27	2.49	16.1	298.9±7.0	3.94
Acenaphthene	Ace	83-32-9		6.04	2.53	3.90	279.0±0.0	3.92
Fluorene	Flu	86-73-7		6.59	1.34	1.69	293.6±10.0	4.18
Phenanthrene	Phe	85-01-8		7.22	0.68	1.15	337.4±9.0	4.46
Anthracene	Ant	120-12-7		7.09	0.69	0.04	337.4±9.0	4.45
Fluoranthene	Flt	206-44-0		8.60	0.13	0.26	375.0±0.0	5.16
Pyrene	Pyr	129-00-0		8.19	0.22	0.14	404.0±0.0	4.88
Benzo(a)anthracene	BaAnt	56-55-3		9.07	0.03	0.009	436.7±12.0	5.76
Chrysene	Chry	218-01-9		9.48	0.03	0.002	448.0±0.0	5.81

Benzo(b)fluoranthene	BbFlt	205-99-2		10.35	0.02	0.002	467.5±12.0	5.78
Benzo(k)fluoranthene	BaFlt	206-44-0		8.60	0.13	0.26	N.A.	5.16
Benzo(a)pyrene	BaPyr	50-32-8		10.86	0.01	0.002	495.0±0.0	6.13
Indeno(1,2,3-cd)pyrene	IPyr	193-39-5		11.55	0.002	0.0002	497.1±12.0	6.70
Dibenzo(ah)anthracene	DBAnt	53-70-3		11.78	0.003	0.001	524.7±17.0	6.54
Benzo(g,h,i)perylene	BPer	191-24-2		11.50	0.003	0.0003	501.0±0.0	6.63
1,4-Naphthoquinone	1,4-NapQ	130-15-4		8.80	2417	N.A.	297.9±40.0	1.71
1-Nitronaphthalene	1-NNap	86-57-7		7.33	45.66	9.18	304.0±0.0	3.19
2-Nitronaphthalene	2-NNap	581-89-5		7.31	41.38	9.24	319.6±11.0	3.24

2-Nitrophenyl	2-NBip	086-00-0		7.75	15.93	N.A.	325.0±11.0	3.57
9-Fluorenone	9-Flu	486-25-9		8.14	3.74	N.A.	341.5±0.0	3.58
4-Nitrophenyl	4-NBip	92-93-3		7.80	9.84	1.23	340.0±11.0	3.82
1,5-Dinitronaphthalene	1.5-DNNap	605-71-0		9.06	89.78	58.0	389.8±22.0	2.58
9,10-Anthraquinone	9,10-AntQ	84-65-1		9.41	3.92	1.35	377.0±12.0	3.39
5-Nitroacenaphthene	5-NAce	602-87-9		8.19	0.72	0.91	377.5±21.0	3.85
4H-Cyclopenta(def)phenanthrene-4-one	cPPhe-4	5737-13-3		9.60	0.94	N.A.	411.6±12.0	4.14
2-Nitrofluorene	2-NFlu	607-57-8		7.94	1.60	0.22	N.A.	3.37
9-Nitroanthracene	9-NAnt	602-60-8		9.86	0.087	0.12	402.9±14.0	4.78

9,10-Phenanthrenequinone	9,10-PheQ	084-11-7		9.48	21.71	400.0	360.0±0.0	2.52
9-Nitrophenanthrene	9-NPhe	954-46-1		9.24	0.29	N.A.	413.3±14.0	4.16
3-Nitrophenanthrene	3-NPhe	17024-19-0		9.24	0.29	N.A.	423.9±14.0	4.16
2-Nitroanthracene	2-NAnt	3586-69-4		9.24	0.29	N.A.	423.9±14.0	4.16
Benzo(a)fluoren-11-one	BaFlu-11	479-79-8		10.30	0.22	N.A.	431.7±12.0	4.73
Benzanthrone	BZT	82-05-3		10.38	0.18	N.A.	436.2±12.0	4.81
2-Nitrofluoranthene	2-NFlt	13177-29-2		8.52	2.12	N.A.	N.A.	4.29
3-Nitrofluoranthene	3-NFlt	892-21-7		10.62	0.068	0.019	445.5±14.0	4.75

4-Nitropyrene	4-NPyr	57835-92-4		10.62	0.068	N.A.	445.5±14.0	4.75
Benzo(a)anthracene-7,12-dione	BaAnt-7,12	2498-66-0		12.30	0.29	N.A.	472.5±15.0	4.40
1-Nitropyrene	1-NPyr	5522-43-0		10.93	0.037	0.012	445.5±14.0	5.06
2,7-Dinitrofluorene	2,7-DNFlu	5405-53-8		10.32	0.95	N.A.	451.5±38.0	3.35
7-Nitrobenz(a)anthracene	7-NBaAnt	20268-51-3		11.43	0.015	N.A.	495.3±14.0	5.34
6H-Benzo(cd)pyren-6-one	BPyr-6	3074-00-8		11.79	0.050	N.A.	509.5±17.0	5.31
6-Nitrochrysene	6-NChry	7496-02-8		11.43	0.015	N.A.	505.0±19.0	5.34
1,3-Dinitropyrene	1,3-DNPyr	95713-52-3		12.85	0.054	N.A.	493.9±25.0	4.57

1,6-Dinitropyrene	1.6-DNPyr	42397-64-8		12.85	0.054	N.A.	515.2±30.0	4.57
1,8-Dinitropyrene	1.8-DNPyr	42397-65-9		12.85	0.054	N.A.	515.2±30.0	4.57
6-Nitrobenzo(a)pyrene	6-NBaPyr	63041-90-7		12.32	0.0091	N.A.	524.1±19.0	5.44

¹⁾ All structures were prepared with ChemDraw Professional, v 15.0.0.106, PerkinElmer Informatics, Inc., Boston, Massachusetts, USA, 2015

²⁾ Acquired from EPI Suite, U.S.EPA; Estimation Programs Interface Suite, v 4.11, United States Environmental Protection Agency, Washington, DC, USA, 2019

³⁾ Predicted data are calculated with ACD/Labs Percepta Platform – PhysChem Module, Toronto, Canada, 2015

Table S4. GC–EI-MS/MS parameters used for PAHs determination and instrumental limits of quantification (LOQ)

Compound	Retention time, min	Precursor ion, m/z	Product ion quantifier, m/z	Product ion qualifier, m/z	Collision energy, eV	LOQ, pg
Naphthalene-d8	6.20	136	136	-	0	-
Naphthalene	6.22	128	102	127	20/20	1.74
Acenaphthylene-d8	7.88	160	160	-	0	-
Acenaphthylene	7.89	152	151	150	25/25	1.29
Acenaphthene-d10	8.07	164	164	-	0	-
Acenaphthene	8.11	154	152	153	35/35	1.27
Fluorene-d10	8.81	176	176	-	0	-
Fluorene	8.86	166	165	164	40/40	1.14
Phenanthrene-d10	10.46	188	188	-	0	-
Phenanthrene	10.50	178	176	152	40/15	1.43
Anthracene-d10	10.56	188	188	-	0	-
Anthracene	10.56	178	176	152	40/15	1.56
Fluoranthene-d10	12.91	212	212	-	0	-
Fluoranthene	12.95	202	201	200	20/20	1.32
Pyrene-d10	13.43	212	212	-	0	-
Pyrene	13.47	202	201	200	20/20	0.98
Benzo(a)anthracene-d12	16.78	240	240	-	0	-
Benzo(a)anthracene	16.84	228	226	227	30/30	3.39
Chrysene-d12	16.86	240	240	-	0	-
Chrysene	16.94	228	226	227	30/30	2.92
Benzo(b+k)fluoranthene-d12	20.45	264	264	-	0	-
Benzo(b+k)fluoranthene	20.50	252	250	251	25/25	2.88
Benzo(a)pyrene-d12	21.45	264	264	-	0	-
Benzo(a)pyrene	21.52	252	250	251	25/25	2.95
Indeno(1,2,3-cd)pyrene-d12	25.14	288	288	-	0	-
Indeno(1,2,3-cd)pyrene	25.22	276	274	275	35/35	3.69
Dibenzo(a,h)anthracene-d12	25.21	292	292	-	0	-
Dibenzo(a,h)anthracene	25.30	278	276	277	25/25	3.54
Benzo(g,h,i)perylene-d14	25.91	288	288	-	0	-
Benzo(g,h,i)perylene	25.98	276	274	275	35/35	3.37

Table S5. GC-ECNI-MS parameters used for nitro- and oxy-PAHs determination and instrumental limits of quantification (LOQ)

Compound	Monitored ion, m/z	Retention time, min	LOQ, pg
1,4-Naphthaquinone-d6	164	5.95	-
1,4-Naphthaquinone	158	5.96	0.12
1-Nitronaphthalene-d7	180	6.50	-
1-Nitronaphthalene	173	6.60	0.09
2-Nitronaphthalene	173	6.90	0.09
2-Nitrobiphenyl-d9	208	6.76	-
2-Nitrobiphenyl	199	6.80	0.13
9-Fluorenone-d8	188	6.90	-
9-Fluorenone	180	7.00	0.49
4-Nitrobiphenyl	199	7.35	0.24
1,5-Dinitronaphthalene	218	7.60	0.23
Anthraquinone-d8	216	7.80	-
9,10-Anthraquinone	208	7.85	0.84
1,2,3,4-Tetrachloronaphthalene RSTD	264	7.80	-
5-Nitroacenaphthene	199	8.00	0.20
4H-Cyclopenta[def]phenanthrene-4-one	204	8.20	0.50
Fluoranthene-d10 RSTD	212	8.30	-
2-Nitrofluorene	211	8.50	0.26
2-Nitrofluorene-d9	220	8.50	-
9-Nitroanthracene-d9	232	8.66	-
9-Nitroanthracene	223	8.70	0.33
9,10-Phenanthrenequinone	208	8.95	26.87
9-Nitrophenanthrene	223	9.20	0.37
3-Nitrophenanthrene	223	9.50	0.57
2-Nitroanthracene	223	9.90	0.58
Benzo[a]fluoren-11-one	230	10.40	0.75
Benanthrone	230	11.90	2.69
3-Nitrofluoranthene-d9	256	12.40	-
2-Nitrofluoranthene	247	12.40	1.36
3-Nitrofluoranthene	247	12.50	1.22
4-Nitropyrene	247	12.70	1.12
Benzo[a]anthracene-7,12-dione	258	13.00	1.62
1-Nitropyrene-d9 RSTD	256	13.20	-
1-Nitropyrene	247	13.20	1.21
2-Nitropyrene	247	13.20	2.30
2,7-Dinitrofluorene	256	13.80	1.41
7-Nitrobenzo[a]anthracene	273	15.70	1.22
6H-Benzo[cd]pyren-6-one	254	16.50	5.35
6-Nitrochrysene-d11	284	16.80	-
6-Nitrochrysene	273	16.90	1.30
1,3-Dinitropyrene	292	17.80	1.27
1,6-Dinitropyrene	292	18.60	2.04
1,8-Dinitropyrene	292	19.10	1.55
6-Nitrobenzo(a)pyrene	297	21.00	1.14

Table S6. Blank values and method detection limits (MDL) for different sampling materials

Compound	UNIS and Adventdalen				Power plant			
	QFF=7		PUF=7		QFF=7		PUF=7	
	Ø = 103 mm, Munktell**		L = 100 mm, Ziemer**		Ø = 47 mm, Pallflex**		L = 75 mm, Ziemer**	
	Mean blank, pg	MDL, pg	Mean blank, pg	MDL, pg	Mean blank, pg	MDL, pg	Mean blank, pg	MDL, pg
Naphthalene	16394 ± 2765	24689	54223 ± 3648	65167	3849 ± 672	5865	33647 ± 5652	50603
Acenaphthylene	n.d.	-	272.1 ± 13.0	310.9	114.8 ± 10.0	144.9	1219.0 ± 231.6	1913.8
Acenaphthene	n.d.	-	307.9 ± 19.7	367.0	32.9 ± 3.9	44.6	211.4 ± 52.0	367.4
Fluorene	51.0 ± 6.6	70.8	6075 ± 508	7599	139.2 ± 9.5	167.7	3783 ± 677	5814
Phenanthrene	7660 ± 779	9997	43073 ± 2155	49538	394.8 ± 41.7	519.9	14051 ± 1731	19244
Anthracene	n.d.	-	n.d.	-	n.d.	-	630.0 ± 134.3	1032.9
Fluoranthene	274.2 ± 18.6	330.1	2389.4 ± 103.5	2699.9	61.9 ± 6.6	81.6	1597.5 ± 142.3	2024.4
Pyrene	259.7 ± 28.9	346.4	4369 ± 353	5428	183.6 ± 29.0	270.6	1089.8 ± 124.7	1463.9
Benzo(a)anthracene	n.d.	-	173.6 ± 13.4	213.7	n.d.	-	117.5 ± 22.0	183.5
Chrysene	77.4 ± 5.1	92.7	157.8 ± 10.7	189.9	n.d.	-	80.3 ± 11.1	113.7
Benzo(b+k)fluoranthene	n.d.	-	n.d.	-	n.d.	-	n.d.	-
Benzo(a)pyrene	n.d.	-	n.d.	-	n.d.	-	n.d.	-
Indeno(1,2,3-cd)pyrene	49.9 ± 5.0	64.9	n.d.	-	n.d.	-	86.8 ± 15.7	134.0
Dibenzo(a,h)anthracene	n.d.	-	n.d.	-	n.d.	-	n.d.	-
Benzo(g,h,i)perylene	53.9 ± 4.1	66.1	n.d.	-	n.d.	-	164.3 ± 27.0	245.3
1-Nitronaphthalene	24.4 ± 1.4	28.6	474.9 ± 24.5	548.4	707.4 ± 101.5	1011.9	238.4 ± 44.5	371.9
2-Nitronaphthalene	11.3 ± 1.3	15.1	255.0 ± 23.4	325.2	44.2 ± 6.9	65.0	94.7 ± 10.0	125
2-Nitrophenyl	4.3 ± 0.3	5.1	199.6 ± 16.4	248.7	48.3 ± 5.4	64.4	59.2 ± 9.9	89.0
9-Fluorenone	3453 ± 367	4554	15754 ± 1085	19009	1190.0 ± 152.4	1647.2	6486 ± 1275	10311
4-Nitrophenyl	n.d.	-	84.0 ± 7.6	106.8	n.d.	-	n.d.	-
1,5-Dinitronaphthalene	22.0 ± 1.7	27.2	152.2 ± 7.6	175.1	n.d.	-	204.1 ± 41.9	329.8
9,10-Anthraquinone	4399 ± 741	6622	10896 ± 724	13068	1106.8 ± 141.9	1532.5	3781 ± 718	5935
5-Nitroacenaphthene	n.d.	-	3.0 ± 3.4	44.2	n.d.	-	n.d.	-
cPPhen-4	695.0 ± 115.7	1042.1	1412.5 ± 110.4	1743.7	92.1 ± 9.7	121.3	446.0 ± 89.6	714.8
2-Nitrofluorene	12.0 ± 1.1	15.3	49.2 ± 3.7	60.3	149218 ± 17607	202039	39.0 ± 3.8	50.5
9-Nitroanthracene	64.1 ± 5.4	80.4	103.0 ± 6.1	121.2	n.d.	-	41.8 ± 4.5	55.4
9,10-Phenanthrenequinone	7799 ± 840	10319	3610 ± 280	4450	n.d.	-	2667 ± 379	3804
9-NPhe	258.4 ± 15.1	303.6	52.5 ± 4.9	67.2	n.d.	-	n.d.	-
3-Nitrophenanthrene	n.d.	-	n.d.	-	n.d.	-	26729 ± 4632	40625
2-Nitroanthracene	n.d.	-	n.d.	-	n.d.	-	85.5 ± 19.7	144.7
Benzo(a)fluoren-11-one	125.0 ± 9.5	153.5	n.d.	-	27.2 ± 3.1	36.5	50.1 ± 7.5	72.7
Benzanthrone	n.d.	-	135.6 ± 9.2	163.2	n.d.	-	179.1 ± 19.2	236.9
2+3-Nitrofluoranthene	1131.5 ± 169.3	1639.4	703.4 ± 58.9	880.1	n.d.	-	86.2 ± 14.0	128.4
4-Nitropyrene	n.d.	-	n.d.	-	n.d.	-	31.9 ± 5.0	47.0
Benzo(a)anthracene-7,12-dione	n.d.	-	n.d.	-	n.d.	-	n.d.	-
1-Nitropyrene	n.d.	-	n.d.	-	n.d.	-	n.d.	-
2,7-Dinitrofluorene	n.d.	-	n.d.	-	n.d.	-	n.d.	-
7-Nitrobenzo(a)anthracene	n.d.	-	n.d.	-	n.d.	-	139.4 ± 17.7	192.6
6H-Benzo(cd)pyren-6-one	n.d.	-	n.d.	-	n.d.	-	n.d.	-
6-Nitrochrysene	n.d.	-	n.d.	-	n.d.	-	n.d.	-

1,3-Dinitropyrene	n.d.	-	n.d.	-	n.d.	-	n.d.	-
1,6-Dinitropyrene	n.d.	-	n.d.	-	n.d.	-	n.d.	-
1,8-Dinitropyrene	n.d.	-	n.d.	-	n.d.	-	n.d.	-
6-Nitrobenzo(a)pyrene	n.d.	-	n.d.	-	n.d.	-	n.d.	-

* MDL = blank + 3*STD

** Sampling material with different size (PUF length or QFF diameter) and producers (Munktell, Ziemer, Pallflex) were used for air sampling

225

Table S7. Average recovery rates (Rec, %) and relative standard deviations (RSTD, %) for spiked samples

Compound	Spiked QFF=4		Spiked PUF=4	
	Mean Rec, %	RSTD, %	Mean Rec, %	RSTD, %
Nap	128.6 ± 10.0	7.8	121.2 ± 9.5	7.8
Acy	79.1 ± 6.8	8.6	93.3 ± 1.6	1.7
Ace	46.2 ± 4.2	9.1	48.0 ± 9.9	20.5
Flu	80.1 ± 9.1	11.3	109 ± 13.4	12.3
Phe	78.2 ± 9.4	12.0	83.7 ± 3.5	4.1
Ant	97.5 ± 4.6	4.7	119.8 ± 4.2	3.5
Flt	37.5 ± 5.4	14.3	43.5 ± 5.1	11.6
Pyr	80.9 ± 4.4	5.4	100.7 ± 2.3	2.3
BaAnt	77.6 ± 5.8	7.5	90.3 ± 4.3	4.8
Chry	78.9 ± 9.1	11.6	77.9 ± 5.8	7.4
BbkFlt	72.4 ± 10.1	13.9	90.9 ± 1.5	1.7
BaPyr	76.5 ± 5.1	6.6	86.0 ± 13.6	15.8
IPyr	75.6 ± 8.4	11.1	78.2 ± 5.7	7.3
DBAnt	86.9 ± 11.1	12.8	89.1 ± 2.1	2.3
BPer	81.1 ± 3.1	3.8	94.6 ± 10.0	10.6
dNap	64.5 ± 3.4	5.2	53.7 ± 11.0	20.4
dAcy	90.1 ± 9.5	10.6	73.0 ± 1.3	1.8
dAce	97.1 ± 8.7	9.0	89.4 ± 11.1	12.5
dFlu	68.9 ± 4.3	6.2	76.2 ± 9.3	12.2
dPhe	68.2 ± 16.4	24.0	82.4 ± 17.2	20.9
dAnt	111.3 ± 7.0	6.3	97.3 ± 5.3	5.4
dFlt	81.9 ± 10.9	13.3	100.4 ± 22.2	22.1
dPyr	107.8 ± 11.0	10.2	76.8 ± 5.0	6.5
dBaAnt	66.9 ± 9.0	13.4	82.6 ± 27.9	33.8
dChry	69.5 ± 9.7	13.9	80.1 ± 11.3	14.1
dBbkFlt	98.0 ± 7.1	7.3	100.6 ± 15.7	15.6
dBaPyr	98.9 ± 7.4	7.4	98.7 ± 5.9	6.0
dIPyr	102.2 ± 15.9	15.6	101.0 ± 17.6	17.5
dDBAnt	93.2 ± 8.4	9.0	89.8 ± 17.0	19.0
dBPer	96.9 ± 17.2	17.8	91.1 ± 9.2	10.1
1-Nnap	51.2 ± 10.9	21.2	72.3 ± 7.1	9.8
2-Nnap	61.4 ± 7.5	12.2	73.3 ± 19.5	26.6
2-NBip	74.4 ± 16.8	22.6	99.5 ± 9.9	9.9
9-Flu	40.1 ± 2.0	5.1	91.5 ± 7.7	8.4
4-NBip	65.9 ± 4.4	6.7	84.5 ± 18.3	21.7

1,5-DNNap	53.1 ± 8.4	15.9	69.0 ± 7.1	10.3
9,10-AntQ	42.0 ± 6.9	16.4	43.2 ± 4.4	10.3
5-NAce	74.3 ± 4.9	6.5	80.2 ± 10.0	12.5
cPPhe-4	44.1 ± 6.5	14.7	48.2 ± 2.4	4.9
2-Nflu	66.6 ± 5.0	7.6	66.3 ± 14.9	22.4
9-Nant	42.5 ± 16.7	39.3	78.0 ± 6.7	8.5
9,10-PheQ	56.8 ± 10.2	18.0	74.0 ± 7.6	10.3
9-NPhe	64.2 ± 6.0	9.3	104.7 ± 15.6	14.8
3-Nphe	65.7 ± 8.4	12.9	87.7 ± 4.9	5.5
2-Nant	46.2 ± 11.6	25.1	107.1 ± 11.0	10.3
BaFlu-11	47.4 ± 3.0	6.3	109.5 ± 20.4	18.6
BZT	37.8 ± 7.2	19.0	43.8 ± 3.1	7.1
2+3-NFlt	59.3 ± 15.4	25.9	79.6 ± 13.5	17.0
4-Npyr	54.6 ± 5.7	10.4	79.2 ± 10.3	13.0
BaAnt-7,12	46.8 ± 12.1	25.8	69.4 ± 4.0	5.8
1-Npyr	49.1 ± 15.5	31.5	56.2 ± 7.9	14.0
7-NBaAnt	69.8 ± 35.2	50.4	100.4 ± 8.5	8.5
BPyr-6	2.0 ± 0.3	13.7	4.1 ± 0.2	5.0
6-Nchry	58.8 ± 5.3	8.9	83.5 ± 8.3	9.9
1,3-DNPyr	17.8 ± 3.0	17.0	104.4 ± 36.8	35.2
1,6-DNPyr	22.6 ± 1.0	4.2	98.6 ± 17.9	18.2
1,8-DNPyr	9.5 ± 0.3	3.2	50.0 ± 12.3	24.5
6-NBaPyr	6.4 ± 0.5	7.1	32.6 ± 7.0	21.5
1-NNap-d7	60.7 ± 1.1	1.7	73.3 ± 9.2	12.5
2-NBP-d9	77.1 ± 3.9	5.1	104.1 ± 12.6	12.1
9-Flu-d8	40.7 ± 5.7	13.9	73.8 ± 8.8	12.0
AntQ-d8	39.6 ± 3.4	8.5	50.3 ± 8.6	17.2
2-NFlu-d9	68.6 ± 9.7	14.2	73.5 ± 6.6	8.9
9-NAnt-d9	39.9 ± 3.4	8.6	69.0 ± 8.3	12.0
3-NFlt-d9	55.3 ± 7.6	13.7	79.6 ± 14.4	18.1
6-NChry-d11	59.4 ± 1.2	2.1	93.1 ± 16.2	17.4

Table S8. Average recovery rates (Rec, %) of internal standards (ISTDs) for *ambient air* samples

ISTD	Rec, %	
	QFF=15	PUF=15
dNap	68.6 ± 11.2	68.4 ± 6.2
dAcy	70.7 ± 7.8	99.1 ± 22.3
dAce	100.2 ± 27.5	74.4 ± 17.9
dFlu	90.8 ± 9.2	76.9 ± 25.8
dPhe	66.3 ± 5.8	100.8 ± 15.9
dAnt	63.3 ± 11.3	91.7 ± 33.0
dFlt	68.6 ± 5.2	93.9 ± 15.8
dPyr	102.4 ± 6.1	84.3 ± 11.6
dBaAnt	94.8 ± 12.6	103.5 ± 21.3
dChry	63.9 ± 7.6	83.2 ± 18.7
dBbkFlt	99.8 ± 15.4	99.3 ± 6.4
dBaPyr	74.9 ± 6.0	97.5 ± 17.0
dIPyr	72.0 ± 4.9	109.1 ± 20.0
dDBAnt	80.1 ± 22.6	101.3 ± 13.1
dBPer	91.1 ± 14.3	79.3 ± 12.9
1-NNap-d7	59.8 ± 3.7	80.3 ± 23.7
2-NBP-d9	70.0 ± 8.0	89.0 ± 4.3
9-Flu-d8	60.6 ± 16.6	67.7 ± 4.3
9,10-AntQ-d8	56.2 ± 12.4	69.0 ± 20.9
2-NFlu-d9	52.7 ± 6.0	84.5 ± 18.1
9-NAnt-d9	74.5 ± 14.8	65.2 ± 6.7
3-NFlt-d9	63.1 ± 5.7	49.3 ± 7.4
6-NChry-d11	44.0 ± 7.7	49.1 ± 9.0

Table S9. Concentrations of PAHs (G+P) and percentage in the particulate phase (%PM) in Longyearbyen power plant (n=6), as well as MDLs for gaseous (PUF) and particulate (QFF) phases, and instrumental LOD and LOQ; all values are in pg m^{-3} *

Variable	Mean conc \pm STD, pg m^{-3}	Median pg m^{-3}	Min – Max pg m^{-3}	Mean %PM	MDL _{OFF} pg m^{-3}	MDL _{PUF} pg m^{-3}	LOD pg m^{-3}	LOQ pg m^{-3}
Naphthalene	51817.0 \pm 10297.0	55629.0	32737.0 - 59824.0	7.4	1515.2	23992.0	0.3	0.9
Acenaphthylene	2301.0 \pm 1059.0	2203.0	1218.0 - 3797.0	0.6	107.9	1024.0	0.2	0.6
Acenaphthene	873.0 \pm 778.0	487.0	300.0 - 2177.0	8.4	29.5	145.2	0.2	0.6
Fluorene	7607.0 \pm 3568.0	6946.0	3680.0 - 12164.0	4.6	62.3	3445.5	0.2	0.6
Phenanthrene	27324.0 \pm 12700.0	27530.0	12015.0 - 44871.0	5.6	159.2	9242.6	0.2	0.7
Anthracene	1055.0 \pm 818.0	925.0	229.2 - 2136.0	0.0	n.d.	458.4	0.3	0.8
Fluoranthene	6991.0 \pm 3754.0	6961.0	1428.0 - 12494.0	3.9	47.7	1126.6	0.2	0.7
Pyrene	4404.0 \pm 2178.0	4700.0	1083.0 - 7348.0	8.3	75.2	717.9	0.2	0.5
Benzo(a)anthracene	130.7 \pm 77.3	156.7	36.4 ²⁾ - 202.8	0.0	n.d.	72.9	0.6	1.7
Chrysene	277.3 \pm 141.4	333.3	60.7 - 421.3	0.0	n.d.	54.7	0.5	1.4
Benzo(b+k)fluoranthene	n.d.	n.d.	n.d.	-	n.d.	n.d.	0.5	1.4
Benzo(a)pyrene	n.d.	n.d.	n.d.	-	n.d.	n.d.	0.5	1.5
Indeno(1,2,3-cd)pyrene	n.d.	n.d.	n.d.	-	n.d.	132.2	0.6	1.8
Dibenzo(a,h)anthracene	n.d.	n.d.	n.d.	-	n.d.	n.d.	0.6	1.8
Benzo(g,h,i)perylene	n.d.	n.d.	n.d.	-	n.d.	225.4	0.6	1.7
1-Nitronaphthalene	2188.0 \pm 1341.0	1729.0	988.0 - 4685.0	61.7	241.0	158.9	0.0	0.0
2-Nitronaphthalene	257.3 \pm 108.8	273.6	105.9 - 395.1	31.7	20.3	74.9	0.0	0.0
2-Nitrobiphenyl	157.4 \pm 75.7	154.2	69.2 - 290.3	39.9	18.8	38.8	0.0	0.1
9-Fluorenone	12352.0 \pm 5258.0	11937.0	5566.0 - 19541.0	19.2	479.0	4368.6	0.1	0.2
4-Nitrobiphenyl	n.d.	n.d.	n.d.	-	n.d.	n.d.	0.0	0.1
1,5-Dinitronaphthalene	n.d.	n.d.	n.d.	-	n.d.	139.7	0.0	0.1
9,10-Anthraquinone	15758.0 \pm 15578.0	10806.0	4595.0 - 46956.0	21.3	446.8	2558.7	0.1	0.4
5-Nitroacenaphthene	n.d.	n.d.	n.d.	-	n.d.	n.d.	0.0	0.1
cPPhen-4	1304.0 \pm 743.0	1320.0	506.0 - 2554.0	15.8	39.3	326.7	0.1	0.2
2-Nitrofluorene	42.5 \pm 54.3	25.0	22.0 ²⁾ - 134.5	0.0	777.5	44.0	0.0	0.1
9-Nitroanthracene	79.6 \pm 77.2	61.4	20.5 ²⁾ - 226.7	0.0	n.d.	41.1	0.1	0.2
9,10-Phenanthrenequinone	2127.0 \pm 1934.0	2061.0	960.1 ²⁾ - 4400.0	0.0	n.d.	1920.2	9.4	28.3
9-Nitrophenanthrene	n.d.	n.d.	n.d.	-	n.d.	n.d.	0.1	0.2
3-Nitrophenanthrene	761.0 \pm 757.0	656.0	0.3 ¹⁾ - 1930.0	96.1	n.d.	76.0	0.1	0.3
2-Nitroanthracene	305.7 \pm 235.5	261.4	66.1 ²⁾ - 620.9	0.0	n.d.	132.2	0.1	0.3
Benzo(a)fluoren-11-one	157.5 \pm 55.2	165.0	75.5 - 227.0	27.6	27.0	32.9	0.1	0.4
Benzanthrone	866.0 \pm 418.0	920.0	135.0 - 1314.0	0.0	n.d.	117.1	0.4	1.3
2+3-Nitrofluoranthene	519.3 \pm 437.1	442.1	61.0 - 1140.3	0.0	n.d.	53.6	0.2	0.6
4-Nitropyrene	114.8 \pm 70.0	151.5	25.7 ²⁾ - 174.5	0.0	n.d.	51.4	0.2	0.6
Benzo(a)anthracene-7,12-dione	n.d.	n.d.	n.d.	-	n.d.	n.d.	0.3	0.8
1-Nitropyrene	n.d.	n.d.	n.d.	-	n.d.	n.d.	0.2	0.6
2,7-Dinitrofluorene	58.8 \pm 53.1	70.5	0.6 ¹⁾ - 141.0	0.0	n.d.	n.d.	0.2	0.6
7-Nitrobenzo(a)anthracene	578.0 \pm 376.0	709.0	114.2 ²⁾ - 932.0	0.0	n.d.	228.5	0.2	0.6
6H-Benzo(cd)pyren-6-one	n.d.	n.d.	n.d.	-	n.d.	n.d.	0.9	2.6
6-Nitrochrysene	n.d.	n.d.	n.d.	-	n.d.	n.d.	0.2	0.6
1,3-Dinitropyrene	n.d.	n.d.	n.d.	-	n.d.	n.d.	0.2	0.6
1,6-Dinitropyrene	n.d.	n.d.	n.d.	-	n.d.	n.d.	0.3	1.0
1,8-Dinitropyrene	n.d.	n.d.	n.d.	-	n.d.	n.d.	0.3	0.8
6-Nitrobenzo(a)pyrene	n.d.	n.d.	n.d.	-	n.d.	n.d.	0.2	0.6
Σ PAHs	102846 \pm 31931		61925 - 139082					
Σ oxy-PAHs	32565 \pm 20963		15767 - 73084					
Σ nitro-PAHs	4451 \pm 2075		2046 - 7752					

235

* LOD, LOQ and MDL in pg (Tables S4-S6) were converted to pg m^{-3} using 2 m^3 as average sample volume
n.d. not detected

¹⁾ equal LOQ

²⁾ $\frac{1}{2}$ of MDL

240 **Table S10. Concentrations of PAHs (G+P) and percentage in the particulate phase (%PM) at UNIS (n=6), as well as MDLs for gaseous (PUF) and particulate (QFF) phases, and instrumental LOD and LOQ; all values are in pg m⁻³***

Variable	Mean conc ± STD, pg m ⁻³	Median pg m ⁻³	Min – Max pg m ⁻³	Mean %PM ± STD	MDL qff ¹ pg m ⁻³	MDL puf ² pg m ⁻³	LOD pg m ⁻³	LOQ pg m ⁻³
Naphthalene	< MDL	< MDL	< MDL	-	45.6	241.8	0.002	0.005
Acenaphthylene	16.9 ± 8.2	16.6	7.1 - 29.2	0 ± 0.0	n.d.	0.8	0.001	0.003
Acenaphthene	48.5 ± 20.5	45.7	24.3 - 73.0	0 ± 0.0	n.d.	0.9	0.001	0.003
Fluorene	170.5 ± 39.6	155.2	136.5 - 236.0	1.1 ± 1.0	0.2	26.6	0.001	0.003
Phenanthrene	409.2 ± 34.3	401.8	368.5 - 470.0	6.5 ± 8.6	32.4	179.6	0.001	0.004
Anthracene	18.0 ± 4.5	17.2	12.3 - 25.5	0 ± 0.0	n.d.	n.d.	0.001	0.004
Fluoranthene	28.5 ± 4.3	27.5	24.1 - 36.1	40.5 ± 19.4	1.2	7.4	0.001	0.004
Pyrene	39.5 ± 6.3	37.9	30.7 - 47.8	26.8 ± 18.6	1.1	12.7	0.001	0.003
Benzo(a)anthracene	2.2 ± 2.6	1.2	0.009 ¹⁾ - 5.8	68.2 ± 2.4	n.d.	0.5	0.003	0.009
Chrysene	7.3 ± 4.3	6.6	2.6 - 13.5	81.7 ± 10.3	0.2	0.4	0.003	0.008
Benzo(b+k)fluoranthene	2.2 ± 2.1	1.8	0.008 ¹⁾ - 5.9	100 ± 0.0	n.d.	n.d.	0.003	0.008
Benzo(a)pyrene	0.9 ± 1.1	0.6	0.008 ¹⁾ - 2.5	100 ± 0.0	n.d.	n.d.	0.003	0.008
Indeno(1,2,3-cd)pyrene	1.6 ± 1.5	1.8	0.07 ²⁾ - 3.8	100 ± 0.0	0.15	n.d.	0.003	0.010
Dibenzo(a,h)anthracene	n.d.	n.d.	n.d.	-	n.d.	n.d.	0.003	0.009
Benzo(g,h,i)perylene	3.9 ± 2.5	3.7	1.4 - 8.1	100 ± 0.0	0.2	n.d.	0.003	0.009
1-Nitronaphthalene	17.0 ± 3.0	16.4	13.4 - 21.5	0.1 ± 0.2	0.1	1.3	0.000	0.001
2-Nitronaphthalene	5.1 ± 2.0	5.1	2.4 - 7.3	3.1 ± 5.6	0.04	1.0	0.000	0.001
2-Nitrophenyl	1.0 ± 0.1	1.0	0.8 - 1.2	10.1 ± 8.3	0.01	0.6	0.000	0.001
9-Fluorenone	270.3 ± 146.9	211.2	128.2 - 543.8	41.7 ± 22.3	14.1	62.1	0.001	0.004
4-Nitrophenyl	2.2 ± 0.5	2.4	1.5 - 2.7	0 ± 0.0	n.d.	0.2	0.001	0.002
1,5-Dinitronaphthalene	0.8 ± 0.9	0.5	0.05 - 2.2	80.0 ± 44.7	0.1	0.4	0.001	0.002
9,10-Anthraquinone	163.5 ± 57.4	159.6	105.2 - 269.1	37.5 ± 22.4	19.3	22.8	0.002	0.007
5-Nitroacenaphthene	0.2 ± 0.1	0.2	0.05 ²⁾ - 0.38	-	n.d.	0.1	0.001	0.002
cPPhen-4	27.2 ± 6.9	25.1	20.2 - 35.8	65.5 ± 10.6	2.8	5.1	0.001	0.004
2-Nitrofluorene	0.2 ± 0.3	0.1	0.07 ²⁾ - 0.8	15.1 ± 7.5	0.04	0.15	0.001	0.002
9-Nitroanthracene	0.6 ± 0.3	0.7	0.2 ²⁾ - 0.9	-	0.2	0.4	0.001	0.003
9,10-Phenanthrenequinone	< MDL	< MDL	< MDL	-	22.5	14.4	0.155	0.464
9-Nitrophenanthrene	0.2 ± 0.2	0.3	0.1 ²⁾ - 0.4	-	1.1	0.2	0.001	0.003
3-Nitrophenanthrene	n.d.	n.d.	n.d.	-	n.d.	n.d.	0.002	0.005
2-Nitroanthracene	n.d.	n.d.	n.d.	-	n.d.	n.d.	0.002	0.005
Benzo(a)fluoren-11-one	6.1 ± 3.6	5.0	1.8 - 11.1	100 ± 0.0	0.6	n.d.	0.002	0.006
Benzanthrone	1.8 ± 1.8	1.7	0.02 ¹⁾ - 4.3	96.7 ± 4.8	n.d.	0.5	0.007	0.022
2+3-Nitrofluoranthene	9.5 ± 1.6	9.7	7.3 - 11.4	94.5 ± 13.5	4.5	2.1	0.003	0.010
4-Nitropyrene	n.d.	n.d.	n.d.	-	n.d.	n.d.	0.003	0.009
Benzo(a)anthracene-7,12-dione	2.2 ± 1.8	2.2	0.01 ¹⁾ - 4.9	100 ± 0.0	n.d.	n.d.	0.004	0.013
1-Nitropyrene	n.d.	n.d.	n.d.	-	n.d.	n.d.	0.003	0.010
2,7-Dinitrofluorene	n.d.	n.d.	n.d.	-	n.d.	n.d.	1.003	3.010
7-Nitrobenzo(a)anthracene	n.d.	n.d.	n.d.	-	n.d.	n.d.	0.003	0.010
6H-Benzo(cd)pyren-6-one	n.d.	n.d.	n.d.	-	n.d.	n.d.	0.014	0.043
6-Nitrochrysene	n.d.	n.d.	n.d.	-	n.d.	n.d.	0.004	0.011
1,3-Dinitropyrene	n.d.	n.d.	n.d.	-	n.d.	n.d.	0.003	0.010
1,6-Dinitropyrene	n.d.	n.d.	n.d.	-	n.d.	n.d.	0.006	0.017
1,8-Dinitropyrene	n.d.	n.d.	n.d.	-	n.d.	n.d.	0.004	0.013
6-Nitrobenzo(a)pyrene	n.d.	n.d.	n.d.	-	n.d.	n.d.	0.003	0.009
∑ PAHs	749.2 ± 72.6		687.4 - 866.9					
∑ oxy-PAHs	471.0 ± 150.8		325.9 - 741.4					
∑ nitro-PAHs	36.76 ± 6.19		30.30 - 46.10					

* LOD, LOQ and MDL in pg (Tables S4-S6) were converted to pg m⁻³ using 370 m³ as average sample volume

245 <MDL below method detection limit

n.d. not detected

¹⁾ equal LOQ

²⁾ ½ of MDL

Table S11. Concentrations of PAHs (G+P) and percentage in the particulate phase (%PM) at Adventdalen (n=6), as well as MDLs for gaseous (PUF) and particulate (QFF) phases, and instrumental LOD and LOQ; all values are in pg m^{-3} *

Variable	Mean conc \pm STD, pg m^{-3}	Median pg m^{-3}	Min – Max pg m^{-3}	Mean %PM \pm STD	MDL qff pg m^{-3}	MDL puf pg m^{-3}	LOD pg m^{-3}	LOQ pg m^{-3}
Naphthalene	< MDL	< MDL	< MDL	-	45.6	241.8	0.002	0.005
Acenaphthylene	2.4 \pm 1.5	2.1	1.1 - 5.1	0 \pm 0	-	0.8	0.001	0.004
Acenaphthene	3.8 \pm 2.5	3.8	1.3 - 6.6	0 \pm 0	-	0.9	0.001	0.003
Fluorene	60.0 \pm 23.2	50.1	38.5 - 95.8	1.8 \pm 3.0	0.2	26.6	0.001	0.003
Phenanthrene	236.3 \pm 31.8	236.2	191.7 - 270.8	3.7 \pm 9.0	32.4	179.6	0.001	0.004
Anthracene	14.3 \pm 3.4	13.9	10.5 - 19.3	3.5 \pm 8.5	-	-	0.001	0.004
Fluoranthene	19.1 \pm 10.0	15.8	10.8 - 38.5	23.2 \pm 9.2	1.2	7.4	0.001	0.004
Pyrene	27.2 \pm 6.4	26.4	20.9 - 35.9	15.8 \pm 11.0	1.1	12.7	0.001	0.003
Benzo(a)anthracene	n.d.	n.d.	n.d.	-	-	0.5	0.003	0.009
Chrysene	3.1 \pm 2.5	2.7	0.1 ¹⁾ - 7.1	64.1 \pm 18.7	0.2	0.4	0.003	0.008
Benzo(b+k)fluoranthene	0.7 \pm 1.2	0.0	0.008 ¹⁾ - 2.785	100 \pm 0	-	-	0.003	0.008
Benzo(a)pyrene	0.3 \pm 0.5	0.0	0.008 ¹⁾ - 1.163	100 \pm 0	-	-	0.003	0.008
Indeno(1,2,3-cd)pyrene	0.7 \pm 1.2	0.0	0.07 ²⁾ - 2.67	100 \pm 0	0.15	-	0.003	0.010
Dibenzo(a,h)anthracene	n.d.	n.d.	n.d.	-	-	-	0.003	0.010
Benzo(g,h,i)perylene	1.2 \pm 1.5	0.8	0.08 ²⁾ - 3.83	100 \pm 0	0.2	-	0.003	0.009
1-Nitronaphthalene	5.0 \pm 3.2	4.2	1.9 - 9.8	1.5 \pm 3.6	0.1	1.3	0.000	0.001
2-Nitronaphthalene	1.9 \pm 0.6	1.7	1.3 - 2.8	5.4 \pm 8.0	0.1	1.0	0.000	0.001
2-Nitrophenyl	1.0 \pm 0.2	0.9	0.8 - 1.3	5.9 \pm 10.0	0.1	0.6	0.000	0.001
9-Fluorenone	139.4 \pm 24.9	137.3	110.2 - 177.2	25.5 \pm 13.4	14.1	62.1	0.001	0.004
4-Nitrophenyl	2.5 \pm 1.2	2.6	0.3 - 4.1	-	-	0.2	0.001	0.002
1,5-Dinitronaphthalene	0.9 \pm 1.4	0.6	0.05 ²⁾ - 3.72	53.9 \pm 53.6	0.1	0.4	0.001	0.002
9,10-Anthraquinone	71.7 \pm 39.2	80.3	11.4 ²⁾ - 118.4	43.9 \pm 1.4	19.3	22.8	0.002	0.007
5-Nitroacenaphthene	0.3 \pm 0.7	0.0	0.05 ²⁾ - 1.62	-	-	0.1	0.001	0.002
cPPhen-4	18.8 \pm 10.2	15.1	12.0 - 39.1	38.1 \pm 20.2	2.8	5.1	0.001	0.004
2-Nitrofluorene	0.6 \pm 0.4	0.7	0.07 ²⁾ - 1.05	4.2 \pm 9.5	0.15	0.1	0.001	0.002
9-Nitroanthracene	2.3 \pm 1.9	1.8	1.0 - 4.7	57.8 \pm 29.7	0.2	0.4	0.001	0.003
9,10-Phenanthrenequinone	n.d.	n.d.	n.d.	-	22.5	14.4	0.155	0.464
9-Nitrophenanthrene	0.4 \pm 0.4	0.4	0.09 ²⁾ - 1.17	25 \pm 50	1.1	0.2	0.001	0.003
3-Nitrophenanthrene	n.d.	n.d.	n.d.	-	-	-	0.002	0.005
2-Nitroanthracene	n.d.	n.d.	n.d.	-	-	-	0.002	0.005
Benzo(a)fluorene-11-one	2.2 \pm 1.7	1.6	0.7 - 4.4	100 \pm 0	0.6	-	0.002	0.006
Benzanthrone	0.1 \pm 0.2	0.0	0.02 ¹⁾ - 0.58	100 \pm 0	-	0.5	0.007	0.022
2+3-Nitrofluoranthene	12.3 \pm 7.7	9.8	4.7 - 26.7	79.8 \pm 16.5	4.5	2.1	0.003	0.010
4-Nitropyrene	n.d.	n.d.	n.d.	-	-	-	0.003	0.009
Benzo(a)anthracene-7,12-dione	0.9 \pm 0.7	0.7	0.01 ¹⁾ - 2.21	100 \pm 0	-	-	0.004	0.013
1-Nitropyrene	n.d.	n.d.	n.d.	-	-	-	0.003	0.010
2,7-Dinitrofluorene	n.d.	n.d.	n.d.	-	-	-	1.003	3.010
7-Nitrobenzo(a)anthracene	n.d.	n.d.	n.d.	-	-	-	0.003	0.010
6H-Benzo(cd)pyren-6-one	n.d.	n.d.	n.d.	-	-	-	0.015	0.043
6-Nitrochrysene	n.d.	n.d.	n.d.	-	-	-	0.004	0.011
1,3-Dinitropyrene	n.d.	n.d.	n.d.	-	-	-	0.003	0.010
1,6-Dinitropyrene	n.d.	n.d.	n.d.	-	-	-	0.006	0.017
1,8-Dinitropyrene	n.d.	n.d.	n.d.	-	-	-	0.004	0.013
6-Nitrobenzo(a)pyrene	n.d.	n.d.	n.d.	-	-	-	0.003	0.009
Σ PAHs	369.1 \pm 66.7		279.0 - 454.5					
Σ oxy-PAHs	233.1 \pm 68.3		124.7 - 337.1					
Σ nitro-PAHs	27.16 \pm 11.14		13.50 - 44.43					

* LOD, LOQ and MDL in pg (Tables S4-S6) were converted to pg m^{-3} using 370 m^3 as average sample volume

<MDL below method detection limit

255 n.d. not detected

¹⁾ equal LOQ

²⁾ $\frac{1}{2}$ of MDL

Table S12. Comparison of Longyearbyen power plant 16 PAH emissions with other coal-burning plants operated worldwide

Power plant	Location	Coal type	Boiler capacity, conditions	Flue gas cleaning	Dust in flue gas, mg m ⁻³	EF, µg kg ⁻¹	ΣPAHs, µg m ⁻³	%PM	Predominant PAHs	PAH profile	References
Energyverket	Longyearbyen, Svalbard	Bituminous, Ro=0.78%, High volatile	68 ton-coal/day, two boilers 32 MW each	SNCR+ESP+WFGD	1.5	1.5	0.106	0.06	Nap+ Phe+ Flu, Flt+ Pyr	53% 2 rings, 36% 3 rings, 11% 4 rings, 5-6 rings n.d.	This work
n.a.	Central Taiwan	Indonesian and Australian	6480 ton-coal/day	SCR+ESP+FGD	6.0	1.5	0.268	n.a.	Nap + Phe, Flt, Pyr + Flu	45% 2 rings, 20% 3 rings, 30% 4 rings, 5% rest n.a.	(Hsu et al., 2016)
Fusina plant	Porto Marghera, Italy	n.a.	n.a.	SCR + ESP + FGD	5.2	n.a.	0.697	n.a.	n.a.	n.a.	(Rigamonti et al., 2012)
n.a.	Netherlands	From different countries	n.a.	ESP+FGD	n.a.	n.a.	1-3	n.a.	n.a.	n.a.	(Meij and Te Winkel, 2007)
Point F	China	Blend	1000 MW	SCR + LLT-ESP + WFGD	4.0	n.a.	5.255	0.09	Nap+ Phe + 6 rings	80% 2 rings	(Li et al., 2016)
Point G	China	Blend	1000 MW	SCR + LLT-ESP + WFGD + WESP	< 1.9	n.a.	0.870	0.51	5 and 6 rings, no Nap	73% 5 and 6 rings	(Li et al., 2016)
HPA-3	Huainan, China	Bituminous	600 MW	ESP + WFGD	10.4	n.a.	11.67	0.39	Nap + Acy, Ant, Phe	n.a.	(Wang et al., 2015)
HPB-2	Huainan, China	Bituminous	600 MW	ESP + WFGD	10.6	n.a.	11.87	0.30	Nap + Acy, Flu	n.a.	(Wang et al., 2015)
HPC-1	Huainan, China	Bituminous	600 MW	ESP + WFGD	11.2	n.a.	8.84	0.32	Nap + Acy, Ant	n.a.	(Wang et al., 2015)

n.a. not available

SCR is selective catalytic reduction system; SNCR is selective non-catalytic reduction system

ESP is electrostatic precipitator; LLT-ESP is low-low temperature ESP

FGD is flue-gas desulfurization scrubber; WFGD is wet FGD

Table S13. UNIS and Adventdalen air concentrations (G+P) of 16 PAHs compared to national and regional background concentrations detected in autumn 2018

Components	UNIS (ng m ⁻³) ²⁾			Adventdalen (ng m ⁻³) ²⁾			Birkenes (ng m ⁻³) ^{1,3)}			Zeppelin (ng m ⁻³) ^{1,4)}		
	Average	Min	Max	Average	Min	Max	Average	Min	Max	Average	Min	Max
Naphthalene	n.q.	n.q.	n.q.	n.q.	n.q.	n.q.	0.034	0.028	0.044	0.094 ⁵⁾	0.081	0.107
Acenaphthylene	0.017	0.007	0.029	0.002	0.001	0.002	0.019	0.002	0.052	n.d.	n.d.	n.d.
Acenaphthene	0.049	0.024	0.073	0.004	0.001	0.007	0.141	0.027	0.301	0.002	0.002	0.002
Fluorene	0.171	0.137	0.236	0.060	0.039	0.096	0.264	0.172	0.334	0.009	0.001	0.014
Phenanthrene	0.409	0.369	0.470	0.236	0.192	0.271	0.675	0.508	0.878	0.009	0.005	0.016
Anthracene	0.018	0.012	0.026	0.014	0.011	0.019	0.009	0.003	0.030	0.001	0.001	0.001
Fluoranthene	0.029	0.024	0.036	0.019	0.011	0.039	0.141	0.113	0.193	0.004	0.003	0.004
Pyrene	0.040	0.031	0.048	0.027	0.021	0.036	0.081	0.055	0.100	0.003	0.002	0.004
Benzo(a)anthracene	0.002	9.0E-06	0.006	n.d.	n.d.	n.d.	0.006	0.003	0.010	n.d.	n.d.	n.d.
Chrysene	0.007	0.003	0.014	0.003	1.00E-04	0.007	0.052	0.025	0.084	n.d.	n.d.	n.d.
Benzo(b+k)fluoranthene	0.002	7.0E-06	0.006	0.001	8.00E-06	0.003	0.050	0.015	0.104	n.d.	n.d.	n.d.
Benzo(a)pyrene	0.001	7.0E-06	0.002	3.00E-04	8.00E-06	0.001	0.004	0.002	0.009	n.d.	n.d.	n.d.
Indeno(123-cd)pyrene	0.002	7.4E-05	0.004	0.001	7.00E-05	0.003	0.014	0.006	0.020	n.d.	n.d.	n.d.
Dibenzo(ah)anthracene	n.d.	n.d.	n.d.	n.d.	n.d.	n.d.	0.004	0.002	0.007	n.d.	n.d.	n.d.
Benzo(ghi)perylene	0.004	0.001	0.008	0.001	8.00E-05	0.004	0.020	0.009	0.029	n.d.	n.d.	n.d.

n.d.: below detection limits

n.q.: high blank contamination

¹⁾ Data acquired from <http://ebas.nilu.no>, last access: 20 June 2020

²⁻⁴⁾ Volume sampled: 350–450 m³, 650 m³, and 1300 m³, respectively

⁵⁾ Possibly influenced by blank levels

NOTE: the chemical profiles are presented as Figure S3

Table S14: Comparison of average concentrations (G+P; $\mu\text{g m}^{-3}$) of PAHs, oxy-PAHs and nitro-PAHs measured in Longyearbyen with those previously reported in the literature for rural sites worldwide

Region	Season	Sampling phase	Type of site	Number of compared compounds*	Average sum concentration ($\mu\text{g m}^{-3}$)	Reference
Parent PAHs						
France, Marseille	Summer 2004	G+P	Rural	13	15959	(Albinet et al., 2007)
Denmark, Riso	Winter 1998	P	Semi-rural	9	4390	(Feilberg et al., 2001)
Eastern England, Weybourne	Winter 2010	G+P	Background	12	2298	(Alam et al., 2014)
Southern China, Wanjingsha	Autumn 2010	G+P	Background	15	88950	(Huang et al., 2014b)
Subarctic, Finland, Pallas	Autumns 1996-2015	G+P	Background	12	403	(Yu et al., 2019)
Arctic, Canada, Alert	Autumns 1992-2015	G+P	Background	15	81	(Yu et al., 2019)
Arctic, Svalbard, Zeppelin	Autumns 1994-2015	G+P	Background, altitude	13	185	(Yu et al., 2019)
Southern Norway, Birkenes	Autumn 2018	G+P	Background	15	1480	(NILU, 2018)
Arctic, Svalbard, Zeppelin	Autumn 2018	G+P	Background, altitude	15	28	(NILU, 2018)
Arctic, Svalbard, UNIS	Autumn 2018	G+P	Semi-urban	15	749	This study
Arctic, Svalbard, Adventdalen	Autumn 2018	G+P	Rural	15	369	This study
Nitro-PAHs						
Northern China	Annual 2010-2011	G+P	Rural	12	**911	(Li et al., 2015)
Southern China, Wanjingsha	Autumn 2010	G+P	Rural	23	4021	(Huang et al., 2014b)
France, Marseille	Summer 2004	G+P	Rural	9	26	(Albinet et al., 2007)
France, The Alps, Chamomix	Winter 2002	P	Rural, altitude	10	9	(Albinet et al., 2008a)
France, The Alps, Maurienne	Winter 2002	G+P	Rural	15	**352	(Albinet et al., 2008a)
Danmark, Riso	Winter 1998	P	Semi-rural	4	152	(Lammel et al., 2020)
Central Europe, Košice	Winter 2017	G+P	Background	8	15	(Lammel et al., 2020)
Southern Sweden, Råö	Spring 2008	G+P	Background	8	40	(Feilberg et al., 2001)
Subarctic Finland, Pallas	Spring 2008	G+P	Background	8	19	(Bronsström-Lundén et al., 2010)
Arctic, Svalbard, UNIS	Autumn 2018	G+P	Semi-urban	11	37	This study
Arctic, Svalbard, Adventdalen	Autumn 2018	G+P	Rural	11	27	This study
Oxy-PAHs						
Northern China	Annual 2010-2011	G+P	Rural	3	**10552	(Li et al., 2015)
Southern China, Wanjingsha	Autumn 2010	G+P	Rural	5	12940	(Huang et al., 2014b)
France, Marseille	Summer 2004	G+P	Rural	4	1093	(Albinet et al., 2007)
France, The Alps, Chamomix	Winter 2002	P	Rural, altitude	5	790	(Albinet et al., 2008a)
France, The Alps, Maurienne	Winter 2002	G+P	Rural	5	**6875	(Albinet et al., 2008a)
Central Europe, Košice	Winter 2017	G+P	Rural	5	336	(Lammel et al., 2020)
Eastern England, Weybourne	Winter 2010	G+P	Rural	4	591	(Alam et al., 2014)
Southern Sweden, Råö	Spring 2008	G+P	Background	4	583	(Bronsström-Lundén et al., 2010)
Subarctic, Finland, Pallas	Spring 2008	G+P	Background	4	239	(Bronsström-Lundén et al., 2010)
Arctic, Svalbard, UNIS	Autumn 2018	G+P	Semi-urban	6	471	This study
Arctic, Svalbard, Adventdalen	Autumn 2018	G+P	Rural	6	233	This study

*within similar detectable compounds

**average of sites within type of site

275 **Table S15. Spearman correlation of selected PAH %PMs with ambient temperature and specific humidity for Adventdalen data (n=6)**

	Temperature	Humidity
%PM Fluorene	-0.030	-0.030
%PM Phenanthrene	0.131	0.131
%PM Anthracene	-0.393	-0.393
%PM Fluoranthene	-0.371	-0.371
%PM Pyrene	-0.429	-0.429
%PM Chrysene	-0.700	-0.700
%PM 1-Nitronaphthale	-0.655	-0.655
%PM 2-Nitronaphthale	-0.698	-0.698
%PM 2-Nitrobiphenyl	-0.455	-0.455
%PM 9-Fluorenone	-0.516	-0.516
%PM 9,10-Anthraquinone	-0.205	-0.205
%PM cPPhen-4	-0.759	-0.759
%PM 2+3-Nitrofluoranthene	-0.872	-0.872
%PM 2-NFlu	-0.030	-0.030
%PM 9-NAnt	0.900	0.900

Table S16. Spearman correlation of selected PAH concentrations (G+P) with precipitation for UNIS data (n=6)

	Precipitation
Pyrene	-0.829
Phenanthrene	-0.543
Fluoranthene	-0.543
Chrysene	-0.943
Benzo(b+k)fluoranthene	-0.886
Indeno(1,2,3-cd)pyrene	-0.812
Benzo(g,h,i)perylene	-0.886
Benzo(a)fluoren-11-one	-0.714
Benzo(a)anthracene-7,12-dione	-0.829

280

Table S17. Spearman correlation of PAH concentrations (G+P) with weather parameters for Adventdalen data (n=6)

	Solar radiation	Temperature	Humidity
Acenaphthylene	-0.829	-1.000	-1.000
Acenaphthene	-0.600	-0.771	-0.771
Fluorene	-0.486	-0.714	-0.714
Phenanthrene	-0.371	-0.657	-0.657
Anthracene	-0.543	-0.714	-0.714
Fluoranthene	-0.943	-0.771	-0.771
Pyrene	-0.886	-0.886	-0.886
Chrysene	-0.600	-0.771	-0.771
1-Nitronaphthale	-0.771	-0.943	-0.943
2-Nitronaphthale	-0.257	-0.429	-0.429
9-Fluorenone	-0.543	-0.829	-0.829
9,10-Anthraquinone	0.086	-0.314	-0.314
cPPen-4	-0.771	-0.771	-0.771
2-Nitrofluorene	0.200	0.086	0.086
9-Nitroanthracene	0.657	0.714	0.714
Benzo(a)fluoren-11-one	-0.600	-0.771	-0.771
2+3-Nitrofluoranthene	0.657	0.657	0.657

285 **Table S18. %PM obtained in this study compared to literature data**

	UNIS ¹⁾	Adventdalen ¹⁾	Southern China ²⁾	Southeastern France ³⁾	The Apls, France ⁴⁾
	Sub-urban, autumn	Rural, autumn	Rural, autumn	Urban, annual	Rural, winter
Acenaphthylene	0 ± 0.0	0 ± 0	0.9	-	-
Acenaphthene	0 ± 0.0	0 ± 0	1.9	5.9	-
Fluorene	1.1 ± 1.0	1.8 ± 3.0	1.3	2.0	-
Phenanthrene	6.5 ± 8.6	3.7 ± 9.0	0.6	3.0	-
Anthracene	0 ± 0.0	3.5 ± 8.5	3.4	4.3	-
Fluoranthene	40.5 ± 19.4	23.2 ± 9.2	11.0	15.7	-
Pyrene	26.8 ± 18.6	15.8 ± 11.0	16.5	20.0	-
Benzo(a)anthracene	68.2 ± 2.4	-	85.3	65.7	-
Chrysene	81.7 ± 10.3	64.1 ± 18.7	85.3	80.7	-
Benzo(b+k)fluoranthene	100 ± 0.0	100 ± 0	98.4	100.0	-
Benzo(a)pyrene	100 ± 0.0	100 ± 0	98.8	100.0	100.0
Indeno(1,2,3-cd)pyrene	100 ± 0.0	100 ± 0	99.6	98.1	-
Dibenzo(a,h)anthracene	-	-	100.0	100.0	-
Benzo(g,h,i)perylene	100 ± 0.0	100 ± 0	99.6	97.8	-
1-Nitronaphthalene	0.1 ± 0.2	1.5 ± 3.6	1.7	2.1	11.3
2-Nitronaphthalene	3.1 ± 5.6	5.4 ± 8.0	0.7	2.3	8.5
2-Nitrobiphenyl	10.1 ± 8.3	5.9 ± 10.0	14.5	0	-
9-Fluorenone	41.7 ± 22.3	25.5 ± 13.4	3.8	2.2	38.8
4-Nitrobiphenyl	0 ± 0.0	-	3.8	-	-
1,5-Dinitronaphthalene	80.0 ± 44.7	53.9 ± 53.6	39.3	100.0	-
9,10-Anthraquinone	37.5 ± 22.4	43.9 ± 1.4	43.0	55.8	97.8
5-Nitroacenaphthene	-	-	95.0	53.3	-
cPPhen-4	65.5 ± 10.6	38.1 ± 20.2	20.4	-	-
2-Nitrofluorene	15.1 ± 7.5	4.2 ± 9.5	-	0.0	87.5
9-Nitroanthracene	-	57.8 ± 29.7	95.0	64.7	95.8
9-Nitrophenanthrene	-	25 ± 50	-	66.7	88.3
Benzo(a)fluoren-11-one	100 ± 0.0	100 ± 0	-	95.5	99.8
Benzanthrone	96.7 ± 4.8	100 ± 0	98.2	100.0	100.0
2+3-Nitrofluoranthene	94.5 ± 13.5	79.8 ± 16.5	97.0	98.6	99.0
Benzo(a)anthracene-7,12-dione	100 ± 0.0	100 ± 0	99.3	99.4	100.0

¹⁾This study; ²⁾ (Huang et al., 2014a); ³⁾ (Tomaz et al., 2016); ⁴⁾ (Albinet et al., 2008b)

Table S19. Combustion engine vehicles in Longyearbyen as of 2018

	Diesel engine	Gasoline engine	Total
Passenger cars	522	553	1114
Vans	276	17	293
Lorry	52	8	60
Buses	26	-	26
Tractors	33	32	65
Recreational Boats	n.a.	n.a.	718

290

Data acquired from Statistics Norway (www.ssb.no), last access: 20 June 2020

n.a. this information is not available

Table S20. Eigenanalysis of the correlation matrix and Eigenvectors for Adventdalen data

Variable	PC1	PC2
Eigenvalue	8,7122	3,8497
Proportion	0,512	0,226
Cumulative	0,512	0,739
Flu/(Flu+Pyr)	-0,002	-0,427
IPyr/(IPyr+BPer)	0,238	0,225
Flu	0,207	-0,366
Phe	0,176	-0,388
Flt	0,243	0,294
Pyr	0,300	0,225
9-Flu	0,170	-0,287
9,10-AntQ	0,153	-0,090
cPPhe-4	0,319	0,096
BaFlu-11	0,285	0,194
BaAnt-7,12	0,240	0,047
1-NNap	0,253	-0,308
9-NAnt	-0,225	0,054
2+3-NFlt	-0,245	-0,252
Temperature	-0,318	0,068
Humidity	-0,287	0,187
Solar Radiation	-0,264	-0,073

295 **Table S21. Spearman correlation of PAH concentrations (G+P; n=6) with diagnostic ratios for Adventdalen data**

	IPyr/(IPyr+BPer) traffic	Flu/(Flu+Pyr) coal burning
Flu	0,270	0,771
Phe	0,101	0,771
Ant	0,845	0,143
Flt	0,541	-0,257
Pyr	0,439	0,257
Chry	0,778	-0,029
1-NNap	0,439	0,429
9-Flu	-0,034	0,314
9,10-AntQ	-0,101	0,257
cPPhe-4	0,778	-0,314
9-NAnt	-0,135	-0,371
9-NPhe	0,789	-0,232
BaFlu-11	0,778	-0,029
2+3-NFlt	-0,778	0,086
BaAnt-7,12	0,845	0,143

Table S22. Extractions from certificate of quality: unleaded gasoline, RON95, Norway, summer

Property	Units	Spec	Results
Appearance	-	Clear % Bright	Clear & Bright
Density at 15 deg. C	kg/m ³	720-775	723.0
Reid Vapour Pressure	kPa	≤ 67.0	66.9
Colour	-	Undyed	Undyed
Odour	-		Merchantable
Total Sulphur	mg/kg	≤ 10.0	3.9
Copper Strip Corrosion 3h at 50 deg. C	-	No.1	No.1
Existent Gum	mg/100ml	≤ 5	≤ 5
Oxidation Stability	min	≥ 360	≥ 360
MTBE	%-vol	≤ 0.5	<0.1
Oxygen content	%-wt	≤ 0.5	<0.1
Other Oxygenates	-	Not allowed	Not added
Lead	mg_Pb/l	≤ 5	≤ 3
Manganese	mg/l	≤ 2	≤ 2
Evaporated at 70 deg. C	%-vol	22.0-48.0	37.4
Evaporated at 100 deg. C	%-vol	46.0-71.0	60.9
Evaporated at 150 deg. C	%-vol	≥ 75.0	90.8
Final Boiling Point	deg. C	≤ 210.0	195.0
Residue	%-vol	≤ 2.0	1.0
Olefins	%-vol	≤ 18.0	17.5
Aromatics	%-vol	≤ 35.0	19.7
Benzene	%-vol	≤ 1.00	0.84
Motor Octane Number	-	≥ 85.0	85.0
Research Octane Number	-	≥ 95.0	95.0
Silver strip corrosion (3h at 50 deg. C)	-	≤ 1	0

300 Table S23. Extractions from certificate of quality: B-base automotive diesel, CFPP-12, Norway

Property	Units	Spec	Results
Appearance at 20 deg. C	-	Clear & Bright	Clear & Bright
Water	ppm-wt	≤ 100	≤ 100
Density at 15 deg. C	kg/m ³	820.0-842.0	840.8
Recovered at 250 deg. C	%-vol	≤ 64	40
Recovered at 350 deg. C	%-vol	≥ 85	98
95% Recovered	deg. C	≤ 360	332
Flash Point	deg. C	≥ 58	62
Total Sulphur	mg/kg	≤ 10.0	9.8
Copper Strip Corrosion 3h at 50 deg. C	-	No. 1	No. 1
Oxidation Stability	g/m ³	≤ 25	≤ 25
Viscosity at 40 deg. C	mm ² /s	2.00-4.00	2.57
Lubricity at 60 deg. C	um	≤ 460	≤ 460
Cloud Point	deg. C	≤ -1	-17
Cold Filter Plugging Point	deg. C	≤ -12	-17
Carbon Residue on 10 % Residue	%-wt	≤ 0.30	≤ 0.30
Ash	%-wt	≤ 0.01	≤ 0.01
Manganese	mg/l	≤ 2.0	≤ 2.0
Particulate Matter	mg/kg	≤ 24	≤ 24
Fatty acid methyl ester	%-vol	≤ 0.2	≤ 0.2
PAH	%-wt	≤ 8.0	3.4
Cetane Index, four variable	-	≥ 46.0	48.8
Cetane Number	-	≥ 51.0	51.6
Aromatics, %-wt	%-wt	Report	26.4
Conductivity	pS/m	≥ 50	218
at temperature	deg. C	Report	22
Stadis 425	mg/l	Report	2.0

Table S24. Ratios of nitro- and oxy-PAH to corresponding parent PAH at three locations

	Power plant (n=6)			UNIS (n=6)			Adventdalen (n=6)		
	Mean	STD	Median	Mean	STD	Median	Mean	STD	Median
9,10-AntQ/Ant	12.16	6.53	10.47	9.44	3.80	7.63	4.02	2.40	4.57
9-NAnt/Ant	0.055	0.020	0.056	0.039	0.026	0.042	0.189	0.171	0.109
9-FluQ/Flu	1.67	0.29	1.72	1.65	0.95	1.30	2.35	0.79	2.15
BaFlu-11/Chry	0.65	0.34	0.58	0.87	0.26	0.82	0.67	0.15	0.63
cPPhen-4/Pyr	0.31	0.10	0.30	0.64	0.30	0.56	0.48	0.06	0.48
9-FluQ/Phe	0.47	0.13	0.42	0.67	0.38	0.51	0.55	0.09	0.56
2+3-NFlt/Flt	0.029	0.023	0.017	0.335	0.043	0.324	0.603	0.326	0.585

Table S25. Spearman correlation of nitro- and oxy-PAH to corresponding parent PAH ratios with weather parameters in Adventdalen (n=6)

305

	Solar radiation	Temperature	Humidity	Pressure
9-Flu/Flu	0.029	0.029	0.029	-0.029
9,10-AntQ/Ant	0.486	-0.029	-0.029	0.429
9-FluQ/Phe	-0.429	-0.486	-0.486	-0.257
9-NAnt/Ant	0.600	0.829	0.829	0.543
2+3-NFlt/Flt	0.886	0.714	0.829	0.943
cPPhen-4/Pyr	0.257	0.257	0.257	-0.029

Table S26. Spearman correlation of concentrations (G+P) of PAHs, nitro- and oxy-PAHs with each other for Adventdalen data (n=6)

	Acy	Ace	Flu	Phe	Ant	Flt	Pyr	Chry	1-Nnap	2-Nnap	9-Flu	9,10-AntQ	cPPhen-4	2-Nflu	9-Nant	9-NPhe	BaFlu-11	2+3-NFlt	BaAnt-7,12	
Acy																				
Ace	0.771																			
Flu	0.714	0.600																		
Phe	0.657	0.314	0.829																	
Ant	0.714	0.943	0.714	0.486																
Flt	0.771	0.714	0.314	0.143	0.600															
Pyr	0.886	0.600	0.657	0.714	0.657	0.771														
Chry	0.771	1.000	0.600	0.314	0.943	0.714	0.600													
1-Nnap	0.943	0.714	0.829	0.829	0.771	0.657	0.943	0.714												
2-Nnap	0.429	0.029	0.714	0.943	0.257	-0.029	0.600	0.029	0.657											
9-Flu	0.829	0.371	0.486	0.714	0.314	0.429	0.714	0.371	0.771	0.543										
9,10-AntQ	0.314	0.429	0.371	0.086	0.257	-0.029	-0.143	0.429	0.143	-0.143	0.257									
cPPhen-4	0.771	0.829	0.314	0.257	0.771	0.886	0.771	0.829	0.714	0.029	0.486	-0.029								
2-Nflu	-0.086	-0.143	0.600	0.429	0.029	-0.429	-0.086	-0.143	0.086	0.543	-0.143	0.257	-0.543							
9-Nant	-0.714	-0.657	-0.714	-0.314	-0.543	-0.600	-0.486	-0.657	-0.600	-0.143	-0.371	-0.600	-0.371	-0.314						
9-NPhe	0.812	0.899	0.406	0.319	0.841	0.841	0.754	0.899	0.754	0.058	0.522	0.116	0.986	-0.464	-0.435					
BaFlu-11	0.771	1.000	0.600	0.314	0.943	0.714	0.600	1.000	0.714	0.029	0.371	0.429	0.829	-0.143	-0.657	0.899				
2+3-NFlt	-0.657	-0.943	-0.543	-0.143	-0.886	-0.771	-0.543	-0.943	-0.600	0.086	-0.143	-0.314	-0.771	0.086	0.714	-0.812	-0.943			
BaAnt-7,12	0.714	0.943	0.714	0.486	1.000	0.600	0.657	0.943	0.771	0.257	0.314	0.257	0.771	0.029	-0.543	0.841	0.943	-0.886		

Table S27. Eigenanalysis of the correlation matrix and Eigenvectors for UNIS data

Variable	PC1	PC2
Eigenvalue	8,9948	3,5126
Proportion	0,529	0,207
Cumulative	0,529	0,736
BbkFlt/BPer	0,235	-0,066
Flu/(Flu+Pyr)	-0,195	-0,326
Flt/(Flt+ Pyr)	-0,062	0,458
Phe	-0,117	-0,426
Flt	0,294	0,162
Pyr	0,308	-0,110
Chry	0,289	-0,217
BaPyr	0,323	0,071
BPer	0,266	-0,284
1-NNap	0,193	-0,057
2-NNap	0,303	0,119
9-Flu	-0,093	0,274
9,10-AntQ	-0,182	-0,374
cPPeh-4	0,076	0,203
BaFlu-11	0,320	-0,056
BZT	0,282	0,100
BaAnt-7,12	0,302	-0,203

Table S28. Spearman correlation of PAH concentrations (G+P; n=6) with diagnostic ratios for UNIS data

	IPyr/(IPyr+BPer) traffic	BbkFlt/BPer diesel/gasoline	Flu/(Flu+Pyr) coal combustion	Flt/(Flt+Pyr) marine fuel
Flu	-0,429	0,143	0,714	-0,714
Phe	0,086	0,200	0,543	-0,200
Flt	0,886	0,771	-0,829	0,143
Pyr	0,771	0,886	-0,714	-0,143
Chry	0,543	0,886	-0,371	-0,486
BbkFlt	0,600	0,943	-0,200	-0,314
BaPyr	0,759	0,880	-0,698	-0,030
IPyr	0,754	0,986	-0,464	-0,232
BPer	0,600	0,943	-0,200	-0,314
1-NNap	0,543	0,429	-0,600	-0,086
2-NNap	0,771	0,657	-0,943	0,086
9-Flu	0,371	0,257	0,029	0,657
9,10-AntQ	-0,829	-0,600	0,657	-0,486
cPPeh-4	0,086	0,314	0,314	<u>0,200</u>
BaFlu-11	0,771	0,886	-0,714	-0,143
BZT	0,754	0,638	-0,696	0,087
BaAnt-7,12	0,714	0,943	-0,543	-0,314

Figure S1. Wind rose diagrams for UNIS (samples U1-U7) and Adventdalen (samples A1-A7) sampling stations

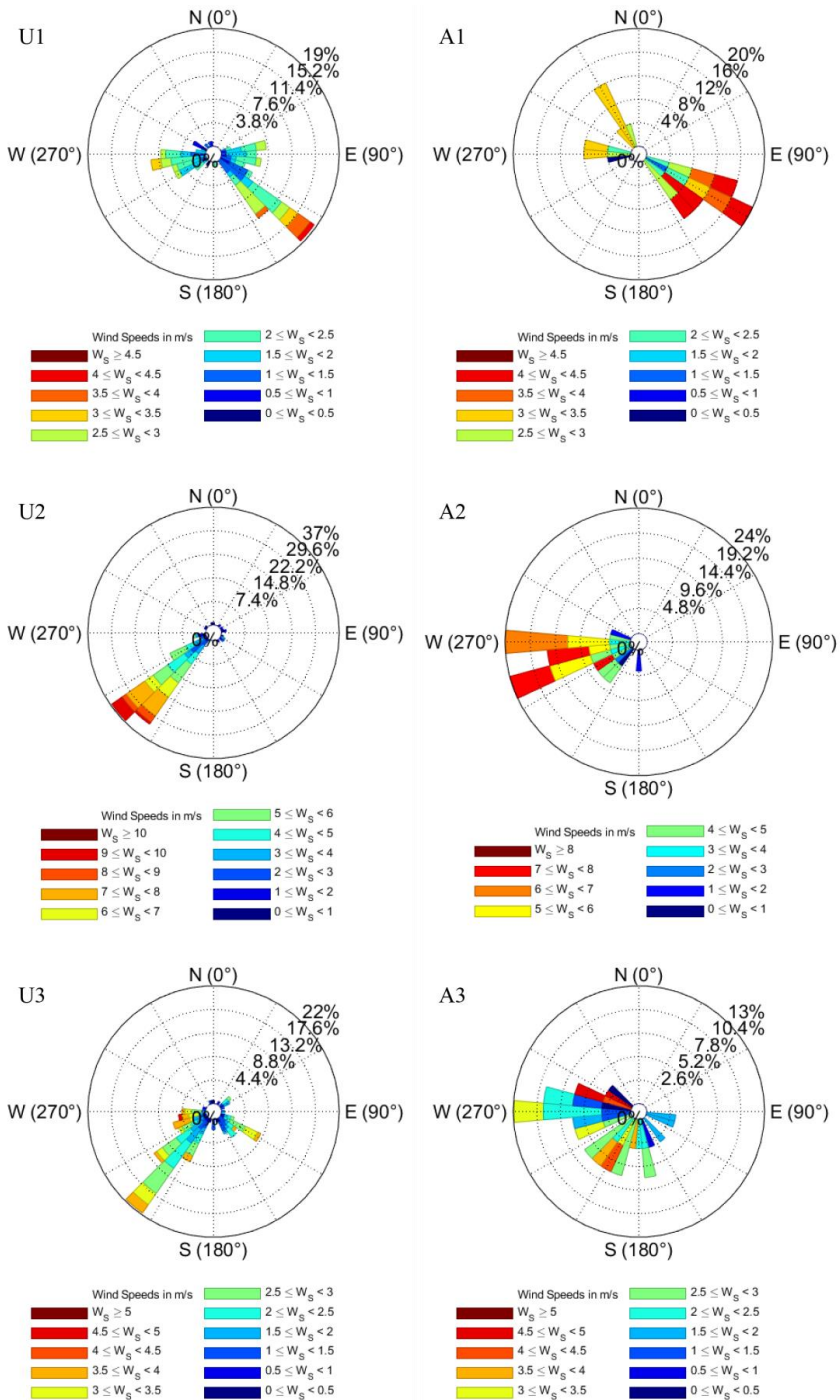


Figure S1 continued

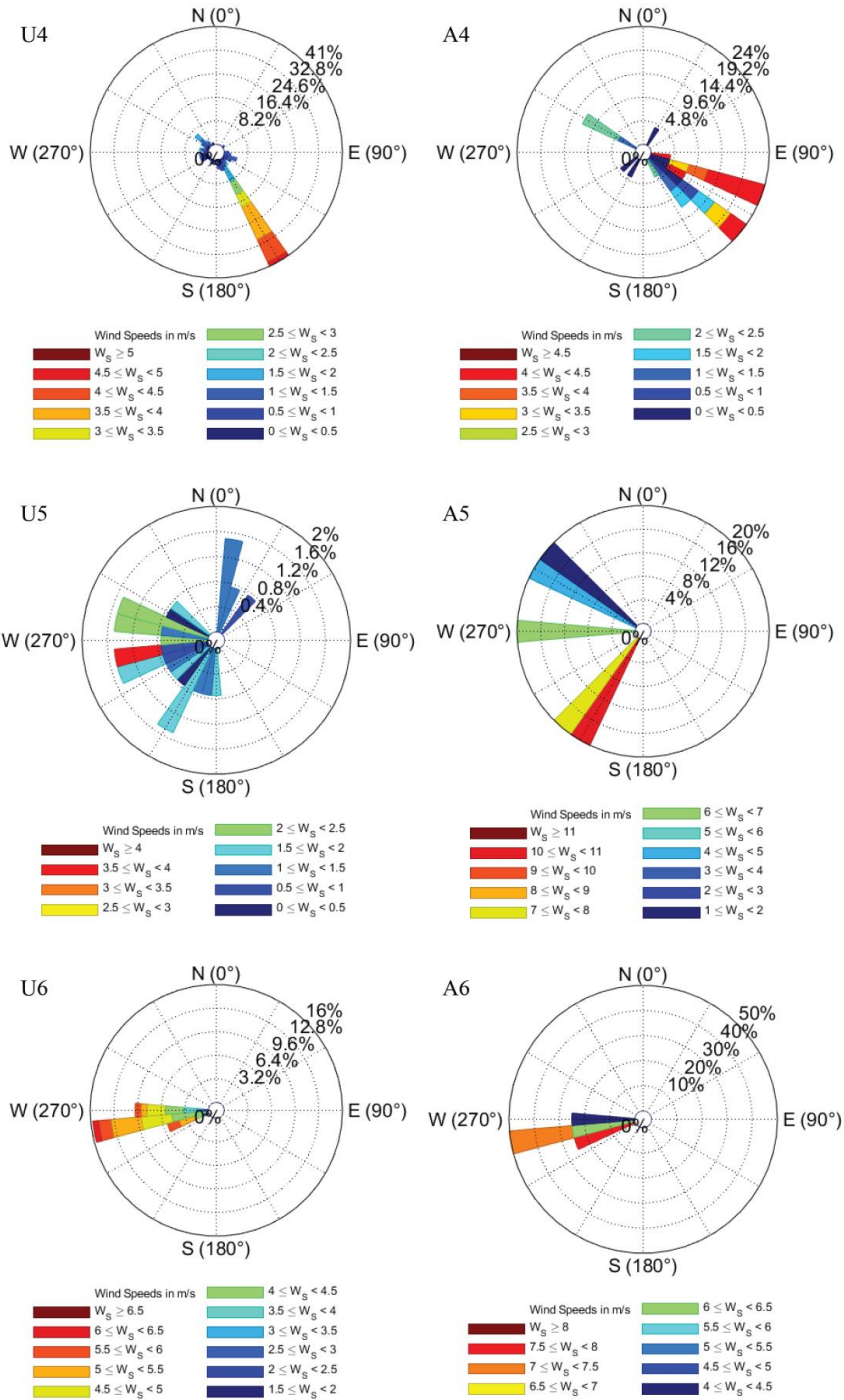


Figure S1 continued

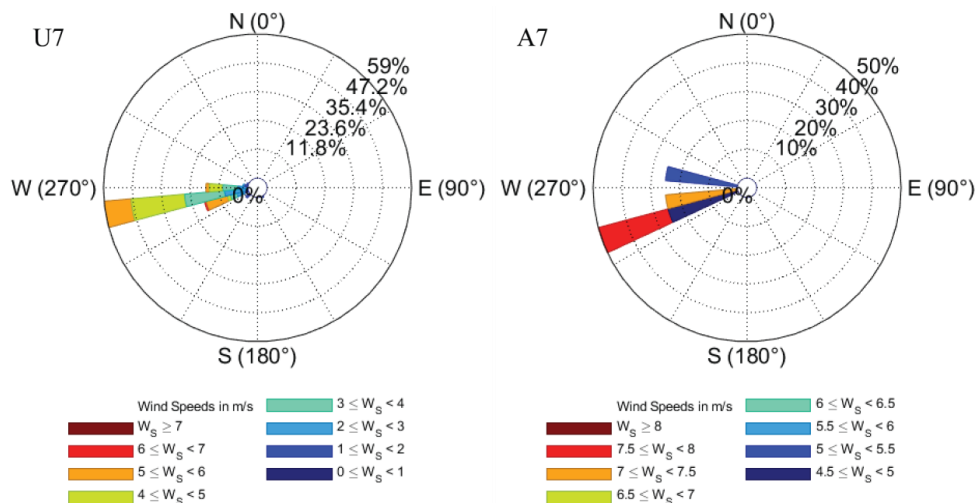


Figure S2. UNIS and Adventdalen chemical profiles of (a) PAHs, (b) oxy-PAHs, and (c) nitro-PAHs

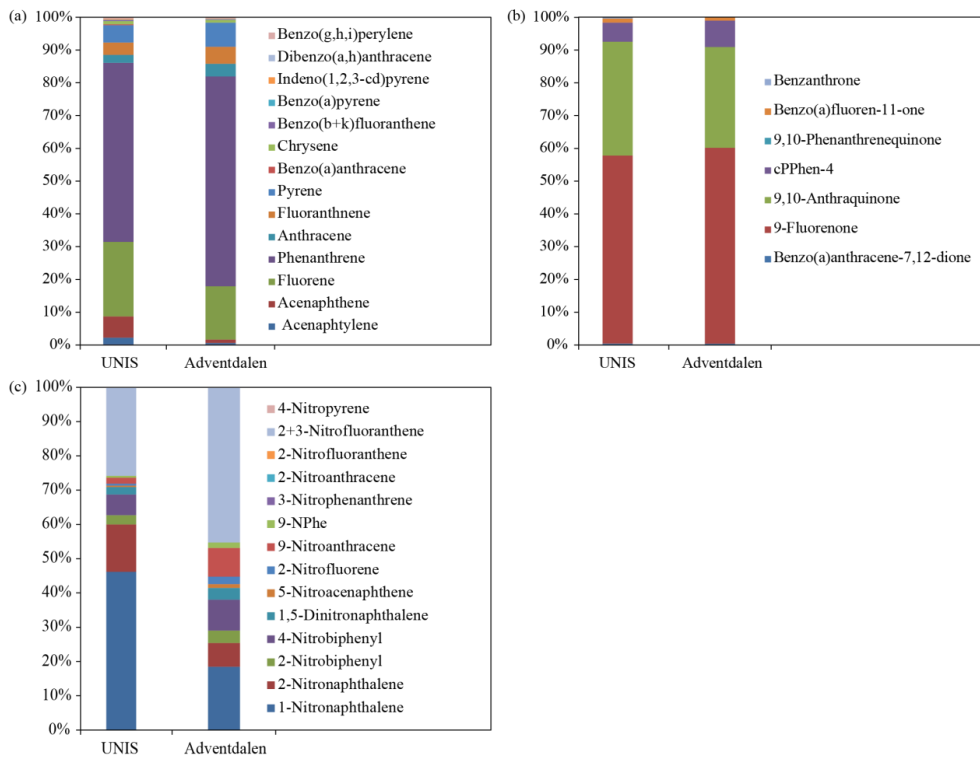
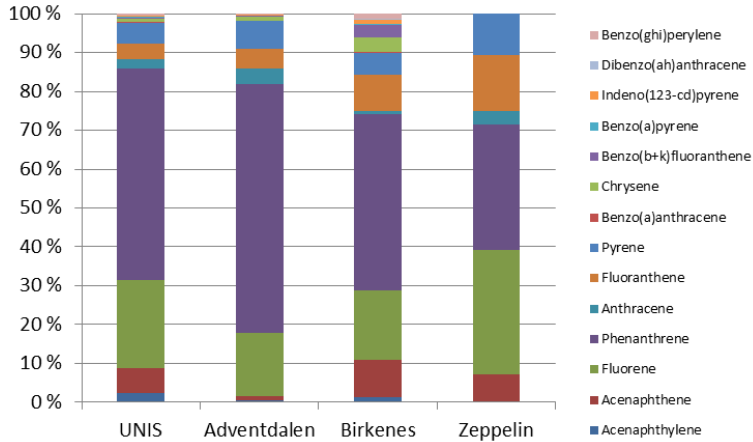


Figure S3. The 15 PAH profiles for different stations in Svalbard (UNIS, Adventdalen, Zeppelin) and the mainland Norway (Birkenes) measured in autumn 2018*



* Based on Table S13 data

330

Figure S4. 5-day back trajectories of Longyearbyen*

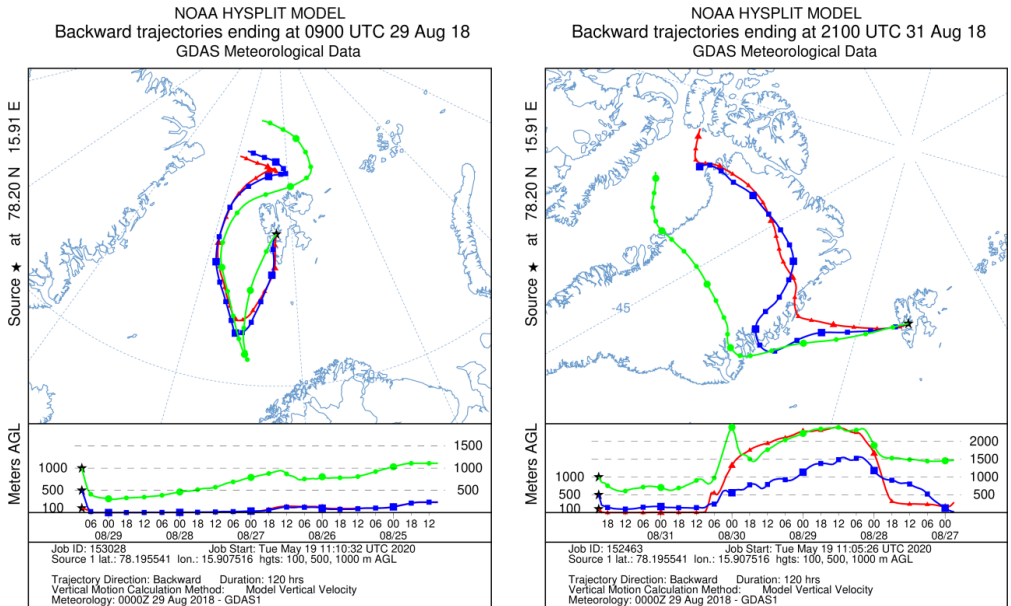


Figure S4 continued

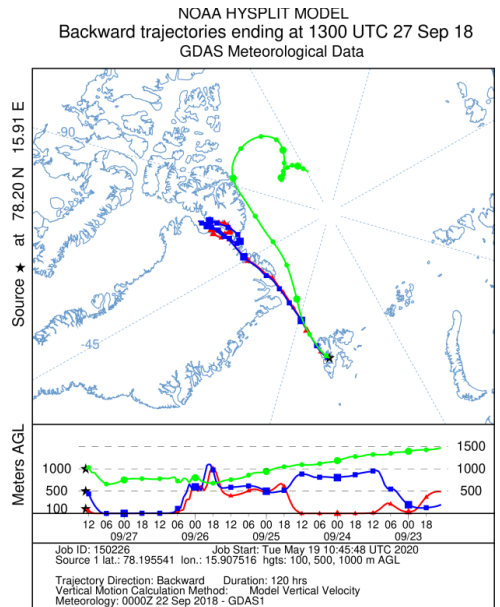
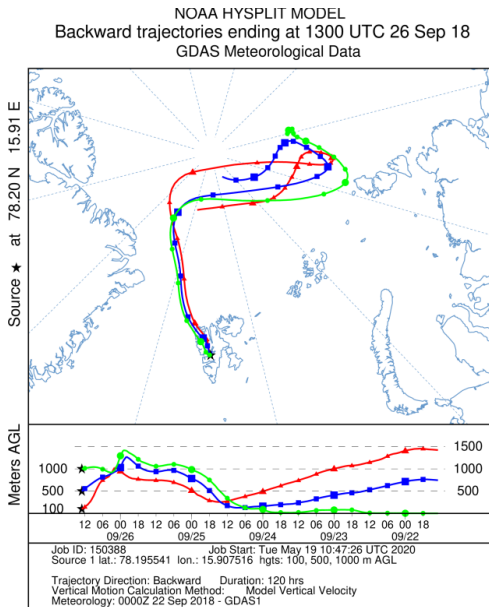
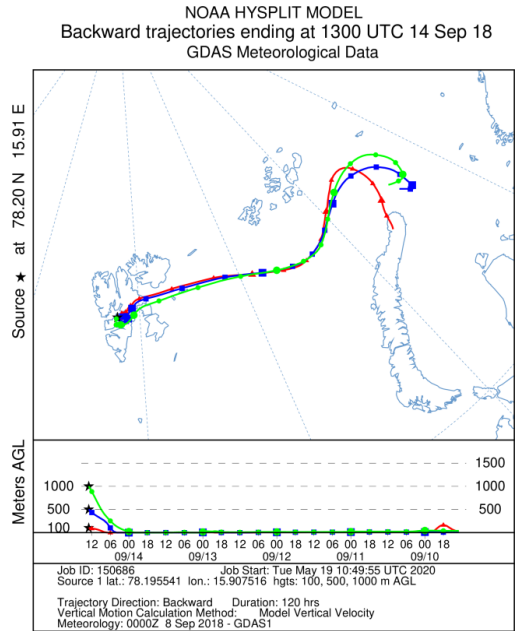
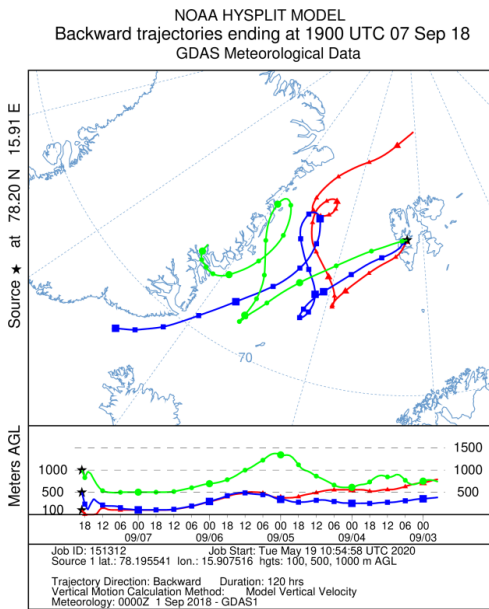
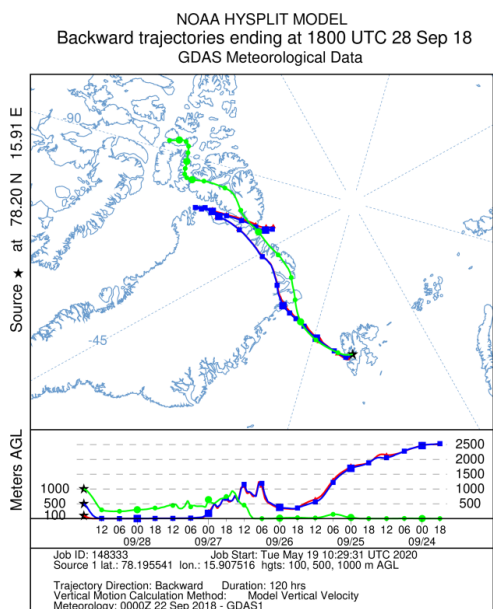
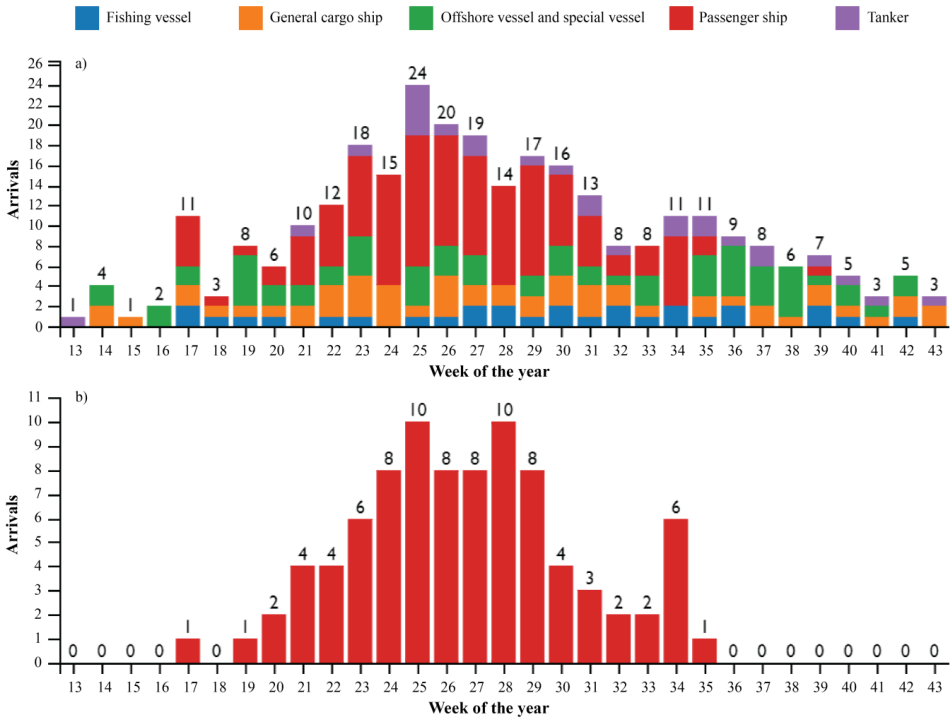


Figure S4 continued



*calculated using the US NOAA Hybrid Single Particle Lagrangian Integrated Trajectory (HYSPLIT) model

335 **Figure S5. Port Longyearbyen statistics 2018**



*data acquired from <https://kystdatahuset.no/>, last access: 30 May 2020

**this study sampling was performed during week 34-38 period

References

- 340 Alam, M. S., Delgado-Saborit, J. M., Stark, C., and Harrison, R. M.: Investigating PAH relative reactivity using congener profiles, quinone measurements and back trajectories, *Atmos. Chem. Phys.*, 14, 2467-2477, <https://doi.org/10.5194/acp-14-2467-2014>, 2014.
- Albinet, A., Leoz-Garziandia, E., Budzinski, H., and Villenave, E.: Simultaneous analysis of oxygenated and nitrated polycyclic aromatic hydrocarbons on standard reference material 1649a (urban dust) and on natural
345 ambient air samples by gas chromatography–mass spectrometry with negative ion chemical ionisation, *J. Chromatogr. A*, 1121, 106-113, <https://doi.org/10.1016/j.chroma.2006.04.043>, 2006.
- Albinet, A., Leoz-Garziandia, E., Budzinski, H., and Villenave, E.: Polycyclic aromatic hydrocarbons (PAHs), nitrated PAHs and oxygenated PAHs in ambient air of the Marseilles area (South of France): Concentrations and sources, *Science of the Total Environment*, 384, 280-292, [10.1016/j.scitotenv.2007.04.028](https://doi.org/10.1016/j.scitotenv.2007.04.028), 2007.
- 350 Albinet, A., Leoz-Garziandia, E., Budzinski, H., Villenave, E., and Jaffrezo, J. L.: Nitrated and oxygenated derivatives of polycyclic aromatic hydrocarbons in the ambient air of two French alpine valleys - Part 1: Concentrations, sources and gas/particle partitioning, *Atmos. Environ.*, 42, 43-54, <https://doi.org/10.1016/j.atmosenv.2007.10.009>, 2008a.
- Albinet, A., Leoz-Garziandia, E., Budzinski, H., Villenave, E., and Jaffrezo, J. L.: Nitrated and oxygenated derivatives of polycyclic aromatic hydrocarbons in the ambient air of two French alpine valleys. Part 1: Concentrations, sources and gas/particle partitioning, *Atmos. Environ.*, 42, 43-54, <http://doi.org/10.1016/j.atmosenv.2007.10.009>, 2008b.
- Albinet, A., Tomaz, S., and Lestremau, F.: A really quick easy cheap effective rugged and safe (QuEChERS) extraction procedure for the analysis of particle-bound PAHs in ambient air and emission samples, *Sci. Total Environ.*, 450-451, 31-38, <https://doi.org/10.1016/j.scitotenv.2013.01.068>, 2013.
- 360 Albinet, A., Nalin, F., Tomaz, S., Beaumont, J., and Lestremau, F.: A simple QuEChERS-like extraction approach for molecular chemical characterization of organic aerosols: application to nitrated and oxygenated PAH derivatives (NPAH and OPAH) quantified by GC–NICIMS, *Anal. Bioanal. Chem.*, 406, 3131-3148, <https://doi.org/10.1007/s00216-014-7760-5>, 2014.
- 365 Brorström-Lundén, E., Remberger, M., Kaj, L., Hansson, K., Palm Cousins, A., and Andersson, H.: Results from the Swedish national screening programme 2008, IVL Swedish Environmental Research Institute, Göteborg, Sweden, 69, 2010.
- Burns, D. T., Danzer, K., and Townshend, A.: Use of the term "recovery" and "apparent recovery" in analytical procedures (IUPAC Recommendations 2002), *Pure Appl. Chem.*, 74, 2201-2205, <https://doi.org/10.1351/pac200274112201>, 2002.
- 370 Feilberg, A., Poulsen, M. W. B., Nielsen, T., and Skov, H.: Occurrence and sources of particulate nitro-polycyclic aromatic hydrocarbons in ambient air in Denmark, *Atmos. Environ.*, 35, 353-366, [https://doi.org/10.1016/s1352-2310\(00\)00142-4](https://doi.org/10.1016/s1352-2310(00)00142-4), 2001.
- Han, M., Kong, J., Yuan, J., He, H., Hu, J., Yang, S., Li, S., Zhang, L., and Sun, C.: Method development for simultaneous analyses of polycyclic aromatic hydrocarbons and their nitro-, oxy-, hydroxy- derivatives in
375 sediments, *Talanta*, 205, 120128, <https://doi.org/10.1016/j.talanta.2019.120128>, 2019.
- Hsu, W. T., Liu, M. C., Hung, P. C., Chang, S. H., and Chang, M. B.: PAH emissions from coal combustion and waste incineration, *J. Hazard. Mater.*, 318, 32-40, <http://doi.org/10.1016/j.jhazmat.2016.06.038>, 2016.
- 380 Huang, B., Liu, M., Bi, X., Chaemfa, C., Ren, Z., Wang, X., Sheng, G., and Fu, J.: Phase distribution, sources and risk assessment of PAHs, NPAHs and OPAHs in a rural site of Pearl River Delta region, China, *Atmos. Pollut. Res.*, 5, 210-218, <https://doi.org/10.5094/APR.2014.026>, 2014a.
- Huang, B., Liu, M., Bi, X. H., Chaemfa, C., Ren, Z. F., Wang, X. M., Sheng, G. Y., and Fu, J. M.: Phase distribution, sources and risk assessment of PAHs, NPAHs and OPAHs in a rural site of Pearl River Delta region, China, *Atmospheric Pollution Research*, 5, 210-218, <https://doi.org/10.5094/apr.2014.026>, 2014b.
- 385 Kanan, R., Andersson, J. T., Receveur, J., Guyomarch, J., Le Floch, S., and Budzinski, H.: Quantification of polycyclic aromatic compounds (PACs), and alkylated derivatives by gas chromatography-tandem mass spectrometry (GC/MS/MS) to qualify a reference oil, in: Proceedings of the Thirty-fifth AMOP technical seminar on environmental contamination and response, Ottawa, Canada, 2012, 616-927, 2012.
- Konieczka, P., and Namieśnik, J.: Limit of detection and limit of quantification, in: Quality assurance and
390 quality control in the analytical chemical laboratory, CRC Press, Taylor & Francis Group, Boca Raton, Florida, USA, 143-160, 2009.
- Lammel, G., Kitanovski, Z., Kukucka, P., Novak, J., Arangio, A. M., Codling, G. P., Filippi, A., Hovorka, J., Kuta, J., Leoni, C., Pribylova, P., Prokes, R., Sanka, O., Shahpoury, P., Tong, H. J., and Wietzoreck, M.: Oxygenated and nitrated polycyclic aromatic hydrocarbons in ambient air-levels, phase partitioning, mass size
395 distributions, and inhalation bioaccessibility, *Environ. Sci. Technol.*, 54, 2615-2625, <https://doi.org/10.1021/acs.est.9b06820>, 2020.

- Launiainen, J., and Vihma, T.: Derivation of turbulent surface fluxes — An iterative flux-profile method allowing arbitrary observing heights, *Environmental Software*, 5, 113-124, [https://doi.org/10.1016/0266-9838\(90\)90021-W](https://doi.org/10.1016/0266-9838(90)90021-W), 1990.
- 400 Li, J., Li, X., Li, M., Lu, S., Yan, J., Xie, W., Liu, C., and Qi, Z.: Influence of air pollution control devices on the polycyclic aromatic hydrocarbon distribution in flue gas from an ultralow-emission coal-fired power plant, *Energy & Fuels*, 30, 9572-9579, <http://doi.org/10.1021/acs.energyfuels.6b01381>, 2016.
- 405 Li, W., Wang, C., Shen, H. Z., Su, S., Shen, G. F., Huang, Y., Zhang, Y. Y., Chen, Y. C., Chen, H., Lin, N., Zhuo, S. J., Zhong, Q. R., Wang, X. L., Liu, J. F., Li, B. G., Liu, W. X., and Tao, S.: Concentrations and origins of nitro-polycyclic aromatic hydrocarbons and oxy-polycyclic aromatic hydrocarbons in ambient air in urban and rural areas in northern China, *Environ. Pollut.*, 197, 156-164, <https://doi.org/10.1016/j.envpol.2014.12.019>, 2015.
- Meij, R., and Te Winkel, H.: The emissions of heavy metals and persistent organic pollutants from modern coal-fired power stations, *Atmos. Environ.*, 41, 9262-9272, <https://doi.org/10.1016/j.atmosenv.2007.04.042>, 2007.
- 410 Observation data of atmospheric PAHs at Zeppelin and Birkenes stations in 2018: <http://ebas.nilu.no>, access: 25 June 2020, 2018.
- Rigamonti, L., Grosso, M., and Biganzoli, L.: Environmental assessment of refuse-derived fuel co-combustion in a coal-fired power plant, *J. Ind. Ecol.*, 16, 748-760, <http://doi.org/10.1111/j.1530-9290.2011.00428.x>, 2012.
- 415 Şengül, Ü.: Comparing determination methods of detection and quantification limits for aflatoxin analysis in hazelnut, *J. Food Drug Anal.*, 24, 56-62, <https://doi.org/10.1016/j.jfda.2015.04.009>, 2016.
- Shrivastava, A., and Gupta, V. B.: Methods for the determination of limit of detection and limit of quantitation of the analytical methods, *Chronicles of young scientists*, 2, 21, <https://doi.org/10.4103/2229-5186.79345>, 2011.
- 420 Tomaz, S., Shahpoury, P., Jaffrezo, J.-L., Lammel, G., Perraudin, E., Villenave, E., and Albinet, A.: One-year study of polycyclic aromatic compounds at an urban site in Grenoble (France): Seasonal variations, gas/particle partitioning and cancer risk estimation, *Sci. Total Environ.*, 565, 1071-1083, <http://doi.org/10.1016/j.scitotenv.2016.05.137>, 2016.
- Wang, R., Liu, G., and Zhang, J.: Variations of emission characterization of PAHs emitted from different utility boilers of coal-fired power plants and risk assessment related to atmospheric PAHs, *Sci. Total Environ.*, 538, 180-190, <http://doi.org/10.1016/j.scitotenv.2015.08.043>, 2015.
- 425 Yu, Y., Katsoyiannis, A., Bohlin-Nizzetto, P., Brorstrom-Lunden, E., Ma, J. M., Zhao, Y., Wu, Z. Y., Tych, W., Mindham, D., Sverko, E., Barresi, E., Dryfhout-Clark, H., Fellin, P., and Hung, H.: Polycyclic Aromatic Hydrocarbons Not Declining in Arctic Air Despite Global Emission Reduction, *Environ. Sci. Technol.*, 53, 2375-2382, [10.1021/acs.est.8b05353](https://doi.org/10.1021/acs.est.8b05353), 2019.

Paper II

Polycyclic aromatic hydrocarbons (PAHs) and their nitrated and oxygenated derivatives in the Arctic boundary layer: seasonal trends and local anthropogenic influence.

Drotikova, T., Dekhtyareva, A., Kallenborn, R., and Albinet, A.

Accepted for final publication.



Polycyclic aromatic hydrocarbons (PAHs) and their nitrated and oxygenated derivatives in the Arctic boundary layer: Seasonal trends and local anthropogenic influence

Tatiana Drotikova^{1,2}, Alena Dekhtyareva³, Roland Kallenborn^{1,2}, and Alexandre Albinet⁴

- 5 ¹Department of Arctic Technology, University Centre in Svalbard (UNIS), Longyearbyen, 9171, Norway
²Faculty of Chemistry, Biotechnology and Food Sciences, Norwegian University of Life Sciences (NMBU), Ås, 1432, Norway
³Geophysical Institute, University of Bergen and Bjerknes Centre for Climate Research, Bergen, 5020, Norway
⁴French National Institute for Industrial Environment and Risks (Ineris), Verneuil en Halatte, 60550, France

Correspondence to: Tatiana Drotikova (tatiana.drotikova@unis.no) and Alexandre Albinet (alexandre.albinet@ineris.fr)

- 10 **Abstract.** 22 PAHs, 29 oxy-PAHs, and 35 nitro-PAHs (polycyclic aromatic compounds, PACs) were measured in gaseous and particulate phases in the ambient air of Longyearbyen, the most populated settlement in Svalbard, the European Arctic. The sampling campaign started in polar night in November 2017 and lasted for 8 months until June 2018, when a light cycle reached a sunlit period with no night. The transport regimes of the near-surface, potentially polluted air masses from midlatitudes to the Arctic and the polar boundary layer meteorology were studied. The data analysis showed the observed
15 winter PAC levels were mainly influenced by the lower latitude sources in northwestern Eurasia, while local emissions dominated in spring and summer. The highest PAC concentrations observed in spring, with PAH concentration levels a factor of 30 higher compared to the measurements at the closest background station in Svalbard (Zeppelin; in 115 km distance to Longyearbyen), were attributed to local snowmobile driving emissions. The lowest PAC concentrations were expected in
20 summer due to enhanced photochemical degradation under the 24 h midnight sun conditions and inhibited long-range atmospheric transport. In contrast, the measured summer concentrations were notably higher than those in winter due to the harbour (ship) emissions.

1 Introduction

- Polycyclic aromatic hydrocarbons (PAHs) are toxic and carcinogenic compounds (IARC, 2010; Kim et al., 2013) released into the atmosphere primarily through incomplete combustion of fossil fuels and biomass (Ravindra et al., 2008). PAHs react with
25 several atmospheric oxidants and form toxic oxygenated and nitrated PAH derivatives (oxy-PAHs and nitro-PAHs; Clergé et al., 2019; WHO, 2003; Bolton et al., 2000; Idowu et al., 2019; IARC, 2012), which can also be present in primary emissions (Keyte et al., 2013; Bandowe and Meusel, 2017; Walgraeve et al., 2010; Abbas et al., 2018). PAHs, nitro- and oxy-PAHs (polycyclic aromatic compounds, PACs) are semi-volatile compounds partitioning between gaseous and particulate phases in response to ambient pressure and temperature, and thus have different photolysis rates and long-range atmospheric transport
30 (LRAT) potentials (Mulder et al., 2019; Tomaz et al., 2016; Albinet et al., 2007; Albinet et al., 2008; Keyte et al., 2013; Nalin et al., 2016; Huang et al., 2014; Odabasi et al., 1999; Shahpoury et al., 2016). Once emitted in the atmosphere, PACs are



35 subjected to dry and wet deposition with different efficiencies depending on compound physical properties (e.g. vapor pressure, water solubility, polarity, particle size and mass), ambient conditions (e.g. air temperature, wind speed, atmospheric stratification), and precipitation intensity (Keyte et al., 2013; Lei and Wania, 2004; Shahpoury et al., 2018). The PACs that escape the listed sink processes disperse via LRAT to remote places, including the Arctic.

The Arctic region is a receptor of gas and particulate phase pollution from diverse source regions at lower latitudes. Though, the lower troposphere of the high Arctic is in general well isolated from the rest of the atmosphere due to the very cold air masses located in this region (Bozem et al., 2019), which build the so-called polar dome with the Arctic front as its boundary, formed by the surfaces of constant potential temperature (Klonecki, 2003; AMAP, 2015). Air masses inside and outside the
40 polar dome have different chemical compositions (Klonecki, 2003; Bozem et al., 2019; Willis et al., 2019), confirming the barrier function of the dome. Only the air masses cooled to similar low potential temperatures as within the polar dome area can penetrate it (Klonecki, 2003).

During the winter and early spring the Arctic front can move as far south as 40° N with its greatest extent over cold areas of northern Eurasia (AMAP, 2015). It allows a direct low-level transport of air masses from the areas located north of the Arctic
45 front (within the polar dome) to the Arctic lower troposphere. This pathway provides the most rapid (about 10-15 days; Stohl, 2006) and efficient pollution delivery to the high Arctic lower troposphere due to low wet scavenging and absence of photochemical degradation processes during winter polar night, which lasts for about 3.5 months. The average precipitation amount per month is only 14-57 mm during winter and spring in different European Arctic areas (Hanssen-Bauer et al., 2019). At polar sunrise, the number of oxidants significantly increases in the Arctic troposphere (Barrie and Platt, 1997; Atlas et al.,
50 2003; Simpson et al., 2007; Monks, 2000). Direct photolysis and reactions with atmospheric oxidants (e.g., hydroxyl and nitrate radicals, ozone, nitrogen dioxide) in the gas phase, and also heterogeneous (gas/particle) reactions, are the dominant loss processes for most PAHs. PAHs' lifetimes towards photochemical degradation range between one hour and 14 days (Keyte et al., 2013). In the Arctic, the atmospheric reactions play a significant role during spring as other sink processes, wet and dry deposition, are limited due to rare precipitation and low vertical turbulence of stably stratified cold air. This may cause
55 the buildup of nitro- and oxy-PAHs though nitro-PAHs degrade quickly (lifetimes of both, particulate and gaseous phase compounds, range between 6 min and 3 h; Reisen and Arey, 2005; Fan et al., 1996) by direct photolysis even under cold conditions. A similar outcome may be presumed for oxy-PAHs based on their photolysis and photochemical degradation rates (Miet et al., 2014; Kameda, 2018; Ringuet et al., 2012; Matsuzawa, 2000).

At the same time, the Arctic front starts receding during spring, and by summer, it has significantly retreated northward to
60 about 73.5° N at longitudes between 134° and 17° W according to the recent estimates (Bozem et al., 2019), though the front is not symmetrical. This means potential air pollution sources are located south of the Arctic front barrier. Also, the wintertime atmospheric transport of air masses from northern Eurasia, promoted by a seasonal intensification of Siberian high and Icelandic low systems, weakens in summer due to a change in land-sea temperature contrasts. Consequently, in summer, the LRAT path to the Arctic shifts to a cleaner one, from the North Atlantic Ocean (Stohl, 2006) with no significant potential
65 impacting PAC sources along the LRAT route. The summer LRAT to the Arctic is a slow process, as uplifted (at source or at



Arctic front) emissions are transported to the higher troposphere with further descent into the Arctic lower troposphere from above through radiative cooling (about 1 K d^{-1} ; Klonecki, 2003). Descent from the upper troposphere to the near-ground layer typically takes several weeks (AMAP, 2015). This is a long time of exposure to 24 h midnight sun Arctic summer conditions. PACs may significantly degrade (Singh et al., 2017; Kameda, 2018; Matsuzawa, 2000; Cvrčková and Ciganek, 2005; Cvrčková et al., 2006; Ringuet et al., 2012). Furthermore, the lifting of polluted air masses at lower latitudes is typically associated with cloud formation and precipitation (AMAP, 2015) by which soluble and particle-associated PACs can be scavenged from the atmosphere before entering the Arctic dome as well as within the Arctic (Willis et al., 2018).

70 Thereby, the Arctic front location and permeability, the large scale circulation in the Arctic, available solar radiation, and precipitation regime affect the magnitude of PAC's LRAT to the Arctic lower troposphere, enhancing transport during winter and inhibiting it during summer (Klonecki, 2003; Stohl, 2006; Bozem et al., 2019). It also depends on the Arctic oscillation mode (Eckhardt et al., 2003; Madonna et al., 2014; Stohl et al., 2002), weather along the transport pathway (sea ice extent, air and ocean temperatures as they influence phase partitioning and vertical turbulence), primary emissions strength at lower latitudes, and local high Arctic meteorological conditions.

75 Svalbard archipelago (74° - 81° N, 10° - 35° E) is the northernmost land in the European Arctic. Due to its location relative to the low-pressure systems in the Norwegian Sea (Hanssen-Bauer et al., 2019), Svalbard frequently receives air masses from Eurasia. Svalbard is located at the gateway of both atmospheric and oceanic heat transport into the Central Arctic (Serreze et al., 2007) as the Gulf Stream and the North Atlantic cyclone track are along its west coast. The region has experienced the greatest temperature increase during the last three decades (Nordli et al., 2014; Isaksen et al., 2016), and it is the warmest location in the Arctic above 76° N latitude (Wickström, 2020) with consequently one of the most visible changes associated with the Arctic amplification (Hanssen-Bauer et al., 2019; Isaksen et al., 2016; van Pelt et al., 2016; Onarheim et al., 2014; Dahlke et al., 2020; Wickström et al., 2020a). Thus, Svalbard is currently identified as an epicenter of climate change and perhaps the main receiver of air pollution from high-latitude Eurasian sources.

80 PAHs are chemicals of emerging concern in the Arctic (Balmer and Muir, 2017). Their occurrence has been monitored at several Arctic stations for over 30 years (Yu et al., 2019; Balmer et al., 2019), including one in Svalbard (Zeppelin station, Ny-Ålesund, $78^{\circ}58' \text{ N}$, $11^{\circ}53' \text{ E}$, 474 m asl). Located on the mountain top, the station is often above a temperature inversion layer, making it ideal for LRAT pollution observations with minimal influence of near-ground pollution plumes (Eckhardt et al., 2013). On the other hand, local source emissions are often not detected at this elevation and are systematically considered negligible though their emissions may significantly contribute to Arctic air pollution (Eckhardt et al., 2013; Aliabadi et al., 2015; Ferrero et al., 2016; Law et al., 2017; Schmale et al., 2018). Thus, the primary purpose of this work was to quantify the occurrence of 86 PACs in the high Arctic lower troposphere, including PAHs, as well as nitro- and oxy-PAHs (a list of the compounds and abbreviations is available in Table S1-S3), which are not yet included in the circum-Arctic monitoring programs. This study was performed over 8 months in Svalbard, 115 km south-west to Ny-Ålesund, in the most populated town of Longyearbyen. During this period, seasonal changes were observed in terms of ambient temperature, absolute humidity, surface albedo, prevailing wind direction, air masses inflow, chemical composition of the troposphere, precipitation



100 type and intensity, clouds height and thickness, as well as an extreme shift from polar night conditions to a completely sunlit period, and a seasonal variation in human activities. The detailed objectives in this work were to investigate the PAC's seasonal variations of concentrations and substance patterns and study the potential influence of local anthropogenic emissions on it, as the air samples (gaseous and particulate phases) were collected within the boundary layer.

2 Material and methods

105 2.1 Sampling site

The study was performed in the Arctic town of Longyearbyen (78.22° N, 15.65° E) on the west coast of Svalbard (Fig. S1) from November 2017 to June 2018. As a result of the high-latitude location, the sun in Longyearbyen remains below the horizon between late-October and mid-February (polar night). On the contrary, it does not set between mid-April and the end of August (midnight sun or polar day; Fig. S2).

110 Longyearbyen is the largest populated among the northernmost settlements, with about 2400 permanent residents (Statistics Norway, 2020) and a seasonal increase due to tourism, mainly in spring and summer. The local coal-fired power plant (30771 ton year⁻¹ of coal and 419 ton year⁻¹ of diesel consumption (Miljødirektoratet, 2018)) and car traffic (1558 vehicles (Statistics Norway, 2018)) are the main permanent local sources of PAC/anthropogenic emissions (Drotikova et al., 2020), while snowmobiles (2135 vehicles (Statistics Norway, 2018)) and marine (718 local boats (Statistics Norway, 2018) and 345
115 cruise ships (Kystdatahuset, 2018)) traffic is seasonal. There is no local waste incineration and wood burning registered in the town.

Svalbard's topography is predominantly mountainous. The prevailing wind direction over the archipelago is from the eastern sector as a consequence of Svalbard's location relative to the low pressure systems in the Norwegian Sea (Isaksen et al., 2016). Influenced by local orography, it creates the predominant southeasterly winds in Longyearbyen. Sampling equipment was
120 installed on the roof of the University Centre in Svalbard (UNIS, 25 m asl), which is considered to represent near-surface air pollution. UNIS is located in Adventdalen valley, 300 m to Adventfjærd, and surrounded by mountaintops primarily below 1000 m (Fig. S1c). Considering south-easterly prevailing wind direction and katabatic winds from Longyearbreen and Larsbreen glaciers, nearly all year-round UNIS is located downwind from the town (600 m distance), and the two main gateways (Adventdalen and Longyeardalen valleys) largely used for snowmobile driving during winter and spring. In summer,
125 the wind direction can temporarily change to northwesterly (Dekhtyareva et al., 2016; Niedźwiedz, 2013), making UNIS position downwind the coal-burning power plant (1 km distance to UNIS) and the harbour (5 km distance to UNIS). UNIS is also surrounded by paved roads that are used by cars all year round (Fig. S1c).

2.2 Sample collection

Particulate and gaseous PACs were collected on quartz fiber filters (QFF; pre-burnt at 450 °C for 6 h; Ø = 103 mm; no binder;
130 Munktell/Ahlstrom, Finland) and polyurethane foams (PUF; Soxhlet pre-cleaned in toluene for 24 h followed by 24 h acetone



wash; $\varnothing = 65$ mm; $L = 100$ mm; Klaus Ziemer GmbH, Germany), respectively, using a high-volume air sampler (TISCH-1000-BLXZ, TISCH Environmental Inc., USA). On average, 370 m^{-3} of ambient air was collected over 24 h per sample (Table S4). Meteorological parameters, including ambient temperature, atmospheric pressure, wind speed and direction, relative humidity, and UV radiation, were recorded at Gruvefjellet ($78^{\circ}12' \text{ N } 15^{\circ}37' \text{ E}$; 464 m asl) and Adventdalen ($78^{\circ}12' \text{ N } 15^{\circ}49'$
135 E; 15 m asl) automatic weather stations in 2.6 and 4.6 km distance to the sampling site, respectively.

A total of 31 samples (31 QFFs and 31 PUFs) and 8 field blanks were collected. All samples were kept intact inside the sampling unit after collection. In order to reduce the risk of post-collection contamination, the unit was sealed in two plastic bags for transportation to the lab, where samples were removed from the unit, sealed with layers of aluminium foil, and stored airtight in two plastic bags. Samples were kept frozen at $-20\text{ }^{\circ}\text{C}$ until sent to the French National Institute for Industrial
140 Environment and Risks (Ineris, France), by express delivery using cool, insulated containers and then stored at $-10\text{ }^{\circ}\text{C}$ until analysis.

2.3 Atmospheric stability, boundary layer height (BLH), and LRAT evaluation

The atmospheric layer between the Adventdalen (17 m asl) and Gruvefjellet (466 m asl) weather stations was studied. The potential temperatures θ at 17 and 466 m asl heights were calculated following Wallace and Hobbs (2006):

$$145 \quad \theta = T \cdot \left(\frac{1000}{p}\right)^k \quad (1)$$

where T is temperature [K], p is pressure [mbar], $k = 0.286$ is a gas constant derived from the Poisson equation. The average temperature inversion strength (TIS, K), expressed as the potential temperature difference $\theta_{466} - \theta_{17}$, was evaluated (Arya, 1999).

Turbulence probability (atmospheric stratification) within the atmospheric layer of 449 m thickness between the stations was
150 assessed via bulk Richardson number (Ri_{bulk}):

$$Ri_{\text{bulk}} = \frac{g}{T_v} \frac{\Delta z \cdot \Delta \theta_v}{\Delta U^2} \quad (2)$$

where T_v is the average virtual potential temperature between the two stations, Δz , $\Delta \theta_v$, and ΔU are the differences in height, virtual potential temperature, and wind speed at the two stations, respectively (Wallace and Hobbs, 2006). As the layer is thick, likely, some sharp gradients of temperature and wind speed in the subregions of this layer are averaged out; a thus higher value
155 of critical Ri_{bulk} was used to assess the probability of turbulence. The turbulence probability decreases linearly as the value of Ri_{bulk} increases from 0.25 to 10.25 (Stull, 1988). The Ri_{bulk} value of 5.25 was used to indicate less than a 50% probability of turbulent mixing within the layer between the two stations, i.e., stable stratification.

ERA5 data have been utilized to investigate the synoptic-scale meteorological conditions and BLH over Svalbard for the measurement period. ERA5 is the global reanalysis dataset with hourly output frequency, the horizontal and vertical resolutions
160 of 31 km and 137 levels, respectively (Copernicus C3S, 2017; Hersbach et al., 2020). BLH in the ERA5 data set is based on



Ri_{bulk} calculations for the specific vertical layer and surface. The values of Ri superior to 0.25 indicate stable stratification, and the BLH is diagnosed where the Ri_{bulk} exceeds this critical value (ECMWF, 2017).

An extended version of the FLEXPART air parcel trajectory data set of Läderach and Sodemann (2016); Fremme and Sodemann (2019) was used to study LRAT of pollutants to the measurement sites. FLEXPART V8.2 is a 3-dimensional
165 Lagrangian particle dispersion model driven with the meteorological data from European Centre for Medium-Range Weather
Forecasts' (ECMWF) ERA-Interim reanalysis (Stohl et al., 2005; Dee et al., 2011) with a spatial resolution of approximately
80 km and temporal resolution of 6 hours. The current FLEXPART data set contains the horizontal and vertical position of 5
million air parcels that represent the global atmosphere.

The 10-day backward trajectories have been extracted from the data set. The trajectories' points corresponding to the first day
170 of the simulation were not considered since most of them were over the Svalbard region. The trajectories start at the height
between 0 and 500 m above the ground in the region covering both Ny-Ålesund and Longyearbyen (from 77.5° N to 79.5° N
and from 10° E to 20° E). The number of trajectories starting in this vertical layer in the data set varied from 1395 and 4659
per season (Table S5). To investigate LRAT of air pollutants from mid-latitudes to Svalbard, only the trajectories that reach
175 latitudes below 70° N and end up below the local BLH were considered. The air masses that fit these criteria are potential
sources of long-range air pollution to the Arctic from ground-based emissions at the lower latitudes. Additionally, in order to
assess atmospheric pollutants' possible removal via precipitation, the specific humidity was extracted at each time step along
the trajectories. The specific humidity reduction on a value of $\Delta q > 0.1 \text{ g kg}^{-1}$ on the consecutive time steps indicates the
removal of water vapor from air masses and precipitation event (Läderach and Sodemann, 2016). The precipitation from the
air parcels with temperatures above (below) 0 °C were considered as rainfall (snowfalls).

180 2.4 Analytical procedures

A detailed description of the analytical protocols used has been published previously (Tomaz et al., 2016; Albinet et al., 2006;
Albinet et al., 2013; Albinet et al., 2014; Srivastava et al., 2018). Slight modifications have been applied here. In brief, a known
amount of several surrogates (6-methylchrysene, 3 deuterated oxy-PAHs, including benzo[a]anthracene-7,12-dione-d4 (98%,
TRC, Canada) to quantify the heavier oxy-PAHs, and 7 deuterated nitro-PAHs) were added to the samples prior to extraction.
185 Gaseous phase PACs were extracted from PUF samples with acetone (two cycles: 80 °C, 100 bars, 5 min heat time, 15 min
static time) using pressurized liquid extraction (ASE 350, Thermo Scientific, USA). Sample extracts were then reduced under
a nitrogen stream to a volume of about 200 μL (Turbovap II, Zymark, USA) and adjusted to 1 mL with acetonitrile. A fraction
(900 μl) was dedicated to the PAH analyses, while another (100 μl) was used for nitro- and oxy-PAHs quantification.
Particulate phase PACs were extracted from a 47 mm diameter QFF sample punch applying a QuEChERS-like (Quick Easy
190 Cheap Effective Rugged and Safe) method with 7 ml acetonitrile (Albinet et al., 2013; Albinet et al., 2014). The 2 and 3.5 ml
of supernatant were then reduced to near dryness under a nitrogen stream and reconstituted into 500 μl and 100 μl of acetonitrile
for PAH and nitro-/oxy-PAH analyses, respectively. The PUF and QFF extracts dedicated to the analysis of oxy- and nitro-



195 PAHs were purified by solid phase extraction before analysis: first with neutral alumina (Al_2O_3 , 500 mg, Macherey Nagel, Germany) and then with unmodified silica gel (SiOH , 500 mg, Macherey Nagel, Germany). All the extract volumes were then reduced to near dryness under a gentle nitrogen stream, reconstituted with acetonitrile (100 μl for PUF and 50 μl for QFF), and spiked with a known amount of 2 labelled internal standards prior to further analysis.

200 The 22 PAHs were analyzed by UHPLC-Fluorescence (Dionex Ultimate 3000, Thermo Scientific, USA) using a C18 UPLC column (Zorbax Eclipse PAH, 2.1 mm \times 150 mm \times 1.8 μm , Agilent, USA; 3 μl injected). GC-NICI/MS under SIM mode (Agilent 7890A GC coupled to 5975C MS, Agilent Technologies, USA) was used to quantify 35 nitro-PAHs and 29 oxy-PAHs. The compounds were separated on a Rxi-PAH column (30 m \times 250 μm \times 0.10 μm , Restek, USA). 1 μl of the purified extracts has been injected into the pulsed splitless mode for analysis. In addition, elemental carbon (EC) and organic carbon (OC) were measured on dedicated 1.5 cm^2 filter punches using a Sunset lab analyzer according to the EUSAAR-2 thermal protocol (Cavalli et al., 2010; CEN, 2017).

2.5 Quality assurance and quality control

205 In order to evaluate the background contamination related to sample collection and analysis, PUF and QFF field ($n = 8$) and laboratory blanks ($n = 6$) were performed. Low contamination of laboratory blanks was confirmed. Field blank contamination higher than 30 % of the seasonal average concentrations was determined for biphenyl-2,2'-dicarboxaldehyde, 2,3-naphthalenedicarboxylic anhydride, and 1,8-naphthalic anhydride for the gaseous phase. These compounds, in this phase, were excluded from the results. No blank correction was performed for the concentration calculations. Samples showing PAC concentrations below limit of quantification (LOQ) were replaced by LOQ/2 for further calculations. The instrumental LOQ was defined as the lowest concentration of the compound that can be determined for a signal to noise ratio $S/N = 10$. This evaluation was performed using the lowest concentrated standard solution.

215 Acceptable PAC surrogate recoveries were obtained and ranged between 53–120 %. Quality of the PAH analyses was assessed following the European Committee for Standardization (CEN) standard procedures EN 15549:2008 and TS 16645:2014 (CEN, 2008, 2014). In addition, Ineris routinely participates in national and European PAH analytical inter-comparison biannual exercises. The last exercise results were in good agreement with reference values, including those for the QuEChERS extraction (Verlhac, 2015; Bailleul and Albinet, 2018).

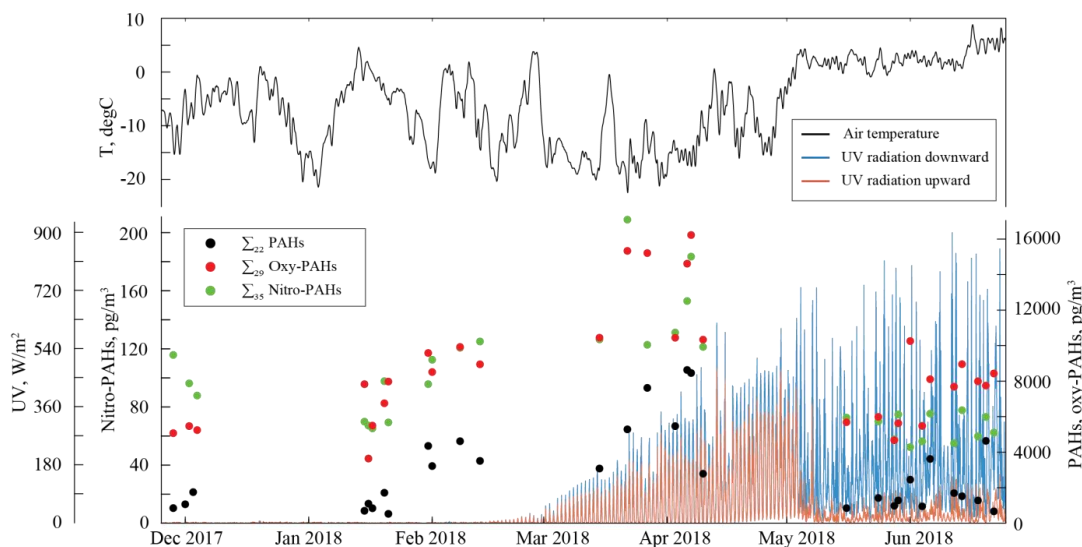
220 The analytical procedures were also validated ($n = 3$) using NIST standard reference material (SRM 1649b, urban dust). The obtained results were in good agreement with NIST certified, reference, or indicative PAC values and those previously reported in the literature for oxy- and nitro-PAHs (Albinet et al., 2013; Albinet et al., 2014) as reference concentration values in SRM do not exist for several compounds.



3 Results and discussion

3.1 Seasonal variations

Individual PAH, oxy- and nitro-PAH, as well as OC and EC average concentrations measured in the ambient air of Longyearbyen are presented in Table S1-S3, and daily values are presented graphically in Figure 1. Large seasonal variations were observed for all the PACs, and the Σ_{20} PAH concentrations trend was found to differ from the long-term observations at the background station at Zeppelin mountain (Fig. S3) in Ny-Ålesund, Svalbard, located 115 km northwest of Longyearbyen. To explain the PAC concentration trends found here, the measurements data set was divided into the four periods (P1-P4) based on weather and light conditions (Fig. S2) and potential sources as follows: November to January (dark winter; P1), February (twilight winter; P2), March to April (day light spring; P3), and May to June (polar day summer; P4). The full details on samples grouping and weather conditions are outlined in the Supplement (Table S4 and S6).



235 **Figure 1.** Atmospheric temperature, UV radiation, and daily total (gaseous + particulate) concentrations of Σ_{22} PAHs, Σ_{29} oxy-PAHs, and Σ_{35} nitro-PAHs in the urban air of Longyearbyen.

3.1.1 Winter and spring cold P1-P3 periods

The winter season (P1-P2) is characterized by the most considerable weather fluctuations due to the large-scale temperature and pressure gradients between midlatitudes and the Arctic (Sjöblom, 2010). During the sampling period the temperatures ranged from -18 °C and +4 °C being -5 °C as average. In winter, the Arctic weather is strongly controlled by extratropical

240

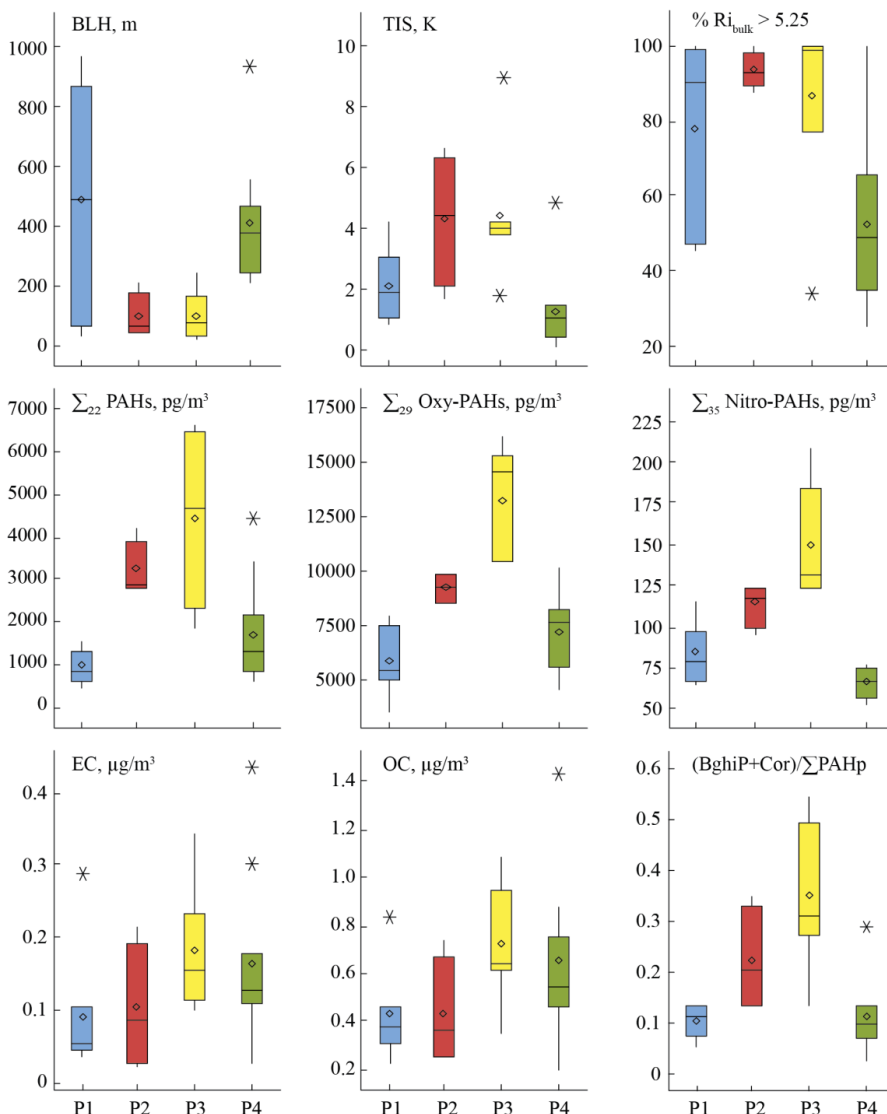


Figure 2. Box plots of atmospheric characteristics (boundary layer height BLH, thermal inversion strength TIS, bulk Richardson number Ri_{bulk} as characteristic of thermal stability of air layer, sum PAC (G+P), EC, OC concentrations, and the gasoline emissions PAH diagnostic ratio values ($(BghiP + Cor)/\sum PAH_p$). Data are for the November-January (P1; n=8), February (P2; n=4), March-April (P3; n=7), and May-June (P4; n=12) periods. The boxes represent the 25th and 75th percentiles of the data. The lines in the boxes and diamond symbols represent the median and the mean, respectively. All the outliers beyond the whiskers are shown individually.

245



cyclones, commonly referred to as low pressure systems, which are at its strongest and the most frequent in December-February (Zhang et al., 2004), and have an increasing tendency in the areas around Svalbard over the last decades (Wickström et al., 2020b). These cyclones are the main atmospheric heat source to the Arctic in winter (Fig. S4), and they are also associated with high winds and precipitation (Wickström, 2020). Such inflows from southern latitudes interrupt the Arctic atmosphere thermal stability and cause the BLH fluctuations (Fig. 2). The southeasterly wind was observed during all the sampling days in the cold P1-P3 periods (Fig. S5a). Thus, the sampling site was upwind the coal-burning emissions at the power plant in winter and spring (Fig. S1c).

The average P1 winter \sum_{22} PAH total (gaseous and particulate; G+P) concentrations were $1068 \pm 449 \text{ pg m}^{-3}$. The level of \sum_{29} oxy-PAH ($5934 \pm 1480 \text{ pg m}^{-3}$) were about 6-fold higher than PAHs, while \sum_{35} nitro-PAHs ($84 \pm 19 \text{ pg m}^{-3}$) were an order of magnitude lower. As discussed earlier, the LRAT of pollutants to the lower Arctic troposphere is maximum in winter, and the PAH multidecadal monitoring data from the Zeppelin station reflects this trend well (Fig. S3 and Yu et al., 2019). The measured PAH concentrations in Longyearbyen were similar (about 19% higher) to those detected at the Zeppelin station (Table S7), confirming LRAT of anthropogenic pollutants as a dominant source of PAHs in the Arctic air during winter. According to the 10 day back-trajectory analysis, the transported air masses in winter mainly originated from the European sector, including the areas of Scandinavia, Northern Europe, Western Russia, and the West Siberian plain (Fig. 3a). Compared to the winter 2018 PAH levels in the background continental air in Northern Finland (Pallas, Matorova station, $68^{\circ}00' \text{ N}$, $24^{\circ}14' \text{ E}$, 340 m asl), where the air masses are frequently delivered from, the Longyearbyen PAH concentrations are a factor of 2 lower (Table S7), which may give us a rough estimation of the PAH's LRAT efficiency though it largely depends on the weather along the transport pathway, as discussed earlier.

At the end of January, the Longyearbyen area starts receiving sunlight. It promotes photochemical processes and notably PAC degradation. As a consequence, a factor of 5 lower PAH concentrations were measured at the Zeppelin station in spring compared to the winter levels (Table S7), also in agreement with earlier studies (Singh et al., 2017; Halsall et al., 1997; Fu et al., 2009). In contrast, a double amount of \sum_{86} PACs ($13277 \pm 1295 \text{ pg m}^{-3}$) was detected in Longyearbyen air in February (P2), and even higher levels ($19281 \pm 4876 \text{ pg m}^{-3}$) were found during the March to April period P3. A pronounced increase of concentrations was revealed for most of the compounds. Compared to the winter levels, a 6-fold increase was detected for \sum_{22} PAHs ($5902 \pm 2421 \text{ pg m}^{-3}$), and 2-fold higher concentrations of \sum_{29} oxy-PAHs ($13229 \pm 2681 \text{ pg m}^{-3}$) and \sum_{35} nitro-PAHs ($150 \pm 34 \text{ pg m}^{-3}$) were determined in spring P3. These levels are about one order of magnitude lower than the average European urban and suburban PAC concentrations measured during cold seasons (Tomaz et al., 2016; Albinet et al., 2008), though the difference is less pronounced with the annual levels in background air (Nežiková et al., 2020): the sum spring concentrations of PAHs ($n=15$) and HMW oxy-PAHs ($n=4$) were about a factor of 2 lower, while LMW oxy-PAHs ($n=4$) and the sum nitro-PAHs ($n=15$) were in a similar range to up to one order of magnitude higher. Several individual PAC concentrations increased by a factor of 2 to 525 (depending on the compound) compared to the winter levels and several of them significantly exceeded (more than twice) the annual mean urban levels in central Europe (Tables S1 to S3; Tomaz et al., 2016; Albinet et al., 2008). As for the Arctic scale, the \sum_{20} PAH concentrations measured at UNIS were a factor of 30 higher than those at the Zeppelin



background station (oxy- and nitro-PAHs are not monitored at the station; Table S7). Such a large difference implies a significant contribution of local emissions to the overall PAC levels in Longyearbyen as the UNIS and Zeppelin stations have similar air masses transport from lower latitudes. According to the backward trajectory probability analysis, in spring, the source regions shifted from east to west and significantly up north: from continental locations in Russia and Europe (P1-P2; Fig. 3a-b) to marine ones over the North Atlantic (Fig. 3c), mainly from the area north of the 75° N latitude with no significant PAC sources. Thus, the influence of local emissions might be prevailing in spring.

Regional high Arctic weather conditions established by spring favor pollution accumulation in the near-ground air layer. Continuous radiative cooling of snow-covered surfaces during several months of polar night results in low temperatures at the ground, which creates thermally very stable air stratification. The median values of R_{bulk} for P2 and P3 periods were significantly higher than 5.25 (Fig. 2), indicating reduced vertical air mixing (Stull, 1988). Strong temperature inversions were frequent during this period with median TIS of about 4.5° K. The inversion events were the most persistent in spring due to

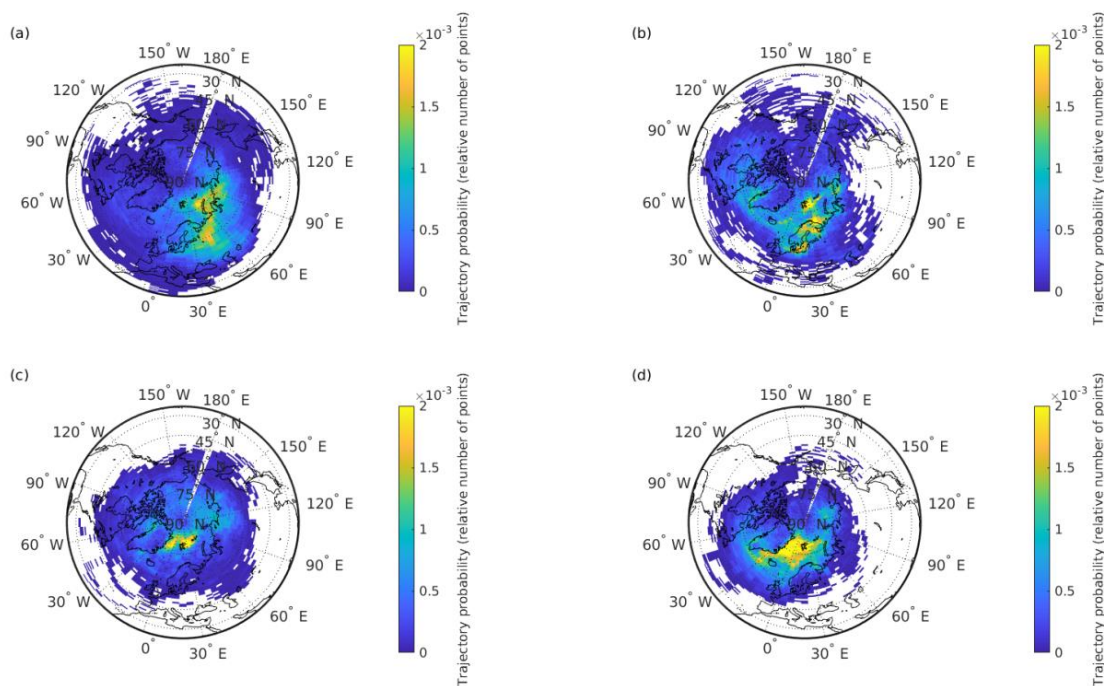


Figure 3. 10-day backward trajectory probability maps for the air masses originated from a source area boundary layer and arrived at 0-500 m above the region of interest in Svalbard. The trajectories' points corresponding to the first day of the simulation are not considered since most of the points for this day are over the Svalbard region. Data are for the November-January P1 (a), February P2 (b), March-April P3 (c), and May-June P4 (d) periods.



typical sustained cold ambient temperatures (-13.8 ± 3.4 °C as average) in March and April (P3). The estimated BLHs were as low as 100 ± 79 m with its minimum of 19 m under calm (1.9 m s^{-1} wind as median), cold conditions (-15.4 °C; Table S6). Thus, the spring near-ground PAC concentrations were greatly influenced by local emissions, which were frequently trapped
300 beneath an inversion layer and their dilution was limited to a very shallow volume of cold air under suppressed vertical mixing conditions. In addition, for secondary species such as nitro- and oxy-PAHs, secondary formation processes could also occur during these periods and might be promoted by such meteorological conditions. This will be further discussed in a forthcoming article.

Similar to PACs, about 2-fold higher EC and OC concentrations were measured in P2 and P3 periods (Fig. 2 and Table S1),
305 and the peak values were found on weekends and during the Easter holidays. This highlights that a large part of OC was probably related to primary combustion emissions in these periods, although secondary processes (formation of secondary organic aerosol) may occur (Hallquist et al., 2009; Heald and Kroll, 2020; Jimenez et al., 2009; Kroll and Seinfeld, 2008). The coal-burning emissions from the power plant were upwind during all the sampling days. Thus, this source probably had no impact on the concentrations and patterns observed. Car traffic intensity is quite steady through winter to spring (P1-P3), and
310 the same emission intensities are presumed as of similarly cold ambient temperatures during these periods. However, significantly higher values of the ratio $(\text{BghiP}+\text{Cor})/\sum\text{PAH}_p$, representative of gasoline emissions (sum of filter concentrations of 12 PAHs mainly present in the particulate phase (PAH_p): from benzo[a]anthracene to coronene according to our observations; Table S1) (Marchand et al., 2004; Albinet et al., 2007) were noticed during and after the polar sunrise (P2 and P3, respectively) compared to the winter period P1 (Fig. 2). Human activities increase greatly with the sun's return. The town
315 residents start driving snowmobiles predominantly for recreational purposes already during the twilight period P2. It is also the main attraction for tourists, the number of which significantly increases during the spring period P3 (about 16000 monthly hotel guest nights are registered in March and April; Statistics Norway, 2016) and the greatest number of snowmobiles (2135 vehicles; Statistics Norway, 2018) are in use.

The Longyearbyen snowmobiles park predominantly consists of 4-stroke engine touring vehicles (60-150 HP) and a small
320 number (about 10%) of 2-stroke modern (sport models) and old snowmobiles (registered before 2010). All the snowmobiles are gasoline driven (10-20 L per 100 km; NS-EN 228 Norwegian standard winter Gasoline 95 No. 2 with up to 15% MTBE (methyl tert-butyl ether); Jøran Storø, LNS Spitsbergen, personal communication, 2020) with an addition of synthetic oil (about 2 L per 100 km) for 2-stroke engines. Snowmobile emissions constitute a significant source of carbon monoxide, nitrogen oxides (NO_x), particles, aldehydes, a large number of aromatic hydrocarbons (Sive et al., 2003; Bishop et al., 2001; Shively et
325 al., 2008; Zhou et al., 2010; GYC, 2011), as well as several studies confirmed significant contamination of snow along a snowmobile track by PAHs (McDaniel and Zielinska, 2014; Rhea et al., 2005; Oanh et al., 2019). Due to potentially hazardous consequences related to the emissions, the use of snowmobiles is regulated and controlled in the USA with the hydrocarbons and carbon monoxide emission limits of $15 \text{ g kW}^{-1}\text{h}^{-1}$ and $90 \text{ g kW}^{-1}\text{h}^{-1}$, respectively (U.S. NPS, 2015). Significantly higher concentrations of numerous aromatic hydrocarbons were measured in Longyearbyen air in spring 2007 caused by snowmobile
330 driving (Reimann et al., 2009). The last decade's shift from 2 to 4-stroke snowmobile engines, including in Svalbard, has



reduced CO emissions. However, the recent inventory of 2017-2021 production year snowmobiles (499-1056 cc engine displacement; EPA, 2020) still shows up to an order of magnitude higher emissions of hydrocarbons (and probably PACs) from 2-stroke modern sleds, the small number of which in Longyearbyen can cause severe air pollution (Reimann et al., 2009). In conclusion, the results obtained here highlighted a strong impact of the snowmobile emissions on the ambient air PAC concentrations levels observed.

3.1.2 Summer P4 period

The Arctic lower troposphere's summer composition is primarily controlled by local Arctic weather conditions and local anthropogenic and natural emission sources due to less efficient LRAT mechanism and enhanced sink processes for PACs. The influence of the midlatitude emissions is more pronounced at higher altitudes because the summer atmospheric transport is directed to the higher troposphere (Klonecki, 2003; Stohl, 2006; Bozem et al., 2019). Arctic age of summer air near the surface north of 75° N is 13-17 days (Stohl, 2006) and the estimated travel time for gaseous pollutants is about three weeks (Bozem et al., 2019), while particles are efficiently scavenged by wet precipitation (Willis et al., 2018; and Table S5). Thus, local emissions are of great importance in summer in the high Arctic.

Increased incoming solar radiation (24 h of sunlight) and warmer ambient temperatures are the most notable changes of the high latitude summer. During the sampling period P4 the temperatures ranged from -0.1 °C and +9.3 °C with the average value of +3.6 °C on the sampling days. Loss of land-based snow cover and retreat of sea ice decrease surface albedo, which consequently creates the dominance of downward short-wave radiation in contrast to the spring period P3 (Fig. 1). Moreover, large areas of open ocean and increased solar insolation create relatively high atmospheric humidity. It allows the formation of low-level liquid-containing clouds (Browse et al., 2012), which are ubiquitous in the Arctic during summer (Lawson et al., 2001; Cesana et al., 2012). These low-level clouds and fogs produce frequent drizzle, which leads to efficient removal of particles associated (Browse et al., 2012), as well as gaseous phase water-soluble pollutants, including the PACs (Lei and Wania, 2004; Shahpoury et al., 2018). Thereby, the Arctic troposphere during summer is generally cleaner than winter (AMAP, 2006; Stohl et al., 2007) and is often considered pristine (Browse et al., 2012; Garrett et al., 2010). The 2-decade atmospheric measurements at several high Arctic monitoring stations confirm that PAH concentrations throughout the year are minimal during summers (Yu et al., 2019). The summer PAH levels are usually 1-2 orders of magnitude lower than in winter and often close to detection limits (Table S7 and Yu et al., 2019; Prevedouros et al., 2004; Singh et al., 2017). Nonetheless, summer Σ_{22} PAHs concentrations ($1779 \pm 1210 \text{ pg m}^{-3}$) measured in Longyearbyen air were about 67% higher than the winter P1 levels (Table S1). The Σ_{29} oxy-PAH ($7219 \pm 1692 \text{ pg m}^{-3}$) concentrations were 22% higher, while the levels of Σ_{35} nitro-PAHs ($66 \pm 9 \text{ pg m}^{-3}$) were 22% lower (Table S2-S3) during P4 compared to winter P1. The PAH levels observed in Longyearbyen were a factor of 19 higher compared to levels measured at the Zeppelin background station during the same period of summer 2018 (Table S7) stresses the predominant contribution of the local anthropogenic emissions. Due to the town's lower demand for electricity and central heating during brighter and warmer midnight sun conditions, coal-burning emissions at the power plant decrease (Bøckman, 2019) as do car traffic emissions (Statistics Norway, 2016), also because of preferences for biking and



walking within the town. Meanwhile, boat traffic increases dramatically, mainly due to tourist cruises (about 53000 vessel
365 passengers during summer season; Statistics Norway, 2016) and cargo delivery, and can significantly contribute to the local
air pollution (Eckhardt et al., 2013; Zhan et al., 2014; Law et al., 2017; Ferrero et al., 2016).

Due to the town's coastal location and the summer-specific land-sea thermal gradient, the northwesterly winds become frequent
during summer. These winds are characterized by lower velocity (4.0 m s^{-1} as median) compared to southeasterly (7.4 m s^{-1} as
median), the annual prevailing wind direction (Table S6). About half of the P4 period air samples were collected under
370 northwesterly wind conditions (Fig. S5c) when the sampling site was downwind the coal power plant and the harbour (Fig. S1
c-d). The Flu/(Flu+Pyr) coal combustion diagnostic ratio values 0.81 ± 0.09 were found similar to the earlier reported
(Drotikova et al., 2020) with low variability over the entire summer sampling period P4 indicating steady contamination from
the power plant. Also, the power plant plumes are emitted at high elevation (95 m asl) and a short distance from UNIS (about
800 m), and thus might not be well detectable at the UNIS sampling site due to higher BLH, less frequent thermal inversion
375 events, increased air layers convection, and generally windy conditions during summer (4.9 m s^{-1} during P4 sampling days).
However, about 29-88 % higher \sum_{86} PACs, EC, and OC concentrations were detected on the days with a northwesterly wind,
and the harbour emissions seemed then likely responsible for it as substantial air pollution can be caused by ship emissions
when docked and during port maneuvering (Huang et al., 2018a). Moreover, these summer PAC concentrations (measured
during the May to June 2018 period P4) were found about 3-fold higher than those reported previously for the autumn
380 (measured during the late August to September 2018 period; Drotikova et al., 2020), when ship traffic in the fjord was already
notably lower as a sailing season was close to its end. The average ($n = 5$) concentrations when the wind blew from the
southeast direction (from Adventdalen valley; $n=5$) were \sum_{22} PAHs 1116 ± 278 , \sum_{29} oxy-PAHs 6557 ± 1821 , and \sum_{35} nitro-
PAHs $65 \pm 10 \text{ pg m}^{-3}$, and likely mainly influenced by local car traffic. On average, a factor of 2 and 1.2 higher concentrations
of \sum_{22} PAHs ($2253 \pm 1416 \text{ pg m}^{-3}$) and \sum_{29} oxy-PAHs ($7691 \pm 1553 \text{ pg m}^{-3}$), respectively, were measured on the days with
385 northwesterly wind (from the harbour; $n = 7$). The \sum_{35} nitro-PAHs ($66 \pm 10 \text{ pg m}^{-3}$) level did not change markedly. The
maximum summer concentrations (\sum_{22} PAHs = 4633, \sum_{29} oxy-PAH = 10256 and \sum_{35} nitro-PAHs = 75 pg m^{-3}) were found
downwind from the harbour when the source strength (summed total tonnage of ships registered in the harbour during the
sampling hours) was maximum and hourly median wind speed varied between 1.8 and 5.7 m s^{-1} . Dispersal of ship plumes and
their visibility at a fixed measurement point is not only dependent on the source strength but also on the atmospheric stability,
390 wind velocity, and turbulence intensity (Contini et al., 2011). Higher local air pollution by ship emissions and its accumulation
can be expected at lower wind speed, similar to the summer 2009 case study in Ny-Ålesund, Svalbard (Eckhardt et al., 2013).
To further highlight ship emissions' influence, samples collected when the moderate wind (4.0 m s^{-1} as median) blew from the
northwesterly sector (292° - 313° ; $n = 7$) were only considered (Fig. 4). The total (arrival + departure) gross tonnage of vessels
(Kystdatahuset, 2018) was used as indicator of local ship traffic. A correspondence was found between the summed total
395 tonnage of ships registered in the harbour during the sampling hours and the Flt/(Flt+Pyr) and BaAnt/(BaAnt+Chry) diagnostic
ratios, providing clear evidence of the harbour emissions' contribution (Zhang et al., 2019; Drotikova et al., 2020). A factor of
4 higher concentrations of the PAHs were measured on the days with northwesterly wind compared to the days when wind



blew from a southeast direction, which is also in agreement with a recent study on ship emissions in the harbour of Longyearbyen (Dekhtyareva, 2019). Such large increase of particle-associated PAHs also suggests the harbour predominant influence as only about 6% of the power plant total PAC emissions (gaseous + particulate phases) were associated to the particulate phase (Drotikova et al., 2020). Finally, a good correlation of the PAHp/OC ratio values with the summed vessels' total tonnage was also found (Fig. 4), highlighting a higher content of PAHs in OC under such harbour influence.

As a last evidence indicating a significant influence from the harbour, the OC/EC ratio values ranged between 2.5 and 7.4 (3.6 as median) on the selected days. Marine fuel quality and engine operated conditions cause large variation of the OC and EC emissions. The OC/EC ratio values between 2 and 5 are often detected for low- and high-power diesel operated vessel plumes, while the higher values are typical for heavy fuel oil engine emissions (Zhang et al., 2019; Zhang et al., 2020; Sippula et al., 2014), as well as for the ship emissions at low-speed maneuvering during the harbour departure and arrival (Zhang et al., 2016; Sippula et al., 2014; Huang et al., 2018b). Furthermore, the plot of the daily OC/EC ratio values versus total tonnage demonstrates the ratio increasing with the tonnage (Fig. S6).

410

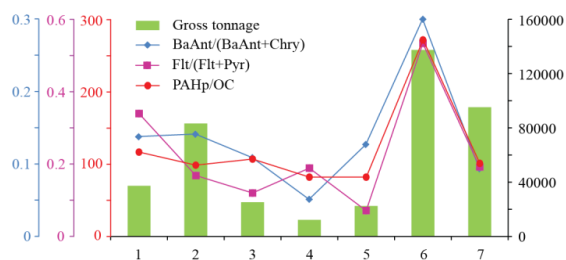


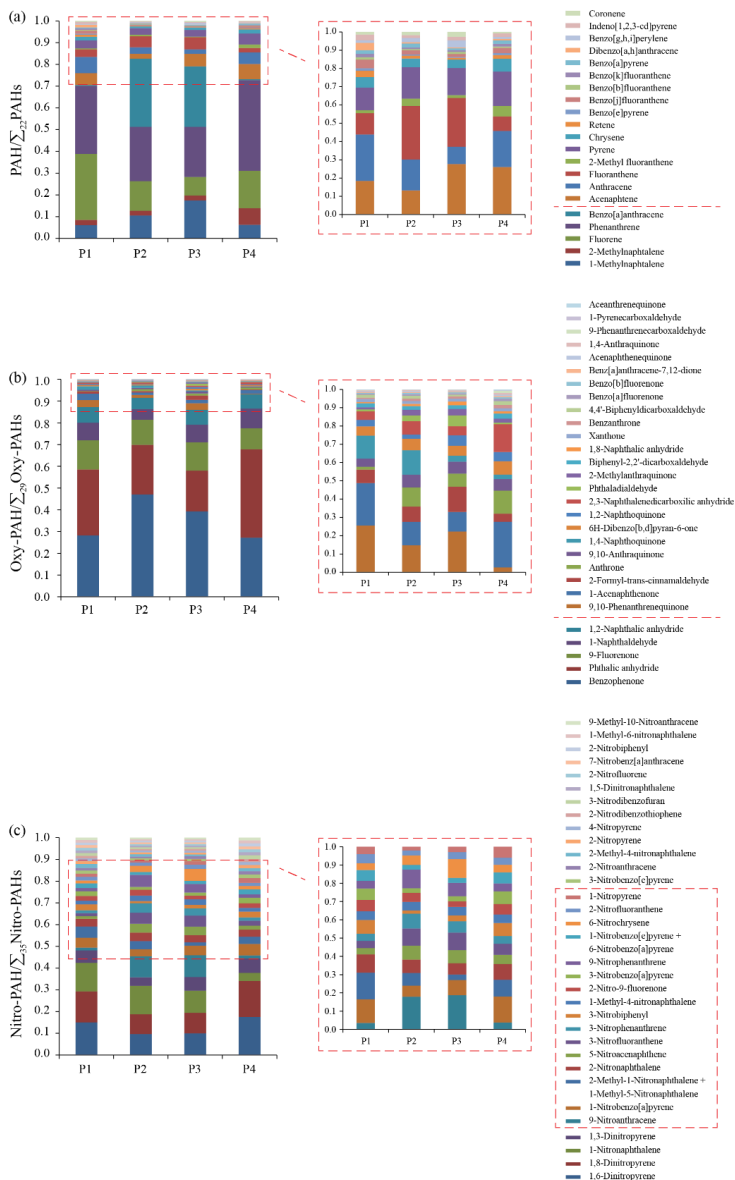
Figure 4. Correlations of the diagnostic ratios and the sum gross tonnage (dimensionless) of vessels arriving and departing the harbour of Longyearbyen during sampling hours on the summer period P4 days when the UNIS station was downwind the harbour (n=7).

415 3.2 PAC chemical profiles and source influences

3.2.1 PAH profiles

Phenanthrene, fluorene, naphthalene, benzo[a]anthracene, and 1-methylnaphtalene accounted for $76 \pm 8\%$ of total PAHs measured in Longyearbyen. Phenanthrene was the predominant compound in all the periods (P1-P4) and accounted for about 30% as the average, being higher in summer. The contribution of naphthalene varied from 5% to 24%, with a higher proportion in the spring period P3. This compound is not included in the further discussion as it is not source-specific.

420 The resulting winter profile P1 (Fig. 5a) was dominated by phenanthrene and fluorene (60%) with a smaller contribution of about 8% of anthracene, which was highest compared to the other periods. Anthracene is one of the most reactive among



425 **Figure 5:** Average chemical profiles based on the total (gaseous + particulate phases) individual concentrations of PAHs (a), oxy-PAHs (b), and nitro-PAHs (c) for the November-January (P1; n=8), February (P2; n=4), March-April (P3; n=7), and May-June (P4; n=12) periods. Further details can be found in the Supplement (Fig. S7-S11).



PAHs (Keyte et al., 2013). Its higher proportion in winter may indicate accumulation of anthracene due to lower level of atmospheric oxidants under dark conditions during the P1 period.

430 The twilight P2 and spring P3 profiles were strongly influenced by benzo[a]anthracene and 1-methylnaphtalene accounted for 40 % of the total PAHs relative compositions with a higher proportion on weekends and public holidays, when snowmobile traffic is increased. Comparing the PAHs spring weekend profiles ($n = 7$) with the rest of the cold period day profiles (P1-P3; $n = 12$) confirmed a significant increase of benzo[a]anthracene proportion caused by snowmobiling, as well as the higher contribution of 1-methylnaphtalene, fluoranthene, acenaphthene, and coronene to the total PAHs profile (Fig. S7). All over,

435 benzo[a]anthracene, phenanthrene, and 1-methylnaphtalene accounted for 68 % of the average PAHs profile of these days with known high snowmobile traffic. The predominance of phenanthrene and methylated PAHs in snow samples contaminated by a snowmobile emissions has being reported earlier (McDaniel and Zielinska, 2014), although the contribution of 2-methylnaphtalene and 2-methylfluoranthene in the present study was found negligible. Different engine technologies and fuel quality may have been responsible for it.

440 Like in winter, phenanthrene and fluorene were the predominant compounds of the summer PAH profile P4 accounted for 59 % of it. The proportion of 2-methylnaphtalene was found higher in summer. The summer profile represents an average picture of two sample groups collected under different wind conditions (direction) and thus influenced by different sources, though car traffic is similar (Fig. S1c). To investigate the source-specific emissions, profiles of the days with northwesterly wind ($n = 7$) were compared with those samples collected when wind was from the Adventdallen valley (south-easterly wind; $n = 5$).

445 The difference between the average profiles was mainly driven by the significantly higher contribution of fluoranthene, 2-methylfluoranthene, and chrysene on the days with northwesterly wind from the harbour and the coal power plant (Fig. S8). As specified above, increased air convection in summer, the sampling site's proximity to the power plant, and it's almost exclusively gaseous emissions mean that the ground-level emissions from the harbour are more detectable at UNIS than the high elevation power plant plumes. Our assumption is supported by frequent reports of fluoranthene and chrysene as major

450 PAHs in ship emissions (Huang et al., 2018b; Zhang et al., 2019; Zhao et al., 2020; Zhao et al., 2019) and an absence of contribution changes of phenanthrene, fluorene, and pyrene, the predominant compounds emitted from the power plant (Drotikova et al., 2020).

3.2.2 Oxy-PAH profiles

Benzophenone, phthalic anhydride, 9-fluorenone, 1-naphthaldehyde, and 1,2-naphthalic anhydride were the predominant

455 substances and accounted for 89 ± 4 % of the total oxy-PAHs in all periods (Fig. 5b). Main changes in the profiles were caused by a 16 % increased contribution of benzophenone in spring and a 17 % higher proportion of phthalic anhydride in summer. Among the minor compounds (ranging from 25 to 400 pg m^{-3}) accounted for about 10 % of the total oxy-PAHs profile, higher proportions of 2,3-naphthalenedicarboxylic anhydride and anthrone were found in summer. Detailed analysis of the average summer profiles based on different prevailing wind directions (Fig. S9) did not reveal any primary local source influence. This

460 may indicate the secondary formation of phthalic anhydride, 2,3-naphthalenedicarboxylic anhydride, and anthrone from PAH



photochemical reactions (Keyte et al., 2013; Chan et al., 2009; Perraudin et al., 2007; Bunce et al., 1997; Lee and Lane, 2009). A higher contribution of 9-fluorenone, 1-naphthaldehyde, 1-acenaphthenone, 6H-dibenzo[b,d]pyran-6-one, 9,10-anthraquinone, 2-methylanthraquinone, and benzantrone to the total oxy-PAHs summer profile was discovered on days with northwesterly wind (Fig. S9). Several of these compounds have earlier been detected in the ship plumes (Zhao et al., 2020; Czeck et al., 2017; Sippula et al., 2014). Note that 9-Fluorenone and 9,10-anthraquinone are the main oxy-PAHs emitted after the local coal burning at the plant (Drotikova et al., 2020).

For the twilight P2 and spring P3 periods, a higher contribution of several oxy-PAHs was found on weekends and public holidays, namely benzophenone, 9,10-phenanthrenequinone, 2-formyl-trans-cinnamaldehyde, anthrone, 9,10-anthraquinone, benzantrone (Fig. S10a), and the greatest proportion increase were found among the minor compounds 1,2-naphthoquinone, phthalaldehyde, 2-methylanthraquinone, and 1,8-naphthalic anhydride (ranged from 33 to 102 $\mu\text{g m}^{-3}$; Fig. S10b). These changes seemed likely to be caused by higher human activities and mostly snowmobile driving, as mentioned above. The use of oxidation catalysts as part of 4-stroke snowmobile exhaust after-treatment (Meldrum, 2017) may lead to efficient oxidation of parent PAHs and consequent formation of their oxygenated derivatives.

3.2.3 Nitro-PAH profiles

1-Nitronaphthalene and dinitropyrenes accounted for $40 \pm 5\%$ of total nitro-PAHs in all periods (Fig. 5c). The contribution of 1-nitronaphthalene decreased in summer while it increased for 1-nitrobenzo[a]pyrene. Different wind directions did not cause notable changes to the P4 summer profile.

The twilight P2 and spring P3 period profiles differ greatly from the winter P1 and summer P4 total nitro-PAHs relative compositions. The P2 and P3 profiles were enhanced by higher proportions of 9-nitroanthracene, 6-nitrochrysene, 3-nitrophenanthrene, 5-nitroacenaphthene, and 3-nitrofluoranthene. A study of daily profiles of the entire cold period (P1-P3) showed evident pattern changes with a significantly greater contribution of the listed nitro-PAHs during non-work days (Fig. S11). No scientific studies on PAC emissions from snowmobiles are reported yet. Nonetheless, snowmobile driving is a well-documented major source of a list of aromatic hydrocarbons (Zhou et al., 2010; Reimann et al., 2009; Eriksson et al., 2003; Shively et al., 2008), and PAHs were detected in snow along snowmobile tracks (McDaniel and Zielinska, 2014; Rhea et al., 2005; Oanh et al., 2019). Moreover, a factor of 3 higher NO_x emissions from snowmobiles compared to gasoline-driven cars in Svalbard are reported by the Norwegian Climate and Pollution Agency (Vestreng et al., 2009) with the main contribution from four-stroke snowmobiles. Modern technology snowmobiles have a significant side effect of high production of NO_x (Ray et al., 2012) due to oxidation reactions in exhaust after-treatment (Aubin et al., 2017). A recent field survey by Dekhtyareva (2019) in Svalbard also confirmed enhanced NO_x emissions from snowmobiles. Excess of NO_x during combustion drives nitration of PAHs producing nitrated PAH derivatives via electrophilic substitution (Ringuet et al., 2012; Heeb et al., 2008; Carrara and Niessner, 2011; Carrara et al., 2010; Hu et al., 2013; Keyte et al., 2013). To note, pattern changes of the daily total nitro-PAHs profiles were the easiest applicable to recognize snowmobile emissions than PAHs and oxy-PAHs, and 9-



nitroanthracene, 6-nitrochrysene, 3-nitrophenanthrene, 5-nitroacenaphthene, and 3-nitrofluoranthene seems to have strong specificity to the source.

495 **4 Summary and conclusion**

LRAT is believed to play a predominant role in Arctic air pollution. Different seasonal mechanisms of air masses' transport to the lower Arctic troposphere determine the annual trend of remote sources' contribution with its maximum in winter and minimum in summer. The results obtained here from air samples collected within a polar boundary layer at an urban site revealed the importance of anthropogenic emissions within the Arctic, which caused a different seasonal trend of PAC concentrations.

While the winter PAC levels were found to be mainly influenced by the north-western Eurasian emissions, the highest concentrations, with comparable and even exceeded the European annual mean levels, were measured in spring, the coldest period in the high Arctic. Low BLH, suppressed vertical mixing (stable stratification), and frequent thermal inversions facilitated the accumulation of near-ground emissions during spring. This period coincided with a significant increase in local human activities followed the several months of winter darkness. Simultaneously, the LRAT dislocated to be mainly from the area north of the 75 °N latitude in the North Atlantic Ocean, with no significant PAC sources. The pollution was primarily attributed to local snowmobile related emissions, resulted in a factor of 30 higher PAH concentrations compared to the Zeppelin background station data. In addition, no typical pristine Arctic summer conditions were observed in Longyearbyen air. The PAC summer levels outreached the winter ones, while they are usually an order of magnitude lower as reported from background stations. Under inhibited LRAT and enhanced PACs' photochemical degradation (24 h sun) conditions during summer, these elevated levels indicated fresh local emissions. The PAC, OC, and EC levels depended on wind direction and were found to correlate with the local marine traffic. When the wind blew from the harbour, the average PAC concentrations were up to twice higher.

To date, this is the most comprehensive data on the phase-separated concentrations of non-monitored emerging contaminants in the Arctic like oxy- and nitro-PAHs. These results provide insights on their global fate, persistence in a cold environment (Röhler et al., 2020), and LRAT potential. Moreover, the here reported study allows the influence of the middle latitude sources (LRAT) to be distinguished from local sources. This knowledge is essential for authorities working on national and regional regulatory monitoring and remediation strategies and might further provide confidence for choosing new candidates to be routinely measured (Wong et al., 2021) in densely populated areas and in the Arctic (Röhler et al., 2020). As increased shipping, industrial development, and further urbanization of local settlements are predicted to substantially increase in the Arctic due to climate change and declining sea ice cover, it is crucial to stay alert on the levels of the emerging contaminants primarily emitted after fossil fuel burning such as the PACs.



Data availability. The dataset used in this paper is included in the Supplement, and further information is available from the
525 corresponding authors at tatiana.drotikova@unis.no and alexandre.albinet@ineris.fr.

Supplement. The supplement related to this article is available online at: XXX.

Author contributions. TD, RK, and AA designed the study. TD conducted and performed the fieldwork. AA led and validated
530 the chemical analyses. AD produced the meteorological data and assisted its interpretation. RK provided academic guidance
and contributed to the paper preparation. TD and AA interpreted the data and wrote the manuscript with inputs from all co-
authors.

Competing interests. The authors declare that they have no conflict of interest.

535
Acknowledgements. The authors thank Valérie Minguet, Arnaud Papin, Ahmad El-Masri, Faustina Fuvel, and Serguei
Stavrovski (Ineris) for sample preparation and EC/OC and PAC analyses. They acknowledge the Norwegian national archive
Norstore (project NS9054K) for the trajectory data retrieved in this study, as well as ECMWF for the ERA5 meteorological
data and personally Michael Sprenger (ETH Zurich) for the support in providing the data. They also acknowledge the Swedish
540 EPA and Katarina Hansson (IVL Swedish Environmental Research Institute) for the PAH concentrations data monitored at
Pallas (Finland) station, and Pernilla Bohlin-Nizzetto and Karl Espen Yttri (NILU) for the PAH, EC, and OC data from the
Zeppelin (Svalbard) station. This research was financially supported by UNIS and the French Ministry of Environment.

References

- 545 Abbas, I., Badran, G., Verdin, A., Ledoux, F., Roumié, M., Courcot, D., and Garçon, G.: Polycyclic aromatic hydrocarbon derivatives in
airborne particulate matter: sources, analysis and toxicity, *Environ. Chem. Lett.*, 1-37, 10.1007/s10311-017-0697-0, 2018.
- Albinet, A., Leoz-Garziandia, E., Budzinski, H., and Villenave, E.: Simultaneous analysis of oxygenated and nitrated polycyclic aromatic
hydrocarbons on standard reference material 1649a (urban dust) and on natural ambient air samples by gas chromatography–mass
spectrometry with negative ion chemical ionisation, *J. Chromatogr. A*, 1121, 106-113, <https://doi.org/10.1016/j.chroma.2006.04.043>, 2006.
- 550 Albinet, A., Leoz-Garziandia, E., Budzinski, H., and Villenave, E.: Polycyclic aromatic hydrocarbons (PAHs), nitrated PAHs and
oxygenated PAHs in ambient air of the Marseilles area (South of France): Concentrations and sources, *Sci. Total Environ.*, 384, 280-292,
<https://doi.org/10.1016/j.scitotenv.2007.04.028>, 2007.
- Albinet, A., Leoz-Garziandia, E., Budzinski, H., Villenave, E., and Jaffrezou, J. L.: Nitrated and oxygenated derivatives of polycyclic aromatic
hydrocarbons in the ambient air of two French alpine valleys. Part I: Concentrations, sources and gas/particle partitioning, *Atmos. Environ.*,
42, 43-54, <http://doi.org/10.1016/j.atmosenv.2007.10.009>, 2008.
- 555 Albinet, A., Tomaz, S., and Lestremau, F.: A really quick easy cheap effective rugged and safe (QuEChERS) extraction procedure for the
analysis of particle-bound PAHs in ambient air and emission samples, *Sci. Total Environ.*, 450-451, 31-38,
<https://doi.org/10.1016/j.scitotenv.2013.01.068>, 2013.
- Albinet, A., Nalin, F., Tomaz, S., Beaumont, J., and Lestremau, F.: A simple QuEChERS-like extraction approach for molecular chemical
characterization of organic aerosols: application to nitrated and oxygenated PAH derivatives (NPAH and OPAH) quantified by GC–NICIMS,
560 *Anal. Bioanal. Chem.*, 406, 3131-3148, <https://doi.org/10.1007/s00216-014-7760-5>, 2014.
- Aliabadi, A. A., Staebler, R. M., and Sharma, S.: Air quality monitoring in communities of the Canadian Arctic during the high shipping
season with a focus on local and marine pollution, *Atmos. Chem. Phys.*, 15, 2651-2673, 10.5194/acp-15-2651-2015, 2015.
- AMAP: AMAP Assessment 2006: Acidifying Pollutants, Arctic Haze, and Acidification in the Arctic, Oslo, Norway, xii+112 pp., 2006.



- AMAP: AMAP Assessment 2015: Black carbon and ozone as Arctic climate forcers, Arctic Monitoring and Assessment Programme (AMAP), Oslo, Norway, 116 pp., 2015.
- 565 Arya, S. P.: Air Pollution and Dispersion Meteorology, Oxford University Press, New York, 310 pp., 1999.
- Atlas, E. L., Ridley, B. A., and Cantrell, C. A.: The tropospheric ozone production about the spring equinox (TOPSE) experiment: introduction, *Journal of Geophysical Research: Atmospheres*, 108, <https://doi.org/10.1029/2002JD003172>, 2003.
- 570 Aubin, C.-P., Girard, E., Langlois, P.-O., Lebreux, Y., and Verner, G.: 4-Stroke IDI Turbocharged Diesel Snowmobile Design, The Clean Snowmobile Challenge 2017 Conference, Ann Arbor, Michigan, United States, March 2017, 2017.
- Bailleul, S., and Albinet, A.: Interlaboratory comparison for the analysis of PAHs in ambient air (2018), LCSQA, <https://www.lcsqa.org/fr/rapport/interlaboratory-comparison-analysis-pah-ambient-air-2018>, 2018.
- Balmer, J., and Muir, D.: Polycyclic aromatic hydrocarbons (PAHs), in: AMAP Assessment 2016: Chemicals of emerging Arctic concern, edited by: Hung, H., Letcher, R., and Yu, Y., Arctic Monitoring and Assessment Programme (AMAP), Oslo, Norway, 219-238, 2017.
- 575 Balmer, J. E., Hung, H., Yu, Y., Letcher, R. J., and Muir, D. C. G.: Sources and environmental fate of pyrogenic polycyclic aromatic hydrocarbons (PAHs) in the Arctic, *Emerging Contaminants*, 5, 128-142, <https://doi.org/10.1016/j.emcon.2019.04.002>, 2019.
- Bandowe, B. A. M., and Meusel, H.: Nitrated polycyclic aromatic hydrocarbons (nitro-PAHs) in the environment – A review, *Sci. Total Environ.*, 581-582, 237-257, <https://doi.org/10.1016/j.scitotenv.2016.12.115>, 2017.
- 580 Barrie, L., and Platt, U.: Arctic tropospheric chemistry: an overview, *Tellus B: Chemical and Physical Meteorology*, 49, 450-454, <https://doi.org/10.3402/tellusb.v49i5.15984>, 1997.
- Bishop, G. A., Morris, J. A., and Stedman, D. H.: Snowmobile contributions to mobile source emissions in Yellowstone National Park, *Environ Sci Technol*, 35, 2874-2881, 10.1021/es101513l, 2001.
- Bolton, J. L., Trush, M. A., Penning, T. M., Dryhurst, G., and Monks, T. J.: Role of Quinones in Toxicology, *Chem. Res. Toxicol.*, 13, 135-160, 10.1021/tx9902082, 2000.
- 585 Bozem, H., Hoor, P., Kunkel, D., Köllner, F., Schneider, J., Herber, A., Schulz, H., Leaitch, W. R., Aliabadi, A. A., Willis, M. D., Burkart, J., and Abbatt, J. P. D.: Characterization of transport regimes and the polar dome during Arctic spring and summer using in situ aircraft measurements, *Atmos. Chem. Phys.*, 19, 15049-15071, 10.5194/acp-19-15049-2019, 2019.
- Browse, J., Carslaw, K. S., Arnold, S. R., Pringle, K., and Boucher, O.: The scavenging processes controlling the seasonal cycle in Arctic sulphate and black carbon aerosol, *Atmos. Chem. Phys.*, 12, 6775-6798, 10.5194/acp-12-6775-2012, 2012.
- 590 Bunce, N. J., Liu, L., Zhu, J., and Lane, D. A.: Reaction of Naphthalene and Its Derivatives with Hydroxyl Radicals in the Gas Phase, *Environ. Sci. Technol.*, 31, 2252-2259, 10.1021/es960813g, 1997.
- Bøckman, R.: Fremtidens energiutfordringer på Svalbard (in Norwegian), Longyearbyen Lokalstyre, Norway, Open file at www.uit.no, last access: 28 January 2020, 10 pp., 2019.
- Carrara, M., Wolf, J.-C., and Niessner, R.: Nitro-PAH formation studied by interacting artificially PAH-coated soot aerosol with NO₂ in the temperature range of 295–523K, *Atmos. Environ.*, 44, 3878-3885, <https://doi.org/10.1016/j.atmosenv.2010.07.032>, 2010.
- 595 Carrara, M., and Niessner, R.: Impact of a NO₂-regenerated diesel particulate filter on PAH and NPAH emissions from an EURO IV heavy duty engine, *J. Environ. Monit.*, 13, 3373-3379, 10.1039/C1EM10573F, 2011.
- Cavalli, F., Viana, M., Yttri, K. E., Genberg, J., and Putaud, J. P.: Toward a standardised thermal-optical protocol for measuring atmospheric organic and elemental carbon: the EUSAAR protocol, *Atmos. Meas. Tech.*, 3, 79-89, 10.5194/amt-3-79-2010, 2010.
- 600 CEN: European Committee for Standardization, EN-15549: 2008 - Air Quality - Standard Method for the Measurement of the Concentration of Benzo[a]pyrene in Air, CEN, Brussels (Belgium), <https://shop.bsigroup.com/ProductDetail?pid=00000000030142046>, 2008.
- CEN: European Committee for Standardization, TS-16645: 2014- Ambient Air – Method for the Measurement of Benzo[a]anthracene, Benzo[b]fluoranthene, Benzo[j]fluoranthene, Benzo[k]fluoranthene, Dibenz[a,h]anthracene, Indeno[1,2,3-cd]pyrene and Benzo[ghi]perylene, CEN, Brussels (Belgium), <https://shop.bsigroup.com/ProductDetail?pid=00000000030277467>, 2014.
- 605 CEN: European Committee for Standardization, EN-16909: 2017 - Ambient air - Measurement of elemental carbon (EC) and organic carbon (OC) collected on filters, CEN, Brussels (Belgium), 2017.
- Cesana, G., Kay, J., Chepfer, H., English, J., and De Boer, G.: Ubiquitous low-level liquid-containing Arctic clouds: New observations and climate model constraints from CALIPSO-GOCCP, *Geophys. Res. Lett.*, 39, <https://doi.org/10.1029/2012GL053385>, 2012.
- 610 Chan, A. W. H., Kautzman, K. E., Chhabra, P. S., Surratt, J. D., Chan, M. N., Crouse, J. D., Kürten, A., Wennberg, P. O., Flagan, R. C., and Seinfeld, J. H.: Secondary organic aerosol formation from photooxidation of naphthalene and alkylnaphthalenes: implications for oxidation of intermediate volatility organic compounds (IVOCs), *Atmos. Chem. Phys.*, 9, 3049-3060, 10.5194/acp-9-3049-2009, 2009.
- Clergé, A., Le Goff, J., Lopez, C., Ledauphin, J., and Delépée, R.: Oxy-PAHs: occurrence in the environment and potential genotoxic/mutagenic risk assessment for human health, *Crit. Rev. Toxicol.*, 1-27, 10.1080/10408444.2019.1605333, 2019.
- 615 Contini, D., Gambaro, A., Belosi, F., De Pieri, S., Cairns, W. R. L., Donato, A., Zanutto, E., and Citron, M.: The direct influence of ship traffic on atmospheric PM_{2.5}, PM₁₀ and PAH in Venice, *J. Environ. Manage.*, 92, 2119-2129, 10.1016/j.jenvman.2011.01.016, 2011.
- Copernicus C3S: Copernicus Climate Change Service (C3S), ERA5: Fifth generation of ECMWF atmospheric reanalyses of the global climate, Copernicus Climate Change Service Climate Data Store (CDS), 2017.



- 620 Cvrčková, O., and Ciganek, M.: PHOTOSTABILITY OF POLYCYCLIC AROMATIC HYDROCARBONS (PAHs) AND NITRATED POLYCYCLIC AROMATIC HYDROCARBONS (NPAHs) IN DICHLOROMETHANE AND ISOCTANE SOLUTIONS, *Polycyclic Aromat. Compd.*, 25, 141-156, 10.1080/10406630590922166, 2005.
- Cvrčková, O., Ciganek, M., and Šimek, Z.: ANTHRACENE, CHRYSENE, THEIR NITRO-AND METHYL-DERIVATIVES PHOTOSTABILITY IN ISOCTANE, *Polycyclic Aromat. Compd.*, 26, 331-344, 10.1080/10406630601028221, 2006.
- 625 Czech, H., Stengel, B., Adam, T., Sklorz, M., Streibel, T., and Zimmermann, R.: A chemometric investigation of aromatic emission profiles from a marine engine in comparison with residential wood combustion and road traffic: Implications for source apportionment inside and outside sulphur emission control areas, *Atmos. Environ.*, 167, 212-222, <https://doi.org/10.1016/j.atmosenv.2017.08.022>, 2017.
- Dahlke, S., Hughes, N. E., Wagner, P. M., Gerland, S., Wawrzyniak, T., Ivanov, B., and Maturilli, M.: The observed recent surface air temperature development across Svalbard and concurring footprints in local sea ice cover, *Int. J. Climatol.*, 40, 5246-5265, <https://doi.org/10.1002/joc.6517>, 2020.
- 630 Dee, D. P., Uppala, S. M., Simmons, A. J., Berrisford, P., Poli, P., Kobayashi, S., Andrae, U., Balmaseda, M. A., Balsamo, G., Bauer, P., Bechtold, P., Beljaars, A. C. M., van de Berg, L., Bidlot, J., Bormann, N., Delsol, C., Dragani, R., Fuentes, M., Geer, A. J., Haimberger, L., Healy, S. B., Hersbach, H., Hólm, E. V., Isaksen, I., Kållberg, P., Köhler, M., Matricardi, M., McNally, A. P., Monge-Sanz, B. M., Morcrette, J.-J., Park, B.-K., Peubey, C., de Rosnay, P., Tavolato, C., Thépaut, J.-N., and Vitart, F.: The ERA-Interim reanalysis: configuration and performance of the data assimilation system, *Q. J. R. Meteorolog. Soc.*, 137, 553-597, <https://doi.org/10.1002/qj.828>, 2011.
- 635 Dekhtyareva, A., Edvardsen, K., Holmén, K., Hermansen, O., and Hansson, H. C.: Influence of local and regional air pollution on atmospheric measurements in Ny-Ålesund, *International Journal of Sustainable Development and Planning*, 11, 578-587, <http://doi.org/10.2495/sdp-v11-n4-578-587>, 2016.
- Dekhtyareva, A.: On local and long-range transported air pollution in Svalbard, *Phylosophiae Doctor, University in Tromsø, UiT The Arctic University of Norway*, 2019.
- 640 Drotikova, T., Ali, A. M., Halse, A. K., Reinardy, H. C., and Kallenborn, R.: Polycyclic aromatic hydrocarbons (PAHs) and oxy- and nitro-PAHs in ambient air of the Arctic town Longyearbyen, Svalbard, *Atmos. Chem. Phys.*, 20, 9997-10014, 10.5194/acp-20-9997-2020, 2020.
- Eckhardt, S., Stohl, A., Beirle, S., Spichtinger, N., James, P., Forster, C., Junker, C., Wagner, T., Platt, U., and Jennings, S. G.: The North Atlantic Oscillation controls air pollution transport to the Arctic, *Atmos. Chem. Phys.*, 3, 1769-1778, 10.5194/acp-3-1769-2003, 2003.
- Eckhardt, S., Hermansen, O., Grythe, H., Fiebig, M., Stebel, K., Cassiani, M., Baecklund, A., and Stohl, A.: The influence of cruise ship emissions on air pollution in Svalbard: a harbinger of a more polluted Arctic?, *Atmos. Chem. Phys.*, 13, 8401-8409, 10.5194/acp-13-8401-2013, 2013.
- 645 ECMWF: European Centre for Medium-Range Weather Forecasts. PART IV: PHYSICAL PROCESSES, in: IFS Documentation CY43R3, IFS Documentation, ECMWF, 221 pp., 2017.
- EPA: United States Environmental Protection Agency. Annual Certification Data for Vehicles, Engines, and Equipment: <https://www.epa.gov/compliance-and-fuel-economy-data/annual-certification-data-vehicles-engines-and-equipment>, access: 22 November, 2020.
- 650 Eriksson, K., Tjärner, D., Marqvardsen, I., and Järvholm, B.: Exposure to benzene, toluene, xylenes and total hydrocarbons among snowmobile drivers in Sweden, *Chemosphere*, 50, 1343-1347, [https://doi.org/10.1016/S0045-6535\(02\)00808-1](https://doi.org/10.1016/S0045-6535(02)00808-1), 2003.
- Fan, Z., Kamens, R. M., Hu, J., Zhang, J., and McDow, S.: Photostability of Nitro-Polycyclic Aromatic Hydrocarbons on Combustion Soot Particles in Sunlight, *Environ. Sci. Technol.*, 30, 1358-1364, 10.1021/es9505964, 1996.
- 655 Ferrero, L., Cappelletti, D., Busetto, M., Mazzola, M., Lupi, A., Lanconelli, C., Becagli, S., Traversi, R., Caiazzo, L., Giardi, F., Moroni, B., Crocchianti, S., Fierz, M., Močnik, G., Sangiorgi, G., Perrone, M. G., Maturilli, M., Vitale, V., Udisti, R., and Bolzacchini, E.: Vertical profiles of aerosol and black carbon in the Arctic: a seasonal phenomenology along 2 years (2011–2012) of field campaigns, *Atmos. Chem. Phys.*, 16, 12601-12629, 10.5194/acp-16-12601-2016, 2016.
- Fremme, A., and Sodemann, H.: The role of land and ocean evaporation on the variability of precipitation in the Yangtze River valley, *Hydrol. Earth Syst. Sci.*, 23, 2525-2540, 10.5194/hess-23-2525-2019, 2019.
- 660 Fu, P., Kawamura, K., and Barrie, L. A.: Photochemical and Other Sources of Organic Compounds in the Canadian High Arctic Aerosol Pollution during Winter–Spring, *Environ. Sci. Technol.*, 43, 286-292, 10.1021/es803046q, 2009.
- Garrett, T., Zhao, C., and Novelli, P.: Assessing the relative contributions of transport efficiency and scavenging to seasonal variability in Arctic aerosol, *Tellus B: Chemical and Physical Meteorology*, 62, 190-196, 10.1111/j.1600-0889.2010.00453.x, 2010.
- 665 GYC: Greater Yellowstone Coalition. Existing Research and Data Regarding the Status of Air Quality in the Greater Yellowstone Ecosystem: A Bibliography, edited by: Hettinger, K., 2011.
- Hallquist, M., Wenger, J. C., Baltensperger, U., Rudich, Y., Simpson, D., Claeys, M., Dommen, J., Donahue, N. M., George, C., Goldstein, A. H., Hamilton, J. F., Herrmann, H., Hoffmann, T., Iinuma, Y., Jang, M., Jenkin, M. E., Jimenez, J. L., Kiendler-Scharr, A., Maenhaut, W., McFiggans, G., Mentel, T. F., Monod, A., Prévôt, A. S. H., Seinfeld, J. H., Surratt, J. D., Szmigielski, R., and Wildt, J.: The formation, performance and impact of secondary organic aerosol: current and emerging issues, *Atmos. Chem. Phys.*, 9, 5155-5236, 10.5194/acp-9-5155-2009, 2009.



- Halsall, C. J., Barrie, L. A., Fellin, P., Muir, D., Billeck, B., Lockhart, L., Rovinsky, F. Y., Kononov, E. Y., and Pastukhov, B.: Spatial and temporal variation of polycyclic aromatic hydrocarbons in the Arctic atmosphere, *Environ. Sci. Technol.*, 31, 3593-3599, <https://doi.org/10.1021/es970342d>, 1997.
- 675 Hanssen-Bauer, I., Førland, E., Hisdal, H., Mayer, S., AB, S., and Sorteberg, A.: Climate in Svalbard 2100 - a knowledge base for climate adaptation. NCCS report no. 1/2019, Norway, 105 pp., 2019.
- Heald, C. L., and Kroll, J. H.: The fuel of atmospheric chemistry: Toward a complete description of reactive organic carbon, *Sci. Adv.*, 6, eaay8967, 10.1126/sciadv.aay8967, 2020.
- 680 Heeb, N. V., Schmid, P., Kohler, M., Gujer, E., Zennegg, M., Wenger, D., Wichser, A., Ulrich, A., Gfeller, U., Honegger, P., Zeyer, K., Emmenegger, L., Petermann, J.-L., Czerwinski, J., Mosimann, T., Kasper, M., and Mayer, A.: Secondary effects of catalytic diesel particulate filters: conversion of PAHs versus formation of nitro-PAHs, *Environ. Sci. Technol.*, 42, 3773-3779, <http://doi.org/10.1021/es7026949>, 2008.
- Hersbach, H., Bell, B., Berrisford, P., Hirahara, S., Horányi, A., Muñoz-Sabater, J., Nicolas, J., Peubey, C., Radu, R., Schepers, D., Simmons, A., Soci, C., Abdalla, S., Abellan, X., Balsamo, G., Bechtold, P., Biavati, G., Bidlot, J., Bonavita, M., De Chiara, G., Dahlgren, P., Dee, D., Diamantakis, M., Dragani, R., Flemming, J., Forbes, R., Fuentes, M., Geer, A., Haimberger, L., Healy, S., Hogan, R. J., Hólm, E., Janisková, M., Keeley, S., Laloyaux, P., Lopez, P., Lupu, C., Radnoti, G., de Rosnay, P., Rozum, I., Vamborg, F., Villaume, S., and Thépaut, J.-N.: The ERA5 global reanalysis, *Q. J. R. Meteorol. Soc.*, 146, 1999-2049, <https://doi.org/10.1002/qj.3803>, 2020.
- 685 Hu, S., Herner, J. D., Robertson, W., Kobayashi, R., Chang, M. C. O., Huang, S.-M., Zielinska, B., Kado, N., Collins, J. F., Rieger, P., Huai, T., and Ayala, A.: Emissions of polycyclic aromatic hydrocarbons (PAHs) and nitro-PAHs from heavy-duty diesel vehicles with DPF and SCR, *Journal of the Air & Waste Management Association*, 63, 984-996, <https://doi.org/10.1080/10962247.2013.795202>, 2013.
- 690 Huang, B., Liu, M., Bi, X., Chaemfa, C., Ren, Z., Wang, X., Sheng, G., and Fu, J.: Phase distribution, sources and risk assessment of PAHs, NPAHs and OPAHs in a rural site of Pearl River Delta region, China, *Atmos. Pollut. Res.*, 5, 210-218, <https://doi.org/10.5094/APR.2014.026>, 2014.
- Huang, C., Hu, Q., Li, Y., Tian, J., Ma, Y., Zhao, Y., Feng, J., An, J., Qiao, L., Wang, H., Jing, S. a., Huang, D., Lou, S., Zhou, M., Zhu, S., Tao, S., and Li, L.: Intermediate Volatility Organic Compound Emissions from a Large Cargo Vessel Operated under Real-World Conditions, *Environ. Sci. Technol.*, 52, 12934-12942, 10.1021/acs.est.8b04418, 2018a.
- 695 Huang, C., Hu, Q., Wang, H., Qiao, L., Jing, S. a., Wang, H., Zhou, M., Zhu, S., Ma, Y., Lou, S., Li, L., Tao, S., Li, Y., and Lou, D.: Emission factors of particulate and gaseous compounds from a large cargo vessel operated under real-world conditions, *Environ. Pollut.*, 242, 667-674, <https://doi.org/10.1016/j.envpol.2018.07.036>, 2018b.
- 700 IARC: International Agency for Research on Cancer. Some non-heterocyclic polycyclic aromatic hydrocarbons and some related exposures, <http://monographs.iarc.fr/ENG/Monographs/vol92/mono92.pdf>, 2010.
- IARC: International Agency for Research on Cancer. Some Chemicals Present in Industrial and Consumer Products, Food and Drinking-water, <http://monographs.iarc.fr/ENG/Monographs/vol101/index.php>, 2012.
- Idowu, O., Semple, K. T., Ramadass, K., O'Connor, W., Hansbro, P., and Thavamani, P.: Beyond the obvious: Environmental health implications of polar polycyclic aromatic hydrocarbons, *Environ. Int.*, 123, 543-557, <https://doi.org/10.1016/j.envint.2018.12.051>, 2019.
- 705 Isaksen, K., Nordli, Ø., Førland, E. J., Lupikasza, E., Eastwood, S., and Niedźwiedz, T.: Recent warming on Spitsbergen—Influence of atmospheric circulation and sea ice cover, *Journal of Geophysical Research: Atmospheres*, 121, 11,913-911,931, <https://doi.org/10.1002/2016JD025606>, 2016.
- Jimenez, J. L., Canagaratna, M. R., Donahue, N. M., Prevot, A. S. H., Zhang, Q., Kroll, J. H., DeCarlo, P. F., Allan, J. D., Coe, H., Ng, N. L., Aiken, A. C., Docherty, K. S., Ulbrich, I. M., Grieshop, A. P., Robinson, A. L., Duplissy, J., Smith, J. D., Wilson, K. R., Lanz, V. A., Collins, D. R., Cubison, M. J., Dunlea, J., Huffman, J. A., Onasch, T. B., Alfarra, M. R., Williams, P. I., Bower, K., Kondo, Y., Schneider, J., Drewnick, F., Borrmann, S., Weimer, S., Demerjian, K., Salcedo, D., Cottrell, L., Griffin, R., Takami, A., Miyoshi, T., Hatakeyama, S., Shimojo, A., Sun, J. Y., Zhang, Y. M., Dzepina, K., Kimmel, J. R., Sueper, D., Jayne, J. T., Herndon, S. C., Trimborn, A. M., Williams, L. R., Wood, E. C., Middlebrook, A. M., Kolb, C. E., Baltensperger, U., and Worsnop, D. R.: Evolution of Organic Aerosols in the Atmosphere, *Science*, 326, 1525-1529, 10.1126/science.1180353, 2009.
- 710 Kameda, T.: Atmospheric Reactions of PAH derivatives: Formation and Degradation, in: *Polycyclic Aromatic Hydrocarbons: Environmental Behavior and Toxicity in East Asia*, edited by: Hayakawa, K., Springer Singapore, Singapore, 75-91, 2018.
- Keyte, I. J., Harrison, R. M., and Lammel, G.: Chemical reactivity and long-range transport potential of polycyclic aromatic hydrocarbons – a review, *Chem. Soc. Rev.*, 42, 9333-9391, <https://doi.org/10.1039/C3CS60147A>, 2013.
- 720 Kim, K.-H., Jahan, S. A., Kabir, E., and Brown, R. J. C.: A review of airborne polycyclic aromatic hydrocarbons (PAHs) and their human health effects, *Environ. Int.*, 60, 71-80, 10.1016/j.envint.2013.07.019, 2013.
- Klonecki, A.: Seasonal changes in the transport of pollutants into the Arctic troposphere-model study, *J. Geophys. Res.*, 108, 8367, <http://doi.org/10.1029/2002jd002199>, 2003.
- 725 Kroll, J. H., and Seinfeld, J. H.: Chemistry of secondary organic aerosol: Formation and evolution of low-volatility organics in the atmosphere, *Atmos. Environ.*, 42, 3593-3624, <https://doi.org/10.1016/j.atmosenv.2008.01.003>, 2008.
- Kystdatahuset. Longyearbyen port traffic as of 2018: <https://kystdatahuset.no/>, access: 05 June 2020, 2018.



- Law, K. S., Roiger, A., Thomas, J. L., Marelle, L., Raut, J.-C., Dalsøren, S., Fuglestedt, J., Tuccella, P., Weinzierl, B., and Schlager, H.: Local Arctic air pollution: Sources and impacts, *Ambio*, 46, 453-463, 10.1007/s13280-017-0962-2, 2017.
- 730 Lawson, R. P., Baker, B. A., Schmitt, C. G., and Jensen, T.: An overview of microphysical properties of Arctic clouds observed in May and July 1998 during FIRE ACE, *Journal of Geophysical Research: Atmospheres*, 106, 14989-15014, <https://doi.org/10.1029/2000JD900789>, 2001.
- Lee, J. Y., and Lane, D. A.: Unique products from the reaction of naphthalene with the hydroxyl radical, *Atmos. Environ.*, 43, 4886-4893, <https://doi.org/10.1016/j.atmosenv.2009.07.018>, 2009.
- 735 Lei, Y. D., and Wania, F.: Is rain or snow a more efficient scavenger of organic chemicals?, *Atmos. Environ.*, 38, 3557-3571, 10.1016/j.atmosenv.2004.03.039, 2004.
- Läderach, A., and Sodemann, H.: A revised picture of the atmospheric moisture residence time, *Geophys. Res. Lett.*, 43, 924-933, <https://doi.org/10.1002/2015GL067449>, 2016.
- Madonna, E., Wernli, H., Joos, H., and Martius, O.: Warm Conveyor Belts in the ERA-Interim Dataset (1979–2010). Part I: Climatology and Potential Vorticity Evolution, *J. Clim.*, 27, 3-26, 10.1175/jcli-d-12-00720.1, 2014.
- 740 Marchand, N., Besombes, J. L., Chevron, N., Masclet, P., Aymoz, G., and Jaffrezo, J. L.: Polycyclic aromatic hydrocarbons (PAHs) in the atmospheres of two French alpine valleys: sources and temporal patterns, *Atmos. Chem. Phys.*, 4, 1167-1181, 10.5194/acp-4-1167-2004, 2004.
- Matsuzawa, S.: Photodegradation of some Oxygenated Polycyclic Aromatic Hydrocarbons, *Polycyclic Aromat. Compd.*, 21, 331-339, 10.1080/10406630008028543, 2000.
- 745 McDaniel, M., and Zielinska, B.: Polycyclic Aromatic Hydrocarbons in the Snowpack and Surface Water in Blackwood Canyon, Lake Tahoe, CA, as Related to Snowmobile Activity, *Polycyclic Aromat. Compd.*, 35, 102-119, 10.1080/10406638.2014.935449, 2014.
- Meldrum, J.: Optimization of a Direct-Injected 2-Stroke Cycle Snowmobile, in: *Clean Snowmobile Challenge: 1 the Early Years, 4-Stroke Engines Make Their Debut*, SAE, 1-14, 2017.
- 750 Miet, K., Albinet, A., Budzinski, H., and Villenave, E.: Atmospheric reactions of 9,10-anthraquinone, *Chemosphere*, 107, 1-6, 10.1016/j.CHEMOSPHERE.2014.02.050, 2014.
- Miljødirektoratet. Longyearbyen power plant coal and diesel consumption as of 2018: <https://www.norskeutslipp.no/no/Diverse/Virksomhet/?CompanyID=5115>, access: 12 November 2020, 2018.
- Monks, P. S.: A review of the observations and origins of the spring ozone maximum, *Atmos. Environ.*, 34, 3545-3561, [https://doi.org/10.1016/S1352-2310\(00\)00129-1](https://doi.org/10.1016/S1352-2310(00)00129-1), 2000.
- 755 Mulder, M. D., Dumanoglu, Y., Efstathiou, C., Kukučka, P., Matejovičová, J., Maurer, C., Příbylová, P., Prokeš, R., Sofuoğlu, A., Sofuoğlu, S. C., Wilson, J., Zetzsch, C., Wotawa, G., and Lammel, G.: Fast Formation of Nitro-PAHs in the Marine Atmosphere Constrained in a Regional-Scale Lagrangian Field Experiment, *Environ. Sci. Technol.*, 53, 8914-8924, 10.1021/acs.est.9b03090, 2019.
- Nalin, F., Golly, B., Besombes, J.-L., Pelletier, C., Aujay-Plouzeau, R., Verhac, S., Dermigny, A., Fievet, A., Karoski, N., Dubois, P., Collet, S., Favez, O., and Albinet, A.: Fast oxidation processes from emission to ambient air introduction of aerosol emitted by residential log wood stoves, *Atmos. Environ.*, 143, 15-26, 10.1016/j.atmosenv.2016.08.002, 2016.
- 760 Nežiková, B., Degrendele, C., Bandowe, B. A. M., Holubová Šmejkalová, A., Kukučka, P., Martiník, J., Mayer, L., Prokeš, R., Příbylová, P., Klánová, J., and Lammel, G.: Three years of atmospheric concentrations of nitrated and oxygenated polycyclic aromatic hydrocarbons and oxygen heterocycles at a central European background site, *Chemosphere*, 128738, <https://doi.org/10.1016/j.chemosphere.2020.128738>, 2020.
- 765 Niedźwiedz, T.: The atmospheric circulation, Climate and Climate Change at Hornsund, Svalbard. The Publishing House of Gdynia Maritime University, Gdynia, 2013.
- Nordli, Ø., Przybylak, R., Ogilvie, A. E. J., and Isaksen, K.: Long-term temperature trends and variability on Spitsbergen: the extended Svalbard Airport temperature series, 1898-2012, *Polar Res.*, 33, 10.3402/polar.v33.21349, 2014.
- 770 Oanh, P. K., Kazushi, N., Yoshie, N., Tatsuya, T., Yusuke, F., Miho, A., Toshimitsu, S., Kenji, K., Hideaki, M., Hien, T. O. T., and Norimichi, T.: Concentrations of polycyclic aromatic hydrocarbons in Antarctic snow polluted by research activities using snow mobiles and diesel electric generators, *Bull. Glaciol. Res.*, 37, 23-30, 10.5331/bgr.19A02, 2019.
- Ođabasi, M., Vardar, N., Sofuoğlu, A., Tasdemir, Y., and Holsen, T. M.: Polycyclic aromatic hydrocarbons (PAHs) in Chicago air, *Sci. Total Environ.*, 227, 57-67, [https://doi.org/10.1016/S0048-9697\(99\)00004-2](https://doi.org/10.1016/S0048-9697(99)00004-2), 1999.
- 775 Onarheim, I. H., Smedsrud, L. H., Ingvaldsen, R. B., and Nilsen, F.: Loss of sea ice during winter north of Svalbard, *Tellus A: Dynamic Meteorology and Oceanography*, 66, 23933, 10.3402/tellusa.v66.23933, 2014.
- Perraudin, E., Budzinski, H., and Villenave, E.: Identification and quantification of ozonation products of anthracene and phenanthrene adsorbed on silica particles, *Atmos. Environ.*, 41, 6005-6017, <https://doi.org/10.1016/j.atmosenv.2007.03.010>, 2007.
- 780 Prevedouros, K., Brorström-Lundén, E., J. Halsall, C., Jones, K. C., Lee, R. G. M., and Sweetman, A. J.: Seasonal and long-term trends in atmospheric PAH concentrations: evidence and implications, *Environ. Pollut.*, 128, 17-27, <https://doi.org/10.1016/j.envpol.2003.08.032>, 2004.
- Ravindra, K., Sokhi, R., and Vangrieken, R.: Atmospheric polycyclic aromatic hydrocarbons: Source attribution, emission factors and regulation, *Atmos. Environ.*, 42, 2895-2921, <http://doi.org/10.1016/j.atmosenv.2007.12.010>, 2008.



- 785 Ray, J. D., Bishop, G., Schuchmann, B., Frey, C., Sandu, G., and Graver, B.: Yellowstone Over-snow Vehicle Emission Tests–2012: Preliminary Report, Natural Resource Technical Report NPS/NRPC/ARD/NRTR—2012. National Park Service, Fort Collins, Colorado, 36 pp., 2012.
- Reimann, S., Kallenborn, R., and Schmidbauer, N.: Severe Aromatic Hydrocarbon Pollution in the Arctic Town of Longyearbyen (Svalbard) Caused by Snowmobile Emissions, *Environ Sci Technol*, 43, 4791–4795, 10.1021/es900449x, 2009.
- 790 Reisen, F., and Arey, J.: Atmospheric Reactions Influence Seasonal PAH and Nitro-PAH Concentrations in the Los Angeles Basin, *Environ. Sci. Technol.*, 39, 64–73, 10.1021/es0354541, 2005.
- Rhea, D. T., Gale, R. W., Orazio, C. E., Peterman, P. H., Harper, D. D., and Farag, A. M.: Polycyclic aromatic hydrocarbons in water, sediment, and snow, from lakes in Grand Teton National Park, Wyoming. Final Report, USGS-CERC-91344, US. Geological Survey, Columbia Environmental Research Center (USGS-CERC), Columbia, South Carolina, USA, 30 pp., 2005.
- 795 Ringuet, J., Albinet, A., Leoz-Garziandia, E., Budzinski, H., and Villenave, E.: Reactivity of polycyclic aromatic compounds (PAHs, NPAHs and OPAHs) adsorbed on natural aerosol particles exposed to atmospheric oxidants, *Atmos. Environ.*, 61, 15–22, <https://doi.org/10.1016/j.atmosenv.2012.07.025>, 2012.
- Röhler, L., Schlabach, M., Haglund, P., Breivik, K., Kallenborn, R., and Bohlin-Nizzetto, P.: Non-target and suspect characterisation of organic contaminants in Arctic air – Part 2: Application of a new tool for identification and prioritisation of chemicals of emerging Arctic concern in air, *Atmos. Chem. Phys.*, 20, 9031–9049, 10.5194/acp-20-9031-2020, 2020.
- 800 Schmale, J., Arnold, S. R., Law, K. S., Thorp, T., Anenberg, S., Simpson, W. R., Mao, J., and Pratt, K. A.: Local Arctic air pollution: A neglected but serious problem, *Earth's Future*, 6, 1385–1412, <https://doi.org/10.1029/2018ef000952>, 2018.
- Serreze, M. C., Barrett, A. P., Slater, A. G., Steele, M., Zhang, J., and Trenberth, K. E.: The large-scale energy budget of the Arctic, *J. Geophys. Res.*, 112, D11122, 10.1029/2006jd008230, 2007.
- 805 Shahpoury, P., Lammel, G., Albinet, A., Sofuoğlu, A., Dumanoglu, Y., Sofuoğlu, S. C., Wagner, Z., and Zdimal, V.: Evaluation of a Conceptual Model for Gas-Particle Partitioning of Polycyclic Aromatic Hydrocarbons Using Polyparameter Linear Free Energy Relationships, *Environ. Sci. Technol.*, 50, 12312–12319, 10.1021/acs.est.6b02158, 2016.
- Shahpoury, P., Kitanovski, Z., Lammel, G. J. A. C., and Physics: Snow scavenging and phase partitioning of nitrated and oxygenated aromatic hydrocarbons in polluted and remote environments in central Europe and the European Arctic, *Atmos. Chem. Phys.*, 18, 13495–13510, <https://doi.org/10.5194/acp-18-13495-2018>, 2018.
- 810 Shively, D. D., Pape, B. M. C., Mower, R. N., Zhou, Y., Russo, R., and Sive, B. C.: Blowing Smoke in Yellowstone: Air Quality Impacts of Oversnow Motorized Recreation in the Park, *Environmental Management*, 41, 183–199, 10.1007/s00267-007-9036-8, 2008.
- Simpson, W. R., von Glasow, R., Riedel, K., Anderson, P., Ariya, P., Bottenheim, J., Burrows, J., Carpenter, L. J., Frieß, U., Goodsite, M. E., Heard, D., Hutterli, M., Jacobi, H. W., Kaleschke, L., Neff, B., Plane, J., Platt, U., Richter, A., Roscoe, H., Sander, R., Shepson, P., Sodeau, J., Steffen, A., Wagner, T., and Wolff, E.: Halogens and their role in polar boundary-layer ozone depletion, *Atmos. Chem. Phys.*, 7, 4375–4418, 10.5194/acp-7-4375-2007, 2007.
- 815 Singh, D. K., Kawamura, K., Yanase, A., and Barrie, L. A.: Distributions of polycyclic aromatic hydrocarbons, aromatic ketones, carboxylic acids, and trace metals in Arctic aerosols: Long-range atmospheric transport, photochemical degradation/production at polar sunrise, *Environ. Sci. Technol.*, 51, 8992–9004, <https://doi.org/10.1021/acs.est.7b01644>, 2017.
- 820 Sippula, O., Stengel, B., Sklorz, M., Streibel, T., Rabe, R., Orasche, J., Lintelmann, J., Michalke, B., Abbaszade, G., Radischat, C., Gröger, T., Schnelle-Kreis, J., Harndorf, H., and Zimmermann, R.: Particle Emissions from a Marine Engine: Chemical Composition and Aromatic Emission Profiles under Various Operating Conditions, *Environ. Sci. Technol.*, 48, 11721–11729, 10.1021/es502484z, 2014.
- Sive, B. C., Shively, D., and Pape, B.: Spatial variation of volatile organic compounds associated with snowmobile emissions in Yellowstone National Park, *National Park Service*, 85 pp., 2003.
- Sjöblom, A.: The Ice-atmosphere boundary layer, *The University Centre in Svalbard, Norway, Longyearbyen*, 30 pp., 2010.
- 825 Srivastava, D., Favez, O., Bonnaire, N., Lucarelli, F., Haeffelin, M., Perraudin, E., Gros, V., Villenave, E., and Albinet, A.: Speciation of organic fractions does matter for aerosol source apportionment. Part 2: Intensive short-term campaign in the Paris area (France), *Sci. Total Environ.*, 634, 267–278, <https://doi.org/10.1016/j.scitotenv.2018.03.296>, 2018.
- Statistics Norway: This is Svalbard 2016. What the figures say, *Statistics Norway*, 28 pp., 2016.
- Statistics Norway. Registered vehicles, by region, statistical variable per year, data for 2018: <https://www.ssb.no/statbank/table/11823/>, access: 05 June 2020, 2018.
- 830 Statistics Norway. Longyearbyen and Ny-Ålesund population as of 2020: <https://www.ssb.no/befolkning/statistikker/befsvsvalbard>, access: 12 November, 2020.
- Stohl, A., Eckhardt, S., Forster, C., James, P., and Spichtinger, N.: On the pathways and timescales of intercontinental air pollution transport, *Journal of Geophysical Research: Atmospheres*, 107, ACH 6-1-ACH 6-17, <https://doi.org/10.1029/2001JD001396>, 2002.
- 835 Stohl, A., Forster, C., Frank, A., Seibert, P., and Wotawa, G.: Technical note: The Lagrangian particle dispersion model FLEXPART version 6.2, *Atmos. Chem. Phys.*, 5, 2461–2474, 10.5194/acp-5-2461-2005, 2005.
- Stohl, A.: Characteristics of atmospheric transport into the Arctic troposphere, *Journal of Geophysical Research: Atmospheres*, 111, 10.1029/2005jd006888, 2006.



- Stohl, A., Berg, T., Burkhart, J. F., Fjérraa, A. M., Forster, C., Herber, A., Hov, Ø., Lunder, C., McMillan, W. W., Oltmans, S., Shiobara, M., Simpson, D., Solberg, S., Stebel, K., Ström, J., Tørseth, K., Treffeisen, R., Virkkunen, K., and Yttri, K. E.: Arctic smoke - record high air pollution levels in the European Arctic due to agricultural fires in Eastern Europe in spring 2006, *Atmos. Chem. Phys.*, 7, 511–534, 10.5194/acp-7-511-2007, 2007.
- 840 Stull, R. B.: An introduction to boundary layer meteorology, Kluwer Academic Publishers, Dordrecht, The Netherlands, 1988.
- Tomaz, S., Shahpoury, P., Jaffrezo, J.-L., Lammel, G., Perraudin, E., Villenave, E., and Albinet, A.: One-year study of polycyclic aromatic compounds at an urban site in Grenoble (France): Seasonal variations, gas/particle partitioning and cancer risk estimation, *Sci. Total Environ.*, 565, 1071–1083, <http://doi.org/10.1016/j.scitotenv.2016.05.137>, 2016.
- 845 U.S. NPS. National Park Service. Best Available Technology (BAT) Snowmobiles as of December 15th, 2015: <https://www.nps.gov/yell/planyourvisit/newbatlist.htm>, access: 30 December 2020, 2015.
- van Pelt, W. J. J., Kohler, J., Liston, G. E., Hagen, J. O., Luks, B., Reijmer, C. H., and Pohjola, V. A.: Multidecadal climate and seasonal snow conditions in Svalbard, *Journal of Geophysical Research: Earth Surface*, 121, 2100–2117, <https://doi.org/10.1002/2016JF003999>, 2016.
- 850 Verlhac, S., Albinet, A., Cabillic, J., Lalère, B. and Fallot, C.,: European Interlaboratory Comparison for the analysis of PAHs in ambient air (2015), LCSQA, <https://www.lcsqa.org/fr/rapport/2015/ineris/european-interlaboratory-comparison-for-the-analysis-of-pah-in-ambient-air>, 2015.
- Vestreng, V., Kallenborn, R., and Økstad, E.: Norwegian Arctic climate: climate influencing emissions, scenarios and mitigation options at Svalbard, 56 pp., 2009.
- 855 Walgraeve, C., Demeestere, K., Dewulf, J., Zimmermann, R., and Van Langenhove, H.: Oxygenated polycyclic aromatic hydrocarbons in atmospheric particulate matter: Molecular characterization and occurrence, *Atmos. Environ.*, 44, 1831–1846, 10.1016/j.atmosenv.2009.12.004, 2010.
- Wallace, J. M., and Hobbs, P. V.: *Atmospheric science: an introductory survey*, Elsevier, 2006.
- WHO: The World Health Organization. Environmental health criteria 229. Selected nitro- and nitro-oxy-polycyclic aromatic hydrocarbons, 511, http://whqlibdoc.who.int/ehc/WHO_EHC_229.pdf, 2003.
- 860 Wickström, S.: Warmer and wetter winters over the high-latitude North Atlantic: an atmospheric circulation perspective, Doctoral thesis, UiB, The University of Bergen, 2020.
- Wickström, S., Jonassen, M. O., Cassano, J. J., and Vihma, T.: Present Temperature, Precipitation, and Rain-on-Snow Climate in Svalbard, *Journal of Geophysical Research: Atmospheres*, 125, e2019JD032155, <https://doi.org/10.1029/2019JD032155>, 2020a.
- 865 Wickström, S., Jonassen, M. O., Vihma, T., and Uotila, P.: Trends in cyclones in the high-latitude North Atlantic during 1979–2016, *Q. J. R. Meteorol. Soc.*, 146, 762–779, <https://doi.org/10.1002/qj.3707>, 2020b.
- Willis, M. D., Leaitch, W. R., and Abbatt, J. P. D.: Processes controlling the composition and abundance of Arctic aerosol, *Rev. Geophys.*, 56, 621–671, <https://doi.org/10.1029/2018rg000602>, 2018.
- Willis, M. D., Bozem, H., Kunkel, D., Lee, A. K. Y., Schulz, H., Burkart, J., Aliabadi, A. A., Herber, A. B., Leaitch, W. R., and Abbatt, J. P. D.: Aircraft-based measurements of High Arctic springtime aerosol show evidence for vertically varying sources, transport and composition, *Atmos. Chem. Phys.*, 19, 57–76, 10.5194/acp-19-57-2019, 2019.
- 870 Wong, F., Hung, H., Dryfhout-Clark, H., Aas, W., Bohlin-Nizzetto, P., Breivik, K., Mastromonaco, M. N., Lundén, E. B., Ólafsdóttir, K., Sigurðsson, Á., Vorkamp, K., Bossi, R., Skov, H., Hakola, H., Barresi, E., Sverko, E., Fellin, P., Li, H., Vlasenko, A., Zapevalov, M., Samsonov, D., and Wilson, S.: Time Trends Of Persistent Organic Pollutants (Pops) And Chemicals Of Emerging Arctic Concern (Ceac) In Arctic Air From 25 Years Of Monitoring, *Sci. Total Environ.*, 145109, <https://doi.org/10.1016/j.scitotenv.2021.145109>, 2021.
- 875 Yu, Y., Katsoyiannis, A., Bohlin-Nizzetto, P., Brorström-Lundén, E., Ma, J., Zhao, Y., Wu, Z., Tych, W., Mindham, D., Sverko, E., Barresi, E., Dryfhout-Clark, H., Fellin, P., and Hung, H.: Polycyclic aromatic hydrocarbons not declining in Arctic air despite global emission reduction, *Environ. Sci. Technol.*, 53, 2375–2382, <https://doi.org/10.1021/acs.est.8b05353>, 2019.
- Zhan, J., Gao, Y., Li, W., Chen, L., Lin, H., and Lin, Q.: Effects of ship emissions on summertime aerosols at Ny–Ålesund in the Arctic, *Atmospheric Pollution Research*, 5, 500–510, 10.5094/apr.2014.059, 2014.
- 880 Zhang, F., Chen, Y., Tian, C., Lou, D., Li, J., Zhang, G., and Matthias, V.: Emission factors for gaseous and particulate pollutants from offshore diesel engine vessels in China, *Atmos. Chem. Phys.*, 16, 6319–6334, 10.5194/acp-16-6319-2016, 2016.
- Zhang, F., Chen, Y., Cui, M., Feng, Y., Yang, X., Chen, J., Zhang, Y., Gao, H., Tian, C., Matthias, V., and Liu, H.: Emission factors and environmental implication of organic pollutants in PM emitted from various vessels in China, *Atmos. Environ.*, 200, 302–311, <http://doi.org/10.1016/j.atmosenv.2018.12.006>, 2019.
- 885 Zhang, F., Guo, H., Chen, Y., Matthias, V., Zhang, Y., Yang, X., and Chen, J.: Size-segregated characteristics of organic carbon (OC), elemental carbon (EC) and organic matter in particulate matter (PM) emitted from different types of ships in China, *Atmos. Chem. Phys.*, 20, 1549–1564, 10.5194/acp-20-1549-2020, 2020.
- Zhang, X., Walsh, J. E., Zhang, J., Bhatt, U. S., and Ikeda, M.: Climatology and Interannual Variability of Arctic Cyclone Activity: 1948–2002, *J. Clim.*, 17, 2300–2317, 10.1175/1520-0442(2004)017<2300:CAIVOA>2.0.CO;2, 2004.
- 890 Zhao, J., Zhang, Y., Wang, T., Sun, L., Yang, Z., Lin, Y., Chen, Y., and Mao, H.: Characterization of PM_{2.5}-bound polycyclic aromatic hydrocarbons and their derivatives (nitro- and oxy-PAHs) emissions from two ship engines under different operating conditions, *Chemosphere*, 225, 43–52, <http://doi.org/10.1016/j.chemosphere.2019.03.022>, 2019.



- 895 Zhao, J., Zhang, Y., Chang, J., Peng, S., Hong, N., Hu, J., Lv, J., Wang, T., and Mao, H.: Emission characteristics and temporal variation of PAHs and their derivatives from an ocean-going cargo vessel, *Chemosphere*, 249, 126194, <http://doi.org/10.1016/j.chemosphere.2020.126194>, 2020.
- Zhou, Y., Shively, D., Mao, H., Russo, R. S., Pape, B., Mower, R. N., Talbot, R., and Sive, B. C.: Air Toxic Emissions from Snowmobiles in Yellowstone National Park, *Environ. Sci. Technol.*, 44, 222-228, 10.1021/es9018578, 2010.

Supplement of Paper II

Table of content

Table S1. Total (G+P) concentrations of PAHs [$\mu\text{g}/\text{m}^3$], %PM, and concentrations of OC and EC [$\mu\text{g}/\text{m}^3$] measured in urban air of Longyearbyen in 2018.....	2
Table S2. Total (G+P) concentrations of oxy-PAHs [pg/m^3] and %PM measured in urban air of Longyearbyen in 2018.....	3
Table S3. Total (G+P) concentrations of nitro-PAHs [pg/m^3] and %PM measured in urban air of Longyearbyen in 2018.....	4
Table S4. Sampling periods and air sample volumes.....	6
Table S5. 10-day backward trajectory probability analysis data.....	7
Table S6. Meteorological data for sampling days.....	8
Table S7. PAH concentrations (G+P; pg/m^3) in the air of Longyearbyen (UNIS) compared to the levels at the background Arctic stations in Svalbard and Finland.....	9
Table S8. PAC concentrations ($\mu\text{g kg}^{-1}$) in SRM 1649b (urban dust).....	10
Figure S1. Maps of the Arctic, Svalbard, vicinity of Longyearbyen, and marine traffic in Isfjorden.	11
Figure S2. Sun diagram for Longyearbyen.....	12
Figure S3. Seasonal trends of weather parameters and $\sum_{20} \text{PAH}^*$ total (G+P) concentrations measured in Svalbard air in 2018 at UNIS and Zeppelin stations.....	13
Figure S4. Synoptic map and 10-day backward trajectories illustrating frequent winter events of the Atlantic warm air masses transport to the Arctic.....	14
Figure S5. Wind rose diagrams typical for the P1-P3 cold and P4 summer periods.....	15
Figure S6. Correlations of the OC/EC ratio and the sum gross tonnage of vessels arriving and departing the harbour of Longyearbyen.....	16
Figure S7. Comparison of the P1-P3 cold period profiles of PAHs based on the snowmobile traffic intensity.....	16
Figure S8. Comparison of the P4 summer profiles of PAHs based on wind direction and the chemical profile proportion increase rates of PAHs as result of ship traffic.....	17
Figure S9. Comparison of the P4 summer profiles of oxy-PAHs based on wind direction and the chemical profile proportion increase rates of selected oxy-PAHs as result of ship traffic.....	18
Figure S10. Comparison of the cold period P1-P3 profiles of oxy-PAHs based on snowmobile traffic intensity and the chemical profile proportion increase rates of selected oxy-PAHs.....	19
Figure S11. Comparison of the cold period P1-P3 profiles of nitro-PAHs based on the snowmobile traffic intensity and the chemical profile proportion increase rates of selected nitro-PAHs.....	20

Table S1. Total (G+P) concentrations of PAHs [$\mu\text{g}/\text{m}^3$], %PM, and concentrations of OC and EC [$\mu\text{g}/\text{m}^3$] measured in urban air of Longyearbyen in 2018.

Compound name	Abbreviated name	Cold period						Warm period						
		Dark winter P1 November-January n=8		Twilight winter P2 February n=4		Daylight spring P3 March-April n=7		%PM cold P1-P3 n=19		Polar day summer P4 May-June n=12		%PM warm P4 n=12		
		Mean	StDev	Median	Mean	StDev	Median	Mean	StDev	Median	Mean	StDev	Median	
Naphthalene	Nap	111.9	78.9	88.6	727.0	550.0	562.0	1533.0	760.0	1671.0	95.9	69.1	77.2	9.3
1-Methylnaphthalene	1-MeNap	58.1	27.6	56.0	336.5	159.6	276.3	890.0	389.0	744.0	105.6	65.7	80.8	38.2
2-Methylnaphthalene	2-MeNap	23.4	18.6	21.4	69.8	78.4	57.9	112.1	71.8	84.3	129.2	108.6	95.6	98.2
Acenaphthene	Ace	51.9	42.9	33.5	73.4	33.6	74.4	283.9	195.5	261.4	117.4	97.9	85.9	2.5
Fluorene	Flu	290.5	141.4	243.0	434.0	100.6	449.1	559.0	402.0	474.0	287.8	172.1	270.2	1.3
Phenanthrene	Phe	298.5	165.1	284.1	798.9	163.5	799.8	1129.0	594.0	1041.0	702.0	490.0	570.0	8.2
Anthracene	Ant	71.5	38.9	71.8	93.9	53.0	87.6	97.4	87.2	78.4	89.2	73.5	62.1	3.2
Fluoranthene	Flt	32.7	15.5	33.1	161.8	59.5	158.8	280.6	202.6	176.1	35.6	82.9	4.2	78.1
2-Methylfluoranthene	2-MeFlt	4.8	2.0	4.0	22.4	17.5	21.7	18.0	14.3	12.1	26.4	58.2	7.9	25.8
Pyrene	Pyr	34.7	21.0	32.8	95.5	63.3	116.1	154.8	76.9	155.2	84.6	78.0	69.1	15.4
Benzo[a]anthracene	BaAnt	3.9	0.3	4.0	1003.0	655.0	834.0	643.0	775.0	406.0	7.5	13.5	3.7	96.8
Chrysene	Chry	16.7	9.9	10.3	26.3	19.1	25.1	46.4	26.9	40.7	31.8	32.2	23.6	78.8
Retene	Ret	9.4	0.8	9.6	8.8	1.5	8.8	11.4	1.5	10.9	9.0	1.1	9.1	n.d.
Benzo[e]pyrene	BePyr	3.9	0.3	4.0	3.6	0.6	3.6	4.6	0.7	4.5	5.2	3.7	3.8	n.d.
Benzo[j]fluoranthene	BjFlt	13.2	1.1	13.5	12.3	2.1	12.3	15.8	2.2	15.2	12.6	1.5	12.7	n.d.
Benzo[b]fluoranthene	BbFlt	3.9	0.3	4.0	3.6	0.6	3.6	11.8	18.7	4.9	3.7	0.5	3.7	n.d.
Benzo[k]fluoranthene	BkFlt	5.3	0.4	5.4	4.9	0.8	4.9	9.6	8.3	6.7	6.4	5.0	5.1	85.6
Benzo[a]pyrene	BaPyr	5.5	4.2	4.0	12.2	9.5	11.8	11.1	10.8	5.4	8.5	9.3	3.9	93.5
Dibenzo[a,h]anthracene	DBahAnt	11.4	21.3	4.0	3.6	0.6	3.6	4.6	0.7	4.5	3.7	0.5	3.7	n.d.
Benzo[ghi]perylene	BghiP	3.9	0.3	4.0	13.3	10.9	12.2	40.0	30.3	34.6	4.8	3.6	3.8	93.5
Indeno[1,2,3-cd]pyrene	IPyr	9.0	0.7	9.2	8.4	1.4	8.4	19.6	22.8	11.5	8.6	1.1	8.7	n.d.
Coronene	Cor	3.9	0.3	4.0	9.8	6.9	8.7	27.3	32.2	5.5	3.7	0.5	3.7	n.d.
Σ22 PAHs		1068.0	449.0	957.0	3923.0	667.0	3929.0	5902.0	2421.0	5466.0	1779.0	1210.0	1352.0	
Elemental carbon	EC	0.09	0.08	0.06	0.10	0.09	0.09	0.18	0.08	0.15	0.16	0.11	0.13	
Organic carbon	OC	0.42	0.18	0.38	0.42	0.23	0.36	0.71	0.24	0.65	0.64	0.31	0.55	

*n.d. is not determined; proper evaluation of %PM was not possible due to the high number of concentration values <LOQ

Table S2. Total (G+P) concentrations of oxy-PAHs [pg/m³] and %pPM measured in urban air of Longyearbyen in 2018.

	Dark winter P1 November-January n=8						Cold period						%pPM cold P1-P3 n=19						Warm period					
	November-January n=8			Twilight winter P2 February n=4			Daylight spring P3 March-April n=7			%pPM cold P1-P3 n=19			Polar day summer P4 May-June n=12			%pPM warm P4 n=12								
	Mean	StDev	Median	Mean	StDev	Median	Mean	StDev	Median	Mean	StDev	Median	Mean	StDev	Median	Mean	StDev	Median						
Phthalic anhydride	1796.0	689.0	1824.0	2101.0	548.0	2063.0	2542.0	621.0	2582.0	37.7	2934.0	670.0	2983.0	20.3										
Benzophenone	1676.0	496.0	1650.0	4354.0	511.0	4269.0	5086.0	1413.0	5200.0	42.8	1962.0	536.0	1879.0	20.6										
1-Naphthaldehyde	478.3	148.0	485.8	454.6	109.8	501.5	1157.0	587.0	1165.0	26.8	656.0	490.0	526.0	5.7										
9-Fluorene	797.7	209.9	794.7	1064.6	134.2	1030.2	1682.0	551.0	1793.0	61.4	694.1	317.4	696.1	35.1										
1,2-Naphthalic anhydride	429.2	135.8	364.3	485.2	99.8	466.5	1003.0	277.0	971.0	37.9	477.0	207.8	396.8	39.5										
9,10-Phenanthrenequinone	194.0	143.4	268.2	115.3	117.5	106.8	271.0	336.0	19.0	80.2	13.0	1.6	13.1	n.d.										
2-Methylanthraquinone	8.1	3.2	7.7	24.4	6.0	25.8	64.7	45.8	47.8	74.5	10.4	8.5	7.8	71.8										
Phthalaldehyde	8.3	3.0	7.8	25.0	25.3	13.0	109.0	126.7	56.4	85.5	4.8	2.2	4.0	62.9										
1,4-Naphthoquinone	95.3	58.6	105.0	105.0	56.4	101.1	58.6	17.0	59.4	53.2	11.9	5.4	11.0	29.2										
2-Formyl-trans-cinnamaldehyde	55.7	63.5	35.0	65.1	14.2	62.0	249.8	151.3	296.3	67.9	21.8	14.9	18.1	80.3										
1,2-Naphthoquinone	26.5	34.8	11.8	19.0	7.6	18.8	103.2	110.5	18.3	0.7	25.7	9.0	27.6	n.d.										
1-Acenaphthene	175.3	96.3	150.4	100.6	17.0	95.0	196.5	111.1	156.7	65.3	123.9	110.5	100.9	20.2										
Biphenyl-2,2-dicarboxaldehyde	17.1	14.2	13.1	16.0	7.1	15.7	35.3	21.3	32.9	57.4	14.0	7.6	12.5	33.8										
2,3-Naphthalenedicarboxylic anhydride	35.5	30.5	32.3	55.8	20.1	54.0	90.1	107.4	38.6	18.3	74.7	56.4	63.7	70.5										
Anthrone	12.0	14.4	5.1	81.1	97.6	43.2	189.6	140.6	190.9	17.2	62.5	99.3	34.8	86.0										
6H-Dibenzo[b,d]pyran-6-one	38.6	24.7	34.7	48.4	22.7	46.2	114.2	42.2	108.5	53.5	36.2	26.5	35.3	79.9										
9,10-Antraquinone	33.3	12.3	32.7	54.9	7.2	55.3	119.3	59.6	109.5	62.6	31.3	13.3	26.9	56.0										
1,8-Naphthalic anhydride	4.8	3.4	2.9	9.6	4.9	8.0	37.1	13.6	36.9	44.0	6.4	6.4	3.5	61.7										
1,4-Antraquinone	4.4	0.4	4.5	4.1	0.7	4.1	5.3	0.7	5.1	n.d.	5.5	3.1	4.3	n.d.										
4,4-Biphenylidene-carboxaldehyde	11.7	4.2	10.2	12.6	3.9	12.7	18.3	3.1	16.9	22.7	9.9	3.0	9.8	21.7										
9-Phenanthrenecarboxaldehyde	1.2	0.6	1.0	1.3	0.5	1.0	2.6	1.4	2.9	71.1	4.9	7.6	2.8	75.8										
Benzo[a]fluorenone	4.3	1.5	4.5	6.8	2.2	6.9	11.6	6.3	12.4	57.6	6.8	5.9	5.3	64.1										
Benzo[b]fluorenone	3.6	1.8	2.9	6.1	1.9	5.7	11.9	6.0	9.0	55.3	4.6	3.2	4.3	65.6										
Benzanthrone	6.2	3.1	5.3	9.9	2.7	10.1	24.2	14.5	22.2	71.3	9.3	7.1	8.4	79.3										
1-Pyrenecarboxaldehyde	0.9	0.1	0.9	0.9	0.1	0.9	2.8	1.9	2.4	n.d.	1.5	1.5	0.9	86.5										
Acenanthrenequinone	1.7	2.3	0.9	0.8	0.1	0.8	1.9	2.2	1.0	n.d.	2.5	2.5	1.0	n.d.										
Benz[a]anthracene-7,12-dione	2.3	1.1	2.6	2.4	1.4	2.4	8.9	7.3	6.0	77.2	2.6	2.2	1.2	85.2										
Xanthone	12.5	5.1	12.9	12.0	2.7	11.9	27.6	11.9	29.6	40.1	7.7	3.1	7.4	69.9										
Acenaphthenequinone	3.6	3.0	2.8	4.7	1.1	4.6	6.0	3.3	5.7	42.9	3.6	1.7	3.0	49.4										
Σ 29 Oxy-PAHs	5934.0	1480.0	5482.0	9241.0	633.0	9264.0	13229.0	2681.0	14612.0		7219.0	1692.0	7717.0											

*n.d. is not determined; proper evaluation of %pPM was not possible due to the high number of concentration values <LOQ

Table S3. Total (G+P) concentrations of nitro-PAHs [pg/m³] and %PM measured in urban air of Longyearbyen in 2018.

	Cold period												Warm period									
	Dark winter P1 November-January n=8				Twilight winter P2 February n=4				Daylight spring P3 March-April n=7				%PM cold P1-P3 n=19			Polar day summer P4 May-June n=12			%PM warm P4 n=12			
	Mean	StDev	Median		Mean	StDev	Median		Mean	StDev	Median		Mean	StDev	Median	Mean	StDev	Median	Mean	StDev	Median	
1-Nitronaphthalene	11.42	7.42	10.69		14.75	7.46	12.87		21.40	14.61	17.45		9.3		2.81	1.83	2.36					1.3
2-Methyl-1-nitronaphthalene + 1-Methyl-5-nitronaphthalene	5.29	3.64	4.85		4.05	2.83	3.32		3.42	3.32	2.26		1.4		2.23	1.28	1.74					n.d.
2-Nitronaphthalene	2.85	0.86	2.62		4.43	1.33	4.58		5.12	3.38	3.60		10.2		2.05	0.75	2.26					n.d.
2-Methyl-4-nitronaphthalene	1.48	0.82	0.97		1.16	0.47	0.95		1.15	0.19	1.16		n.d.		0.85	0.10	0.85					n.d.
1-Methyl-4-nitronaphthalene	1.95	1.81	0.96		2.77	0.80	2.62		3.94	3.49	3.17		73.8		1.12	0.68	0.85					n.d.
1-Methyl-6-nitronaphthalene	1.10	0.62	0.90		0.82	0.14	0.83		0.96	0.43	1.12		n.d.		0.98	0.47	0.86					n.d.
1.5-Dinitronaphthalene	1.13	0.64	0.93		0.85	0.14	0.85		1.10	0.14	1.05		n.d.		1.01	0.48	0.89					n.d.
2-Nitrophenyl	0.92	0.07	0.93		0.85	0.14	0.86		1.44	0.97	1.06		n.d.		1.02	0.51	0.88					n.d.
3-Nitrophenyl	2.13	0.88	2.46		1.59	1.02	1.14		2.66	2.11	1.53		4.1		1.64	0.72	1.60					n.d.
3-Nitrodibenzofuran	1.15	0.63	0.93		0.85	0.14	0.85		1.46	0.95	1.16		n.d.		1.16	0.66	0.89					n.d.
5-Nitroacenaphthene	1.31	1.08	1.32		4.31	3.93	4.30		5.65	4.33	4.75		0.8		1.35	0.77	1.20					1.3
2-Nitro-9-fluorenone	1.85	1.59	0.96		2.88	1.49	3.09		2.29	1.26	2.90		1.6		1.38	0.81	0.95					n.d.
2-Nitrofluorene	0.94	0.14	0.92		0.86	0.10	0.84		1.09	0.14	1.03		n.d.		0.86	0.11	0.86					n.d.
9-Nitroanthracene	1.32	0.96	1.00		11.74	12.66	11.09		16.92	12.55	17.67		13.2		1.00	0.32	0.92					n.d.
9-Nitrophenanthrene	1.15	0.13	1.14		6.07	2.04	6.53		3.14	2.24	2.90		3.0		1.03	0.14	1.02					n.d.
2-Nitrodibenzothiophene	0.90	0.07	0.92		0.84	0.14	0.84		1.36	0.71	1.14		n.d.		0.86	0.11	0.87					n.d.
3-Nitrophenanthrene	1.09	0.12	1.08		5.26	5.07	4.69		4.79	3.56	3.94		3.1		1.14	0.56	0.96					n.d.
2-Nitroanthracene	0.92	0.05	0.93		0.84	0.14	0.85		3.33	3.95	1.27		1.2		1.07	0.50	0.93					n.d.
9-Methyl-10-nitroanthracene	0.87	0.07	0.89		0.81	0.14	0.81		1.06	0.14	1.00		n.d.		0.83	0.10	0.84					n.d.
2-Nitrofluoranthene	1.37	0.63	1.07		1.74	1.04	1.70		2.89	0.74	3.06		65.9		0.92	0.16	0.88					n.d.
3-Nitrofluoranthene	1.09	0.09	1.11		5.75	1.41	5.27		3.85	1.29	3.89		4.2		1.46	0.78	1.07					n.d.
4-Nitropyrene	1.17	0.64	0.95		1.18	0.52	0.98		1.15	0.15	1.18		n.d.		1.05	0.61	0.90					n.d.
1-Nitropyrene	1.55	1.13	0.98		1.19	0.48	0.98		2.44	1.45	1.51		72.8		1.38	0.67	1.00					67.7
2-Nitropyrene	0.99	0.06	0.97		0.95	0.11	0.98		1.25	0.23	1.24		n.d.		0.96	0.11	0.94					n.d.
7-Nitrobenz[a]anthracene	0.94	0.06	0.94		0.86	0.14	0.86		1.37	0.87	1.06		n.d.		0.88	0.11	0.89					n.d.
6-Nitrochrysene	1.22	0.62	1.05		2.11	0.84	2.31		8.09	6.73	3.89		n.d.		0.98	0.17	0.96					n.d.
1.3-Dinitropyrene	4.47	0.48	4.46		4.38	0.43	4.43		9.01	4.20	6.14		n.d.		4.24	0.52	4.30					n.d.

Table S3 (continued)

	Cold period												Warm period																			
	Dark winter P1 November-January n=8				Twilight winter P2 February n=4				Daylight spring P3 March-April n=7				%PM cold P1-P3 n=19				Polar day summer P4 May-June n=12				%PM warm P4 n=12											
	Mean	StDev	Median		Mean	StDev	Median		Mean	StDev	Median		Mean	StDev	Median		Mean	StDev	Median		Mean	StDev	Median		Mean	StDev	Median					
1,6-Dinitropyrene	11.71	0.96	11.93		10.87	1.83	10.92		14.18	1.83	13.50		n.d.				11.20	1.37	11.24		n.d.				n.d.				n.d.			
1,8-Dinitropyrene	11.10	0.91	11.31		10.30	1.74	10.35		13.44	1.74	12.79		n.d.				10.61	1.30	10.65		n.d.				n.d.				n.d.			
1-Nitrobenzo[e]pyrene + 6-Nitrobenzo[a]pyrene	1.92	1.00	1.59		1.48	0.14	1.49		2.04	0.23	2.01		n.d.				1.45	0.23	1.45		n.d.				n.d.				n.d.			
3-Nitrobenzo[e]pyrene	1.13	0.07	1.13		1.13	0.26	1.12		1.43	0.20	1.48		n.d.				1.08	0.17	1.06		n.d.				n.d.				n.d.			
1-Nitrobenzo[a]pyrene	3.54	0.29	3.60		3.53	0.34	3.54		4.08	0.74	4.08		n.d.				3.38	0.41	3.40		n.d.				n.d.				n.d.			
3-Nitrobenzo[a]pyrene	1.71	0.14	1.74		2.27	1.33	1.79		2.07	0.27	1.97		n.d.				1.64	0.20	1.64		n.d.				n.d.				n.d.			
Σ35 Nitro-PAHs	83.7	18.6	78.9		113.5	13.0	116.6		149.6	34.3	131.2						65.6	9.2	66.2										66.2			

*n.d. is not determined; proper evaluation of %PM was not possible due to the high number of concentration values <LOQ

Table S4. Sampling periods and air sample volumes.

Period	Sample	Sampling start		Sampling stop		Sample volume [m ³]
		Date	Local time	Date	Local time	
P1	UNIS_1	28.11.2017	14:45	29.11.2017	14:55	342.9
P1	UNIS_2	01.12.2017	15:11	02.12.2017	16:32	353.9
P1	UNIS_3	03.12.2017	12:18	04.12.2017	10:53	318.9
P1	UNIS_4	15.01.2018	13:17	16.01.2018	15:21	392.4
P1	UNIS_5	16.01.2018	15:26	17.01.2018	15:07	350.9
P1	UNIS_6	17.01.2018	15:10	18.01.2018	15:48	368.2
P1	UNIS_7	20.01.2018	13:52	21.01.2018	12:42	352.2
P1	UNIS_8	21.01.2018	13:17	22.01.2018	15:34	417.1
P2	UNIS_9	31.01.2018	16:15	01.02.2018	16:03	410.3
P2	UNIS_10	01.02.2018	16:05	02.02.2018	22:02	485.5
P2	UNIS_11	08.02.2018	20:20	09.02.2018	21:58	324.9
P2	UNIS_12	13.02.2018	15:49	14.02.2018	21:42	364.3
P3	UNIS_13	15.03.2018	15:27	16.03.2018	13:37	256.2
P3	UNIS_14	22.03.2018	10:50	23.03.2018	13:22	312.1
P3	UNIS_15	27.03.2018	15:43	28.03.2018	15:24	283.7
P3	UNIS_16	03.04.2018	13:47	04.04.2018	16:01	370.4
P3	UNIS_17	06.04.2018	21:48	07.04.2018	20:11	335.0
P3	UNIS_18	07.04.2018	20:15	08.04.2018	22:13	369.5
P3	UNIS_19	10.04.2018	21:21	11.04.2018	15:48	257.2
P4	UNIS_20	16.05.2018	22:10	17.05.2018	21:58	356.6
P4	UNIS_21	24.05.2018	15:20	25.05.2018	16:21	344.1
P4	UNIS_22	28.05.2018	13:38	29.05.2018	15:55	397.6
P4	UNIS_23	29.05.2018	15:59	30.05.2018	16:05	369.7
P4	UNIS_24	01.06.2018	14:31	02.06.2018	22:56	476.0
P4	UNIS_25	04.06.2018	13:44	05.06.2018	16:01	420.0
P4	UNIS_26	06.06.2018	15:47	07.06.2018	16:01	361.6
P4	UNIS_27	12.06.2018	15:46	13.06.2018	23:24	439.2
P4	UNIS_28	14.06.2018	14:43	15.06.2018	13:38	319.4
P4	UNIS_29	18.06.2018	11:49	19.06.2018	15:01	400.4
P4	UNIS_30	20.06.2018	17:21	21.06.2018	16:20	315.1
P4	UNIS_31	22.06.2018	15:53	23.06.2018	18:50	380.0

Table S5. 10-day backward trajectory probability analysis data.

	Period 2017/2018	Number of trajectories*	Percentage of trajectories that fit to the LRAT criteria	Median number of rain precipitation events	Median rain precipitation events efficiency, Δq , [g·kg ⁻¹]	Median number of snow precipitation events	Median snow precipitation events efficiency, Δq , [g·kg ⁻¹]
P1	Nov– Jan	4659	48	0	0.49	8	0.27
P2	February	1395	56	1	0.57	8	0.32
P3	March-April	2565	23	1	0.46	3	0.27
P4	May-June	2523	48	13	0.46	0	0.28

* starting at the specified height (within a source area boundary layer) over the region

Table S6. Meteorological data for sampling days.

Period	24 h sampling start		Ambient temperature, [°C]			Pressure, [hPa]	Relative humidity RH, [%]		Specific humidity H_{spec} , [g/kg]		Wind speed, [m/s]			Wind from, [degree]	UV, [W/m ²]
	Date		min	max	median		mean	mean	min	max	median	mean			
P1	28.11.2017		-14.1	-6.3	-9.7	1012.3	68.8	1.1	0.6	6.5	3.8	3.8	113	0.8	
P1	01.12.2017		-8.3	-3.4	-6.2	989.0	83.0	1.9	0.0	7.2	1.2	1.7	113	0.4	
P1	03.12.2017		-4.6	1.0	-0.1	991.0	73.0	2.8	1.6	11.5	5.5	5.8	76	0.5	
P1	15.01.2018		1.1	4.0	1.7	994.5	76.1	3.5	2.6	10.2	7.1	7.0	125	0.3	
P1	16.01.2018		-0.7	1.0	0.2	1000.5	73.1	3.0	5.3	12.0	9.4	9.1	93	0.2	
P1	17.01.2018		-1.6	0.6	-0.6	1009.8	73.8	2.8	5.7	10.4	8.3	8.4	112	0.2	
P1	20.01.2018		-6.5	-2.7	-4.3	1013.1	81.6	2.1	0.2	4.8	1.6	2.0	120	0.9	
P1	21.01.2018		-5.3	-1.8	-2.7	1015.3	71.3	2.2	1.9	7.5	6.4	6.1	133	0.7	
P2	31.01.2018		-16.9	-15.1	-15.4	1024.6	57.3	0.6	3.1	7.6	6.4	6.0	136	0.8	
P2	01.02.2018		-18.0	-5.5	-13.4	1019.7	65.6	1.0	0.6	7.2	4.2	4.1	118	0.3	
P2	08.02.2018		-9.8	1.2	-2.7	993.3	67.3	2.0	2.6	10.6	7.7	7.3	126	0.6	
P2	13.02.2018		-8.4	-4.3	-5.7	1012.4	72.7	1.7	6.0	13.2	10.8	10.4	126	0.7	
P3	15.03.2018		-9.9	-6.1	-7.4	1019.4	71.9	1.4	3.6	10.1	7.5	7.2	122	18.4	
P3	22.03.2018		-15.9	-10.3	-11.6	1007.1	61.4	0.8	1.2	8.4	3.4	4.5	284	120.1	
P3	27.03.2018		-13.3	-9.4	-11.0	1006.0	75.2	1.1	1.0	7.0	3.8	3.9	125	91.0	
P3	03.04.2018		-16.4	-12.8	-14.8	1024.7	57.7	0.7	7.2	11.8	9.7	9.7	129	186.5	
P3	06.04.2018		-17.1	-9.8	-15.1	1018.6	53.6	0.6	0.6	5.9	1.9	2.7	125	207.9	
P3	07.04.2018		-17.0	-7.5	-12.6	1016.5	66.3	0.9	0.6	6.2	2.7	2.8	116	163.1	
P3	10.04.2018		-12.6	-4.7	-8.6	1006.7	68.5	1.4	2.7	7.9	5.2	5.2	124	166.6	
P4	16.05.2018		3.8	5.6	4.9	999.6	68.4	3.9	6.7	16.7	11.5	11.8	91	145.9	
P4	24.05.2018		-0.1	4.5	1.9	1008.5	75.1	3.5	2.3	10.4	5.2	5.5	228	262.4	
P4	28.05.2018		1.3	4.2	2.9	1014.4	73.5	3.6	1.9	11.4	7.1	7.3	102	202.5	
P4	29.05.2018		1.1	4.4	1.9	1021.1	80.2	3.7	0.4	5.5	3.3	3.2	302	158.7	
P4	01.06.2018		1.5	5.0	3.2	1000.7	80.9	4.1	0.5	8.0	3.1	3.3	292	134.6	
P4	04.06.2018		1.1	3.5	1.9	1013.8	69.9	3.3	0.6	9.5	6.5	5.8	112	174.5	
P4	06.06.2018		2.8	4.3	3.4	1003.7	66.5	3.5	2.6	9.2	5.4	5.8	294	366.4	
P4	12.06.2018		0.3	2.3	1.6	998.9	72.3	3.3	1.6	6.2	4.6	4.2	304	186.2	
P4	14.06.2018		3.0	5.7	3.7	1006.2	60.8	3.4	0.5	11.8	3.9	5.2	120	272.8	
P4	18.06.2018		4.9	7.0	6.3	1005.6	62.2	4.0	2.3	13.7	7.9	7.6	116	275.4	
P4	20.06.2018		5.1	6.5	5.8	1006.8	84.5	5.0	1.8	5.7	3.8	3.6	304	178.9	
P4	22.06.2018		3.0	9.3	6.2	1010.5	92.2	5.1	0.8	7.1	3.0	2.9	313	301.6	

Table S7. PAH concentrations (G+P; pg/m³) in the air of Longyearbyen (UNIS) compared to the levels at the background Arctic stations in Svalbard and Finland measured during the same period in 2017/2018. The determined periods are November-January (P1), February (P2), March-April (P3), and May-June (P4).

N of compounds	Location	Coordinates	Period	N samples	Mean	SD	Minimum	Median	Maximum
Σ20* PAHs	Zeppelin, Svalbard	78°58' N, 11°53' E, 474 m asl	P1	9	736	357	275	742	1227
	Zeppelin, Svalbard		P2	4	411	105	297	397	551
	Zeppelin, Svalbard		P3	6	141	42	88	151	191
	Zeppelin, Svalbard		P4	10	72	21	46	69	111
Σ20 PAH	UNIS, Svalbard	78.22° N, 15.65° E, 25 m asl	P1	8	951	388	477	863	1573
	UNIS, Svalbard		P2	4	3173	656	2797	2871	4155
	UNIS, Svalbard		P3	7	4351	2037	1829	4659	6611
	UNIS, Svalbard		P4	12	1657	1110	626	1311	4198
Σ11** PAHs	Pallas, Finland	68°00' N, 24°14' E, 340 m asl	P1	3	1102	92	999	1131	1176
	Pallas, Finland		P2	-	-	-	-	-	-
	Pallas, Finland		P3	2	341	156	231	341	452
	Pallas, Finland		P4	3	209	65	136	230	261
Σ11 PAH	UNIS, Svalbard	78.22° N, 15.65° E, 25 m asl	P1	8	488	209	239	474	847
	UNIS, Svalbard		P2	4	2217	730	1546	2033	3255
	UNIS, Svalbard		P3	7	2428	1266	905	3073	3597
	UNIS, Svalbard		P4	12	978	742	286	732	2725

Data acquired from <http://ebas.nilu.no>. last access: 20 December 2020

*Summed compounds are 1-MeNap, 2-MeNap, Ace, Flu, Phe, Ant, Flt, Pyr, BaAnt, Chry, Ret, BePyr, BbFlt, BkFlt, BbFlt, BkFlt, BaPyr, DBAnt, BghiP, IPyr, Cor

**Summed compounds are Ant, BaAnt, BaPyr, BbFlt, BghiP, BkFlt, Chry, DBAnt, Flt, Phe, Pyr

Table S8. PAC concentrations ($\mu\text{g kg}^{-1}$) in SRM 1649b (urban dust)

	This work		Certified/reference/indicative NIST 1649b		QuEChERS (Albinet, 2014)	
	Mean	SD	Mean	SD	Mean	SD
Naphtalene	0.81	0.09	0.95	0.09		
Acenaphtene	0.15	0.01	0.20	0.04		
Fluorene	0.20	0.02	0.22	0.04		
Phenanthrene	4.19	0.34	4.03	0.06		
Anthracene	0.41	0.02	0.41	0.00		
Fluoranthene	6.46	0.59	6.24	0.08		
Pyrene	5.52	0.52	4.98	0.14		
Benzo[a]anthracene	2.02	0.08	2.11	0.05		
Chrysene	4.31	0.21	3.05	0.03		
Benzo[b]fluoranthene	7.08	0.51	6.18	0.18		
Benzo[k]fluoranthene	1.70	0.14	1.70	0.05		
Benzo[a]pyrene	2.44	0.09	2.47	0.24		
Benzo[g,h,i]perylene	3.20	0.25	3.97	0.04		
Indeno[1,2,3-cd]pyrene	2.94	0.15	2.89	0.16		
Dibenzo[a,h]anthracene	0.28	0.01	0.29	0.00		
1-Methylnaphtalene	0.38	0.07	0.90	0.01		
2-Methylnaphtalene	1.08	0.84	0.96	0.02		
2-Methylfluoranthene	0.24	0.03	NA	NA		
Retene	1.32	0.08	0.24	0.01		
Benzo[e]pyrene	3.18	0.16	2.97	0.05		
Benzo[j]fluoranthene	2.08	0.17	1.73	0.04		
Coronene	2.83	0.09	3.16	0.05		
9-Nitrophenanthrene	10.23	4.28	1.8	0.1	11.4	4.6
5-Nitroacenaphthene	8.71	2.68	3.1	0.0	12.5	2.1
3-Nitrofluoranthene	4.60	0.25	4.7	0.7	NA	NA
4-Nitropyrene	4.83	0.37	5.6	0.1	27.3	7.1
7-Nitrobenz[a]anthracene	27.82	0.35	24.4	0.4	35.2	3.1
1-Nitropyrene	60.30	3.45	74.8	1.9	60.9	9.0
2-Nitrofluoranthene	293.10	7.09	304.0	25.0	261.9	29.7
2-Nitronaphthalene	8.40	2.24	11.8	0.4	14.4	5.1
1-Nitronaphthalene	4.31	0.60	7.3	0.0	9.2	3.4
6-Nitrochrysene	6.50	1.16	3.6	0.2	18.8	6.9
3-Nitrobiphenyl	6.98	1.62	3.7	0.2	15.7	5.8
2-Nitropyrene	138.50	11.19	10.9	0.1	42.0	3.2
3-Nitrophenanthrene	65.43	3.88	21.8	1.2	29.2	9.0
9-Nitroanthracene	107.61	45.60	37.0	4.4	25.7	3.6
9-Fluorenone	1712.51	816.37	1400.0	NA	715.0	88.0
Benz[a]anthracene-7,12-dione	3018.30	186.48	3600.0	NA	4862.0	442.0
9,10-Anthraquinone	787.35	34.32	1800.0	NA	1748.0	37.0
Benzanthrone	2899.67	189.68	1600.0	NA	6977.0	59.0

Figure S1. Maps of the Arctic (a), Svalbard (b), vicinity of Longyearbyen (c), and marine traffic in Isfjorden (d) (North-West to the UNIS sampling station).

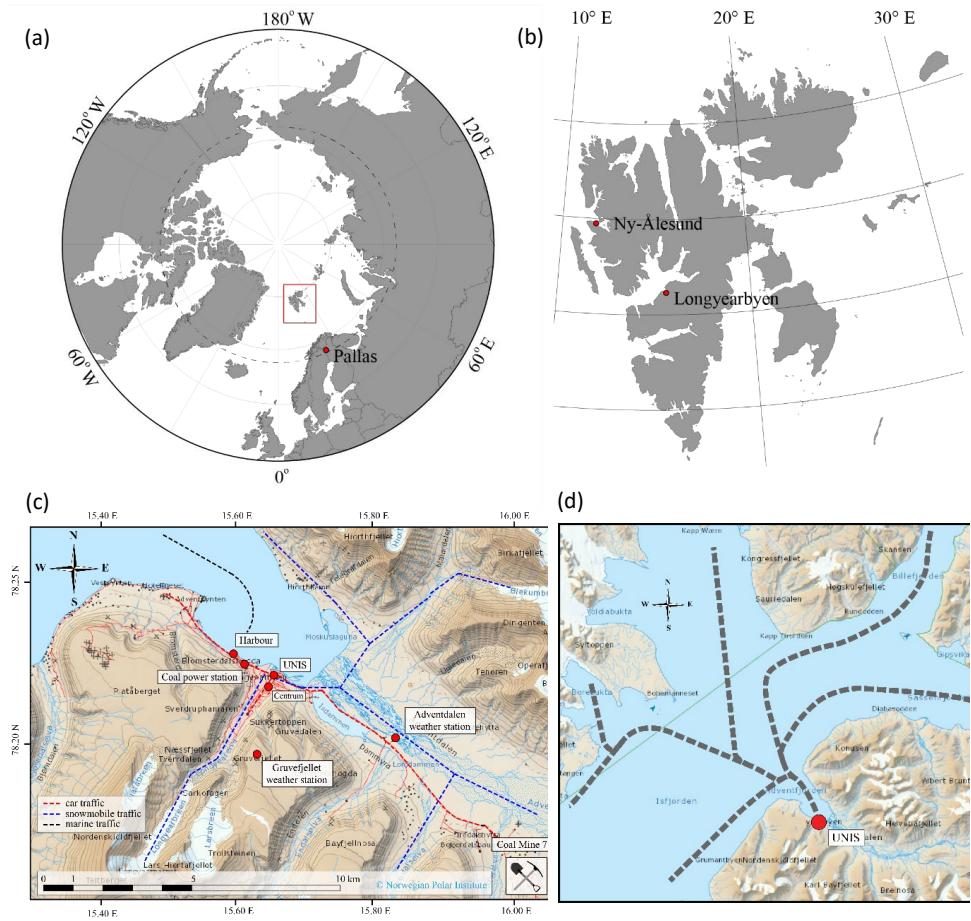


Figure S2. Sun diagram for Longyearbyen.

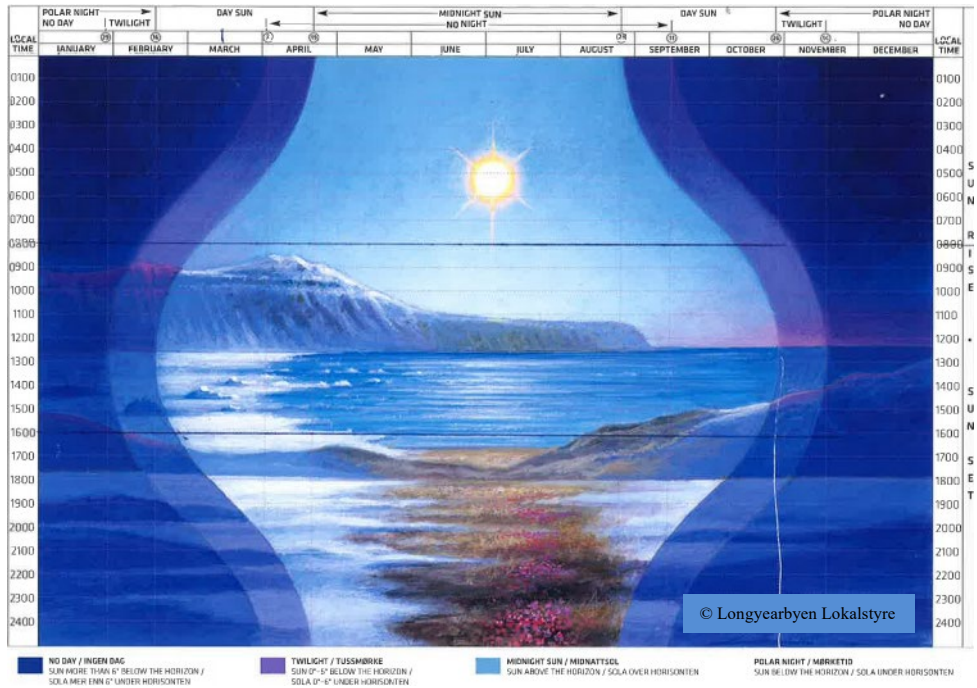
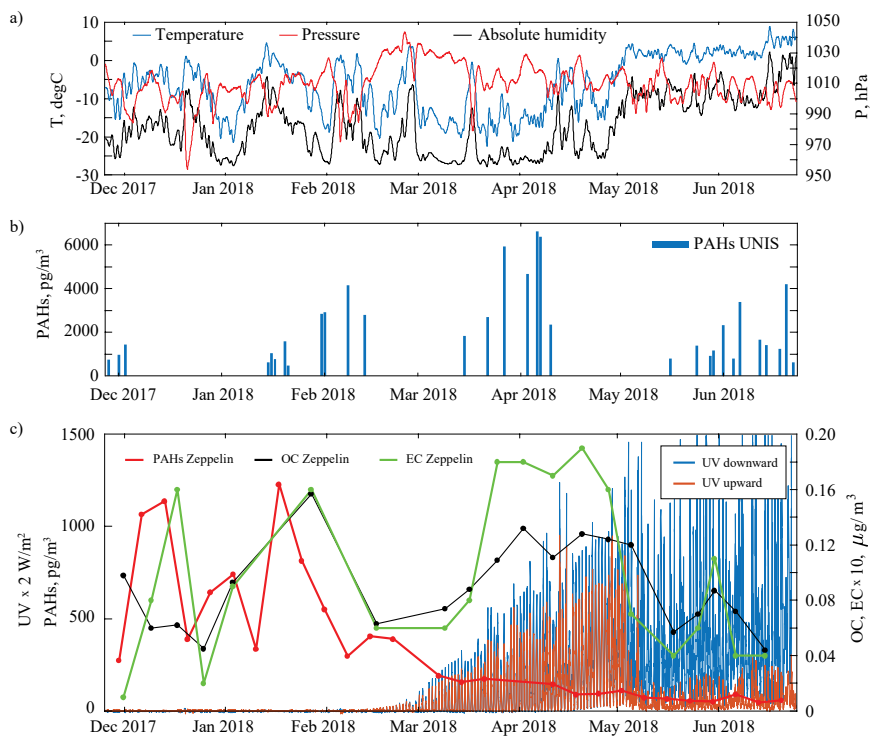
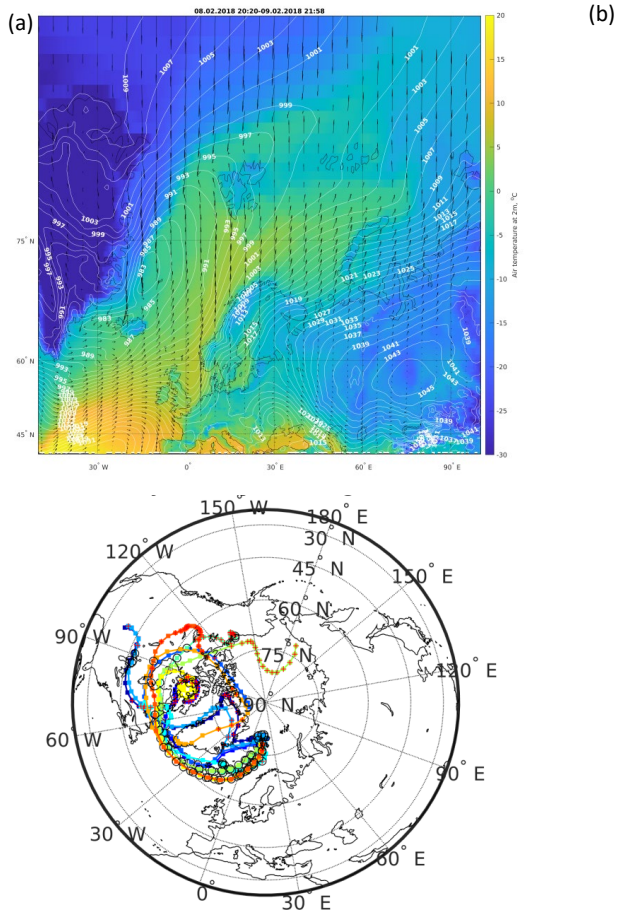


Figure S3. Seasonal trends of weather parameters (a) and Σ_{20} PAH* total (G+P) concentrations measured in Svalbard air in 2018 at UNIS (Longyearbyen; urban) (b) and Zeppelin (Ny-Ålesund; background) (c) stations.



*Summed compounds are 1-MeNap, 2-MeNap, Ace, Flu, Phe, Ant, Flt, Pyr, BaAnt, Chry, Ret, BePyr, BjFlt, BbFlt, BkFlt, BaPyr, DBAnt, BghiP, IPyr, Cor

Figure S4. Synoptic map (a) and 10-day backward trajectories (b) illustrating frequent winter events of the Atlantic warm air masses transport to the Arctic.



Note: An ambient temperature increase of 13.3 °C was registered during the 24 h of air sampling in Longyearbyen started on the 8th of February 2018 (the example on the plots).

Figure S5. Wind rose diagrams typical for the P1-P3 cold (a) and P4 summer (b-c) periods.

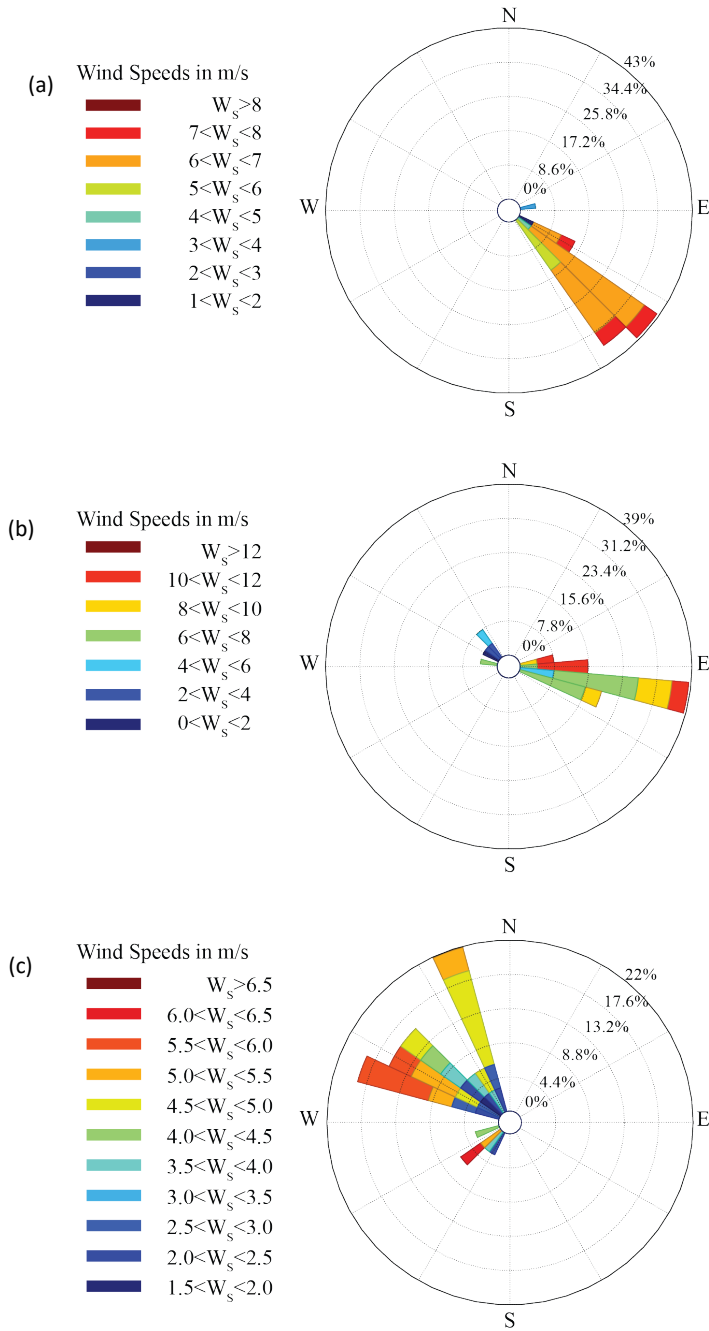


Figure S6. Correlations of the OC/EC ratio and the sum gross tonnage (dimensionless) of vessels arriving and departing the harbour of Longyearbyen during sampling hours on summer days when the UNIS station was downwind the harbour (P4; n=7).

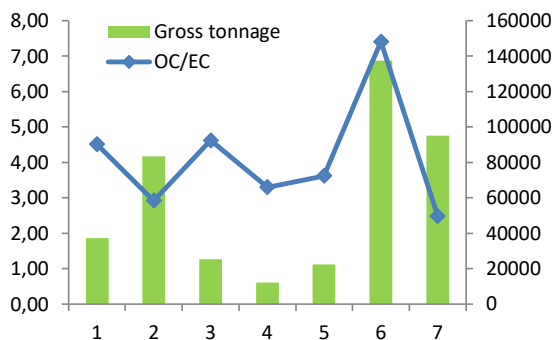


Figure S7. Comparison of the P1-P3 cold period profiles of PAHs based on the snowmobile traffic intensity.

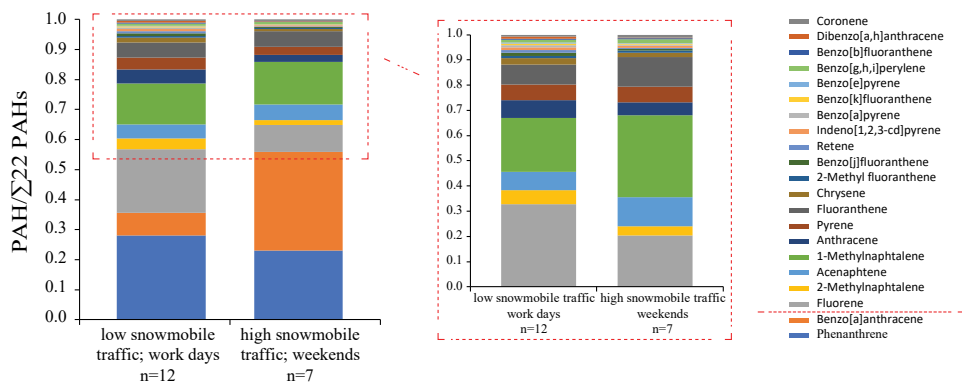
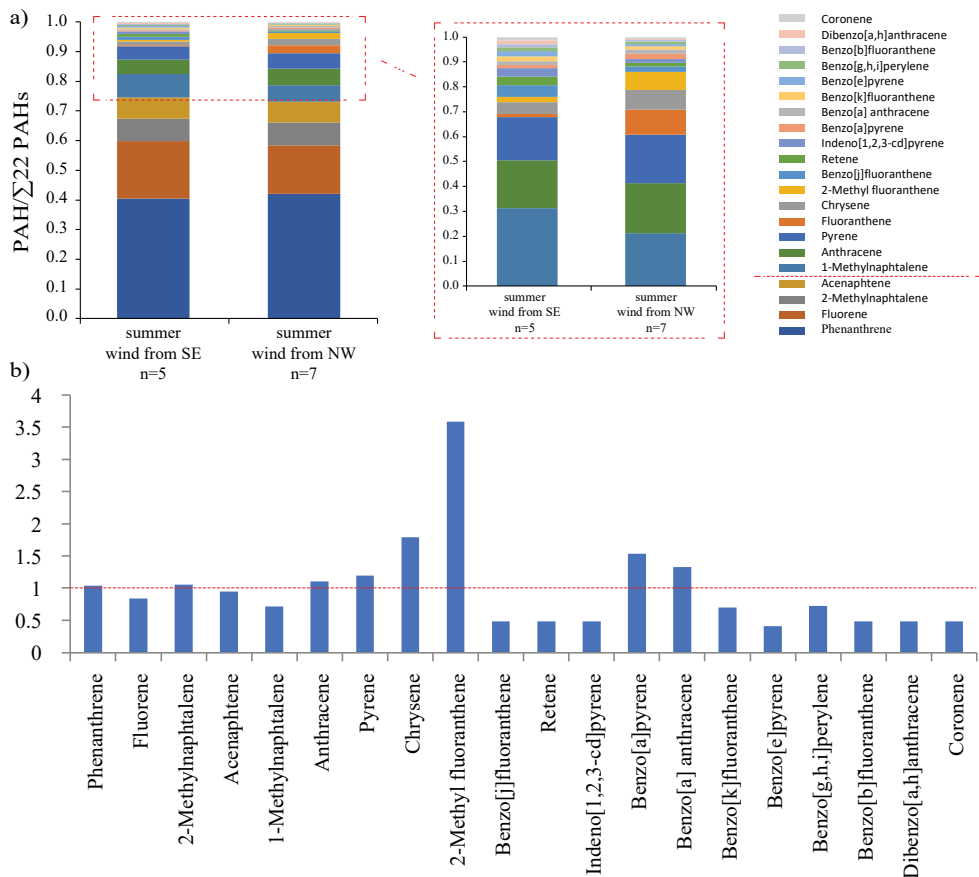
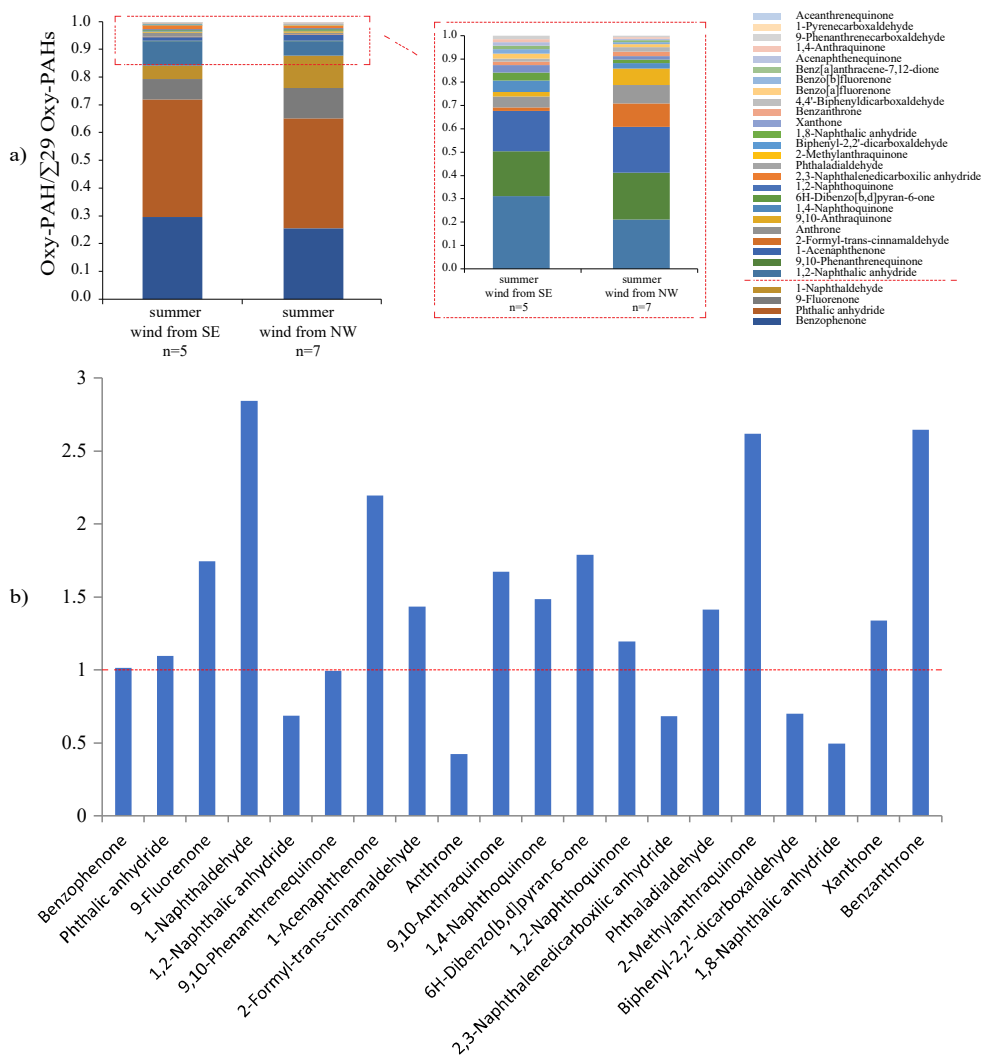


Figure S8. Comparison of the P4 summer profiles of PAHs based on wind direction (a) and the chemical profile proportion increase rates of PAHs (b) as result of ship traffic (NW wind) in the harbour of Longyearbyen.



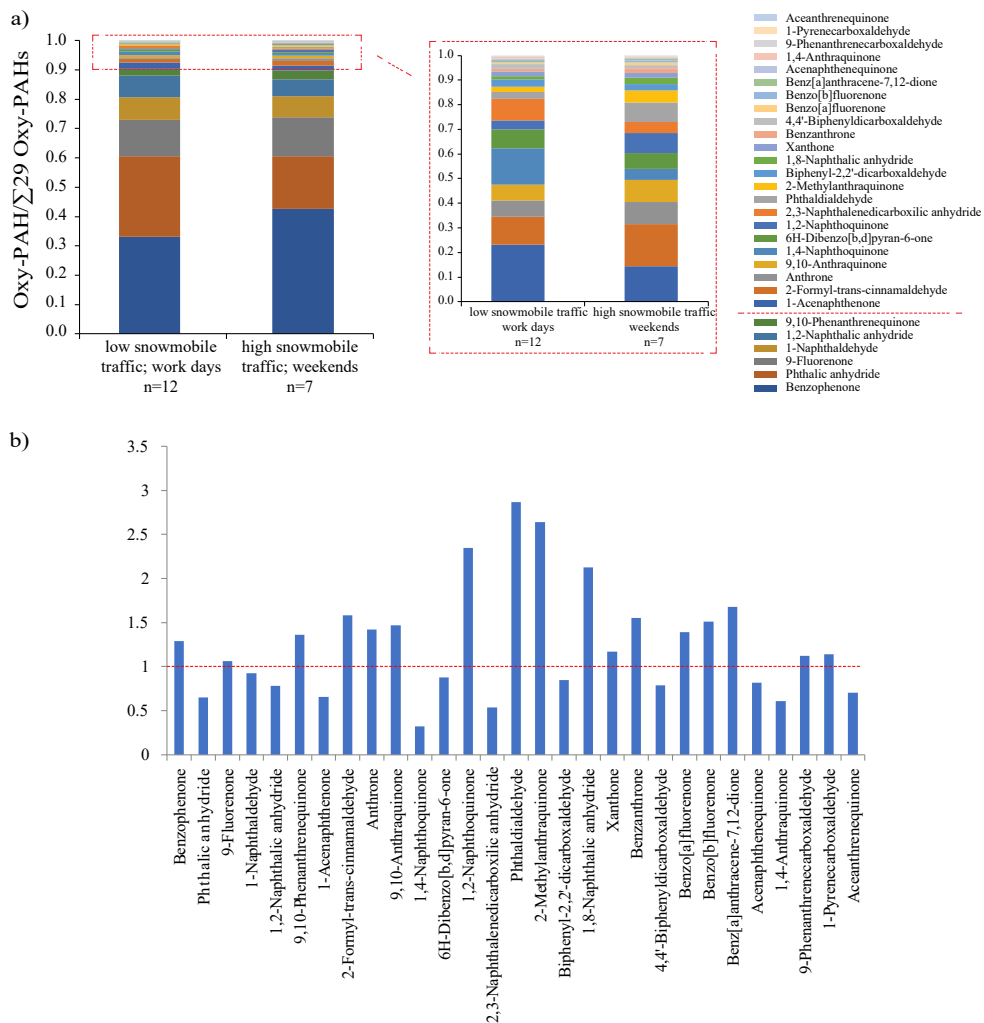
Note: The proportion increase rate of Flt (7.5) is not included to scale the picture. Rate >1 indicates enhanced rate of increase of a compound proportion in the total PAHs profile on the days with NW wind from the harbour

Figure S9. Comparison of the P4 summer profiles of oxy-PAHs based on wind direction (a) and the chemical profile proportion increase rates of selected oxy-PAHs (with concentration > 10 pg/m³) (b) as result of ship traffic (NW wind) in the harbour of Longyearbyen.



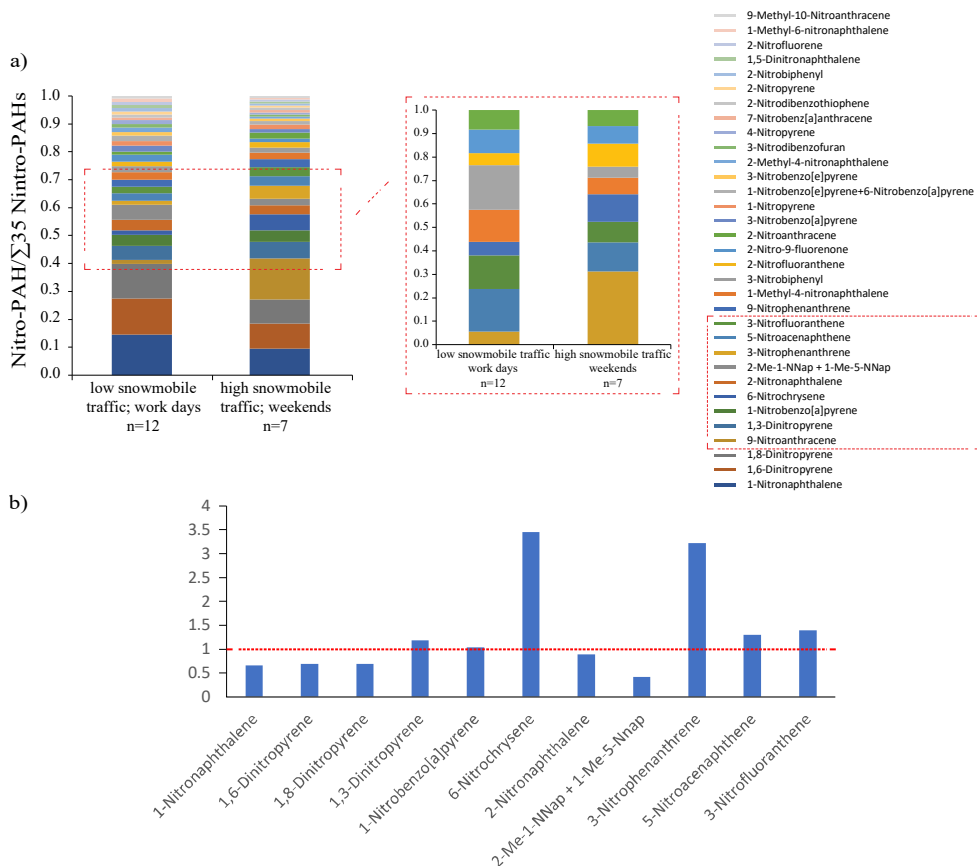
Note: Rate >1 indicates enhanced rate of increase of a compound proportion in the total oxy-PAHs profile on the days with NW wind from the harbour

Figure S10. Comparison of the cold period P1-P3 profiles of oxy-PAHs based on snowmobile traffic intensity (a) and the chemical profile proportion increase rates of selected oxy-PAHs (with concentration > 10 pg/m3) (b).



Note: Rate >1 indicates enhanced rate of increase of a compound proportion in the total oxy-PAHs profile compared to the days with low or no snowmobiles driving.

Figure S11. Comparison of the cold period P1-P3 profiles of nitro-PAHs based on the snowmobile traffic intensity (a) and the chemical profile proportion increase rates of selected nitro-PAHs (b).



Note: The proportion increase rate of 9-nitroanthracene (9.6) is not included to scale the picture. Rate >1 indicates enhanced rate of increase of a compound proportion in the total nitro-PAHs profile compared to the days with low or no snowmobiles driving

Paper III

Insights the physicochemical processes of atmospheric polycyclic aromatic hydrocarbons (PAHs) and their derivatives under polar conditions in Svalbard.

Drotikova, T., Kallenborn, R., and Albinet A.

In preparation.

Insights the physicochemical processes of atmospheric polycyclic aromatic hydrocarbons (PAHs) and their derivatives under polar conditions in Svalbard

Tatiana Drotikova^{1,2}, Roland Kallenborn^{1,2}, and Alexandre Albinet³

¹Department of Arctic Technology, University Centre in Svalbard (UNIS), Longyearbyen, 9171, Norway

²Faculty of Chemistry, Biotechnology and Food Sciences, Norwegian University of Life Sciences (NMBU), Ås, 1432, Norway

³French National Institute for Industrial Environment and Risks (Ineris), Verneuil en Halatte, 60550, France

Abstract. Arctic air contamination by PACs was investigated on the local scale of the largest Arctic settlement of Longyearbyen in Svalbard (Norwegian Arctic). Gaseous and particulate air samples were collected at three different locations from November 2017 until July 2018. Target compounds included 22 polycyclic aromatic hydrocarbons (PAHs), 29 oxy-PAHs, and 35 nitro-PAHs. Results showed long-range atmospheric transport predominance in winter and significant contribution of local anthropogenic sources in spring and summer. Significant phase partitioning of number of PACs in response to ambient conditions change was observed. Secondary formation of oxy-PAHs under polar conditions in winter (polar night), spring (daylight), and summer (full polar day) was revealed.

1. Introduction

The Arctic is the main sensor of global climate change, a receptor for global pollution, and a driver for global climate system (Strong et al., 2020). Polycyclic aromatic hydrocarbons (PAHs) are ubiquitous pollutants and chemicals of emerging concern in the Arctic (AMAP, 2017). They primarily enter the atmosphere through incomplete combustion of fossil fuels and biomass (Ravindra et al., 2008). PAHs react with a number of atmospheric oxidants, most notably the hydroxyl radical, ozone, the nitrate radical, and nitrogen dioxide (Keyte et al., 2013). This leads to their transformation into more toxic oxygenated and nitrated PAH derivatives (oxy-PAHs and nitro-PAHs) (Idowu et al., 2019), which can also be present in primary emissions (Ravindra et al., 2008; Bandowe and Meusel, 2017). The recent studies in the European Arctic on Svalbard (74°-81° N, 10°-35° E), revealed high air pollution by PAHs, nitro- and oxy-PAHs (polycyclic aromatic compounds, PACs) transported from midlatitude Eurasian sources, as well as significant contribution of local fossil fuel combustion emissions in spring (snowmobiles) and summer (ships) (Drotikova et al., 2021; Drotikova et al., 2020; Dekhtyareva, 2019; Röhler et al., 2020).

Being a remote region with highly seasonal variations in ambient temperature, absolute humidity, solar radiation, surface conditions, and long-range atmospheric transport (LRAT), the Arctic is an exceptional natural laboratory to study atmospheric processes (Barrie and Platt, 1997; Simpson et al., 2007; Fu et al., 2009). Due to the axial tilt of the Earth and high latitude location, the Arctic is obscured from the sun during winter, when the region experiences polar night conditions. For the areas at latitudes above 75°N, the period of complete darkness (when the sun is more than 6° below horizon) lasts over two months. During this period, the Arctic atmosphere is an excellent night-time chemistry natural laboratory, substituted by reactants and reagents via their efficient delivery from remote sources, dictated by a seasonal LRAT mechanism and reduced photodegradation and wet scavenging (Stohl, 2006; AMAP, 2015). Stably stratified cold spring conditions coincide with polar sunrise, which triggers regional photochemistry and significantly increases the oxidation capacity of the Arctic troposphere, especially within a very shallow polar boundary layer (100-200 m; Mao et al., 2010; Drotikova et al., 2021), where snow chemistry plays an additional role (Abbatt et al., 2012; Grannas et al., 2007; Sumner et al., 2002; Mao et al., 2010; Zhou et al., 2001). Further in summer, a stagnant atmosphere, with minimal input of LRAT (Stohl, 2006), is greatly suitable for understanding local emissions evolution under continuous sunlit conditions and enhanced ocean-to-air exchange of heat, water vapour, and marine biogenic gases (Barrie and Platt, 1997).

The herein study was carried in Longyearbyen on Svalbard. The main objectives of the work were to understand the pathways and the main seasonal drivers of the PACs' atmospheric chemical transformation processes under polar winter, spring, and summer conditions. In addition, the difference of the background, rural, and urban seasonal concentrations of 86 PACs was studied, and the compounds' gas-to-particle repartitioning in response to meteorological conditions was evaluated.

2. Experimental

2.1 Sample collection

Atmospheric samples were collected in the vicinity of Longyearbyen town on Svalbard (78.22° N, 15.65° E; Fig. S1), the largest settlement and the administrative centre of Svalbard, with population about 2400 permanent residents (Statistics Norway, 2020) and high tourism activities (Statistics Norway, 2016). Sampling was performed in the period of November 2017 to July 2018, at three field sites (Fig. S2): the roof of the University Centre in Svalbard (UNIS,

25 m asl, urban location, 250 m from the fjord), the former northern lights observatory in Adventdalen valley (Adventdalen, 10 m asl, rural location, 4.6 km upwind UNIS), and Svalbard satellite station on Platåberget mountain by the antenna №1 (Svalsat, 450 m asl, background altitudinal location, 6 km downwind UNIS). The prevailing wind direction in Longyearbyen is from the southeast. In summer, it can temporarily change to northwesterly. Sampling was not simultaneous unless specified. Due to high avalanche danger, sampling at Svalsat was not possible to perform in spring.

For the Longyearbyen latitude (Fig. S3), the period of 24 h of complete darkness lasts for 2.5 months from the middle of November until the end of January (polar night, winter; P1), followed by the about 3 weeks long twilight period, when the sun become less than 6° below the horizon (twilight, winter; P2). Sun returns to the town by the mid of February and the light conditions increase gradually until April (daylight, spring; P3), when the period of 5 months of midnight sun begins (polar day, summer; P4).

A high-volume air sampler (TISCH1000-BLXZ, TISCH Environmental Inc., USA) was used to collect the samples for 24 h at a flow rate giving a total sample volume of about 400 m³. Particulate phase compounds were trapped on quartz fiber filters (QFF; pre-burnt at 450 °C for 6 h; Ø = 103 mm; no binder; Munktell/Ahlstrom, Finland) and gaseous phase compounds were collected on polyurethane foams (PUF; Soxhlet pre-cleaned in toluene for 24 h followed by 24 h acetone wash; Ø = 65 mm; L = 100 mm; Klaus Ziemer GmbH, Germany). Meteorological data were recorded at the two local stations at different altitudes: Gruvefjellet (78°12' N 15°37' E; 464 m asl) and Adventdalen (78°12' N 15°49' E; 15 m asl).

A total of 59 samples (59 QFFs and 59 PUFs; Table S5) and 11 field blanks were collected. All samples were kept intact inside the sampling unit after collection. In order to reduce the risk of post-collection contamination, the unit was sealed in two plastic bags for transportation to the lab, where samples were removed from the unit, sealed with layers of aluminium foil, and stored airtight in two plastic bags. Samples were kept frozen at -20 °C until sent to the French National Institute for Industrial Environment and Risks (Ineris, France), by express delivery using cool, insulated containers and then stored at -10 °C until analysis.

2.2 Sample preparation and analysis

The analytical protocols used has been published previously (Drotikova et al., 2021; Tomaz et al., 2016; Albinet et al., 2006; Albinet et al., 2013; Albinet et al., 2014; Srivastava et al., 2018a). In brief, a known amount of several surrogates (6-methylchrysene, 3 deuterated oxy-PAHs, and 7 deuterated nitro-PAHs) were added to the samples prior to extraction. Gaseous

phase PACs were extracted from PUF samples with acetone (two cycles: 80 °C, 100 bars, 5 min heat time, 15 min static time) using pressurized liquid extraction (ASE 350, Thermo Scientific, USA). Sample extracts were then reduced under a nitrogen stream to a volume of about 200 µL (Turbovap II, Zymark, USA) and adjusted to 1 mL with acetonitrile. A fraction (900 µl) was dedicated to the PAH analyses, while another (100 µl) was used for nitro- and oxy-PAHs quantification. Particulate phase PACs were extracted from a 47 mm diameter QFF sample punch applying a QuEChERS-like (Quick Easy Cheap Effective Rugged and Safe) method with 7 ml acetonitrile (Albinet et al., 2013; Albinet et al., 2014). The 2 and 3.5 ml of supernatant were then reduced to near dryness under a nitrogen stream and reconstituted into 500 µl and 100 µl of acetonitrile for PAH and nitro-/oxy-PAH analyses, respectively. The PUF and QFF extracts dedicated to the analysis of oxy- and nitro-PAHs were purified by solid phase extraction before analysis: first with neutral alumina (Al₂O₃, 500 mg, Macherey Nagel, Germany) and then with unmodified silica gel (SiOH, 500 mg, Macherey Nagel, Germany). All the extract volumes were then reduced to near dryness under a gentle nitrogen stream, reconstituted with acetonitrile (100 µl for PUF and 50 µl for QFF), and spiked with a known amount of 2 labelled internal standards prior to further analysis.

The 22 PAHs were analyzed by UHPLC-Fluorescence (Dionex Ultimate 3000, Thermo Scientific, USA) using a C18 UPLC column (Zorbax Eclipse PAH, 2.1 mm × 150 mm × 1.8 µm, Agilent, USA; 3 µl injected). GC-NICI/MS under SIM mode (Agilent 7890A GC coupled to 5975C MS, Agilent Technologies, USA) was used to quantify 35 nitro-PAHs and 29 oxy-PAHs. The compounds were separated on a Rxi-PAH column (30 m × 250 µm × 0.10 µm, Restek, USA). 1 µl of the purified extracts has been injected into the pulsed splitless mode for analysis. In addition, elemental carbon (EC) and organic carbon (OC) were measured on dedicated 1.5 cm² filter punches using a Sunset lab analyzer according to the EUSAAR-2 thermal protocol (Cavalli et al., 2010; CEN, 2017).

2.3 Quality assurance

In order to evaluate the background contamination related to sample collection and analysis, PUF and QFF field (n = 8) and laboratory blanks (n = 6) were performed. Low contamination of laboratory blanks was confirmed. Field blank contamination higher than 30 % of the seasonal average concentrations was determined for biphenyl-2,2'-dicarboxaldehyde, 2,3-naphthalenedicarboxylic anhydride, and 1,8-naphthalic anhydride for the gaseous phase. These compounds, in this phase, were excluded from the results. No blank correction was performed for the concentration calculations. Samples showing PAC concentrations below

limit of quantification (LOQ) were replaced by LOQ/2 for further calculations. The instrumental LOQ was defined as the lowest concentration of the compound that can be determined for a signal to noise ratio $S/N = 10$. This evaluation was performed using the lowest concentrated standard solution.

Acceptable PAC surrogate recoveries were obtained and ranged between 53–120 %. Quality of the PAH analyses was assessed following the European Committee for Standardization (CEN) standard procedures EN 15549:2008 and TS 16645:2014 (CEN, 2008, 2014). In addition, Ineris routinely participates in national and European PAH analytical inter-comparison biannual exercises. The last exercise results were in good agreement with reference values, including those for the QuEChERS extraction (Verlhac et al., 2015; Bailleul and Albinet, 2018).

The analytical procedures were also validated ($n = 3$) using NIST standard reference material (SRM 1649b, urban dust). The obtained results (earlier reported in Table S8 in Drotikova et al., 2021) were in good agreement with NIST certified, reference, or indicative PAC values and those previously reported in the literature for oxy- and nitro-PAHs (Albinet et al., 2013; Albinet et al., 2014) as reference concentration values in SRM do not exist for several compounds.

3. Results and discussion

3.1 Concentration levels of PACs

Individual total (gaseous and particulate; G+P) PAC concentrations and proportions in particulate phase (%PM), as well as OC and EC concentrations determined at urban (UNIS), rural (Adventdalen), and altitudinal background (Svalsat) sites are presented in Tables S1-S3, Tables S7-S9, Table S4, respectively, and Figures 1-2. The data are for the four defined periods based on weather and light conditions (Fig. S3): November to January (dark winter; P1), February (twilight winter; P2), March to April (day light spring; P3), and May to June (polar day summer; P4). The PAC seasonal concentrations measured at the urban site (UNIS) have been discussed in detail previously (Drotikova et al., 2021) and, thus, are not in the main focus herein.

Based on the seasonal sum concentrations basis, higher levels of primary species, PAHs and EC, as well as OC were determined at urban location, followed by the rural and altitudinal levels, highlighting notable contribution of local emissions in Longyearbyen (town, cars, snowmobiles, coal burning, ships). Predominance of primary emissions of oxy- and nitro-

PAHs were less obvious, as the sum concentrations were at comparable or even higher levels at the rural and altitudinal sites than at UNIS. In contrast to PAHs, which only degrade after they were emitted, the level of the derivatives can also be substituted by the secondary atmospheric processes during their LRAT or locally by photochemical oxidation of PAH primary emissions within the Arctic.

At background Arctic sites, the PAH levels peak in winter, decreasing throughout spring, with annual minimal levels during summers (Prevedouros et al., 2004; Singh et al., 2017; Yu et al., 2019; Fu et al., 2009). This seasonal trend in the polar atmosphere is mainly driven by LRAT seasonality (Klonecki, 2003; Stohl, 2006) and an increased photolysis and number of atmospheric oxidants with return of sun light in the Arctic (Barrie, 1996; Kawamura et al., 1995) during late winter and spring (P2-P3). Such PAH concentrations' annual trend was also observed at the Zeppelin background station in Svalbard in 2018 (Fig. S3 in Drotikova et al., 2021), though it was different at the three sites in Longyearbyen. Due to increased local emissions, the annual greatest concentrations of PACs, OC, and EC were found in late winter and spring (P2-P3) at urban and rural sites (no samples from Svalsat were taken during these periods) (Fig. 1). As expected, due to increased photolysis, the concentrations of PAHs and nitro-PAHs were lowest in summer ($P3 > P1 > P4$) except the UNIS location ($P3 > P2 > P4 > P1$), largely affected by the fresh harbour emissions (Drotikova et al., 2021). The summer concentrations of OC and EC at UNIS were significantly higher those in winter as well (Fig. 2), confirming the primary emissions influence. At Svalsat and Adventdalen, the OC and EC levels were 20-70% higher in winter than in summer ($P3 > P1 > P4$), though the EC summer concentrations at Svalsat were twice higher the winter levels ($P4 > P1$) suggesting local emissions contribution during summer, as LRAT is low (Klonecki, 2003). In contrast to PAHs and nitro-PAHs with minimal levels in summer (though not at the urban location), the summer sum concentrations of oxy-PAHs were marginally higher those in the polar night winter P1 period at all the sites ($P3 > P2 > P4 > P1$). As LRAT of PACs is very limited in summer (Drotikova et al., 2021), this observation suggests enhanced secondary production of oxy-PAHs or higher primary local emissions of oxy-PAHs during summer.

High air pollution in spring was caused by local snowmobile driving emissions, accumulated within a very shallow polar boundary layer (less than 200 m; Drotikova et al., 2021). Spring is the coldest season in the high Arctic and the period with less synoptic-scale disturbances for Svalbard than in winter (Wickström et al., 2020). During this period the polar air is stably stratified, vertical mixing is minimal, and thermal inversions are deep and persistent, preventing the fresh emissions dilution and its deposition. Spring snowmobile traffic is

equally high at UNIS and Adventdalen sites (Fig. S2). As the UNIS located downwind Adventdalen nearly all year round, 40-80 % higher sum concentrations of PAHs, nitro-PAHs, EC, and OC were measured at UNIS compared to the levels in the valley (Adventdalen; $\sum 22$ PAHs is 3452 ± 2637 pg/m³ and $\sum 35$ nitro-PAHs is 103 ± 21 pg/m³). The $\sum 29$ oxy-PAH spring concentrations at rural site were as high as at the urban (13317 ± 3179 pg/m³; P3) being at the comparable level as in the European air as has been indicated previously (Drotikova et al., 2021).

In winter, a small difference between the PAC concentrations at the three sites was observed. The $\sum 22$ PAHs winter concentrations were similar at the urban and rural locations (1016 ± 321 pg/m³), being only 16 % higher the background levels at Svalsat (897 ± 453 pg/m³). The EC and OC concentrations were also lowest at Svalsat. By comparison to the Zeppelin mountain background site (475 m asl, located in Ny-Ålesund, 115 km NW of Longyearbyen), the winter average $\sum 20$ PAHs concentrations measured were in good agreement for the same period and same compounds considered (Table S6). Such a small difference between the Svalsat and the Zeppelin stations, as well as with the other two local sites in Longyearbyen, implies the dominant role of lower latitude sources in Arctic air pollution during winter. This conclusion is also supported by the back-trajectory probability analysis for the Longyearbyen and Ny-Ålesund areas (Drotikova et al., 2021), as well as by the earlier research on the European Arctic air pollution (Stohl, 2006). Furthermore, a small difference was observed for the concentration levels of the PAH derivatives between the Longyearbyen sites, though the nitro- and oxy-PAHs were 10-20 % at the mountain. Higher levels at Svalsat rule out the primary sources' influence on the elevated levels and support the LRAT predominance. As the sampling was not simultaneous at the three sites, daily variabilities of LRAT inflow may explain the results fluctuations. To highlight, the winter highest $\sum 22$ PAH concentrations of about 1.8 ng/m³ were determined at UNIS and Svalsat in December 3-5th 2017 due to quick and efficient low-level transport from a source boundary layer of polluted air masses from central Russia and Siberia (Fig. S4).

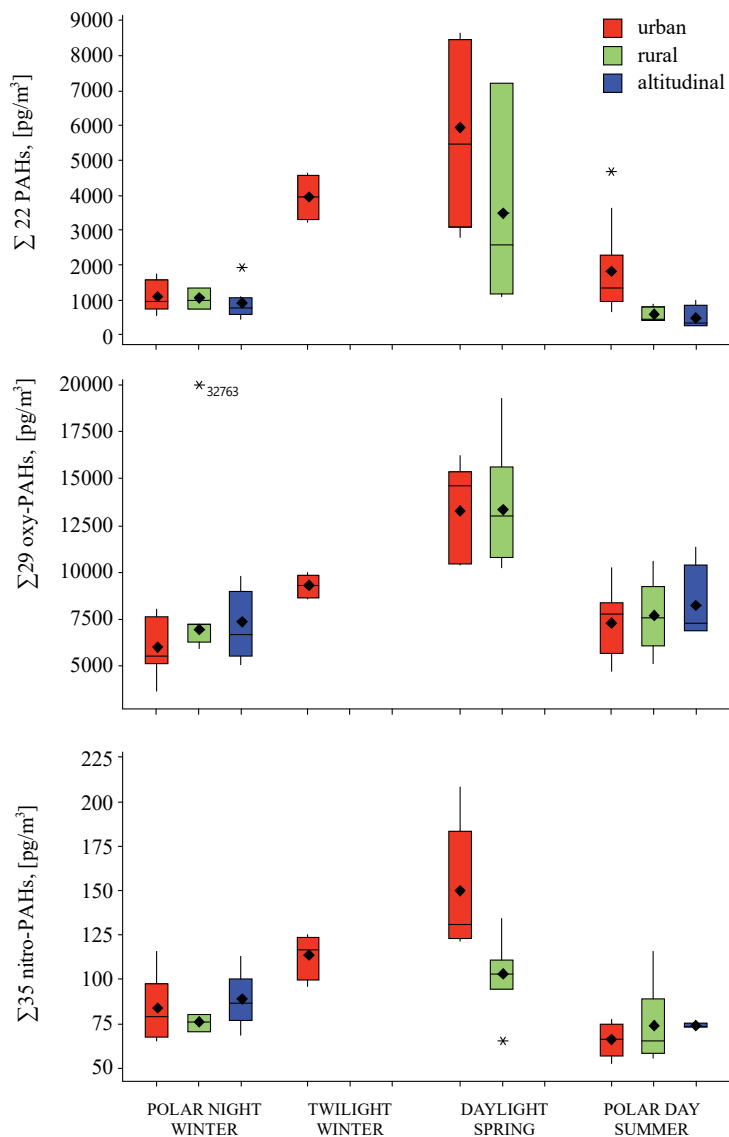


Figure 1. Box plots of sum seasonal total (G+P) concentrations (pg/m^3) of 22 PAHs, 29 oxy-PAHs, and 35 nitro-PAHs at the three sites in Longyearbyen. Data are for the November-January (P1), February (P2), March-April (P3), and May-July (P4) periods in 2017/2018. The boxes represent the 25th and 75th percentiles of the data. The lines in the boxes and diamond symbols represent the median and the mean, respectively. All the outliers beyond the whiskers are shown individually.

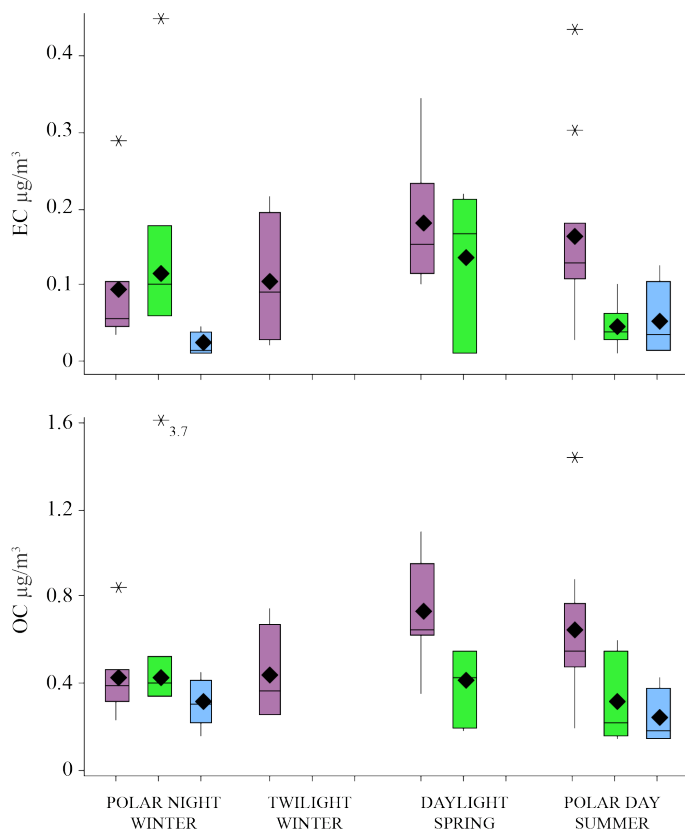


Figure 2. Box plots of seasonal concentrations ($\mu\text{g}/\text{m}^3$) of elemental carbon (EC) and organic carbon (OC) in the air samples from the three sites in Longyearbyen: urban (purple), rural (green), and background (blue).

Local emissions are of great importance in summer in the Arctic, when LRAT is limited (Drotikova et al., 2021; AMAP, 2015). After a snow melt, surface albedo decreases and warmed surface heats the air. Warm air rises, causing turbulence, and thus increasing vertical mixing of local plumes. Furthermore, wind direction is unstable in Longyearbyen area during summer (Drotikova et al., 2020; Drotikova et al., 2021). Due to channeling inside the fjord, the main summer directions are NW and SE, which are along with the three sampling sites, local coal-burning power plant, and the harbour (Fig. S2). Thereby, good pollutants dispersion can be expected in summer in the absence of precipitation events. Indeed, uniform distribution of nitro- and oxy-PAHs, EC, and OC between the three sites was observed, and the difference of the $\Sigma 22$ PAHs concentrations in Adventdalen and Svalsat did not exceed 20 % being higher

at the lower altitude site. However, a factor of 3 higher summer average $\Sigma 22$ PAHs concentrations were determined at UNIS, as well as the levels of OC and EC were twice to four times higher. This site is the closest to the harbour and thus substantially affected by the ship emissions. A factor of 4 higher concentrations of particulate phase PAHs were measured on the days, when UNIS was downwind the harbour (Drotikova et al., 2021). Furthermore, the $\Sigma 20$ PAHs concentrations at Svalsat were on average a factor of 4 higher the Svalbard background levels measured at Zeppelin during the same summer period (Table S6), and the difference was up to one order of magnitude, when several cruise boats were present in the harbour of Longyearbyen. Due to increased vertical mixing, buoyant exhaust from large ships equipped with high smokestacks can likely reach the Svalsat sampling site on the mountain plateau. Gaseous phase compounds, Flu (41 pg/m^3) and Phe (99 pg/m^3), were the most abundant in the air samples from Svalsat, which might indicate the coal power plant emissions contribution, as Flu and Phe are the main PAHs determined in the plant exhaust samples (Drotikova et al., 2020).

Local meteorological events can induce strong pollution episodes. To highlight, severe air pollution in Longyearbyen was caused by stormy conditions at the end of November 2017 (Fig. S5), when large amount of local ground dust particles was suspended in the air due to negligible snow cover. It resulted in extreme (a factor of 5 higher the seasonal mean) $\Sigma 29$ oxy-PAH concentrations of about 33 ng/m^3 at Adventdalen, which are twice higher the average urban winter levels of oxy-PAHs in central Europe (Tomaz et al., 2016; same compounds considered). The concentrations of EC and OC were an order of magnitude higher the seasonal mean (P1), and the PAH levels were found elevated too. Such dusty events are frequent in Svalbard in autumn and early winter due to sparse snow cover and dynamical processes in the Arctic atmosphere: global-scale winds bring pollution from remote sources, which mix with local Arctic dust lifted by strong winds.

3.2 Phase distribution of PACs

Many PACs are semi-volatile compounds repartitioning between gaseous and particulate phases in response to changing meteorological conditions. It plays a crucial role in their lifetimes and environmental fate as each phase removal efficiency from air differs. Percentage of PAC mass determined in particulate phase (%PM) during the cold and warm periods are given in Table S7-S9. Statistically reliable evaluation of %PM for many nitro-PAHs was not

possible due to high number of concentration values below method quantification limit. Thus, they were not considered for further discussion.

During the sampling campaign from the end of November until beginning of July the air temperatures ranged from -18 °C and +6 °C (dT is 24 °C) being -9 °C and +3 °C as average for the cold (P1-P3) and warm (P4) periods, respectively. Compared to the earlier reported data for midlatitude European winters (Tomaz et al., 2016; Nežiková et al., 2020), notably higher %PM was found for several semi-volatile PACs including Flt, PhtA, 1-NapA, 2-FCinA, 1-AceO, 9-FluO, 2,2-BiphA, and Xan. Up to 30% repartitioning between phases was determined for these compounds. Cold ambient conditions favor condensation of semi-volatile compounds to particles. Due to increased solar insolation and large areas of open ocean available after sea ice melt, the mass of water vapour in the air (specific humidity) increased by a factor of 3 in summer, which may affect phase distribution of water-soluble PACs (Hu et al., 2019; Shahpoury et al., 2018). Furthermore, though days with precipitation events were avoided for samples' collection, fog and drizzle are frequent in summer in the high Arctic with different scavenging rates for the gaseous and particulate phases. Statistically significant (Spearman correlation, $n=57$, $p < 0.05$) negative correlations of %PM with ambient temperature and absolute humidity were confirmed for most of these compounds (except Flt, 2-FCinA, and Xan), reflecting their repartitioning to a particulate phase at colder conditions and migration to a vapor phase at warmer and wetter Arctic conditions in summer. Fresh pollution plumes (local or LRAT) of Flt, 2-FCinA, and Xan and their rates' variabilities might have been responsible for the different outcome.

To be considered, the %PM of LMW PACs with molecular mass below 210 g/mol (Biph-2,2-A; > 60 % in gaseous phase in summer) were in agreement with the literature data for temperate climate, meaning their prevailing presence in gas phase and thus high tendency to be re-volatilized from polluted surfaces like ocean, snow, ice, and soil. It is of particular importance for the Arctic due to its quick warming (Yu et al., 2019; Muir and Galarnau, 2021).

3.3 Evidence of secondary formation processes

In order to get insights atmospheric photooxidation processes of PACs, seasonal evolution of the product/parent PAC ratios based on total individual concentrations has been investigated for all the three sampling sites. The results obtained are discussed below separately and combined with literature knowledge, OC/EC ratio, and meteorological parameters (ambient

temperature, humidity, precipitation, UV radiation, wind direction, boundary layer height, atmospheric stratification) in order to highlight specific origin or reactivity (Alam et al., 2014; Nalin et al., 2016; Tomaz et al., 2017).

3.3.1 Polar night winter season/nighttime transformation

As many PAH derivatives can also be primary emitted, the background site (Svalsat) data with no direct emission sources provides strong evidence on the secondary process to appear. The OC/EC ratio is a suitable tracer for evaluation of origin of carbonaceous matter in atmosphere (Srivastava et al., 2018b; Wu and Yu, 2016; Pio et al., 2011). While EC has only primary origin from carbon fuel-based combustion processes, OC can also be secondary formed. Thus, high winter OC/EC ratio values at Svalsat (24.3 as median for P1; Table S4) reveal great potential of atmospheric formation processes during a polar night.

Permanent nighttime conditions prevent photochemistry. In many environments the nitrate radical is the dominant nocturnal oxidant (standard electrode potential $E^0 = 2.3$ V; Ma et al., 2018) and may initiate the night-time removal of PACs from atmosphere (Keyte et al., 2013). However, NO_2 (the main precursor of NO_3 radical) (Brown and Stutz, 2012) values are very low in the Arctic (unless fresh local emissions), and nitrogen oxides are primarily present in stable reservoir forms like N_2O_5 , peroxyacetyl nitrate (PAN), HNO_3 , and others (Solberg et al., 1997; AMAP, 2015; Björkman et al., 2013). Thermal and photolytic decompositions of the reservoir species are reduced under low temperature dark conditions (Brown and Stutz, 2012; Thompson et al., 2015; Simpson et al., 2007), thus NO_3 radical production is likely weak during the permanent nighttime period (Solberg et al., 1997; Brown et al., 2011). Gas and heterogeneous reactions of PAHs with N_2O_5 may occur resulting into nitro-PAHs (Kamens et al., 1990; Zielinska et al., 1989; Arey et al., 1989). The major loss pathways for N_2O_5 are heterogeneous hydrolysis, dry deposition, and heterogeneous reactions with chlorine (Brown and Stutz, 2012; McNamara et al., 2019; Huff et al., 2011). In the polar night troposphere, N_2O_5 is at the level of a few tens of pptv (Solberg et al., 1997; Huff et al., 2011), and thus was considered as of negligible importance. Furthermore, investigation of the ratios of nitro-product/parent PAH did not show a clear evidence of the night-time formation of nitro-PAHs under polar conditions. Thereby, it was presumed that the chemistry was mainly driven by ozone ($E^0 = 2.08$ V; Vione et al., 2004) during the P1 period.

Ozone is a well-known secondary pollutant, which is photochemically produced from volatile hydrocarbons and nitrogen oxides at mid-latitudes and transported to the Arctic lower

troposphere during winter, when long-range atmospheric transport to the region is enhanced (AMAP, 2016). Background concentrations of surface O₃ in the northern hemisphere are in the range 35–40 ppbv increasing with altitude due to the increasing influence of the stratosphere (Bottenheim et al., 2002; Fioletov, 2008; Brown and Stutz, 2012; Hirdman et al., 2010), and the concentrations are higher at the polluted source area. Low-altitude transport of pollution from northern Eurasia to the Arctic is on the time scale of 10 to 15 days, wherein time in darkness is about 10 days (for the lowest 100 m air) (Stohl, 2006) with no photochemical loss of ozone. This is a long time of PAHs' exposure to a nighttime ozone chemistry during LRAT and locally within the Arctic, which may cause their transformation into ring-opened (anhydrides, aldehydes) and ring-retaining (ketones, quinones) oxygenated derivatives (Keyte et al., 2013; Reisen and Arey, 2002; Riva et al., 2016).

The observed ratios of 1,4-NapQ/Nap, PhtAn/2-MeNap, 1-NapA/1-MeNap, BaAnt-7,12/BaAnt, and 9-PheA/Pyr were notably higher in winter at Svalsat and also at the other two locations (Fig. 3 & Fig. S6), suggesting nighttime formation of these compounds, most likely via direct reaction with ozone. Reaction of PAHs with ozone is enhanced on particles in comparison with reactions in the gas phase (Keyte et al., 2013). Experimental studies have reported high loss of BaAnt and Pyr under exposure to O₃ (Ringuet et al., 2012; Jariyasopit et al., 2014) and 1,4-NapQ, PhtAn, 1-NapA, 9-PheA, and BaAnt-7,12 were found among products of ozonation of PAHs (Reisen and Arey, 2002; Riva et al., 2016; Kramer et al., 2019; Perraudin et al., 2007; Rindone et al., 2010; Cochran et al., 2016). Furthermore, BaAnt-7,12 was confirmed to be exclusively formed by ozonation of BaAnt unlike by the reaction with OH radicals (Ringuet et al., 2012).

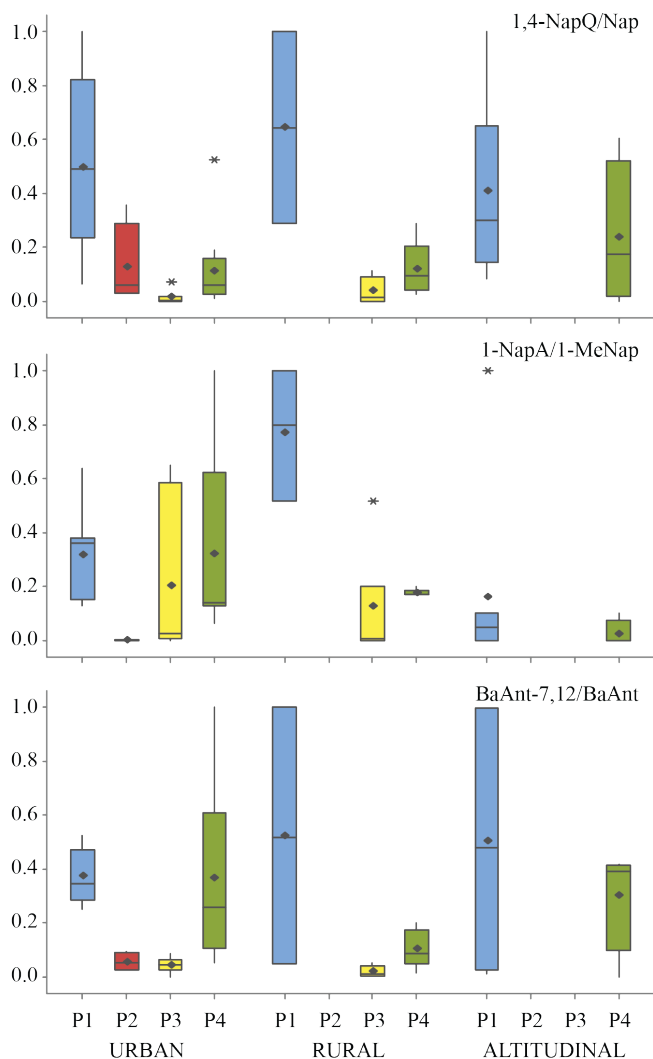


Figure 3. Seasonal evolution of product to reactant concentration ratios at three sites indicating PACs oxidation during polar night in winter (P1).

3.3.2 Day-light spring season/effect of polar sunrise

With return of sunlight (P3), photochemical reactions modify chemical composition of the atmosphere and induce snow chemistry. Due to ubiquitous presence of saline surfaces, such as coastal snowpack, sea ice surfaces, and sea salt aerosol (Abbatt et al., 2012), the Arctic region is indeed a rich source of atmospheric reactive halogen species (Monks, 2005; AMAP, 2016; Zhao et al., 2016; Sihler et al., 2012; Begoin et al., 2010). Up to 400 pptv of molecular chlorine concentrations were systematically measured at Barrow, Alaska (71.30°N,

156.77°W) (Liao et al., 2014). The spring time-integrated concentrations of Br atoms up to 10^{14} cm⁻³ s and molecular chlorine up to 10^9 cm⁻³ s, also in the Arctic Alaska, were reported by Hornbrook et al. (2016), which are up to 4 orders of magnitude higher the concentrations in midlatitude coastal areas. High concentrations of BrO, 1.3×10^{14} molecules/cm³ were also observed by (Simpson et al., 2018). The molecular halogens rapidly photolyze (lifetime \approx 10 min) (Liao et al., 2014; Liao et al., 2012). The steady state calculated concentrations of Cl and Br atoms were in the range of 10^5 and 10^9 atoms/cm³, respectively (Hornbrook et al., 2016). In such conditions, despite of O₃ formation from precursors accumulated in Arctic lower and middle troposphere during winter (AMAP, 2016), active halogen photochemistry causes significant titration of ozone with frequent near zero surface O₃ concentrations, which may last over several days (Thompson et al., 2015). Thereby, a polar sunrise brought a large seasonal shift in the atmospheric chemistry between winter nocturnal oxidation pathways (likely controlled by ozone) and the halogen-dominated spring photochemistry (Simpson et al., 2007; Solberg et al., 1996). It significantly increased the oxidative capacity of polar boundary layer (Simpson et al., 2007; Hornbrook et al., 2016; Peterson et al., 2015; Simpson et al., 2017; Thompson et al., 2015) and thus altered lifetime of organic species, such as PAHs, and changed their fates in environment.

While bromine and iodine atoms are primarily responsible for ozone depletion (Simpson et al., 2015; Strong et al., 2020; Thompson et al., 2015), large chemical flux of carbonyl compounds as oxidation products of extensive chlorine-atom processing of numerous saturated and unsaturated organics (including aromatic) is widely reported (Grannas et al., 2002; Simpson et al., 2007; Hornbrook et al., 2016; Thompson et al., 2015). Dang and He (2016) highlighted that the Cl addition reactions with PAHs are highly exothermic with no potential barriers, which indicate that they can occur readily in the atmosphere and several studies reported photochemical reactions as major generation mechanism of atmospheric halogenated PAHs (Vuong et al., 2020a; Ohura et al., 2005; Vuong et al., 2020b). For example, the calculated rate constant of an adduct formation with Cl is a factor of 3 higher than with OH for Ace and Acy and the easier formation of NAnt and NPy_r via Cl-initiated mechanism was concluded (Dang and He, 2016).

The chlorine-initiated oxidation of PAHs in the atmosphere proceeds via H atom abstraction or Cl addition (adduct formed) reaction pathways followed by further reaction with available reactive species such as Cl*, O₂, HO₂, NO_x (Riva et al., 2015; Dang and He, 2016). Laboratory test studies observed chlorinated PAH by-products, as well as ring-retaining (ketone, quinone, nitro-PAHs) and ring-opened products (aldehyde, anhydride) (Dang and

He, 2016; Riva et al., 2015). The later one reaction (ring-opening) is energetically more favorable pathway (Dang and He, 2016).

The snowpack has been shown to be an additional source of OH in the Arctic (Abbatt et al., 2019). During ozone depletion, the concentrations of Cl and Br atoms are usually few orders of magnitude higher than OH (Hornbrook et al., 2016) and halogen-atom chemistry is likely to dominate. However, if the OH and Cl/Br radical concentrations are equal, the OH-adduct of Ant, as an example, will be formed 20 times faster based on the reaction rate coefficients (Jin et al., 2020) and the OH and Cl chemistry may be along, potentially leading to faster oxidation of PAH similar to the enhanced transformation of ethane into acetaldehyde by the combined chemistry (Hornbrook et al., 2016).

Here, significantly greater ratios of 9,10-AntQ/Ant, ANO/Ant, Xan/Ant, 9-Fluo/Ant, and PhtA/2-FCinA were determined for the spring P3 period compared to the dark/twilight P1-P2 and summer P4 periods at urban and remote sites (Fig. 4 and Fig. S7; no samples were taken at the background site). As the polar chemistry differed largely between the seasons, this result suggested the secondary formation of 9,10-AntQ, ANO, Xan, 9-Fluo and PhtA from the reaction of the parent PAH Ant triggered by halogen radical attack under daylight polar conditions. Ant has sterically unhindered molecule and it is one of the most reactive PAHs (Keyte et al., 2013). In addition, the Cl atom-initiated atmospheric oxidation of Ant is highly exothermic, with no potential barrier process (Dang and He, 2016) and significant degradation of Ant was revealed during a simulated tidal flat conditions experiment on photochemical halogenation of PAHs (Sankoda et al., 2013). Formation of 9,10-AntQ and ANO as products of chlorination of Ant has earlier been proposed by Jin et al. (2020). The same conclusions can be made for PhtA and 2-FCinA. The PhtA/2-FCinA ratio showed significant higher values during the P3 period. PhtA is reported in the literature as a second-generation product resulting from further oxidation of 2-FCinA (Chan et al., 2009; Tomaz et al., 2017), which is the main by-product from the OH-initiated oxidation of Nap (Qu et al., 2006; Keyte et al., 2013). Here, we showed that these compounds can be formed by halogen initiated reaction pathways. Under cold, very dry and ozone depleted spring Arctic conditions as observed during our study, halogen radical-initiated reactions probably played a dominant role in the atmospheric oxidation of PAHs. Simultaneous degradation of PAHs and increase of oxidation by-products (acids) in the high Canadian Arctic in spring have earlier been observed (Fu et al., 2009; Singh et al., 2017). The effect may have been significant as (due to continuous radiative surface cooling over several months and stabilized synoptic conditions) the BLH was minimal in spring (50-150 m), while local primary emissions from snowmobile driving

were high (Drotikova et al., 2021) and dispersion of pollutants was limited by suppressed vertical mixing of stably stratified air and strong thermal inversions. It should also be highlighted that the fresh snowmobile emissions contain large amount of NO_x (Vestreng et al., 2009), which is the key sink reactant for OH (Keyte et al., 2013) as well as a stimulator of halogen production in the Arctic (McNamara et al., 2019), increasing by that an influence of the halogen chemistry. N₂O₅, produced overnight, quickly reacts on chlorine-containing aerosols (McNamara et al., 2019; Brown and Stutz, 2012) and, thus, it is not available for direct reactions with PAHs.

Blowing saline snow and sea salt aerosol particles are responsible for a halogen chemistry inland, far from marine influence (Strong et al., 2020), however, the impact is presumed to be higher at coastal sites with greater seawater spray influence, sea salt aerosol concentrations, and halogens' release by marine organisms at low tide (Simpson et al., 2015). High spring ratios of BbFluo/Flu, DPone/Flu, DPone/9Fluo, DPone/Phen, 1,2-NapQ/Ant, ANO/9,10-AntQ were obtained at UNIS located 250 m from the fjord (no sea ice; 12 h tide period) (Fig. S8), while it was less evident at Adventadlen site located at 3.5 km distance from the sea (Fig. S2). These data strongly imply a higher exposure to halogens, as well as revealing secondary production of BbFluo, DPone, 1,2NapQ, and ANO under polar spring conditions and so halogen initiated reactions. All these compounds have been previously reported in the literature as by-products of the oxidation of PAHs and/or oxy-PAHs by OH and O₃ (Perraudin et al., 2007; Lee and Lane, 2009; Lee et al., 2012). DPone was also suggested as marker of PAH oxidation processes in the atmosphere (Tomaz et al., 2017).

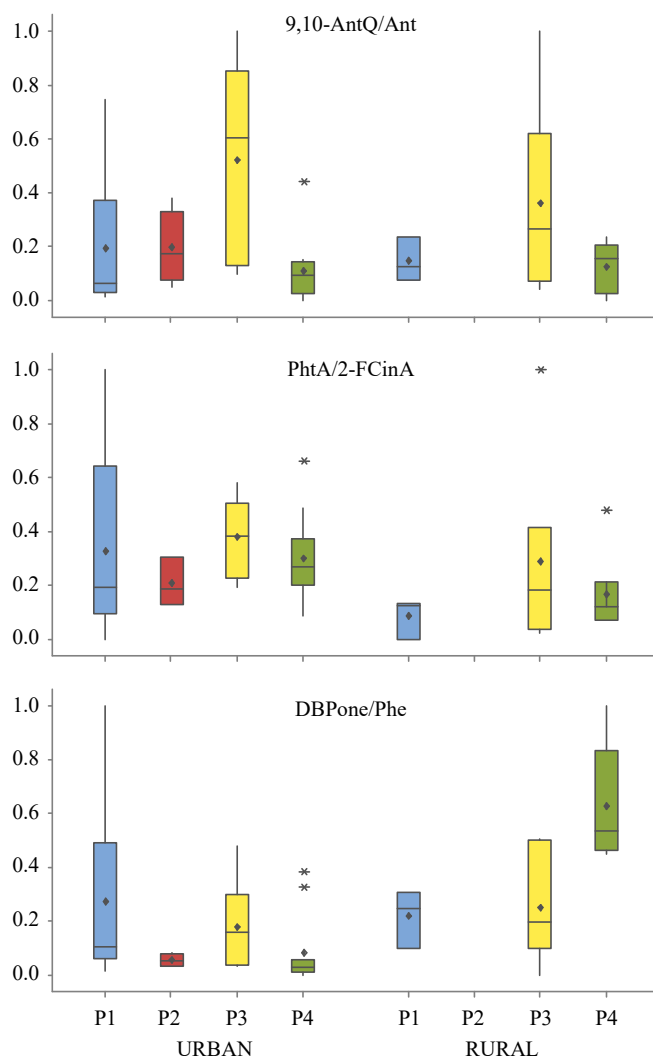


Figure 4. Seasonal evolution of product to reactant concentration ratios at two sites indicating PACs oxidation during spring (P3).

3.3.3 Polar day summer season/effect of increased humidity

A transition from the annual coldest P3 to the warmest P4 season, with a 15-20 °C average ambient temperature higher in summer, altered the main drivers of polar atmospheric chemistry.

In such season, snow and sea ice loss terminate the halogen chemistry, and thus the ozone destruction. Evaporation from large areas of open ocean and frequent drizzle precipitation increase air humidity (Drotikova et al., 2021). Higher air temperatures also magnify the

moisture content of the atmosphere. A 1 °C temperature increase leads to approximately 7% water vapor increase (Strong et al., 2020). Photolysis of ozone in the presence of water vapor produces OH radical, which peaks in concentration in summer (Solberg et al., 1996), while ozone levels become minimal and NO₃ radical (react directly with PAH; Keyte et al., 2013) is rapidly photolyzed (within few seconds) under a midnight sun conditions (Solberg et al., 1997; Monks and Hey, 2020) and so is not present in the atmosphere.

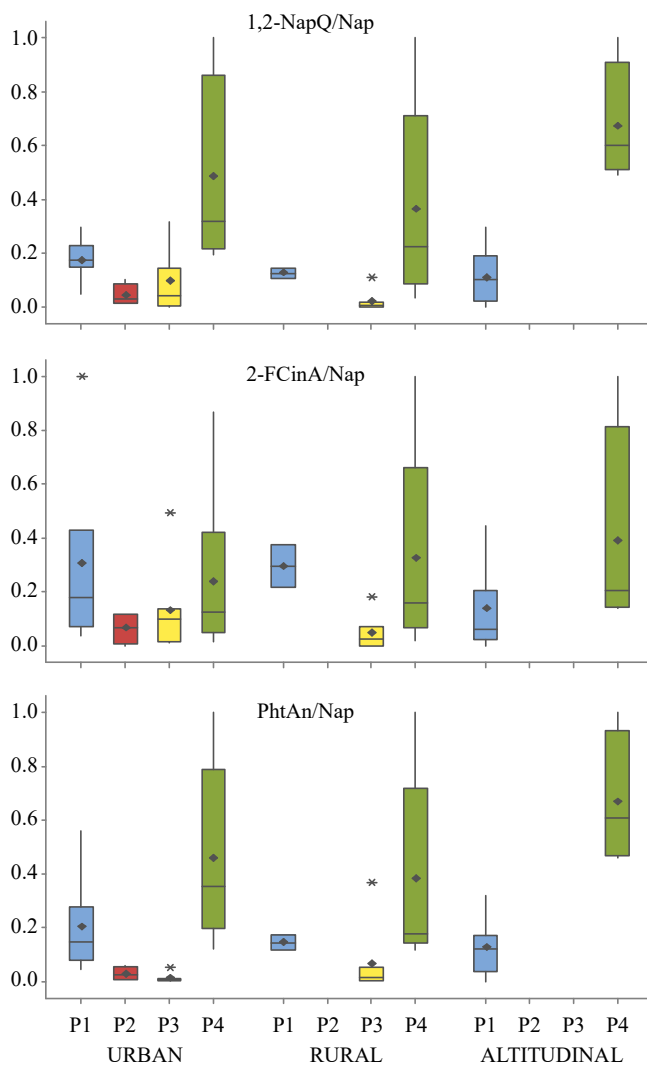


Figure 5. Seasonal evolution of product to reactant concentration ratios at three sites indicating PACs oxidation during summer (P4).

Thereby, the PACs' degradation in the polar atmosphere was during P4 period mainly controlled by photolysis and reaction with OH radicals ($E^0 = 2.59$ V; Vione et al., 2004), as well as wet scavenging. Warmer air temperatures favored re-partitioning of semi-volatile PACs into a gaseous phase, thus enhancing their loss via a reaction with OH radical. Furthermore, LRAT influence is suppressed in summer (Drotikova et al., 2021) and the air in the polar BLH was 13-17 days old (north of 75° N; Stohl, 2006). Thus, the summer air samples mainly represented local (within the Arctic) atmospheric processing of PACs. The ratios of 1,2-NapQ/Nap, 1-NapA/Nap, 2-FCinA/Nap, PhtAn/Nap, and PhtAn/PhtA increased significantly in this period, reflecting oxidation of Nap and a further atmospheric transformation of its secondary product PhtA, driven by reactions with OH radical. The 1,2-NapQ, 1-NapA, 2-FCinA, PhtAn, and PhtA may originate from both primary and secondary sources (Perraudin et al., 2007; Chan et al., 2009; Reisen and Arey, 2002; Lee and Lane, 2009; Lee et al., 2012; Oda et al., 2001; Jakober et al., 2007). As the ratios were also high at the rural and the background sites, located upwind and downwind UNIS (urban), it indeed showed the evidence of the secondary formation of these compounds, most likely as an additional source to their primary emissions. 1-NapA (428 pg/m^3 as summer average for the three sampling sites) was reported earlier to be emitted after a ship traffic at the local harbour (Drotikova et al., 2021).

4. Conclusions

Significantly higher PAC concentrations were detected in urban air of Longyearbyen, emphasizing notable contribution of local fossil fuel burning emissions. The PAC concentrations difference between the three sites in Longyearbyen and the Zeppelin station in Ny-Ålesund was low in winter, when LRAT was the primary source of pollution in the Arctic. Furthermore, the large seasonal difference in the Arctic ambient temperature (dT is 20°C) and humidity ($\times 3$) conditions enabled us to reveal significant phase repartitioning of several semi-volatile PACs, which controls their environmental persistence (LRAT potential) and atmospheric reactivity.

PAHs undergo various transformation processes during their intercontinental air transport to the North, as well as atmospheric chemistry within the Arctic plays a significant role in the PACs' pattern modification. In winter, the oxidation capacity of the polar troposphere is driven by ozone, as nitrogen oxides mainly exist in thermostable reservoir form (N_2O_5), and low concentrations are reported. Ozonation of PAHs under permanent night-time conditions (few months long) may result in their substantial oxidation. Secondary production of 1,4-

NapQ from Nap, PhtAn from 2-MeNap, 1-NapA from 1-MeNap, BaAnt-7,12 from BaAnt, and 9-PheA from Pyr during this period was concluded.

With return of sunlight in spring, the polar chemistry shifts towards the halogen dominant oxidation processes. For the first time, based on the ambient air samples, we show evidence of the halogen-initiated oxidation of PAHs (or perhaps a combination of OH and halogen chemistry). The oxidation of Ant into 9,10-AntQ, anthrone, Xan, 9-Fluo, 1,2-NapAn was evident at all the sampling sites in spring, as this compound is one of the most reactive PAH. Furthermore, the impact is presumed to be higher at coastal sites, and enhanced production of oxy-PAHs (BbFlu and DBPone) from Flu and Phe was also observed. Further oxidation of several oxy-PAHs caused generation of more oxidized species: DBPone from 9-Fluo, PhA from 2-FCinA, anthrone from 9,10-AntQ. Further studies are needed to confirm it, as well as to quantify the atmospheric concentrations of the halogenated PAHs formed along, as this new derivative group of PAHs recently became of significant concern due to their high toxicity (Vuong et al., 2020b). The effect of secondary production of the oxygenated and halogenated PAH derivatives in spring can be significant as the local PAH emissions are high, while their dilution is limited to a very low air volume (BLH is below 150 m) capped by an inversion layer.

Atmospheric degradation of the local summer PAC emissions was driven by photolysis and OH radical chemistry, as ozone and nitrogen oxides are photolyzed (full polar day conditions) and can also be hydrolyzed. Secondary formation of 1,2-NapQ, 1-NapA, 2-FCinA, and PhtAn from Nap, as well as PhtAn from PhtA was determined at the three sampling sites.

The present study provides an extensive data set of the phase-separated seasonal concentrations of 22 PAH, 29 oxy-PAHs, 35 nitro-PAHs, OC, and EC, measured in the urban, rural, and altitudinal Arctic air. Our results demonstrate the great potential of the polar troposphere in the PACs' pattern transformation, which should be considered in modelling studies that aim to assess the extent and impacts of Arctic atmospheric contaminants. Further studies should aim to quantify toxic halogenated PAHs. Since nothing is known about these contaminants occurrence in the Arctic, non-target screening analysis of high-volume air samples (Röhler et al., 2020) would have been of great help for identifying target compounds to be quantified.

Acknowledgments. The authors gratefully acknowledge Kongsberg Svalbard satellite station (SvalSat) for collaboration and support in performing air sampling; Sebastian Sikora and Jessica Birkeland (UNIS) for on-site assistance; Valérie Minguet, Arnaud Papin, Ahmad El-

Masri, Faustina Fuvel, and Serguei Stavrovski (Ineris) for sample preparation and EC/OC and PAC analyses. They acknowledge the Norwegian Institute for Air Research (NILU) for the PAH concentrations data monitored at the Zeppelin (Svalbard) station. This research was financially supported by UNIS and the French Ministry of Environment.

References

Abbatt, J. P. D., Thomas, J. L., Abrahamsson, K., Boxe, C., Granfors, A., Jones, A. E., King, M. D., Saiz-Lopez, A., Shepson, P. B., Sodeau, J., Toohey, D. W., Toubin, C., von Glasow, R., Wren, S. N., and Yang, X.: Halogen activation via interactions with environmental ice and snow in the polar lower troposphere and other regions, *Atmos. Chem. Phys.*, 12, 6237-6271, <https://doi.org/10.5194/acp-12-6237-2012>, 2012.

Abbatt, J. P. D., Leaitch, W. R., Aliabadi, A. A., Bertram, A. K., Blanchet, J. P., Boivin-Rioux, A., Bozem, H., Burkart, J., Chang, R. Y. W., Charette, J., Chaubey, J. P., Christensen, R. J., Cirisan, A., Collins, D. B., Croft, B., Dionne, J., Evans, G. J., Fletcher, C. G., Galí, M., Ghahremaninezhad, R., Girard, E., Gong, W., Gosselin, M., Gourdal, M., Hanna, S. J., Hayashida, H., Herber, A. B., Hesaraki, S., Hoor, P., Huang, L., Hussherr, R., Irish, V. E., Keita, S. A., Kodros, J. K., Köllner, F., Kolonjari, F., Kunkel, D., Ladino, L. A., Law, K., Levasseur, M., Libois, Q., Liggio, J., Lizotte, M., Macdonald, K. M., Mahmood, R., Martin, R. V., Mason, R. H., Miller, L. A., Moravek, A., Mortenson, E., Mungall, E. L., Murphy, J. G., Namazi, M., Norman, A. L., O'Neill, N. T., Pierce, J. R., Russell, L. M., Schneider, J., Schulz, H., Sharma, S., Si, M., Staebler, R. M., Steiner, N. S., Thomas, J. L., von Salzen, K., Wentzell, J. J. B., Willis, M. D., Wentworth, G. R., Xu, J. W., and Yakobi-Hancock, J. D.: Overview paper: New insights into aerosol and climate in the Arctic, *Atmos. Chem. Phys.*, 19, 2527-2560, [10.5194/acp-19-2527-2019](https://doi.org/10.5194/acp-19-2527-2019), 2019.

Alam, M. S., Delgado-Saborit, J. M., Stark, C., and Harrison, R. M.: Investigating PAH relative reactivity using congener profiles, quinone measurements and back trajectories, *Atmos. Chem. Phys.*, 14, 2467-2477, <https://doi.org/10.5194/acp-14-2467-2014>, 2014.

Albinet, A., Leoz-Garziandia, E., Budzinski, H., and Villenave, E.: Simultaneous analysis of oxygenated and nitrated polycyclic aromatic hydrocarbons on standard reference material 1649a (urban dust) and on natural ambient air samples by gas chromatography–mass spectrometry with negative ion chemical ionisation, *J. Chromatogr. A*, 1121, 106-113, <https://doi.org/10.1016/j.chroma.2006.04.043>, 2006.

Albinet, A., Tomaz, S., and Lestremau, F.: A really quick easy cheap effective rugged and safe (QuEChERS) extraction procedure for the analysis of particle-bound PAHs in ambient air and emission samples, *Sci. Total Environ.*, 450-451, 31-38, <https://doi.org/10.1016/j.scitotenv.2013.01.068>, 2013.

Albinet, A., Nalin, F., Tomaz, S., Beaumont, J., and Lestremau, F.: A simple QuEChERS-like extraction approach for molecular chemical characterization of organic aerosols: application to nitrated and oxygenated PAH derivatives (NPAH and OPAH) quantified by GC–NICIMS, *Anal. Bioanal. Chem.*, 406, 3131-3148, <https://doi.org/10.1007/s00216-014-7760-5>, 2014.

AMAP: AMAP Assessment 2015: Black carbon and ozone as Arctic climate forcers, Arctic Monitoring and Assessment Programme (AMAP), Oslo, Norway, vii + 116 pp., 2015.

AMAP: AMAP Assessment 2015: Temporal trends in persistent organic pollutants in the Arctic, Arctic Monitoring and Assessment Programme (AMAP), Oslo, Norway, vi + 71 pp., 2016.

AMAP: AMAP Assessment 2016: Chemicals of Emerging Arctic Concern, Arctic Monitoring and Assessment Programme (AMAP), Oslo, Norway, xvi + 353 pp., 2017.

Arey, J., Zielinska, B., Atkinson, R., and Aschmann, S. M.: Nitroarene products from the gas-phase reactions of volatile polycyclic aromatic hydrocarbons with the OH radical and N₂O₅, *Int. J. Chem. Kinet.*, 21, 775-799, 1989.

Bailleul, S., and Albinet, A.: Interlaboratory comparison for the analysis of PAHs in ambient air (2018), LCSQA, <https://www.lcsqa.org/fr/rapport/interlaboratory-comparison-analysis-pah-ambient-air-2018>, 2018.

Bandowe, B. A. M., and Meusel, H.: Nitrated polycyclic aromatic hydrocarbons (nitro-PAHs) in the environment – A review, *Sci. Total Environ.*, 581-582, 237-257, <https://doi.org/10.1016/J.SCITOTENV.2016.12.115>, 2017.

Barrie, L., and Platt, U.: Arctic tropospheric chemistry: an overview, *Tellus Ser. B*, 49, 450-454, <https://doi.org/10.3402/tellusb.v49i5.15984>, 1997.

Barrie, L. A.: Occurrence And Trends of Pollution in the Arctic Troposphere, in: *Chemical Exchange Between the Atmosphere and Polar Snow*. NATO ASI Series (Series I: Global Environmental Change), edited by: Wolff, E. W., and Bales, R. C., 43, Springer, Berlin, Heidelberg, 93-129, https://doi.org/10.1007/978-3-642-61171-1_5, 1996.

Begoin, M., Richter, A., Weber, M., Kaleschke, L., Tian-Kunze, X., Stohl, A., Theys, N., and Burrows, J. P.: Satellite observations of long range transport of a large BrO plume in the Arctic, 2010.

Björkman, M., Kühnel, R., Partridge, D., Roberts, T., Aas, W., Mazzola, M., Viola, A., Hodson, A., Ström, J., and Isaksson, E.: Nitrate dry deposition in Svalbard, *Tellus Ser. B*, 65, 19071, <https://doi.org/10.3402/tellusb.v65i0.19071>, 2013.

Bottenheim, J. W., Fuentes, J. D., Tarasick, D. W., and Anlauf, K. G.: Ozone in the Arctic lower troposphere during winter and spring 2000 (ALERT2000), *Atmos. Environ.*, 36, 2535-2544, [https://doi.org/10.1016/S1352-2310\(02\)00121-8](https://doi.org/10.1016/S1352-2310(02)00121-8), 2002.

Brown, S. S., Dubé, W. P., Peischl, J., Ryerson, T. B., Atlas, E., Warneke, C., de Gouw, J. A., te Lintel Hekkert, S., Brock, C. A., Flocke, F., Trainer, M., Parrish, D. D., Feshenfeld, F. C., and Ravishankara, A. R.: Budgets for nocturnal VOC oxidation by nitrate radicals aloft during the 2006 Texas Air Quality Study, *J. Geophys. Res. Atmos.*, 116, D24305, <https://doi.org/10.1029/2011JD016544>, 2011.

Brown, S. S., and Stutz, J.: Nighttime radical observations and chemistry, *Chem. Soc. Rev.*, 41, 6405-6447, <https://doi.org/10.1039/C2CS35181A>, 2012.

Cavalli, F., Viana, M., Yttri, K. E., Genberg, J., and Putaud, J. P.: Toward a standardised thermal-optical protocol for measuring atmospheric organic and elemental carbon: the EUSAAR protocol, *Atmos. Meas. Tech.*, 3, 79-89, 10.5194/amt-3-79-2010, 2010.

CEN: European Committee for Standardization (CEN, French: Comité Européen de Normalisation), EN 15549:2008 Air quality - Standard method for the measurement of the concentration of benzo[a]pyrene in ambient air, CEN, Brussels, Belgium, 50 pp., 2008.

CEN: European Committee for Standardization (CEN, French: Comité Européen de Normalisation), PB CEN/TS16645:2014 Ambient Air – Method for the measurement of benz[a]anthracene, benzo[b]fluoranthene, benzo[j]fluoranthene, benzo[k]fluoranthene, dibenz[a,h]anthracene, indeno[1,2,3-cd]pyrene and benzo[ghi]perylene, CEN, Brussels, Belgium, 51 pp., 2014.

CEN: European Committee for Standardization, EN-16909: 2017 - Ambient air - Measurement of elemental carbon (EC) and organic carbon (OC) collected on filters, CEN, Brussels (Belgium), 2017.

Chan, A. W. H., Kautzman, K. E., Chhabra, P. S., Surratt, J. D., Chan, M. N., Crouse, J. D., Kürten, A., Wennberg, P. O., Flagan, R. C., and Seinfeld, J. H.: Secondary organic aerosol formation from photooxidation of naphthalene and alkylnaphthalenes: implications for oxidation of intermediate volatility organic compounds (IVOCs), *Atmos. Chem. Phys.*, 9, 3049-3060, <https://doi.org/10.5194/acp-9-3049-2009>, 2009.

Cochran, R. E., Jeong, H., Haddadi, S., Fisseha Derseh, R., Gowan, A., Beránek, J., and Kubátová, A.: Identification of products formed during the heterogeneous nitration and ozonation of polycyclic aromatic hydrocarbons, *Atmos. Environ.*, 128, 92-103, <https://doi.org/10.1016/j.atmosenv.2015.12.036>, 2016.

Dang, J., and He, M.: Mechanisms and kinetic parameters for the gas-phase reactions of anthracene and pyrene with Cl atoms in the presence of NO_x, *RSC Adv.*, 6, 17345-17353, <https://doi.org/10.1039/C5RA25959B>, 2016.

Dekhtyareva, A.: On local and long-range transported air pollution in Svalbard, Doctoral thesis, The Arctic University of Norway (UiT), Tromsø, Norway, 191 pp., <https://hdl.handle.net/10037/16297>, 2019.

Drotikova, T., Ali, A. M., Halse, A. K., Reinardy, H. C., and Kallenborn, R.: Polycyclic aromatic hydrocarbons (PAHs) and oxy- and nitro-PAHs in ambient air of the Arctic town Longyearbyen, Svalbard, *Atmos. Chem. Phys.*, 20, 9997-10014, 10.5194/acp-20-9997-2020, 2020.

Drotikova, T., Dekhtyareva, A., Kallenborn, R., and Albinet, A.: Polycyclic aromatic hydrocarbons (PAHs) and their nitrated and oxygenated derivatives in the Arctic boundary layer: Seasonal trends and local anthropogenic influence, *Atmos. Chem. Phys. Discuss.*, 2021, 1-27, 10.5194/acp-2021-193, 2021.

Fioletov, V. E.: Ozone climatology, trends, and substances that control ozone, *Atmos. Ocean*, 46, 39-67, 10.3137/ao.460103, 2008.

Fu, P., Kawamura, K., and Barrie, L. A.: Photochemical and Other Sources of Organic Compounds in the Canadian High Arctic Aerosol Pollution during Winter–Spring, *Environ. Sci. Technol.*, 43, 286-292, <https://doi.org/10.1021/es803046q>, 2009.

Grannas, A. M., Shepson, P. B., Guimbaud, C., Sumner, A. L., Albert, M., Simpson, W., Dominé, F., Boudries, H., Bottenheim, J., Beine, H. J., Honrath, R., and Zhou, X.: A study of photochemical and physical processes affecting carbonyl compounds in the Arctic atmospheric boundary layer, *Atmos. Environ.*, 36, 2733-2742, [https://doi.org/10.1016/S1352-2310\(02\)00134-6](https://doi.org/10.1016/S1352-2310(02)00134-6), 2002.

Grannas, A. M., Jones, A. E., Dibb, J., Ammann, M., Anastasio, C., Beine, H. J., Bergin, M., Bottenheim, J., Boxe, C. S., Carver, G., Chen, G., Crawford, J. H., Dominé, F., Frey, M. M., Guzmán, M. I., Heard, D. E., Helmig, D., Hoffmann, M. R., Honrath, R. E., Huey, L. G., Hutterli, M., Jacobi, H. W., Klán, P., Lefer, B., McConnell, J., Plane, J., Sander, R., Savarino, J., Shepson, P. B., Simpson, W. R., Sodeau, J. R., von Glasow, R., Weller, R., Wolff, E. W., and Zhu, T.: An overview of snow photochemistry: evidence, mechanisms and impacts, *Atmos. Chem. Phys.*, 7, 4329-4373, <https://doi.org/10.5194/acp-7-4329-2007>, 2007.

Hirdman, D., Sodemann, H., Eckhardt, S., Burkhart, J. F., Jefferson, A., Mefford, T., Quinn, P. K., Sharma, S., Ström, J., and Stohl, A.: Source identification of short-lived air pollutants in the Arctic using statistical analysis of measurement data and particle dispersion model output, *Atmos. Chem. Phys.*, 10, 669-693, <https://doi.org/10.5194/acp-10-669-2010>, 2010.

Hornbrook, R. S., Hills, A. J., Riemer, D. D., Abdelhamid, A., Flocke, F. M., Hall, S. R., Huey, L. G., Knapp, D. J., Liao, J., Mauldin III, R. L., Montzka, D. D., Orlando, J. J., Shepson, P. B., Sive, B., Staebler, R. M., Tanner, D. J., Thompson, C. R., Turnipseed, A., Ullmann, K., Weinheimer, A. J., and Apel, E. C.: Arctic springtime observations of volatile organic compounds during the OASIS-2009 campaign, *J. Geophys. Res. Atmos.*, 121, 9789-9813, <https://doi.org/10.1002/2015JD024360>, 2016.

Hu, H., Tian, M., Zhang, L., Yang, F., Peng, C., Chen, Y., Shi, G., Yao, X., Jiang, C., and Wang, J.: Sources and gas-particle partitioning of atmospheric parent, oxygenated, and nitrated polycyclic aromatic hydrocarbons in a humid city in southwest China, *Atmos. Environ.*, 206, 1-10, <https://doi.org/10.1016/j.atmosenv.2019.02.041>, 2019.

Huff, D. M., Joyce, P. L., Fochesatto, G. J., and Simpson, W. R.: Deposition of dinitrogen pentoxide, N₂O₅, to the snowpack at high latitudes, *Atmos. Chem. Phys.*, 11, 4929-4938, 10.5194/acp-11-4929-2011, 2011.

Idowu, O., Semple, K. T., Ramadass, K., O'Connor, W., Hansbro, P., and Thavamani, P.: Beyond the obvious: Environmental health implications of polar polycyclic aromatic hydrocarbons, *Environ. Int.*, 123, 543-557, <https://doi.org/10.1016/j.envint.2018.12.051>, 2019.

Jakober, C. A., Riddle, S. G., Robert, M. A., Destailats, H., Charles, M. J., Green, P. G., and Kleeman, M. J.: Quinone Emissions from Gasoline and Diesel Motor Vehicles, *Environ. Sci. Technol.*, 41, 4548-4554, <https://doi.org/10.1021/es062967u>, 2007.

Jariyasopit, N., Zimmermann, K., Schrlau, J., Arey, J., Atkinson, R., Yu, T.-W., Dashwood, R. H., Tao, S., and Simonich, S. L. M.: Heterogeneous Reactions of Particulate Matter-Bound PAHs and NPAHs with NO₃/N₂O₅, OH Radicals, and O₃ under Simulated Long-Range Atmospheric Transport Conditions: Reactivity and Mutagenicity, *Environ. Sci. Technol.*, 48, 10155-10164, <https://doi.org/10.1021/es5015407>, 2014.

Jin, R., Zheng, M., Lammel, G., Bandowe, B. A. M., and Liu, G.: Chlorinated and brominated polycyclic aromatic hydrocarbons: Sources, formation mechanisms, and occurrence in the environment, *Prog. Energy Combust. Sci.*, 76, 100803, <https://doi.org/10.1016/j.peccs.2019.100803>, 2020.

Kamens, R. M., Guo, J., Guo, Z., and McDow, S. R.: Polynuclear aromatic hydrocarbon degradation by heterogeneous reactions with N₂O₅ on atmospheric particles, *Atmos. Environ. A-Gen*, 24, 1161-1173, [https://doi.org/10.1016/0960-1686\(90\)90081-W](https://doi.org/10.1016/0960-1686(90)90081-W), 1990.

Kawamura, K., Kasukabe, H., Yasui, O., and Barrie, L. A.: Production of dicarboxylic acids in the Arctic atmosphere at polar sunrise, *Geophys. Res. Lett.*, 22, 1253-1256, <https://doi.org/10.1029/95GL00880>, 1995.

Keyte, I. J., Harrison, R. M., and Lammel, G.: Chemical reactivity and long-range transport potential of polycyclic aromatic hydrocarbons – a review, *Chem. Soc. Rev.*, 42, 9333-9391, <https://doi.org/10.1039/C3CS60147A>, 2013.

Klonecki, A.: Seasonal changes in the transport of pollutants into the Arctic troposphere-model study, *J. Geophys. Res.*, 108, 8367, <http://doi.org/10.1029/2002jd002199>, 2003.

Kramer, A. L., Suski, K. J., Bell, D. M., Zelenyuk, A., and Massey Simonich, S. L.: Formation of Polycyclic Aromatic Hydrocarbon Oxidation Products in α -Pinene Secondary Organic Aerosol Particles Formed through Ozonolysis, *Environ. Sci. Technol.*, 53, 6669-6677, <https://doi.org/10.1021/acs.est.9b01732>, 2019.

Lee, J. Y., and Lane, D. A.: Unique products from the reaction of naphthalene with the hydroxyl radical, *Atmos. Environ.*, 43, 4886-4893, <https://doi.org/10.1016/j.atmosenv.2009.07.018>, 2009.

Lee, J. Y., Lane, D. A., Heo, J. B., Yi, S.-M., and Kim, Y. P.: Quantification and seasonal pattern of atmospheric reaction products of gas phase PAHs in PM_{2.5}, *Atmos. Environ.*, 55, 17-25, <https://doi.org/10.1016/j.atmosenv.2012.03.007>, 2012.

Liao, J., Huey, L. G., Tanner, D. J., Flocke, F. M., Orlando, J. J., Neuman, J. A., Nowak, J. B., Weinheimer, A. J., Hall, S. R., Smith, J. N., Fried, A., Staebler, R. M., Wang, Y., Koo, J.-H., Cantrell, C. A., Weibring, P., Walega, J., Knapp, D. J., Shepson, P. B., and Stephens, C. R.: Observations of inorganic bromine (HOBr, BrO, and Br₂) speciation at Barrow, Alaska, in spring 2009, *J. Geophys. Res. Atmos.*, 117, <https://doi.org/10.1029/2011JD016641>, 2012.

Liao, J., Huey, L. G., Liu, Z., Tanner, D. J., Cantrell, C. A., Orlando, J. J., Flocke, F. M., Shepson, P. B., Weinheimer, A. J., Hall, S. R., Ullmann, K., Beine, H. J., Wang, Y., Ingall, E. D., Stephens, C. R., Hornbrook, R. S., Apel, E. C., Riemer, D., Fried, A., Mauldin, R. L., Smith, J. N., Staebler, R. M., Neuman, J. A., and Nowak, J. B.: High levels of molecular chlorine in the Arctic atmosphere, *Nat. Geosci.*, 7, 91-94, <https://doi.org/10.1038/ngeo2046>, 2014.

Ma, J., Wang, F., and Mostafavi, M.: Ultrafast chemistry of water radical cation, H₂O^{•+}, in aqueous solutions, *Molecules*, 23, 244, 2018.

Mao, J., Jacob, D. J., Evans, M. J., Olson, J. R., Ren, X., Brune, W. H., Clair, J. M. S., Crouse, J. D., Spencer, K. M., Beaver, M. R., Wennberg, P. O., Cubison, M. J., Jimenez, J. L., Fried, A., Weibring, P., Walega, J. G., Hall, S. R., Weinheimer, A. J., Cohen, R. C., Chen, G., Crawford, J. H., McNaughton, C., Clarke, A. D., Jaeglé, L., Fisher, J. A., Yantosca, R. M., Le Sager, P., and Carouge, C.: Chemistry of hydrogen oxide radicals (HOx) in the Arctic troposphere in spring, *Atmos. Chem. Phys.*, 10, 5823-5838, [10.5194/acp-10-5823-2010](https://doi.org/10.5194/acp-10-5823-2010), 2010.

McNamara, S. M., W. Raso, A. R., Wang, S., Thanekar, S., Boone, E. J., Kolesar, K. R., Peterson, P. K., Simpson, W. R., Fuentes, J. D., Shepson, P. B., and Pratt, K. A.: Springtime Nitrogen Oxide-Influenced Chlorine Chemistry in the Coastal Arctic, *Environ. Sci. Technol.*, 53, 8057-8067, <https://doi.org/10.1021/acs.est.9b01797>, 2019.

Monks, P., and Hey, J. V.: Tropospheric chemistry and air pollution, in: *Atmospheric science for environmental scientists*, 2 ed., edited by: Hewitt, C. N., and Jackson, A. V., Wiley-Blackwell, UK, 159-202, 2020.

Monks, P. S.: Gas-phase radical chemistry in the troposphere, *Chem. Soc. Rev.*, 34, 376-395, <https://doi.org/10.1039/b307982c>, 2005.

Muir, D. C. G., and Galarnau, E.: Polycyclic aromatic compounds (PACs) in the Canadian environment: Links to global change, *Environ. Pollut.*, 273, 116425, <https://doi.org/10.1016/j.envpol.2021.116425>, 2021.

Nalin, F., Golly, B., Besombes, J.-L., Pelletier, C., Aujay-Plouzeau, R., Verlhac, S., Dermigny, A., Fievet, A., Karoski, N., Dubois, P., Collet, S., Favez, O., and Albinet, A.: Fast oxidation processes from emission to ambient air introduction of aerosol emitted by residential log wood stoves, *Atmos. Environ.*, 143, 15-26, <https://doi.org/10.1016/j.atmosenv.2016.08.002>, 2016.

Nežiková, B., Degrendele, C., Bandowe, B. A. M., Holubová Šmejkalová, A., Kukučka, P., Martiník, J., Mayer, L., Prokeš, R., Příbylová, P., Klánová, J., and Lammel, G.: Three years of atmospheric concentrations of nitrated and oxygenated polycyclic aromatic hydrocarbons and oxygen

heterocycles at a central European background site, *Chemosphere*, 269, 128738, <https://doi.org/10.1016/j.chemosphere.2020.128738>, 2020.

Oda, J., Nomura, S., Yasuhara, A., and Shibamoto, T.: Mobile sources of atmospheric polycyclic aromatic hydrocarbons in a roadway tunnel, *Atmos. Environ.*, 35, 4819-4827, [https://doi.org/10.1016/S1352-2310\(01\)00262-X](https://doi.org/10.1016/S1352-2310(01)00262-X), 2001.

Ohura, T., Kitazawa, A., Amagai, T., and Makino, M.: Occurrence, profiles, and photostabilities of chlorinated polycyclic aromatic hydrocarbons associated with particulates in urban air, *Environ. Sci. Technol.*, 39, 85-91, 2005.

Perraudin, E., Budzinski, H., and Villenave, E.: Identification and quantification of ozonation products of anthracene and phenanthrene adsorbed on silica particles, *Atmos. Environ.*, 41, 6005-6017, <https://doi.org/10.1016/j.atmosenv.2007.03.010>, 2007.

Peterson, P. K., Simpson, W. R., Pratt, K. A., Shepson, P. B., Frieß, U., Zielcke, J., Platt, U., Walsh, S. J., and Nghiem, S. V.: Dependence of the vertical distribution of bromine monoxide in the lower troposphere on meteorological factors such as wind speed and stability, *Atmos. Chem. Phys.*, 15, 2119-2137, <https://doi.org/10.5194/acp-15-2119-2015>, 2015.

Pio, C., Cerqueira, M., Harrison, R. M., Nunes, T., Mirante, F., Alves, C., Oliveira, C., Sanchez De La Campa, A., Artíñano, B., and Matos, M.: OC/EC ratio observations in Europe: Re-thinking the approach for apportionment between primary and secondary organic carbon, *Atmos. Environ.*, 45, 6121-6132, <https://doi.org/10.1016/j.atmosenv.2011.08.045>, 2011.

Prevedouros, K., Brorström-Lundén, E., J. Halsall, C., Jones, K. C., Lee, R. G. M., and Sweetman, A. J.: Seasonal and long-term trends in atmospheric PAH concentrations: evidence and implications, *Environ. Pollut.*, 128, 17-27, <https://doi.org/10.1016/j.envpol.2003.08.032>, 2004.

Qu, X., Zhang, Q., and Wang, W.: Mechanism for OH-initiated photooxidation of naphthalene in the presence of O₂ and NO_x: A DFT study, *Chem. Phys. Lett.*, 429, 77-85, <https://doi.org/10.1016/j.cplett.2006.08.036>, 2006.

Ravindra, K., Sokhi, R., and Vangrieken, R.: Atmospheric polycyclic aromatic hydrocarbons: Source attribution, emission factors and regulation, *Atmos. Environ.*, 42, 2895-2921, <http://doi.org/10.1016/j.atmosenv.2007.12.010>, 2008.

Reisen, F., and Arey, J.: Reactions of Hydroxyl Radicals and Ozone with Acenaphthene and Acenaphthylene, *Environ. Sci. Technol.*, 36, 4302-4311, <https://doi.org/10.1021/es025761b>, 2002.

Rindone, B., Saliu, F., and Suarez-Bertoa, R.: The Synthesis of Phthalic Anhydride via Ozonation of Naphthalene, *Ozone Sci. Eng.*, 32, 161-165, <https://doi.org/10.1080/01919511003788001>, 2010.

Ringuet, J., Albinet, A., Leoz-Garziandia, E., Budzinski, H., and Villenave, E.: Reactivity of polycyclic aromatic compounds (PAHs, NPAHs and OPAHs) adsorbed on natural aerosol particles exposed to atmospheric oxidants, *Atmos. Environ.*, 61, 15-22, <https://doi.org/10.1016/j.atmosenv.2012.07.025>, 2012.

Riva, M., Healy, R. M., Flaud, P.-M., Perraudin, E., Wenger, J. C., and Villenave, E.: Gas- and Particle-Phase Products from the Chlorine-Initiated Oxidation of Polycyclic Aromatic Hydrocarbons, *J. Phys. Chem. A*, 119, 11170-11181, <https://doi.org/10.1021/acs.jpca.5b04610>, 2015.

Riva, M., Healy, R. M., Tomaz, S., Flaud, P.-M., Perraudin, E., Wenger, J. C., and Villenave, E.: Gas and particulate phase products from the ozonolysis of acenaphthylene, *Atmos. Environ.*, 142, 104-113, <https://doi.org/10.1016/j.atmosenv.2016.07.012>, 2016.

Röhler, L., Schlabach, M., Haglund, P., Breivik, K., Kallenborn, R., and Bohlin-Nizzetto, P.: Non-target and suspect characterisation of organic contaminants in Arctic air – Part 2: Application of a new tool for identification and prioritisation of chemicals of emerging Arctic concern in air, *Atmos. Chem. Phys.*, 20, 9031-9049, <https://doi.org/10.5194/acp-20-9031-2020>, 2020.

Sankoda, K., Nomiya, K., Kuribayashi, T., and Shinohara, R.: Halogenation of Polycyclic Aromatic Hydrocarbons by Photochemical Reaction under Simulated Tidal Flat Conditions, *Polycyclic Aromat. Compd.*, 33, 236-253, <https://doi.org/10.1080/10406638.2013.770406>, 2013.

Shahpoury, P., Kitanovski, Z., Lammel, G. J. A. C., and Physics: Snow scavenging and phase partitioning of nitrated and oxygenated aromatic hydrocarbons in polluted and remote environments in central Europe and the European Arctic, *Atmos. Chem. Phys.*, 18, 13495-13510, <https://doi.org/10.5194/acp-18-13495-2018>, 2018.

Sihler, H., Platt, U., Beirle, S., Marbach, T., Kühl, S., Dörner, S., Verschaeve, J., Frieß, U., Pöhler, D., Vogel, L., Sander, R., and Wagner, T.: Tropospheric BrO column densities in the Arctic derived

from satellite: retrieval and comparison to ground-based measurements, *Atmos. Meas. Tech.*, 5, 2779-2807, <https://doi.org/10.5194/amt-5-2779-2012>, 2012.

Simpson, W. R., von Glasow, R., Riedel, K., Anderson, P., Ariya, P., Bottenheim, J., Burrows, J., Carpenter, L. J., Frieß, U., Goodsite, M. E., Heard, D., Hutterli, M., Jacobi, H. W., Kaleschke, L., Neff, B., Plane, J., Platt, U., Richter, A., Roscoe, H., Sander, R., Shepson, P., Sodeau, J., Steffen, A., Wagner, T., and Wolff, E.: Halogens and their role in polar boundary-layer ozone depletion, *Atmos. Chem. Phys.*, 7, 4375-4418, <https://doi.org/10.5194/acp-7-4375-2007>, 2007.

Simpson, W. R., Brown, S. S., Saiz-Lopez, A., Thornton, J. A., and von Glasow, R.: Tropospheric Halogen Chemistry: Sources, Cycling, and Impacts, *Chem. Rev.*, 115, 4035-4062, <https://doi.org/10.1021/cr5006638>, 2015.

Simpson, W. R., Peterson, P. K., Frieß, U., Sihler, H., Lampel, J., Platt, U., Moore, C., Pratt, K., Shepson, P., Halfacre, J., and Nghiem, S. V.: Horizontal and vertical structure of reactive bromine events probed by bromine monoxide MAX-DOAS, *Atmos. Chem. Phys.*, 17, 9291-9309, <https://doi.org/10.5194/acp-17-9291-2017>, 2017.

Simpson, W. R., Frieß, U., Thomas, J. L., Lampel, J., and Platt, U.: Polar Nighttime Chemistry Produces Intense Reactive Bromine Events, *Geophys. Res. Lett.*, 45, 9987-9994, <https://doi.org/10.1029/2018GL079444>, 2018.

Singh, D. K., Kawamura, K., Yanase, A., and Barrie, L. A.: Distributions of polycyclic aromatic hydrocarbons, aromatic ketones, carboxylic acids, and trace metals in Arctic aerosols: Long-range atmospheric transport, photochemical degradation/production at polar sunrise, *Environ. Sci. Technol.*, 51, 8992-9004, <https://doi.org/10.1021/acs.est.7b01644>, 2017.

Solberg, S., Schmidbauer, N., Semb, A., Stordal, F., and Hov, Ø.: Boundary-layer ozone depletion as seen in the Norwegian Arctic in spring, *J. Atmos. Chem.*, 23, 301-332, 1996.

Solberg, S., Krognest, T., Stordal, F., Hov, O., Beine, H. J., Jaffe, D. A., Clemmishaw, K. C., and Penkett, S. A.: Reactive Nitrogen Compounds at Spitsbergen in the Norwegian Arctic, *J. Atmos. Chem.*, 28, 209-225, <https://doi.org/10.1023/A:1005883323285>, 1997.

Srivastava, D., Favez, O., Bonnaire, N., Lucarelli, F., Haeffelin, M., Perraudin, E., Gros, V., Villenave, E., and Albinet, A.: Speciation of organic fractions does matter for aerosol source apportionment. Part 2: Intensive short-term campaign in the Paris area (France), *Sci. Total Environ.*, 634, 267-278, <https://doi.org/10.1016/j.scitotenv.2018.03.296>, 2018a.

Srivastava, D., Favez, O., Perraudin, E., Villenave, E., and Albinet, A.: Comparison of Measurement-Based Methodologies to Apportion Secondary Organic Carbon (SOC) in PM_{2.5}: A Review of Recent Studies, *Atmosphere*, 9, 452, <https://doi.org/10.3390/atmos9110452>, 2018b.

Statistics Norway: This is Svalbard 2016. What the figures say, Oslo, Norway, 28 pp., <https://www.ssb.no/en/befolkning/artikler-og-publikasjoner/this-is-svalbard-2016>, 2016.

Statistics Norway. Longyearbyen and Ny-Ålesund population as of 2020: <https://www.ssb.no/befolkning/statistikker/befsvvalbard> (last access: 12 November), 2020.

Stohl, A.: Characteristics of atmospheric transport into the Arctic troposphere, *J. Geophys. Res. Atmos.*, 111, D11306, <https://doi.org/10.1029/2005jd006888>, 2006.

Strong, K., Simpson, W. R., Bognar, K., Lindenmaier, R., and Roche, S.: Trace Gases in the Arctic Atmosphere, in: *Physics and Chemistry of the Arctic Atmosphere*, edited by: Kokhanovsky, A., and Tomasi, C., Springer International Publishing, Cham, Switzerland, 153-207, https://doi.org/10.1007/978-3-030-33566-3_3, 2020.

Sumner, A. L., Shepson, P. B., Grannas, A. M., Bottenheim, J. W., Anlauf, K. G., Worthy, D., Schroeder, W. H., Steffen, A., Dominé, F., Perrier, S., and Houdier, S.: Atmospheric chemistry of formaldehyde in the Arctic troposphere at Polar Sunrise, and the influence of the snowpack, *Atmos. Environ.*, 36, 2553-2562, [https://doi.org/10.1016/S1352-2310\(02\)00105-X](https://doi.org/10.1016/S1352-2310(02)00105-X), 2002.

Thompson, C. R., Shepson, P. B., Liao, J., Huey, L. G., Apel, E. C., Cantrell, C. A., Flocke, F., Orlando, J., Fried, A., Hall, S. R., Hornbrook, R. S., Knapp, D. J., Mauldin III, R. L., Montzka, D. D., Sive, B. C., Ullmann, K., Weibring, P., and Weinheimer, A.: Interactions of bromine, chlorine, and iodine photochemistry during ozone depletions in Barrow, Alaska, *Atmos. Chem. Phys.*, 15, 9651-9679, <https://doi.org/10.5194/acp-15-9651-2015>, 2015.

Tomaz, S., Shahpoury, P., Jaffrezo, J.-L., Lammel, G., Perraudin, E., Villenave, E., and Albinet, A.: One-year study of polycyclic aromatic compounds at an urban site in Grenoble (France): Seasonal

variations, gas/particle partitioning and cancer risk estimation, *Sci. Total Environ.*, 565, 1071-1083, <https://doi.org/10.1016/j.scitotenv.2016.05.137>, 2016.

Tomaz, S., Jaffrezo, J.-L., Favez, O., Perraudin, E., Villenave, E., and Albinet, A.: Sources and atmospheric chemistry of oxy- and nitro-PAHs in the ambient air of Grenoble (France), *Atmos. Environ.*, 161, 144-154, <https://doi.org/10.1016/j.atmosenv.2017.04.042>, 2017.

Verlhac, S., Albinet, A., Cabillic, J., Lalère, B., and Fallot, C.: European Interlaboratory Comparison for the analysis of PAHs in ambient air (2015), LCSQA, <https://www.lcsqa.org/fr/rapport/2015/ineris/european-interlaboratory-comparison-for-the-analysis-of-pah-in-ambient-air>, 2015.

Vestreng, V., Kallenborn, R., and Økstad, E.: Norwegian Arctic climate: climate influencing emissions, scenarios and mitigation options at Svalbard, Miljødirektoratet, Oslo, Norway, 56 pp., <https://www.miljodirektoratet.no/globalassets/publikasjoner/klif2/publikasjoner/2552/ta2552.pdf>, 2009.

Vione, D., Barra, S., de Gennaro, G., de Rienzo, M., Gilardoni, S., Perrone, M. G., and Pozzoli, L.: Polycyclic Aromatic Hydrocarbons in the Atmosphere: Monitoring, Sources, Sinks and Fate. II: Sinks and Fate, *Ann. Chim. (Rome)*, 94, 257-268, <https://doi.org/10.1002/adic.200490031>, 2004.

Vuong, Q. T., Kim, S.-J., Nguyen, T. N. T., Thang, P. Q., Lee, S.-J., Ohura, T., and Choi, S.-D.: Passive air sampling of halogenated polycyclic aromatic hydrocarbons in the largest industrial city in Korea: Spatial distributions and source identification, *J. Hazard. Mater.*, 382, 121238, 2020a.

Vuong, Q. T., Thang, P. Q., Ohura, T., and Choi, S.-D.: Chlorinated and brominated polycyclic aromatic hydrocarbons in ambient air: seasonal variation, profiles, potential sources, and size distribution, *Reviews in Environmental Science and Bio/Technology*, 19, 259-273, 10.1007/s11157-020-09535-z, 2020b.

Wickström, S., Jonassen, M. O., Vihma, T., and Uotila, P.: Trends in cyclones in the high-latitude North Atlantic during 1979–2016, *Q. J. R. Meteorolog. Soc.*, 146, 762-779, <https://doi.org/10.1002/qj.3707>, 2020.

Wu, C., and Yu, J. Z.: Determination of primary combustion source organic carbon-to-elemental carbon (OC/EC) ratio using ambient OC and EC measurements: secondary OC-EC correlation minimization method, *Atmos. Chem. Phys.*, 16, 5453-5465, <https://doi.org/10.5194/acp-16-5453-2016>, 2016.

Yu, Y., Katsoyiannis, A., Bohlin-Nizzetto, P., Brorström-Lundén, E., Ma, J., Zhao, Y., Wu, Z., Tych, W., Mindham, D., Sverko, E., Barresi, E., Dryfhout-Clark, H., Fellin, P., and Hung, H.: Polycyclic aromatic hydrocarbons not declining in Arctic air despite global emission reduction, *Environ. Sci. Technol.*, 53, 2375-2382, <https://doi.org/10.1021/acs.est.8b05353>, 2019.

Zhao, X., Strong, K., Adams, C., Schofield, R., Yang, X., Richter, A., Friess, U., Blechschmidt, A.-M., and Koo, J.-H.: A case study of a transported bromine explosion event in the Canadian high arctic, *J. Geophys. Res. Atmos.*, 121, 457-477, <https://doi.org/10.1002/2015JD023711>, 2016.

Zhou, X., Beine, H. J., Honrath, R. E., Fuentes, J. D., Simpson, W., Shepson, P. B., and Bottenheim, J. W.: Snowpack photochemical production of HONO: A major source of OH in the Arctic boundary layer in springtime, *Geophys. Res. Lett.*, 28, 4087-4090, 10.1029/2001gl013531, 2001.

Zielinska, B., Arey, J., Atkinson, R., and McElroy, P. A.: Formation of methylnitronaphthalenes from the gas-phase reactions of 1-and 2-methylnaphthalene with hydroxyl radicals and nitrogen oxide (N₂O₅) and their occurrence in ambient air, *Environ. Sci. Technol.*, 23, 723-729, <https://doi.org/10.1021/es00064a011>, 1989.

Supplement of Paper III

Table of content

Table S1. Individual seasonal concentrations (G+P; pg/m^3) of PAHs measured in urban, rural, and background air of Longyearbyen in 2017/2018.	2
Table S2. Individual seasonal concentrations (G+P; pg/m^3) of oxy-PAHs measured in urban, rural, and background air of Longyearbyen in 2017/2018.	4
Table S3. Individual seasonal concentrations (G+P; pg/m^3) of nitro-PAHs measured in urban, rural, and background air of Longyearbyen in 2017/2018.	6
Table S4. Seasonal sum concentrations (G+P) of PAHs, oxy-PAHs, and nitro-PAHs [pg/m^3], and OC and EC [$\mu\text{g}/\text{m}^3$] measured in urban, rural, and background (altitudinal) air of Longyearbyen in 2017/2018.	9
Table S5. Sampling periods and air sample volumes.	10
Table S6. Svalbard background air concentrations (G+P; pg/m^3) of $\Sigma 20$ PAHs measured in Longyearbyen (Svalsat) and Ny-Ålesund (Zeppelin) in 2017/2018.	11
Table S7. %PM of PAHs during cold and warm periods.	12
Table S8. %PM of oxy-PAHs during cold and warm periods.	13
Table S9. %PM of nitro-PAHs during cold and warm periods.	14
Figure S1. Location of Svalbard in the Arctic.	15
Figure S2. Air sampling sites in Longyearbyen: urban (UNIS), rural (Adventdalen), altitudinal (Svalsat).	15
Figure S3. Annual sun diagram for Longyearbyen location.	16
Figure S4. 10-day backward trajectories for the air pollution event in Longyearbyen on 5 th of December 2017.	17
Figure S5. 10-day backward trajectories and wind rose for the dust event in Longyearbyen on 29 th of November 2017.	17
Figure S6. Seasonal evolution of product to reactant concentration ratios at three sites indicating PAC's oxidation during <i>polar night</i> in winter (P1).	18
Figure S7. Seasonal evolution of product to reactant concentration ratios at two sites indicating PAC's oxidation during <i>spring</i> (P3).	19
Figure S8. Seasonal evolution of product to reactant concentration ratios at two sites indicating PAC's oxidation during <i>spring</i> (P3) mostly at UNIS.	20
Figure S9. Seasonal evolution of product to reactant concentration ratios at three sites indicating PAC's oxidation during <i>summer</i> (P4).	21

Table S1. Individual seasonal concentrations (G+P; pg/m³) of PAHs measured in urban, rural, and background air of Longyearbyen in 2017/2018.

Compound name	Cold period						Warm period				
	Dark winter P1 November-January			Twilight winter P2 February			Daylight spring P3 March-April		Polar day summer P4 May-June		Svalsat (altitudinal)
	UNIS (urban)	Adventdalen (rural)	Svalsat (altitudinal)	UNIS (urban)	Adventdalen (rural)	UNIS (urban)	Adventdalen (rural)	UNIS (urban)	Adventdalen (rural)		
	n=8	n=4	n=8	n=4	n=7	n=7	n=12	n=6	n=4		
	mean ± std (median)	mean ± std (median)	mean ± std (median)	mean ± std (median)	mean ± std (median)	mean ± std (median)	mean ± std (median)	mean ± std (median)	mean ± std (median)	mean ± std (median)	
Naphthalene	112 ± 79 (89)	77 ± 47 (99)	247 ± 194 (189)	727 ± 550 (562)	1533 ± 760 (1671)	1549 ± 1198 (1305)	96 ± 69 (77)	70 ± 67 (52)	34 ± 8 (35)		
1-Methylnaphthalene	58 ± 28 (56)	68 ± 39 (63)	64 ± 67 (47)	337 ± 160 (276)	890 ± 389 (744)	567 ± 438 (450)	106 ± 66 (81)	46 ± 42 (30)	21 ± 33 (4)		
2-Methylnaphthalene	23 ± 19 (21)	173 ± 146 (248)	6.5 ± 5.7 (4.6)	70 ± 78 (58)	112 ± 72 (84)	57 ± 73 (4)	129 ± 109 (96)	40 ± 55 (17)	36 ± 63 (4)		
Acenaphthene	52 ± 43 (34)	17 ± 5 (16)	29 ± 18 (21)	73 ± 34 (74)	284 ± 196 (261)	117 ± 81 (100)	117 ± 98 (86)	10 ± 5 (10)	21 ± 29 (7)		
Fluorene	291 ± 141 (243)	120 ± 60 (99)	296 ± 144 (281)	434 ± 101 (449)	559 ± 402 (474)	137 ± 95 (114)	288 ± 172 (270)	43 ± 26 (41)	67 ± 56 (49)		
Phenanthrene	299 ± 165 (284)	359 ± 184 (256)	119 ± 42 (111)	799 ± 164 (800)	1129 ± 594 (1041)	464 ± 399 (332)	702 ± 490 (570)	133 ± 98 (118)	166 ± 137 (122)		
Anthracene	72 ± 39 (72)	22 ± 4 (22)	21 ± 8 (21)	94 ± 53 (88)	97 ± 87 (78)	24 ± 21 (13)	89 ± 74 (62)	24 ± 16 (20)	15 ± 12 (12)		
Fluoranthene	33 ± 15 (33)	30 ± 12 (24)	13 ± 13 (5)	162 ± 60 (159)	281 ± 203 (176)	155 ± 277 (29)	36 ± 83 (4)	4.4 ± 1.5 (3.9)	4.4 ± 0.1 (4.4)		
2-Methylfluoranthene	4.8 ± 2.0 (4.0)	4.1 ± 0.4 (4.4)	4.5 ± 0.4 (4.5)	22 ± 17 (22)	18 ± 14 (12)	4.8 ± 1.4 (3.9)	26 ± 58 (8)	4.8 ± 1.4 (4.4)	5.5 ± 2.2 (4.4)		
Pyrene	35 ± 21 (33)	39 ± 13 (37)	10 ± 6 (8)	96 ± 63 (116)	155 ± 77 (155)	30 ± 35 (8)	85 ± 78 (69)	39 ± 43 (18)	14 ± 6 (15)		
Benzo[<i>a</i>]anthracene	3.9 ± 0.3 (3.9)	4.1 ± 0.4 (4.4)	4.5 ± 0.3 (4.6)	1003 ± 655 (834)	643 ± 775 (406)	268 ± 300 (219)	7.5 ± 13.5 (3.7)	4.4 ± 1.5 (3.9)	4.4 ± 0.1 (4.4)		

Chrysene	Chry	17 ± 10 (10)	29 ± 2 (29)	11 ± 1 (11)	26 ± 19 (25)	46 ± 27 (41)	11 ± 2 (10)	32 ± 32 (24)	11 ± 4 (9)	10.7 ± 0.2 (10.7)
Retene	Ret	9.4 ± 0.8 (9.6)	10 ± 1 (11)	11 ± 1 (11)	8.8 ± 1.5 (8.8)	11 ± 2 (11)	11 ± 2 (10)	9.0 ± 1.1 (9.1)	11 ± 4 (9)	10.7 ± 0.2 (10.7)
Benzo[e]pyrene	BePyr	3.9 ± 0.3 (3.9)	4.1 ± 0.4 (4.4)	4.5 ± 0.4 (4.6)	3.6 ± 0.6 (3.6)	4.6 ± 0.7 (4.5)	4.4 ± 0.9 (3.9)	5.2 ± 3.7 (3.8)	4.4 ± 1.5 (3.9)	4.4 ± 0.1 (4.4)
Benzo[j]fluoranthene	BjFit	13 ± 1 (13)	14 ± 2 (15)	15 ± 1 (16)	12 ± 2 (12)	16 ± 2 (15)	15 ± 3 (13)	13 ± 2 (13)	15 ± 5 (13)	14.9 ± 0.2 (15.0)
Benzo[b]fluoranthene	BbFit	3.9 ± 0.3 (3.9)	10 ± 11 (4)	4.5 ± 0.4 (4.6)	3.6 ± 0.6 (3.6)	12 ± 19 (5)	4.4 ± 0.9 (3.9)	3.7 ± 0.5 (3.7)	4.4 ± 1.5 (3.9)	4.4 ± 0.1 (4.4)
Benzo[k]fluoranthene	BkFit	5.3 ± 0.4 (5.4)	5.6 ± 0.6 (5.9)	6.2 ± 0.5 (6.2)	4.9 ± 0.8 (5)	10 ± 8 (7)	5.9 ± 1.3 (5.3)	6.4 ± 5.0 (5.1)	6.0 ± 2.0 (5.3)	5.9 ± 0.1 (5.9)
Benzo[a]pyrene	BaP	5.5 ± 4.2 (4.0)	9.3 ± 9.1 (4.4)	4.5 ± 0.4 (4.5)	12 ± 9 (12)	11 ± 11 (5)	4.4 ± 0.9 (3.9)	8.5 ± 9.3 (3.9)	4.4 ± 1.5 (3.9)	4.4 ± 0.1 (4.4)
Dibenzo[a,h]anthracene	DBAnt	11 ± 21 (4)	4.1 ± 0.4 (4.4)	4.5 ± 0.3 (4.5)	3.6 ± 0.6 (3.6)	4.6 ± 0.7 (4.5)	4.4 ± 0.9 (3.9)	3.7 ± 0.5 (3.7)	4.4 ± 1.5 (3.9)	4.4 ± 0.1 (4.4)
Benzo[g,h,i]perylene	BghiP	3.9 ± 0.3 (3.9)	4.1 ± 0.4 (4.4)	4.5 ± 0.3 (4.5)	13 ± 11 (12)	40 ± 30 (35)	4.4 ± 0.9 (3.9)	4.8 ± 3.6 (3.8)	4.4 ± 1.5 (3.9)	4.4 ± 0.1 (4.4)
Indeno[1,2,3-cd]pyrene	IPyr	8.4 ± 1.4 (8.4)	10 ± 1 (10)	11 ± 1 (11)	8.4 ± 1.4 (8.4)	20 ± 23 (11)	10 ± 2 (9)	8.6 ± 1.1 (8.7)	10 ± 3 (9)	10.2 ± 0.2 (10.2)
Coronene	Cor	3.9 ± 0.3 (3.9)	4.1 ± 0.4 (4.4)	4.5 ± 0.3 (4.5)	10 ± 7 (9)	27 ± 32 (6)	5.6 ± 2.5 (4.8)	3.7 ± 0.5 (3.7)	4.4 ± 1.5 (3.9)	4.4 ± 0.1 (4.4)
Σ22 PAHs		1068 ± 449 (957)	1016 ± 321 (988)	897 ± 453 (765)	3923 ± 667 (3929)	5902 ± 2421 (5466)	3452 ± 2637 (2569)	1779 ± 1210 (1352)	576 ± 216 (438)	467 ± 339 (333)
Σ14 EPA PAHs (no Nap and Acy)		839 ± 366 (772)	663 ± 258 (537)	540 ± 206 (504)	2733 ± 772 (2483)	3290 ± 1721 (4040)	1239 ± 1057 (844)	1392 ± 998 (1091)	351 ± 123 (322)	337 ± 237 (257)

Table S2. Individual seasonal concentrations (G+P; pg/m³) of oxy-PAHs measured in urban, rural, and background air of Longyearbyen in 2017/2018.

Compound name	Abbreviated name	Cold period						Warm period					
		Dark winter P1 November-January			Twilight winter P2 February			Daylight spring P3 March-April			Polar day summer P4 May-June		
		n=8 UNIS (urban) mean ± std (median)	n=4 Adventdalen (rural) mean ± std (median)	n=8 Svalsat (altitudinal) mean ± std (median)	n=4 UNIS (urban) mean ± std (median)	n=4 Adventdalen (rural) mean ± std (median)	n=8 Svalsat (altitudinal) mean ± std (median)	n=7 UNIS (urban) mean ± std (median)	n=7 Adventdalen (rural) mean ± std (median)	n=7 UNIS (urban) mean ± std (median)	n=7 Adventdalen (rural) mean ± std (median)	n=12 UNIS (urban) mean ± std (median)	n=6 Adventdalen (rural) mean ± std (median)
Phthalaldehyde	PhA	8.3 ± 3.0 (7.8)	1.5 ± 1.6 (8)	2.0 ± 1.2 (1.3)	25 ± 2.5 (13)	109 ± 127 (56)	26 ± 4.4 (8)	4.8 ± 2.2 (4)	3.3 ± 2.8 (2.5)	2.5 ± 1.8 (2.1)			
Phthalic anhydride	PhAn	1796 ± 689 (1824)	7399 ± 7711 (3631)	3968 ± 1498 (3857)	2101 ± 548 (2063)	2542 ± 621 (2582)	5169 ± 989 (5303)	2934 ± 670 (2988)	3221 ± 1219 (3413)	4838 ± 2022 (3966)			
1,4-Naphthoquinone	1,4-NapQ	95 ± 59 (105)	49 ± 27 (42)	63 ± 35 (52)	105 ± 56 (101)	59 ± 17 (59)	40 ± 28 (35)	12 ± 5 (11)	6.2 ± 4.0 (5.3)	9.3 ± 8.4 (6.6)			
1-Naphthaldehyde	1-NapA	478 ± 148 (486)	704 ± 533 (600)	293 ± 136 (311)	455 ± 110 (502)	1157 ± 587 (1165)	362 ± 210 (287)	656 ± 490 (526)	206 ± 119 (193)	79 ± 45 (57)			
2-Formyl-trans-cinnamaldehyde	2-FCinA	56 ± 64 (35)	38 ± 39 (20)	9.5 ± 4.4 (9.7)	65 ± 14 (62)	250 ± 151 (296)	37 ± 49 (19)	22 ± 15 (18)	8.3 ± 9.0 (3.8)	6.1 ± 7.1 (2.5)			
1,2-Naphthoquinone	1,2-NapQ	27 ± 35 (12)	59 ± 46 (35)	20 ± 13 (13)	19 ± 8 (19)	103 ± 111 (18)	35 ± 7 (31)	26 ± 9 (28)	38 ± 20 (35)	13 ± 0 (13)			
Benzophenone	BZPh	1676 ± 496 (1650)	4186 ± 3565 (2297)	1701 ± 301 (1681)	4354 ± 511 (4269)	5086 ± 1413 (5200)	4807 ± 1384 (5141)	1962 ± 536 (1879)	2697 ± 753 (2669)	2059 ± 270 (1992)			
1-Acenaphthenone	1-AceO	175 ± 96 (150)	230 ± 176 (223)	53 ± 15 (58)	101 ± 17 (95)	197 ± 111 (157)	74 ± 23 (65)	124 ± 111 (101)	60 ± 25 (62)	28 ± 9 (29)			
9-Fluorenone	9-FluO	798 ± 210 (795)	1196 ± 911 (963)	281 ± 56 (285)	1065 ± 134 (1030)	1682 ± 551 (1793)	790 ± 227 (747)	694 ± 317 (696)	403 ± 112 (457)	214 ± 54 (221)			
1,2-Naphthalic anhydride	1,2-NapAn	429 ± 136 (364)	1632 ± 1885 (628)	575 ± 158 (575)	485 ± 100 (467)	1003 ± 277 (971)	651 ± 213 (583)	477 ± 208 (397)	843 ± 274 (858)	594 ± 151 (540)			
2,2'-Biphenyldicarboxaldehyde	2,2'-BPhA	17 ± 14 (13)	23 ± 6 (25)	20 ± 5 (19)	16 ± 7 (16)	35 ± 21 (33)	29 ± 18 (22)	14 ± 8 (13)	18 ± 9 (17)	28 ± 17 (22)			
Xanthone	Xan	13 ± 5 (13)	6.2 ± 1.3 (6.4)	3.1 ± 1.9 (2.4)	12 ± 3 (12)	28 ± 12 (30)	11 ± 6 (9)	7.7 ± 3.1 (7.4)	3.9 ± 3.3 (2.1)	3.4 ± 2.1 (2.3)			

Acenaphthenequinone	AceQ	3.6 ± 3.0 (2.8)	4.9 ± 0.9 (4.6)	3.5 ± 1.6 (3.1)	4.7 ± 1.1 (4.6)	6.0 ± 3.3 (5.7)	6.1 ± 3.4 (4.9)	3.6 ± 1.7 (3.0)	2.3 ± 1.2 (2.2)	4.0 ± 1.3 (3.8)
2,3-Naphthalenedicarboxylic anhydride	2,3-NapAn	36 ± 31 (32)	64 ± 8 (65)	78 ± 42 (76)	56 ± 20 (54)	90 ± 107 (39)	44 ± 27 (35)	75 ± 56 (64)	50 ± 13 (50)	89 ± 17 (84)
Anthrone	ANO	12 ± 14 (5)	4.8 ± 0.5 (5.1)	17 ± 28 (6)	81 ± 98 (43)	190 ± 141 (191)	18 ± 33 (5)	63 ± 99 (35)	5.4 ± 1.6 (5.0)	5.1 ± 0.1 (5.2)
6H-Dibenzof[<i>b</i> , <i>d</i>]pyran-6-one	DBPone	39 ± 25 (35)	12 ± 1 (13)	26 ± 16 (15)	48 ± 23 (46)	114 ± 42 (109)	13 ± 3 (11)	36 ± 26 (35)	18 ± 12 (14)	67 ± 67 (43)
9,10-Anthraquinone	9,10-AntQ	33 ± 12 (33)	19 ± 4 (18)	61 ± 49 (45)	55 ± 7 (55)	119 ± 60 (110)	33 ± 13 (30)	31 ± 13 (27)	20 ± 5 (20)	20 ± 2 (20)
1,8-Naphthalic anhydride	1,8-NapAn	4.8 ± 3.4 (2.9)	4.9 ± 0.9 (4.5)	9.5 ± 4.5 (8.6)	10 ± 5 (8)	37 ± 14 (37)	6.9 ± 4.0 (5.2)	6.4 ± 6.4 (3.5)	5.9 ± 2.2 (5.8)	8.1 ± 6.1 (6.2)
1,4-Anthraquinone	1,4-AntQ	4.4 ± 0.4 (4.5)	4.7 ± 0.5 (4.9)	5.1 ± 0.4 (5.2)	4.1 ± 0.7 (4.1)	5.3 ± 0.7 (5.1)	4.9 ± 1.0 (4.4)	5.5 ± 3.1 (4.3)	5.0 ± 1.7 (4.4)	5.0 ± 0.1 (5)
4,4'-Biphenyldicarboxaldehyde	4,4-BPhA	12 ± 4 (10)	8.6 ± 1.9 (9.3)	7.1 ± 4.3 (4.7)	13 ± 4 (13)	18 ± 3 (17)	11 ± 4 (13)	10 ± 3 (10)	6.1 ± 2.4 (6.8)	6.6 ± 3.1 (6.4)
2-Methylanthraquinone	2-MeAntQ	8.1 ± 3.2 (7.7)	8.2 ± 2.4 (7.3)	3.8 ± 1.0 (3.5)	24 ± 6 (26)	65 ± 46 (48)	12 ± 7 (9)	10 ± 9 (8)	5.9 ± 4.3 (4)	4.7 ± 1.3 (5.1)
9-Phenanthrenecarboxaldehyde	9-PheA	1.2 ± 0.6 (1.0)	1.7 ± 1.3 (1.0)	1.0 ± 0.1 (1.0)	1.3 ± 0.5 (1.0)	2.6 ± 1.4 (2.9)	1.6 ± 1.2 (1.0)	4.9 ± 7.6 (2.8)	1.9 ± 2.0 (1.0)	1.0 ± 0.1 (1.0)
9,10-Phenanthrenequinone	9,10-PheQ	194 ± 143 (268)	14 ± 2 (15)	80 ± 69 (44)	115 ± 118 (107)	271 ± 336 (19)	15 ± 3 (14)	13 ± 2 (13)	13 ± 4 (12)	55 ± 37 (37)
Benzof[<i>a</i>]fluorenone	BaFluO	4.3 ± 1.5 (4.5)	12 ± 11 (7)	1.7 ± 1.1 (1.2)	6.8 ± 2.2 (6.9)	12 ± 6 (12)	5.5 ± 1.9 (4.5)	6.8 ± 5.9 (5.3)	4.2 ± 2.2 (3.5)	1.6 ± 1.0 (1.1)
Benzof[<i>b</i>]fluorenone	BbFluO	3.6 ± 1.8 (2.9)	6.8 ± 1.8 (6.6)	1.2 ± 0.1 (1.2)	6.1 ± 1.9 (5.7)	12 ± 6 (9)	4.0 ± 2.5 (4.5)	4.6 ± 3.2 (4.3)	2.6 ± 1.2 (2.8)	1.1 ± 0.1 (1.1)
Benzanthrone	BZT	6.2 ± 3.1 (5.3)	8.0 ± 3.4 (6.7)	3.9 ± 2.7 (3.6)	10 ± 3 (10)	24 ± 14 (22)	6.7 ± 3.2 (6.7)	9.3 ± 7.1 (8.4)	4.4 ± 2.0 (4.1)	1.7 ± 1.0 (1.2)
1-Pyrenecarboxaldehyde	1-PyrA	0.9 ± 0.1 (0.9)	1.1 ± 0.1 (1.2)	1.3 ± 0.7 (1.0)	0.9 ± 0.1 (0.9)	2.8 ± 1.9 (2.4)	1.1 ± 0.2 (1.0)	1.5 ± 1.5 (0.9)	1.0 ± 0.3 (0.9)	1.0 ± 0.1 (1.0)
Acenanthrenequinone	AAntQ	1.7 ± 2.3 (0.9)	2.7 ± 2.9 (1.0)	1.1 ± 0.1 (1.1)	0.8 ± 0.1 (0.8)	1.9 ± 2.2 (1.0)	1.0 ± 0.2 (0.9)	2.5 ± 2.5 (1.0)	1.1 ± 0.3 (1.0)	1.1 ± 0.1 (1.0)
Benz[<i>a</i>]anthracene-7,12-dione	BaA-7,12Q	2.3 ± 1.1 (2.6)	4.6 ± 1.8 (4.9)	1.2 ± 0.2 (1.3)	2.4 ± 1.4 (2.4)	8.9 ± 7.3 (6.0)	2.7 ± 1.7 (2.9)	2.6 ± 2.2 (1.2)	1.1 ± 0.3 (1.0)	1.1 ± 0.1 (1.1)
Σ29 Oxy-PAHs		5934 ± 1480 (5482)	7197 ± 27 (7197)	7288 ± 1790 (6622)	9241 ± 633 (9264)	13229 ± 2681 (14612)	13317 ± 3179 (12976)	7219 ± 1692 (7717)	7656 ± 1975 (7548)	8146 ± 2124 (7253)

Table S3 Individual seasonal concentrations (G+P; pg/m³) of nitro-PAHs measured in urban, rural, and background air of Longyearbyen in 2017/2018.

Compound name	Abbreviated name	Cold period						Warm period			
		Dark winter P1 November-January			Twilight winter P2 February			Daylight spring P3 March-April		Polar day summer P4 May-June	
		n=8 UNIS (urban)	n=4 Adventdalen (rural)	n=8 Svalsat (altitudinal)	n=4 UNIS (urban)	n=4 UNIS (urban)	n=7 Adventdalen (rural)	n=12 UNIS (urban)	n=6 Adventdalen (rural)	n=4 Svalsat (altitudinal)	
		mean ± std (median)	mean ± std (median)	mean ± std (median)	mean ± std (median)	mean ± std (median)	mean ± std (median)	mean ± std (median)	mean ± std (median)		
1-Nitronaphthalene	1-NNap	11 ± 7 (11)	2.7 ± 0.3 (2.9)	4.1 ± 2.4 (3.2)	15 ± 7 (13)	21 ± 15 (17)	2.8 ± 1.8 (2.4)	1.9 ± 0.9 (1.9)	2.9 ± 0.1 (2.9)		
2-Methyl-1-nitronaphthalene + 1-Methyl-5-nitronaphthalene	2-Me-1-NNap + 1-Me-5-NNap	5.3 ± 3.6 (4.9)	2.9 ± 1.5 (2.0)	5.4 ± 1.4 (5.8)	4.1 ± 2.8 (3.3)	3.4 ± 3.3 (2.3)	2.2 ± 1.3 (1.7)	3.0 ± 1.5 (2.8)	5.7 ± 0.1 (5.7)		
2-Nitronaphthalene	2-NNap	2.8 ± 0.9 (2.6)	2.7 ± 0.3 (2.9)	2.1 ± 1.2 (2.0)	4.4 ± 1.3 (4.6)	5.1 ± 3.4 (3.6)	2.0 ± 0.8 (2.3)	1.7 ± 0.7 (1.7)	1.0 ± 0.1 (1.0)		
2-Methyl-4-nitronaphthalene	2-Me-4-NNap	1.5 ± 0.8 (1)	1.4 ± 0.8 (1.0)	1.7 ± 0.9 (1.1)	1.2 ± 0.5 (1.0)	1.2 ± 0.2 (1.2)	0.8 ± 0.1 (0.9)	1.0 ± 0.3 (0.9)	1.0 ± 0.1 (1.0)		
1-Methyl-4-nitronaphthalene	1-Me-4-NNap	2.0 ± 1.8 (1.0)	1.5 ± 0.9 (1.0)	1.0 ± 0.1 (1.0)	2.8 ± 0.8 (2.6)	3.9 ± 3.5 (3.2)	1.1 ± 0.7 (0.9)	1.0 ± 0.3 (0.9)	1.0 ± 0.1 (1.0)		
1-Methyl-6-nitronaphthalene	1-Me-6-NNap	1.1 ± 0.6 (0.9)	2.7 ± 0.3 (2.8)	1.3 ± 0.7 (1.1)	0.8 ± 0.1 (0.8)	1.0 ± 0.4 (1.1)	1.0 ± 0.5 (0.9)	1.4 ± 0.6 (1.2)	1.0 ± 0.1 (1.0)		
1,5-Dinitronaphthalene	1,5-DNNap	1.1 ± 0.6 (0.9)	2.7 ± 0.3 (2.9)	1.1 ± 0.1 (1.1)	0.8 ± 0.1 (0.9)	1.1 ± 0.1 (1.1)	1.0 ± 0.2 (0.9)	1.0 ± 0.3 (0.9)	1.0 ± 0.1 (1.0)		
2-Nitrobiphenyl	2-NBPh	0.9 ± 0.1 (0.9)	1.0 ± 0.1 (1.0)	3.8 ± 7.7 (1.1)	0.9 ± 0.1 (0.9)	1.4 ± 1.0 (1.1)	1.0 ± 0.5 (0.9)	1.0 ± 0.3 (0.9)	1.0 ± 0.1 (1.0)		
3-Nitrobiphenyl	3-NBPh	2.1 ± 0.9 (2.5)	2.8 ± 0.4 (2.9)	2.7 ± 2.3 (2.2)	1.6 ± 1.0 (1.1)	2.7 ± 2.1 (1.5)	1.6 ± 0.7 (1.6)	2.7 ± 1.3 (2.5)	1.0 ± 0.1 (1.0)		
3-Nitrodibenzofuran	3-NDBF	1.1 ± 0.6 (0.9)	1.0 ± 0.1 (1.0)	2.1 ± 0.9 (2.0)	0.8 ± 0.1 (0.9)	1.5 ± 1.0 (1.2)	1.2 ± 0.7 (0.9)	1.0 ± 0.3 (0.9)	2.0 ± 1.0 (2.0)		

5-Nitroacenaphthene	5-NAce	1.3 ± 1.1 (1.3)	1.1 ± 0.5 (1.2)	1.2 ± 1.4 (0.6)	4.3 ± 3.9 (4.3)	5.7 ± 4.3 (4.8)	4.0 ± 2.2 (3.9)	1.4 ± 0.8 (1.2)	1.4 ± 0.7 (1.3)	0.5 ± 0.1 (0.5)
2-Nitro-9-fluorenone	2-N-9-FluO	1.8 ± 1.6 (1.0)	0.9 ± 0.1 (1.0)	4.3 ± 8.5 (1.1)	2.9 ± 1.5 (3.1)	2.3 ± 1.3 (2.9)	1.6 ± 1.5 (0.9)	1.4 ± 0.8 (0.9)	1.0 ± 0.3 (1.0)	1.0 ± 0.1 (1.0)
2-Nitrofluorene	2-NFlu	0.9 ± 0.1 (0.9)	1.0 ± 0.1 (1.0)	1.0 ± 0.1 (1.1)	0.9 ± 0.1 (0.8)	1.1 ± 0.1 (1)	1.0 ± 0.2 (0.9)	0.9 ± 0.1 (0.9)	1.0 ± 0.3 (0.9)	1.0 ± 0.1 (1.0)
9-Nitroanthracene	9-NAnt	1.3 ± 1.0 (1.0)	1.0 ± 0.1 (1.0)	1.1 ± 0.1 (1.1)	12 ± 13 (11)	17 ± 13 (18)	13 ± 9 (13)	1.0 ± 0.3 (0.9)	1.1 ± 0.4 (0.9)	1.1 ± 0.1 (1.1)
9-Nitrophenanthrene	9-NPhe	1.2 ± 0.1 (1.1)	1.1 ± 0.1 (1.2)	1.2 ± 0.1 (1.2)	6.1 ± 2 (6.5)	3.1 ± 2.2 (2.9)	1.2 ± 0.3 (1.1)	1.0 ± 0.1 (1.0)	1.2 ± 0.4 (1.1)	1.2 ± 0.1 (1.2)
2-Nitrodibenzothiophene	2-NDBT	0.9 ± 0.1 (0.9)	1.0 ± 0.1 (1.0)	1.1 ± 0.1 (1.1)	0.8 ± 0.1 (0.8)	1.4 ± 0.7 (1.1)	1.0 ± 0.2 (0.9)	0.9 ± 0.1 (0.9)	1.0 ± 0.3 (0.9)	1.0 ± 0.1 (1.0)
3-Nitrophenanthrene	3-NPhe	1.1 ± 0.1 (1.1)	1.1 ± 0.1 (1.1)	1.4 ± 0.8 (1.2)	5.3 ± 5.1 (4.7)	4.8 ± 3.6 (3.9)	1.2 ± 0.3 (1.0)	1.1 ± 0.6 (1.0)	1.1 ± 0.4 (1)	1.1 ± 0.1 (1.1)
2-Nitroanthracene	2-NAnt	0.9 ± 0.1 (0.9)	1.0 ± 0.1 (1.0)	1.1 ± 0.1 (1.1)	0.8 ± 0.1 (0.8)	3.3 ± 4.0 (1.3)	1.1 ± 0.3 (0.9)	1.1 ± 0.5 (0.9)	1.0 ± 0.3 (0.9)	1.0 ± 0.1 (1.0)
9-Methyl-10-Nitroanthracene	9-Me-10-NAnt	0.9 ± 0.1 (0.9)	0.9 ± 0.1 (1.0)	1.0 ± 0.1 (1.0)	0.8 ± 0.1 (0.8)	1.1 ± 0.1 (1.0)	1.0 ± 0.2 (0.9)	0.8 ± 0.1 (0.8)	1.0 ± 0.3 (0.9)	1.0 ± 0.1 (1.0)
2-Nitrofluoranthene	2-NFlu	1.4 ± 0.6 (1.1)	1.0 ± 0.2 (1.0)	1.1 ± 0.1 (1.1)	1.7 ± 1.0 (1.7)	2.9 ± 0.7 (3.1)	1.0 ± 0.2 (0.9)	0.9 ± 0.2 (0.9)	1.0 ± 0.3 (0.9)	1.1 ± 0.1 (1)
3-Nitrofluoranthene	3-NFlu	1.1 ± 0.1 (1.1)	1.2 ± 0.1 (1.2)	1.1 ± 0.1 (1.1)	5.8 ± 1.4 (5.3)	3.9 ± 1.3 (3.9)	3.9 ± 4.8 (1.1)	1.5 ± 0.8 (1.1)	1.1 ± 0.3 (0.9)	1.0 ± 0.1 (1.0)
4-Nitropyrene	4-NPyr	1.2 ± 0.6 (1.0)	1.0 ± 0.1 (1.0)	1.1 ± 0.1 (1.1)	1.2 ± 0.5 (1.0)	1.2 ± 0.1 (1.2)	1.0 ± 0.2 (0.9)	1.1 ± 0.6 (0.9)	1.1 ± 0.4 (0.9)	1.1 ± 0.1 (1.1)
1-Nitropyrene	1-NPyr	1.5 ± 1.1 (1.0)	1.6 ± 1.2 (1.0)	2.0 ± 1.1 (2.1)	1.2 ± 0.5 (1.0)	2.4 ± 1.4 (1.5)	1.1 ± 0.2 (1.1)	1.4 ± 0.7 (1.0)	1.1 ± 0.3 (0.9)	1.0 ± 0.1 (1.0)
2-Nitropyrene	2-NPyr	1.0 ± 0.1 (1.0)	1.0 ± 0.1 (1.0)	1.3 ± 0.7 (1.1)	1.0 ± 0.1 (1.0)	1.3 ± 0.2 (1.2)	1.1 ± 0.3 (0.9)	1.0 ± 0.1 (0.9)	1.1 ± 0.5 (1.0)	1.0 ± 0.1 (1.0)
7-Nitrobenz[a]anthracene	7-NBaA	0.9 ± 0.1 (0.9)	1.0 ± 0.1 (1.0)	1.1 ± 0.1 (1.1)	0.9 ± 0.1 (0.9)	1.4 ± 0.9 (1.1)	7.6 ± 6.0 (8.0)	0.9 ± 0.1 (0.9)	1.1 ± 0.3 (0.9)	1.0 ± 0.1 (1.0)
6-Nitrochrysene	6-NChry	1.2 ± 0.6 (1.1)	1.2 ± 0.1 (1.2)	1.1 ± 0.1 (1.1)	2.1 ± 0.8 (2.3)	8.1 ± 6.7 (3.9)	3.5 ± 2.6 (2.5)	1.0 ± 0.2 (1.0)	1.1 ± 0.3 (0.9)	1.0 ± 0.1 (1.0)
1,3-Dinitropyrene	1,3-DNPyr	4.5 ± 0.5 (4.5)	4.6 ± 0.5 (4.9)	5.1 ± 0.4 (5.1)	4.4 ± 0.4 (4.4)	9.0 ± 4.2 (6.1)	4.9 ± 1.0 (4.4)	4.2 ± 0.5 (4.3)	5.0 ± 1.7 (4.4)	5.0 ± 0.1 (5.0)

Table S3 (continued)

Compound name	Abbreviated name	Cold period						Warm period		
		Dark winter P1 November-January		Twilight winter P2 February		Daylight spring P3 March-April		Polar day summer P4 May-June		
		n=8 UNIS (urban)	n=4 Adventdalen (rural)	n=8 Svalsat (altitudinal)	n=4 UNIS (urban)	n=7 UNIS (urban)	n=7 Adventdalen (rural)	n=12 UNIS (urban)	n=6 Adventdalen (rural)	n=4 Svalsat (altitudinal)
	mean \pm std (median)	mean \pm std (median)	mean \pm std (median)	mean \pm std (median)	mean \pm std (median)	mean \pm std (median)	mean \pm std (median)	mean \pm std (median)	mean \pm std (median)	
1,6-Dinitropyrene	1,6-DNPyr	12 \pm 1 (12)	12 \pm 1 (13)	14 \pm 1 (14)	11 \pm 2 (11)	14 \pm 2 (13)	13 \pm 3 (12)	11 \pm 1 (11)	13 \pm 4 (12)	13 \pm 0.1 (13)
1,8-Dinitropyrene	1,8-DNPyr	11 \pm 1 (11)	12 \pm 1 (12)	13 \pm 1 (13)	10 \pm 2 (10)	13 \pm 2 (13)	12 \pm 3 (11)	11 \pm 1 (11)	13 \pm 4 (11)	13 \pm 0.1 (13)
1-Nitrobenzo[e]pyrene + 6-Nitrobenzo[a]pyrene	1-NBePyr + 6-NBaPyr	1.9 \pm 1.0 (1.6)	1.7 \pm 0.3 (1.6)	1.8 \pm 0.2 (1.8)	1.5 \pm 0.1 (1.5)	2.0 \pm 0.2 (2.0)	1.9 \pm 0.4 (1.7)	1.5 \pm 0.2 (1.4)	1.9 \pm 0.5 (1.6)	1.7 \pm 0.1 (1.7)
3-Nitrobenzo[e]pyrene	3-NBePyr	1.1 \pm 0.1 (1.1)	1.2 \pm 0.1 (1.2)	1.3 \pm 0.1 (1.3)	1.1 \pm 0.3 (1.1)	1.4 \pm 0.2 (1.5)	1.2 \pm 0.3 (1.1)	1.1 \pm 0.2 (1.1)	1.3 \pm 0.4 (1.1)	1.3 \pm 0.1 (1.3)
1-Nitrobenzo[a]pyrene	1-NBaPyr	3.5 \pm 0.3 (3.6)	3.8 \pm 0.4 (4.0)	4.1 \pm 0.3 (4.2)	3.5 \pm 0.3 (3.5)	4.1 \pm 0.7 (4.1)	5.4 \pm 3.2 (3.7)	3.4 \pm 0.4 (3.4)	4.0 \pm 1.3 (3.5)	4.0 \pm 0.1 (4.0)
3-Nitrobenzo[a]pyrene	3-NBaPyr	1.7 \pm 0.1 (1.7)	1.8 \pm 0.2 (1.9)	2.0 \pm 0.2 (2.0)	2.3 \pm 1.3 (1.8)	2.1 \pm 0.3 (2.0)	1.9 \pm 0.4 (1.7)	1.6 \pm 0.2 (1.6)	2.0 \pm 0.6 (1.7)	1.9 \pm 0.1 (1.9)
Σ35 Nitro-PAHs		83.7 \pm 18.6 (78.9)	75.6 \pm 5.2 (75.9)	88.5 \pm 14.8 (86.9)	113.5 \pm 12.9 (116.6)	149.6 \pm 34.3 (131.2)	102.6 \pm 20.8 (103.1)	65.6 \pm 9.2 (66.2)	73.6 \pm 22.5 (65.6)	73.8 \pm 1.3 (73.3)

Table S4. Seasonal sum concentrations (G+P) of PAHs, oxy-PAHs, and nitro-PAHs [$\mu\text{g}/\text{m}^3$], and OC and EC [$\mu\text{g}/\text{m}^3$] measured in urban, rural, and background (altitudinal) air of Longyearbyen in 2017/2018.

Compound name	Cold period				Warm period				
	Dark winter P1 November-January		Twilight winter P2 February		Daylight spring P3 March-April		Polar day summer P4 May-June		
	n=8 UNIS (urban)	n=4 Adventdalen (rural)	n=8 Svalsat (altitudinal)	n=4 UNIS (urban)	n=7 UNIS (urban)	n=7 Adventdalen (rural)	n=6 Adventdalen (rural)	n=4 Svalsat (altitudinal)	
	mean \pm std (median)	mean \pm std (median)	mean \pm std (median)	mean \pm std (median)	mean \pm std (median)	mean \pm std (median)	mean \pm std (median)	mean \pm std (median)	
$\Sigma 22$ PAHs	1068 \pm 449 (957)	1016 \pm 321 (988)	897 \pm 453 (765)	3923 \pm 667 (3929)	5902 \pm 2421 (5466)	3452 \pm 2637 (2569)	1779 \pm 1210 (1352)	576 \pm 216 (438)	467 \pm 339 (333)
$\Sigma 14$ EPA PAHs (no Nap and Acy)	839 \pm 366 (772)	663 \pm 258 (537)	540 \pm 206 (504)	2733 \pm 772 (2483)	3290 \pm 1721 (4040)	1239 \pm 1057 (844)	1392 \pm 998 (1091)	351 \pm 123 (322)	337 \pm 237 (257)
$\Sigma 29$ oxy-PAHs	5934 \pm 1480 (5482)	7197 \pm 27 (7197)	7288 \pm 1790 (6622)	9241 \pm 633 (9264)	13229 \pm 2681 (14612)	13317 \pm 3179 (12976)	7219 \pm 1692 (7717)	7656 \pm 1975 (7548)	8146 \pm 2124 (7253)
$\Sigma 35$ nitro-PAHs	83.7 \pm 18.6 (78.9)	75.6 \pm 5.2 (75.9)	88.5 \pm 14.8 (86.9)	113.5 \pm 12.9 (116.6)	149.6 \pm 34.3 (131.2)	102.6 \pm 20.8 (103.1)	65.6 \pm 9.2 (66.2)	73.6 \pm 22.5 (65.6)	73.8 \pm 1.3 (73.3)
Elemental carbon EC	0.09 \pm 0.08 (0.06)	0.11 \pm 0.06 (0.1)	0.02 \pm 0.02 (0.01)	0.10 \pm 0.09 (0.09)	0.18 \pm 0.08 (0.15)	0.13 \pm 0.09 (0.17)	0.16 \pm 0.11 (0.13)	0.04 \pm 0.03 (0.04)	0.05 \pm 0.05 (0.03)
Organic carbon OC	0.42 \pm 0.18 (0.38)	0.42 \pm 0.09 (0.4)	0.31 \pm 0.11 (0.3)	0.42 \pm 0.23 (0.36)	0.71 \pm 0.2 (0.65)	0.4 \pm 0.16 (0.42)	0.64 \pm 0.31 (0.55)	0.31 \pm 0.2 (0.21)	0.23 \pm 0.13 (0.18)
OC/EC	6.1 \pm 2.8 (5)	5.0 \pm 1.8 (5.7)	22.6 \pm 13.9 (24.3)	6.1 \pm 4.2 (4.4)	4.3 \pm 1.2 (3.7)	8.0 \pm 8.9 (3.3)	4.8 \pm 2.3 (4.1)	8.6 \pm 5.4 (5.2)	7.7 \pm 5.4 (6.6)

Table S5. Sampling periods and air sample volumes.

Period	Sample	Sampling start		Sampling stop		T mean, [°C]	Sample volume, [m ³]
		Date	Local time	Date	Local time		
P1	UNIS 1	28.11.2017	14:45	29.11.2017	14:55	-10.2	342.9
P1	UNIS 2	01.12.2017	15:11	02.12.2017	16:32	-6.0	353.9
P1	UNIS 3	03.12.2017	12:18	04.12.2017	10:53	-0.5	318.9
P1	UNIS 4	15.01.2018	13:17	16.01.2018	15:21	2.0	392.4
P1	UNIS 5	16.01.2018	15:26	17.01.2018	15:07	0.2	350.9
P1	UNIS 6	17.01.2018	15:10	18.01.2018	15:48	-0.6	368.2
P1	UNIS 7	20.01.2018	13:52	21.01.2018	12:42	-4.5	352.2
P1	UNIS 8	21.01.2018	13:17	22.01.2018	15:34	-2.7	417.1
P1	ADVENT 1	28.11.2017	11:55	29.11.2017	14:00	-11.8	386.9
P1	ADVENT 2	29.11.2017	14:17	30.11.2017	12:48	-11.0	321.6
P1	ADVENT 3	22.01.2018	13:20	23.01.2018	14:02	-3.4	316.9
P1	SVALSAT 1	04.12.2017	12:22	05.12.2017	13:04	-7.8	306.6
P1	SVALSAT 2	06.12.2017	12:32	07.12.2017	11:21	-8.6	291.4
P1	SVALSAT 3	09.12.2017	15:29	10.12.2017	13:18	-7.6	270.1
P1	SVALSAT 4	10.12.2017	13:21	11.12.2017	13:12	-7.3	305.8
P1	SVALSAT 5	11.12.2017	13:12	12.12.2017	13:20	-5.1	299.7
P1	SVALSAT 6	12.12.2017	14:12	13.12.2017	12:35	-7.8	313.5
P1	SVALSAT 7	09.01.2018	12:09	10.01.2018	12:20	-6.6	334.3
P1	SVALSAT 8	10.01.2018	12:20	11.01.2018	13:55	-3.5	356.9
P2	UNIS 9	31.01.2018	16:15	01.02.2018	16:03	-15.6	410.3
P2	UNIS 10	01.02.2018	16:05	02.02.2018	22:02	-12.4	485.5
P2	UNIS 11	08.02.2018	20:20	09.02.2018	21:58	-3.2	324.9
P2	UNIS 12	13.02.2018	15:49	14.02.2018	21:42	-5.9	364.3
P3	UNIS 13	15.03.2018	15:27	16.03.2018	13:37	-7.6	256.2
P3	UNIS 14	22.03.2018	10:50	23.03.2018	13:22	-12.9	312.1
P3	UNIS 15	27.03.2018	15:43	28.03.2018	15:24	-11.2	283.7
P3	UNIS 16	03.04.2018	13:47	04.04.2018	16:01	-14.7	370.4
P3	UNIS 17	06.04.2018	21:48	07.04.2018	20:11	-14.4	335.0
P3	UNIS 18	07.04.2018	20:15	08.04.2018	22:13	-12.7	369.5
P3	UNIS 19	10.04.2018	21:21	11.04.2018	15:48	-8.3	257.2
P3	ADVENT 4	23.02.2018	14:38	24.02.2018	14:46	-3.2	357.0
P3	ADVENT 5	24.02.2018	14:50	25.02.2018	15:37	-3.8	370.6
P3	ADVENT 6	03.04.2018	14:32	04.04.2018	16:43	-15.7	345.8
P3	ADVENT 7	04.04.2018	16:47	05.04.2018	20:49	-15.3	367.0
P3	ADVENT 8	06.04.2018	22:13	07.04.2018	19:48	-15.4	291.6
P3	ADVENT 9	09.04.2018	17:42	10.04.2018	21:50	-10.7	362.9

Table S5 (continued)

P3	ADVENT 10	10.04.2018	21:55	11.04.2018	15:12	-9.2	222.0
P4	UNIS 20	16.05.2018	22:10	17.05.2018	21:58	4.7	356.6
P4	UNIS 21	24.05.2018	15:20	25.05.2018	16:21	1.7	344.1
P4	UNIS 22	28.05.2018	13:38	29.05.2018	15:55	2.7	397.6
P4	UNIS 23	29.05.2018	15:59	30.05.2018	16:05	2.2	369.7
P4	UNIS 24	01.06.2018	14:31	02.06.2018	22:56	3.4	476.0
P4	UNIS 25	04.06.2018	13:44	05.06.2018	16:01	2.1	420.0
P4	UNIS 26	06.06.2018	15:47	07.06.2018	16:01	3.4	361.6
P4	UNIS 27	12.06.2018	15:46	13.06.2018	23:24	1.5	439.2
P4	UNIS 28	14.06.2018	14:43	15.06.2018	13:38	4.1	319.4
P4	UNIS 29	18.06.2018	11:49	19.06.2018	15:01	6.2	400.4
P4	UNIS 30	20.06.2018	17:21	21.06.2018	16:20	5.8	315.1
P4	UNIS 31	22.06.2018	15:53	23.06.2018	18:50	5.4	380.0
P4	ADVENT 11	01.06.2018	15:01	02.06.2018	22:21	3.1	419.3
P4	ADVENT 12	04.06.2018	14:46	05.06.2018	17:40	1.8	369.7
P4	ADVENT 13	06.06.2018	15:07	07.06.2018	17:01	3.3	351.5
P4	ADVENT 14	12.06.2018	16:07	13.06.2018	23:10	1.3	401.2
P4	ADVENT 15	14.06.2018	15:06	15.06.2018	17:05	4.0	290.0
P4	ADVENT 16	18.06.2018	12:20	19.06.2018	03:01	6.1	193.0
P4	SVALSAT 9	20.06.2018	13:41	21.06.2018	13:54	2.9	323.8
P4	SVALSAT 10	21.06.2018	14:00	22.06.2018	14:06	3.0	312.5
P4	SVALSAT 11	28.06.2018	09:01	29.06.2018	09:01	1.7	318.4
P4	SVALSAT 12	04.07.2018	15:09	05.07.2018	15:18	3.7	315.0

Table S6. Svalbard background air concentrations (G+P; $\mu\text{g}/\text{m}^3$) of $\Sigma 20$ PAHs measured in Longyearbyen (Svalsat) and Ny-Ålesund (Zeppelin) in 2017/2018.

Location	Season	N samples	Mean	Std	Min	Median	Max
Svalsat	winter P1	8	645	273	338	604	1260
Zeppelin	winter P1	6	719	334	335	692	1137
Svalsat	summer P4	4	428	332	193	300	919
Zeppelin	summer P4	4	68	20	46	67	91

Zeppelin data was acquired from <http://ebas.nilu.no>, last access: 20 December 2020

Summed compounds are 1-MeNap, 2-MeNap, Ace, Flu, Phe, Ant, Flt, Pyr, BaAnt, Chry, Ret, BePyr, BjFlt, BbFlt, BkFlt, BaP, DBAnt, BghiP, IPyr, Cor

For accurate comparison, samples from the same winter (Dec-Jan 2017/2018) and summer (June-July 2018) periods were considered

Table S7. %PM of PAHs during cold and warm periods.

	COLD period (November-April) n=35		WARM period (May-July) n=21	
	Mean	Std	Mean	Std
Naphtalene	2.8	3.8	9.8	8.9
1-Methylnaphtalene	13.2	21.2	27.6	16.4
2-Methylnaphtalene	97.1	1.2	98.2	0.8
Acenaphtene	2.7	2.5	2.7	1.4
Fluorene	1.5	1.1	2.9	2.5
Phenanthrene	9.6	10.1	6.7	6.8
Anthracene	3.3	1.4	3.6	1.9
Fluoranthene	65.5	37.4	78.1	32.2
2-Methylfluoranthene	27.5	14.0	27.8	11.2
Pyrene	37.9	26.2	16.7	13.8
Benzo[a]anthracene	n.d.	-	96.8	0.2
Chrysene	78.4	5.7	78.8	8.9
Retene	n.d.	-	n.d.	-
Benzo[e]pyrene	n.d.	-	n.d.	-
Benzo[j]fluoranthene	n.d.	-	n.d.	-
Benzo[b]fluoranthene	92.9	1.2	85.6	0.3
Benzo[k]fluoranthene	n.d.	-	85.6	0.8
Benzo[a]pyrene	93.8	1.1	93.5	1.2
Dibenzo[a,h]anthracene	97.7	1.2	n.d.	-
Benzo[g,h,i]perylene	94.7	1.3	93.5	0.6
Indeno[1,2,3-cd]pyrene	n.d.	-	n.d.	-
Coronene	94.0	2.4	n.d.	-

Table S8. %PM of oxy-PAHs during cold and warm periods.

	COLD period (November-April) n=35		WARM period (May-July) n=22	
	Mean	Std	Mean	Std
Phthalaldehyde	77.9	23.5	63.9	16.4
Phthalic anhydride	26.4	18.0	19.8	12.0
1,4-Naphthoquinone	53.2	26.9	29.2	28.5
1-Naphthaldehyde	21.8	23.1	6.8	6.5
2-Formyl-trans-cinnamaldehyde	75.6	24.5	81.9	14.3
1,2-Naphthoquinone	0.6	0.4	54.3	-
Benzophenone	15.7	24.3	17.1	12.3
1-Acenaphthenone	50.9	23.7	23.6	14.9
9-Fluorenone	48.3	22.2	33.3	16.6
1,2-Naphthalic anhydride	27.1	15.1	32.4	18.5
Biphenyl-2,2'-dicarboxaldehyde	68.8	20.8	45.2	18.1
Xanthone	52.9	24.3	70.7	18.6
Acenaphthenequinone	40.3	21.3	45.8	19.3
2,3-Naphthalenedicarboxylic anhydride	48.0	31.2	52.5	33.4
Anthrone	48.8	39.7	57.5	42.9
6H-Dibenzo[b,d]pyran-6-one	56.5	26.1	71.8	25.0
9,10-Anthraquinone	44.9	25.4	44.5	21.8
1,8-Naphthalic anhydride	42.5	20.6	42.4	23.5
1,4-Anthraquinone	n.d.	-	n.d.	-
4,4'-Biphenyldicarboxaldehyde	23.1	9.8	26.1	13.7
2-Methylanthraquinone	63.4	17.0	67.5	15.9
9-Phenanthrenecarboxaldehyde	71.4	27.8	77.3	13.1
9,10-Phenanthrenequinone	77.9	11.4	72.6	11.1
Benzo[a]fluorenone	56.1	16.9	63.5	15.5
Benzo[b]fluorenone	56.7	16.3	57.6	23.0
Benzanthrone	67.2	14.8	75.5	10.4
1-Pyrenecarboxaldehyde	n.d.	-	86.5	5.2
Aceanthrenequinone	n.d.	-	n.d.	-
Benz[a]anthracene-7,12-dione	67.3	20.4	85.2	2.2

Table S9. %PM of nitro-PAHs during cold and warm periods.

	COLD period (November-April)		WARM period (May-July)	
	Mean	Std	Mean	Std
1-Nitronaphthalene	7.9	13.8	1.3	0.3
2-Methyl-1-Nitronaphthalene + 1-Methyl-5-Nitronaphthalene	17.2	27.4		
2-Nitronaphthalene	28.1	22.0		
1-Methyl-4-nitronaphthalene	73.8	13.5		
2-Nitrobiphenyl	0.4	0.2		
3-Nitrobiphenyl	36.9	31.3		
5-Nitroacenaphthene	0.9	0.3	1.3	0.3
2-Nitro-9-fluorenone	1.6	0.0		
9-Nitroanthracene	7.5	22.9		
9-Nitrophenanthrene	3.0	1.1		
3-Nitrophenanthrene	1.1	0.2		
2-Nitroanthracene	1.2	0.3		
2-Nitrofluoranthene	65.9	5.2		
3-Nitrofluoranthene	3.8	0.9		
1-Nitropyrene	71.8	6.2	67.7	1.0
7-Nitrobenz[a]anthracene	0.8	0.2		
6-Nitrochrysene	1.4	0.3		
1-Nitrobenzo[a]pyrene	5.1	1.7		

Figure S1. Location of Svalbard in the Arctic.

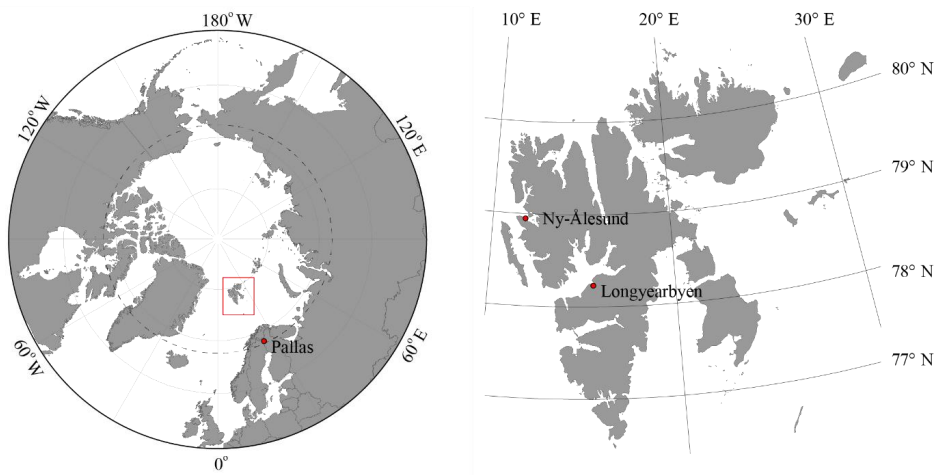


Figure S2. Air sampling sites in Longyearbyen: urban (UNIS), rural (Adventdalen), altitudinal (Svalsat).

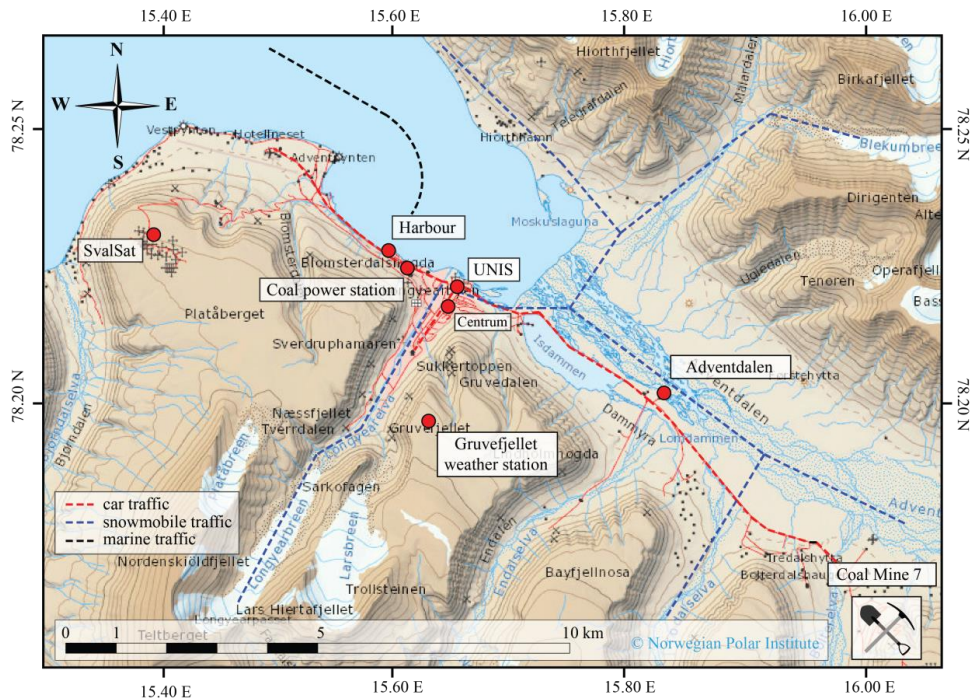


Figure S3. Annual sun diagram for Longyearbyen location.

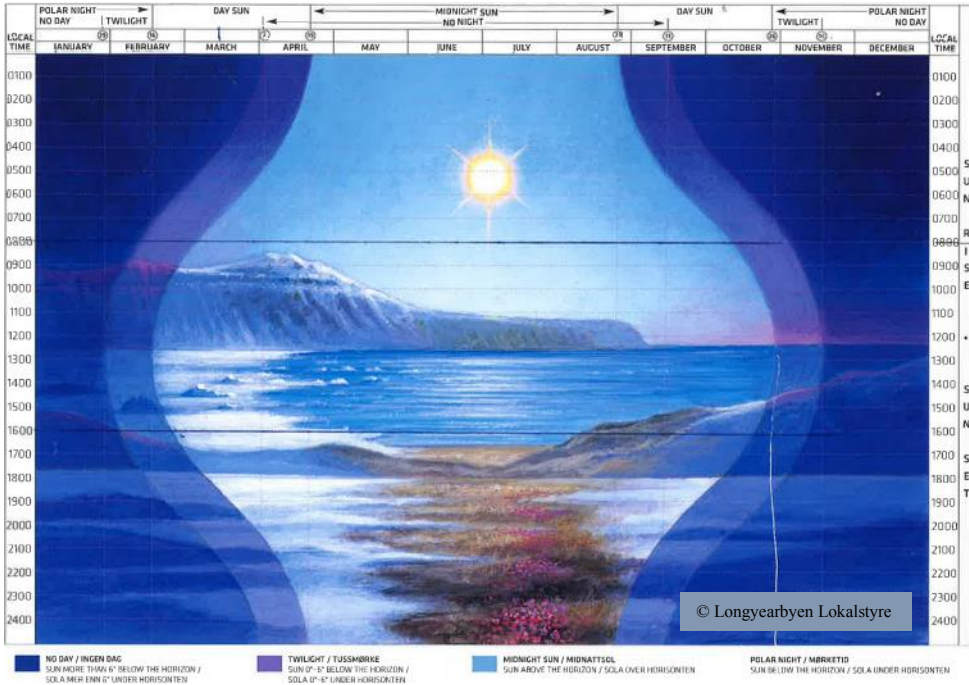
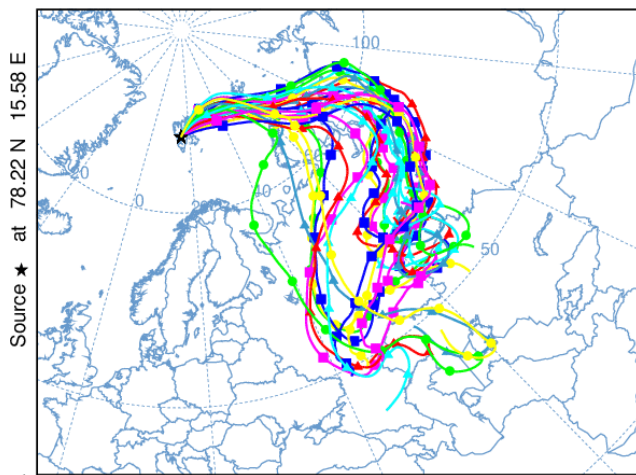
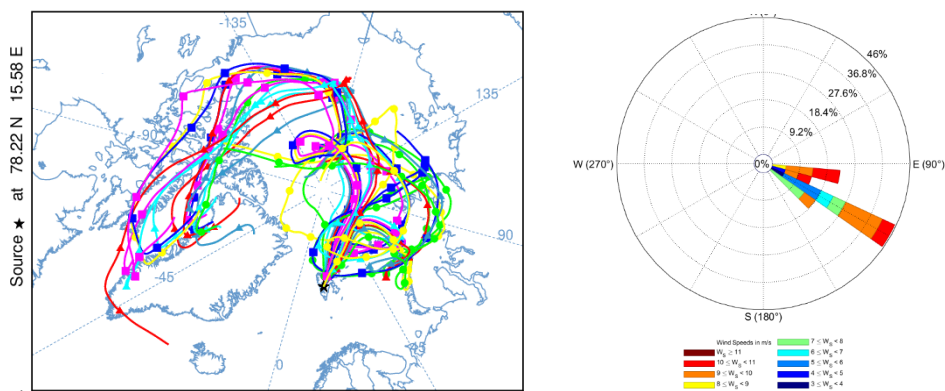


Figure S4. 10-day backward trajectories for the air pollution event in Longyearbyen on 5th of December 2017.



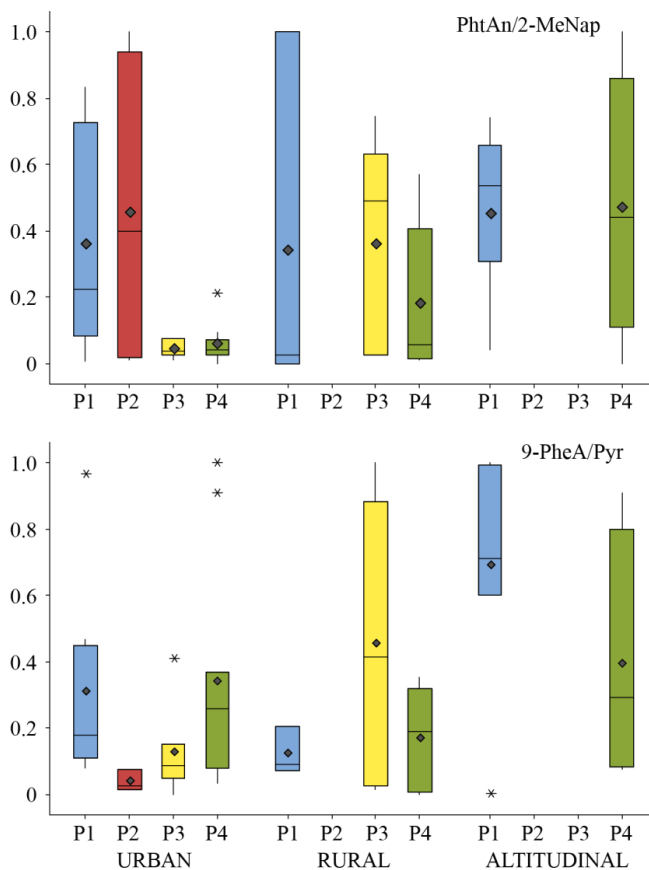
Back-trajectories were calculated for air arriving at the 500 m height above sampling site using the US NOAA Hybrid Single Particle Lagrangian Integrated Trajectory (HYSPLIT) model.

Figure S5. 10-day backward trajectories and wind rose for the dust event in Longyearbyen on 29th of November 2017.



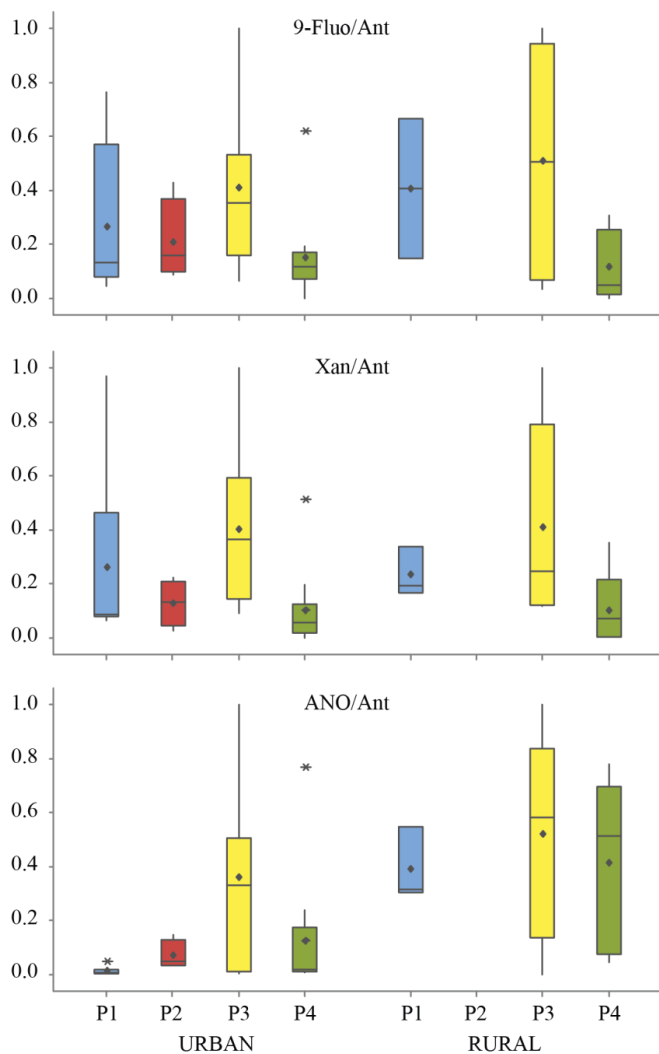
Back-trajectories were calculated for air arriving at the 500 m height above sampling site using the US NOAA Hybrid Single Particle Lagrangian Integrated Trajectory (HYSPLIT) model. A 24-hour wind rose was plotted in MATLAB software (R2020a, The MathWorks Inc., Natick, MA, USA) using hourly-registered data at Adventdalen weather station.

Figure S6. Seasonal evolution of product to reactant concentration ratios at three sites indicating PAC's oxidation during *polar night* in winter (P1).



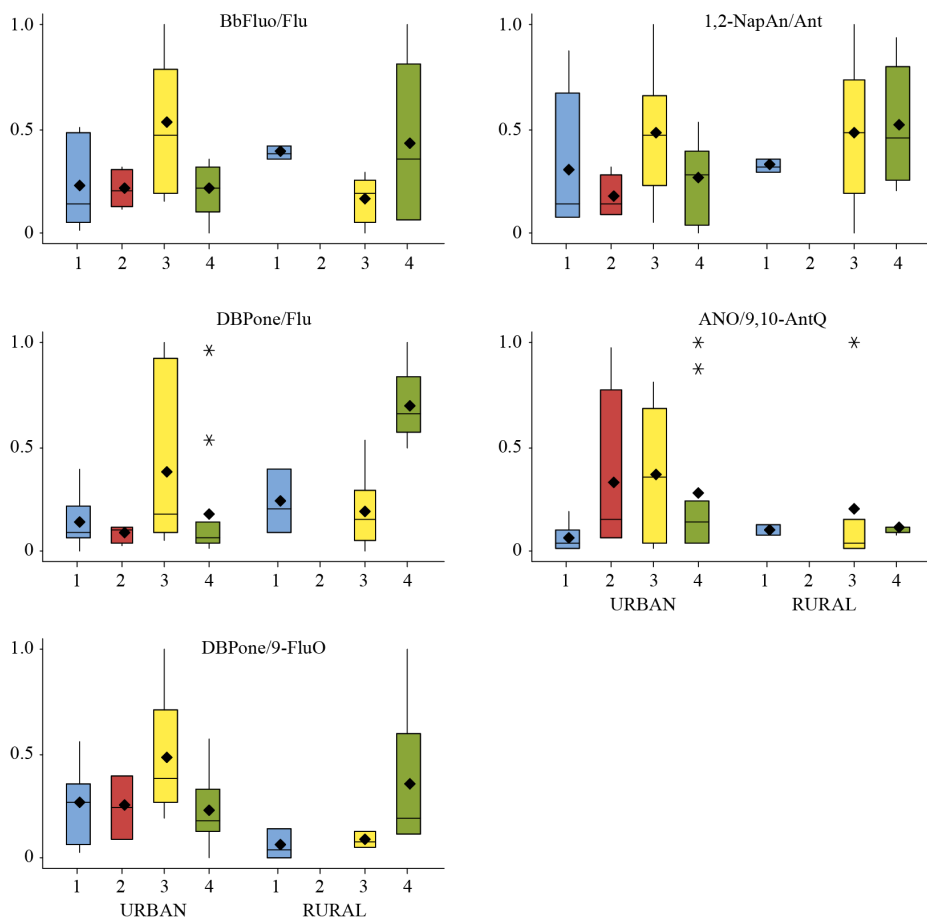
Note: Data are for the November-January (P1), February (P2), March-April (P3), and May-June (P4) periods.

Figure S7. Seasonal evolution of product to reactant concentration ratios at two sites indicating PAC's oxidation during *spring* (P3).



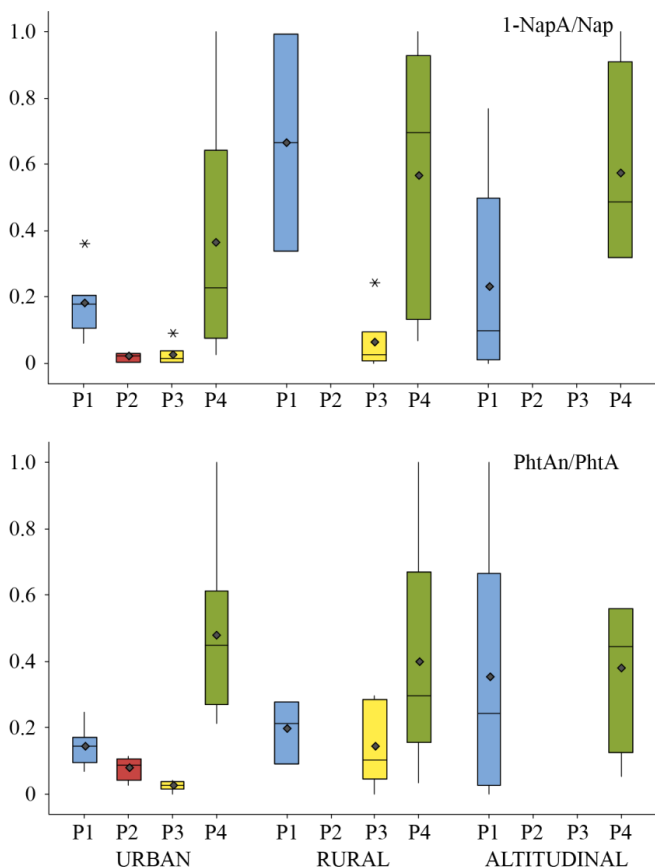
Note: Data are for the November-January (P1), February (P2), March-April (P3), and May-June (P4) periods. No samples at Svalvat site were taken in spring due to high avalanche danger.

Figure S8. Seasonal evolution of product to reactant concentration ratios at two sites indicating PAC's oxidation during *spring* (P3) mostly at UNIS.



Note: Data are for the November-January (P1), February (P2), March-April (P3), and May-June (P4) periods. No samples at Svalsat site were taken in spring due to high avalanche danger.

Figure S9. Seasonal evolution of product to reactant concentration ratios at three sites indicating PAC's oxidation during *summer* (P4).



Note: Data are for the November-January (P1), February (P2), March-April (P3), and May-June (P4) periods.

ISBN: 978-82-575-1857-8

ISSN: 1894-6402



The University Centre in Svalbard (UNIS)
Telephone: +47 79 02 33 00
www.unis.no
E-mail: post@unis.no / webmaster@unis.no
Address: P.O. Box 156 N-9171 Longyearbyen
Org. no. 985 204 454



Norwegian University
of Life Sciences

Postboks 5003
NO-1432 Ås, Norway
+47 67 23 00 00
www.nmbu.no